SUPERCRITICAL WATER GASIFICATION OF WOOD-RELATED PRODUCTS: A THERMODYNAMIC AND EXPERIMENTAL STUDY

by

Jeanne Louw

Dissertation presented for the Degree

of

DOCTOR OF PHILOSOPHY
(Chemical Engineering)

in the Faculty of Engineering
at Stellenbosch University

Supervisor
Prof. A.J. Burger

Co-Supervisor
Prof. C.E. Schwarz

December 2016

DECLARATION

By submitting this dissertation electronically, I declare that the entirety of the work contained therein is my own, original work, that I am the sole author thereof (save to the extent explicitly otherwise stated), that reproduction and publication thereof by Stellenbosch University will not infringe any third party rights and that I have not previously in its entirety or in part submitted it for obtaining any qualification.

Date: ……..

This dissertation includes 3 original papers published in peer-reviewed journals or books and 0 unpublished publications. The development and writing of the papers (published and unpublished) were the principal responsibility of myself and, for each of the cases where this is not the case, a declaration is included in the dissertation including the nature and extend of the contributions of co-authors.

ABSTRACT

Supercritical water gasification (SCWG) is a method through which energy can be harvested, allowing high-energy gases such as hydrogen and methane to be generated from wet organic materials without prior energy-intensive drying. This thesis provides new insight into and an improved understanding of both the thermodynamic equilibrium and practical kinetic behaviour during SCWG of three wood-derived products, namely wood chips, primary paper sludge and wood-based pyrolysis char.

A method, based on thermodynamic equilibrium calculations and the feedstock composition (molar H/C and O/C ratio) was developed to aid in the selection of suitable feed material and operating conditions for SCWG[1]. It was shown that, thermodynamically, feed material containing less oxygen, such as pyrolysis char, might be a promising feed material to achieve high H_2 and CH_4 yields as well as a gas product with a high calorific value.

Experimental and theoretical thermodynamic equilibrium results are presented for SCWG of primary paper waste sludge (PWS)[2], *E.grandis* wood chips and various related pyrolysis chars[3]. The effect of various parameters that may influence the kinetic behaviour were assessed, including catalyst type, catalyst loading, reaction time and feedstock composition (specifically O/C ratio and volatile matter content).

A gas product relatively close to the calculated thermodynamic composition was produced during SCWG of PWS and *E.grandis* using a high loading of heterogeneous catalyst (0.5 – 1

[1] Louw, J., Schwarz, C.E., Knoetze, J.H., Burger, A.J., *Thermodynamic modelling of supercritical water gasification: Investigating the effect of biomass composition to aid in the selection of appropriate feedstock material*. Bioresource Technology, Vol 174 (2014), pp 11-23 (DOI: 10.1016/j.biortech.2014.09.129).

[2] Louw, J., Schwarz, C.E., Burger, A.J., *Catalytic supercritical water gasification of primary paper sludge using a homogeneous and heterogeneous catalyst: Experimental vs thermodynamic equilibrium results*. Bioresource Technology, Vol 201 (2016), pp 111-120 (DOI: 10.1016/j.biortech.2015.11.043).

[3] Louw, J., Schwarz, C.E., Burger, A.J., *Supercritical water gasification of Eucalyptus grandis and related pyrolysis char: Effect of feedstock composition*. Bioresource Technology, Vol 216 (2016), pp 1030-1039 (DOI: 10.1016/j.biortech.2016.06.062).

$g/g_{feed,dry}$ Ni/Al_2O_3-SiO_2) and longer reaction times (60 – 120 min). Furthermore, significantly higher conversion of carbon to the gas phase was achieved with Ni/Al_2O_3-SiO_2 than with a homogeneous catalyst (K_2CO_3). While feed material with lower O/C ratios typically resulted in higher thermodynamic equilibrium CH_4 yields and gasification efficiencies, these feed material resulted in the lowest experimental CH_4 yields and gasification efficiencies. Furthermore, a linear relationship between the carbon efficiency (CE) and both the volatile matter content and O/C ratio of the feed material was found to hold true in both catalytic and non-catalytic experiments. The results suggest that, although thermodynamic calculations disregard the volatile matter content of the feed material, very useful predictive information can still be obtained from such calculations. It should therefore not be disregarded when considering a specific material as possible feedstock for SCWG.

To summarise, this dissertation provides more insight into both the thermodynamic equilibrium and possible kinetic effects associated with SCWG for various wood-related products. The major contributions are encapsulated in three peer reviewed journal publications[1-3].

OPSOMMING

Superkritiese water vergassing (SKWVG) is 'n metode waardeur hoë-energie gasse soos waterstof en metaan geproduseer kan word deur van nat organiese materiaal as voer materiaal gebruik te maak sonder energie-intensiewe drogingsproses. Hierdie tesis bied nuwe insig in en 'n beter begrip van beide die termodinamiese ewewig en praktiese kinetiese gedrag tydens SCWG van drie houtagtige produkte, naamlik houtsaagsels, primêre papierafval slyk en houtskool geproduseer tydens pirolise van hout saagsels.

'n Metode, gebaseer op termodinamiese ewewigsberekeninge en die voermateriaal samestelling (molêre H/C en O/C verhoudings) is ontwikkel om te help met die keuse van geskikte voer materiaal en bedryfstoestande vir SKWVG. Termodinamiese ewewigsberekeninge het getoon dat voer materiaal wat minder suurstof bevat (soos houtskool), 'n belowende voer materiaal vir SKWVG kan wees aangesien dit ’n gasproduk met hoë H_2 en CH_4 inhoud produseer. Gevolglik het hierdie gasproduk ’n hoë kalorie waarde.

Beide eksperimentele- en teoretiese termodinamiese ewewigsresultate wanneer primêre afval papier slyk, *E.grandis* houtsaagsels en verskeie verwante houtskool voer materiale as voer materiaal gebruik is, word in hierdie proefskrif bespreek. Die bespreking sluit die effek wat verskillende faktore soos die soort katalisator, katalisator lading, reaksie tyd sowel as die samestelling van die roumateriaal samestelling (spesifiek O / C-verhouding en vlugtige materiaal inhoud) in.

'n Gasproduk met samestelling relatief naby aan die berekende termodinamiese samestelling kan geproduseer word tydens SKWVG van papier slyk en *E.grandis* wanneer 'n hoë heterogene katalisator (0.5 – 1 $g/g_{voer,droog}$ Ni/Al_2O_3-SiO_2) en langer reaksie tye (60 – 120 min). Aansienlike hoër omsetting van koolstof na die gasfase is behaal wanneer Ni/Al_2O_3-SiO_2 as katalisator gebruik word, in vergelyking met wanneer 'n homogene katalisator (K_2CO_3) gebruik word. Voer materiale met laer O/C verhoudings het hoër CH_4 termodinamiese ewewigopbrengste en vergassingsdoeltreffendheid tot gevoel gehad het. Hierdie selfde voer materiale het egter die laagste eksperimentele CH_4 opbrengste en vergassingdoeltreffendheid tot gevolg gehad. Verder

is 'n lineêre verwantskap tussen die koolstofvergassingsdoeltreffendheid en beide die vlugtige materiaal inhoud en die O/C verhouding van die voer materiaal is gevind. Die resultate dui daarop dat, hoewel termodinamiese ewewigsberekeninge nie die vlugtige materiaal inhoud van die voer materiaal in ag neem nie, dit 'n belangrike rol speel in hoe maklik 'n sekere voer materiaal in superkritiese water omgesit word na ’n gas. Dit moet dus nie buite rekening gelaat word wanneer 'n spesifieke materiaal as moontlike voermateriaal vir SKWVG oorweeg word nie.

Ter opsomming, hierdie verhandeling bied meer insig in beide die termodinamiese ewewig en moontlike kinetiese effekte wat verband hou met SKWVG vir verskeie hout-verwante produkte. Die groot bydraes is vervat in drie portuurbeoordeelde joernaalpublikasies.

ACKNOWLEDGEMENTS

I could not have completed this project without the assistance, encouragement and support of my family, friends and colleagues. I would like to thank and honour the following people and institutions:

My supervisor, Prof André Burger: We started out this project without any prior knowledge in this specific research field and you warned me that it will sometimes be a lonely journey. Thank you for all the financial and moral support as well as practical engineering advice.

My co-supervisor, Prof Cara Schwarz: Even though you were only recently appointed as an official supervisor, your input throughout the whole project was of great value (especially in the high pressure equipment design and supercritical fluid field).

The National Research Foundation (NRF) and Sasol-Stellenbosch 2020: Thank you for the financial support throughout various stages of this project.

The workshop staff at Process Engineering, Mr. Jos Weerdenberg and Mr Anton Cordier: Without the technical staff at the Process Engineering Department, we would not be able to do any experimental work. Throughout the duration of my experimental work I spent a fair amount of time in the workshop. Thank you for all your assistance during the experimental part of the project and for helping me with the closing and opening of my reactor and also for the construction of the mechanical swivel arm, which I could use to insert my reactor safely into the hot sand bath.

The analytical staff at Process Engineering, Mrs. Hanlie Botha and Mrs. Levine Simmers: Thank you for assisting me in various analytical activities and for all your advice.

The Separations Technology research group colleagues: Thank you for all the good conversations and coffees that we could share in the office.

Herman Franken, Nardus Uys, Jason Smit and Frederick Fourie: Thank you for providing practical and technical assistance during the experimental phase of my project.

Prof Johan Görgens and Dr. Eugene van Rensburg: Thank you for allowing me to use the Techne fluidised sand bath as well as the paper sludge for my experimental work.

On a more personal note, the greatest appreciation goes to my husband, Francois: Although you were also busy with your PhD, you always had a willing ear to listen to my ideas and also a strong shoulder on which I could often cry. Thank you for all your love, encouragement, help and each cup of coffee in bed in the morning. I love you very much and life would be less colourful without you.

Then to all my friends: especially Salomé, Mandrie, Leana, Celeste, Janneke and Ruenda. Thank you for the privilege of sharing in your lives and that I can also share my life and this PhD journey with you. Thank you for all your support and for helping me to keep perspective in life.

To my family, Marike, PJ, Johann, Mamma, Pappa and Ma Irma: Thank you for all your love and support throughout my life. Thank you for encouraging me during the times that I was physically ill and wanted to give up. Thank you for all your prayers and love. I am really privileged to have all of you in my life.

Then lastly, to my Heavenly Father: Thank you for being a Good Father and for being perfect in all of Your ways. Thank you for Your amazing grace and that You are faithful even when I am sometimes faithless.

TABLE OF CONTENT

CHAPTER 1 ..... **1**

INTRODUCTION **1**

1.1 BACKGROUND *1*

1.2 PROJECT MOTIVATION *4*

1.2.1 The Role of Thermodynamic Equilibrium Calculations 4

1.2.2 Wood Derived Products as Feedstock for SCWG 5

1.3 PROJECT OBJECTIVES *7*

1.4 PROJECT SCOPE *7*

1.4.1 Thermodynamic Equilibrium Calculations 8

1.4.2 Experimental Tests 8

1.5 DISSERTATION LAYOUT *9*

CHAPTER 2 ..... **10**

LITERATURE REVIEW **10**

2.1 INTRODUCTION *10*

2.2 PROPERTIES OF SUPERCRITICAL WATER *10*

2.3 BACKGROUND ON SCWG *14*

2.4 THE CHEMISTRY OF SCWG *16*

2.5 OPERATING TEMPERATURES OF SCWG *17*

2.6 THE USE OF CATALYSTS DURING SCWG *19*

2.6.1 Homogenous catalysts 19

2.6.2 Heterogeneous catalysts 21

2.7 Feed Materials Used for SCWG *24*

2.7.1 The Use of Model Compounds 24

2.7.2 Real Feedstock Material Used in SCWG Experimental Tests 26

a) Paper sludge as feedstock for SCWG 27

b) Wood as feedstock for SCWG 28

c) Pyrolysis char as feedstock for SCWG 32

d) Effect of feedstock composition 32

2.8 Additional Factors Influencing SCWG *34*

2.9 Modelling Approaches to SCWG *36*

2.9.1 Thermodynamic Modelling 36

2.9.2 Process Modelling 40

2.10 Current Status and Challenges of SCWG *43*

2.11 Outcome of this Chapter *44*

a) Thermodynamic modelling of SCWG 44

b) Practical kinetic effects and feedstock composition 45

CHAPTER 3 47

Thermodynamic Modelling of SCWG – Effect of Feedstock composition 47

3.1 Introduction *47*

3.2 Materials and Methods *48*

3.2.1 Biomass Feedstock Properties 48

a) Determining the calorific value of the feed material 49

3.2.2 Model Description 51

3.2.3 Property Method Selection 52

3.2.4 Comparison of Model Results with Experimental Data 56

b) High temperature SCWG (600 – 800 °C) 56

c) Low temperature SCWG (400 – 550 °C) 58

3.2.5 Model Implementation 59

3.3 Evaluation of Results 61

3.4 Results and Discussion 62

3.4.1 H_2 yield 63

3.4.2 CH_4 yield 69

3.4.3 CO Yield 75

3.4.4 CO_2 Yield 81

3.4.5 Total gas yield 86

3.4.6 Calorific Value of Product Gas (HHV) 91

3.4.7 Heat Required for Isothermal Operations 97

3.4.8 Energy Recovery (Cold Gas Efficiency) 102

3.4.9 Overall Thermal Efficiency 107

3.5 Practical Method to Selecting Appropriate Operating Conditions For a Specific Feedstock Material for SCWG 113

3.5.1 Method Description 113

3.5.2 Example of Method Implementation 114

3.6 Outcome of this Chapter 117

CHAPTER 4 119

Materials and Methods for Experimental Tests 119

4.1 Introduction 119

4.2 Feedstock Characterisation 119

4.2.1 Proximate Analysis 120

4.2.2 Ultimate Analysis 121

4.2.3 Lignocellulosic Composition 124

4.3 Catalysts 125

4.3.1 Heterogeneous catalyst (Ni/Al_2O_3-SiO_2) 125

a) Homogeneous catalyst (K_2CO_3) 125

4.4 Batch Reactor Apparatus 127

4.5 Experimental Procedure 127

4.6 Separation and Analysis of Products 131

4.6.1 Product gas analysis 131

4.6.2 Liquid Phase Analyses 132

4.6.3 Solid Phase Analyses 133

4.7 Data Interpretation and Calculations 133

4.8 Experimental Design 136

4.9 Outcome of this Chapter 138

CHAPTER 5 139

SCWG of Primary Paper Sludge 139

5.1 Introduction 139

5.2 Determining the Thermodynamic Equilibrium Limits for PWS 140

5.3 Results and Discussion 143

5.3.1 Thermodynamic Equilibrium Yields 144

5.3.2 Reproducibility of Experimental Results 145

5.3.3 Deviation from Equilibrium yields 148

5.3.4 Effect of Catalyst Type and Catalyst Loading 148

a) Effect of K_2CO_3 loading on SCWG of PWS 148

b) Effect of Ni/Al_2O_3-SiO_2 loading on SCWG of PWS 152

c) Comparison between K_2CO_3 and Ni/Al_2O_3-SiO_2 153

5.3.5 Effect of hold time 154

a) Gas yields and H_2 selectivity 154

b) Gas composition 156

c) Carbon distribution between the gas, liquid and solid phases 157

d) Gasification Efficiencies 158

5.3.6 Effect of PWS feed concentration during Ni/Al_2O_3-SiO_2 catalysed SCWG 160

5.3.7 Energy potential from SCWG of Primary Paper Sludge based on thermodynamic equilibrium calculations 163

5.4 Outcome of this Chapter 166

CHAPTER 6 167

SCWG of *E.grandis* and related pyrolysis char: Effect of feedstock composition 167

6.1 Introduction 167

6.2 Effect of Feedstock Elemental Composition on the Thermodynamic Equilibrium Yields at 450 °C 168

6.3 Experimental Results 171

6.3.1 Effect of Elemental Composition and Volatile Matter Content of Feed Material . 174

6.3.2 Effect of Ni/Al_2O_3-SiO_2 Loading 184

6.3.3 Effect of Reaction Time 188

6.4 Outcome of This Chapter 193

CHAPTER 7 195

Conclusions and Recommended Future Work 195

7.1 Reviewing the Objectives of this Project 195

7.2 Objective 1: Development of a Method To Aid In The Selection of Feedstock material for SCWG 196

7.3 Objective 2: SCWG of Primary Paper Sludge: Effect of Reaction Time and Catalyst Type and Loading 197

7.4 Objective 3: SCWG of E.grandis and related Pyrolysis Char – Effect of Feedstock Composition 198

7.5 Original Contributions 199

7.6 Publication list 200

7.6.1 Journal Publications 200

7.6.2 Conference Talks and Poster Presentations 201

7.7 Recommended Future Work 201

REFERENCES 203

APPENDIX A 218

Additional Information: Thermodynamic Modelling 218

A.1 Biomass Feedstock Properties 218

A.2 PR-BM Property Method applying Gibbs-free Energy Minimisation 223

A.3 Gibbs Free Energy Minimisation 225

A.4 Properties of all 120 cases of feed material used 226

APPENDIX B 232

Additional Results: Thermodynamic Modelling 232

B.1 Comparison between mass and molar basis results 232

B.2 Additional results 237

B.3 Result at 450 °C and 25 MPa 249

B.4 Results at 500 °C and 25 MPa 256

B.5 Additional results at 700 °C and 25 MPa *264*

APPENDIX C **272**

Detailed Experimental Setup and Procedure **272**

C.1 Experimental setup *272*

C.2 Detailed Experimental Procedure *274*

C.3 Gas Analysis *278*

C.4 Detailed Sample Calculations *289*

APPENDIX D **301**

Additional Results for SCWG of PWS **301**

GLOSSARY

SYMBOL	DESCRIPTION	REFERENCE TO EQUATION
CE	CARBON GASIFICATION EFFICIENCY	EQ. 4-7
$\dot{E}_{chemical,produced}$	CHEMICAL ENERGY PRODUCED	EQ. 5-3
$\dot{E}_{chemical,produced}$	CHEMICAL ENERGY ADDED	EQ. 5-4
$\dot{E}_{in}$	ENERGY INPUT	
$\dot{E}_{out}$	ENERGY PRODUCED	
EOS	EQUATION OF STATE	
EQ	EQUILIBRIUM	
ER	ENERGY RECOVERY	EQ. 3-11 & EQ. 4-9
EXP	EXPERIMENTAL	
FC	FIXED CARBON	
GE	GASIFICATION EFFICIENCY	EQ. 4-6
HE	HYDROGEN GASIFICATION EFFICIENCY	EQ. 4-8
$HHV_{feed,dry}$	HIGHER HEATING VALUE OF FEED MATERIAL	
HHV_{milne}	MILNE CORRELATION FOR THE HHV	EQ. 3-1
HHV_{Dulong}	DULONG CORRELATION FOR THE HHV	EQ. 3-2
HHV_{Boie}	BOIE CORRELATION FOR THE HHV	EQ. 3-3
HHV_{Friedl}	FRIEDL CORRELATION FOR THE HHV	EQ. 3-4
$HHV_{gas\ product}$	HHV OF THE PRODUCT GAS	EQ. 3-10
HTC	HYDROTHERMAL CARBONISATION	

SYMBOL	DESCRIPTION	REFERENCE TO EQUATION
H/C	HYDROGEN-TO-CARBON RATIO (MOLAR)	
k_H	HENRY'S CONSTANT	EQ. 4-3
K_w	IONIC PRODUCT OF WATER	
$LHV_{feed,dry}$	LOWER HEATING VALUE OF DRY FEED MATERIAL	EQ. 3-12
$LHV_{gas\ product}$	LHV OF PRODUCT GAS	
$n_{i,diss}$	MOLES OF COMPONENT i DISSOLVED IN LIQUID PHASE	EQ. 4-2
n_i	MOLES OF COMPONENT i	
n_{N_2}	MOLES OF N_2 IN REACTOR	EQ. 4-1
m_i	MASS OF COMPONENT i	
O/C	OXYGEN-TO-CARBON RATIO (MOLAR)	
P	PRESSURE	
PR	PENG-ROBINSON	
$PR-BM$	PENG-ROBINSON WITH BOSTON MATHIAS MODIFICATION	
Q_{req}	HEAT REQUIRED FOR ISOTHERMAL OPERATION	EQ. 3-13
R	UNIVERSAL GAS CONSTANT	
$RMSE$	ROOT MEAN SQUARE ERROR	EQ. 3-5
r	PEARSON'S CORRELATION COEFFICIENT	EQ. 3-6
S_{H_2}	HYDROGEN SELECTIVITY	EQ. 4-10
SCW	SUPERCRITICAL WATER	
$SCWG$	SUPERCRITICAL WATER GASIFICATION	
T	TEMPERATURE	

SYMBOL	DESCRIPTION	REFERENCE TO EQUATION
V	VOLUME	
VM	VOLATILE MATTER	
Y_i	YIELD OF COMPONENT i	EQ. 3-8 & EQ. 4-5
y_i	MOLE FRACTION OF COMPONENT i	EQ. 4-4
Y_{total}		EQ. 3-7
z	COMPRESSIBILITY FACTOR	
$\eta_{overall}$	OVERALL EFFICIENCY	EQ. 5-2
$\dot{\xi}$	RESIDENCE TIME DEPENDENCE BIOMASS-TO-CATALYST RATIO	EQ. 2-15

Chapter 1

INTRODUCTION

1.1 BACKGROUND

Fossil fuels such as coal, oil and natural gas have been used as effective energy sources for centuries. Due to the increasing greenhouse effects of these energy sources, the decrease in its supply as well as the increase in the global energy demand, the utilisation of alternative renewable energy sources, such as biomass is crucial (L. Zhang et al., 2010a). According to the World Bioenergy Association's Global Bioenergy Statistics report of 2014, the global energy supply increased from 426 EJ in the year 2000 to 522 EJ in 2011 (World Bioenergy Association, 2014).

When replacing or supplementing existing fossil fuel resources with biomass as an energy source, the generation of greenhouse gases is greatly reduced and the limited fossil fuel resources are conserved. This will ultimately result in a reduction of the reliance on fossil fuels both locally and globally. Additionally, the fuel supply of the world can be diversified as a wide variety of fuels can be produced from various biomass sources (Crocker, 2010).

Biomass can include anything from trees, grass, insects, animal wastes or agricultural resources (Basu, 2010a). Ideally, potential biomass for energy production should be inexpensive and should have low input energy for cultivation of the biomass as well as a low nutrient requirement. It should also contain little or no contaminants. The main properties of biomass that are important for energy generation is the calorific value, moisture content, ash content, metal content, cellulose/lignin ratio and the fraction of fixed carbon and volatiles (McKendry, 2002). Typical biomass energy sources can include agricultural feedstock and wood, petroleum

coke, solid organic wastes, reclaimed oil, biogas, waste cooking oil, ethanol from wood or agricultural feedstock material (McGowan 2009).

The three main types of energy sources that can be derived from biomass include liquid products (such as bio-ethanol, biodiesel, methanol and pyrolysis oil), gaseous products (such as biogas, syngas and producer gas) and solid products (such as torrefied biomass and char). The four main applications for these products are electricity generation, heat generation, transportation fuels and chemicals (such as chemicals for the textile industry, fertiliser and synthetic fibres) (Basu, 2010a).

A wide variety of biomass conversion process technologies are available, all in various stages of development. These biomass conversion processes can be divided into two main conversion routes, *viz.* biochemical conversion and thermochemical conversion. Each of these conversion routes can be subdivided into several other conversion processes (see Figure 1-1).

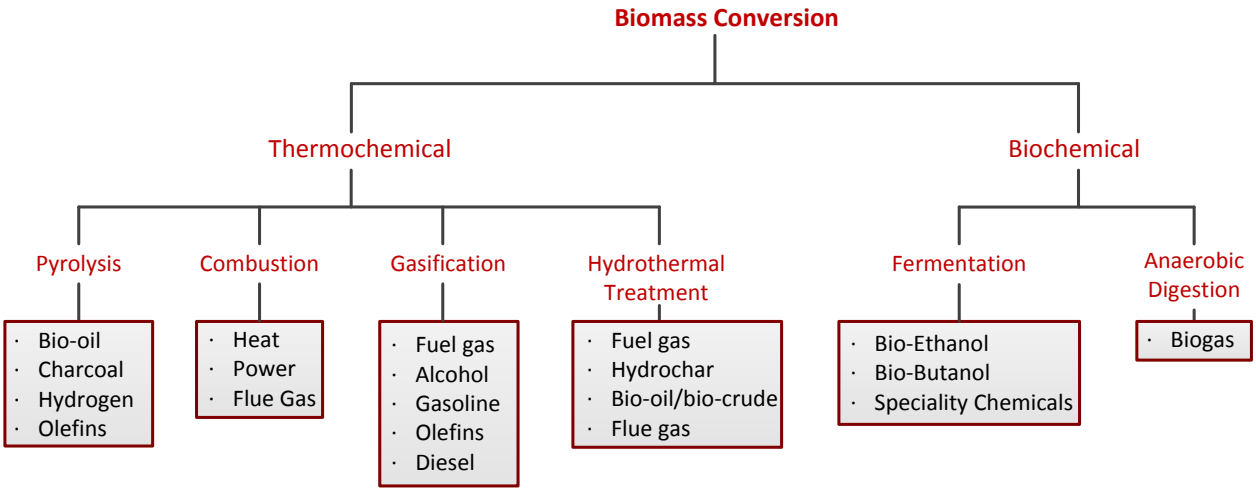

FIGURE 1-1 THERMOCHEMICAL CONVERSION PROCESSES (ADAPTED FROM MENON AND RAO (2012))

Biochemical conversion includes anaerobic digestion, fermentation and hydrolysis. Thermochemical conversion includes pyrolysis, gasification, hydrothermal treatment and combustion. Although thermochemical conversion processes typically operates at higher temperatures than biochemical conversion processes, the conversion time for thermochemical process is much shorter than for biochemical processes. For instance, the typical residence time for anaerobic digestion is 14 – 28 days, while that of thermochemical processes are typically

only a few minutes. Another advantage of thermochemical conversion technologies is the fact that a much wider variety of biomass can be processed (including agricultural or forestry residues, organic municipal wastes and by-products from the food, bio-refinery or any bio-processing industry) and the product gases formed can be used as substitutes for a variety of fuels and chemicals. A disadvantage however, is the presence of undesirable pollutants in the product (such as tar), which must be removed. Furthermore, feedstock material with moisture content typically higher than 10 wt.%, must first be dried before it is suitable for conventional thermochemical processes such as conventional gasification and pyrolysis.

Gasification of biomass in supercritical water - also referred to as ***hydrothermal gasification*** or ***supercritical water gasification (SCWG)*** - shows great potential for the conversion of wet organic waste streams such as sewage sludge, manure, paper waste sludge or wet forestry remains. During SCWG, biomass molecules are broken down into smaller molecules such as H_2, CH_4, CO and CO_2 in the presence of supercritical water, typically between 400 – 800 °C and 22 – 35 MPa (see Figure 1-2). These gases can be utilised directly as energy sources, or in the subsequent synthesis of more complex liquid fuels. Water acts as a reaction medium as well as a reactant by providing the hydrogen needed for the hydrolysis reaction (Kruse, 2008).

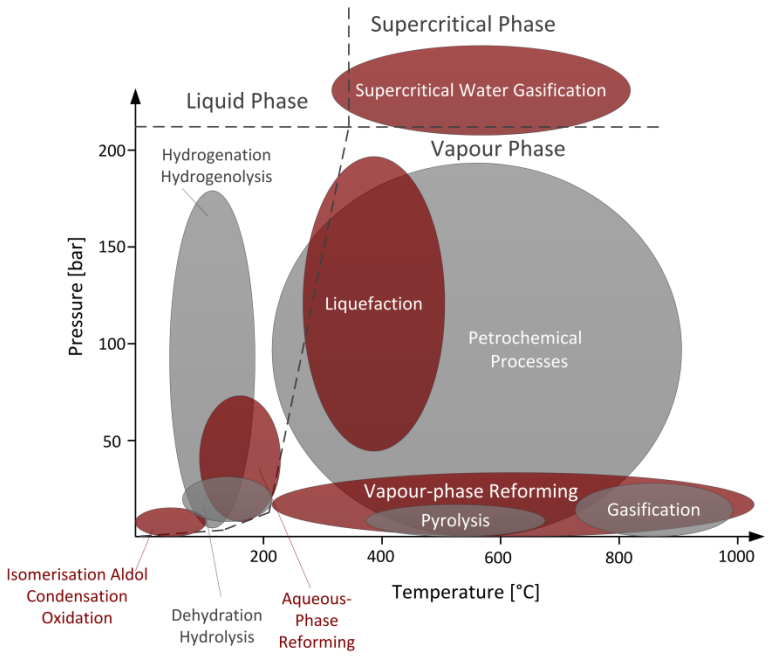

FIGURE 1-2 OPERATING CONDITIONS OF VARIOUS THERMOCHEMICAL PROCESSES COMPARED TO THE PHASE DIAGRAM OF WATER (REDRAWN FROM CHHEDA ET AL., 2007)

If carried out correctly, complete conversion of carbon to the gas phase can be achieved, resulting in minimal char or coke formation. No drying of the feedstock material is required prior to gasification. Due to the change in the transport properties of water above its critical point, minimal resistance to inter-phase mass transfer exists. Furthermore, efficient separation of different by-product streams can be achieved due to elevated operating pressures (Peterson et al., 2008). Lastly, shorter reaction times and the ability to convert lignin compounds make SCWG a promising alternative for the conversion of wet organic waste streams.

Yoshida et al. (2003) compared the efficiency of SCWG with that of anaerobic digestion, liquefaction, pyrolysis and dry gasification for electricity generation (see Table 1-1). The energy conversion efficiency decreases as the moisture content in the feed increases for all of the processes, except for SCWG and anaerobic digestion. ***For biomass with moisture content higher than 30%, SCWG was the most promising technology***. Furthermore, in a thermo-economic study, Gassner et al. (2011) showed that hydrothermal gasification can compete with conventional gasification of dry biomass, which can reach efficiencies up to 76 – 80%.

TABLE 1-1 COMPARING ENERGY CONVERSION EFFICIENCY OF VARIOUS BIOMASS CONVERSION PROCESSES (ORIGINAL DATA FROM YOSHIDA ET AL. (2003))

MOISTURE CONTENT IN FEED [WT.%]	THERMAL GASIFICATION	PYROLYSIS	ANAEROBIC DIGESTION	SCWG	LIQUEFACTION
5	61%	57%	31%	55%	39%
30	55%	53%	31%	55%	37%
55	47%	45%	31%	55%	36%
75	27%	27%	31%	55%	34%

1.2 PROJECT MOTIVATION

1.2.1 THE ROLE OF THERMODYNAMIC EQUILIBRIUM CALCULATIONS

The assumption of ***thermodynamic equilibrium*** during SCWG are often used in order to determine optimum operating conditions (such as temperature and biomass-to-water ratio) for hydrogen and/or methane production and to determine the energy efficiency of the process (Castello and Fiori, 2011; Lu et al., 2007; Tang and Kitagawa, 2005; Yan et al., 2006). However, the effect of the ***feedstock composition in terms of its elemental analysis*** (*i.e.*, its C, H and O

content) on the gas yields has not been investigated extensively before. Knowledge of the thermodynamic equilibrium yields that can be achieved through SCWG of a specific feedstock can act as a screening tool which can give an indication of whether a potential feedstock material is a worth-while candidate to consider as an option for SCWG.

However, although thermodynamic equilibrium calculations are valuable for providing the thermodynamic limits for the gas yields from a certain feedstock material at specific operating conditions, in reality, the ***composition of the feedstock*** as well as ***kinetic effects***, such as ***reaction time***, ***catalyst type*** and ***catalyst loading*** plays in important role during SCWG experiments. Hence, comparing actual experimental results with that of theoretical equilibrium results is a good indication of the influence of these aforementioned effects at the specific operating conditions. It also provides an understanding of which type of feed material will result in gas yields close to the calculated equilibrium yields, when reasonable operating times and catalyst loadings are employed.

1.2.2 Wood Derived Products as Feedstock for SCWG

Eucalyptus wood species are popular feedstock material used in the South African pulp and paper industry as well as the solid wood market, mainly due to the fast growth rate, low production cost and the good quality of the fibres (Joubert, 2013). For the same reasons, Eucalyptus species have also been identified as a potential wood fuel resource (Leslie et al., 2012). In the 2014 financial year, approximately 9.9 million tons of Eucalyptus species were sold as round wood, approximately 7 million tons as pulp wood and around 0.62 million tons as sawlogs (Godsmark, 2015). Joubert (2013) investigated the use of ***Eucalyptus Grandis*** (*E.grandis*) as feed material for slow, vacuum and fast pyrolysis. However, no study could be found in which *E.grandis* was considered as feed material for SCWG.

Furthermore, large quantities of solid wastes and sludge products are produced from the pulp and paper industry. The quantity and composition of the waste streams are greatly dependent on the origin of cellulose fibres used (virgin wood or recycled paper), the grade of paper produced and the methods applied for the paper production (Bajpai, 2015). The main waste products are ***wood wastes*** (sawdust, bark, pins and fibres from chip screening and woodyard

waste), black liquor, pulp rejects (also known as fibre sludge or ***primary paper sludge***), biological sludge from wastewater treatment (known as secondary paper sludge) and de-inking sludge from de-inking of recycled paper (Gavrilscu, 2008).

Prins et al. (2007) suggested that, thermodynamically, biomass with low O/C ratios (typically below 0.4) were preferred for maximum thermodynamic efficiency during conventional dry gasification process. They further suggested that it would be an attractive option to modify the properties of biomass (which is highly oxygenated) prior to gasification in order to obtain higher gasification efficiencies. A typical "modified" biomass material is the solid product produced during pyrolysis (referred to as ***pyrolysis char*** from here onwards). Currently, pyrolysis char is most commonly used as a solid fuel, soil amendment agent (biochar) or an adsorbent during gas clean-up or wastewater treatment (Carrier et al., 2011; Uras et al., 2012; Kambo and Dutta, 2015). Furthermore, it has also been considered as an alternative to coal for energy production by means of steam gasification (Encinar et al., 2001).

Ramsurn et al. (2011) and Castello et al. (2014) both investigated the possible use of hydrochar, the solid product produced during hydrothermal carbonisation (HTC) of biomass, as a feedstock material for SCWG. However, the possibility of using pyrolysis char, the solid product produced during pyrolysis, as a feedstock material for SCWG has, as far as my knowledge, not yet been considered. The compositions of hydrochar and pyrolysis char differ significantly due to the difference in the prevailing reactions taking place during pyrolysis and HTC (Kambo and Dutta, 2015). During pyrolysis, decomposition of hemicellulose and cellulose typically occurs between 200-300 °C and 300-400 °C, respectively, while lignin decomposition only occurs around 600 °C (Saha, 2003). However, in the presence of hot, compressed water the degradation of cellulose and hemicellulose occurs between 160-180 °C, while lignin degradation occurs around the critical point of water (Bobleter, 1994).

1.3 Project Objectives

The overall aim of this project is to provide improved understanding and new insight into the thermodynamic and practical kinetic behaviour during SCWG of wood-related produced sourced at three different stages of the wood utility cycle. These are: wood chips (E.grandis), primary paper sludge and wood-based pyrolysis char.

From the overall aim of the project, the objectives can be summarised:

1. ***To develop a method (based on the assumption of thermodynamic equilibrium) to aid in the selection of appropriate operating conditions for a specific feed material, in terms of its elemental composition (more specifically, the O/C and H/C ratio of the feed material).***
2. ***To determine whether the calculated equilibrium yields can be achieved applying a reasonable catalyst loading and reaction time when using primary paper waste sludge (PWS) as feed material during SCWG experiments (specifically at a low operating temperature).***
3. ***To determine the possible kinetic influence of the feedstock composition (O/C ratio and volatile matter content) on the gas yields and gasification efficiencies by using wood (E.grandis) and various wood-derived pyrolysis chars as feed material for SCWG.***

With these main project objectives in mind, the project scope and the dissertation layout are presented in the sections to follow. The project scope provides the boundaries within which the project was conducted. The dissertation layout provides a summary of each chapter as well as how each chapter is linked to the main project objectives.

1.4 Project Scope

This project focusses exclusively on addressing various theoretical and practical aspects of SCWG. Comparison of SCWG of other thermochemical technologies such as pyrolysis or conventional gasification is therefore beyond the scope of this project.

1.4.1 THERMODYNAMIC EQUILIBRIUM CALCULATIONS

Concerning the developed thermodynamic equilibrium model, only cubic equations (more specifically the Peng-Ronbinson and Redlick-Kwong-Soave equations of state (EoSs) were considered. These two EOSs are typically used for oil and gas production, medium pressure refinery applications, hydrogen-rich refinery systems and hydrocarbon separations (gas phase) (Finlayson, 2014). Furthermore, although cubic EoSs typically perform poorly around the critical point of a specific component, operating conditions in this study were significantly higher than the critical point of water (22.1 MPa and 374 °C).

Concerning the operating conditions, the operating temperature and dry feed concentration ranges were chosen as 400 – 800 °C and 5 – 20 wt.%, respectively. The feed material composition in terms of the O/C and H/C molar content ranges were 0.08 to 1.33 and 0.45 to 3.97, respectively (discussed in more detail in Chapter 3). All of the thermodynamic equilibrium calculations for the developed model were conducted at a constant pressure of 25 MPa.

1.4.2 EXPERIMENTAL TESTS

Concerning the experimental tests, due to batch reactor operations and isochoric heat-up phase, the pressure inside the reactor could not be kept constant. The end pressure in the reactor for all experiments ranged between 25 and 28 MPa. The three kinetic effects investigated are catalyst type, catalyst loading as well as reaction time. A catalyst screening study was beyond the scope of this project. Hence, only two types of catalysts were used, namely a homogeneous catalyst (K_2CO_3) and a heterogeneous catalyst (Ni/Al_2O_3-SiO_2). The catalyst loading was varied between 0 and 1 $g/g_{feed,dry}$ and the reaction time ranged from 15 to 120 minutes. While the highest catalyst loading of 1 $g/g_{feed,dry}$ is in a practical sense not feasible, it was chosen in order to determine if equilibrium yields can be achieved at such high loadings. Although a wide variety of feedstock properties can possibly influence the kinetics of SCWG, the elemental composition (C, H and O content) and the volatile matter content are of specific interest in this study. Furthermore, experiments were conducted at a low operating temperature of 450 °C with the production of natural gas, rich in methane being the end application for heat and/or power generation.

1.5 Dissertation Layout

Figure 1-3 provides a layout of the structure of the thesis together with comments on how the chapters relate to one another and where each of the main objectives presented in section 1.3 relate to each chapter in the dissertation.

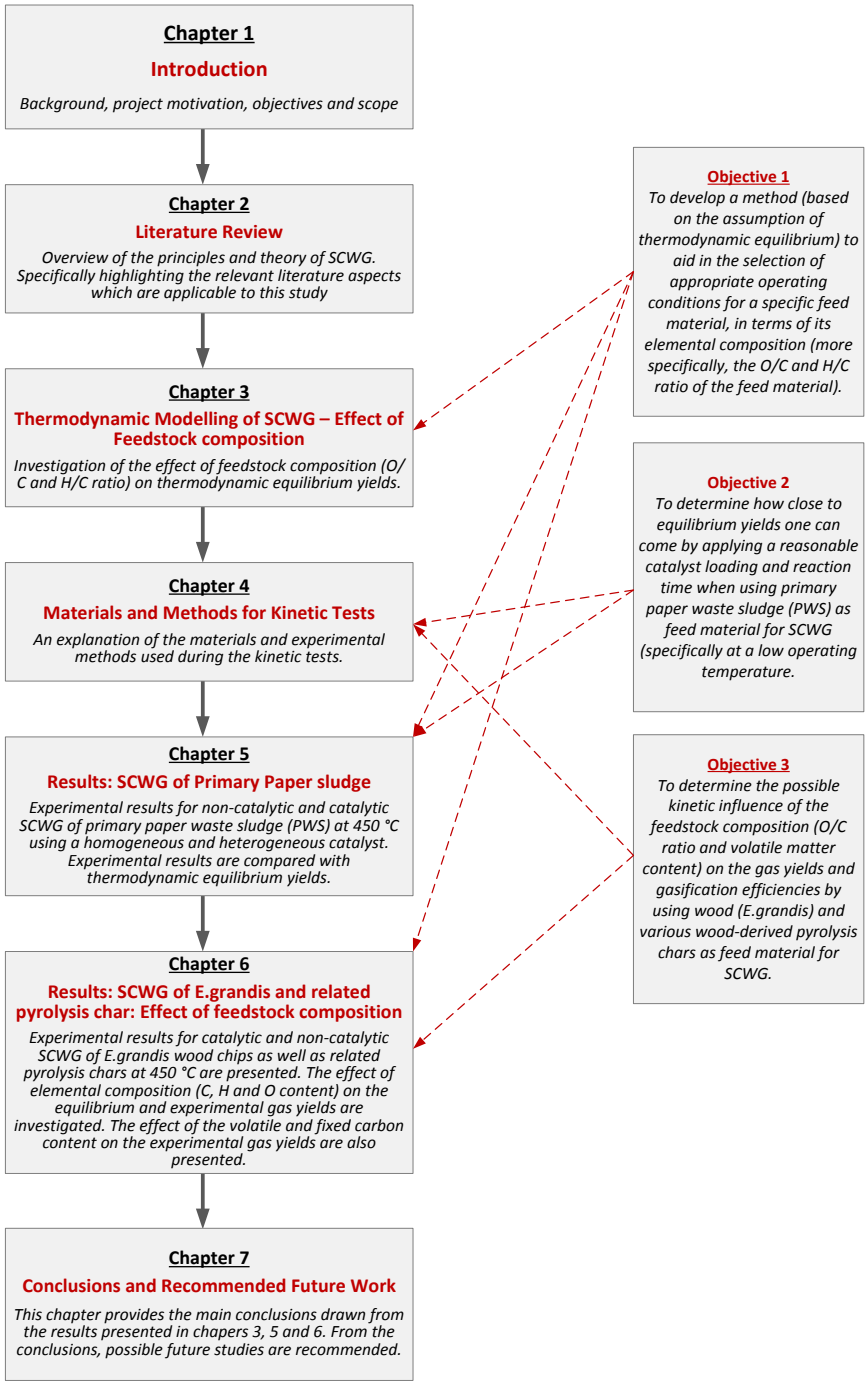

Figure 1-3 Schematic of dissertation outline

Chapter 2

LITERATURE REVIEW

2.1 INTRODUCTION

A wide variety of literature is available on various aspects of gasification of organic material in supercritical water and a number of review articles has been published on SCWG (Azadi and Farnood, 2011; Elliott, 2008; Y. Guo et al., 2010; Kruse, 2009, 2008; Matsumura et al., 2005; Reddy et al., 2014; Yakaboylu et al., 2015). The aim of this chapter is not to review all the aspects of SCWG, but to provide a critical analysis of previous research relevant to the work done in this study, to identify trends and shortcomings and design the research approach accordingly.

2.2 PROPERTIES OF SUPERCRITICAL WATER

Above the critical point of water, (374.1 °C and 22.1 MPa), water is referred to as ***supercritical water (SCW)***. A typical phase diagram of water is shown in Figure 2-1. Water or steam below the critical temperature or pressure is referred to as ***subcritical water***. Once above the critical point, the line separating liquid and vapour phases disappears (Basu, 2010b)

Significant changes in the thermo-physical and transport properties of water are notable as it changes from the sub-critical to the supercritical phase (see Table 2-1 and Figure 2-2). Transport properties of SCW exhibit liquid- as well as gas-like behaviour. At subcritical pressures (0.1 and 5 MPa), a significant drop in the density is noted once the temperature is increased above the supercritical temperature (Figure 2-2(a)). However, at supercritical pressures (25 and 50 MPa), the density decreases more gradually (without a jump as in the case of subcritical pressures) from 0.74 g/cm^3 (at 300 °C and 25 MPa) to 0.17 g/cm^3 (at 400 °C and 25 MPa).

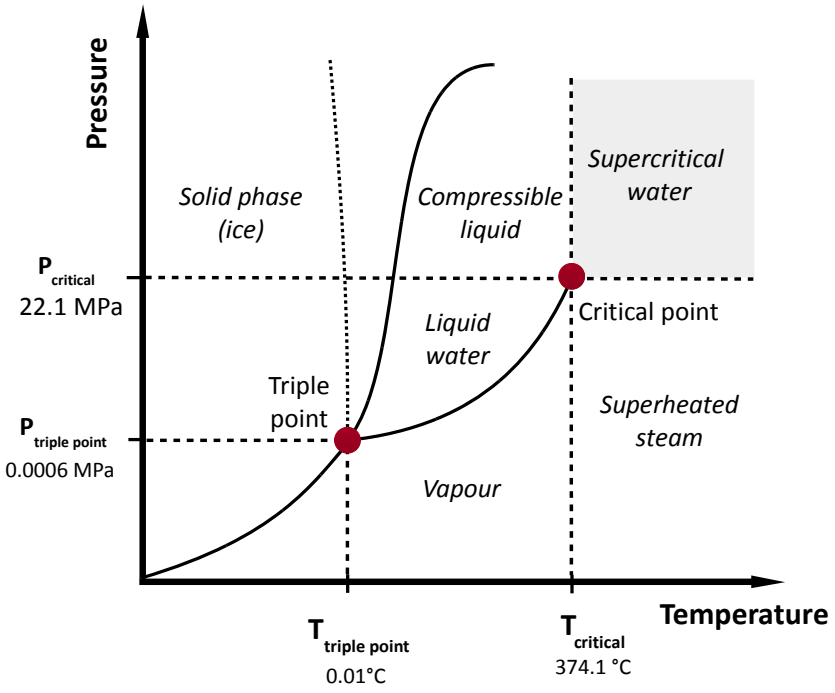

FIGURE 2-1 PHASE DIAGRAM OF WATER

TABLE 2-1 PROPERTIES OF SUBCRITICAL STEAM, SUBCRITICAL WATER AND SUBCRITICAL STEAM (ADAPTED FROM BRÖLL ET AL., 1999)

PROPERTY	UNITS	WATER CONDITION				
		AMBIENT	SUB-CRITICAL	SUPER-CRITICAL	SUPER-CRITICAL	SUPER-HEATED
Temperature	°C	25	250	400	400	400
Pressure	MPa	0.1	5	25	50	0.1
Density	g/cm^3	0.997	0.80	0.170	0.580	3.0×10^{-4}
Dynamic viscosity	mPa.s	0.89	0.11	0.03	0.07	0.02
Dielectric constant		78.5	27.1	5.9	10.5	1
Ionic product		14.0	11.2	19.4	11.9	-
Heat capacity	kJ/(kg·K)	4.22	4.86	13	6.8	2.1
Thermal conductivity	W/(m·K)	0.608	0.620	0.160	0.438	0.055

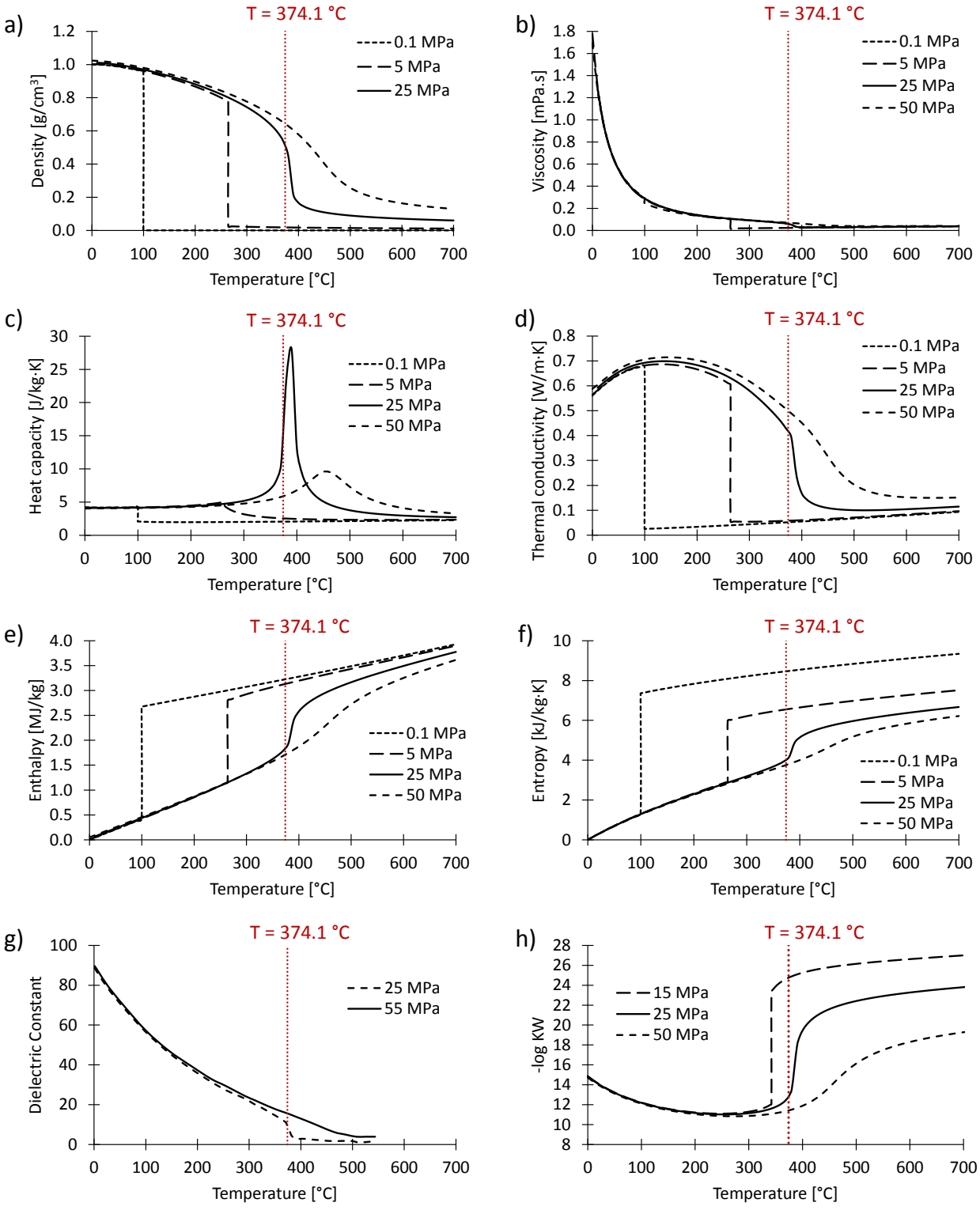

FIGURE 2-2 TRANSPORT PROPERTIES OF WATER AS A FUNCTION OF TEMPERATURE AND PRESSURE (DATA FROM LEMMON ET AL. (2011); MARSHALL AND FRANCK (1981); UEMATSU AND FRANCK (1980))

The dynamic viscosity of SCW is an order of magnitude lower than that of sub-critical water (Figure 2-2(b)), which significantly enhances diffusion and mass transfer when operating at supercritical conditions (Yong and Matsumura, 2012a).

The heat capacity of water (Figure 2-2(c)) shows a sudden spike in the region where water changes from subcritical to a supercritical fluid. Unlike in the case of low pressure gases and liquids in which the heat capacity is a weak function of pressure, in the supercritical region, the heat capacity is greatly influenced by both the temperature and the pressure. This phenomenon can aid in diminishing the hotspot problem which especially occurs in highly exothermic reactions - for example partial oxidation in SCW (Bröll et al., 1999).

As in the case of density, the thermal conductivity (Figure 2-2(d)) of water also drops more gradually during the phase change between 370 °C (0.43 W/m.K) and 400°C (0.170 W/m.K) at a pressure of 25 MPa, as appose to the sudden jump visible at subcritical pressures (0.1 and 5 MPa).

Concerning the enthalpy (Figure 2-2(e)) and entropy (Figure 2-2(f)) of water, the energy needed to heat compressed water at 50 MPa from 25 to supercritical water at 700°C is nearly the same as the energy needed to heat liquid water at 0.1 MPa and 25 °C to superheated steam at 700 °C, which includes a phase change of liquid water to vapour (*i.e.* evaporation). When water is heated to 700°C at 50 MPa, evaporation does not occur, but water changes from a compressed liquid directly to the supercritical phase. The absence of evaporation at supercritical conditions (especially high pressures) allows one to avoid the energy transfer associated with a phase change at a constant temperature, and thus, the heat exchanger efficiency can be increased (Kruse, 2008).

The dielectric constant of water changes from 80 at atmospheric conditions, to close to 5 at 400°C and 25 MPa (see Table 2-1 and Figure 2-2(g)). This drop in the dielectric constant causes water to change from being a highly polar solvent at conditions below the critical point to a non-polar solvent at supercritical conditions (Basu and Mettanant, 2009). SCW is therefore a good solvent for non-polar substances that shows poor solubility at subcritical conditions (such as carbohydrates and lignin).

As soon as organic material (such as lignocellulosic compounds) has dissolved in SCW, cellulose bonds are effectively broken by SCW, which result in the formation of gaseous products. SCW is therefore an effective reaction medium offering enhanced mixing and rapid and effective dissolution of organic compounds (Yesodharan, 2002). Hence, polar inorganic compounds such as such as NaCl, KCl and $CaSO_4$, which have a high solubility in water under subcritical conditions, shows poor solubility under supercritical conditions. For example, the solubility of NaCl decreases from 40 wt.% at 300°C to 100 ppm at 450°C, while the solubility of $CaCl_2$ in water decreases from 70 wt.% in liquid water to 10 ppm at 500 °C (Yesodharan, 2002). Additionally, gases and organic compounds are almost completely miscible with SCW (Kruse and Dinjus, 2007a).

The ionic product of water (K_w) also varies significantly between sub- and supercritical conditions as it is greatly dependent on the temperature and density of water (Bröll et al., 1999). When the temperature is increased from ambient temperature (at 25 MPa) to 300°C, K_w increases from 10^{-14} to approximately 10^{-11} (see Figure 2-2(h)). However, when the temperature is further increased above the supercritical temperature, water becomes a non-ionic solvent as K_w decreases to 10^{-22} at 500 °C and to 10^{-24} at 700 °C (both at a pressure of 25 MPa). The high self-dissociation property of supercritical water allows it to catalyse various decomposition reactions (for example glycerol decomposition) (Basu and Mettanant, 2009).

Due to its physical and transport properties, sub- and supercritical water are used in various biomass conversion methods including hydrothermal carbonisation, hydrothermal liquefaction, supercritical water oxidation and supercritical water gasification (Yakaboylu et al., 2015). For the purposes of this specific study, only SCWG and its applications are be discussed further.

2.3 Background on SCWG

Supercritical water gasification (SCWG), also referred to as hydrothermal gasification, is the conversion of organic material to gases such as H_2, CH_4, CO and CO_2 in the presence of supercritical water with or without the use of a catalyst. The first work done on SCWG was by Modell (1985), who demonstrated that, when maple sawdust is immersed in supercritical water,

it decomposes to tar and gas without char formation. Since then, various research groups have investigated different aspects of SCWG.

The features drawing much attention to SCWG were discussed in great detail in a review by Peterson et al. (2008), and can be summarised as follow:

- Biomass feedstock used in conventional thermochemical processes (such as pyrolysis and conventional gasification) includes material such as agriculture residues, food processing waste and sewage sludges. These feed materials all contain high amounts of moisture, which needs to be removed beforehand. Water is typically removed from the biomass by means of vaporization, distillation or drying prior to any of the conventional processes, requiring large amounts of additional energy. SCWG however requires minimal or no drying prior to gasification.
- Feedstock material containing a wide variety of components such as fatty acids, lignocelluloses (wood or forestry waste) and compounds derived from proteins can be treated in SCW to produce hydrogen and methane, that can be used as commercial fuel sources.
- When operating at near-critical or supercritical conditions, resistance to inter-phase mass transfer is greatly reduced or even removed. A reduction in the energy consumption may also be evident due to improved transport properties of water at supercritical conditions, as well as improved selectivity of high energy compounds such as methane and hydrogen.
- The significant change in the physical properties of water associated with the increase in temperature and pressure around the critical point can aid in efficient separation of different product and by-product streams, ultimately reducing energy usage associated with conventional product purification steps.
- A product gas, rich in H_2 with low CO composition can be produced by changing operating conditions so that the water gas-shift reaction is favoured. The produced gas is then available at a high pressure (due to the nature of the process), which eliminates the need for additional pressurisation for storage.

- Atoms such as S, N and halogens leave the process in the liquid phase, aiding in cost reduction as an expensive gas cleaning is not required (Kruse & Dinjus 2007).

2.4 The Chemistry of SCWG

The chemical reactions taking place during SCWG are complex and it is not easy to quantify all reactions taking place. However, the overall reaction can be represented by Eq. 2-1 (Guo et al., 2007):

Overall reaction: $$CH_xO_y + (2-y)H_2O \rightarrow CO_2 + \left(2 - y + \frac{x}{2}\right)H_2 \quad 2\text{-}1$$

It is agreed in literature that the three main reactions taking place during SCWG are steam reforming of biomass to form CO and H_2 (Eq. 2-2), water-gas shift reaction between CO and water to form CO_2 and H_2 (Eq. 2-3), and methanation of CO and H_2 to form CH_4 (Eq. 2-4) (Yan et al., 2006).

Steam reforming: $$CH_xO_y + (1-y)H_2O \rightarrow CO + \left(1 - y + \frac{x}{2}\right)H_2 \quad 2\text{-}2$$

Water-gas shift: $$CO + H_2O \leftrightarrows CO_2 + H_2 \quad 2\text{-}3$$

Methanation of CO and H_2: $$CO + 3H_2 \leftrightarrows CH_4 + H_2O \quad 2\text{-}4$$

The mechanisms through which the water-gas shift reaction occur in supercritical water are shown in Eq. 2-5 and Eq. 2-6 (as described by Penninger and Rep (2006)). Above the critical point, water dissociates to release OH^- ions. The OH^- ions then react with CO (formed during steam reforming) to produce $COOH^-$ anions. The $COOH^-$ anions then decompose to form CO_2 and H^- (2-5). The hydrated anions (H^-) react with water to form H_2 and OH^- (Eq. 2-6).

$$OH^- + CO \leftrightarrows HCOO^- \leftrightarrows H^- + CO_2 \quad 2\text{-}5$$

$$H^- + H_2O \rightleftarrows H_2 + OH^- \quad 2\text{-}6$$

A number of authors have also confirmed the formation of CH_4 *via* the methanation of CO_2 and H_2 in the presence of transition metal catalyst (Eq. 2-7) (Minowa et al., 1994; Waldner and Vogel, 2005).

Methanation of CO_2 and H_2: $$CO_2 + 4H_2 \leftrightarrow CH_4 + 2H_2O \quad (2\text{-}7)$$

2.5 Operating Temperatures of SCWG

The temperature at which the SCWG reactions take place is probably the most important factor that affects the SCWG process. Three operating temperature ranges generally exists for SCWG, (see Table 2-2), namely subcritical water gasification (below 374 °C), low temperature SCWG (typically between 374 – 550 °C) and high temperature SCWG (typically between 550 – 700 °C) (Azadi and Farnood, 2011). The dominant reaction mechanism is dependent on the operating temperature and changes from ionic at low temperatures to free-radical at high operating temperatures (see Figure 2-3).

Table 2-2 Gasification regions adapted from Kruse (2008) and Basu & Mettanant (2009)

Region	Temperature Range	Catalyst	Main Product
Region I	T < 374°C	Yes	Gases from small organic molecules
Region II	374°C < T < 550°C	Yes	Methane rich gas
Region III	T > 500°C	No	Hydrogen rich gas

When operating at temperatures higher than 550°C, a catalyst is not necessarily required for complete gasification and the product gas will be rich in hydrogen. However, when operating at lower temperatures (between 374 and 550°C), the product gas will be richer in methane and a catalyst is required to achieve complete gasification (Elliott, 2008). Apart from the higher energy requirement when operating at higher temperatures, another drawback is that it requires reactors with thicker walls due to the decrease in the yield strength of a metal with an increase in temperature. This will result in higher investment costs due to the high cost for alloy material suitable for operation at these conditions. Hence, in terms of investment costs, operating at lower temperatures closer to the supercritical point has a clear advantage over high temperature SCWG (Gasafi et al., 2008). However, at low temperatures, a catalyst is required to

overcome the slow gasification rates. A number of authors have in fact shown that complete conversion of carbon to the gas phase is possible at low operating temperatures with the use of a catalyst (see Table 2-3 for a summary).

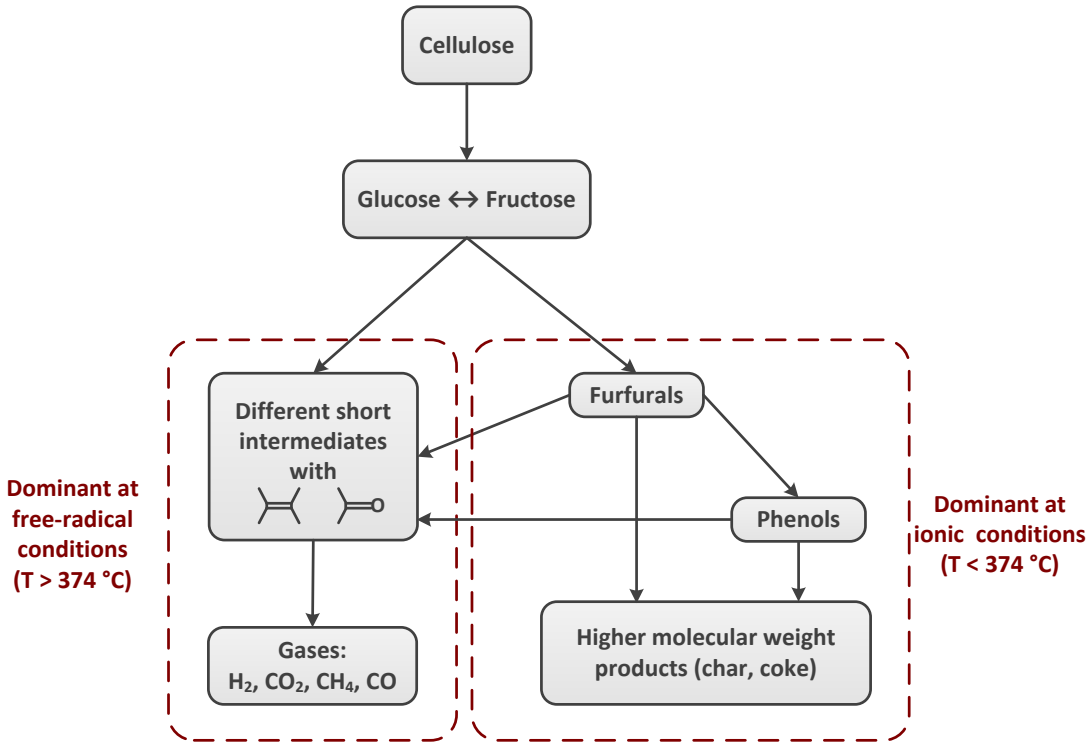

FIGURE 2-3 KEY SUBSTANCES REACTION MECHANISM FOR SCWG OF CELLULOSE (ADAPTED FROM KRUSE AND DINJUS (2007B))

TABLE 2-3 SUMMARY OF STUDIES ACHIEVING COMPLETE CARBON CONVERSION IN BATCH REACTORS AT LOW OPERATING TEMPERATURES

FEEDSTOCK	TEMPERATURE	CATALYST	REFERENCE
Polypropylene, Phenyl Ether, Dibenzofuran, Polyethylene, Polystyrene	450 °C	RuO_2	Park and Tomiyasu (2003)
Wood sawdust	410 °C	Raney nickel	Waldner and Vogel (2005)
Microalgae	400 °C	Ru/C	Stucki et al. (2009)
Glucose	380 °C	Raney nickel	Azadi et al. (2012)
Cellulose	380 °C	Raney nickel	Azadi et al. (2012)
Fermentation residue	410 °C	Ru/C	Zöhrer and Vogel (2013)
Macroalgae	500 °C	Ru/Al_2O_3	Cherad et al. (2014)

2.6 THE USE OF CATALYSTS DURING SCWG

Two comprehensive reviews on the catalytic gasification in SCW are provided by Elliott (2008) and Y. Guo et al. (2010). Hence, only a brief discussion will be given here. Two main types of catalyst that are frequently used in SCWG experiments are ***homogeneous catalysts*** (alkali metal catalysts usually soluble in water at atmospheric conditions) and ***heterogeneous catalysts*** (transition metal catalysts, usually not soluble in water at atmospheric conditions).

2.6.1 HOMOGENOUS CATALYSTS

Various researchers have used alkali metal salts such as $Ca(OH)_2$, $CaCO_3$, NaOH, Na_2CO_3, KOH, K_2CO_3, $KHCO_3$ and LiOH on SCWG as catalysts during SCWG experiments of real and model biomass compounds (Cao et al., 2013; Castello et al., 2014; Garcia Jarana et al., 2008; Ge et al., 2014; Guo et al., 2007, 2012; Hao et al., 2003; Jin et al., 2014; Kersten et al., 2006; Kruse et al., 2000; Madenoğlu et al., 2013; Ramsurn et al., 2011; Rönnlund et al., 2011; Schmieder et al., 2000; Sınağ et al., 2004, 2003; Yanik et al., 2008). All of these studies are in agreement that the presence of these alkali metal salts increases hydrogen yields and decreases CO yields by accelerating the water-gas shift reaction (Matsumura et al., 2005).

Numerous studies have compared the activity of several alkali catalysts during SCWG (Ge et al., 2014; Guo et al., 2007; Jin et al., 2014; Muangrat et al., 2010a). Guo et al. (2007) compared the effect of $Ca(OH)_2$, and K_2CO_3 on the gasification of cellulose in SCW at 500 °C and 10 wt.% cellulose loading at various catalyst loadings (0 – 0.8 $g_{catalyst}/g_{cellulose}$ for K_2CO_3 and 0 – 3.2 $g/g_{cellulose}$ for $Ca(OH)_2$). The catalytic activity for the formation of hydrogen was much higher for K_2CO_3 than for $Ca(OH)_2$ at the same catalyst loading. Despite the significant lower activity of $Ca(OH)_2$ for hydrogen formation, it showed significantly lower CO_2 yields compared to K_2CO_3. They suggested that $Ca(OH)_2$ not only acts as a catalyst, but also a sorbent for CO_2 to form $CaCO_3$ and water.

Ge et al. (2014) compared the activity of various alkali catalysts on the H_2 yield during batch gasification of lignite coal in SCW at 700 °C and 23 MPa with 1 $g_{catalyst}/g_{coal}$. The activity of the catalysts used in terms of H_2 yield were $K_2CO_3 \approx KOH \approx NaOH > N_2CO_3 > Ca(OH)_2$. In contrast to the results from Guo et al. (2007) and Ge et al. (2014), Muangrat et al. (2010) found that the

catalytic effect, in terms of H_2 yield, for various alkali catalysts were NaOH > KOH > $Ca(OH)_2$ > K_2CO_3 > Na_2CO_3 during the sub-critical gasification of glucose by partial oxidation of glucose at 330 °C and 13.5 MPa using 1.33 $g_{catalyst}/g_{glucose}$. In addition, Jin et al. (2014) found the catalytic effect on the hydrogen yield for the gasification of glucose in SCW at 400 °C and 23 MPa with catalyst loading of 0.2 $g_{catalyst}/g_{glucose}$ to be KOH > $Ca(OH)_2$ > K_2CO_3 > LiOH > NaOH > Na_2CO_3.

This dissimilarity in the activity of the alkali catalyst suggests that the operating conditions (supercritical vs. sub-critical), type of feedstock material used (coal, glucose or cellulose), the presence of an oxidant as well as the catalyst loading can affect the activity of alkali catalysts for the production of hydrogen.

Amongst all the of the various alkali catalysts available, K_2CO_3 has been investigated most extensively. Sınağ et al. (2004) investigated the effect of K_2CO_3 on the formation of intermediate products during the SCWG of glucose. They showed that in the presence of K_2CO_3, the decomposition of glucose to formic acid is enhanced while the formation of furfurals is restrained (furfurals are known to be converted to phenols from which tar and char is formed). Hence, when K_2CO_3 is present, the formation of tars and chars are supressed while gas formation is enhanced. They ascribed the catalytic effect of K_2CO_3 to the production of potassium formate (HCOOK) *via* the reaction of K_2CO_3 with water to form $KHCO_3$ and KOH (Eq. 2-8), and then the reaction of KOH with CO to form HCOOK (Eq. 2-9):

$$K_2CO_3 + H_2O \rightarrow KHCO_3 + KOH \qquad 2\text{-}8$$

$$KOH + CO \rightarrow HCOOK \qquad 2\text{-}9$$

Hydrogen and $KHCO_3$ are then formed *via* the reaction of potassium formate with water (Eq. 2-10), followed by the decomposition of $KHCO_3$ to water, K_2CO_3 and CO_2 (Eq. 2-11).

$$HCOOK + H_2O \rightarrow KHCO_3 + H_2 \qquad 2\text{-}10$$

$$2KHCO_3 \rightarrow H_2O + K_2CO_3 + CO_2 \qquad 2\text{-}11$$

$$KOH + CO \rightarrow HCOOK \qquad 2\text{-}12$$

From these reactions, the most important reaction is the formation of potassium formate, as it is needed for the production of hydrogen (Eq. 2-10). However, CO is needed for the formation of potassium formate (Eq. 2-12). The early formation of CO (generally through steam reforming) is therefore essential for hydrogen production during alkali-catalysed SCWG by means of K_2CO_3. The overall nett reaction showing the catalytic effect of K_2CO_3 is shown in reaction (Eq. 2-13):

$$H_2O + CO \leftrightarrow HCOOH \leftrightarrow H_2 + CO_2 \qquad 2\text{-}13$$

2.6.2 HETEROGENEOUS CATALYSTS

Heterogeneous catalysts typically used to aid in SCWG are transition metals, which are known to catalyse steam reforming and methanation reactions. However, activated carbon has also been used as a heterogeneous catalyst in SCWG applications (Yanagida et al., 2009; Yong and Matsumura, 2012a). Although a wide variety of transition metals has been used as catalyst in SCWG experiments, nickel (Ni) and ruthernium (Ru) have shown to be the most active catalysts (Elliott, 2008). Despite the fact that Ru catalysts have shown the highest activity towards SCWG, Ni catalysts are often preferred due to their relatively lower cost compared to Ru (Azadi and Farnood, 2011). An extensive review on the various types of Ru and Ni catalysts and supports are given by Azadi and Farnood (2011) and by Elliott (2008).

Mass transfer limitations are typically associated with heterogeneous catalyst for the transfer of gas phase molecules to the solid surface of the catalyst. However, in supercritical water, these mass transfer limitations are minimal due to the gas-like viscosity of supercritical water (see section 2.2).

Minowa et al. (1994) were the first to report experimental data for SCWG using a reduced nickel catalyst on kieselguhr and sodium carbonate support. Their results suggest that the reduced nickel catalyses the formation of CO_2 and CH_4. Minowa and Ogi (1998) proposed a reaction scheme for Ni-catalysed gasification of cellulose in sub- and supercritical water, showing that Ni promotes the methanation of CO_2 with H_2 to form CH_4 (see Eq. 2-14).

$$\text{Cellulose} \xrightarrow{\text{decomposition}} \text{water} - \text{soluble products} \xrightarrow{\text{gasification/Ni}} H_2 + CO_2 \xrightarrow{\text{methanation/Ni}} CH_4 + CO_2 \qquad 2\text{-}14$$

Table 2-4 provides a summary of the various Ni catalyst types that have been used in batch experimental studies at low gasification temperatures (below 550 °C). Many studies have focussed on the development of novel Ni catalysts and support material suited for the SCWG of various feed material (Azadi et al., 2012; Chowdhury et al., 2011; Furusawa et al., 2007; Li et al., 2011; Lu et al., 2014, 2013, 2010). In these studies, the mechanical, catalytic and chemicophysical properties of the catalyst were taken into account to test various catalysts and support materials specifically for the application in SCWG. The development of catalyst support for SCWG is however outside the scope of this project.

A number of studies have used commercially available catalysts in SCWG studies. The most popular commercial Ni catalyst used in SCWG studies is skeletal Raney nickel, a pyrophoric porous nickel catalyst with a small amount of aluminium residue, typically used for hydrogenation reactions (Afif et al., 2011; Jin et al., 2014; Pei et al., 2007; Sınağ et al., 2004; Waldner and Vogel, 2005; Yanik et al., 2008). However, other authors have shown that a commercially available, safer powdered Ni catalyst on Al_2O_3/SiO_2 support (a popular catalyst support material used in a wide variety of disciplines) can also be used as catalyst during SCWG (Guan et al., 2014; Taylor et al., 2009; Youssef et al., 2010).

Zöhrer and Vogel (2013) suggested a residence time dependent biomass-to-catalyst ratio ($\dot{\xi}$) – to serve as first estimate of the minimum weight hourly space velocity (WHSV) when changing from a batch to a continuous setup (see Eq. 2-15). The residence time (τ) was defined as the time that the temperature of the reactor content exceeds 300 °C. They showed that almost complete conversion of carbon can be achieved during SCWG of fermentation residue at 410 °C with $\dot{\xi}$ < 0.45 $g.g^{-1}h^{-1}$ when Ru/C catalyst is used at a reaction time of 25 minutes or less (this corresponds to a total catalyst loading of 6.3 g/g_{FR} Ru/C).

$$\dot{\xi}[g.g^{-1}.h^{-1}] = \frac{m_{feed,dry}}{m_{catalyst}\tau} \qquad 2\text{-}15$$

TABLE 2-4 SUMMARY OF STUDIES USING NI CATALYST IN SCWG EXPERIMENTS

FEEDSTOCK	CATALYST	CATALYST LOAD [$G_{CATALYST}/G_{FEED,DRY}$]	FEED CONC. [WT.%]	TEMP [°C]	HOLD TIME [MIN]	CGE [%]	YIELD [MOL/KG_{FEED}]		REFERENCE
							Y_{CH_4}	Y_{H_2}	
Cellulose	Ni on Kieselguhr	0.2	33	400	60	67	10.6	3.5	Minowa et al. (1994)
Cellulose	Ni5132-Engel	1.3		400	20	90	14	8	Yoshida et al. (2004)
Lignin	Ni5132-Engel	0.8		400	20	14	1	3	Yoshida et al. (2004)
Glucose	Raney Ni	0.1	5	500	60	45	4	8.3	Sınağ et al. (2004)
Sawdust	Raney Ni	0.5	10	400	92	100	20.1	3.3	Waldner and Vogel (2005)
Peanut shell	Raney Ni + Mo	0.5	2	450	50	94	13	17	Pei et al. (2007)
Lignin	Ni/MgO	1	5.5	400	120	15	2.5	5	Furusawa et al. (2007)
Sunflower stalk	Raney Ni	0.1	6	500	60		3.2	8	Yanik et al. (2008)
Cellulose	Ni/SiO_2-Al_2O_3	0.63	9	500	15	50	9	11	Taylor et al. (2009)
Cellulose	Ni wire	125 mm^2/g	5	500	10	45	1.8	3.5	Resende and Savage (2010)
Cellulose	Ni wire	240 mm^2/g	1	500	10	51	6	6	Resende and Savage (2010)
Glucose	Ni/γ-Al_2O_3	1	9	400	25	33	2.5	10.5	Lu et al. (2010)
Glucose	Ni/SiO_2-Al_2O_3	0.16	4.5	500	30	78	4.1	6.2	Youssef et al. (2010)
Sludge	Raney Ni	2	3	380	16	68	11.7	11.8	Afif et al. (2011)
Glucose	Ni-Cu/γ-Al_2O_3	0.2	10	400	60	60	11	1.9	Li et al. (2011)
Cellulose	Ni/α-Al_2O_3	0.6	2	380	60	88	9	40	Azadi et al. (2012)
Glucose	Ni/CeO_2-Al_2O_3	0.2	9.1	400	20	33	2	13	Lu et al. (2013)
Lignin	Ni/SiO_2-Al_2O_3	0.5	5	500	60	28	2.9	6.9	Guan et al. (2014)
Peanut shell	Raney Ni	1	10	550	20	67	12.1	9.6	Jin et al. (2014)
Sewage sludge	Ni powder	0.22	5	400	10	8	0.45	3.6	Gong et al. (2014)
Glucose	Ni/CeO_2-Al_2O_3	0.1	10	400	20	18	0.3	1.4	Lu et al. (2014)

2.7 Feed Materials Used for SCWG

2.7.1 The Use of Model Compounds

Identifying and understanding all of the chemical reactions that take place during the conversion of biomass in SCW are difficult due to the complexity and variability of biomass mixtures. Kruse and Dinjus (2007) proposed a method to deal with this issue. They proposed that "key substances" (which are typical intermediate products) should be identified. These key substances can help in identifying reaction pathways for the conversion of more complex feed material.

The three major constituent of biomass are cellulose, hemicelluloses and lignin (Figure 2-4). Of these, cellulose and hemicelluloses are carbohydrates, while lignin contains aromatic rings (Guo et al. 2010). When cellulose undergoes hydrolysis near the critical point of water, glucose is the main product that forms, and thus, glucose and cellulose yield similar gasification products. Therefore, although cellulose is the main constituent of biomass, glucose has been used more frequently as model compound for cellulose during SCWG experiments (Guo et al. 2010).

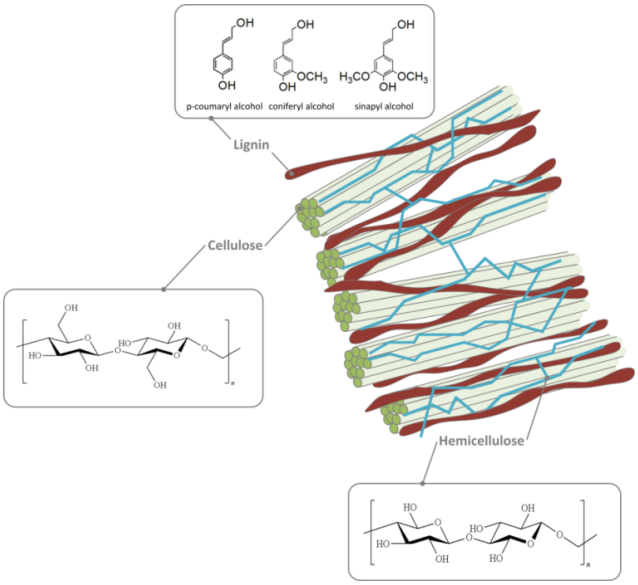

Figure 2-4 Schematic of the microscopic structure of biomass

Probably the most widely used model compound in SCWG studies is glucose (Azadi et al., 2009; Castello et al., 2013; Ding et al., 2014a; Goodwin and Rorrer, 2008; Hao et al., 2003; Hendry et al., 2011; Lee et al., 2002; Promdej et al., 2010; Susanti et al., 2012; Watanabe et al., 2002;

Williams and Onwudili, 2006, 2005; Yu et al., 1993; Yu-Wu et al., 2013). A reaction scheme was proposed by Chuntanapum and Matsumura (2010) for the decomposition of glucose in sub- and supercritical water at 300 and 400 °C (see Figure 2-5).

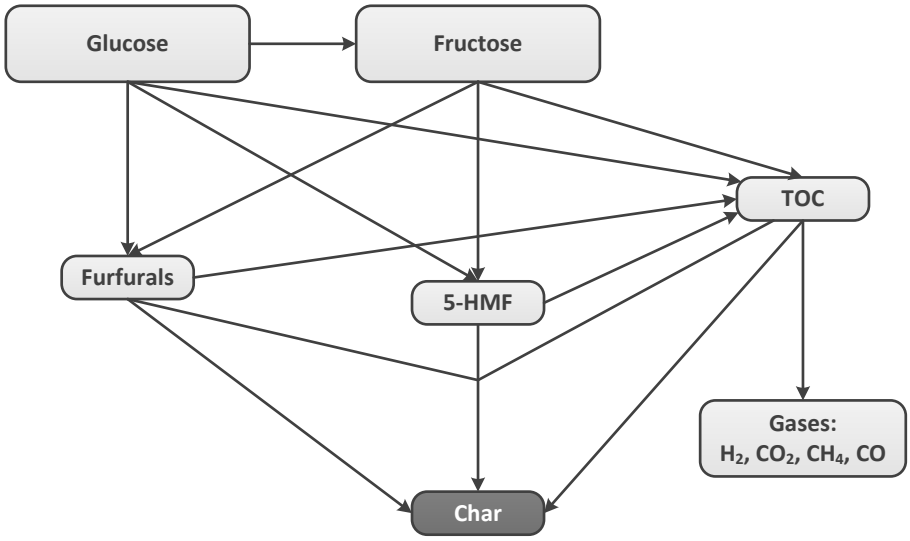

FIGURE 2-5 REACTION PATHWAY FOR THE DECOMPOSITION OF GLUCOSE IN SUB- AND SUPERCRITICAL WATER AT 300 AND 400 °C, AS PROPOSED BY CHUNTANAPUM AND MATSUMURA (2010)

The reaction mechanism of lignin in SCW with and without the presence of catalysts has also been investigated in various studies (Furusawa et al., 2007; Guan et al., 2014; Osada et al., 2007; Resende et al., 2008; Saisu et al., 2003; Yong and Matsumura, 2012b). As in the case of cellulose, the decomposition of lignin in SCW also starts by means of hydrolysis reactions, but forms guaiacol instead of glucose/fructose. Guaiacol then further decomposes to phenol and/or catechol. Hence a number of studies focussed on the the gasification of guaiacol or phenols in SCW as a model compound for lignin (DiLeo et al., 2008; Huelsman and Savage, 2012; Selvi Gökkaya et al., 2015). Compared to cellulose and lignin, very little work on the SCWG of hemicellulose (or xylose/xylan) has been conducted (Aida et al., 2010; Goodwin and Rorrer, 2010; Guo et al., 2007).

The interaction of several model compound mixtures to understand the reaction mechanisms associated with possible interactions between biomass constituents has also been reported (Castello et al., 2015; Goodwin and Rorrer, 2009; Kruse et al., 2005; Su et al., 2015; Weiss-

Hortala et al., 2010; Yoshida and Matsumura, 2001). Mixtures of xylan and cellulose resulted in experimental yields close to that predicted by standard mixing rule correlations developed from the experimental data from SCWG of pure xylan and cellulose. However, the addition of lignin to xylan and cellulose resulted in gasification efficiencies and H_2 production lower than the predicted values (Yoshida et al., 2004; Yoshida and Matsumura, 2001). Furthermore, Yong and Matsumura (2012) observed high char yields during the SCWG of lignin. They suggested that the char originated most likely from the phenolic compounds. Phenols are more likely to polymerise to char than to gasify (especially if the temperature is still below the critical temperature of water – see Figure 2-3).

2.7.2 Real Feedstock Material Used in SCWG Experimental Tests

Despite some similarities between the experimental results of model compounds and mixtures of model compounds to represent real biomass, SCWG of real and model compounds may result in considerable variation in experimental results due to the presence of inorganic components (ash) as well as the possible presence of sulphur, which can lead to catalyst deactivation during catalytic SCWG (Azadi and Farnood, 2011). Hence, it is essential to generate experimental data using real biomass as feedstock material for SCWG.

Various types of real biomass materials have been used as feedstock material in SCWG experiments (batch or continuous setups). These organic materials include:

- ***Agricultural residue material***, including potato wastes (Antal et al., 2000) corn starch, clover grass and corn silage (Boukis et al., 2007; D'Jesus et al., 2006), tobacco-, corn-, cotton- and sunflower stalk (Madenoğlu et al., 2012; Yanik et al., 2007) and bagasse (Barati et al., 2014);
- ***Animal waste material***, including chicken manure (Nakamura et al., 2008; Yanagida et al., 2009; Yong and Matsumura, 2012a), swine manure (Waldner, 2007) and tannery waste (Yanik et al., 2007);
- ***Food industry waste*** such as fruit shells (Demirbas, 2004), molasses and rice bran (Muangrat et al., 2010b) and soybean fibre and restaurant waste (Munetsuna et al. 2010);

- Various ***Algae*** species, including *Chlorella Vulgaris* (Chakinala et al., 2010), *Laminaria hyperborea* (Cherad et al., 2014), *Nannochloropsis* (Guan et al., 2012a), *Spirulina* (Miller et al., 2012), *Chlorella*, *Spirulina* and *Saccharina* (Onwudili et al., 2013), *Spirulina platensis* (Stucki et al., 2009);
- ***Sewage sludge*** including studies from Acelas et al. (2014), Afif et al. (2011), Chen et al. (2013a), Chen et al. (2013b), Gong et al. (2014a), Gong et al. (2014b), Qian et al. (2015), Schmieder et al. (2000), Vostrikov et al. (2008), Wilkinson et al. (2012), Xu and Antal (1998), Xu et al. (2013), Xu et al. (2012) and Zhu et al. (2011);
- ***Wastewater*** from a updraft wood gasifiers (Blasi et al., 2007), olive mill (Kıpçak et al., 2011), amino acid production (Lee and Ihm, 2010), an electronic process (Nakagawa et al., 2007) and wastewater containing *o*-cresols (Wei et al., 2006);
- Various ***coal*** and ***lignite*** including studies by Cao et al. (2015), Cheng et al. (2004), Jin et al. (2015), Lan et al. (2014) and Li et al. (2010);

A number of experiments have been conducted in small-scale batch reactors at low gasification temperatures (e.g. Afif et al., 2011; Castello et al., 2013; Waldner and Vogel, 2005; Zöhrer and Vogel, 2013). Typically, a batch reactor will not be used on industrial scale for SCWG. Experiments in small batch reactors can however be used to demonstrate the suitability and viability of a specific organic material as feedstock material for SCWG. Furthermore, optimum operating conditions can be determined, which may then later be confirmed in a continuous system.

a) Paper sludge as feedstock for SCWG

A wide variety of studies focussed on the SCWG of waste sludge – specifically sewage sludge and secondary paper sludge, which consists mainly of microbial biomass, non-biodegradable lignin solids and cell-decay products (Afif et al., 2011; Chen et al., 2013a; Gong et al., 2014a; Xu et al., 2013; L. Zhang et al., 2010b). However, only one study has previously focussed on the SCWG of primary paper sludge, which consists mainly of rejected wood fibres (Rönnlund et al., 2011). The work by Rönnlund et al. (2011) was conducted at high operating temperatures (500 – 650 °C) and low dry matter feed concentrations (2 – 3 wt.%) using three alkali catalysts, including KOH, NaOH, or K_2CO_3.

L. Zhang et al. (2010) conducted a comprehensive study on the gasification of various industrial sludge products (primary sewage sludge, secondary sewage sludge, digested sewage sludge and secondary pulp/paper-mill sludge) in SCW at various operating temperatures (400 – 550 °C) and reaction time (20 – 120min) in a Hastelloy alloy batch reactor without added catalyst. The water content of all four feedstock materials were between 95.5 and 98 wt.%. Their results showed that, amongst the feedstock used, the secondary pulp/paper-mill sludge exhibited the greatest potential for the production of H_2 and energy recovery, due to the high volatile content and the presence of alkali salts which catalysed the water-gas shift reaction. They further showed that a low dry matter content (around 2 wt.%) favoured H_2 and total gas yields compared to higher dry matter content (around 8.8 wt.%). In addition, by adding a few drops of NaOH solution as alkali catalyst to the primary sewage sludge, the H_2 yield increased significantly from 1 to 8 mol/kg_{sludge} (when operating at a temperature of 500°C).

Rönnlund et al. (2011) investigated the gasification of paper sludge (with a very low amount inorganic material) and black liquor (with high amount of inorganic material around 40%) in SCW at various operating temperatures (500 – 600 °C) in a small scale semi-batch reactor made from Inconel 625. Their results showed that the gas yields increased only slightly with an increase in the temperature without added catalyst during SCWG of paper sludge. However, by adding various alkali catalysts (0.4-0.47 $g_{catalyst}/g_{sludge}$ KOH, NaOH or K_2CO_3), the gas yields and the cold gas efficiency increased significantly. Amongst the catalysts used, K_2CO_3 had the most significant effect on the gas yields and cold gas efficiency. In another study by the same research group, Myréen et al. (2011) investigated different integration scenarios of SCWG of paper sludge into an existing pulp and paper mill process in Finland. Their calculations suggested that the thermal efficiency of the paper mill can be increased by 50% (from 5MW to 7.5 MW) by integrating the SCWG of their primary paper sludge into the existing process plant.

b) Wood as feedstock for SCWG

Various authors have used wood (specifically wood sawdust) as feedstock material during SCWG experiments. The earliest work done on gasification of wood in sub- and supercritical water was by Sealock and Elliott (1991). Since then, many researchers have carried out gasification

experiments in SCW using various wood species as feed material. A summary of the experimental conditions as well as the results achieved in these studies are given in Table 2-5.

Waldner and Vogel (2005) proposed a reaction mechanism for the SCWG of wood in the presence of Raney nickel catalyst (see Figure 2-6). Firstly, cellulose decomposes to glucose, hemicellulose to xylose and glucuronic acid and lignin to phenolics (all through hydrolysis reactions). Dehydration of phenolics leads to the formation of aromatic components (such as toluene, benzene and xylenes). The aromatics may undergo polymerisation to from coke (or char). The phenolics can also hydrolyse to form polyphenols. Dehydration of glucose leads to the formation of 5-hydroxymethyl furfural (5-HMF). The 5-HMF can form polyphenols such as 1,2,4-trihodroxybenzene. Polyphenols typically form tar-like substances through condensation reactions. However, under catalytic conditions, the 5-HMF and polyphenols are assumed to decompose to small molecules such as carboxylic acids, aldehydes, alcohols and ketones. These small, low molecular weight molecules can be directly reformed to H_2, CO, CO_2 and CH_4 on a nickel catalyst. Furthermore, formic acid and acetic acid can undergo carboxylation to form CH_4, CO_2 and H_2. These gas products can then further react with water and each other through the equilibrium reactions (water gas shift reaction and methanation reactions – Eq. 2-3, Eq. 2-4 and Eq. 2-10).

The only study in which the gasification of *Eucalyptus* wood in SCW was investigated was that by Yong and Matsumura (2012a). In their work, they investigated the effect of wood addition to poultry manure for SCWG in a continuous flow system at 550 – 650 °C in the presence of activated carbon catalyst. Their results showed that *Eucalyptus* wood was more easily gasified in SCW than poultry manure.

TABLE 2-5 SUMMARY OF STUDIES USING WOOD AS FEEDSTOCK MATERIAL FOR SCWG EXPERIMENTS

REACTOR TYPE	REACTOR TYPE	OPERATING CONDITIONS	CATALYST	MAIN RESULTS	REFERENCE
Wood flour	Batch	300 – 450 °C, 34 MPa 10 wt.%	Harshaw Ni	Y_{CH_4} = 13.7 mol/kg$_{wood}$	Sealock and Elliott (1991)
Wood sawdust	Batch	450 °C , 31.5 – 35 MPa 120 min TOC$_{feed}$ = 4900 ppm	None	CE = 98%	Schmieder et al. (2000)
Poplar wood sawdust & corn starch	Flow type	650 °C, 22 MPa 1 – 4 g/min 15.4 wt.%	Activated carbon	CE = 100% Y_{gas} = 1.4 g/g$_{wood}$	Antal et al. (2000)
Wood sawdust	Batch	400 °C, 25 MPa 20 min	0.4 – 1.2 g/g$_{sawdust}$ Ni catalyst	CE = 51% Y_{CH_4} = 6 mol/kg$_{wood}$ Y_{H_2} = 7 mol/kg$_{wood}$	Yoshida et al. (2004)
Bark-free fir and spruce chip mixture	Batch	400 °C, 30 MPa 0 – 92 min 10 – 30 wt.%	0.5 g/g$_{wood}$ Raney Ni	CE = 96 – 103%	Waldner and Vogel (2005)
Sawdust	Batch	500 °C, 27 MPa 20 min 10 wt.%	0.2 g/g$_{sawdust}$ Ru/C	CE = 77.2% Y_{CH_4} = 11.2 mol/kg$_{wood}$ Y_{H_2} = 12.7 mol/kg$_{wood}$	Hao et al. (2005)
Bark from birchwood	Batch	380 °C, 23 MPa 5 – 60 min 2 wt.%	0.6 g$_{Ni}$/g$_{wood}$ Raney Ni	CE = 80%	Azadi et al. (2012)
Eucalyptus wood & poultry manure mixtures	Flow type	550 – 650 °C, 25 MPa 86 – 105 s 0.1 – 0.5 wt.%	0.2 – 0.8 wt.% Activated carbon	CE = 52%	Yong and Matsumura (2012)
Wood sawdust	Batch	550 °C, 36 – 40 MPa 28 min 0.5 wt.%	1 g/g$_{sawust}$ Ru/α-Al_2O_3 + 1.07 M CaO	CE = 99% Y_{CH_4} = 9 mol/kg$_{wood}$ Y_{H_2} = 10.5 mol/kg$_{wood}$	Onwudili and Williams (2013)
Beech wood	Batch	350 & 400 °C, 30 MPa 60 – 300 min 15 wt.%	None	Y_{H_2} = 1.3 mol/kg$_{wood}$	Castello et al. (2013)
Pine wood	Batch	550 °C 30 min 25 wt.%	1 g/g$_{wood}$ Ni/CeO_2/Al_2O_3 1 g/g$_{wood}$ Dolomite 1.67 M KOH	CE = 99% Y_{CH_4} = 2 mol/kg$_{wood}$ Y_{H_2} = 5.6 mol/kg$_{wood}$	Ding et al. (2014a)

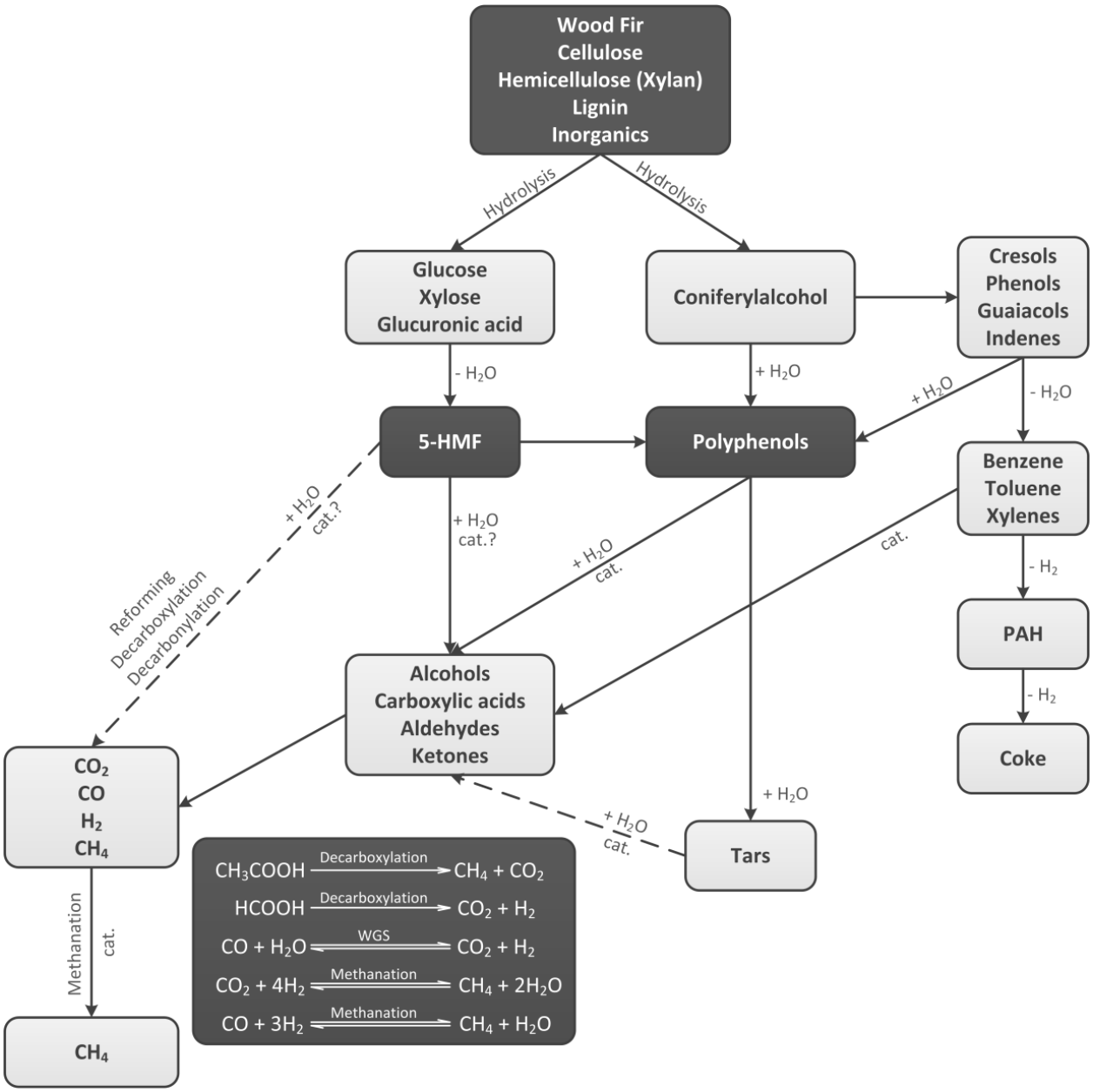

FIGURE 2-6 PROPOSED SIMPLIFIED REACTION PATHWAY FOR GASIFICATION OF WOOD IN SUPERCRITICAL WATER (REDRAWN FROM WALDNER AND VOGEL (2005)). THE TERM "CAT." DENOTES THE PATHWAYS THAT ARE AFFECTED BY THE PRESENCE OF A CATALYST, WHILE THE TERM "CAT.?" INDICATE THE TERMS THAT ARE ASSUMED TO BE CATALYTICALLY DRIVEN.

c) Pyrolysis char as feedstock for SCWG

Pyrolysis is the process in which the volatile matter in solid fuel is liberated during heating in an inert environment (without oxygen) to form a non-condensable product (fuel gas), liquid (bio-oil) and solid (char) product (Aboyade et al., 2013). While the liquid product can be upgraded for liquid fuel, the solid product is considered as a soil amendment agent, an adsorbent during gas clean-up or wastewater treatment or as charcoal (Uras et al., 2012; Kambo and Dutta, 2015). Furthermore, it has also been considered as an alternative to coal for energy production by means of steam gasification (Encinar et al., 2001).

Ramsurn et al. (2011) used hydrochar produced during HTC of switchgrass as feed material to compare the gasification efficiencies achieved during conventional dry gasification and SCWG. Significantly higher carbon gasification efficiencies were achieved during SCWG of hydrochar compared to that of dry gasification. Castello et al. (2014) gasified hydrochar from HTC of maize silage in SCW at 400 °C. Their results showed that, contrary to what has been believed, hydrochar from HTC is not an inert in SCW and the gas product produced during SCWG is non-negligible. Lu and Savage (2015) further showed that the recovery of energy within an algal bio-refinery is possible *via* the SCWG of lipid-extracted algal hydrochar produced during HTC of microalgae followed by an ethanol extraction step. They achieved up to 75% energy recovery and complete recovery of organic nitrogen to ammonium in the aqueous phase during SCWG.

d) Effect of feedstock composition

Park and Tomiyasu (2003) were the first to investigate the effect of the composition of organic components on the gas yields. In their study, nine model compounds were used as feed material in SCWG experiments (see Table 2-6 for more detail on the organic components used). Experiments were conducted in a batch autoclave at 450 °C and 44 MPa over a RuO_2 catalyst and a residence time of 120 minutes. Their results suggest that a feedstock with a lower O/C ratio and higher H/C ratio will result in an increase in the CH_4/CO_2 product ratio.

TABLE 2-6 SUMMARY OF STUDIES INVESTIGATING THE EFFECT OF FEEDSTOCK COMPOSITION

	PARK AND TOMIYASU (2003)	DEMIRBAS (2004)	YANIK ET AL. (2007)
Feed type	Naphthalene, carbazole, phenyl ether, dibenzofuran, polyethylene, polypropylene, polystyrene, polyethylene terephthalate & cellulose	Almond, cotton cocoon, hazelnut, sunflower & walnut	Tobacco stalk, corn stalk, cotton stalk, sunflower stalk, corncob and oregano stalk, chromium-tanned & vegetable-tanned waste
O/C	0 – 0.83	0.53 – 0.65	0.60 – 0.85
H/C	0.75 – 2.0	1.2 – 1.6	1.4 – 1.8
Cellulose	n/a	27.0 – 48.5 wt.%	26.3 – 52.0 wt.%
Lignin	n/a	3.0 – 11.1 wt.%	17.5 – 53.8 wt.%
Hemicellulose	n/a	7.4 – 31.7 wt.%	10.5 – 35.6 wt.%
Temperature	450 °C	377 – 477 °C	500 °C
Pressure	44 MPa	23 – 48 MPa	28 – 34 MPa
Catalyst	RuO_2	None	None

Demirbas (2004) used real biomass as feed material and investigated the effect of the cellulose content in the feed material on the H_2 yield at various operating temperatures, while using five different empty fruit shells as feed material without any catalyst. A correlation between the H_2 yield and the cellulose content were developed, depending on the gasification temperature. Unfortunately, they did not report the CH_4 yields.

Yanik et al. (2007) investigated the difference in the gas yields during SCWG at 500 °C of various lignocellulosic materials as well as tannery waste materials in a batch reactor at 500 °C without the use of a catalyst. Despite the wide range of lignocellulosic composition, the range of the feedstock composition in terms of the O/C and H/C ratios was not very broad and no conclusion could be drawn regarding the effect of the elemental composition (C, H and O content) on the gas yields. Furthermore, the proximate analysis of the feed material in terms of the fixed carbon and volatile matter was not provided. Hence, no conclusion could be drawn regarding the effect of the volatile matter and fixed carbon content on the gas yields.

None of these previous studies compared the actual experimental results with the theoretical equilibrium results in order to determine the effect of the O/C ratio and the volatile matter content on the yields. Park and Tomiyasu (2003) only considered a variety of model compounds and could therefore not show the effect of the volatile matter content in the feed material on the gasification efficiencies. Yanik et al. (2007) focussed more on the cellulose, lignin and hemi cellulose content. Although they also reported the elemental composition and the proximate analysis of each of the feed materials, they did not relate it to the gas yields achieved for each feed material. Hence, all these previous studies focussed on the effect of the operating conditions such as temperature and dry feedstock concentration. They did not consider the composition of the feed material as a variable.

2.8 Additional Factors Influencing SCWG

Apart from operating temperature, the use of catalyst and the effect of the type of feedstock used, a number of other parameters influence the outcome of the SCWG. These parameters include the operating pressure, the type, size and material of construction of the reactor, residence time, feedstock concentration, heating rate, feed particles size and feed composition. An extensive review of the effect of these parameters are given in a review article by Basu and Mettanant (2009) as well as a book chapter by Basu (2010b). While the most important factors that are applicable to this study (temperature, catalyst and feedstock type) have been discussed in the preceding sections, a brief summary of the effects of the other parameters, are given in Table 2-7.

TABLE 2-7 SUMMARY OF THE EFFECT OF OPERATING PARAMETERS ON SCWG

PARAMETER	MAIN EFFECT	REFERENCE
Pressure	• Majority of studies showed that there is not a significant effect on gas yields above the critical pressure	Kruse et al. (2003) Lu et al. (2006)
Reactor type	• Batch reactors operations are not isothermal • Unwanted reactions may take place during the heat-up phase • Continuous plug-flow reactors requires shorter residence times but may plug more easily • Fluidised bed reactor may overcome some problems associated with batch and plug-flow reactors	Kruse et al. (2000) Susanti et al. (2010) Chen et al. (2013a) Chen et al. (2013b)
Reactor material	• Reactors made from metal alloys (especially those which contains Ni) catalysed gasification reactions • The presence of chromium negatively affected the gas yields	Antal et al. (2000) Yanik et al. (2007) Castello et al. (2013)
Heating rate	• Lower heating rates resulted in an increase in the formation of tar and char • Higher heating rates resulted in an increase in the gas yields and gasification efficiencies	Sınağ et al. (2004) Matsumura et al. (2006) Lu et al. (2006) Barbier et al. (2011)
Reaction time	• Increase in reaction time resulted in an increase in the performance of the SCWG reactor • After certain time (different for every setup) no further improvement in performance was evident	Williams and Onwudili (2005) Lu et al. (2006) Cherad et al. (2014)
Feed concen-tration	• The results in literature do not all show the same effect that an increase in solid concentration has on the SCWG reactor performance • The type and size of reactor, mixing method as well as type of feedstock plays an important role in the difference in the results	Kruse et al. (2003) Cherad et al. (2014)
Particle size	• SCWG of smaller particles resulted in higher hydrogen yield, CE and GE • Issues regarding pumpability of feed material as well as extra energy required to reduce particles size must be taken into account before concluding that smaller particles will result in a higher process efficiency	D'Jesús et al. (2005) Lu et al. (2006)

2.9 Modelling Approaches to SCWG

A number of modelling approaches have been followed to investigate equipment performance as well as to predict the production formation at various operation conditions during SCWG. Apart from thermodynamic equilibrium modelling and process modelling, some studies have also a focussed on kinetic modelling of SCWG (Bühler et al., 2002; Castello and Fiori, 2012; Guan et al., 2012b; Resende and Savage, 2010) as well as computational fluid dynamics (CFD) simulations (Azadi et al., 2011; Goodwin and Rorrer, 2011; Yoshida and Matsumura, 2009). For the purposes of this specific project, only studies relating to thermodynamic modelling and process modelling will be discussed.

2.9.1 Thermodynamic Modelling

Thermodynamic analysis of the SCWG process is very useful in presenting theoretical predictions for optimisation of the process and can include both thermodynamic equilibrium calculations as well as exergy analysis of the process. SCWG is known to be influenced by kinetics, especially at low operating temperatures without the use of catalysts (Kruse, 2008). However, knowing the thermodynamic limit of the gas yields that can be attained from a specific feedstock material prior to conducting experimental work can be of great help. Knowing such information can aid in more effective design of experiments. Furthermore, once experimental data is available, it can be compared with equilibrium results to determine the deviation from equilibrium (Gutiérrez Ortiz et al., 2011a).

Two general approaches are commonly followed for equilibrium modelling namely the stoichiometric approach and the non-stoichiometric approach. When using the stoichiometric approach, one requires prior knowledge of all the species involved in the process, chemical reactions taking place as well as information on the reaction rates. Once this information is known, the equilibrium constants for all the reactions are calculated. When using the non-stoichiometric approach, one only requires knowledge about the reactor temperature, pressure and the elemental composition of the feedstock (which can be determined by means of an elemental analysis). The non-stoichiometric approach uses molar balance constraints as well as the Gibbs-free energy minimization of the system at a specific temperature and pressure to

estimate the composition of the product leaving the reactor. Despite the difference in the non-stoichiometric and stoichiometric approaches, it has been shown that these two methods in essence, are equivalent (Smith & Missen 1982).

The earliest study using the non-stoichiometric approach was done by Tang and Kitagawa (2005) on the SCWG of cellulose, glucose and methanol. They used the Peng-Robinson equation of state (EoS) together with the van der Waals mixing rules to determine the product gas composition at different input temperatures and feed concentrations. Their results were in good agreement with experimental data from Boukis et al. (2003). Since then, a number of other authors have implemented similar methods to determine the thermodynamic yields at various operating conditions using a variety of mathematical modelling methods and equations of states – See Table 2-8 (Castello and Fiori, 2011; Freitas and Guirardello, 2013; Lu et al., 2007; Voll et al., 2009; Yakaboylu et al., 2014, 2013; Yan et al., 2006; Yanagida et al., 2008).

Although the results from all these studies vary slightly, depending on the EoS used and the approach followed, the general trends are in agreement (see Figure 2-7):

- An increase in the feedstock concentration typically results in an increase in the CH_4 and CO yields and a decrease in the H_2 and CO_2 yields;
- An increase in the operating temperature typically causes an in an increase in the H_2 and CO_2 yields and a decrease in the CH_4 yield;
- An increase in temperature results in an initial increase in the CO yield, but a further increase resulted in a decrease in the CO yield;
- An increase in the operating pressure above the critical pressure of water does not seem to have a significant effect on the gas yields.

TABLE 2-8 SUMMARY OF THERMODYNAMIC EQUILIBRIUM MODELLING STUDIES CONDUCTED ON SCWG

FEEDSTOCK	METHOD	EOS	OPERATING CONDITIONS	CONTRIBUTION	REFERENCE
Methanol & Glucose	Non-stoichiometric	Peng-Robinson EoS	630 – 750 °C, 27.6 – 28 MPa	• Developed first thermodynamic model for SCWG. • Only took gas phase into account	Tang & Kitagawa (2005)
Glucose	Non-stoichiometric	Duan EoS	377 – 777 °C 20 – 35 MPa	• Trend of the model prediction is in good comparison with experimental data. • The predictions suggest that an increase in C/O ratio will offer high theoretical H_2 yield. • Only took gas phase into account	Yan et al. (2006)
Wood sawdust	Non-stoichiometric	Duan EoS	400 – 800 °C, 25 MPa	• Developed first model which took formation of solid carbon into account • High temperature favours H_2 production • CH_4 and H_2 yields decrease with oxygen addition	Lu et al. (2007)
Poultry manure	Non-stoichiometric	Did not mention	600 °C, 30 MPa	• Determined the behaviour of inorganic elements (N, Ca, K, P, S Cl and Si) into account • All of the N, K and Cl were present in the liquid phase while all of the Ca, P and Si were present in the solid phase	Yanagida et al. (2008)
Methanol, Ethanol, Glycerol, Cellulose	Non-stoichiometric	Ideal EoS	380 – 440 °C, 650 – 800 °C, 22.1, 24.1 & 27.6 MPa	• Did not take non-ideality into account. • Results very close to results when non-ideality is taken into account. • Took gas and solid phase into account	Voll et al. (2009)
Methanol, Glucose and Sewage sludge	Stoichiometric	Peng-Robinson EoS	550 – 740 °C, 27.6 – 28 MPa	• Developed first stoichiometric model using reaction equilibrium method • 7 chemical reactions were considered • Above 740°C (glucose) and 700°C (methanol), the model fits experimental results from literature well	Letellier et al. (2010)
Glycerol & Spirulina	Non-stoichiometric	Peng-Robinson EoS	400 – 1200 °C, 0 – 50 MPa	• Determined at which conditions char formation occurs • Model predicts H_2 and CH_4 very well, but other gasses not that well	Castello & Fiori (2011)
Pig & Cow manure	Non-stoichiometric	Viral EoS	100 – 580 °C, 24 MPa	• Second paper to take the inorganic components into account • Investigated the partitioning of elements in different phases	Yakaboylu et al. (2013)
Microalgae	Non-stoichiometric	Peng-Robinson EoS (gas phase) HKF EoS (aqueous phase)	200 – 600 °C, 25 – 30 MPa	• First study to incorporate the sub- and supercritical regions into a multi-phase mathematical model	Yakaboylu et al. (2014)

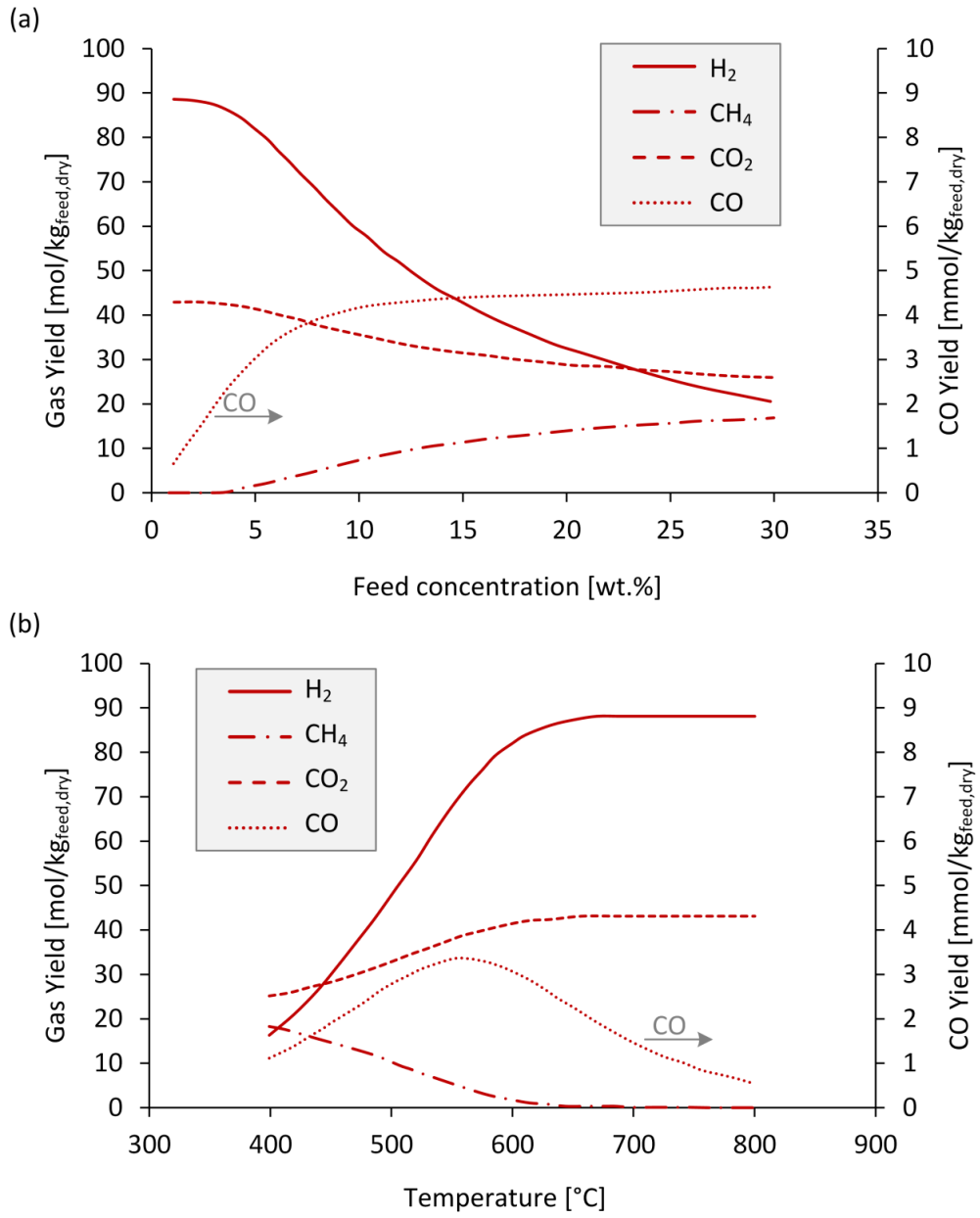

FIGURE 2-7 (A) EQUILIBRIUM GAS YIELDS AS A FUNCTION OF DRY FEED CONCENTRATION DURING SCWG OF WOOD SAWDUST ($CH_{1.35}O_{0.617}$) AT 600 °C AND 25 MPA; (B) EQUILIBRIUM GAS YIELDS AS A FUNCTION OF TEMPERATURE DURING SCWG OF 5WT.% WOOD SAWDUST AT 25 MPA (GRAPH REDRAWN WITH DATA FROM LU ET AL. (2007))

2.9.2 Process Modelling

Apart from thermodynamic equilibrium calculations, various authors have conducted process modelling studies on SCWG to determine the energetic or exergetic efficiency of the process at various operating conditions (Feng et al., 2004; Fiori et al., 2012; Gassner et al., 2011; Gutiérrez Ortiz et al., 2011a, 2011b; Luterbacher et al., 2009; Marias et al., 2011; Withag et al., 2012). Process modelling provides an indication of the performance of the whole SCWG plant.

Gassner et al. (2011) conducted a thermo-economic process modelling analysis on the catalytic gasification of sewage sludge, wood, lignin slurry, manure and microalgae in SCW at 400 °C for the production of Synthetic Natural Gas (SNG) and electricity. Their results showed that an economically and energetically feasible process with overall chemical efficiencies up to 78% can be achieved, depending on the substrate (see Table 2-9).

Table 2-9 Chemical Efficiency for hydrothermal gasification of various substrates (data from Gassner et al. (2011))

Substrate	Overall Chemical Efficiency
Wood	68 – 75%
Sewage sludge	60 – 70%
Manure	45 – 68%
Coffee grounds	75 – 78%
Lignin slurry	72 – 78%
Microalgae	67 – 74%

Gutiérrez Ortiz et al. (2011) used the simulation package Aspen Plus® to model the continuous SCWG process for the reforming of glycerol. The predictive Soave-Redlich-Kwong (PSRK) equation of state together with the generalized Mathais-Copeman α-functions was proposed to be the most suitable EoS to use for their specific application. They showed that the optimum conditions for maximum hydrogen yield was when the reactor was operated at 900°C and 1 mole % glycerol was fed to the reactor. A summary of the process modelling studies conducted on SCWG is shown in Table 2-10.

TABLE 2-10 SUMMARY OF PROCESS MODELLING STUDIES CONDUCTED ON SCWG

FEEDSTOCK	METHOD AND SOFTWARE	EOS	OPERATING CONDITIONS	CONTRIBUTION	REFERENCE
Cellulose	Mathematical model using Non-stoichiometric	SAFT EoS	600 – 750 °C 24 & 35 MPa	• First study to incorporate the gas-liquid separator into the model and perform thermodynamic calculations on SCWG pilot plant • Also the first study to perform an exergy analysis on the system • An optimised heat-exchanger network was design • Exergy efficiency of 40.6% at 600 °C and 35 MPa	Feng et al. (2004)
Wood & Manure	AspenPlus™ and OSMOSE	Did not mention	400 °C 30 MPa	• First study to perform a life cycle assessment on a SCWG pilot plant • Energy recoveries of 62 – 71% were obtained	Luterbacher et al. (2009)
Glycerol & Methanol	AspenPlus™ using R-Gibbs reactor	Predictive Soave-REdlich-Kwong (PSRK)	400 – 1000 °C 24.3 – 30.4 MPa	• Thermodynamically, the best conditions for optimum H_2 production are feeding a glycerol concentration of 1 mole% glycerol and operating at 900°C • Operating pressure did not seem to affect the results significantly	Gutiérrez-Ortiz et al. (2011)
Various lingo-cellulosic materials	In-house software using MILP	Lee-Kesler EoS	400 °C 25 – 25 MPa	• Extensive thermo-economic analysis and optimisation of SCWG for production of SNG • 75% conversion efficiency achieved when microalgae was used as feed material	Gassner et al. (2011)
Vinasse	Mathematical model using the stoichiometric method	Peng-Robinson EoS	500 – 900 °C	• Took solid, liquid and gas phase into account • LHV of gas of 5 MJ/kg achieved with efficiency of 85% • With addition of 0.225 kg/kg air, auto-thermal conditions was achieved	Marias et al. (2011)
Microalgae, Sewage sludge, Grape marc, Glycerol & Phenol	AspenPlus™ using R-Gibbs reactor		500 – 900 °C 25 – 35 MPa 5 – 25 wt.%	• Determine the conditions at which the process is energetically self-sustainable with maximum H_2 production • Feed concentrations between 15 – 25 wt.% resulted in an energy self-sustainable process	Fiori et al. (2012)
Methanol, Glucose & Cellulose	AspenPlus™ using R-Gibbs reactor	Peng-Robinson EoS & Soave-Redlich-Kwong EoS	200 – 900 °C 10 – 40 MPa 0 – 30 wt.%	• Tested variations of the Peng-Robinson EoS & Soave-Redlich-Kwong EoS • Concluded that a feed concentration of 14.5 wt.% methanol and 25 wt.% cellulose and glucose will result in thermal efficiency of 60% at reactor conditions of 600 °C and 30 MPa	Withag et al. (2012)

Withag et al. (2012) developed a system model for SCWG in AspenPlus®. They showed the H_2 mole composition in the gas phase varied in a bandwidth of only 3.5% when the Ideal gas law and two cubic equations of state (Peng-Robinson and Soave Redlich–Kwong) with various mixing rules (Wong–Sandler, modified Huron–Vidal and Boston–Mathias). The thermal efficiency increased as the feed concentration methanol was increased, but stabilised at a concentration at 40 wt.%. They further showed that, in order to achieve a thermal efficiency of 60%, when a 75% heat exchanger efficiency is assumed, the minimum feedstock concentration of 25 wt.% and 14.5 wt.% for cellulose and methanol should be used, respectively.

Fiori et al. (2012) proposed a lay-out for a SCWG pilot plant with 100 kg/h throughput and the process was simulated in AspenPlus® in order to investigate the influence of biomass concentration and type of biomass (glycerol, grape marc, phenol, *Spirulina* microalgae and sewage sludge) on the process. They investigated various process parameters such as temperature (500 – 700 °C), pressure (25 – 30 MPa) and feed concentrations (5 – 25 wt.%) in order to determine the conditions at which the process will be energetically self-sustainable (*i.e.* the conditions at which enough heat was produced to result in isothermal operations of the reactor). At an operating temperature of 700 °C and pressure of 30 MPa, process self-sustainability was achieved at relatively high biomass feed concentrations between 11.4 and 22.9 wt.%, depending on the feedstock type. Energy recovery (one of the key issues in SCWG) as well as the possibility of separating hydrogen from the product gas and feeding it to a fuel cell was investigated through the process simulation.

2.10 CURRENT STATUS AND CHALLENGES OF SCWG

The SCWG process is still in the early stages of its development and a number of process challenges still needs to be overcome. The first process challenge is to ensure that the feed material (typically a slurry-type material) can be pumped efficiently in order to reach the required pressure. A number of pre-treatment methods such as steam-explosion, liquefaction or electroporation are suggested, which can change the feed material into a solution that can be pumped more easily (Kruse, 2008).

Reactor plugging, caused either by salts undissolved in SCW or char formed during slow heat-up phase, is another process challenge associated with SCWG. The addition of a salt separator prior to the gasification reactor in which the salt can precipitate has been proposed to overcome this challenge (Schubert et al., 2012, 2010a, 2010b).

Another process challenge is corrosion of the process equipment. Various methods of minimising corrosion during SCWO are proposed by Marrone and Hong (2009), which can also be applied for the SCWG process. These methods include the usage of high corrosion resistant materials (such as Inconel 625 or Hastelloy C-276) or designing the reactor mixing process in such a way to prevent the corrosive materials to get into contact with the reactor surface (for example a vortex/circulating flow reactor). Furthermore, the operating temperature can be reduced to 400 °C to allow the usage of corrosive resistant metal liners, sacrificial liners, or the application of a coating to some surfaces.

Due to the slight endothermic nature of the SCWG reactions, employing heat integration in the process design is crucial to make the process energy efficient. Various ways of integrating SCWG into existing processes in order to harvest some of the waste heat, or to utilise concentrated solar power for heat generation, have been proposed by (Chen et al., 2010)

Despite these challenges, a number of continuous bench and pilot scale systems have been successfully operated, ranging from a capacity of 1 kg/h at the Paul Schrerrer Institute (Switzerland) to the VARENA plant at Forschungzentrum in Karsruhe (Germany) with a capacity of 100 kg/h (see Table 2-11).

TABLE 2-11 SUMMARY OF LARGER SCALE SCWG SETUPS AND PILOT PLANT SETUPS

INSTITUTE	CAPACITY	OPERATING CONDITIONS	FEEDSTOCK	REFERENCE
FzK (Germany)	100 kg/h	600 – 700 °C, 28 MPa, 20 wt.%	Ethanol & Corn silage	Boukis et al. (2007)
Higashihiroshima (Japan)	46 L/h	600 °C, 25 MPa, 2 & 10 wt.%	Chicken manure	Nakamura et al. (2008)
Paul Scherrer Institut (Switzerland)	1 kg/h	350 – 450 °C, 25 – 35 MPa	Synthetic liquefied wood	Vogel et al., (2007)
State Key Laboratory of Multiphase Flow in Power Engineering (China)	4.8 kg/h	500 - 650 °C, 30 MPa, 2 wt.%	Corn meal Wheat stalk	Chen et al. (2010)
BTG Biomass Technology group (Netherlands)	5 – 30 L/h	600 °C, 30 MPa, 5 wt.%	Glycerol	van Bennekom et al. (2011)
University of Burningham (UK)	4.7 L/h	400 – 550 °C, 17 – 25 MPa, 2 – 30 wt.%	Glycerol	Tapah et al. (2014)

2.11 OUTCOME OF THIS CHAPTER

Although SCWG is still in early phases of development, a lot of work has been done in recent years in order to extend the knowledge related to the process. The overall aim of this chapter was to provide the reader with the necessary background information on SCWG and to highlight the areas in which this study will attempt extend the current understanding in the specific research field. The most important findings of this chapter can be summarised below:

a) Thermodynamic modelling of SCWG

Calculated ***thermodynamic equilibrium yields*** serve as important benchmarks for potential experimental yields, thereby assisting with the selection of suitable operating conditions (*i.e.*, operating temperature and dry feedstock concentration) for a specific feedstock material.

Despite all the work done on thermodynamic modelling, most of these studies only focussed on the effect of the operating conditions such as temperature, pressure and dry feed concentration (also referred to as the biomass-to-water ratio) on the equilibrium product gas composition and gas yields. No in-depth investigation on the combined effect of the composition of the biomass in terms of its ***elemental composition*** (more specifically, its C, H and O content) and operating conditions on the equilibrium gas composition or yields of SCWG have been reported thus far.

Understanding the effect of the feedstock composition on the thermodynamic gas yields can assist with the selection of suitable feedstock material for SCWG prior to conducting experimental work. Although a study on developing such a tool for the selection of appropriate feedstock material for conventional gasification of biomass has been proposed by Vaezi et al. (2012), no work has been published on the development of such a tool for SCWG.

This finding will be addressed by developing a tool to predict the thermodynamic equilibrium composition of a specific feedstock material based on its elemental composition (***Objective 1***, addressed in Chapter 3).

b) Practical kinetic effects and feedstock composition

Thermodynamic studies only take into account the ***elemental composition*** of the feed material and completely ignore the proximate analysis (*i.e.* ***fixed carbon*** and ***volatile composition***). It also assumes that infinite time is available for the system to reach equilibrium. Hence, possible kinetic effects such as ***reaction time***, ***catalyst type*** and ***catalyst loading*** are not taken into account.

A wide variety of organic materials have been used as feedstock material during SCWG experiments. However, work done on wood related waste materials, more specifically ***E.grandis*** **wood** ***chips, primary paper sludge*** and ***pyrolysis char*** is limited. Furthermore, as far as could be ascertained, no previous study has focussed on determining both the effect of ***feedstock composition*** (proximate and ultimate analysis) as well as ***practical kinetic effects*** (catalyst type, catalyst loading and reaction time) by using the calculated thermodynamic equilibrium results as a benchmark.

- These findings are addressed by: Providing both thermodynamic equilibrium and experimental results for the gasification of primary paper sludge in SCW in order to determine how close one can come to the equilibrium limits within a reasonable catalyst loading and reaction time (***Objective 2***, addressed in Chapter 5).
- Providing experimental and thermodynamic equilibrium results for SCWG of *E.grandis* wood chips and wood related pyrolysis char in terms of the gas yields and gasification

efficiencies in order to asses possibility of using these materials as feedstock for SCWG (***Objective 3,*** addressed in Chapter 6).

- Showing the influence of the composition of the feed material (specifically the ultimate and proximate analysis) on the gas yields and gasification efficiencies and comparing the results with the calculated thermodynamic equilibrium results (***Objective 3***, addressed in Chapter 6).

Chapter 3

THERMODYNAMIC MODELLING OF SCWG – EFFECT OF FEEDSTOCK COMPOSITION§

3.1 INTRODUCTION

The aim of this chapter is to develop a method, based on the thermodynamic equilibrium yields, in order to aid in the selection of appropriate feedstock material for SCWG (***Objective 1***). This is done by providing more insight on the effect of the feedstock elemental composition (C, H and O content) on the thermodynamic equilibrium gas yields at various operating temperatures (400 – 800 °C) and dry feedstock concentrations (5 – 20 wt.%). Knowing the thermodynamic yields of a specific feedstock material can serve as a screening method to indicate whether a specific feedstock material is worth-while to be considered as a feedstock material for SCWG.

This chapter is divided into three parts. The first part being the methodology followed to develop the process model as well as the comparison of the model results to experimental results from studies found in literature (Sections 3.2 and 3.3). In the second part, the results showing the effect of feedstock composition at various operating conditions are presented in generalised contour plots and discussed (Section 0). In the third part, the method for utilising the developed contour plots to determine the thermodynamic limits of a specific feedstock material for SCWG is proposed (Section 3.5).

§ Part of this chapter has been published in: Louw, J., Schwarz, C.E., Knoetze, J.H., Burger, A.J., *Thermodynamic modelling of supercritical water gasification: Investigating the effect of biomass composition to aid in the selection of appropriate feedstock material*. Bioresource Technology, Vol 174 (2014), pp 11-23.

3.2 Materials and Methods

3.2.1 Biomass Feedstock Properties

In total, 54 organic compounds were considered as possible feedstock material for SCWG. Of these, five were model biomass components including glycerol, ethanol, glucose, methanol and cellulose. The rest of the 49 materials considered are real biomass compounds, including, amongst others, sewage sludge, black liquor, grape residue, olive residue, pulp and paper mill sludge, various livestock manure, pyrolysis char from sugarcane bagasse, coffee waste, animal blood, leather waste, micro algae, organic wet fraction of municipal waste, crude glycerol from biodiesel production, palm leaves, straw and torrified wood chips. The ultimate and proximate analysis of these materials was obtained from the Phyllis database administrated by the Energy research Centre of the Netherlands (Phyllis2, 2012).

Table 3-1 provides a summary of the ranges and average values of the properties of the feedstock material considered (ultimate and proximate analysis). Figure 3-1 provides the van Krevelen diagram of the 54 feedstock material considered. These properties were considered on a dry, ash-free (daf) basis in order to obtain comparable results only in terms of the effect of the elemental composition of organic material. The ultimate and proximate analysis of each of the 54 feedstock material can be found in Table A-1 and Table A-2 in Appendix A, respectively.

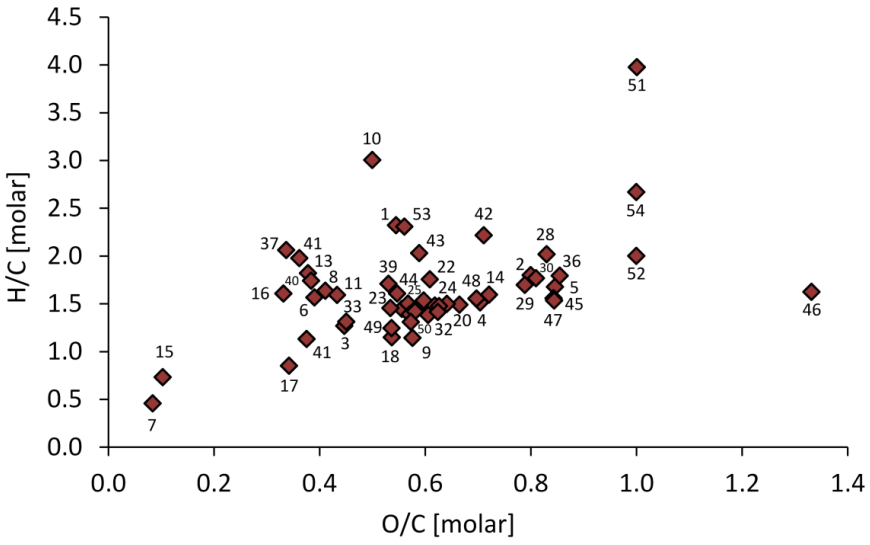

Figure 3-1 Van Krevelen diagram showing the O/C and H/C ratios of all 54 feedstock material considered

TABLE 3-1 EXTREME AND AVERAGE VALUES OF THE COMPOSITION OF THE 54 BIOMASS MATERIALS CONSIDERED

BIOMASS PROPERTIES	MIN	MAX	AVERAGE
Ultimate Analysis (daf) wt.%			
C	34.17	86.26	51.19
H	3.28	13.13	6.86
O	9.63	60.59	38.74
N	0.00	13.99	0.53
S	0.00	7.02	2.32
Proximate analysis (daf) wt.%			
Fix carbon (FC)	0.36	89.70	21.72
Volatile matter (VM)	10.30	99.64	78.28
Ratios (daf) wt.%			
C/H	3.00	26.29	8.02
Molar ratios			
O/C	0.08	1.33	0.60
H/C	0.45	3.97	1.65
HHV_{Milne} [MJ/kg]	10.02	32.91	21.64

a) Determining the calorific value of the feed material

The measured higher heating value (HHV) was not available for all of the components on the Phyllis database and therefore had to be estimated by an empirical correlation. Four empirical correlations (see Eq. 3-1 to Eq. 3-4) which predict the HHV based on the composition of the biomass in terms of its main elements (wt.% C, H, O, N and ash), were examined. These include HHV_{Milne} from (Phyllis2, 2012), HHV_{Dulong}, HHV_{Boie}, HHV_{Friedl} and $HHV_{Gaur\&Reed}$ from (Friedl et al., 2005).

$$HHV_{Milne} = 0.341C + 1.322H - 0.120O - 0.12N + 0.0686S - 0.0153Ash \quad 3\text{-}1$$

$$HHV_{Dulong} = 0.33823C + 1.4225H - 0.18031O + 0.09419S \quad 3\text{-}2$$

$$HHV_{Boie} = 0.3516C + 1.16225H - 0.1109O + 0.0628N + 0.10465S \quad 3\text{-}3$$

$$HHV_{Friedl} = -0.232C^2 - 2.23C + 0.0512H + 0.131CH + 20.6N \quad 3\text{-}4$$

The Pearson's correlation factor (r – see Eq. 3-5) and the root mean squared error ($RMSE$ – see Eq. 3-6) were used to evaluate the accuracy of fit of the correlations. The $RMSE$ provides an absolute fit for the correlations. The smaller the value of $RMSE$ and the closer the value of r is to unity, the better the accuracy of the data (Hameed et al., 2007). Figure 3-2 shows the predicted HHV *vs.* the analytical HHV (obtained from the Pyllis database) for all four correlations considered. It is evident from Table 3-2 that the correlation proposed by Milne is the most accurate with the smallest $RMSE$ (1.81 MJ/kg) and the largest r value (0.940). Hence, HHV_{Milne} was chosen to estimate the calorific value of each biomass component.

$$r = \frac{N\sum exp \times pred - \sum exp \times \sum pred}{\sqrt{[N\sum exp^2 - (\sum exp)^2] \times [N\sum pred^2 - (\sum pred)^2]}} \quad 3\text{-}5$$

$$RMSE = \sqrt{\frac{\sum_{i=1}^{N}(Experimental_i - Model_i)^2}{number\ of\ data\ points}} \quad 3\text{-}6$$

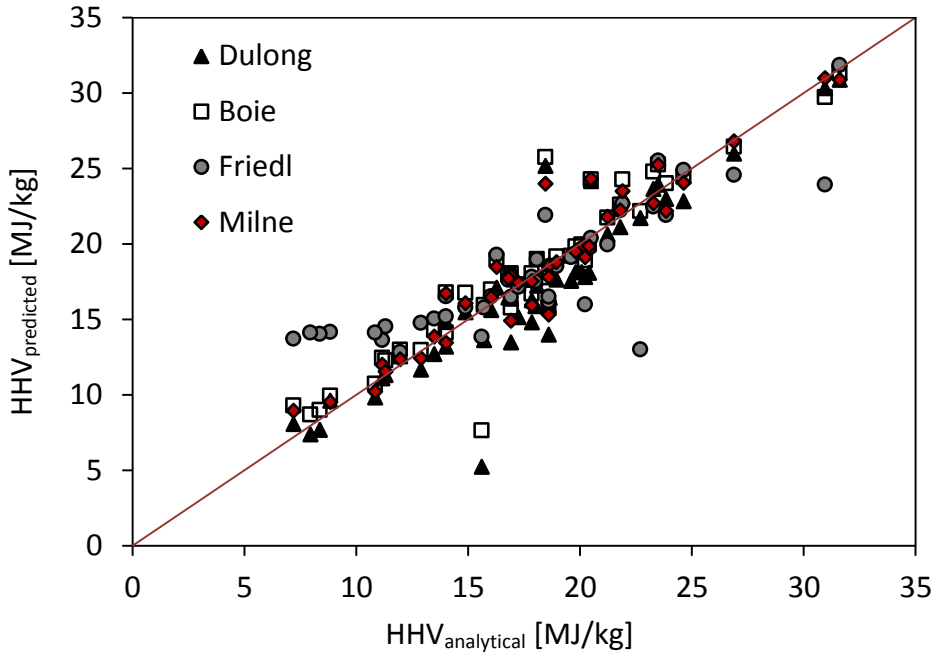

FIGURE 3-2 PREDICTED HHV VS. ANALYTICALLY DETERMINED HHV (ANALYTICAL DATA FROM PHYLLIS2 (2012))

TABLE 3-2 $RMSE$ AND r FOR VARIOUS CORRELATIONS TO DETERMINE THE HHV OF BIOMASS

CORRELATION	$RMSE$ [MJ/KG]	r
HHV_{Milne}	1.81	0.940
HHV_{Dulong}	2.31	0.919
HHV_{Boie}	1.93	0.933
HHV_{Friedl}	2.78	0.849

3.2.2 MODEL DESCRIPTION

A schematic flow sheet of the SCWG process (developed in Aspen Plus®) is shown in Figure 3-3. This flow sheet is a representation of a typical experimental setup used in various SCWG experimental studies (Byrd et al., 2008, 2007; Xu and Antal, 1998; R. Zhang et al., 2010).

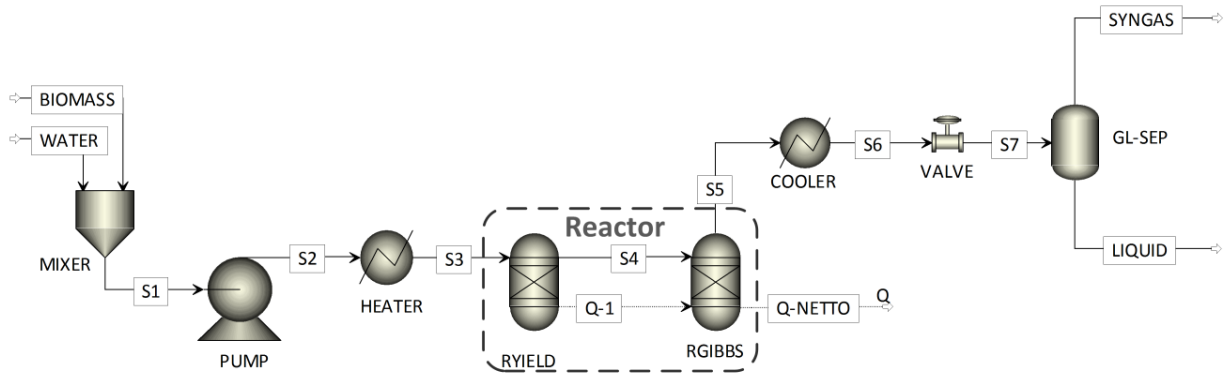

FIGURE 3-3 SCHEMATIC FLOW SHEET FOR SCWG PROCESS USED IN ASPEN PLUS® SIMULATION

Biomass (on a dry, ash-free basis) and water are mixed (MIXER), pressurised (PUMP) and heated (HEATER) to the reactor operating temperature after which it reacts in the SCWG reactor (consisting of RYIELD and RGIBBS). The product stream from RGIBBS (S5) is cooled (COOLER) to room temperature after which it is depressurised to atmospheric pressure in an expansion valve (VALVE). The liquid (LIQUID) and gas (SYNGAS) products are then separated in a gas-liquid (GL-SEP) separator at atmospheric conditions.

Biomass (defined as a heterogeneous solid in Aspen Plus®) does not have a defined molecular weight and is regarded as a non-conventional stream. In order for Aspen Plus® to incorporate such a stream, the RYIELD reactor block is used to decompose it into its elementary,

conventional components (C, H_2, O_2, N_2, Cl and S). The RGIBBS reactor block employs Gibbs free energy minimization calculations in order to model chemical equilibrium at a specified temperature and pressure. The species considered as products from RGIBBS (S5) include H_2O, H_2, CO, CO_2, CH_4, C_2H_6, N_2, N_2O, NO_2, NO, NH_3, SO_2, SO_3, HCl, Cl_2, O_2, and $C_{(s)}$. Catalytic effects were not considered and the reactors were assumed to operate under isothermal and isobaric conditions. Additionally, it was assumed that any char that will form will only consist of solid carbon.

A heat stream (Q-1) is used to transfer the heat of reaction from RYIELD to RGIBBS, while another heat stream (Q-NETTO) provides the net required amount of heat for the reactions to be operated isothermally.

3.2.3 Property Method Selection

A large variety of property methods are available in Aspen Plus®, including both activity coefficient methods and equation of state (EoS) methods. In the case of SCWG, the operating pressure (> 22 MPa) is too high for the use of activity coefficient methods. An EoS method is therefore more suitable. Both the Peng-Robinson EoS and the Redlich-Kwong EoS have been used in thermodynamic equilibrium calculations for SCWG in previous work (Castello and Fiori, 2011; Withag et al., 2012). Although cubic equations of state often perform poorly at conditions close to a component's critical point, the operating temperatures were significantly higher than that of the critical temperature of water (374 °C). Hence, reliable predictions could be generated with the Peng-Robinson and Redlick-Kwong-Soave EoS. These two EoSs are also commonly recommended for gas processing (hydrocarbon separations), hydrogen rich refinery systems, oil and gas production as well as medium pressure refinery applications (Finlayson, 2014).

A number of variations of the Peng-Robinson and Redlick-Kwong-Soave EoS as well as the ideal gas law were used as property method to determine the equilibrium yields of H_2, CO, CO_2 and CH_4 of SCWG of ethanol and water at various feed concentrations and temperatures and a constant pressure of 22.1 MPa. Table 3-3 provides a description of each of the property methods used as well as the Pearson's correlation factor (r) obtained for each property method

for the prediction of the gas yields (H_2, CO, CO_2 and CH_4), when compared to experimental data obtained by Byrd et al. (2007) during SCWG of ethanol using Ru/Al_2O_3 as catalyst. Figure 3-4 and Figure 3-5 provides a graphical comparison of the experimental gas yields and gas yields obtained using the different property methods.

TABLE 3-3 COMPARISON OF VARIOUS PROPERTY METHODS FOR THE CALCULATION OF THE THEORETICAL H_2, CO, CO_2 AND CH_4 YIELDS FOR SCWG OF ETHANOL

PROPERTY METHOD	DESCRIPTION	r
PENG-ROB	Peng Robinson	0.993
PR-BM	Peng Robinson with Boston-Mathias modifications	0.993
PR-MHV2	Peng Robinson with modified Huron-Vidal mixing rules	0.992
PSRK	Predictive Redlich-Kwong-Soave	0.983
RKS-BM	Redlich-Kwong-Soave with Boston-Mathias modification	0.993
RKS-MHV2	Redlich-Kwong-Soave with modified Huron-Vidal mixing rules	0.993
RK-ASPEN	Redlich-Kwong-Soave with Mathias mixing rule	0.993
IDEAL	Ideal gas low	0.991

All of the considered property methods predicted the H_2 yield very well throughout the whole range of ethanol feed concentrations and temperatures (see Figure 3-4(a) and Figure 3-5(a)). Despite following the same trend as the experimental data, the CH_4 yield was somewhat over-predicted at the highest feed concentration and the lowest temperature (Figure 3-4(b) and Figure 3-5(b)). Additionally, all of the property methods except the PSRK method predicted the CO_2 yield very well (see Figure 3-4(c) and Figure 3-5(c)).

Although the trends for the prediction of the CO yield were the same as the experimental data, all of the property methods over-predicted the CO yield (Figure 3-4(d) and Figure 3-5(d)). Despite the poor prediction of the CO yields for all of the property methods, the r-value was greater than 0.990 for all of the cases except when the PSRK property method was used (see Table 3-3). The results for the PENG-ROB, PR-BM, RKS-BM, RKS-MHV2 and RK-ASPEN property methods were the closest to the experimental data with r-values of 0.993. It was decided to use the PR-BM method for the remainder of this study. A detailed description of the PR-BM property method is given in Section A.2 Appendix A.

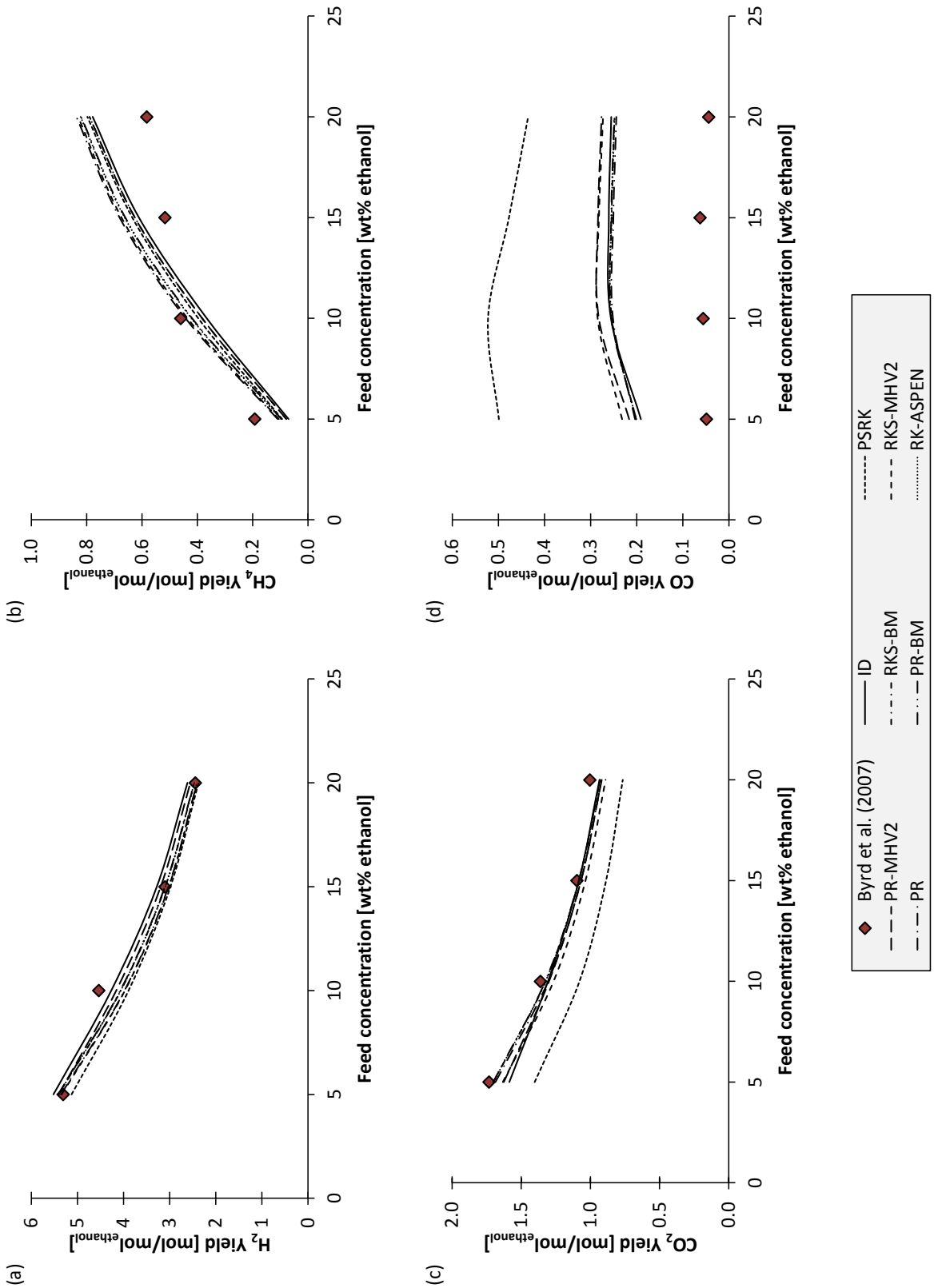

FIGURE 3-4 COMPARISON BETWEEN VARIOUS PROPERTY METHODS AND EXPERIMENTAL DATA FROM THE SCWG OF ETHANOL AT 800 °C AND 22.1 MPA. EXPERIMENTAL DATA FROM BYRD ET AL. (2007).

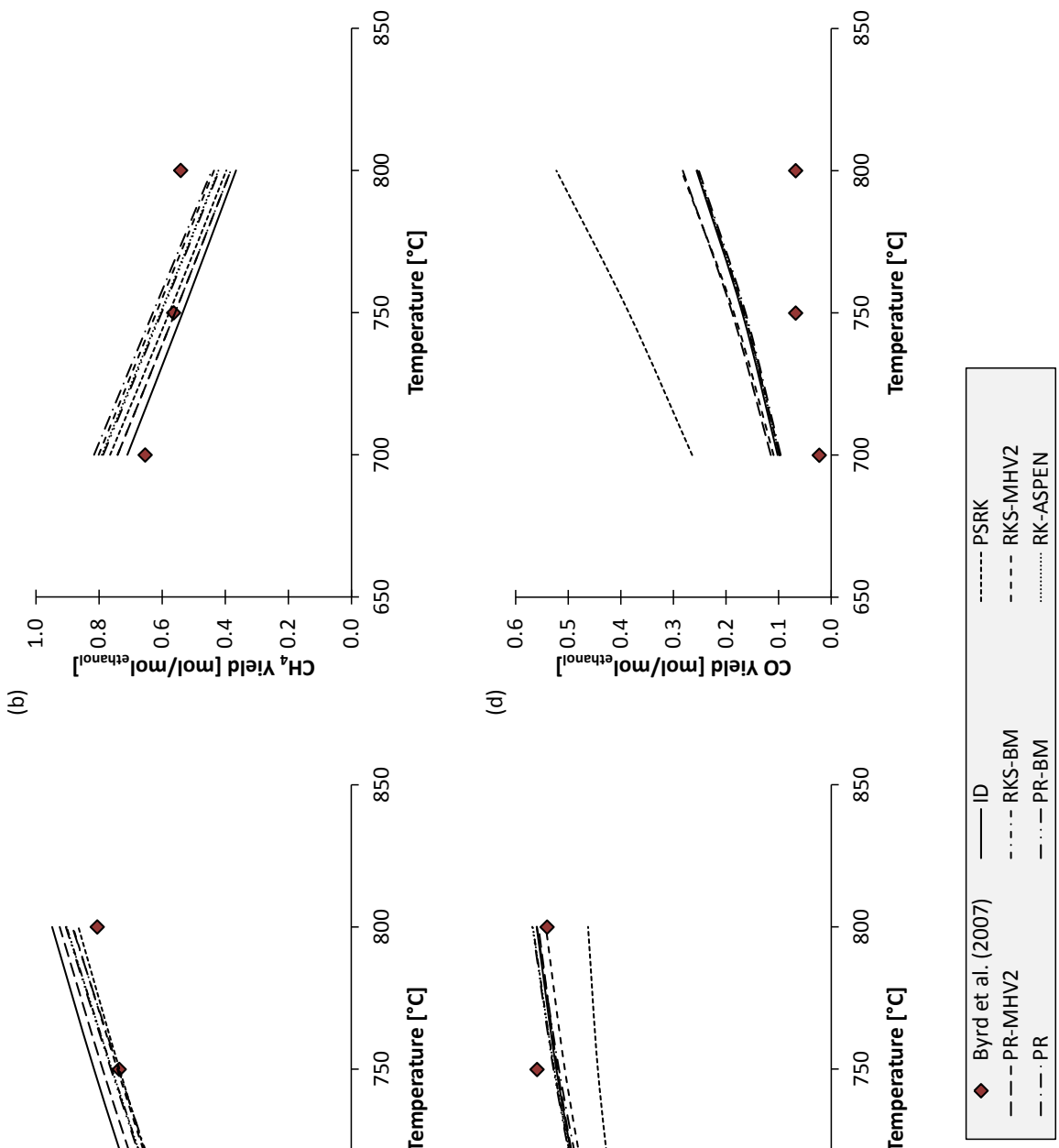

FIGURE 3-5 COMPARISON BETWEEN VARIOUS PROPERTY METHODS AND EXPERIMENTAL DATA FROM THE SCWG OF ETHANOL AS A FUNCTION OF TEMPERATURE, FEEDING 10 WT.% ETHANOL AT 22.1 MPA. EXPERIMENTAL DATA FROM BYRD ET AL. (2007).

3.2.4 Comparison of Model Results with Experimental Data

In order to validate the developed process model, the results from the model using the PR-BM property method were compared to other existing experimental data from both high temperature SCWG (600 – 800 °C) and low temperature SCWG (400 – 550 °C). The experimental data used for the comparison, were specifically chosen as it showed carbon gasification efficiencies close to 100% can be achieved at the appropriate operating conditions with the use of a catalyst.

b) High temperature SCWG (600 – 800 °C)

Table 3-4 shows a summary of the experimental conditions of the reference data. For the SCWG of glycerol (Table 3-5), the equilibrium H_2 and CH_4 yields are in very good agreement with the experimental values from literature (r = 0.98 for both cases). Although the equilibrium yields of CO_2 (r = 0.83) and CO (r = 0.77) do not agree as well, they are still acceptable. The calculated equilibrium product gas composition (mole %) for SCWG of corn starch and saw dust mixtures (Table 3-6), also agree well with the experimental data from literature, especially for the H_2 (r = 0.94) and CO (r = 0.99) content. The process model also predicts the H_2 and CH_4 composition of the gas phase for the SCWG of micro algae at 600 °C accurately (Table 3-7). However, the CO and CO_2 content deviate somewhat from the experimental data from literature.

Table 3-4 Summary of experimental data from literature used to validate the model

Feedstock	Feed solid concentration	Catalyst	Operating conditions		Literature data
			T [°C]	P [MPa]	
Glycerol	5 – 40 wt.%	Ru/Al_2O_3	700 – 800	24.1	Byrd et al. (2008)
CS[a]	10.4 & 13.7 wt.%	Activated Carbon	650 & 715	28.0	Antal et al. (2000)
CS + SD[b]	10.72% SD + 4.01% CS	Activated Carbon	685	28.0	Antal et al. (2000)
Micro algae	7.3 wt.%	Ru/TiO_2	600	24.0	Chakinala et al. (2010)

[a]Corn starch
[b]Saw dust

TABLE 3-5 CALCULATED THERMODYNAMIC EQUILIBRIUM YIELDS (EQUIL) *VS* EXPERIMENTAL (EXP LIT) GAS YIELDS (MOL/$MOL_{GLYCEROL}$) FOR SCWG OF GLYCEROL (EXPERIMENTAL DATA FROM BYRD ET AL. (2008))

CONDITIONS		PRODUCT YIELD [MOL/$MOL_{GLYCEROL}$]							
		H_2		CH_4		CO		CO_2	
FEED WT.%	T [°C]	EXP LIT	EQUIL	EXP. LIT	EQUIL	EXP. LIT	EQUIL	EXP LIT	EQUIL
5	800	6.54	6.69	0.32	0.028	0.1	0.2	2.36	2.77
15	800	4.13	4.63	0.72	0.50	0.04	0.36	2.21	2.14
20	800	3.94	3.78	0.81	0.71	0.17	0.38	2.42	1.91
30	800	2.87	2.66	0.92	0.99	0.21	0.38	2.07	1.63
35	800	2.60	2.28	0.95	1.08	0.24	0.38	1.93	1.53
40	800	2.18	1.99	0.94	1.16	0.24	0.39	1.79	1.46
5	700	5.12	6.07	0.49	0.20	0.02	0.12	2.34	2.64
5	750	5.81	6.52	0.29	0.08	0.01	0.16	2.50	2.74
r		0.98		0.98		0.77		0.83	

TABLE 3-6 CALCULATED THERMODYNAMIC EQUILIBRIUM (EQUIL) *VS* EXPERIMENTAL (EXP) GAS COMPOSITION (DRY MOLE %) FOR SCWG OF CORN STARCH (CS) AND SAWDUST (SD) (EXPERIMENTAL DATA FROM ANTAL ET AL. (2000))

FEED WT.%	T [°C]	H_2		CH_4		CO		CO_2	
		EXP LIT	EQUIL	EXP LIT	EQUIL	EXP LIT	EQUIL	EXP LIT	EQUIL
10.4% CS	650	47	48	15	13	2	1	37	38
13.7% CS	715	55	51	6	11	3	3	34	36
10.7% SD + 4.0% CS	685	43	43	17	19	3	3	38	37
	r	0.94		0.87		0.99		0.89	

TABLE 3-7 CALCULATED THERMODYNAMIC EQUILIBRIUM (EQUIL) *VS* EXPERIMENTAL (EXP LIT) DRY MOLAR GAS COMPOSITION FOR SCWG OF 7.3 WT.% MICRO ALGAE AT 600°C AND 24 MPA (EXPERIMENTAL DATA FROM CHAKINALA ET AL. (2010))

COMPONENT	GAS COMPOSITION [MOLE%]	
	EXP. LIT.	EQUIL
H_2	46.06	47.96
CO	3.00	0.80
CH_4	18.10	18.83
CO_2	28.10	32.45
r	0.995	

c) Low temperature SCWG (400 – 550 °C)

Results obtained from the model were also compared to experimental data from literature at low operating temperatures (*i.e.* below 550 °C). The results were specifically compared to cases where complete conversion of carbon to the gas phase was achieved. Table 3-8 provides a summary of the conditions of the literature data used.

TABLE 3-8 SUMMARY OF EXPERIMENTAL DATA FROM LITERATURE USED TO VALIDATE THE MODEL

FEEDSTOCK	FEED CONC.	CATALYST	OPERATING CONDITIONS		LITERATURE DATA
			T [°C]	P [MPA]	
Sawdust	10 wt.%	Raney Ni	404	31.0	Waldner and Vogel (2005)
Lignin	10 wt.%	Ru/C	400	37.1	Yamaguchi et al. (2009)
Glucose	2 wt.%	Ru/C	450	20.0	Azadi et al. (2010)

TABLE 3-9 CALCULATED THERMODYNAMIC EQUILIBRIUM GAS COMPOSITION COMPARED TO EXPERIMENTAL GAS COMPOSITION FROM LITERATURE (DRY MOLE %) FOR SCWG OF SAWDUST AT 404 °C AND 31 MPA (EXPERIMENTAL DATA FROM WALDNER AND VOGEL (2005))

COMPONENT	GAS COMPOSITION [MOLE%]	
	EXP LIT	EQUILIBRIUM
H_2	7.1	4.3
CO	< 0.1	0.02
CH_4	46.4	48.2
CO_2	46.5	47.4
Y_{CH_4} [g/g$_{wood}$]	0.33	0.33

The model results agree well with experimental data from literature for the SCWG of 10 wt.% sawdust at 404 °C (Table 3-9). The H_2 composition was somewhat over-predicted while the exact CO composition of the experimental data was not given (< 0.1%). The calculated product gas composition from SCWG of 10 wt.% lignin at 400 °C, as well as the calculated gas yields from the SCWG of 2 wt.% glucose at 450 °C, also agree well with the experimental data with an overall r value of 0.992 in both cases (Table 3-10 and Table 3-11).

TABLE 3-10 CALCULATED THERMODYNAMIC EQUILIBRIUM (EQUIL) GAS COMPOSITION COMPARED TO EXPERIMENTAL GAS COMPOSITION FROM LITERATURE (EXP LIT) FOR SCWG OF 10 WT.% LIGNIN AT 400 °C AND 37.1 MPA. EXPERIMENTAL DATA OBTAINED FROM YAMAGUCHI ET AL. (2009).

COMPONENT	GAS COMPOSITION [MOLE%]	
	EXP LIT	EQUIL
H_2	3.4	2.4
CO	0	0.03
CH_4	49.4	54.4
CO_2	46.8	43.1
r	0.992	

TABLE 3-11 CALCULATED EQUILIBRIUM YIELDS (EQUIL) COMPARED TO EXPERIMENTAL YIELDS FROM LITERATURE (EXP LIT) FOR SCWG OF 2 WT.% GLUCOSE AT 450 °C AND 20 MPA (EXPERIMENTAL DATA OBTAINED FROM AZADI ET AL. (2010))

COMPONENT	GAS YIELD [MOL/$KG_{GLUCOSE}$]	
	EXP LIT	EQUIL
H_2	33	29
CO	0.03	0.05
CH_4	6.5	9.4
CO_2	26	23.7
r	0.992	

From these results, it is clear that the equilibrium results obtained from the process model are in good agreement with experimental data from previous studies where gasification efficiencies close to 100% were achieved.

3.2.5 MODEL IMPLEMENTATION

Carbon (C), hydrogen (H) and oxygen (O) are the three major constituents of biomass, while nitrogen (N), sulphur (S) and chlorine (Cl) usually form part of the minor components. Hence, only the C, H and O content of the feed material were varied, while constant values for N, S and Cl were assumed. These constant values were taken as the average values of the 54 organic waste materials, which were 0.5 wt.%, 2.3 wt.% and 0.4 wt.%, respectively (see Table 3-1). Although using constant values for N, S and Cl might influence the accuracy of the results slightly, previous studies have shown that the yields of the gases containing nitrogen and

sulphur were orders of magnitude lower than that of the main product gases from SCWG, namely H_2, CH_4 and CO_2 (Yakaboylu et al., 2013).

Additionally, a dry, ash-free basis was considered in order to obtain comparable results only in terms of the C, H and O content. Hence, the C, H and O content combined comprised of 96.8 wt.% of the feedstock materials. Although adding salts and ash will not influence the expected product yields (as it was determined per mass of dry, ash-free biomass), it might influence the energy required for the process, as well as the sizing of equipment. In a study by Yakaboylu et al. (2013), it was shown that phosphorus, silicon, calcium and magnesium will all be in the stable solid form while chlorine, potassium and sodium will be stable in the aqueous liquid form. It was also shown in previous experimental work by Kruse et al. (2010) that, inorganic salts and char will typically be drained from a SCWG reactor after collecting at the bottom of the reactor. Furthermore, using a salt separator prior to the gasification reactor has shown great potential to remove concentrated brines prior to gasification (Schubert et al., 2012, 2010a, 2010b).

The C and H content are incorporated into two variables, namely the H/C and O/C molar ratios. This allows one to represent the results on a generalised contour plot in terms of two variables while still varying all three variables (C, H and O content). Furthermore, it also allows one to plot the results in the same manner as the classic Van Krevelen diagram, as proposed by Van Krevelen (1950) for the purpose of coal processing. On these plots, the C, H and O contents of the biomass feed material are varied between the extreme values of the 54 organic waste materials (see Table 3-1). These variations entail eight constant H/C molar ratios, namely, 5.96, 1.99, 1.19, 0.85, 0.66, 0.54, 0.46, 0.40 corresponding to eight constant C/H mass ratios of 2, 6, 10, 14, 18, 22, 26 and 30). In other words, the C content varies between 34.2 and 86.3 wt.%, the H content between 3.3 and 13.1 wt.% and the O content between 9.6 and 60.6 wt.%, while maintaining a total mass balance where C, H and O add up to a total of 96.8 wt.% (the balance 3.2% consisting of the N, S and Cl content). In total, 120 cases with different H/C and O/C ratios were used as feed material in the model. Table A-3 in Appendix A provides the properties of the feed material of each of 120 cases when the C, H and O content were varied.

The model was investigated at various operating temperatures (400, 450, 500, 600, 700 and 800 °C) and feed concentrations (5, 10, 15 and 20 wt.%). The pressure was kept constant at 25

MPa for each run, as it was shown in previous studies not to have a significant effect on the equilibrium results of SCWG (Withag et al., 2012).

3.3 Evaluation of Results

The total gas yield (Y_{Total}) and individual component gas yields (Y_{H_2},Y_{CH_4}, Y_{CO} and Y_{CO_2}) were calculated by means of Eq. 3-7 and Eq. 3-8, respectively. In this case $n_{total\ product\ gas}$, $\dot{n}_i$, $\dot{m}_i$and $\dot{m}_{feed,dry}$ are the total gas product molar flow rate, individual molar flow, individual mass flow rate and total mass flow rate of the product gas, respectively.

$$Y_{Total}[\frac{mol}{kg_{biomass}}] = \frac{\dot{n}_{total\ product\ gas}}{\dot{m}_{feed,dry}} \quad 3\text{-}7$$

$$Y_i\ [\frac{mol}{kg_{biomass}}] = \frac{\dot{n}_i}{\dot{m}_{feed,dry}} \quad 3\text{-}8$$

$$x_i[mole\%] = \frac{n_i}{n_{total}} \quad 3\text{-}9$$

The calorific value of the product gas ($HHV_{product\ gas}$) gives an indication of the energetic value of the gas produced (at atmospheric conditions) per mass of biomass fed and was calculated by means of Eq. 3-10. HHV_i is the calorific value of the individual gaseous component in the product gas stream.

$$HHV_{product\ gas}\ [\frac{MJ}{kg_{biomass,daf}}] = \frac{\sum \dot{m}_i HHV_i}{\dot{m}_{feed,dry}} \quad 3\text{-}10$$

The energy recovery (ER) is the fraction of the heat of combustion of the biomass that will be available in the product gas at atmospheric conditions. It was calculated from Eq. 3-11, where LHV_i is the lower heating value of the individual gases in the product gas.

$$ER\ [\%] = \frac{\sum \dot{m}_i LHV_i}{\dot{m}_{feed,dry} LHV_{feed,dry}} \times 100 \quad 3\text{-}11$$

The $LHV_{feed,dry}$ is defined as the HHV of the biomass minus the latent heat of water vapour formed in the combustion of hydrocarbon fuels (in this case, 2.26 MJ/kg). It was calculated from Eq. 3-12, where $H_{wt.\%}$ is the hydrogen content of the biomass.

$$LHV_{feed,dry}[\frac{MJ}{kg}] = HHV_{feed,dry} - 2.26 \times 9\left(\frac{H_{wt.\%\,feed,dry}}{100}\right) \quad 3\text{-}12$$

Previous studies have shown that the SCWG reactions are mostly endothermic, which means that the reactor requires external heat to operate isothermally (Castello and Fiori, 2011; Fiori et al., 2012). The heat required for the process (Q_{Req}) is the sum of the heat needed to heat the feed stream to the reactor temperature (*i.e.*, the duty of HEATER, referred to as Q_{hx}) and the nett heat required to operate RYIELD and RGIBBS isothermally (*i.e.*, Q-NETTO, referred to as Q_{Net}) and was calculated from Eq. 3-13.

$$Q_{Req}\,[\frac{MJ}{kg_{feed,dry}}] = \frac{Q_{hx} + (-Q_{Net})}{\dot{m}_{feed,dry}} \quad 3\text{-}13$$

The overall efficiency of the process was consequently determined by means of Eq. 3-14.

$$\eta_{overall} = \frac{\dot{m}_{H_2}LHV_{H_2} + \dot{m}_{CH_4}LHV_{CH_4} + \dot{m}_{CO}LHV_{CO} + \frac{HR}{100}\dot{Q}_{Cooler}}{\dot{m}_{PWS}LHV_{PWS} + \dot{Q}_{Heater} + \dot{Q}_{Netto} + \dot{W}_{pump}} \quad 3\text{-}14$$

3.4 Results and Discussion

In this dissertation, the results for the gas yields and other performance indicators are presented in terms of the molar O/C and H/C ratios of the feed material. Results for each feed concentration (5, 10, 15 and 20 wt.%) at gasification temperatures of 400, 600 and 800 °C are presented in this section. The results for the gas composition at these conditions are given in Section B.2 in Appendix B while the results for gasification temperatures of 450, 500 and 700 °C are given in Section B.3, B.4 and B.5, respectively in Appendix B.

For each case, the product gas consisted of mainly H_2, CH_4, CO, CO_2 and N_2 (99 % on a mass and mole basis). Furthermore, the N_2 yield was more or less constant at 0.71 mol/$kg_{feed,dry}$ for all 25

cases due to the constant N content in the feed material. Hence, only the results for the H_2, CH_4, CO, CO_2 and total gas yields are presented.

3.4.1 H_2 YIELD

Figure 3-6, Figure 3-7 and Figure 3-8 show the generalised contour plots as a function of the O/C and H/C ratios for the H_2 yield for 400, 600 and 800 °C, respectively. The H_2 yield in terms of the oxygen content in the feed material at various H/C ratios is shown in Figure 3-9, Figure 3-10 and Figure 3-11.

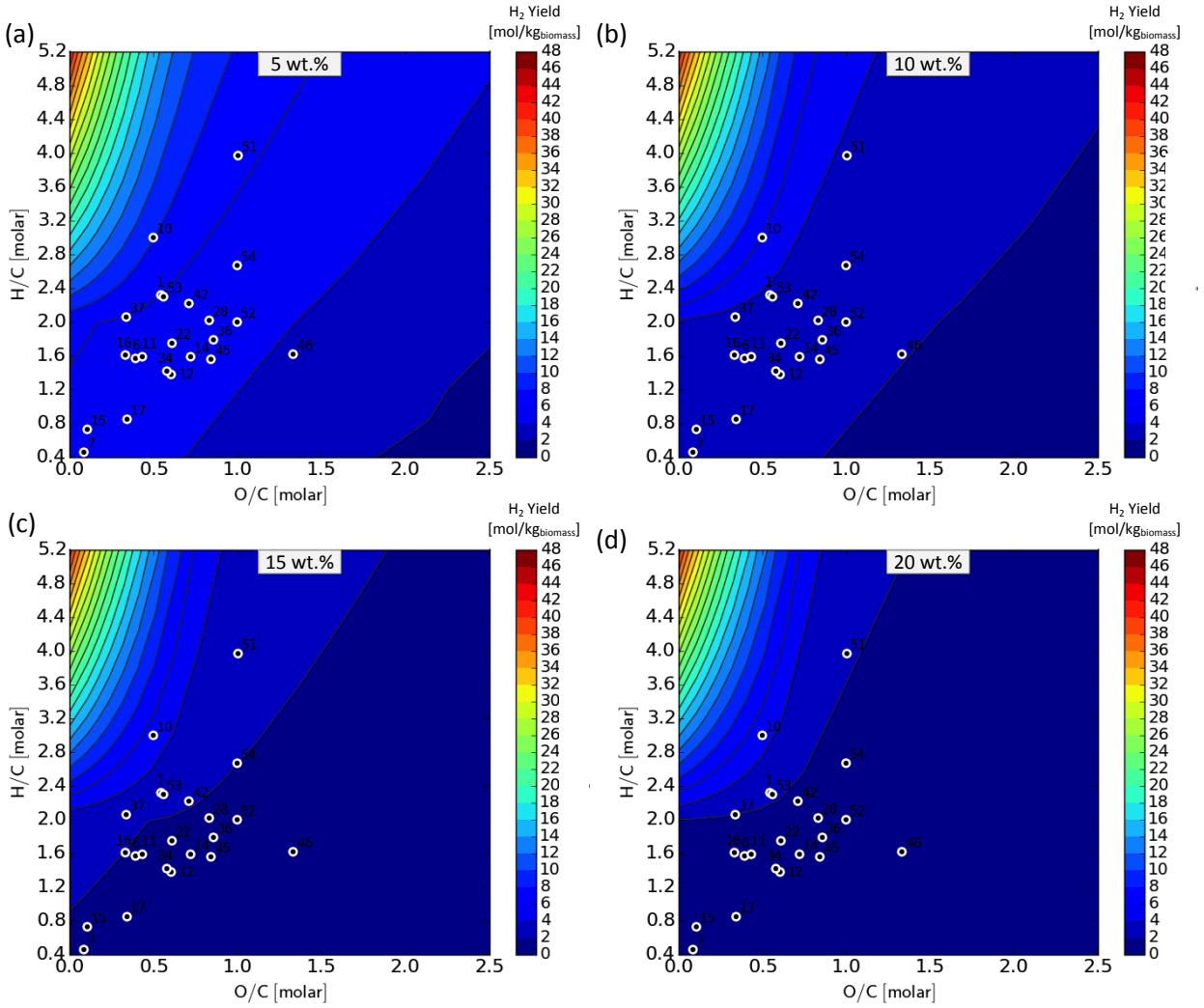

FIGURE 3-6 EFFECT OF FEEDSTOCK COMPOSITION ON THE THERMODYNAMIC EQUILIBRIUM H_2 YIELD DURING SCWG AT 400 °C, 25 MPA AND A DRY FEED CONCENTRATION OF (A) 5 WT.%; (B) 10 WT.%; (C) 15 WT.%; AND (D) 20 WT.%

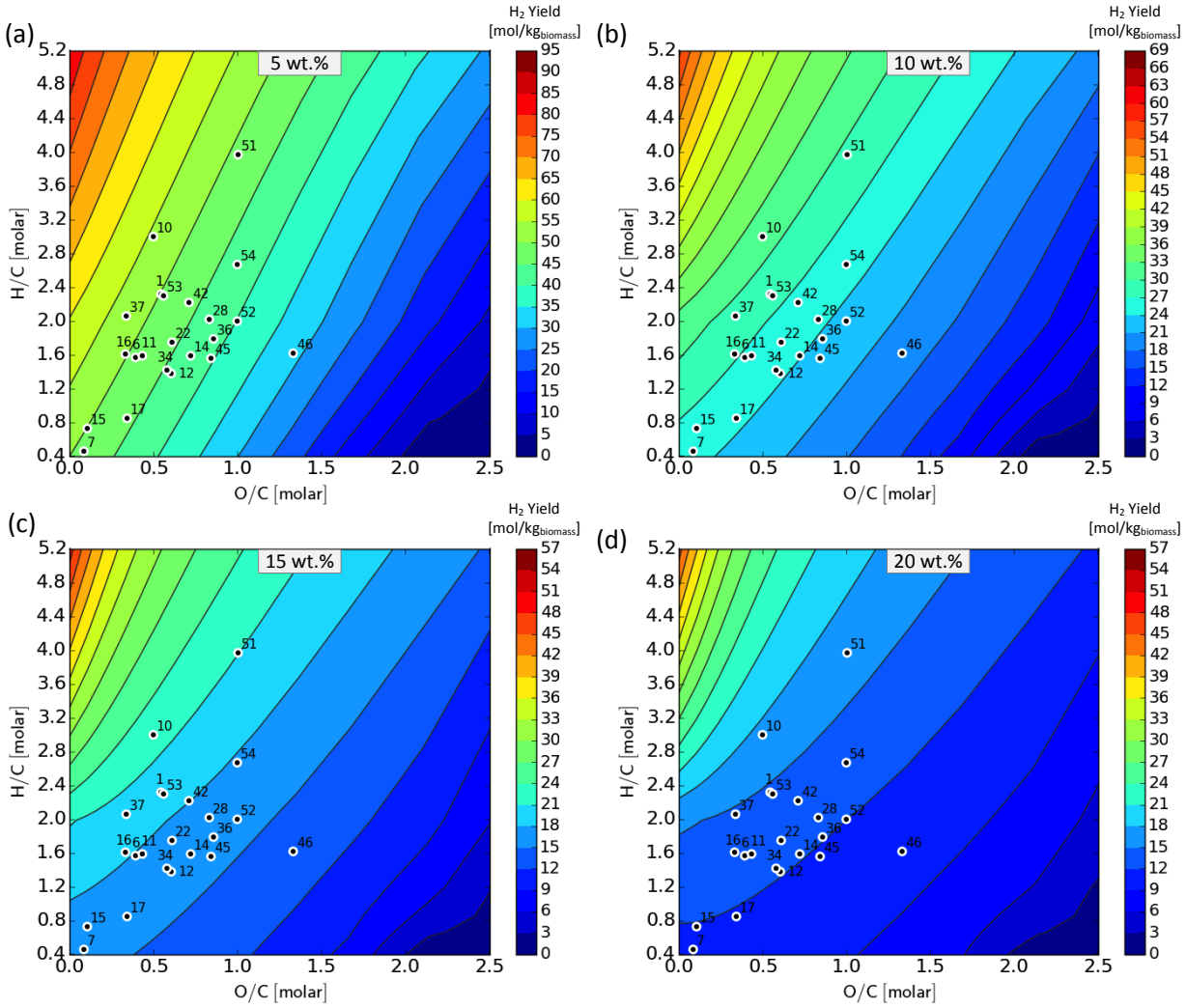

FIGURE 3-7 EFFECT OF FEEDSTOCK COMPOSITION ON THE THERMODYNAMIC EQUILIBRIUM H_2 YIELD DURING SCWG AT 600 °C, 25 MPA AND A DRY FEED CONCENTRATION OF (A) 5 WT.%; (B) 10 WT.%; (C) 15 WT.%; AND (D) 20 WT.%

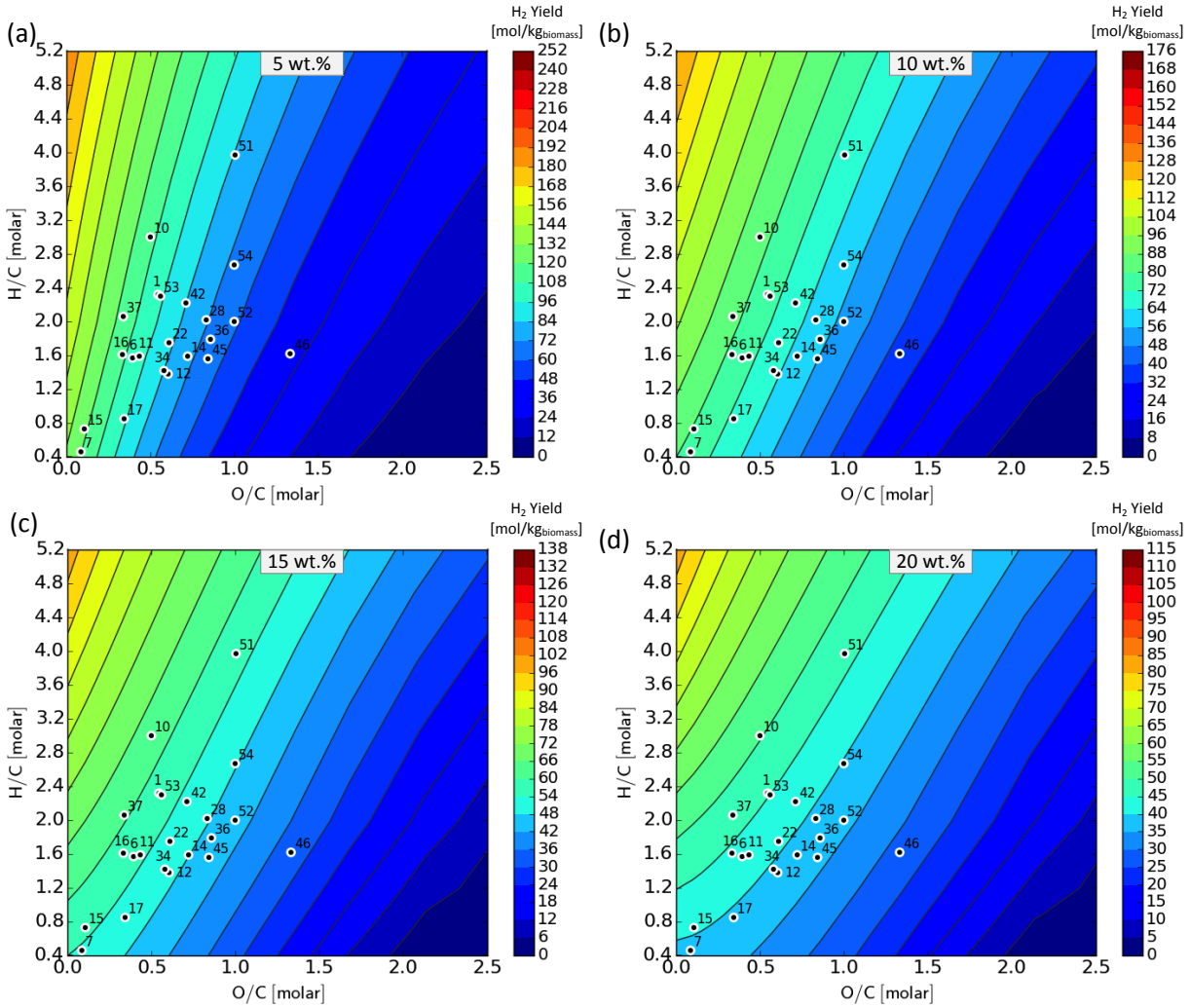

FIGURE 3-8 EFFECT OF FEEDSTOCK COMPOSITION ON THE THERMODYNAMIC EQUILIBRIUM H_2 YIELD DURING SCWG AT 800 °C, 25 MPA AND A DRY FEED CONCENTRATION OF (A) 5 WT.%; (B) 10 WT.%; (C) 15 WT.%; AND (D) 20 WT.%

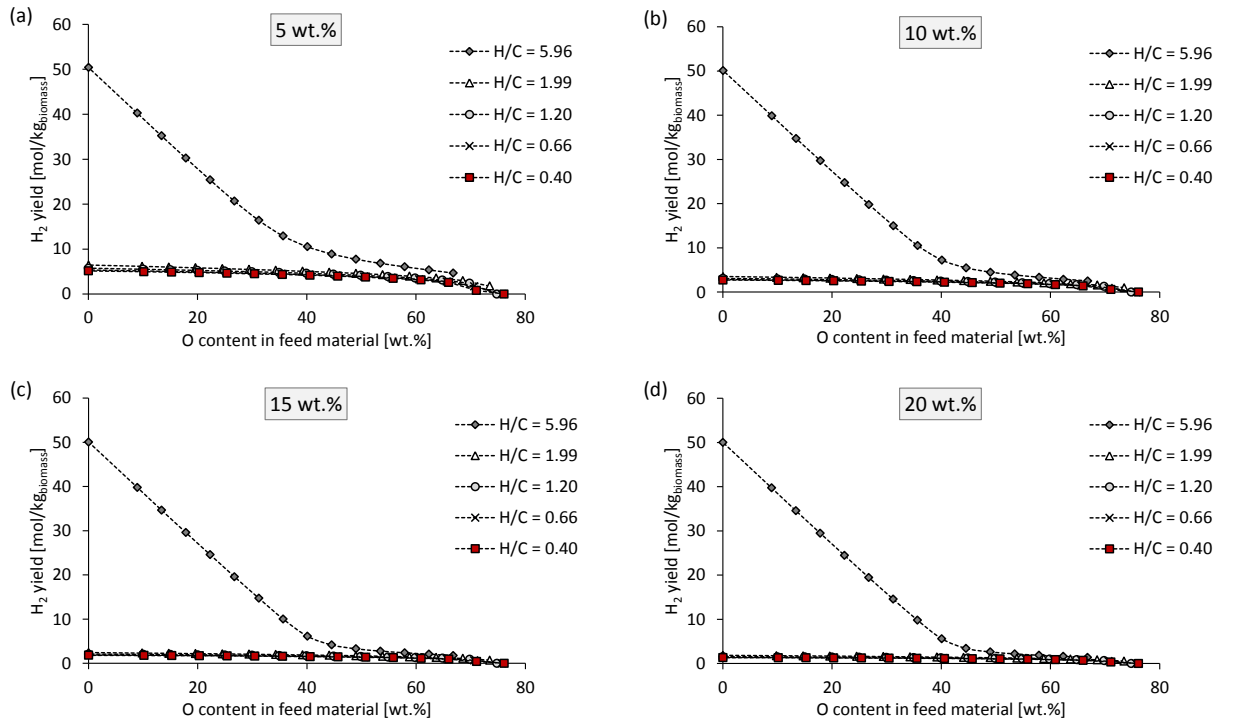

FIGURE 3-9 EFFECT OF OXYGEN CONTENT AND H/C RATIO OF THE FEED MATERIAL ON THE H_2 YIELD DURING SCWG AT 400 °C AND A DRY FEED CONCENTRATION OF (A) 5 WT.%; (B) 10 WT.%; (C) 15 WT.%; AND (D) 20 WT.%

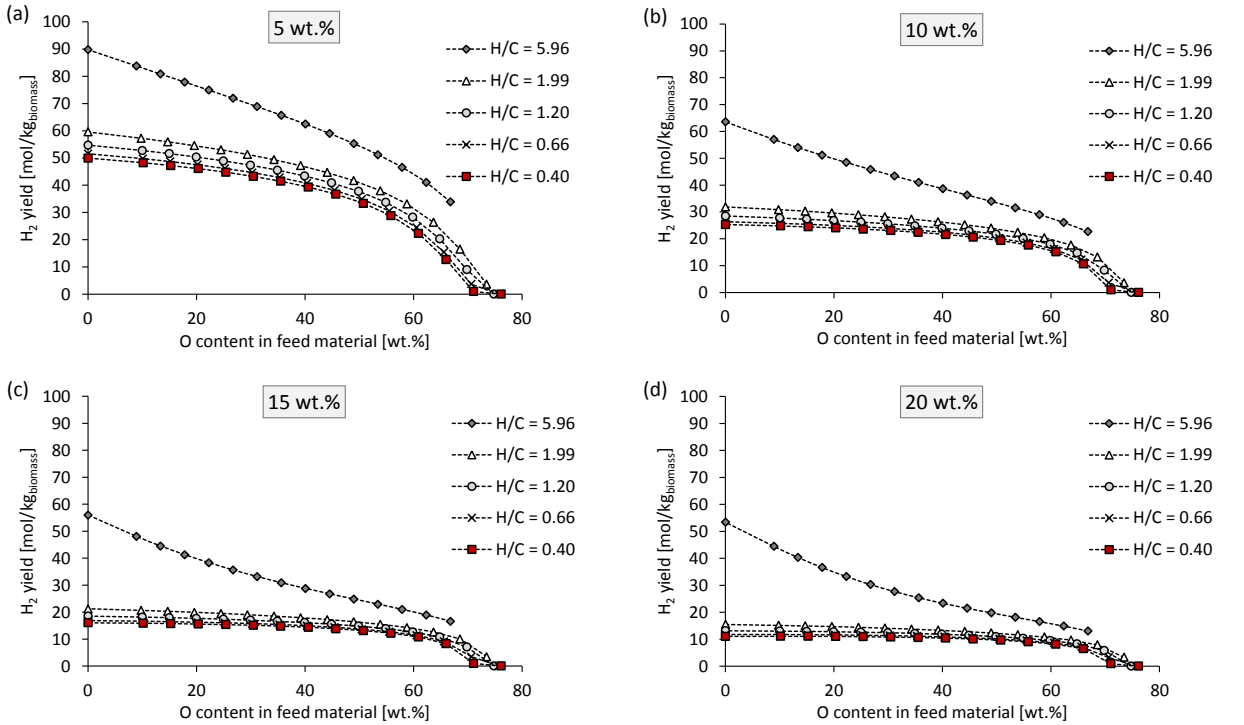

FIGURE 3-10 EFFECT OF OXYGEN CONTENT AND H/C RATIO OF THE FEED MATERIAL ON THE H_2 YIELD DURING SCWG AT 600 °C AND A DRY FEED CONCENTRATION OF (A) 5 WT.%; (B) 10 WT.%; (C) 15 WT.%; AND (D) 20 WT.%

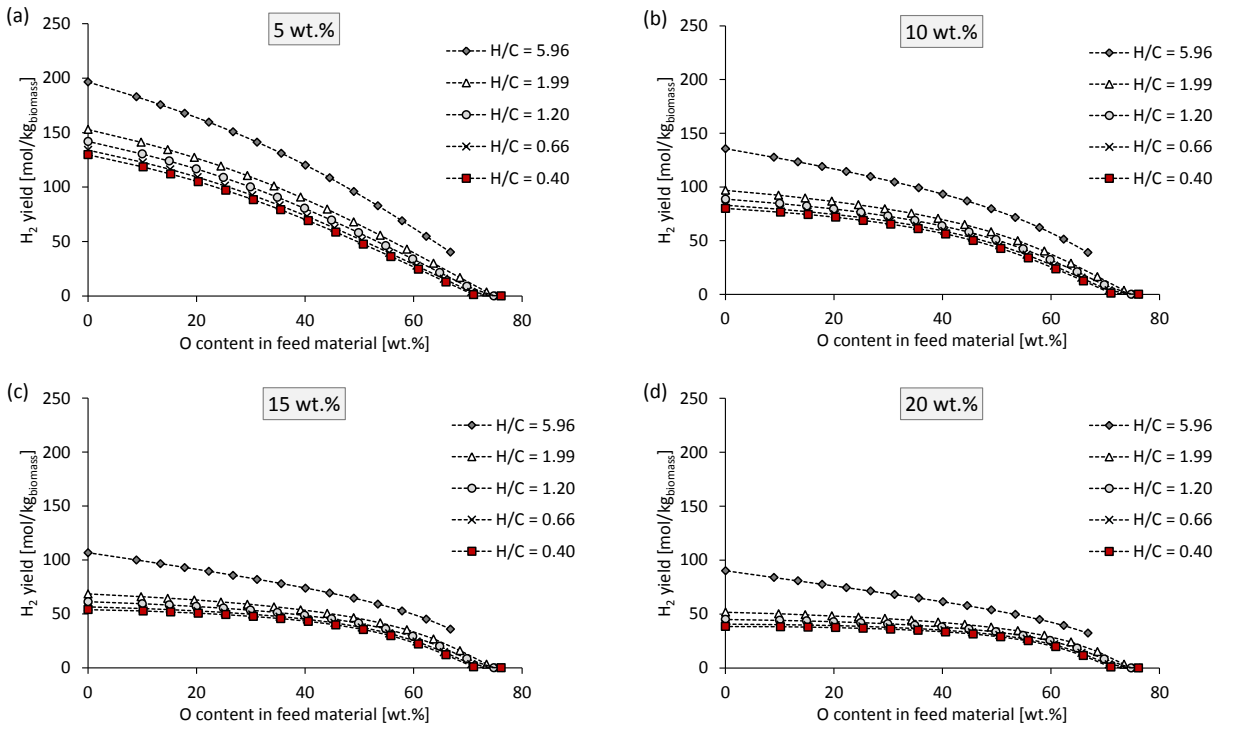

FIGURE 3-11 EFFECT OF OXYGEN CONTENT AND H/C RATIO OF THE FEED MATERIAL ON THE H_2 YIELD DURING SCWG AT 800 °C AND A DRY FEED CONCENTRATION OF (A) 5 WT.%; (B) 10 WT.%; (C) 15 WT.%; AND (D) 20 WT.%

Concerning the effect of feedstock composition on the H_2 yield, it can be said that feed material with low O/C and high H/C ratios typically results in the highest H_2 yields (*i.e.*, the top left hand corner of the contour plots). Hence, the lower the oxygen content and the higher the hydrogen content in the feed material, the higher the H_2 yield at all operating conditions. The same is true for the CH_4 yield (see Section 3.4.2). This due to the fact that, if less oxygen available in the system, the formation of oxygen containing gases (CO and CO_2) will be limited and the formation of hydrogen containing gases (such as H_2 and CH_4) will be higher. This is clear from Figure 3-9, Figure 3-10 and Figure 3-11, which shows the H_2 yield in terms of the oxygen content of the feed material for various H/C ratios (molar) at 400, 600 and 800 °C, respectively. The highest H_2 yields are achieved at the lowest oxygen content in the feed material for all H/C ratios at all of the operating conditions considered. When comparing the H2 yields at different H/C ratios and constant oxygen content, it is clear that the H_2 yield is higher for feed material with higher H/C ratios. This is because more hydrogen is available in feed material with a higher

H/C ratio (5.96 for example) compared to a lower H/C ratio (0.4 for example) at a constant oxygen content.

Yan et al. (2006) compared the thermodynamic equilibrium H_2 yields of seven different feed materials in terms of their O/C ratios, including polyethylene, ethanol, wood type 1, wood type 2, cellulose, corn starch and glucose. Their results also suggested that feed material with a lower O/C ratio will result in the highest H_2 yield. However, they only investigated this aspect at one set of operating conditions (600 °C and 34.5 MPa) and could therefore not make any conclusion regarding the effect of the O/C ratio of the feed material at other operating conditions.

The slope of the contour lines (*i.e.*, the effect of the H/C ratio on the H_2 yield) becomes steeper as the operating temperature is increased at a constant dry feed concentration (compare for example Figure 3-6(a), Figure 3-7(a) and Figure 3-8(a)). Hence, the H_2 yield becomes less dependent on the H/C ratio of the feed material as the operating temperature is increased. Furthermore, at a constant temperature, the slope of the contour plots becomes less steep with an increase in the feed concentration. Hence, the H_2 yield becomes less dependent on the H/C ratio of the feed material with an increase in the feed concentration. It must be noted that, during SCWG, the H_2 that is formed may also originate from the excess of water present. Hence, the increase in the H_2 yield with a decrease in the feed concentration is most likely due to the fact that more water is present in the system and, therefore, more hydrogen molecules.

Considering the combination of feed composition and operating conditions and the different biomass material considered as feed material (as shown with the bullet points on the graph), the highest H_2 yields (120 – 132 mol/$kg_{biomass}$) are achieved when char from vacuum pyrolysis of sugarcane bagasse (feedstock #7) or bituminous coal (#15) are used as feed material. These results are achieved when operating at 800 °C and 5 wt.%.

3.4.2 CH_4 YIELD

The CH_4 yield in terms of the O/C and H/C ratio of the feed material at operating temperature of 400, 600 and 800 °C and feed concentrations of 5, 10, 15 and 20 wt.% are shown in Figure 3-12 – Figure 3-14, while Figure 3-15 – Figure 3-17 shows the effect of the oxygen content on the CH_4 yield at 400, 600 and 800 °C.

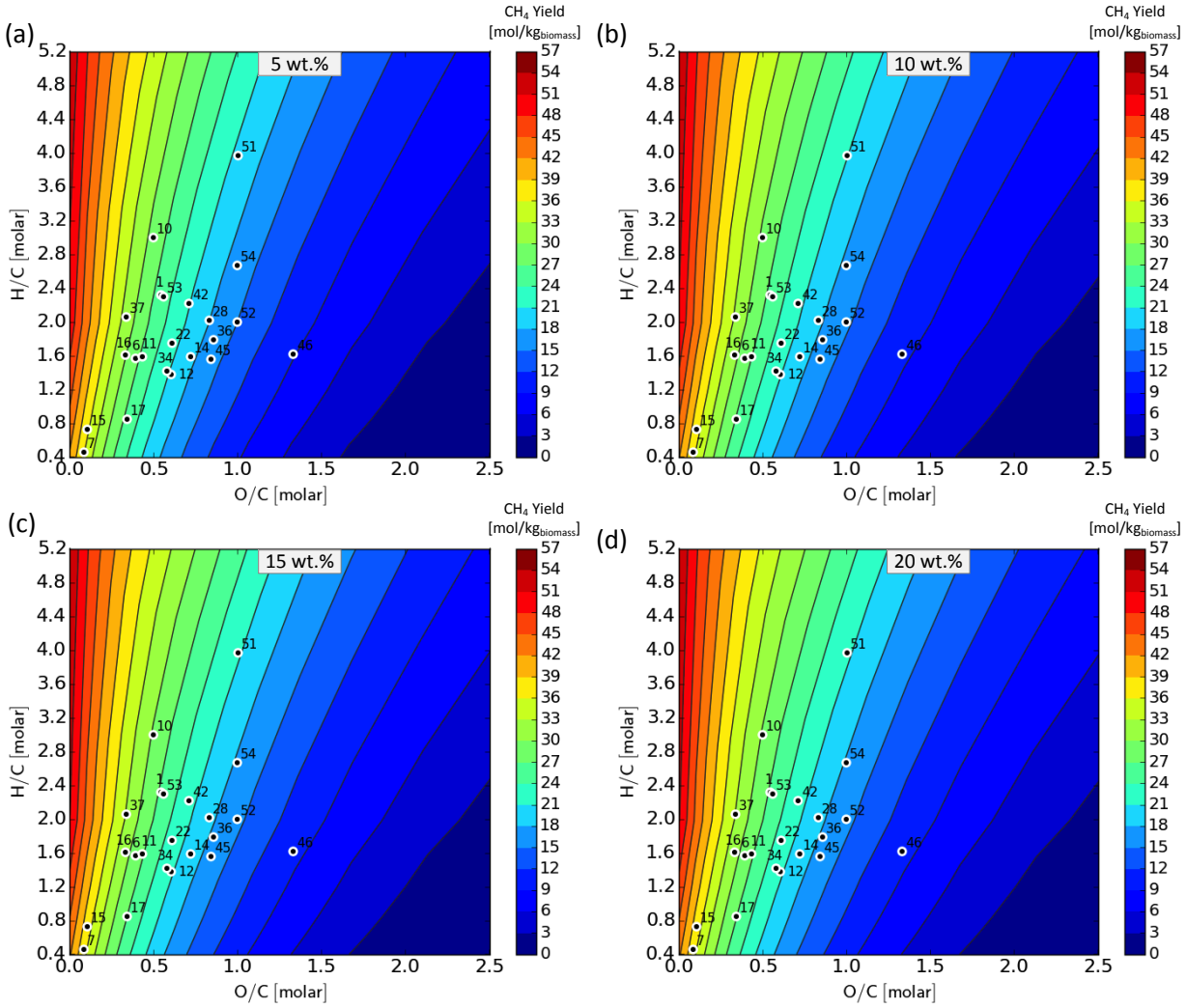

FIGURE 3-12 EFFECT OF FEEDSTOCK COMPOSITION ON THE THERMODYNAMIC EQUILIBRIUM CH_4 YIELD DURING SCWG AT 400 °C, 25 MPA AND A DRY FEED CONCENTRATION OF (A) 5 WT.%; (B) 10 WT.%; (C) 15 WT.%; AND (D) 20 WT.%

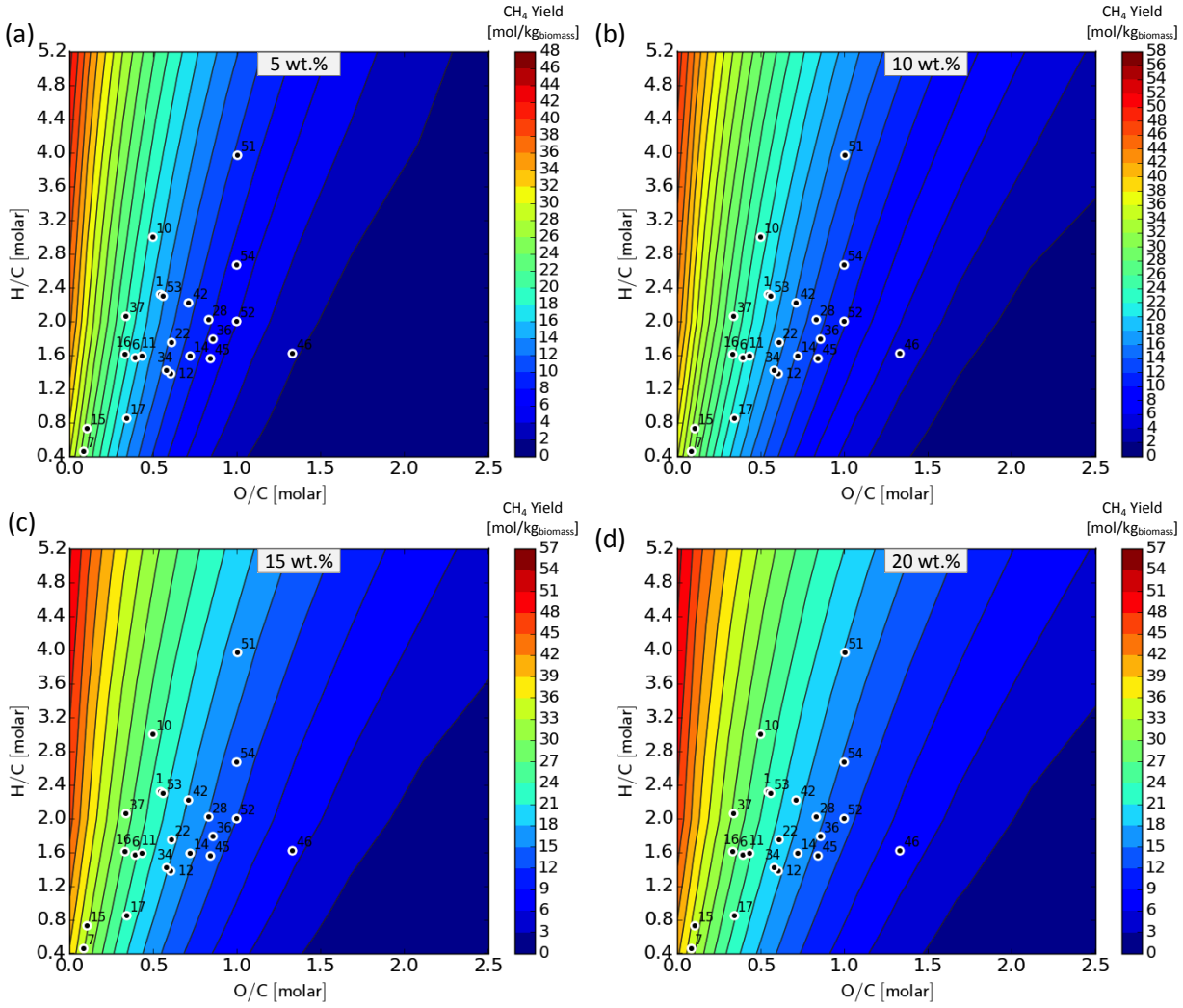

FIGURE 3-13 EFFECT OF FEEDSTOCK COMPOSITION ON THE THERMODYNAMIC EQUILIBRIUM CH_4 YIELD DURING SCWG AT 600 °C, 25 MPA AND A DRY FEED CONCENTRATION OF (A) 5 WT.%; (B) 10 WT.%; (C) 15 WT.%; AND (D) 20 WT.%

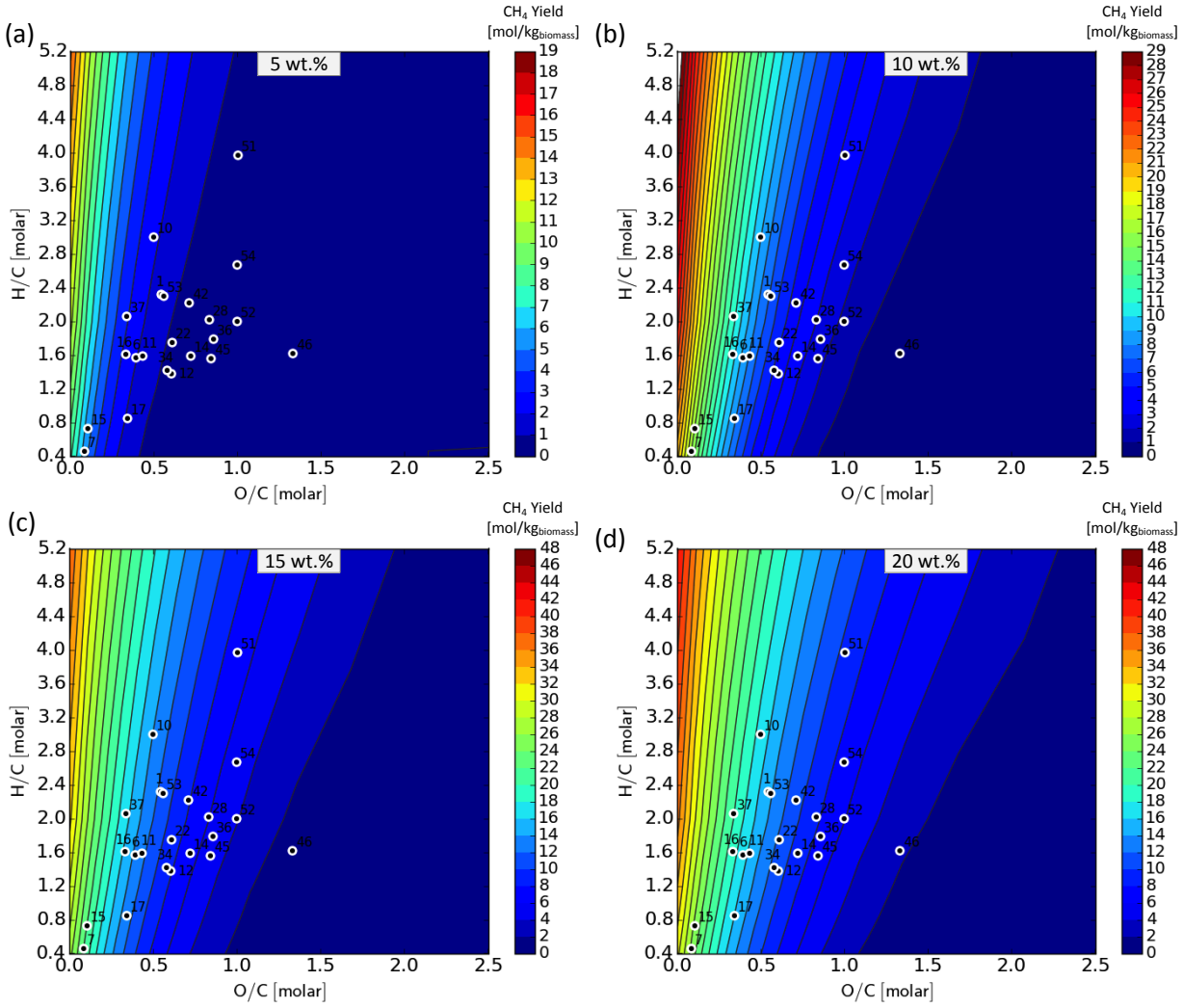

FIGURE 3-14 EFFECT OF FEEDSTOCK COMPOSITION ON THE THERMODYNAMIC EQUILIBRIUM CH_4 YIELD DURING SCWG AT 800 °C, 25 MPA AND A DRY FEED CONCENTRATION OF (A) 5 WT.%; (B) 10 WT.%; (C) 15 WT.%; AND (D) 20 WT.%

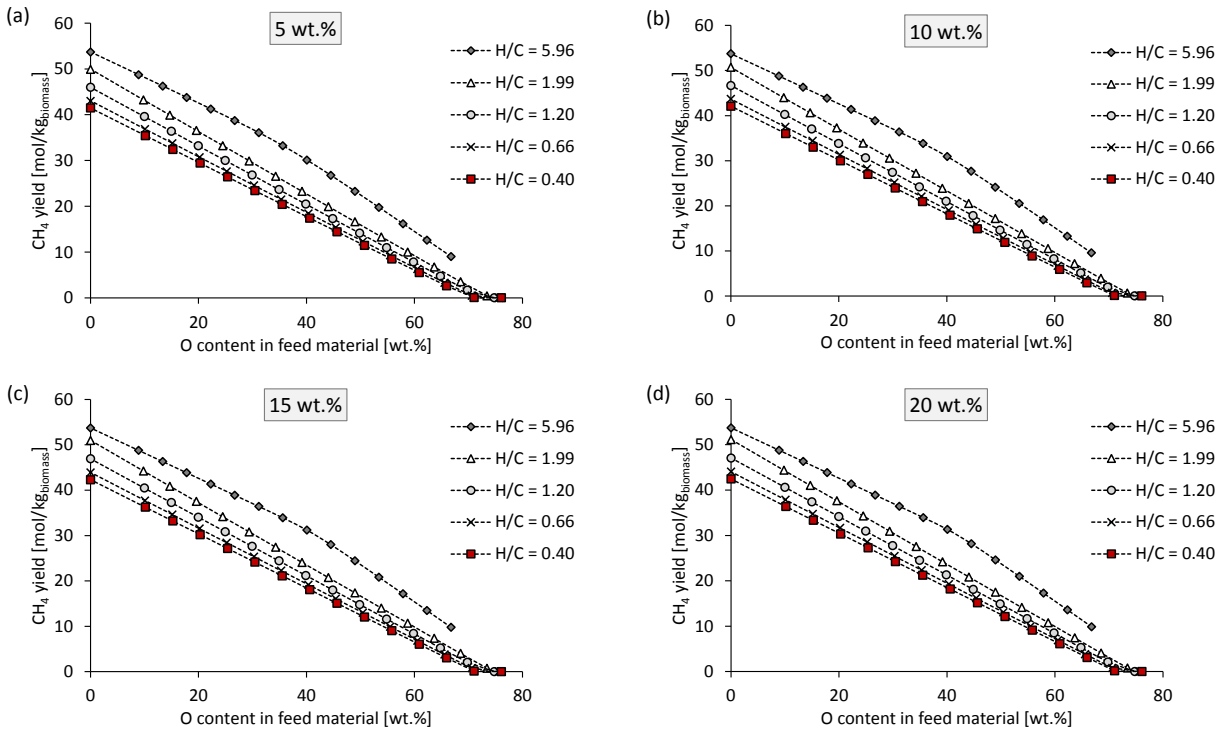

FIGURE 3-15 EFFECT OF OXYGEN CONTENT AND H/C RATIO OF THE FEED MATERIAL ON THE CH_4 YIELD DURING SCWG AT 400 °C AND A DRY FEED CONCENTRATION OF (A) 5 WT.%; (B) 10 WT.%; (C) 15 WT.%; AND (D) 20 WT.%

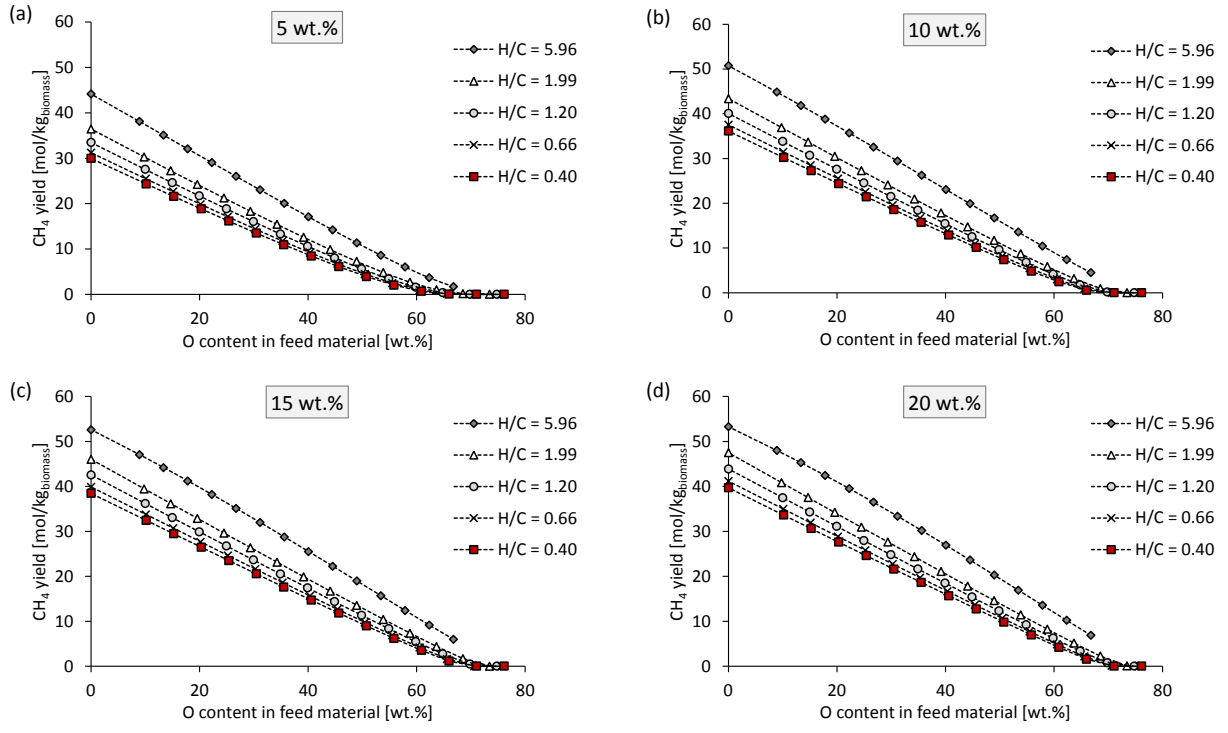

FIGURE 3-16 EFFECT OF OXYGEN CONTENT AND H/C RATIO OF THE FEED MATERIAL ON THE CH_4 YIELD DURING SCWG AT 600 °C AND A DRY FEED CONCENTRATION OF (A) 5 WT.%; (B) 10 WT.%; (C) 15 WT.%; AND (D) 20 WT.%

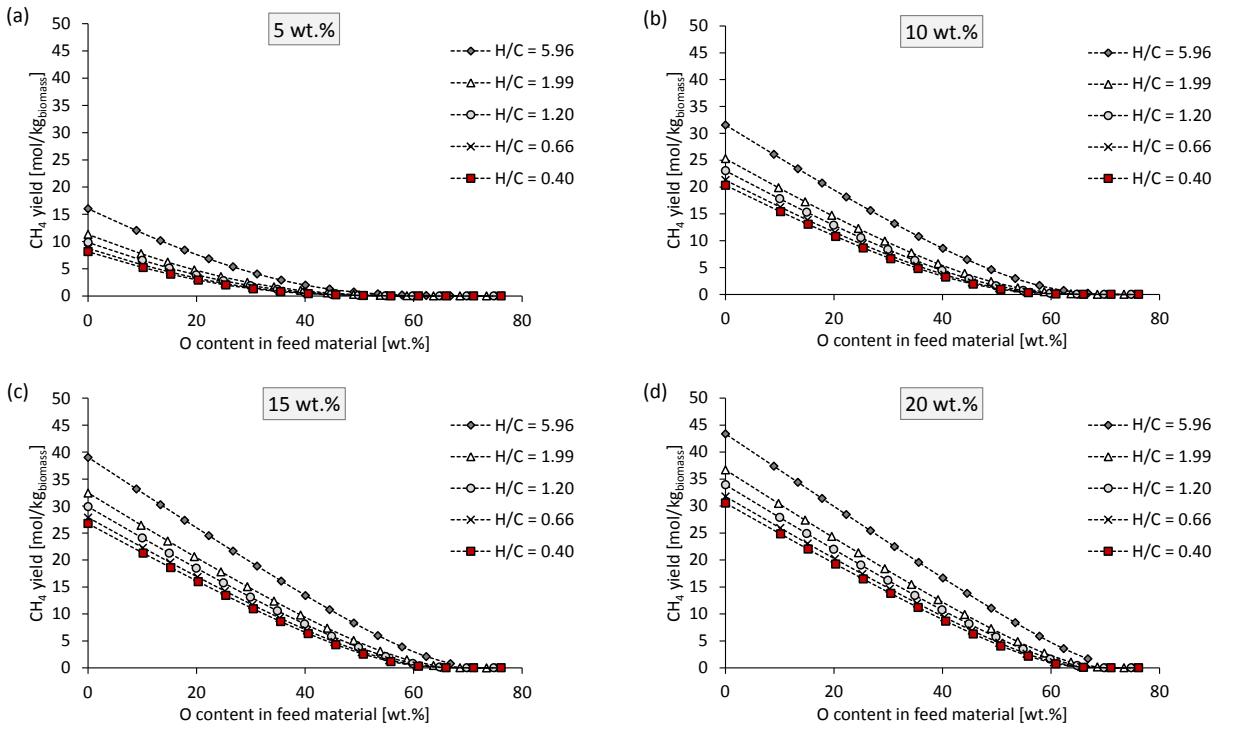

FIGURE 3-17 EFFECT OF OXYGEN CONTENT AND H/C RATIO OF THE FEED MATERIAL ON THE CH_4 YIELD DURING SCWG AT 800 °C AND A DRY FEED CONCENTRATION OF (A) 5 WT.%; (B) 10 WT.%; (C) 15 WT.%; AND (D) 20 WT.%

Furthermore, concerning the feedstock composition, the highest CH_4 yields are achieved when feed material with relatively low O/C ratio is used as feed material. Although the H/C ratio of the feed material also affects the CH_4 yield, its effect is not as prominent as the O/C ratio. For instance, consider an operating temperature of 400 °C (see Figure 3-12). Ethanol (feedstock #10) and lignite coal (feedstock #17) have comparable O/C ratios but differ significantly in terms of their H/C ratios. Nevertheless, the CH_4 yield achieved with these two feed material are comparable. However, when considering bituminous coal (feedstock #15) and lignite coal, which have comparable H/C ratios but differ slightly in terms of their O/C ratios, it is evident that in all cases, the bituminous coal (which has a lower O/C ratio) delivers higher CH_4 yields.

As in the case of the H_2 yield, the lower the oxygen content and the higher the H/C ratio in the feed material, the higher the CH_4 yield (see Figure 3-15, Figure 3-16 and Figure 3-17). An almost linear relationship between the oxygen content in the feed material and the CH_4 yield is observed for all H/C ratios, especially at an operating temperature of 400 and 600 °C and an oxygen content less than 60 wt.%. Furthermore, the effect of the oxygen content on the CH_4

yield is more prominent than that of the H/C content. When more oxygen is present in the feed material, more CO_2 or CO will form and hence, less carbon will be available to form CH_4, compared to when less oxygen is present.

From the results it is clear that highly oxygenated feed material will result in the lowest CH_4 yield. This suggests that, modifying highly oxygenated feed material, such as conventional biomass, prior to SCWG may result in higher CH_4 and H_2 yields (as was also suggested by Prins et al. (2007) to improve the energy efficiency when using biomass during conventional dry gasification).

Amongst the possible biomass materials considered, char from sugarcane bagasse (feedstock #7) and bituminous coal (feedstock #15) are examples of feedstock materials that will result in the highest CH_4 yields (38 mol/$kg_{biomass}$) at 400 °C and 20 wt.%.

3.4.3 CO YIELD

Figure 3-18, Figure 3-19 and Figure 3-20 show the CO yield as a function of the O/C and H/C for an operating temperature of 400, 600 and 800 °C, respectively. Furthermore, the effect of the oxygen content on the CO yield at various molar H/C ratios at 400, 600 and 800 °C are given in Figure 3-21, Figure 3-22 and Figure 3-23, respectively.

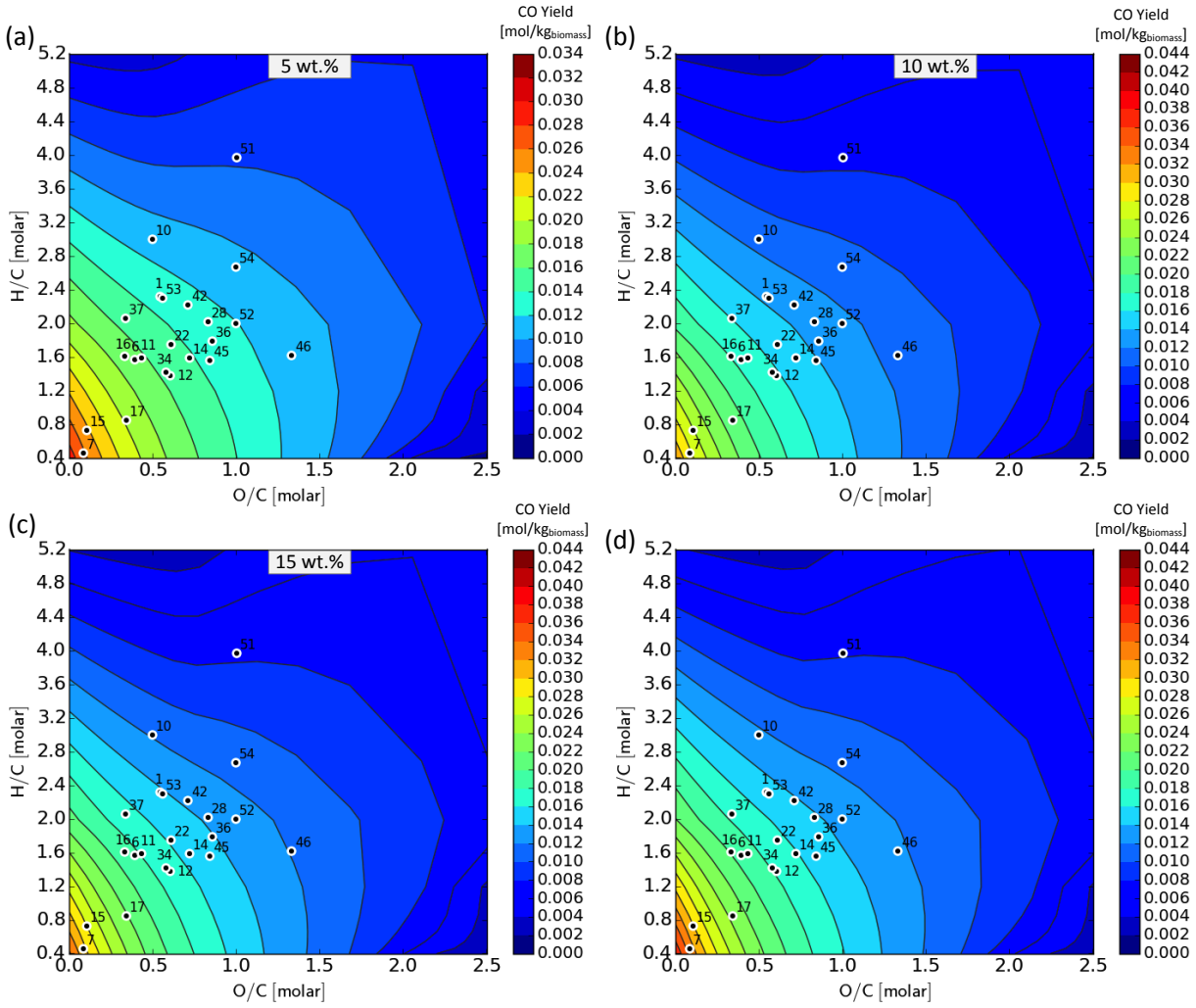

FIGURE 3-18 EFFECT OF FEEDSTOCK COMPOSITION ON THE THERMODYNAMIC EQUILIBRIUM CO YIELD DURING SCWG AT 400 °C, 25 MPA AND A DRY FEED CONCENTRATION OF (A) 5 WT.%; (B) 10 WT.%; (C) 15 WT.%; AND (D) 20 WT.%

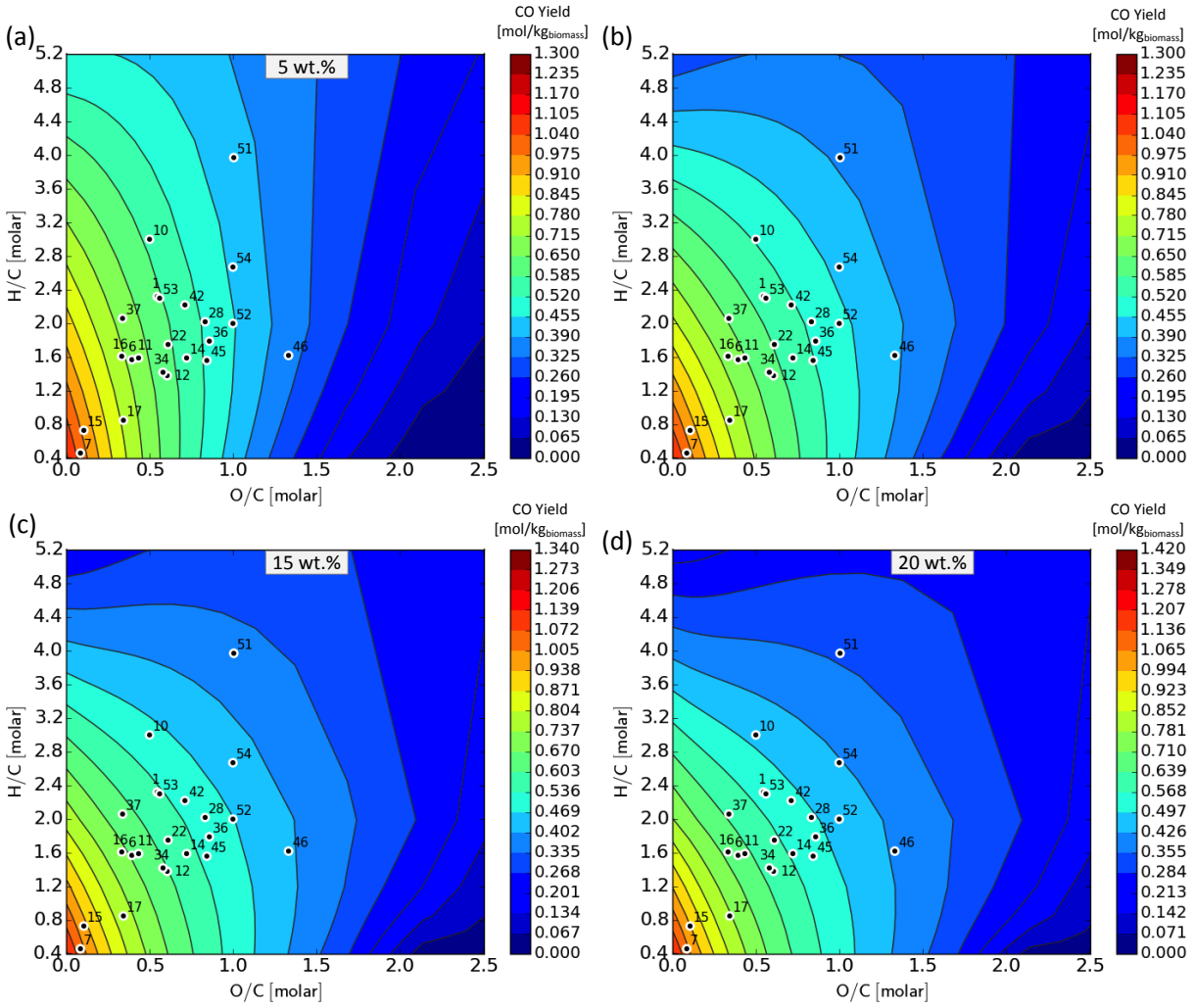

FIGURE 3-19 EFFECT OF FEEDSTOCK COMPOSITION ON THE THERMODYNAMIC EQUILIBRIUM CO YIELD DURING SCWG AT 600 °C, 25 MPA AND A DRY FEED CONCENTRATION OF (A) 5 WT.%; (B) 10 WT.%; (C) 15 WT.%; AND (D) 20 WT.%

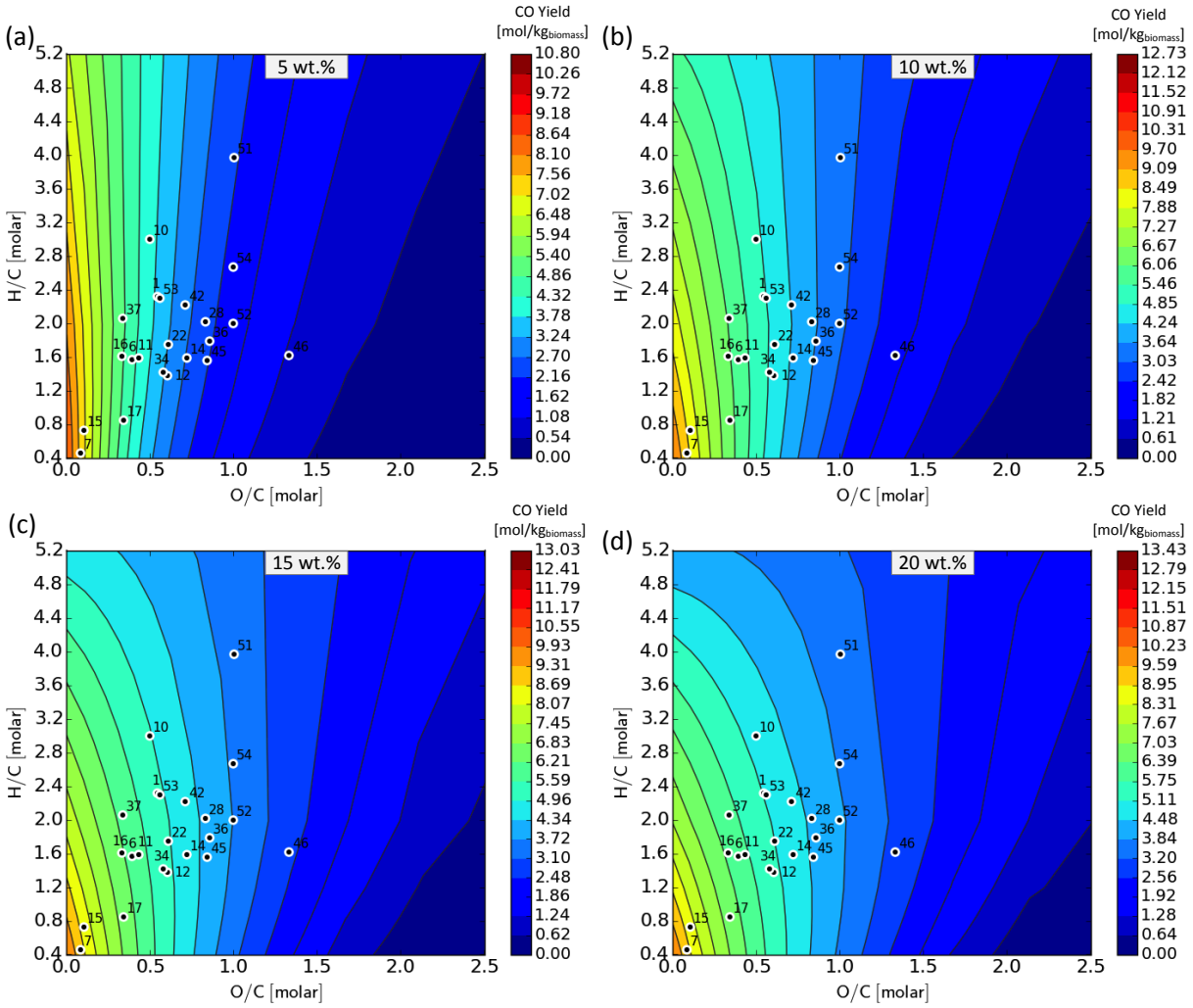

FIGURE 3-20 EFFECT OF FEEDSTOCK COMPOSITION ON THE THERMODYNAMIC EQUILIBRIUM CO YIELD DURING SCWG AT 800 °C, 25 MPA AND A DRY FEED CONCENTRATION OF (A) 5 WT.%; (B) 10 WT.%; (C) 15 WT.%; AND (D) 20 WT.%

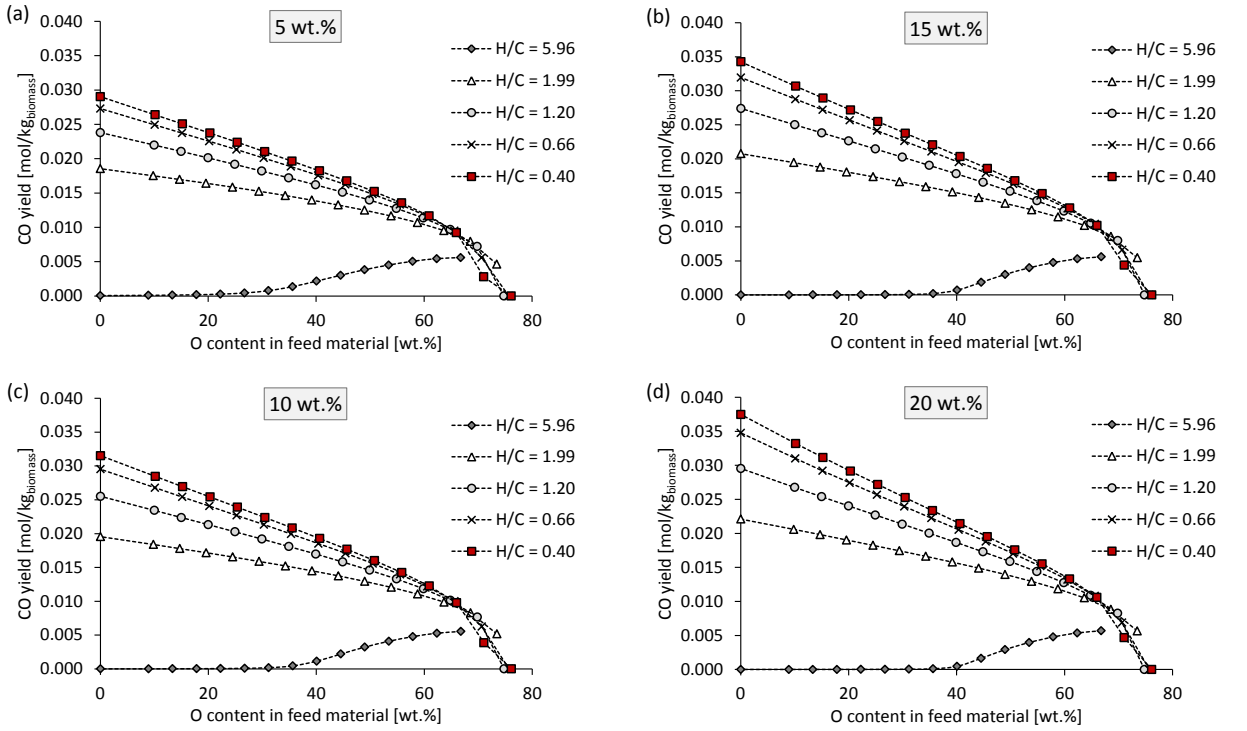

FIGURE 3-21 EFFECT OF OXYGEN CONTENT AND H/C RATIO OF THE FEED MATERIAL ON THE CO YIELD DURING SCWG AT 400 °C AND A DRY FEED CONCENTRATION OF (A) 5 WT.%; (B) 10 WT.%; (C) 15 WT.%; AND (D) 20 WT.%

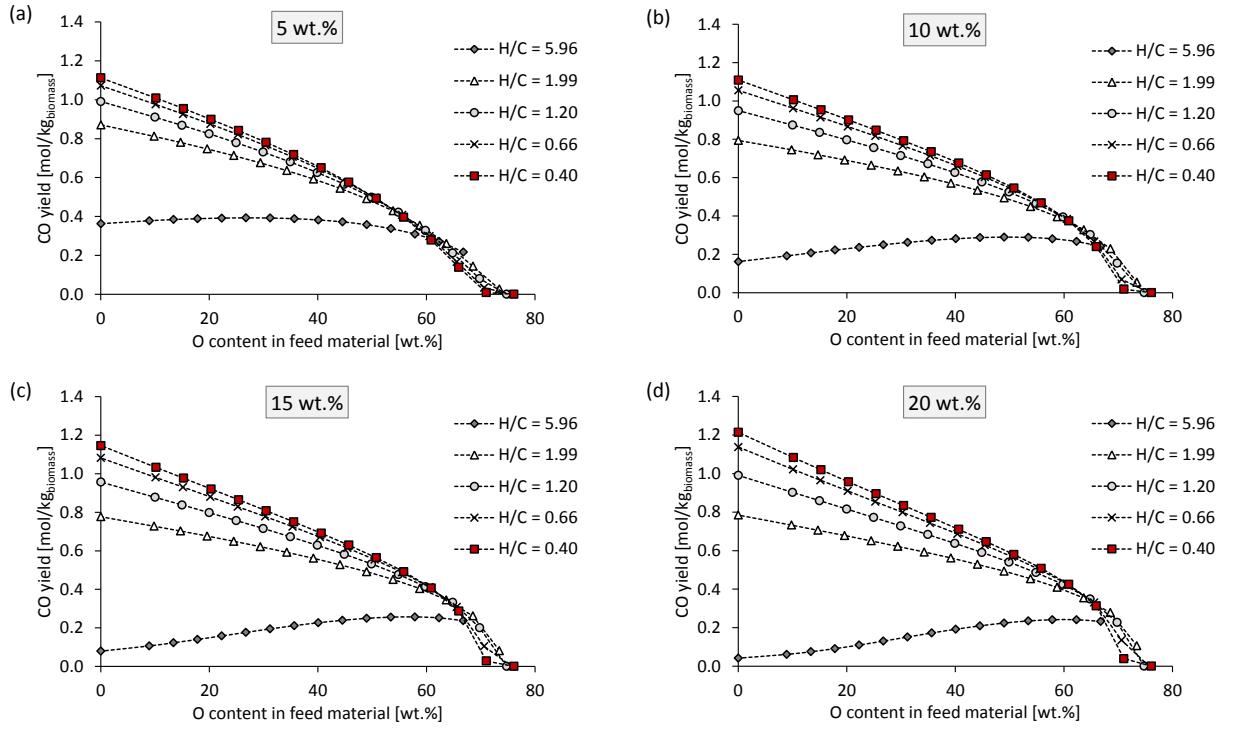

FIGURE 3-22 EFFECT OF OXYGEN CONTENT AND H/C RATIO OF THE FEED MATERIAL ON THE CO YIELD DURING SCWG AT 600 °C AND A DRY FEED CONCENTRATION OF (A) 5 WT.%; (B) 10 WT.%; (C) 15 WT.%; AND (D) 20 WT.%

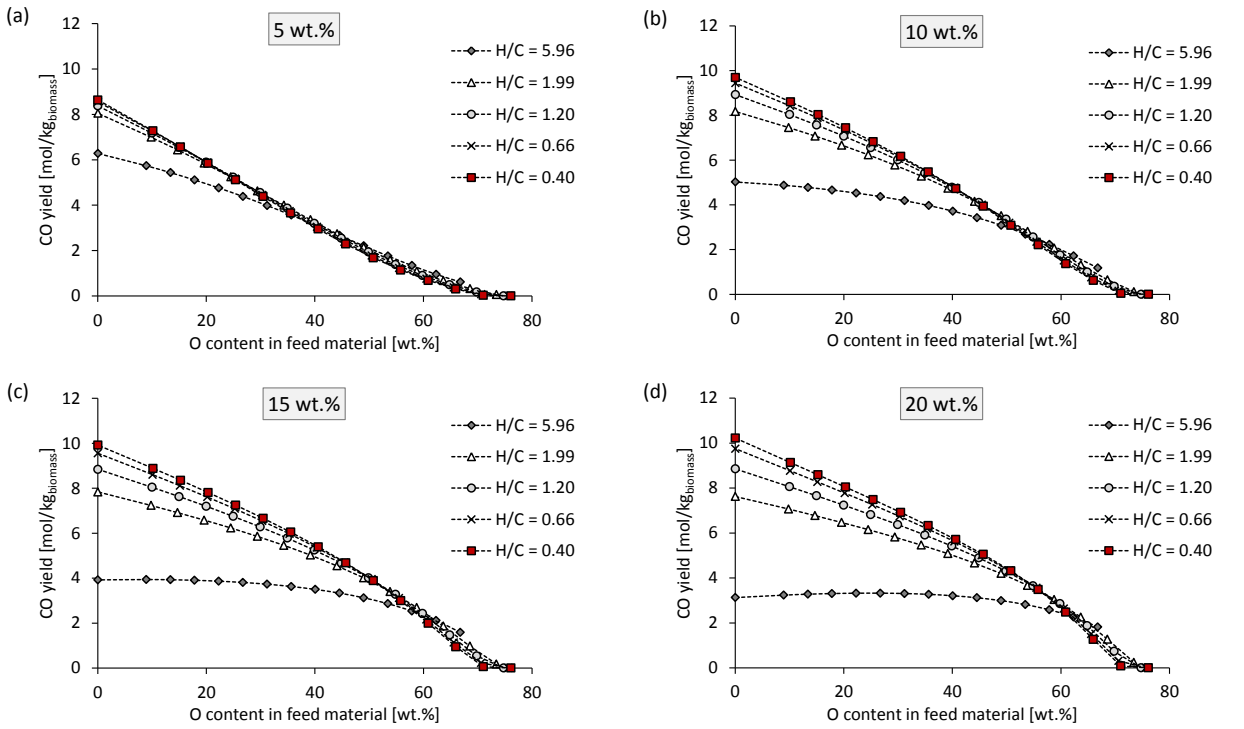

FIGURE 3-23 EFFECT OF OXYGEN CONTENT AND H/C RATIO OF THE FEED MATERIAL ON THE CO YIELD DURING SCWG AT 800 °C AND A DRY FEED CONCENTRATION OF (A) 5 WT.%; (B) 10 WT.%; (C) 15 WT.%; AND (D) 20 WT.%

The effect of the C, H and O composition on the CO yield follows a different trend than that of the H_2 and CH_4 yields, mainly due to the presence of oxygen in the CO molecules. Furthermore, the trend of the contour plots varies at different operating conditions. At 400 and 600 °C, the CO yield is dependent on both the O/C and H/C ratios, especially at O/C ratios lower than 1.5 and H/C ratios lower than 4.0 (see Figure 3-18). At these conditions, the highest CO yields can be achieved when feed material with low O/C and H/C ratios are used as feed material (*i.e.*, bottom left corner of the graphs).

At a constant H/C ratio, the CO yield typically decreases with an increase in the oxygen content in the feed material, expect for the case at the highest H/C ratio. The same trend is observed for the CO_2 yield (see Section 3.4.4). Furthermore, at the highest H/C ratio and 400 °C, the CO and CO_2 yields are almost zero when the oxygen content is less than 40 wt.% (see Figure 3-21 and Figure 3-27). This is due to the fact that more hydrogen is available at these (10 – 32 wt.%) conditions and the formation of CH_4 will therefore be favoured. At all the other H/C ratios, the CO yield typically decreases with an increase in the oxygen content of the feed material (at a

constant H/C ratio). This is due to the fact that, as the oxygen content increases at a constant H/C ratio, both the hydrogen and carbon content will decrease. Hence, less carbon will be available for the formation of both CO and CO_2, even though more than enough oxygen is available. The CO and CO_2 yields typically increase with a decrease in the H/C ratio (at a constant oxygen content in the feed material). This is due to the fact that more carbon and less hydrogen is available at lower H/C ratios than at higher H/C ratios.

At 800 °C and 5 wt.%, the CO yield is almost completely independent of the H/C ratio and completely dependent on the oxygen content, especially at H/C ratios of less than 5.96 (see Figure 3-23). Hence, at these conditions, only the oxygen content in the feed material affects the CO yield. As the feed concentration increases, the CO yield becomes more dependent on the H/C ratio due to the fact that more carbon is available at higher feed concentrations.

Considering the possible feed material and operating conditions, the highest CO yields are achieved when char from sugarcane bagasse (feedstock #7) and bituminous coal (feedstock #15) are used as feedstock material at an operating temperature of 800 °C and feed concentration of 5 wt.% (7.0 – 7.6 mol/$kg_{biomass}$).

3.4.4 CO_2 Yield

The generalised contour plots for the CO_2 yield are shown in Figure 3-24 – Figure 3-26. The CO_2 yields in terms of the oxygen content in the feed material at various H/C ratios are shown in Figure 3-27, Figure 3-28 and Figure 3-29, respectively.

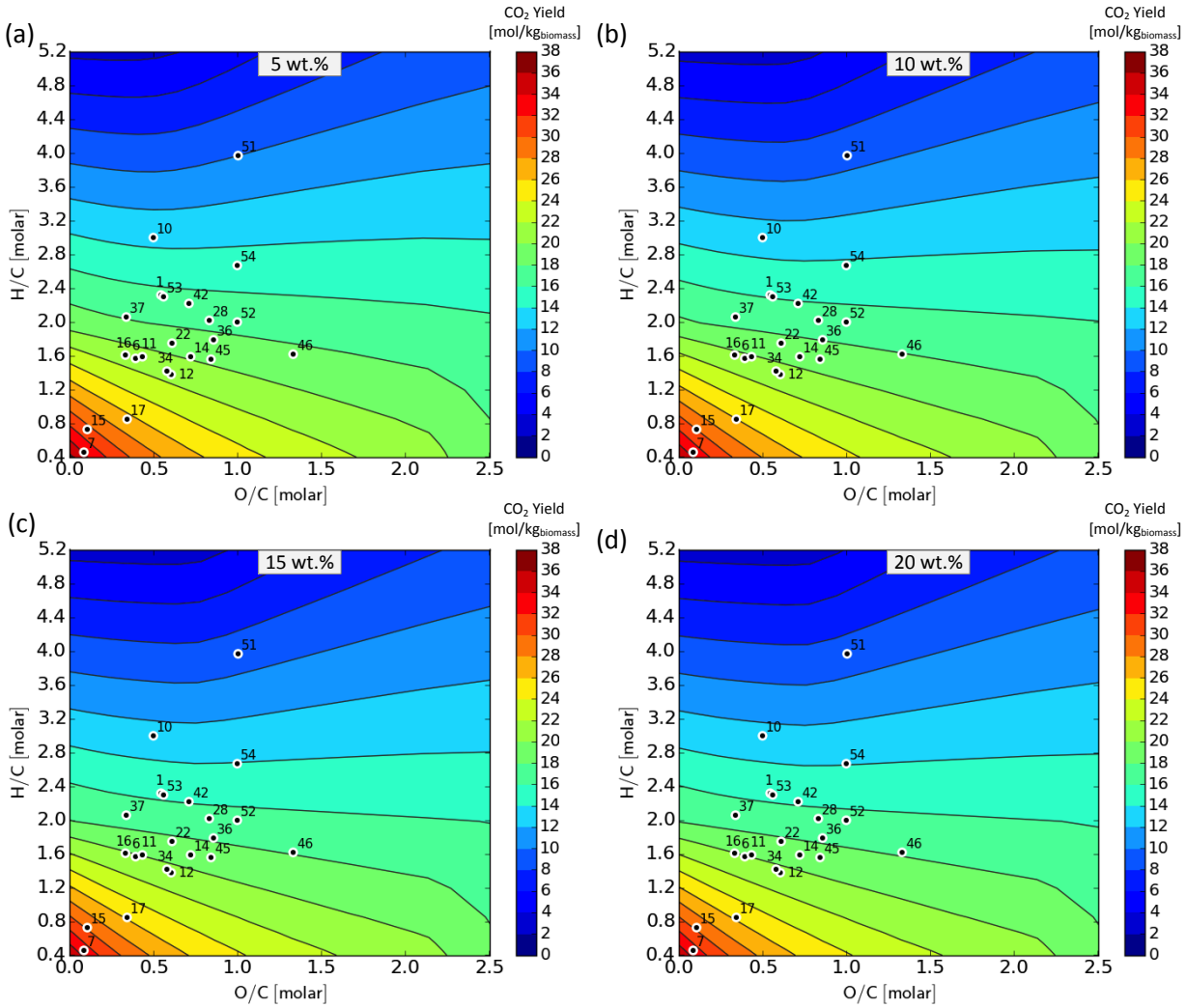

FIGURE 3-24 EFFECT OF FEEDSTOCK COMPOSITION ON THE THERMODYNAMIC EQUILIBRIUM CO_2 YIELD DURING SCWG AT 400 °C, 25 MPA AND A DRY FEED CONCENTRATION OF (A) 5 WT.%; (B) 10 WT.%; (C) 15 WT.%; AND (D) 20 WT.%

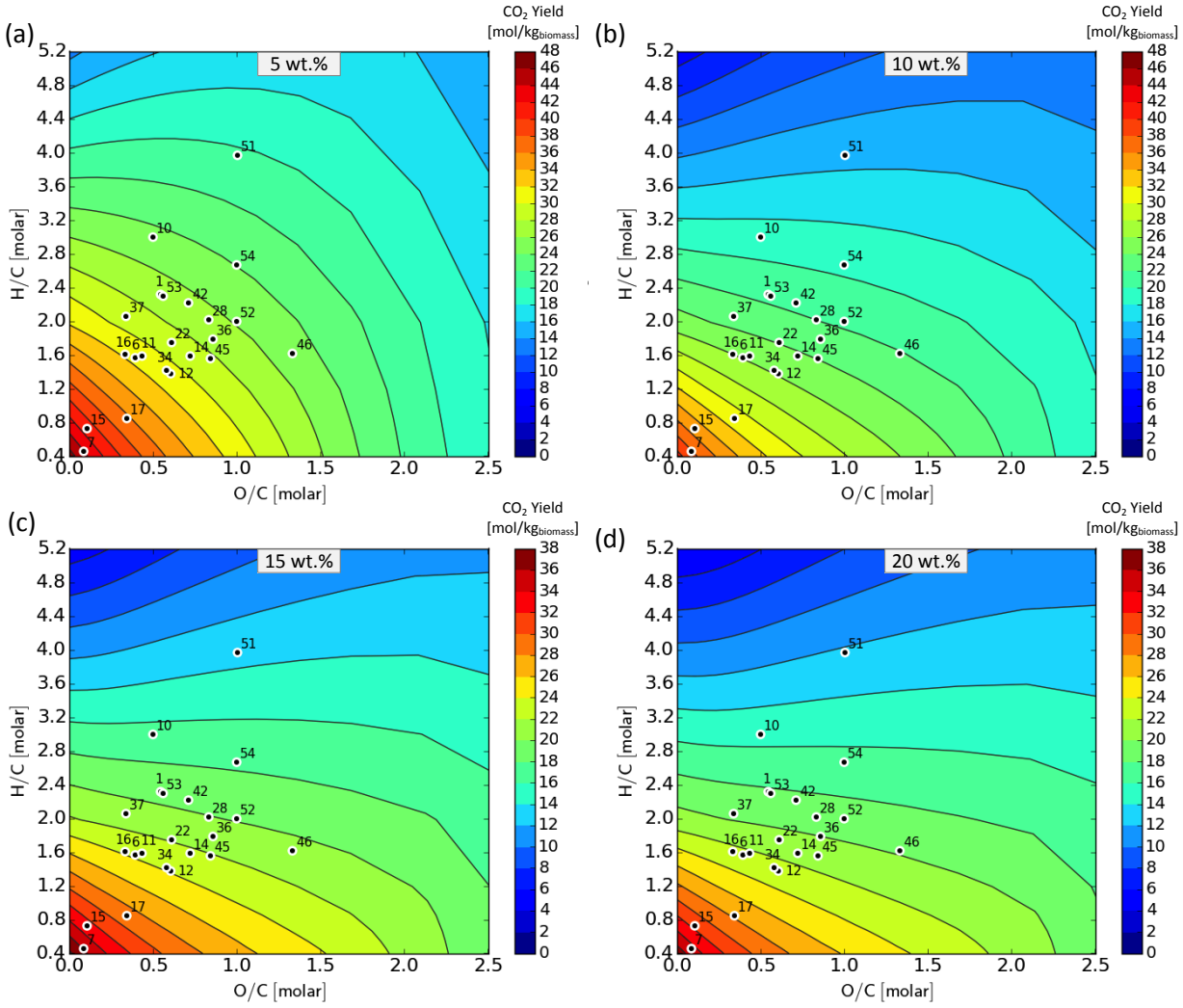

FIGURE 3-25 EFFECT OF FEEDSTOCK COMPOSITION ON THE THERMODYNAMIC EQUILIBRIUM CO_2 YIELD DURING SCWG AT 600 °C, 25 MPA AND A DRY FEED CONCENTRATION OF (A) 5 WT.%; (B) 10 WT.%; (C) 15 WT.%; AND (D) 20 WT.%

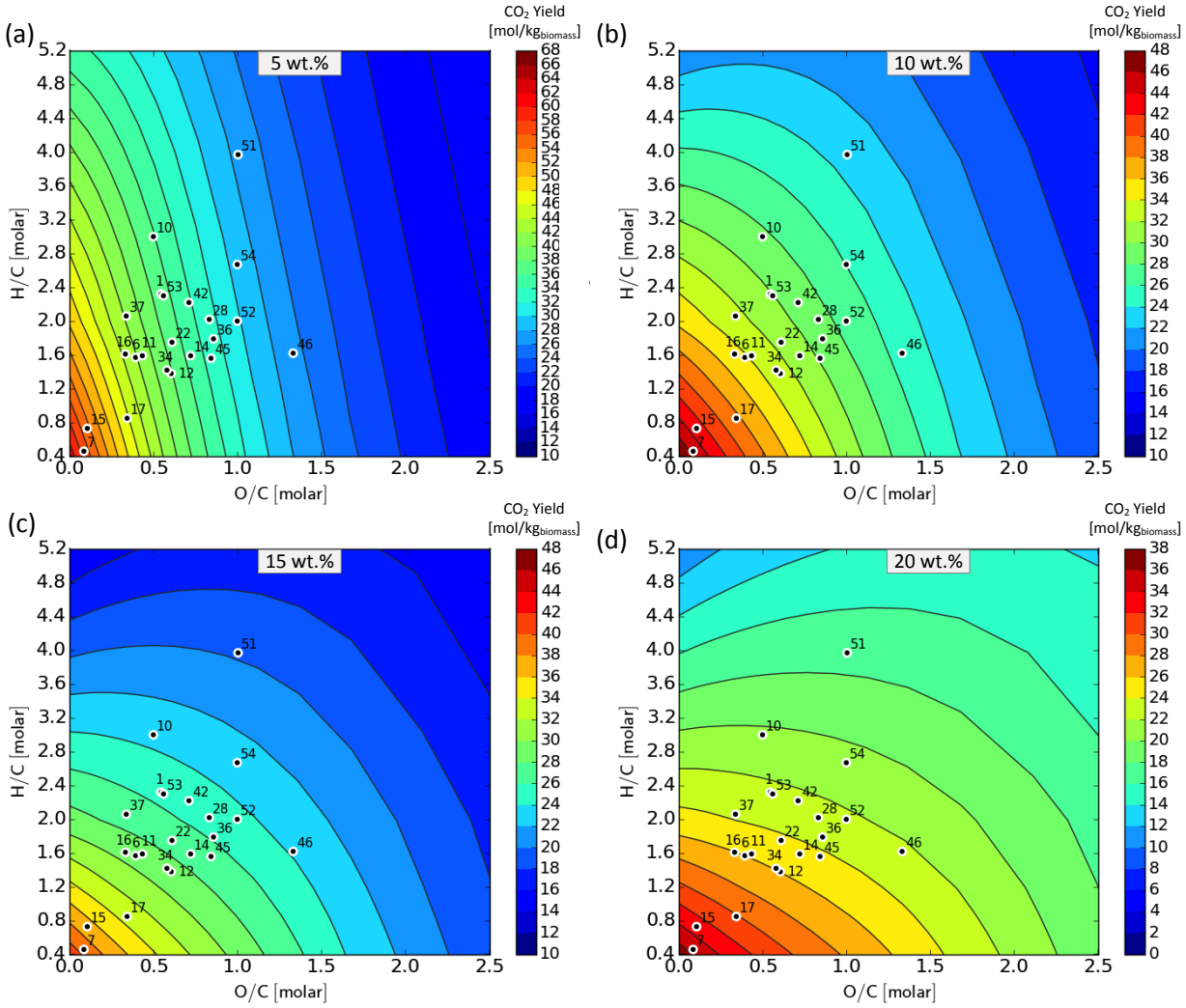

FIGURE 3-26 EFFECT OF FEEDSTOCK COMPOSITION ON THE THERMODYNAMIC EQUILIBRIUM CO_2 YIELD DURING SCWG AT 800 °C, 25 MPA AND A DRY FEED CONCENTRATION OF (A) 5 WT.%; (B) 10 WT.%; (C) 15 WT.%; AND (D) 20 WT.%

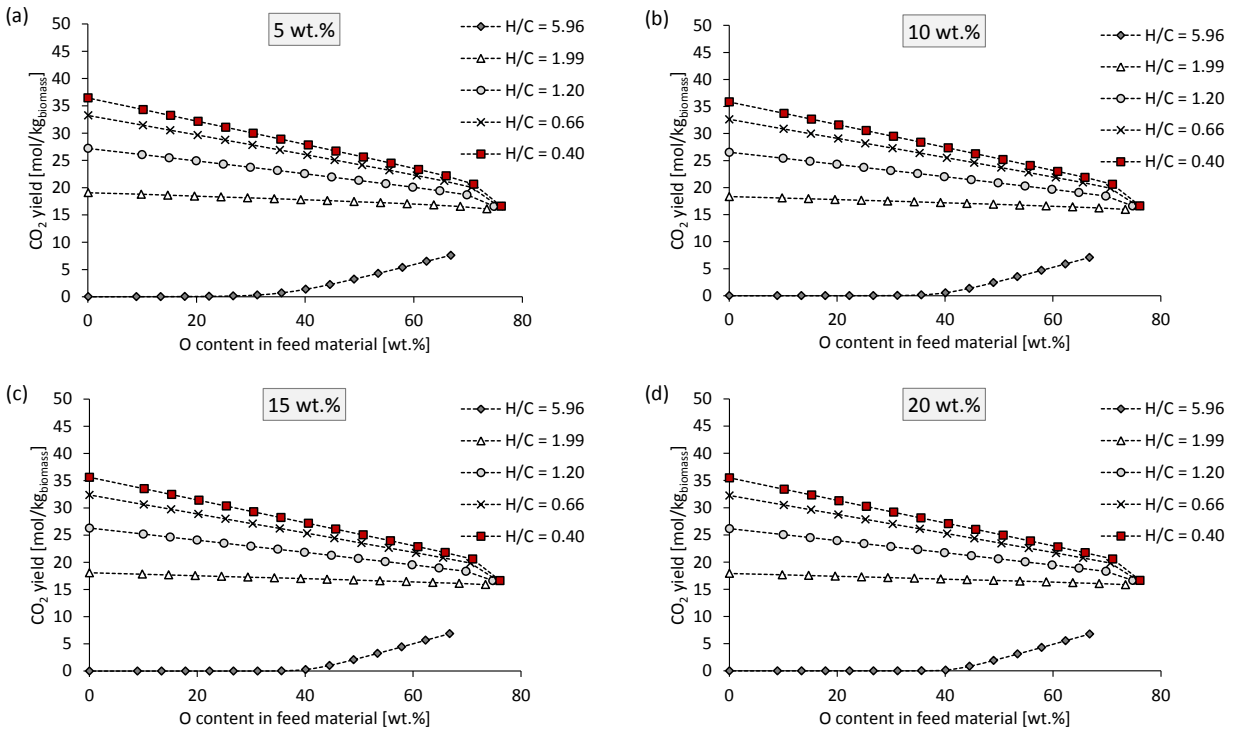

FIGURE 3-27 EFFECT OF OXYGEN CONTENT AND H/C RATIO OF THE FEED MATERIAL ON THE CO_2 YIELD DURING SCWG AT 400 °C AND A DRY FEED CONCENTRATION OF (A) 5 WT.%; (B) 10 WT.%; (C) 15 WT.%; AND (D) 20 WT.%

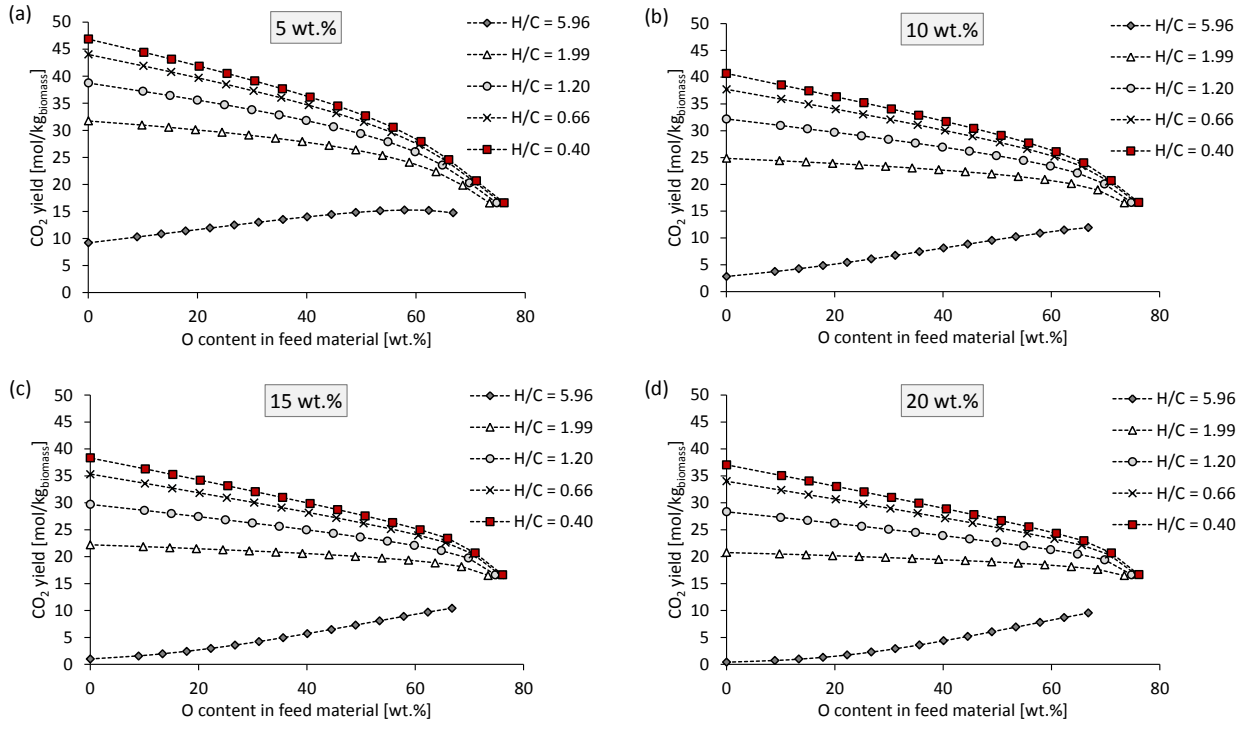

FIGURE 3-28 EFFECT OF OXYGEN CONTENT AND H/C RATIO OF THE FEED MATERIAL ON THE CO_2 YIELD DURING SCWG AT 600 °C AND A DRY FEED CONCENTRATION OF (A) 5 WT.%; (B) 10 WT.%; (C) 15 WT.%; AND (D) 20 WT.%

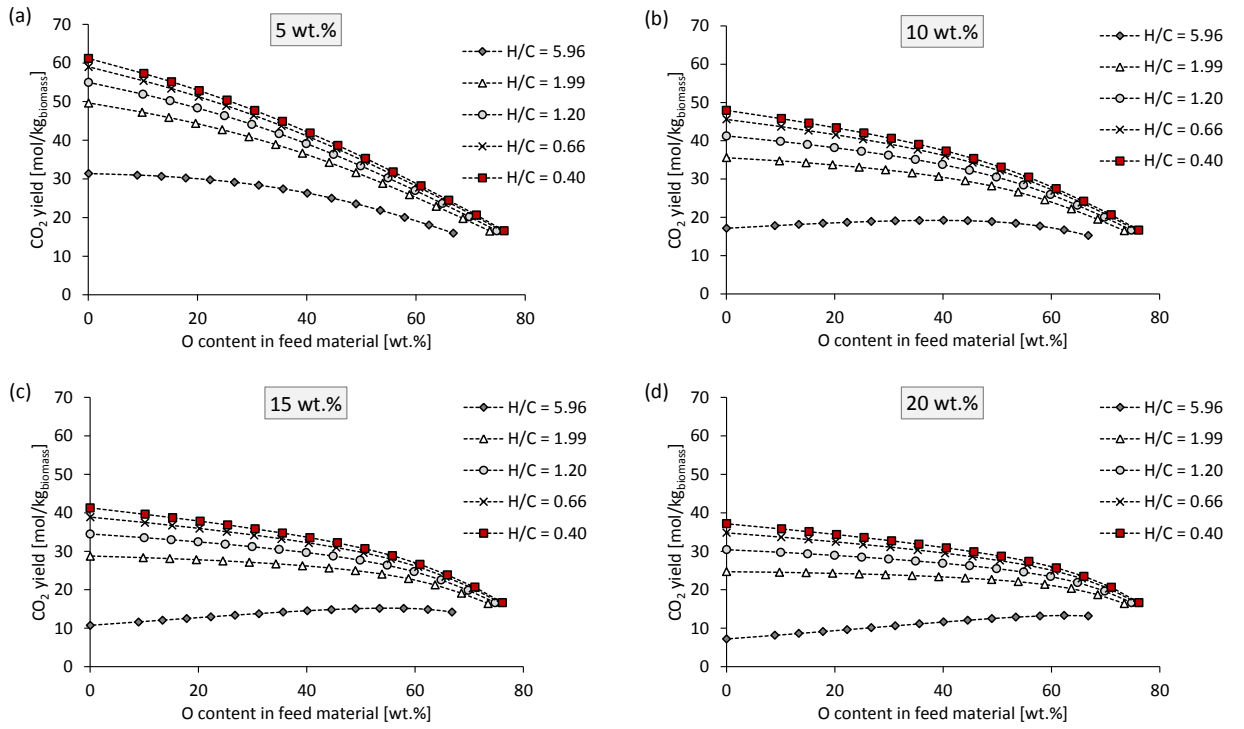

FIGURE 3-29 EFFECT OF OXYGEN CONTENT AND H/C RATIO OF THE FEED MATERIAL ON THE CO_2 YIELD DURING SCWG AT 800 °C AND A DRY FEED CONCENTRATION OF (A) 5 WT.%; (B) 10 WT.%; (C) 15 WT.%; AND (D) 20 WT.%

Due to the fact that CO_2 does not have an energy value, it must be separated from the other gas products during downstream processing. Hence, higher CO_2 yield will result in larger downstream processing equipment. However, the same operating conditions which result in the highest CO_2 yields also results in the highest H_2 yields. Hence, a trade-off between producing high H_2 yields and having bigger downstream processing equipment exists.

The CO_2 yield follows the same trend in terms of the oxygen content and the H/C ratio as that of the CO yield (compare Figure 3-21 and Figure 3-27 as well as Figure 3-22 and Figure 3-28). Once again, the reason for the lower CO_2 yields at the highest H/C ratio is due to the fact that more hydrogen is available (10 – 32 wt.%) compare to the 3 to 13 wt.% hydrogen that is available at a H/C ratios of 1.99. Furthermore, the CO_2 yield typically decreases with a decrease in the H/C ratio of the feed material (at a constant oxygen content). This is due to the fact that, when the H/C ratio increases at a constant oxygen content, the carbon content will increase and the hydrogen content will decrease. More oxygen and carbon will be available for the formation of CO_2 and CO.

Unfortunately, the same biomass materials that yield the highest H_2, CH_4 and CO yields also result in the highest CO_2 yields (feedstock #7 and #15). Additionally, the highest CO_2 yields are also achieved at the same operating conditions at which maximum H_2 and CO yields are achieved, namely at 800 °C and 5 wt.%. At these conditions, the equilibrium CO_2 yields achieved with char from sugarcane bagasse (#7) and bituminous coal (#15) will be 55.0 – 58.2 mol/$kg_{biomass}$. The lowest CO_2 yields are achieved at the same conditions at which the highest CH_4 yields are achieved (*i.e.* at 400 °C and 20 wt.%). Methanol (feedstock #51) and ethanol (feedstock #10) yields the least amount of CO_2 (8.9 – 10.7 mol/$kg_{feed,dry}$ and 12.4 – 14.2 mol/$kg_{feed,dry}$, respectively) at these conditions.

3.4.5 TOTAL GAS YIELD

Figure 3-30 – Figure 3-32 shows the generalised contour plots as a function of the O/C and H/C ratios for the total gas yield while Figure 3-33 – Figure 3-35 shows the total yield in terms of the oxygen content at various H/C ratios.

At all the gasification temperatures and feed concentrations, the highest total gas yields were achieved when using biomass with relatively low O/C ratios, typically < 0.5 (*i.e.* the left hand side of each contour plot). Furthermore, the total yield typically decreases with an increase in the oxygen content of the feed material for all H/C ratios investigated, at all operating temperatures and feed concentrations. No significant increase in the total gas yield is observed at H/C ratios between 0.4 and 1.99. At 400 °C, the total yield decreases almost linearly with an increase in the oxygen content for all H/C ratios, except at the highest H/C ratio. The higher total yields at a the highest H/C ratio and oxygen content lower than 40 wt.% is due to the high H_2 and CH_4 yields achieved at these conditions (see Figure 3-9 and Figure 3-11). However, when the oxygen content is higher than 40 wt.%, the total yield is the lowest at a H/C ratio of 5.96. This is due to the smaller contribution made by the H_2 yield at these conditions.

At 600 °C and 800 °C, the total yield seems to be almost completely independent of the H/C ratio, especially at H/C ratios of 1.99 and lower. Hence, the oxygen content in the feed material has a significant influence on the total gas yield. The lower the oxygen content, the lower the total gas yield. This is true for H_2 and CH_4 at all H/C ratios as well as CO_2 at H/C ratios of 1.99 and

less. Char produced from vacuum pyrolysis of sugarcane bagasse (feedstock #7) and bituminous coal (feedstock #15) are examples of a feedstock material that yields the highest equilibrium gas yields of 192 – 194 mol/$kg_{biomass}$ at 800°C and 5 wt.%.

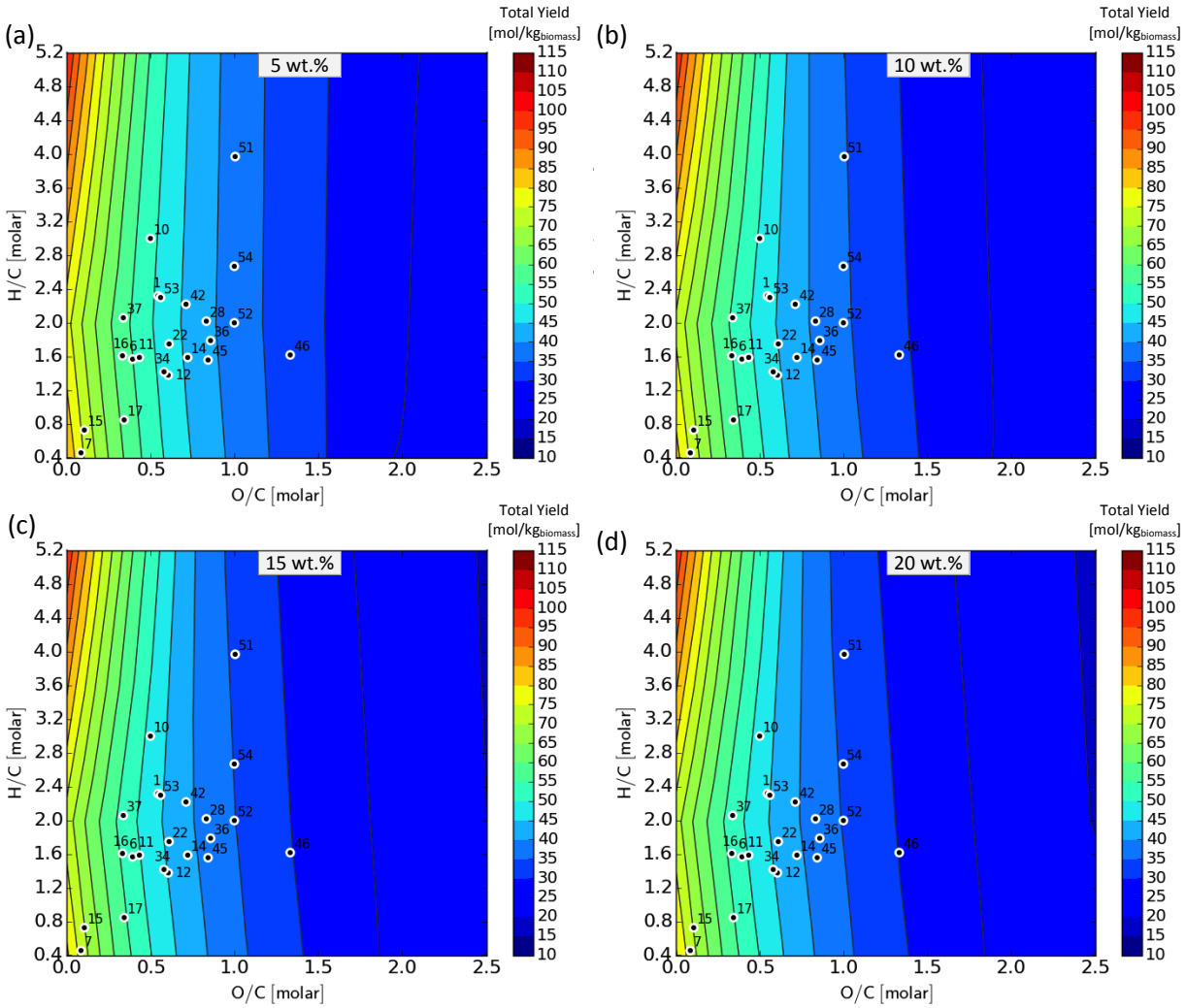

FIGURE 3-30 EFFECT OF FEEDSTOCK COMPOSITION ON THE THERMODYNAMIC EQUILIBRIUM TOTAL YIELD DURING SCWG AT 400 °C, 25 MPA AND A DRY FEED CONCENTRATION OF (A) 5 WT.%; (B) 10 WT.%; (C) 15 WT.%; AND (D) 20 WT.%

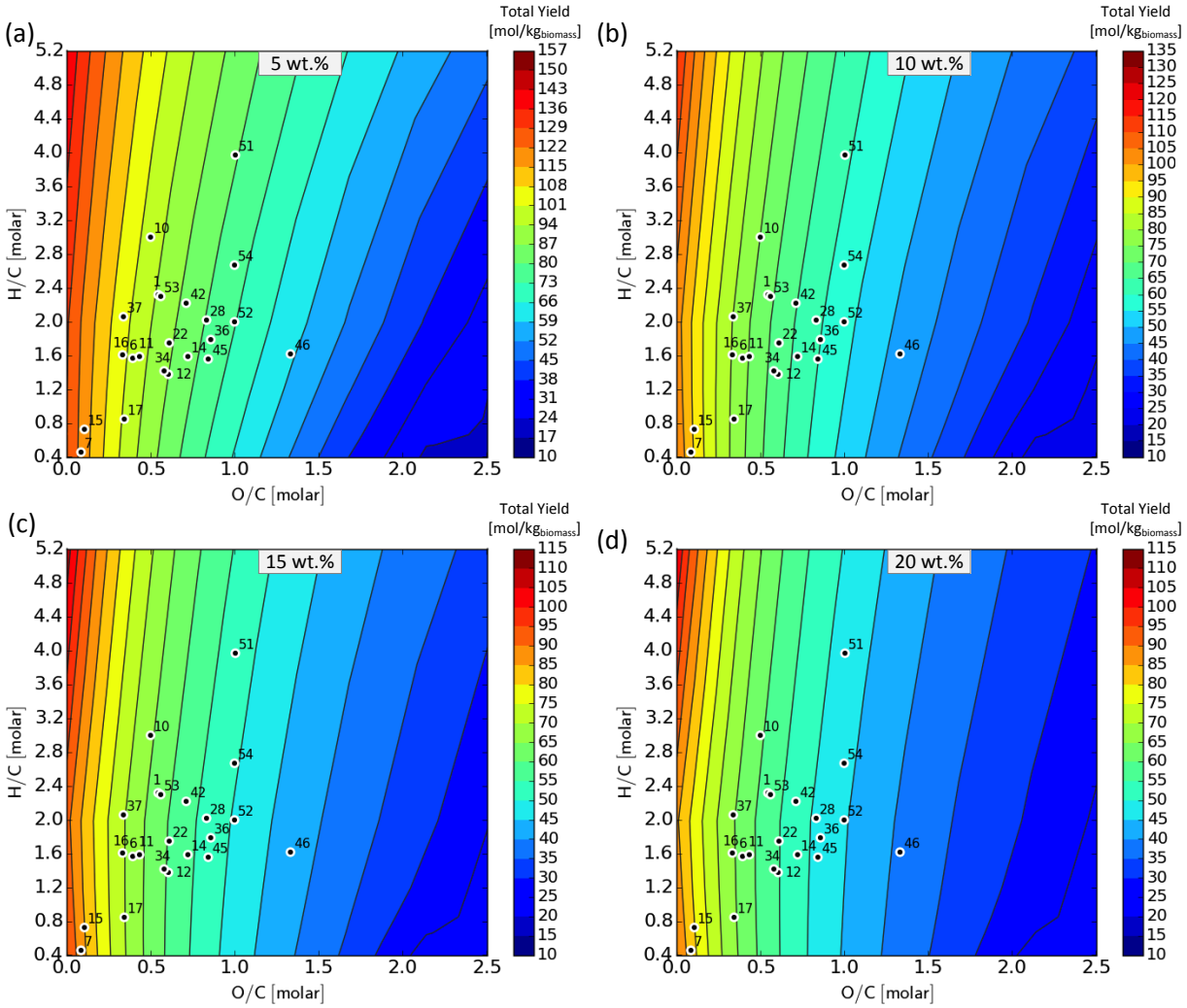

FIGURE 3-31 EFFECT OF FEEDSTOCK COMPOSITION ON THE THERMODYNAMIC EQUILIBRIUM TOTAL YIELD DURING SCWG AT 600 °C, 25 MPA AND A DRY FEED CONCENTRATION OF (A) 5 WT.%; (B) 10 WT.%; (C) 15 WT.%; AND (D) 20 WT.%

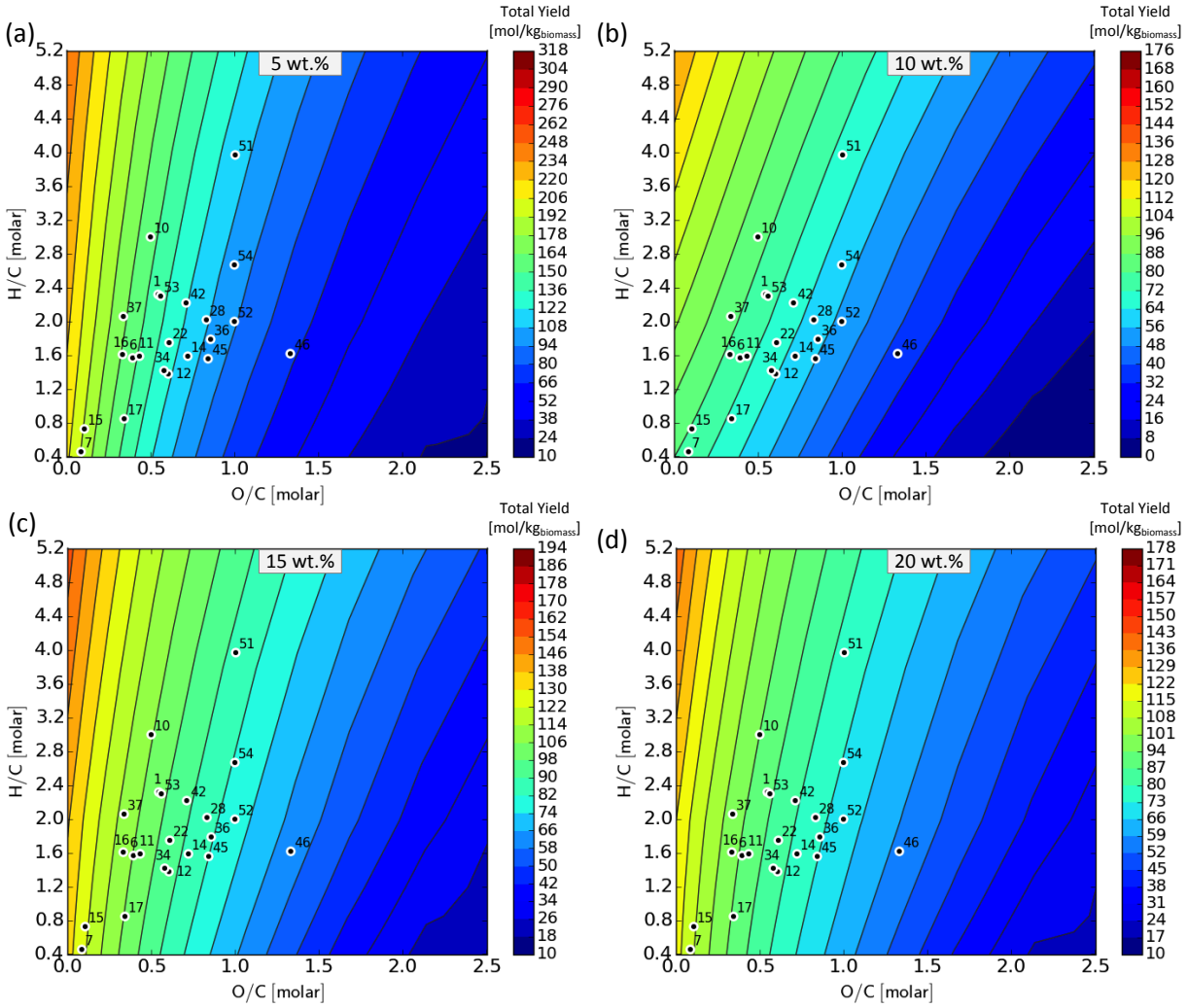

FIGURE 3-32 EFFECT OF FEEDSTOCK COMPOSITION ON THE THERMODYNAMIC EQUILIBRIUM TOTAL YIELD DURING SCWG AT 800 °C, 25 MPA AND A DRY FEED CONCENTRATION OF (A) 5 WT.%; (B) 10 WT.%; (C) 15 WT.%; AND (D) 20 WT.%

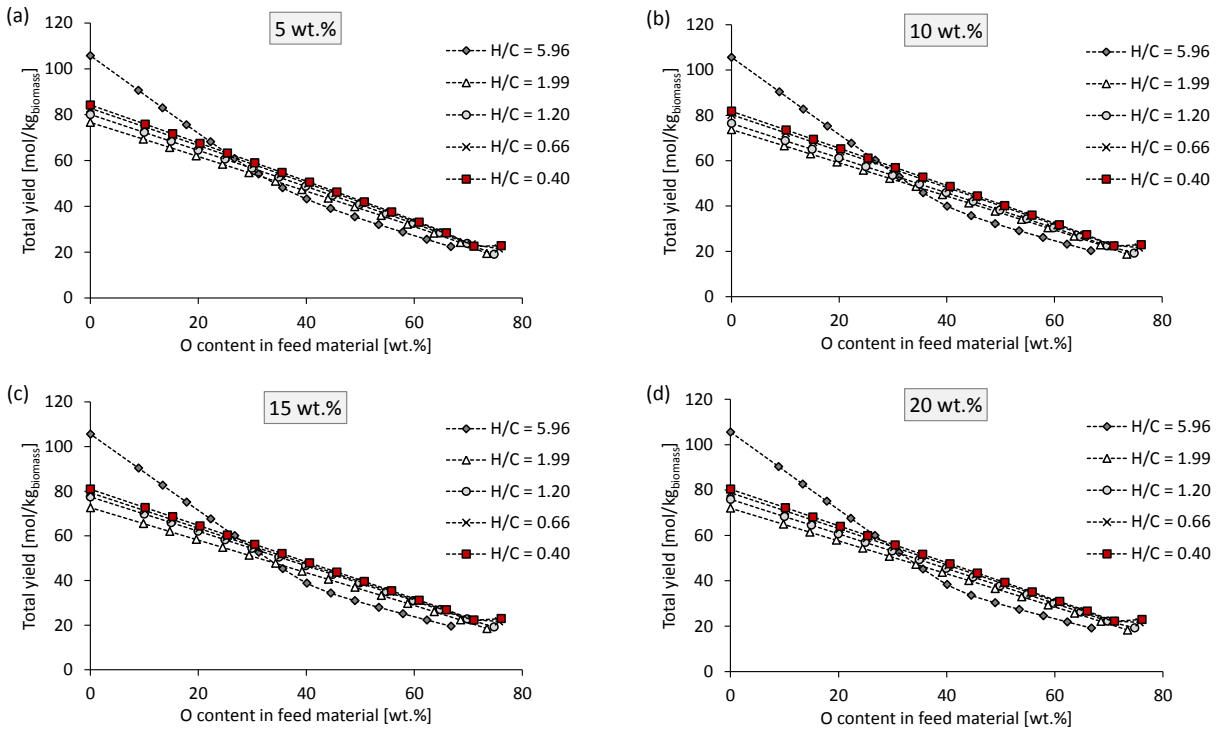

FIGURE 3-33 EFFECT OF OXYGEN CONTENT AND H/C RATIO OF THE FEED MATERIAL ON THE TOTAL YIELD DURING SCWG AT 400 °C AND A DRY FEED CONCENTRATION OF (A) 5 WT.%; (B) 10 WT.%; (C) 15 WT.%; AND (D) 20 WT.%

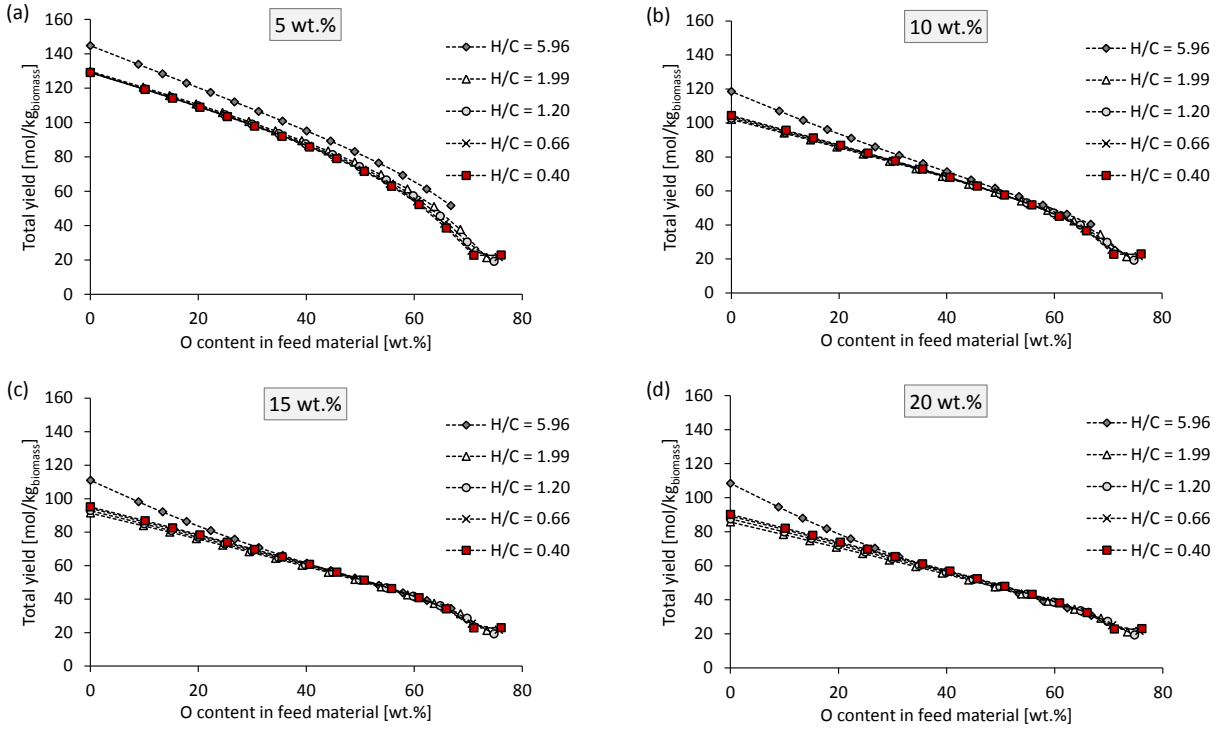

FIGURE 3-34 EFFECT OF OXYGEN CONTENT AND H/C RATIO OF THE FEED MATERIAL ON THE TOTAL YIELD DURING SCWG AT 600 °C AND A DRY FEED CONCENTRATION OF (A) 5 WT.%; (B) 10 WT.%; (C) 15 WT.%; AND (D) 20 WT.%

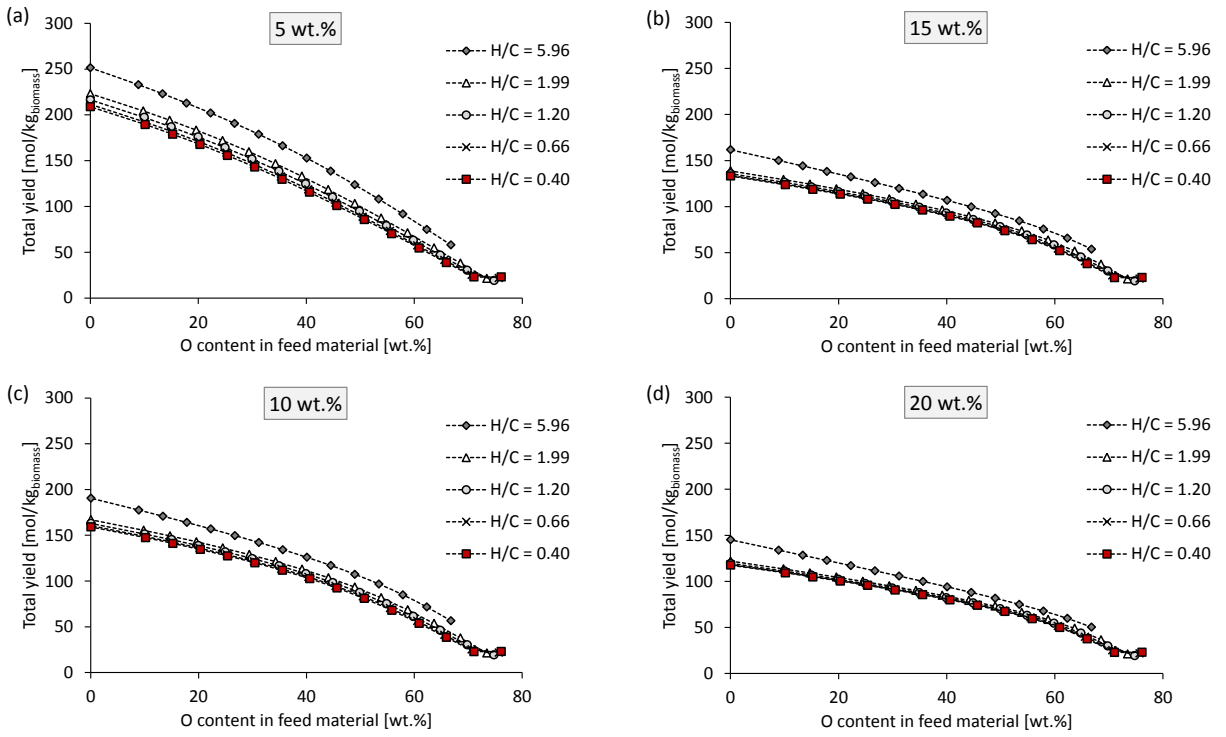

FIGURE 3-35 EFFECT OF OXYGEN CONTENT AND H/C RATIO OF THE FEED MATERIAL ON THE TOTAL YIELD DURING SCWG AT 800 °C AND A DRY FEED CONCENTRATION OF (A) 5 WT.%; (B) 10 WT.%; (C) 15 WT.%; AND (D) 20 WT.%

3.4.6 CALORIFIC VALUE OF PRODUCT GAS (HHV)

The generalised contour plots as a function of the O/C and H/C ratios for the HHV at 400, 600 and 800 °C are shown in Figure 3-36 – Figure 3-38, while the HHV in terms of the oxygen content at a various H/C ratios and 400, 600 and 800 °C are shown in Figure 3-39 - Figure 3-41.

With respect to the operating temperature, it is evident that the same trend is followed for the HHV as for the H_2 yield. In other words, an increase in the gasification temperature leads to an increase in the HHV. The effect of the feed concentration on the HHV of the product gas seems to be less significant than the gasification temperature. The highest calorific value is produced when operating at highest operating temperature of 800 °C and the lowest feed concentration 5 wt.% (*i.e.* at the same conditions where maximum H_2 yields are achieved).

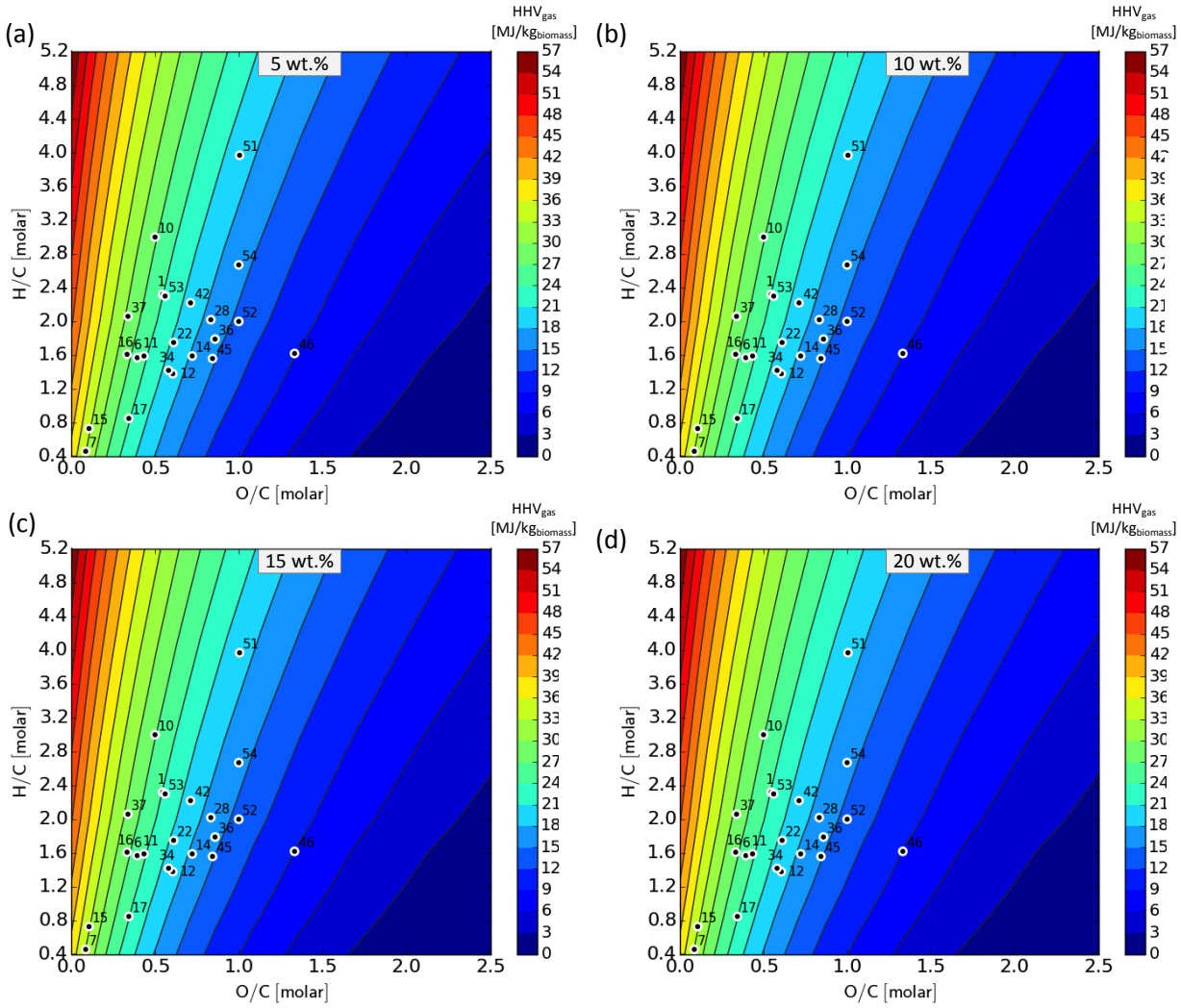

FIGURE 3-36 EFFECT OF FEEDSTOCK COMPOSITION ON THE THERMODYNAMIC EQUILIBRIUM HHV OF THE GAS DURING SCWG AT 400 °C, 25 MPA AND A DRY FEED CONCENTRATION OF (A) 5 WT.%; (B) 10 WT.%; (C) 15 WT.%; AND (D) 20 WT.%

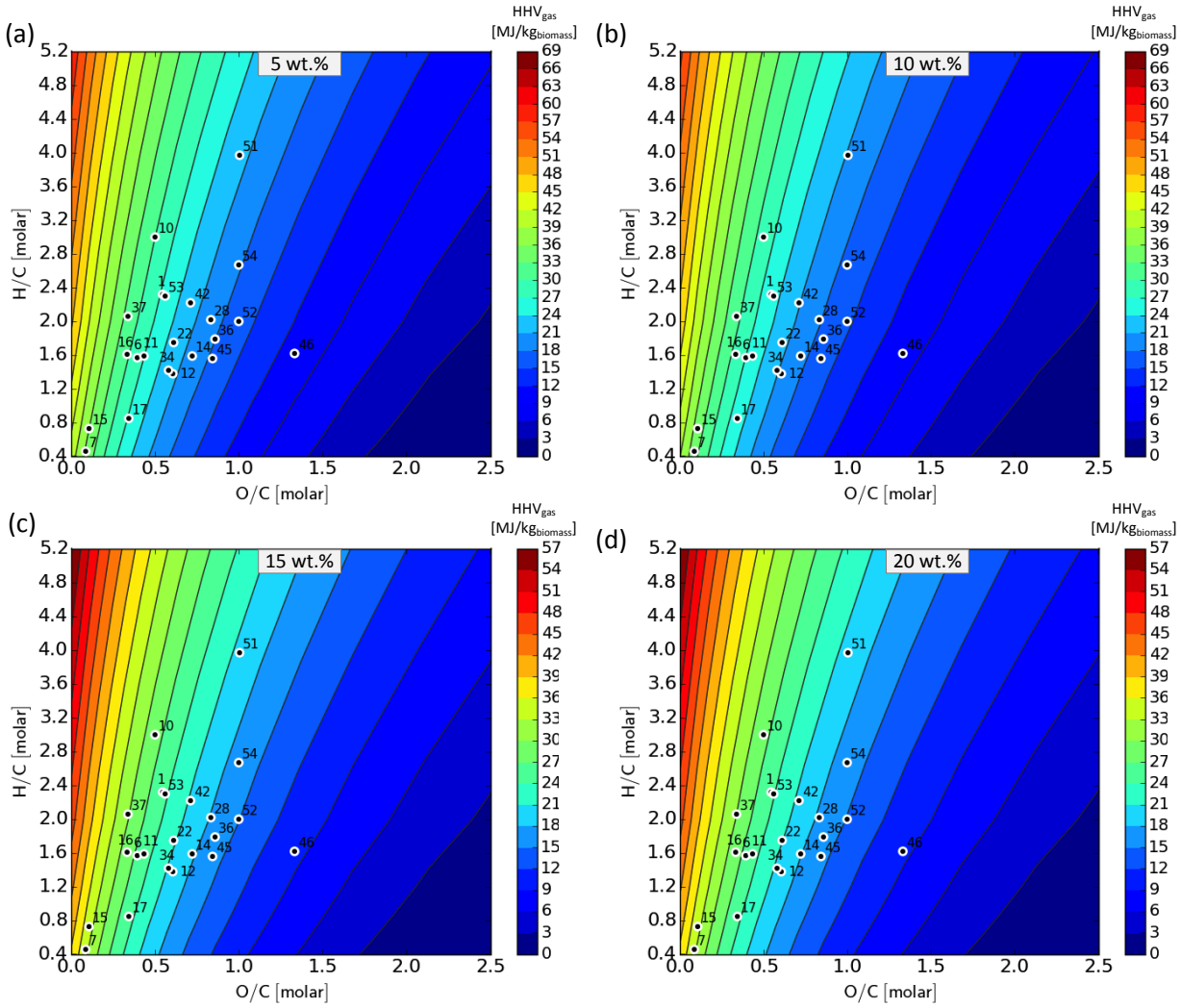

FIGURE 3-37 EFFECT OF FEEDSTOCK COMPOSITION ON THE THERMODYNAMIC EQUILIBRIUM HHV OF THE GAS DURING SCWG AT 600 °C, 25 MPA AND A DRY FEED CONCENTRATION OF (A) 5 WT.%; (B) 10 WT.%; (C) 15 WT.%; AND (D) 20 WT.%

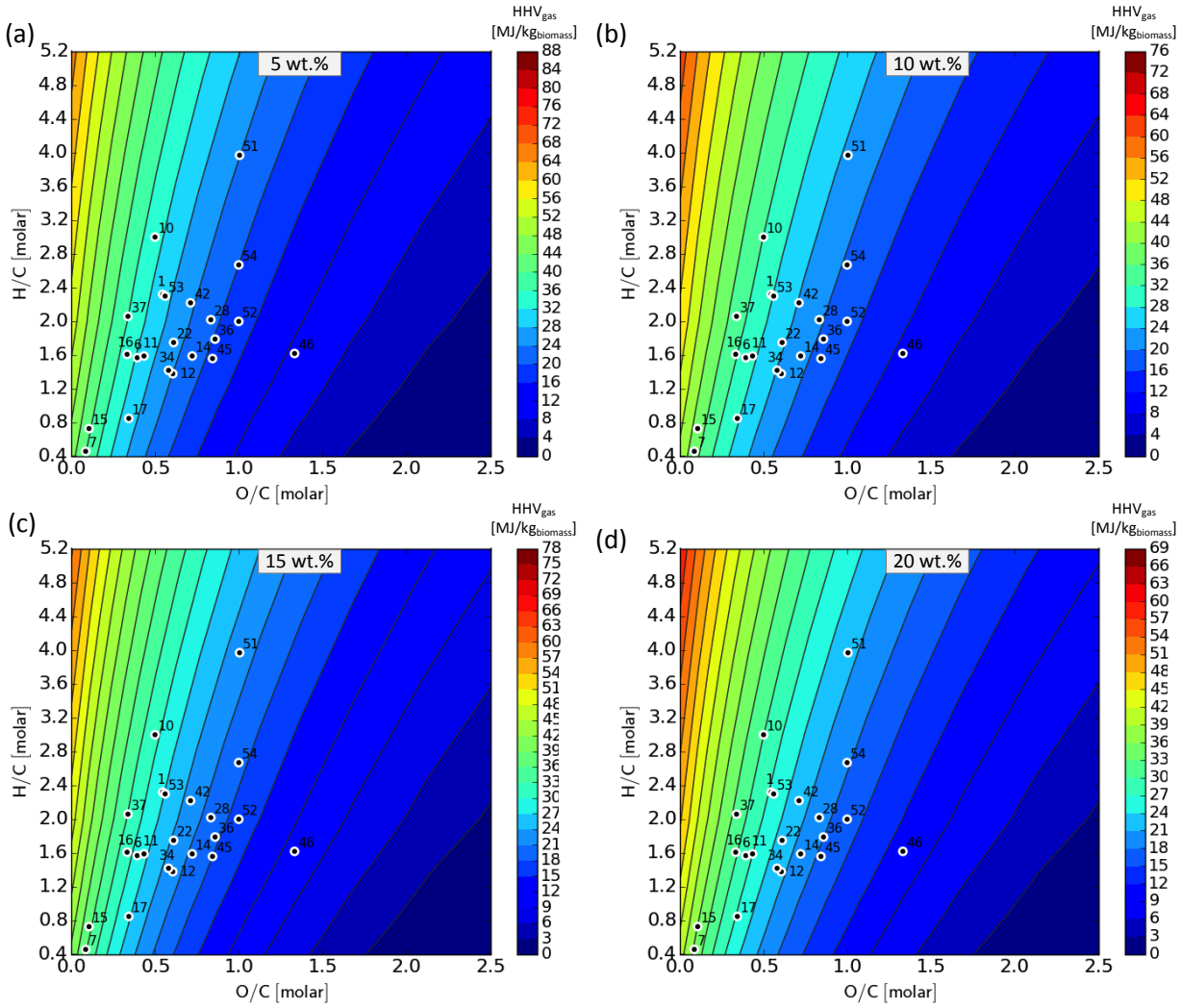

FIGURE 3-38 EFFECT OF FEEDSTOCK COMPOSITION ON THE THERMODYNAMIC EQUILIBRIUM HHV OF THE GAS DURING SCWG AT 800 °C, 25 MPA AND A DRY FEED CONCENTRATION OF (A) 5 WT.%; (B) 10 WT.%; (C) 15 WT.%; AND (D) 20 WT.%

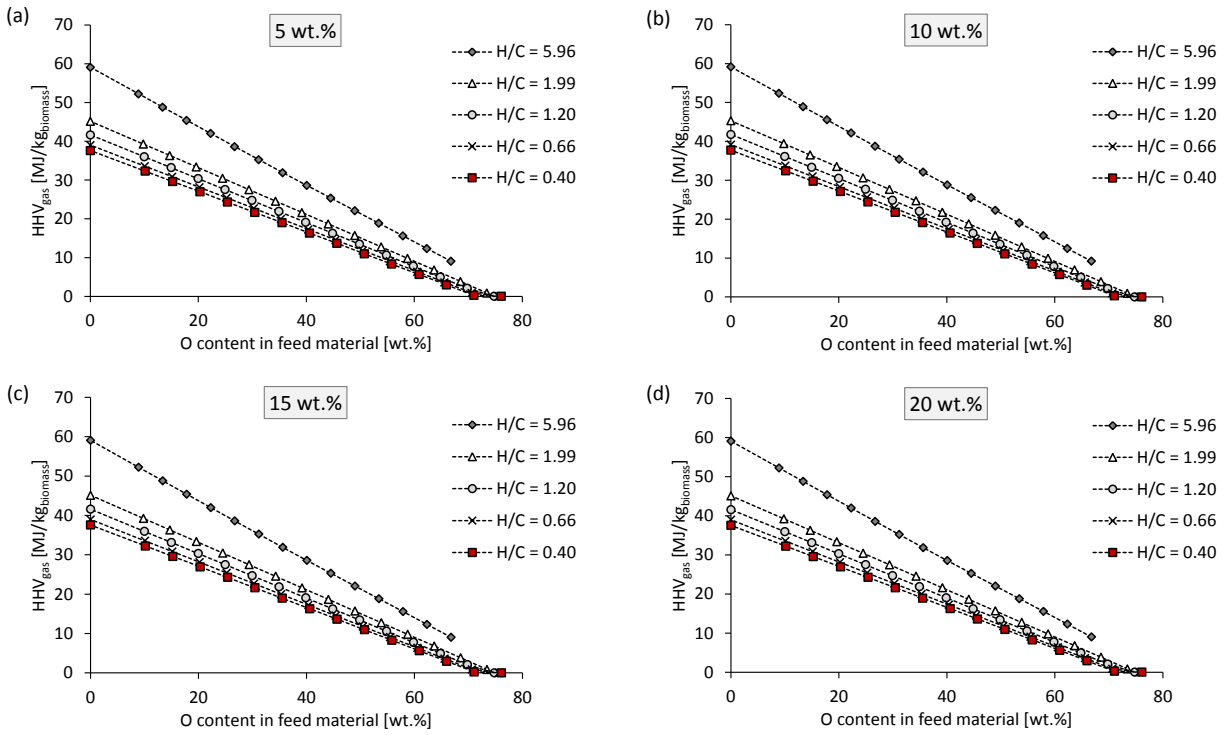

FIGURE 3-39 EFFECT OF OXYGEN CONTENT AND H/C RATIO OF THE FEED MATERIAL ON THE HHV OF THE GAS DURING SCWG AT 400 °C AND A DRY FEED CONCENTRATION OF (A) 5 WT.%; (B) 10 WT.%; (C) 15 WT.%; AND (D) 20 WT.%

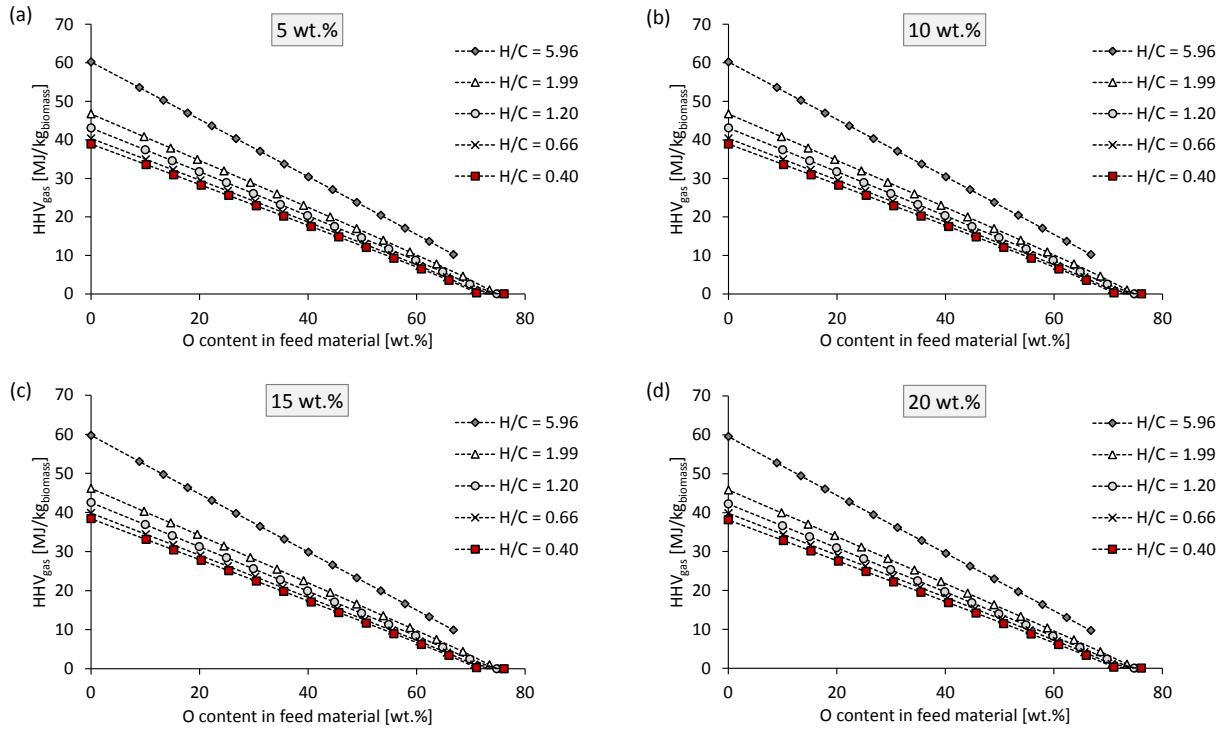

FIGURE 3-40 EFFECT OF OXYGEN CONTENT AND H/C RATIO OF THE FEED MATERIAL ON THE HHV OF THE GAS DURING SCWG AT 600 °C AND A DRY FEED CONCENTRATION OF (A) 5 WT.%; (B) 10 WT.%; (C) 15 WT.%; AND (D) 20 WT.%

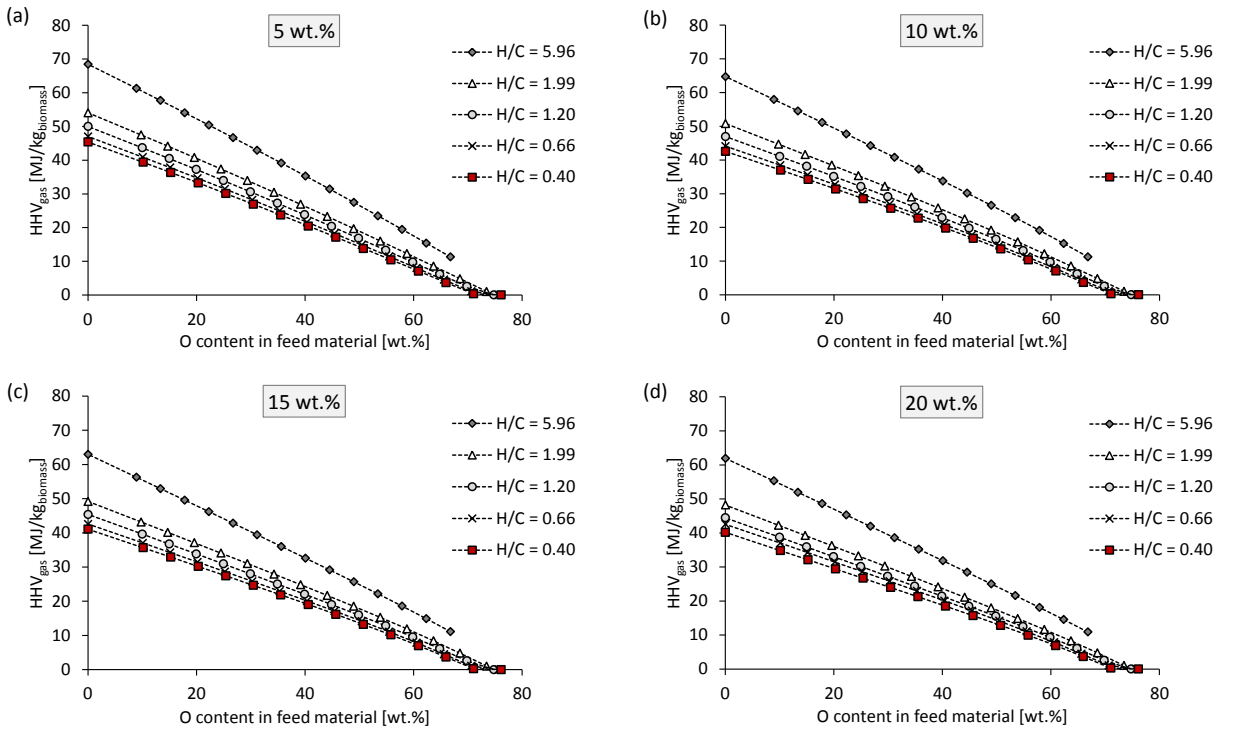

FIGURE 3-41 EFFECT OF OXYGEN CONTENT AND H/C RATIO OF THE FEED MATERIAL ON THE HHV OF THE GAS DURING SCWG AT 800 °C AND A DRY FEED CONCENTRATION OF (A) 5 WT.%; (B) 10 WT.%; (C) 15 WT.%; AND (D) 20 WT.%

A product gas with the highest calorific value is produced at high H/C ratios and low O/C (*i.e*. top left hand corner of the plots). Similar trends are observed for the HHV than for the CH_4 and H_2 yield with respect to the effect of H/C and O/C ratios of the feed material. Hence, feed material that will result in maximum H_2 and CH_4 yields will also result in a gas product with a maximum calorific value. This is due to the fact that the HHV of the product gas is calculated as the sum of the HHV of H_2, CH_4 and CO in the product gas. The CO yield is typically very low compared to that of H_2 and CH_4 at all operating conditions. Hence, its contribution to the HHV is not as significant as that of H_2 and CH_4.

The HHV of the product gas typically decreases almost linearly with an increase in the oxygen content in the feed material (at a constant H/C ratio). Hence, the lower the oxygen content in the feed material, the higher the HHV of the product gas. This is due to the fact that, at higher oxygen content in the feed material, the CO_2 yield (which contains no energy value) is also higher. As in the case of the H_2 and CH_4 yields, the HHV of the product gas is significantly higher at a H/C ratio of 5.96 than at H/C ratios of 1.99 and lower at all feed concentrations and

operating temperatures. Hence, highly oxygenated feed material will typically result in a gas product with a lower calorific value due to the lower H_2 and CH_4 yields.

Taking into account the considered possible feed materials, a product gas with the highest calorific value can be produced when char from pyrolysis of sugarcane bagasse (feedstock #7) and bituminous coal (feedstock #15) are used as feedstock material (41.1 – 44.5 MJ/$kg_{biomass}$) at 800 °C and 5 wt.%.

3.4.7 Heat Required for Isothermal Operations

The amount of heat required for the process (Q_{Req}) is the sum of the heat required to heat the feed stream to the reactor operating temperature (Q_{hx}) and the heat required for isothermal operation of the reactor (Q_{netto} – see Figure 3-3 and Eq. 3-13). These results do however not take into account the possibility of heat recovery. Figure 3-42 – Figure 3-44 shows the generalised contour plots for Q_{Req} at 400, 600 and 800 °C. Figure 3-45 - Figure 3-47 shows Q_{Req} as a function of the oxygen content of the feed material at 400, 600 and 800 °C.

When considering the operating temperature and feed concentration, the least heat is required for the process when operating at a relatively low temperature and using a high biomass feed concentration (*i.e.* at when operating at 400 °C and feed concentration of 20 wt.%). The required heat decreases significantly with an increase in biomass concentration, but increases only slightly with an increase in operating temperature. The significant decrease in the required heat with an increase in the biomass concentration is due to the fact that more water is present in the feed stream at lower biomass concentrations than at higher biomass concentrations.

Interestingly, for all the cases under investigation, the most heat is required for the process when biomass with a high H/C ratio and low O/C content is used as feedstock (*i.e.*, the top left corner of the plot). Furthermore, the required heat for isothermal operating decreases with an increase in the oxygen content of the feed material. This corresponds to the same biomass composition where maximum equilibrium H_2 and CH_4 yields are achieved and, hence, a product gas with the highest calorific value is produced. A trade-off between achieving high H_2 and CH_4 yields and using as little energy as possible therefore exists.

When considering the operating conditions and the feed materials considered, using paper mill sludge cake (feedstock #46) as feed material at 400 °C and 20 wt.% will require the least heat for isothermal operation of the process (17.8 – 21.0 MJ/$kg_{biomass}$), without taking heat recovery into account.

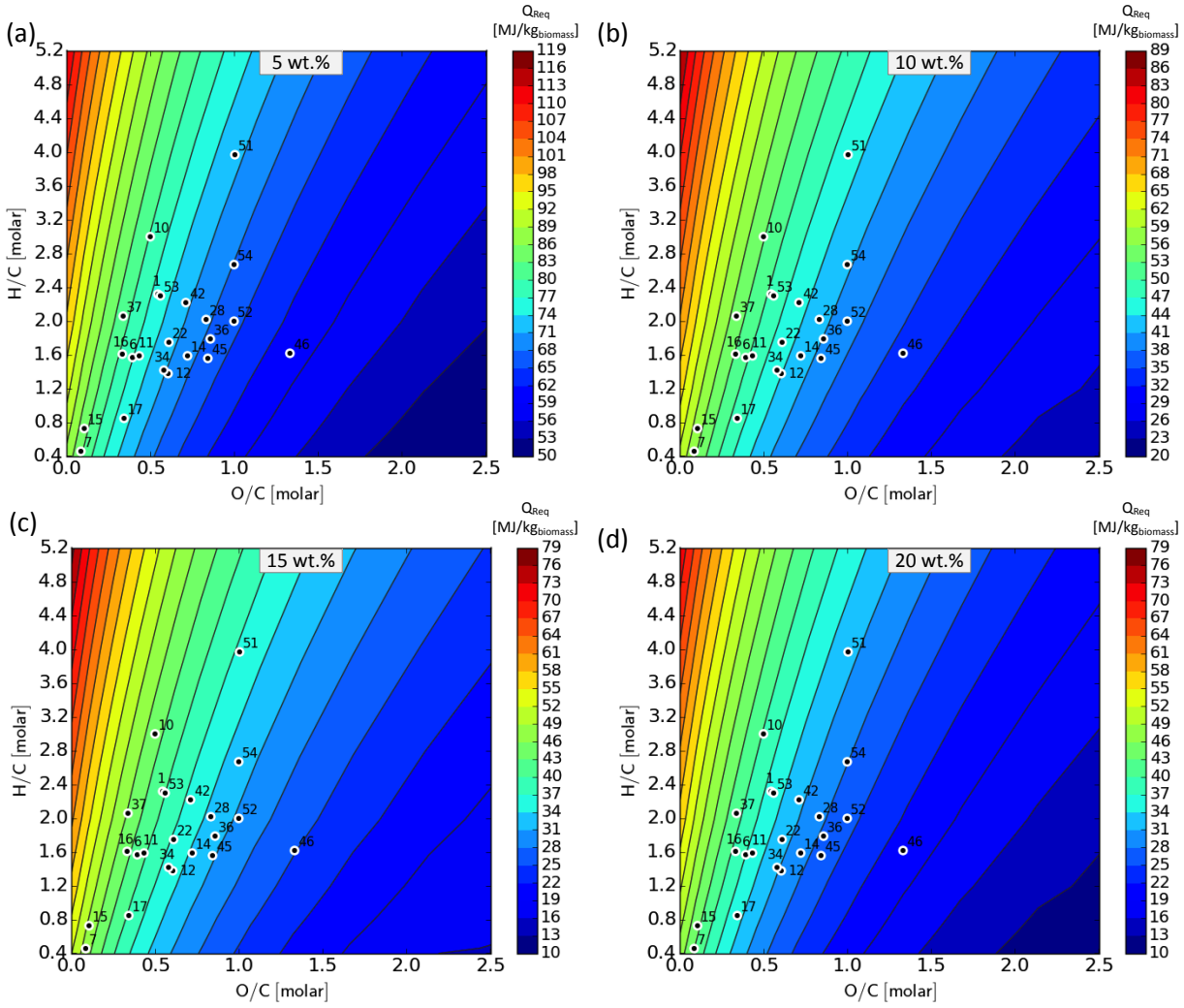

FIGURE 3-42 EFFECT OF FEEDSTOCK COMPOSITION ON THE HEAT REQUIRED FOR ISOTHERMAL OPERATION AT 400 °C, 25 MPA AND A DRY FEED CONCENTRATION OF (A) 5 WT.%; (B) 10 WT.%; (C) 15 WT.%; AND (D) 20 WT.%

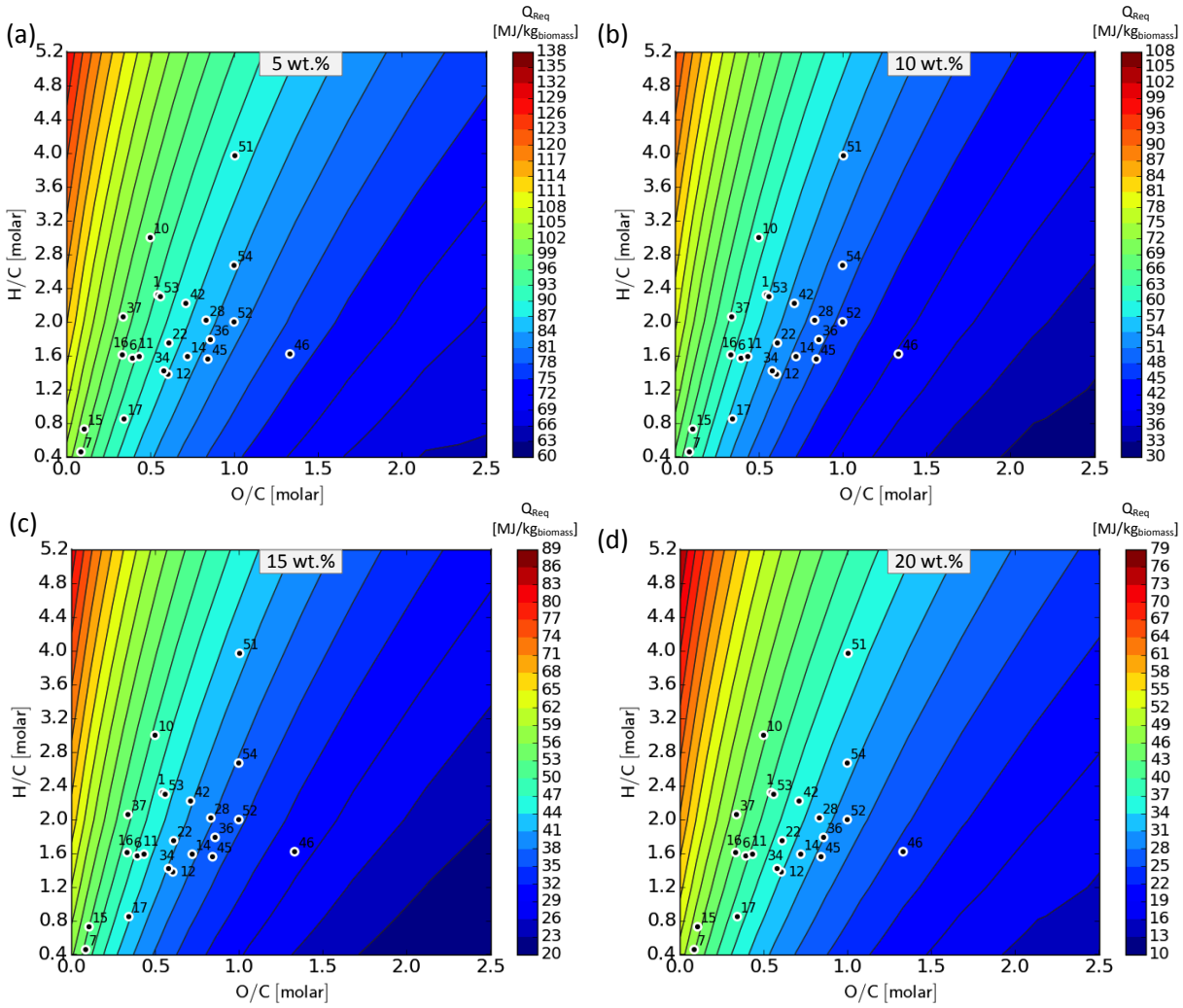

FIGURE 3-43 EFFECT OF FEEDSTOCK COMPOSITION ON THE HEAT REQUIRED FOR ISOTHERMAL OPERATION AT 600 °C, 25 MPA AND A DRY FEED CONCENTRATION OF (A) 5 WT.%; (B) 10 WT.%; (C) 15 WT.%; AND (D) 20 WT.%

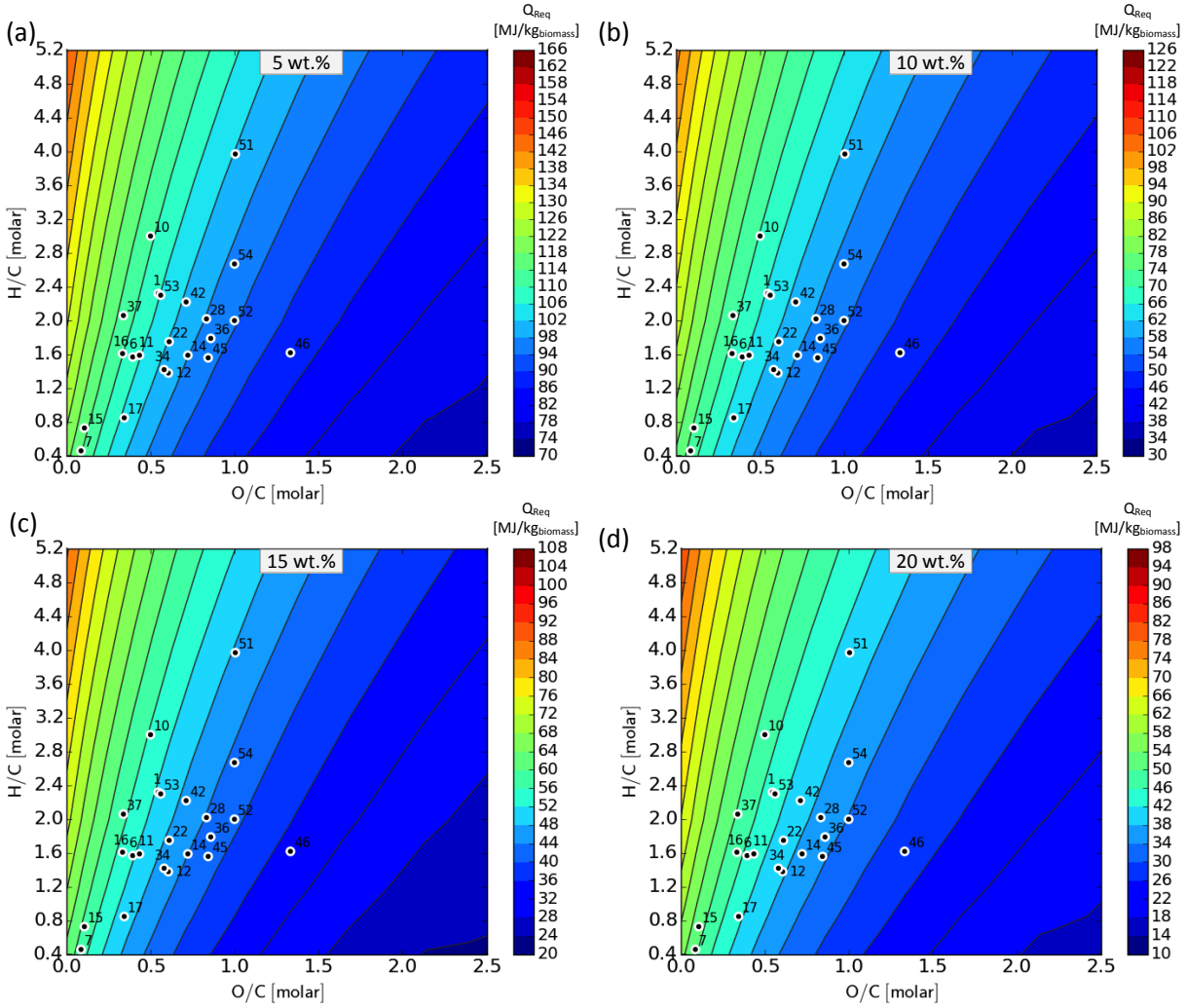

FIGURE 3-44 EFFECT OF FEEDSTOCK COMPOSITION ON THE HEAT REQUIRED FOR ISOTHERMAL OPERATION AT 800 °C, 25 MPA AND A DRY FEED CONCENTRATION OF (A) 5 WT.%; (B) 10 WT.%; (C) 15 WT.%; AND (D) 20 WT.%

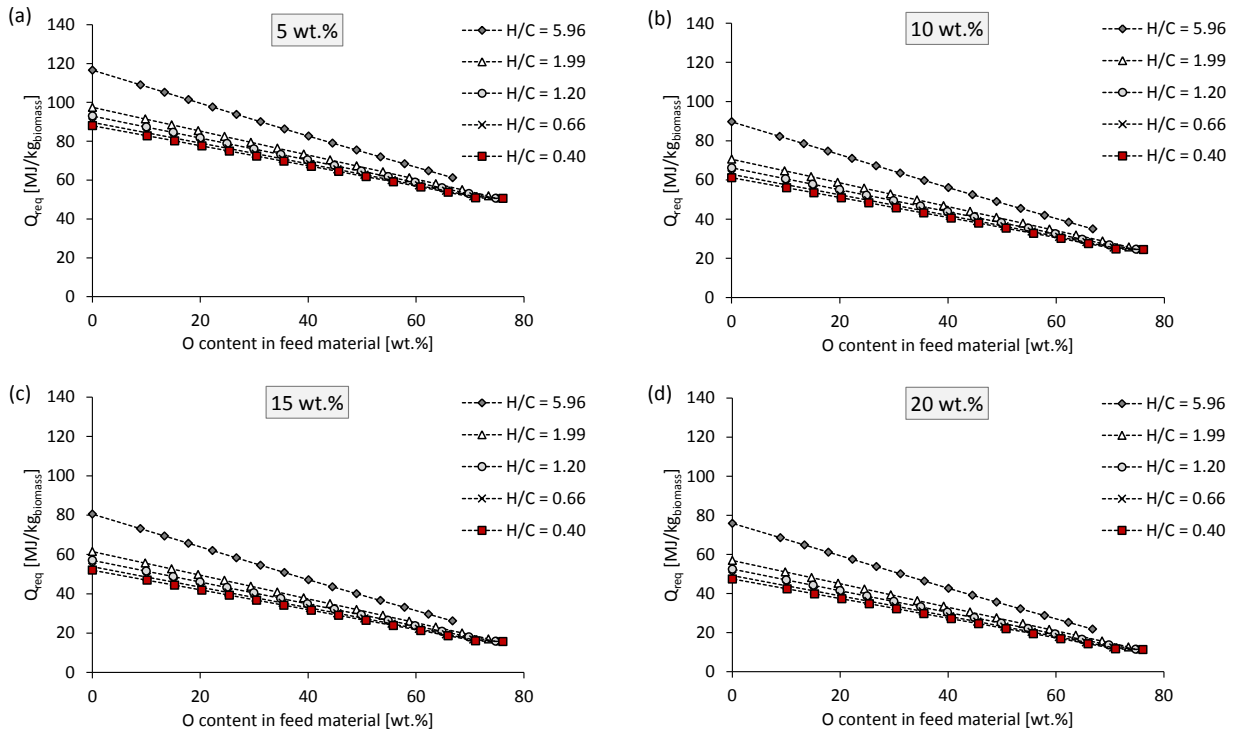

FIGURE 3-45 EFFECT OF OXYGEN CONTENT AND H/C RATIO OF THE FEED MATERIAL ON Q_{REQ} DURING SCWG AT 400 °C AND A DRY FEED CONCENTRATION OF (A) 5 WT.%; (B) 10 WT.%; (C) 15 WT.%; AND (D) 20 WT.%

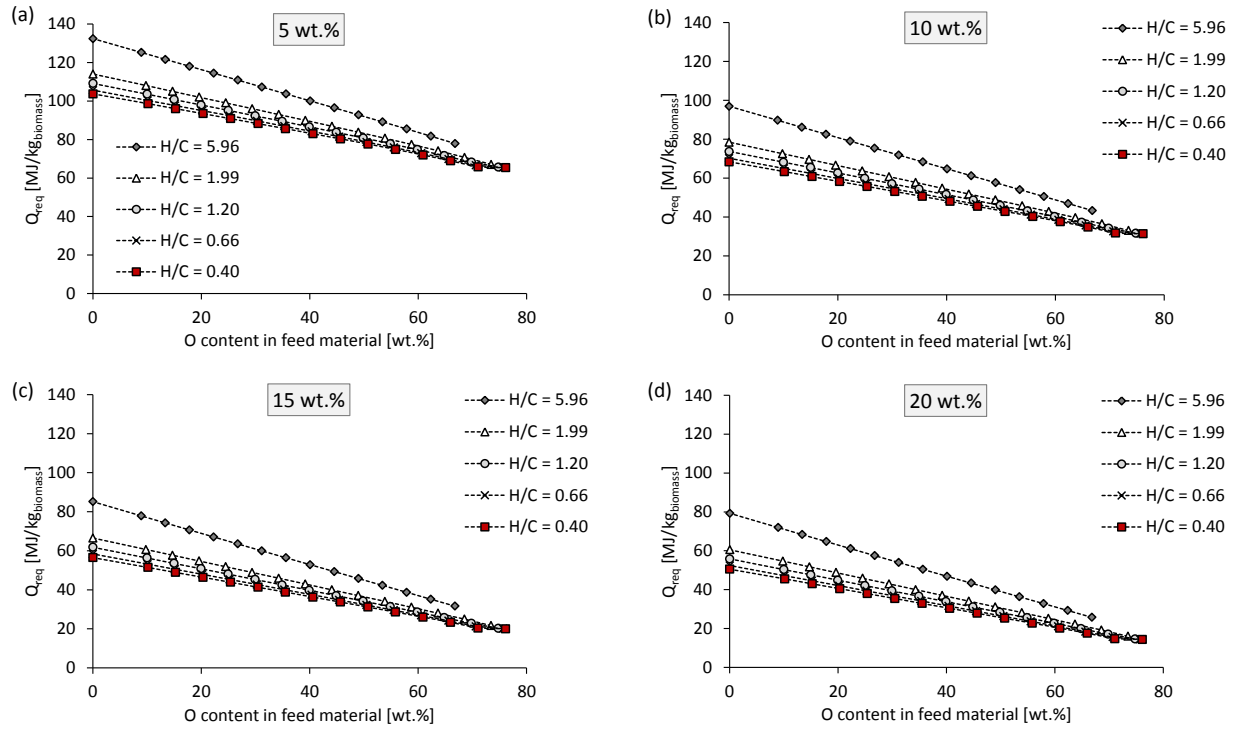

FIGURE 3-46 EFFECT OF OXYGEN CONTENT AND H/C RATIO OF THE FEED MATERIAL ON Q_{REQ} DURING SCWG AT 600 °C AND A DRY FEED CONCENTRATION OF (A) 5 WT.%; (B) 10 WT.%; (C) 15 WT.%; AND (D) 20 WT.%

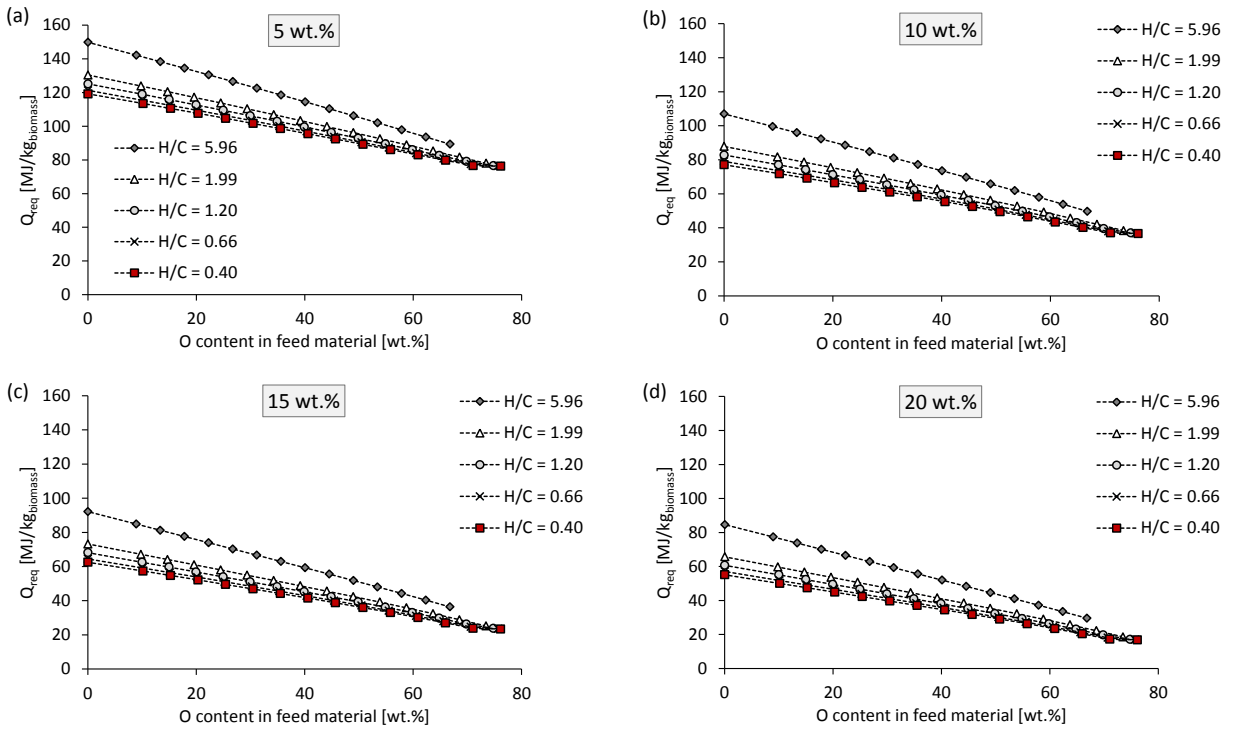

FIGURE 3-47 EFFECT OF OXYGEN CONTENT AND H/C RATIO OF THE FEED MATERIAL ON Q_{REQ} DURING SCWG AT 800 °C AND A DRY FEED CONCENTRATION OF (A) 5 WT.%; (B) 10 WT.%; (C) 15 WT.%; AND (D) 20 WT.%

3.4.8 ENERGY RECOVERY (COLD GAS EFFICIENCY)

Figure 3-48 – Figure 3-50 shows the generalised contour plots for energy recovery (ER) in terms of the O/C and H/C content of the feed material at 400, 600 and 800 °C. The ER in terms of the oxygen content of the feed material at 400, 600 and 800 °C are shown in Figure 3-51 – Figure 3-53.

The ER typically decreases with an increase in the feed concentration, while an increase in the ER is evident with an increase in the operating temperature. At an operating of 400 °C, the ER is greater than 88% for all feed concentrations when feed material with an O/C ratio less than 1.5 was used, irrespective of the H/C ratio of the feed material (see Figure 3-48). At operating temperatures of 600 and 800 °C, the ER is greater than 89% and 98% respectively, for feed material with O/C ratios less than 1.5 (see Figure 3-49 and Figure 3-50).

The ER stays relatively constant with an increase in the oxygen content up to approximately 70 wt.% at all operating temperatures. A sharp drop in the ER is visible at oxygen contents higher

than 60 wt.%. This is due to the fact that the H_2 and CH_4 yields are almost zero at very high oxygen content in the feed material (typically > 70 wt.%). The ER decreases slightly with an increase in the H/C ratio at a constant oxygen content.

Maximum ER of 110.4 – 116.2% is achieved at a feed concentration of 5 wt.% and temperature of 800 °C when all of the feed materials except paper mill sludge cape (feedstock #46) and methanol (feedstock #51) are used. The reason why the ER is the highest at these conditions (800 °C and 5 wt.%) is due to the fact that these are the same conditions for which the H_2 yield, which has a very high energy value, is also at its highest.

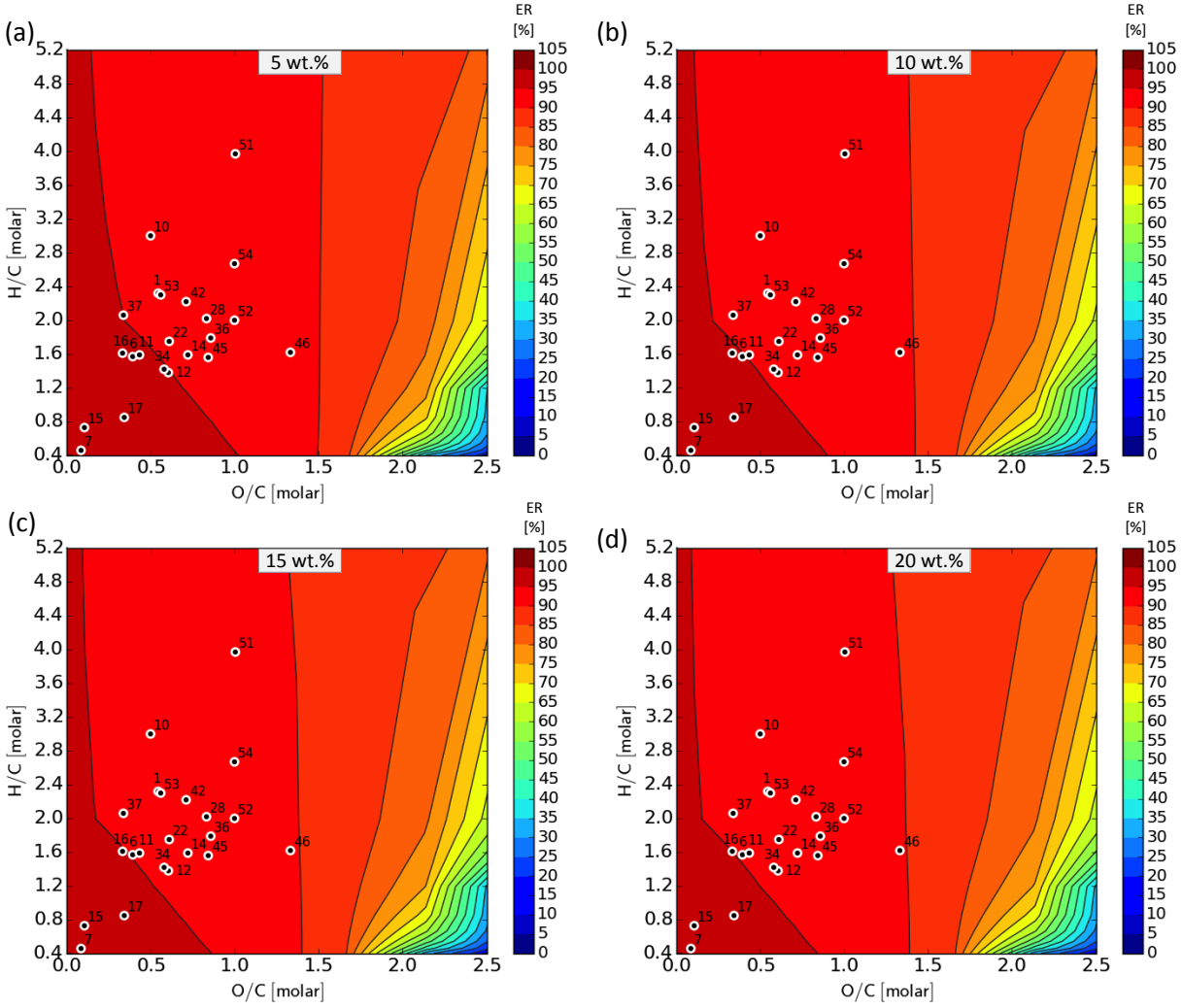

FIGURE 3-48 EFFECT OF FEEDSTOCK COMPOSITION ON THE ENERGY RECOVERY DURING SCWG AT 400 °C, 25 MPA AND A DRY FEED CONCENTRATION OF (A) 5 WT.%; (B) 10 WT.%; (C) 15 WT.%; AND (D) 20 WT.%

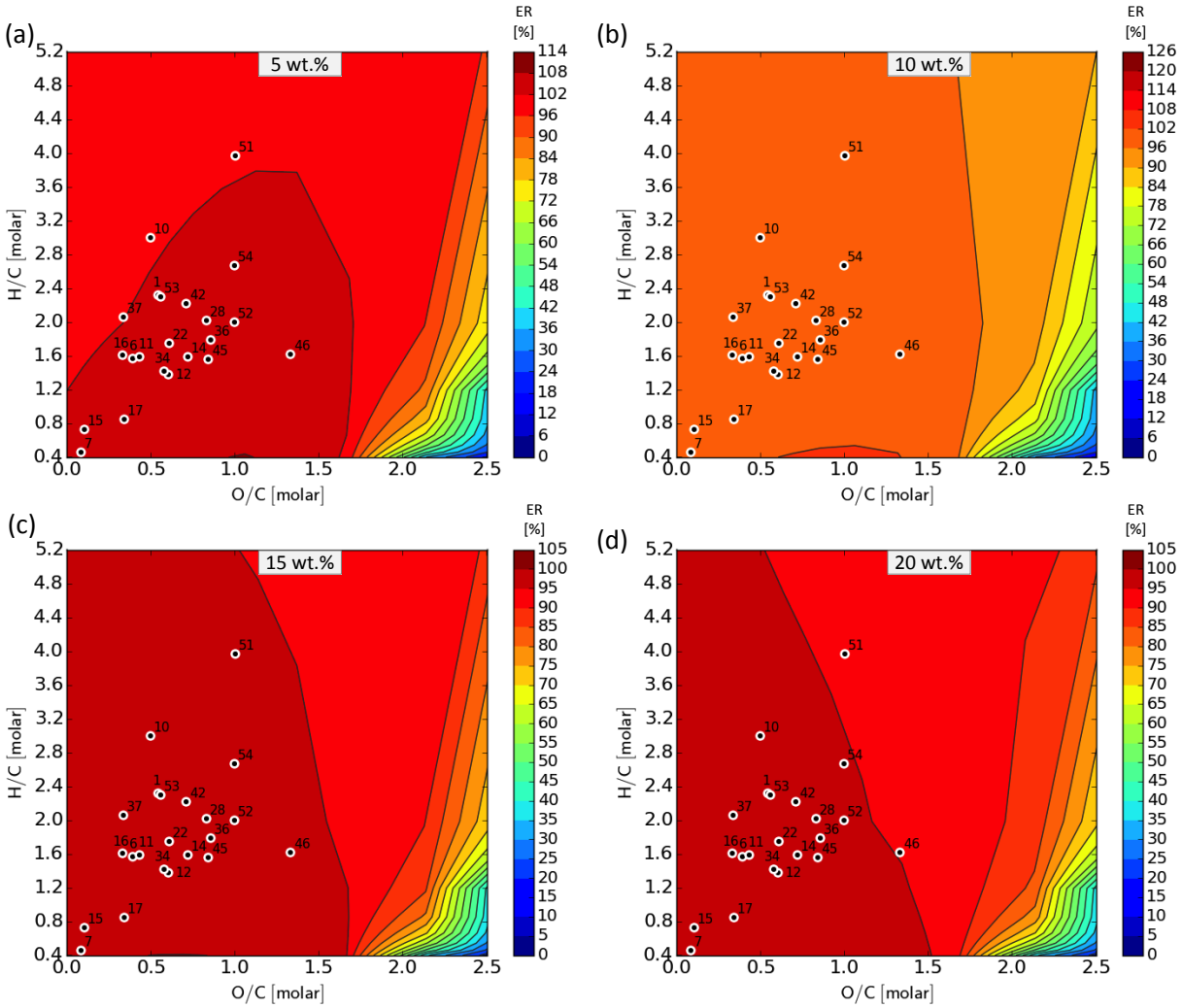

FIGURE 3-49 EFFECT OF FEEDSTOCK COMPOSITION ON THE ENERGY RECOVERY DURING SCWG AT 600 °C, 25 MPA AND A DRY FEED CONCENTRATION OF (A) 5 WT.%; (B) 10 WT.%; (C) 15 WT.%; AND (D) 20 WT.%

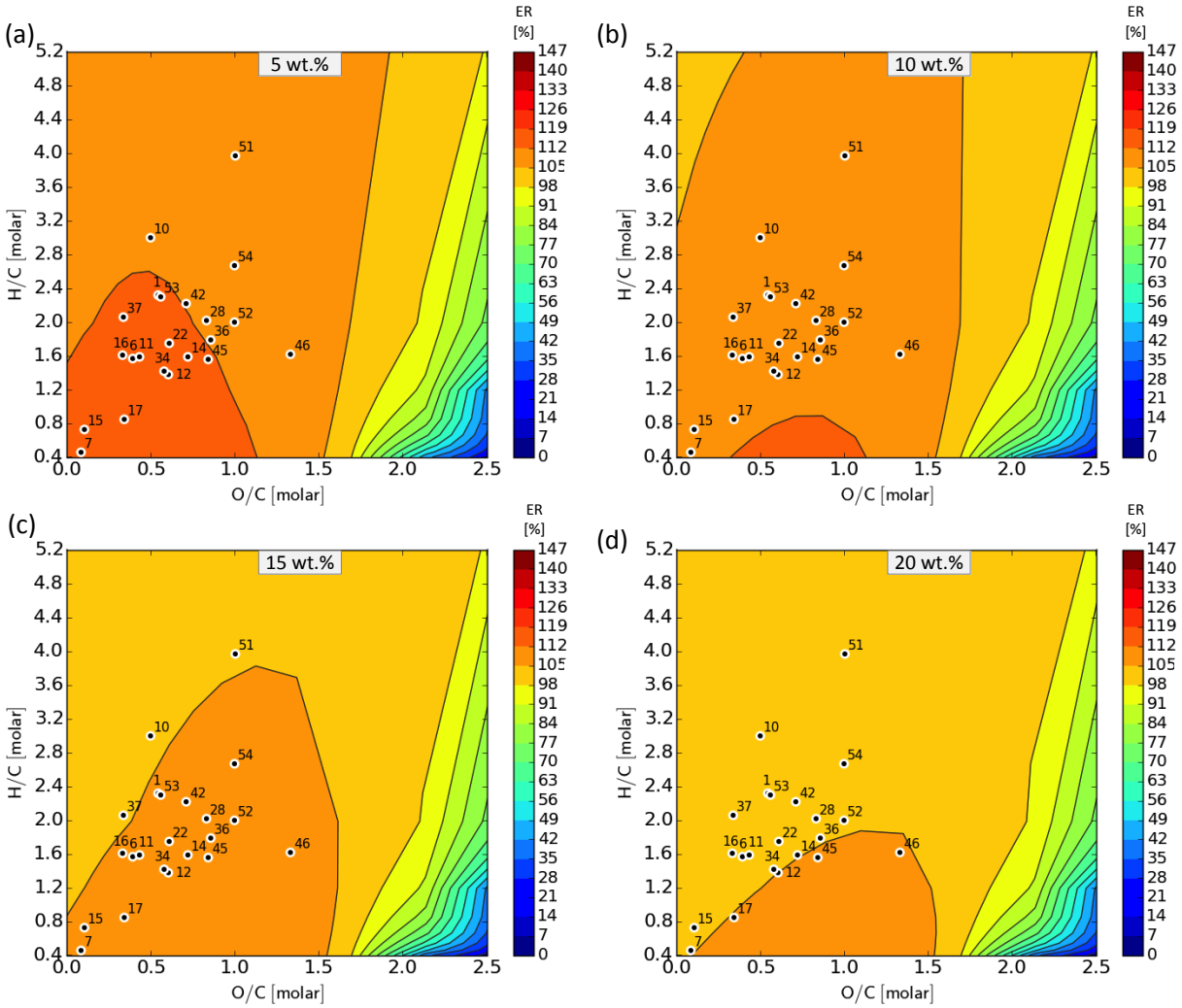

FIGURE 3-50 EFFECT OF FEEDSTOCK COMPOSITION ON THE ENERGY RECOVERY DURING SCWG AT 800 °C, 25 MPA AND A DRY FEED CONCENTRATION OF (A) 5 WT.%; (B) 10 WT.%; (C) 15 WT.%; AND (D) 20 WT.%

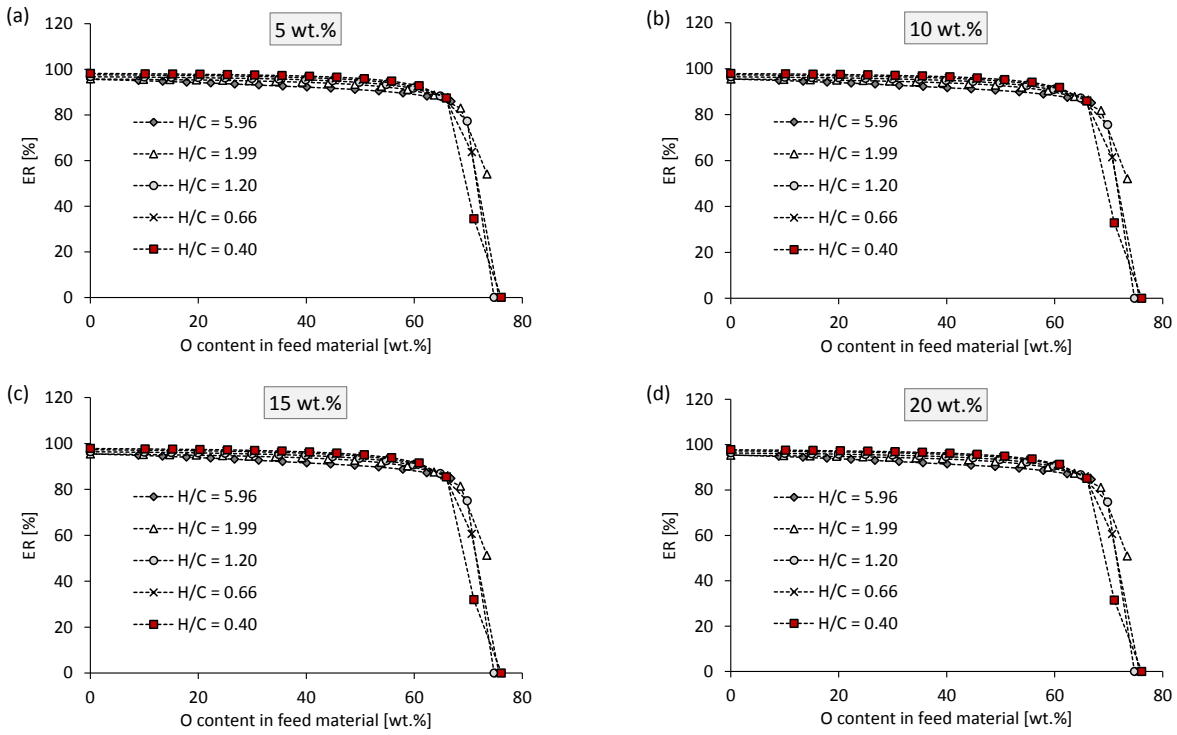

FIGURE 3-51 EFFECT OF OXYGEN CONTENT AND H/C RATIO OF THE FEED MATERIAL ON THE ENERGY RECOVERY (ER) DURING SCWG AT 400 °C AND A DRY FEED CONCENTRATION OF (A) 5 WT.%; (B) 10 WT.%; (C) 15 WT.%; AND (D) 20 WT.%

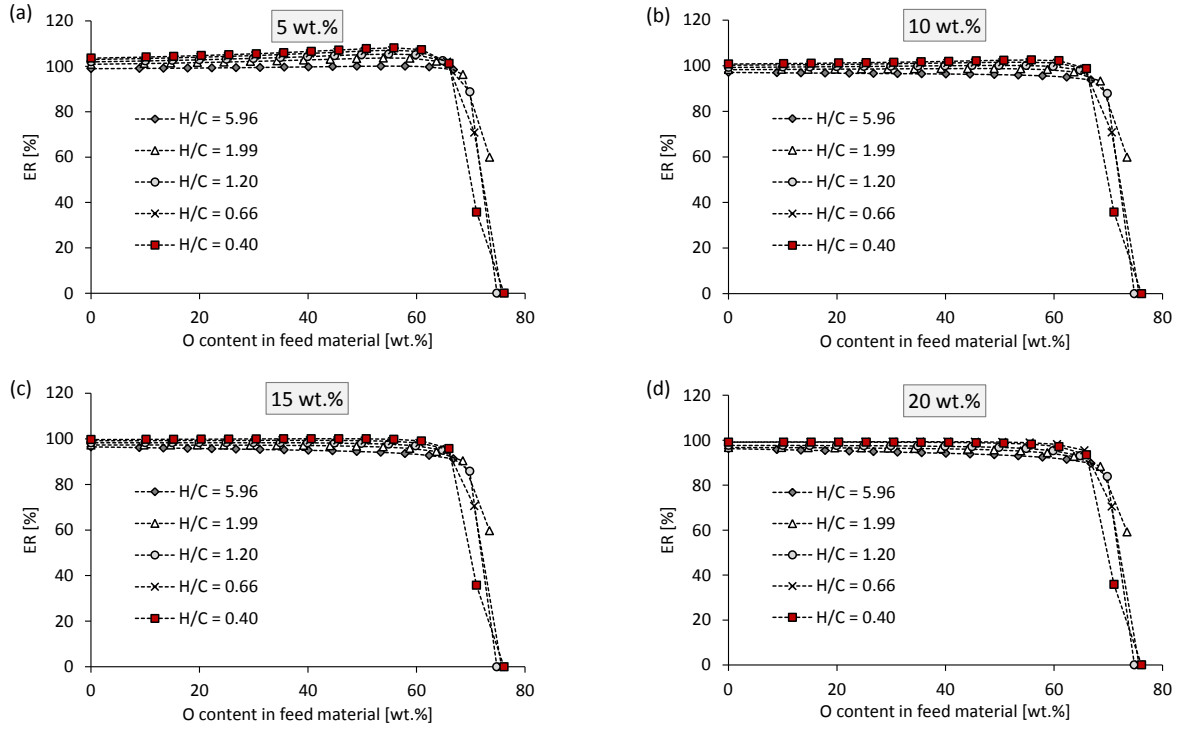

FIGURE 3-52 EFFECT OF OXYGEN CONTENT AND H/C RATIO OF THE FEED MATERIAL ON THE ENERGY RECOVERY (ER) DURING SCWG AT 600 °C AND A DRY FEED CONCENTRATION OF (A) 5 WT.%; (B) 10 WT.%; (C) 15 WT.%; AND (D) 20 WT.%

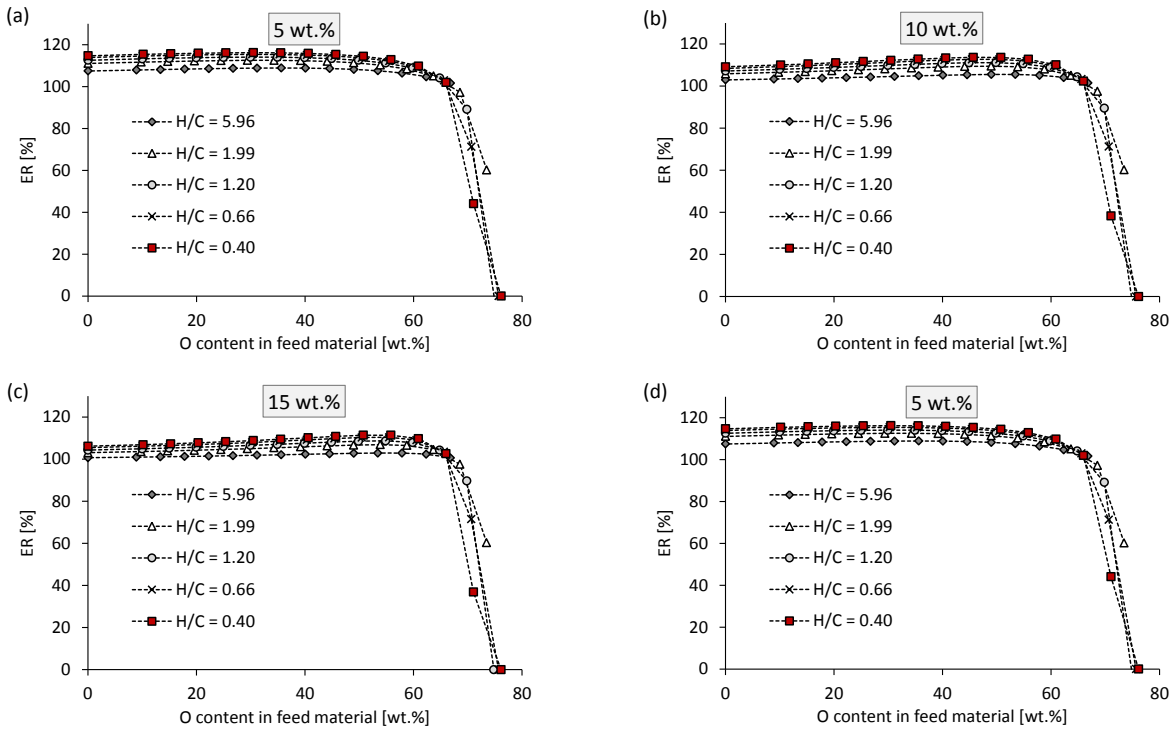

FIGURE 3-53 EFFECT OF OXYGEN CONTENT AND H/C RATIO OF THE FEED MATERIAL ON THE ENERGY RECOVERY (ER) DURING SCWG AT 800 °C AND A DRY FEED CONCENTRATION OF (A) 5 WT.%; (B) 10 WT.%; (C) 15 WT.%; AND (D) 20 WT.%

3.4.9 OVERALL THERMAL EFFICIENCY

The effect of the O/C and H/C content of the feed material on the overall thermal efficiency at 400, 600 and 800 °C are shown in Figure 3-54, Figure 3-55 and Figure 3-56, respectively. The overall thermal efficiency in terms of the oxygen content of the feed material is shown in Figure 3-57 to Figure 3-59.

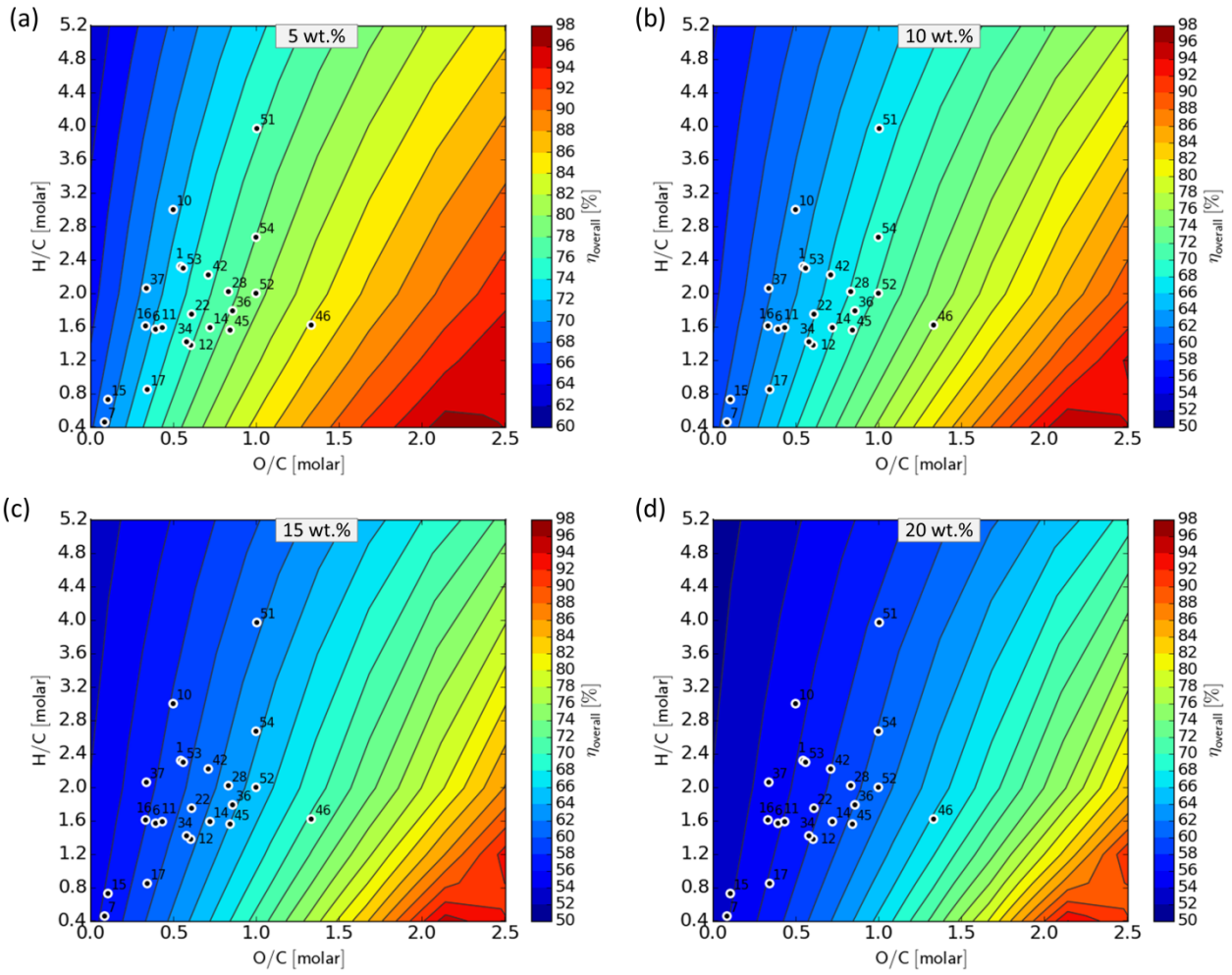

FIGURE 3-54 EFFECT OF FEEDSTOCK COMPOSITION ON THE OVERALL THERMAL EFFICIENCY DURING SCWG AT 400 °C, 25 MPA AND A DRY FEED CONCENTRATION OF (A) 5 WT.%; (B) 10 WT.%; (C) 15 WT.%; AND (D) 20 WT.%

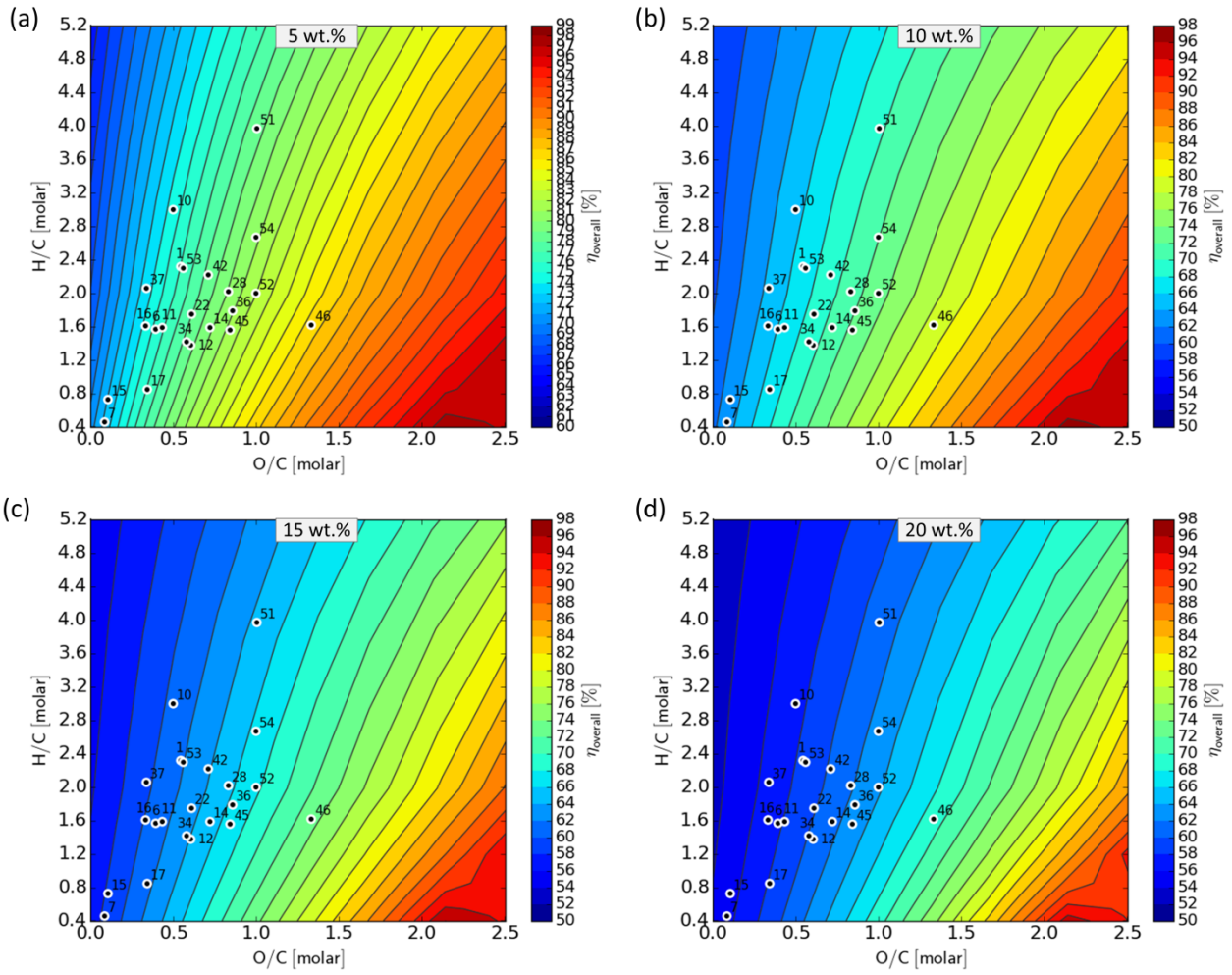

FIGURE 3-55 EFFECT OF FEEDSTOCK COMPOSITION ON THE OVERALL THERMAL EFFICIENCY DURING SCWG AT 600 °C, 25 MPA AND A DRY FEED CONCENTRATION OF (A) 5 WT.%; (B) 10 WT.%; (C) 15 WT.%; AND (D) 20 WT.%

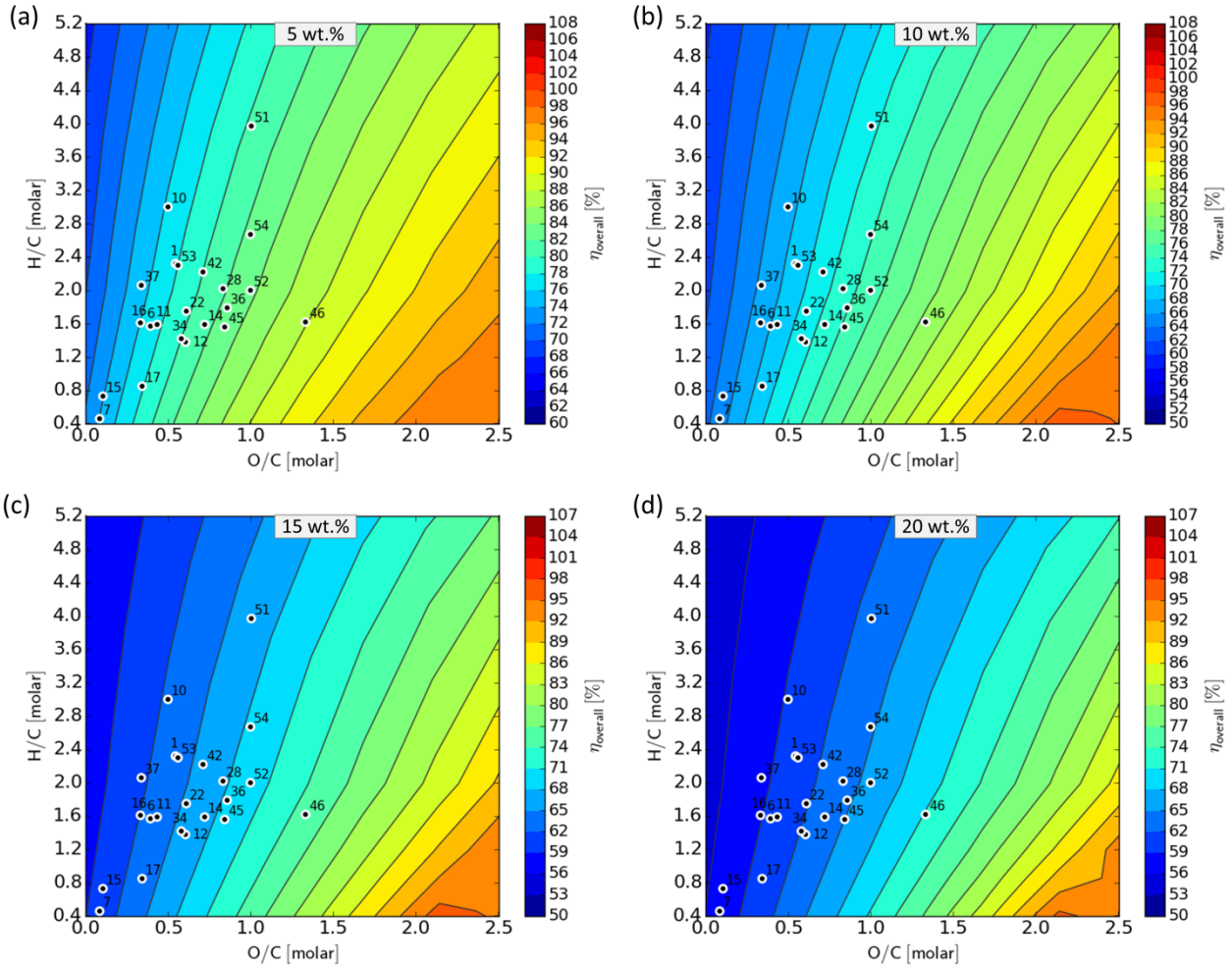

FIGURE 3-56 EFFECT OF FEEDSTOCK COMPOSITION ON THE OVERALL THERMAL EFFICIENCY DURING SCWG AT 800 °C, 25 MPA AND A DRY FEED CONCENTRATION OF (A) 5 WT.%; (B) 10 WT.%; (C) 15 WT.%; AND (D) 20 WT.%

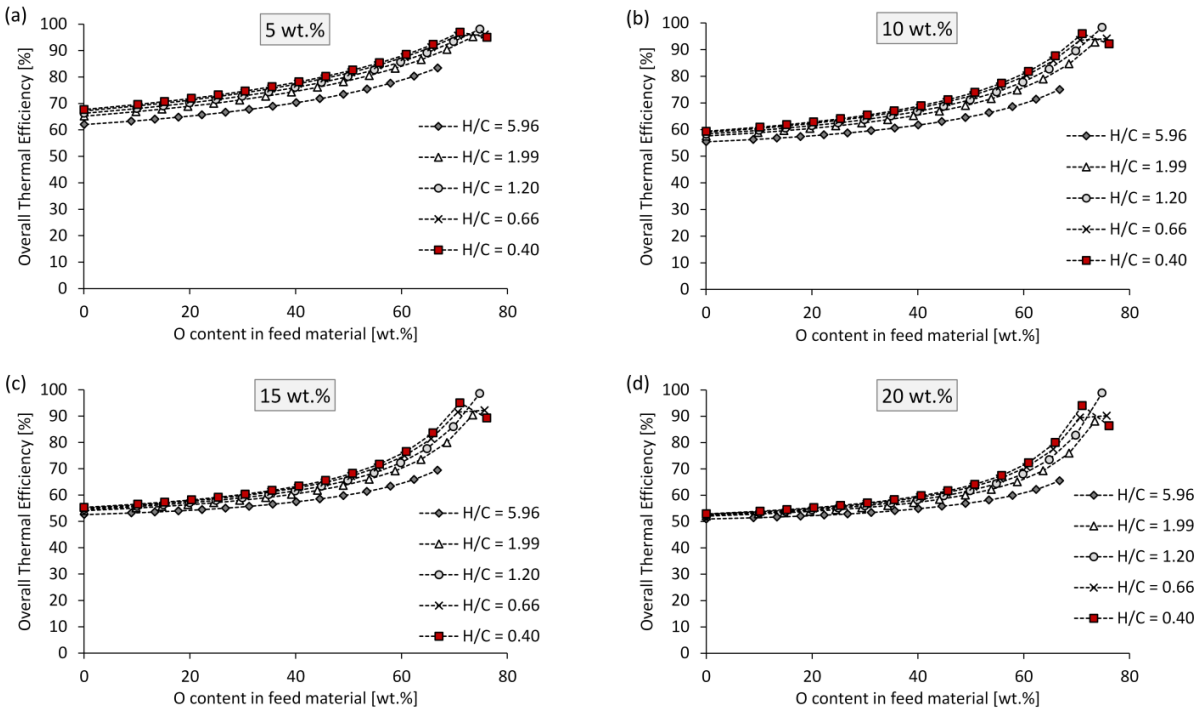

FIGURE 3-57 EFFECT OF OXYGEN CONTENT AND H/C RATIO OF THE FEED MATERIAL ON THE OVERALL THERMAL EFFICIENCY DURING SCWG AT 400 °C AND A DRY FEED CONCENTRATION OF (A) 5 WT.%; (B) 10 WT.%; (C) 15 WT.%; AND (D) 20 WT.%

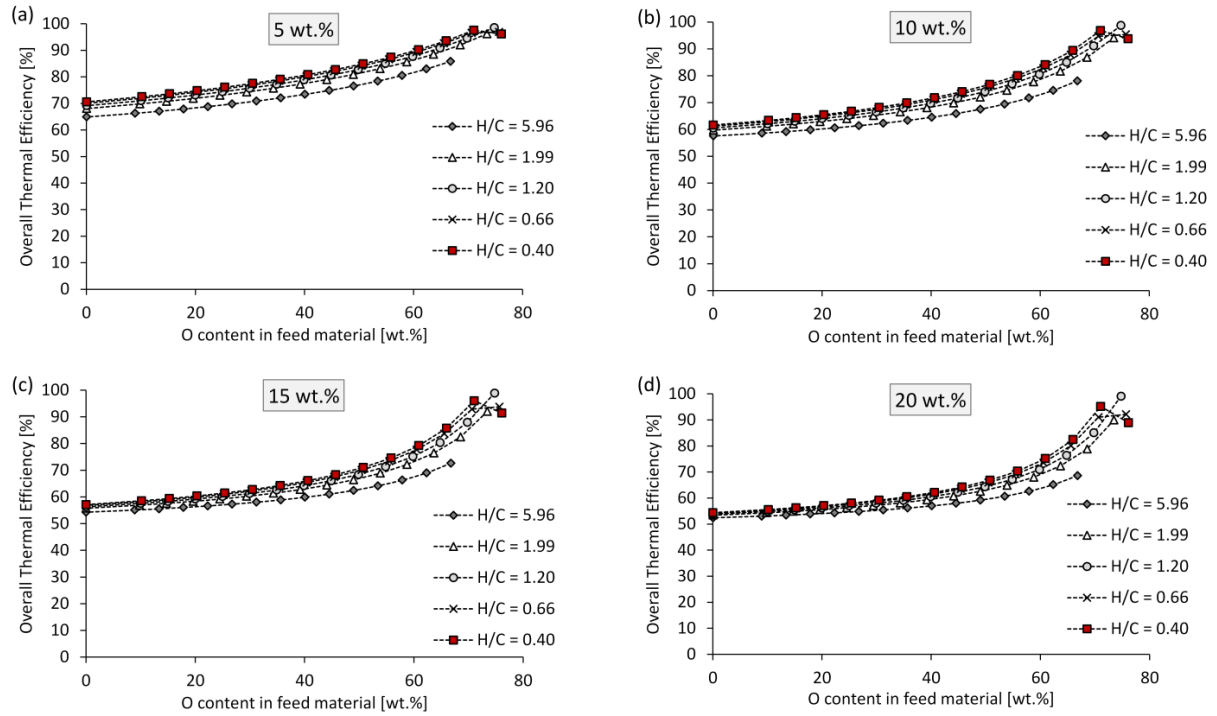

FIGURE 3-58 EFFECT OF OXYGEN CONTENT AND H/C RATIO OF THE FEED MATERIAL ON THE OVERALL THERMAL EFFICIENCY DURING SCWG AT 600 °C AND A DRY FEED CONCENTRATION OF (A) 5 WT.%; (B) 10 WT.%; (C) 15 WT.%; AND (D) 20 WT.%

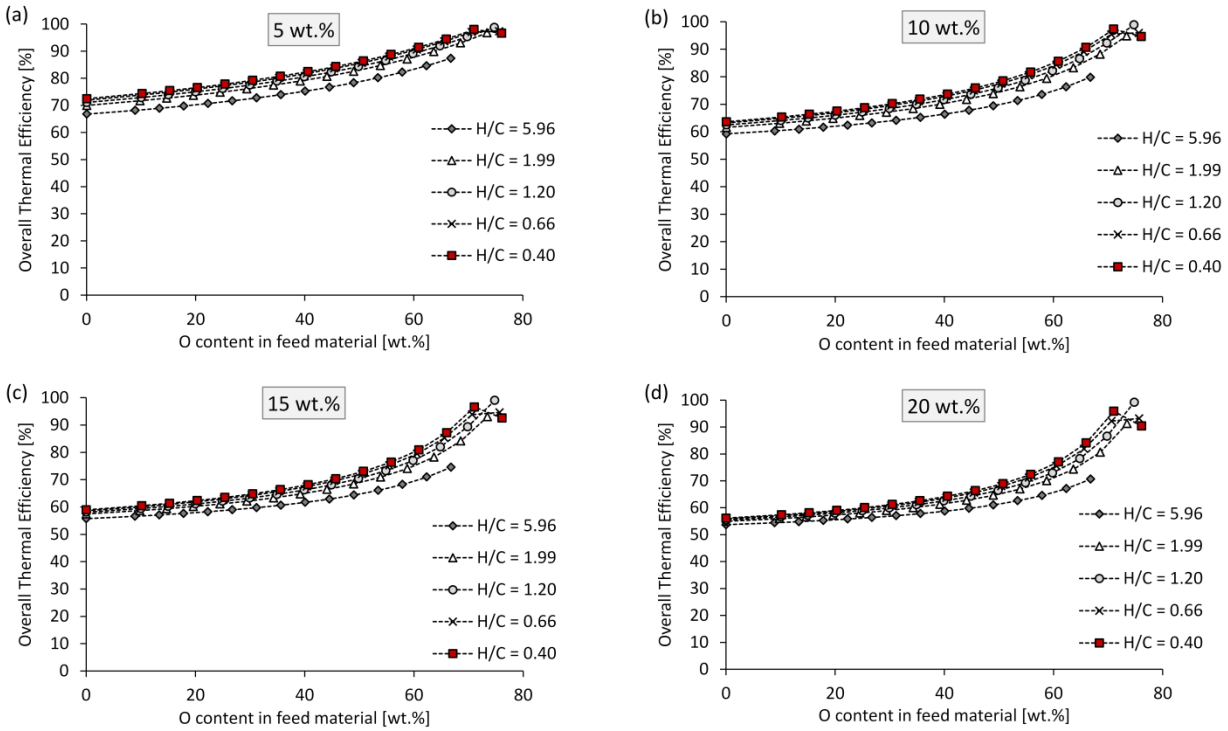

FIGURE 3-59 EFFECT OF OXYGEN CONTENT AND H/C RATIO OF THE FEED MATERIAL ON THE OVERALL THERMAL EFFICIENCY DURING SCWG AT 800 °C AND A DRY FEED CONCENTRATION OF (A) 5 WT.%; (B) 10 WT.%; (C) 15 WT.%; AND (D) 20 WT.%

In contrast to the calorific value of the product gas, the process seems to be most efficient when feed material with a low O/C ratio and low H/C ratio is used as feed material at all operating conditions (*i.e.* right bottom corner of the contour plot). This is the same combination of operating conditions and feed compositions at which the least heat is required for isothermal operation (see Section 3.4.7). An increase in the oxygen content of the feed material typically resulted in a decrease in the calorific value of the product gas as well as a decrease in the heat required for isothermal operations (see Section 3.4.6 and 3.4.7). However, an increase in the oxygen content typically resulted in a slight increase in the overall thermal efficiency of the process (see Figure 3-57 to Figure 3-59). The overall thermal efficiency typically increases with an increase in the operating temperature and decreases with an increase in the dry feed concentration.

Considering the combination of feed composition and operating conditions and the different biomass material considered as feed material (as shown with the bullet points on the graph), the highest overall thermal efficiency (84 – 86%) is achieved when using paper mill sludge cake (feedstock #46) as feed material. These results are achieved when operating at 800 °C and 5 wt.%. These are the same conditions at which the highest H_2 and CH_4 yields as well as the gas product with the highest calorific value can be produced. However, compared to all the feed material considered, the lowest H_2 and CH_4 yields – and hence the gas product with the lowest calorific value – was achieved when using paper mill sludge cake at these conditions.

3.5 Practical Method to Selecting Appropriate Operating Conditions For a Specific Feedstock Material for SCWG

3.5.1 Method Description

In order to utilise the developed contour plots to determine the thermodynamic equilibrium yields at various operating conditions for a specific feed material, the following steps can be followed:

- ***Step 1:*** Determine the ash and the moisture content of the considered feed material. This is usually done by means of the NREL/TP-510-42621 (moisture content) and NREL/TP-510-42622 (ash content).
- ***Step 2:*** Determine the elemental composition (ultimate analysis – C, H, O, N and S content) of the considered feed material on a dry, ash-free (daf) basis. This is usually done by means of an elemental analyser (as described in Section 4.2.2).
- ***Step 3:*** Determine the molar H/C and O/C ratios of the considered material from the ultimate analysis results (dry, ash-free basis).
- ***Step 4:*** Determine the gas yields, ER, HHV of the product gas as well as the heat required for isothermal operations at different combinations of feed concentrations (5, 10, 15 and 20 wt.%) and temperatures (400, 500, 600, 700 and 800 °C) using the developed contour plots (as presented in Section 0 in this chapter as well as Section B.2 and B.5 in Appendix B).

3.5.2 Example of Method Implementation

To illustrate how these contour plots can be used, consider beet pulp (feedstock #14) as a possible feedstock for SCWG. The elemental composition, O/C and H/C ratios, proximate analysis as well as the HHV and LHV of beet pulp, are given in Table 3-12.

A summary of the results when operating at 400, 500, 600, 700 and 800 °C for all four feed concentrations are summarised in Table 3-13 to Table 3-17.

Table 3-12 Properties of beet pulp (data from Phyllis2 (2012) – ID-number #1361)

Composition	Value
Elemental composition: *(wt.%, daf)*	
C	35.50
H	4.74
O	34.09
N	1.28
S	0
***Molar ratios*:**	
O/C	0.72
H/C	1.59
Proximate analysis composition: *(wt.%)*	
Moisture content	83.30
Ash content	4.07
Volatile matter content	10.27
Fixed carbon content	2.36

The maximum thermodynamic limits for the total gas yield (108 - 122 mol/$kg_{feed,daf}$), H_2 yield (72 – 84 mol/$kg_{feed,daf}$) and HHV (20 – 24 MJ/$kg_{feed,daf}$) are achieved at 800 °C and 5 wt.%. The maximum thermodynamic limit for the CH_4 yield (18 – 21 mol/$kg_{feed,daf}$) is achieved at 400 °C (all feed concentrations) as well as at 500 °C and 20 wt.%. Furthermore, the energy recovery is the highest when operating at 800 °C and 5 wt.% (108 – 122%) while the least is required for the process to operate isothermally (28 – 31 MJ/ $kg_{feed,daf}$) when operating at both 400 and 500 °C and 20 wt.%. However, measuring the heat required for isothermal operations in terms of energy per dry, ash-free feed is not always an accurate representation, as water is also present

in the total feed and the water also needs to be heated. Hence, the heat required for isothermal operation per kg of total feed (water and biomass) is also shown in the tables. Taking into account the total feed rate (water and feed material), the least heat is required when operating at 400 °C and 5 wt.% (3.4 – 3.55 MJ/ $kg_{total\ feed}$)

TABLE 3-13 RESULTS FOR THE THERMODYNAMIC LIMITS FOR SCWG OF BEET PULP WHEN OPERATING AT 400 °C

FEED CONCENTRATION	**5 WT.%**	**10 WT.%**	**15 WT.%**	**20 WT.%**
Yields [mol/$kg_{feed,daf}$]				
Total	40 – 45	40 – 45	40 – 45	40 – 45
H_2	4 – 6	2 – 4	0 – 2.5	0 – 2
CH_4	18 – 21	18 – 21	18 – 21	18 – 21
CO	0.014 – 0.016	0.014 – 0.016	0.014 – 0.016	0.016 – 0.018
CO_2	18 – 20	18 – 20	18 – 20	18 – 20
Energy				
ER [%]	90 – 95	90 – 95	90 – 95	90 – 95
HHV [MJ/$kg_{feed,daf}$]	15 – 18	15 – 18	15 – 18	15 – 18
Q_{req} [MJ/$kg_{feed,daf}$]	68 – 71	41 – 44	31 – 34	28 – 31
Q_{req} [MJ/$kg_{feed,total}$]	3.40 – 3.55	4.10 – 4.40	4.65 – 5.10	5.60 – 6.20

TABLE 3-14 RESULTS FOR THE THERMODYNAMIC LIMITS FOR SCWG OF BEET PULP WHEN OPERATING AT 500 °C

FEED CONCENTRATION	**5 WT.%**	**10 WT.%**	**15 WT.%**	**20 WT.%**
Yields [mol/$kg_{feed,daf}$]				
Total	55 – 60	45 – 50	45 – 50	40 – 45
H_2	18 – 21	9 – 12	6 – 9	6 – 8
CH_4	15 – 18	15 – 18	15 – 18	18 – 21
CO	0.117 – 0.130	0.112 – 0.126	0.112 – 0.126	0.105 – 0.120
CO_2	22 – 24	20 – 22	20 – 22	18 – 20
Energy				
ER [%]	95 – 100	95 – 100	90 – 95	90 – 95
HHV [MJ/$kg_{feed,daf}$]	18 – 21	18 – 21	15 – 18	15 – 18
Q_{req} [MJ/$kg_{feed,daf}$]	77 – 80	44 – 47	34 – 37	28 – 31
Q_{req} [MJ/$kg_{feed,total}$]	3.85 – 4.0	4.4 – 4.7	5.10 – 5.55	5.6 – 6.2

TABLE 3-15 RESULTS FOR THE THERMODYNAMIC LIMITS FOR SCWG OF BEET PULP WHEN OPERATING AT 600 °C

FEED CONCENTRATION	5 WT.%	10 WT.%	15 WT.%	20 WT.%
Yields [mol/kg$_{feed,daf}$]				
Total	80 – 87	60 – 65	55 – 60	50 – 55
H_2	40 – 45	24 - 27	15 – 18	12 – 15
CH_4	8 – 10	12 – 14	15 – 18	15 – 18
CO	0.52 – 0.59	0.52 – 0.59	0.54 – 0.60	0.49 – 0.57
CO_2	28 – 30	24 – 26	22 – 24	20 – 22
Energy				
ER [%]	102 – 108	96 – 102	95 – 100	95 – 100
HHV [MJ/kg$_{feed,daf}$]	18 – 21	18 – 21	18 – 21	18 – 21
Q_{req} [MJ/kg$_{feed,daf}$]	81 – 84	48 – 51	38 – 41	31 – 34
Q_{req} [MJ/kg$_{feed,total}$]	4.05 – 4.20	4.80 – 5.10	5.7 – 6.15	6.20 – 6.80

TABLE 3-16 RESULTS FOR THE THERMODYNAMIC LIMITS FOR SCWG OF BEET PULP WHEN OPERATING AT 700 °C

FEED CONCENTRATION	5 WT.%	10 WT.%	15 WT.%	20 WT.%
Yields [mol/kg$_{feed,daf}$]				
Total	98 – 109	74 – 82	70 – 76	58 – 64
H_2	64 – 72	40 – 45	28 – 32	20 – 24
CH_4	3 – 4	8 – 10	12 – 14	12 – 15
CO	1.54 – 1.76	1.78 – 2.0	1.81 – 2.03	1.88 – 2.11
CO_2	34 – 36	28 – 30	24 – 26	22 – 24
Energy				
ER [%]	105 – 112	102 – 108	96 – 102	96 – 102
HHV [MJ/kg$_{feed,daf}$]	20 – 24	18 – 21	18 – 21	18 – 21
Q_{req} [MJ/kg$_{feed,daf}$]	90 – 94	50 – 54	40 – 44	30 – 34
Q_{req} [MJ/kg$_{feed,total}$]	4.5 – 4.7	5.0 – 5.4	6.0 – 6.6	6.0 – 6.8

TABLE 3-17 RESULTS FOR THE THERMODYNAMIC LIMITS FOR SCWG OF BEET PULP WHEN OPERATING AT 800 °C

FEED CONCENTRATION	5 WT.%	10 WT.%	15 WT.%	20 WT.%
Yields [mol/kg$_{feed,daf}$]				
Total	108 – 122	100 – 110	80 – 90	74 – 82
H_2	72 – 84	56 – 64	42 – 49	36 – 42
CH_4	0 – 1	3 – 4	6 – 8	9 -12
CO	2.7 – 3.24	3.64 – 4.24	4.34 – 4.96	4.48 – 5.11
CO_2	34 – 36	30 – 32	26.0 – 28	24 – 26
Energy				
ER [%]	112 – 119	105 – 112	105 – 112	98 – 105
HHV [MJ/kg$_{feed,daf}$]	20 – 24	20 – 24	20 – 24	20 – 24
Q_{req} [MJ/kg$_{feed,daf}$]	94 – 98	54 – 58	40 – 44	34 – 38
Q_{req} [MJ/kg$_{feed,total}$]	4.70 – 4.90	5.40 – 5.80	6.0 – 6.60	6.80 – 7.60

3.6 OUTCOME OF THIS CHAPTER

The aim of this chapter was to develop a method for the selection of appropriate feedstock material for SCWG based on its thermodynamic equilibrium yields (Refer back to ***Objective 1*** in Section 1.3). The key conclusions that are drawn from this chapter are:

- Both the operating conditions as well as the feedstock composition affect the outcome of the SCWG process significantly.
- The highest CH_4 yields are achieved when operating at a low gasification temperature (400 °C) and using a high dry feedstock concentration (20 wt.%).
- The highest H_2 yields and the product gas with the highest calorific value is achieved when operating at 800 °C and using a low dry feedstock concentration (5 wt.%).
- For the highest thermodynamic equilibrium CH_4 and H_2 yields (and consequently, a gas product with the highest calorific value), material with low oxygen content should be used as feedstock material. Hence, modified biomass material, such as pyrolysis char shows great potential as a possible feedstock material for SCWG, based on its composition and thermodynamic equilibrium yields.

- The contour plots developed in this study can aid in determining the thermodynamic limits for the product gas yields before a specific biomass material is considered as a possible feedstock material for SCWG. However, the screening method developed have only considers thermodynamic equilibria and no kinetic predictions or effect of feedstock composition (such as volatile matter content) are offered.

Although knowledge of the thermodynamic limits for the gas yields can serve as a primary indicator if the specific biomass material is a viable feedstock option for SCWG, these guidelines should always be verified by means of experimental work in order to consider the kinetic effects of the feedstock material. The next three chapters deal with these kinetic effects in more detail.

Chapter 4

MATERIALS AND METHODS FOR EXPERIMENTAL TESTS

4.1 INTRODUCTION

Although thermodynamic modelling is a powerful tool which can aid in the selection of suitable feed material for SCWG, it should always be verified with experimental work. Thermodynamic equilibrium modelling does not take into account the volatile matter or fixed carbon content in the feed material. These properties might have a significant influence on how easily a certain feed material is gasified in SCW (*i.e.* an indication of the kinetic effects).

The main aim of this chapter is to provide an overview of the experimental and analytical methods used during the SCWG kinetic tests conducted in this project using various wood-related materials as feedstock (primary paper sludge, *E.grandis* wood chips and char derived from pyrolysis of *E.grandis* wood (refer to ***Objectives 2 & 3***). Firstly, the origin of the feedstock materials and the methods used to characterise the feedstock material are provided. Secondly, the experimental setup is discussed with details regarding the small scale batch reactor. Thirdly, the experimental procedure and methods used to analyse the reaction products are provided, as well as the equations used to interpret the data.

4.2 FEEDSTOCK CHARACTERISATION

Primary paper waste sludge (PWS), *Eucalyptus Grandis* (*E.grandis* - EG) sawdust, as well as char products produced during slow and vacuum pyrolysis of *E.grandis* were used as feed material for SCWG experiments.

The PWS was obtained from a typical South African Kraft pulp mill, with 90% of the hardwood at the mill consisting of *Eucalyptus* species. The as-received PWS was dried in an oven at 105 °C for 12 hours to determine the moisture content (80.9 wt.%). In order to separate the clumped fibres, the PWS was milled with a Retsch hammer mill (2mm sieve).

Eucalyptus wood chips (specifically *E.grandis*) were also provided by a typical South African Kraft mill. The wood chips were milled with a Retsch hammer mill (2 mm). Once milled, the wood particles were separated according to size in an AS 200 Retsch shaker. The size of the wood chips used in the experiments was in the range between 425 and 600 µm.

The various pyrolysis char materials used in this study were produced from slow and vacuum pyrolysis of *E.grandis* during a previous study by Joubert (2013). Table 4-1 shows a summary of the conditions at which each of the pyrolysis char materials (SP1, SP3, VP1 and VP3) were produced, as well as the char, liquid and gas yields achieved, as reported by Joubert (2013). A detailed description of the pyrolysis equipment and methods used to produce these chars can be found elsewhere (Carrier et al., 2011).

TABLE 4-1 DETAILS OF PYROLYSIS METHOD USED TO PRODUCE THE VARIOUS CHAR PRODUCTS (DATA FROM JOUBERT (2013))

SPECIFICATION	VP1	SP1	SP3	VP3
Pyrolysis method	Vacuum	Slow	Slow	Vacuum
Temperature [°C]	300	300	450	450
Heating rate [°C/min]	7	7	7	7
Char yield [wt.% daf]	75.9	60	29.7	24.4
Liquid yield [wt.% daf]	9.2	13.2	31.7	52.7
Gas yield [wt.% daf]	14.9	26.8	38.6	22.9

4.2.1 PROXIMATE ANALYSIS

The proximate analysis of the feedstock samples was done by means of a TGA/DSC 1-LF1100 system (Mettler–Toledo) according to the ASTM E1131 standard method. This method measures the weight loss (in percentage) of a certain mass of sample (10 - 50 mg) during the heating of the sample to a specific temperature in the presence of an inert and oxidation gas.

The percentage weight loss in the different stages relates to the moisture content, volatile matter, fixed carbon and ash content. The sample is firstly heated from ambient to 110 °C under a N_2 flow rate of 50 ml/min. The temperature is maintained at 110 °C for 5 minutes to remove the moisture from the sample. The temperature is then increased to 900 °C to remove the volatile matter. Once the temperature reaches 900 °C, oxygen is introduced in the place of N_2 (for 5 minutes) to allow for complete combustion of the fixed carbon. The mass of sample left after combustion is the ash content. Table 4-2 provides a summary of the proximate analysis for each component.

TABLE 4-2 PROXIMATE ANALYSIS OF FEEDSTOCK MATERIAL

PROXIMATE ANALYSIS	PWS	EG	VP1	SP1	VP3	SP3
Volatile matter (VM)	78.70	83.26	68.26	74.55	30.65	26.62
Fixed Carbon (FC)	15.50	16.65	31.17	25.23	67.93	72.02
Ash content (AC)	5.80	0.09	0.57	0.22	1.52	1.36
VM/FC	5.07	5.00	2.19	2.95	0.45	0.37

4.2.2 ULTIMATE ANALYSIS

An ultimate analysis is typically used to measure the C, H, N, O and S content in biomass or coal. However, often only the C, H and N content are measured and the O and S content are determined by balance (Carrier et al., 2011). The C, H, N and S content of the PWS was determined by a TruSpec Micro elemental analyser (LECO) by the Central Analytical Facilities (CAF) at Stellenbosch University. The ultimate analysis of the E.grandis and pyrolysis char samples was determined using a CE-440 elemental analyser (Exteter Analytical) at North West University in Potchefstroom. Furthermore, the E.grandis and some of the pyrolysis samples were also analysed using a CHN628 elemental analyser (LECO) located at the Rhodes University located in Grahamstown, resulting in satisfactory reproducibility. All three of these machines use the same method based on the classical Pregl-Dumas method. During this method, a certain weight of sample is combusted in the presence of pure oxygen to form combustion gases such as N_2, NO_x, CO_2, H_2O and SO_2. A carrier gas is then used to sweep these gases over heated copper in order to remove the excess O_2 and to convert the NO_x to N_2. These gases then pass

through a series of adsorbent traps to remove products such as HCl in order to purify the gas to only CO_2, N_2, H_2O and SO_2. The gas product is then analysed by means of a GC after which the C, H, N and S (depending on the method) content are calculated based on the quantity of each combustion gas product produced. Table 4-3 provides the ultimate analysis of the feed material used in this study.

Figure 4-1(a) shows the comparison of the composition of these feed materials in terms of its molar O/C and H/C ratio (in the format of the Van Krevelen diagram). A picture of each of the feed materials is also shown on Figure 4-1(a) next to the bullet showing the composition. Figure 4-1(b) shows the fixed carbon as a function of the volatile matter content of each of the feed materials. Figure 4-2 shows the correlation between the volatile matter content of the feed material and the O/C ratios.

TABLE 4-3 ULTIMATE ANALYSIS OF FEED MATERIALS USED IN THIS STUDY

ULTIMATE ANALYSIS	PWS	EG	VP1	SP1	SP3	VP3
C	49.37	47.19	56.06	54.62	77.96	74.48
H	5.92	5.77	4.88	5.37	3.33	2.73
N	0.08	0.21	0.26	0.24	0.38	0.35
O[a]	44.63	46.82	38.80	39.77	18.34	22.44
Molar ratios						
H/C	1.43	1.46	1.04	1.17	0.51	0.44
O/C	0.68	0.75	0.52	0.55	0.18	0.23
O/H	0.48	0.51	0.50	0.47	0.35	0.52

[a]Obtained by difference

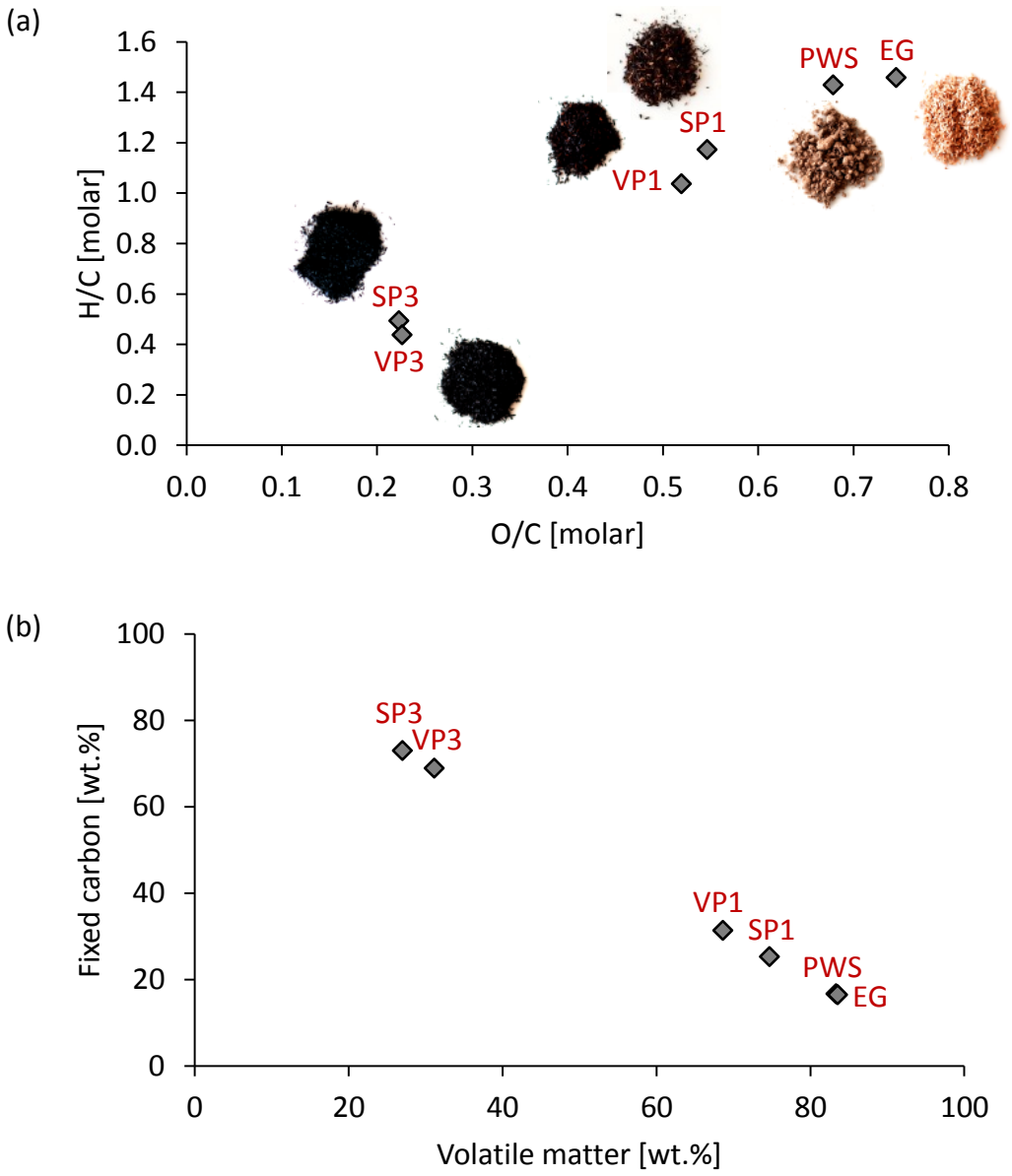

FIGURE 4-1 (A) VAN KREVELEN DIAGRAM SHOWING THE O/C AND H/C CONTENT OF EACH OF THE FEEDSTOCK MATERIAL USED; (B) COMPARISON OF FIXED CARBON AND VOLATILE MATTER CONTENT OF EACH OF THE FEEDSTOCK MATERIAL USED

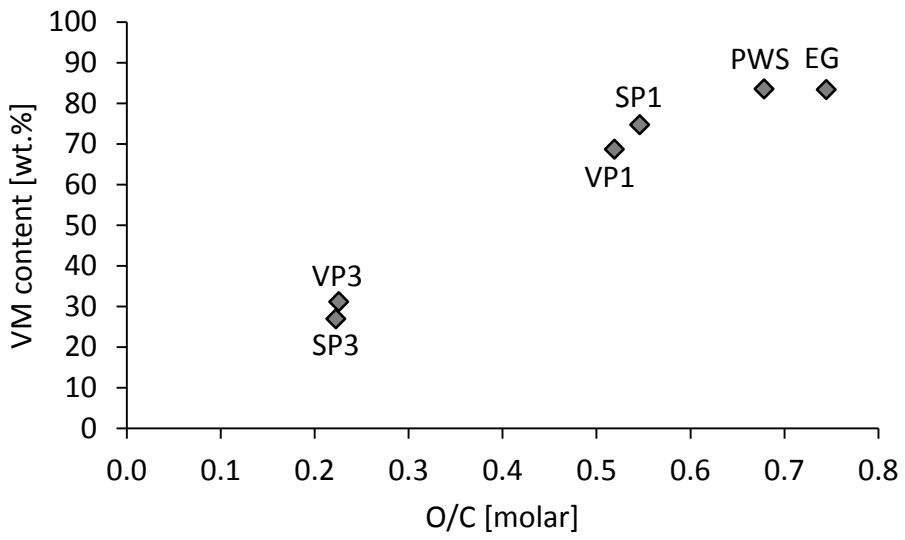

FIGURE 4-2 CORRELATION BETWEEN THE VOLATILE MATTER CONTENT AND THE O/C RATIO IN THE FEED MATERIAL

4.2.3 LIGNOCELLULOSIC COMPOSITION

The lignocellulosic compositions of the *E.grandis* wood and the PWS were determined externally in accordance to the National Renewable Energy Laboratory (NREL) standard procedures NREL/TP-510-52618, as described in Sluiter et al. (2005), and NREL/TP-510-42619, as described in Sluiter et al. (2011) and . Table 4-4 provides the lignocellulosic composition of the PWS and *E.grandis*.

TABLE 4-4 LIGNOCELLULOSIC COMPOSITION OF PWS AND *E.GRANDIS* WOOD USED IN THIS STUDY (DRY, ASH-FREE BASIS)

COMPONENT	PWS	EG WOOD
Extractives	6.3	5.28
Lignin	20.1	32.46
Glucan	58.7	50.47
Xylan	15.3	11.80
Extractives	6.30	4.74

4.3 CATALYSTS

4.3.1 HETEROGENEOUS CATALYST (Ni/Al_2O_3-SiO_2)

The Ni/Al_2O_3-SiO_2, commercially available heterogeneous catalyst, used in this study was purchased from Sigma Aldrich (product number: 208779). The catalyst consist of 65 wt.% nickel on silica/alumina support.

The Brunauer-Emmett Teller (BET) surface area of the catalyst was obtained by means of N_2 adsorption using a 3Flex Surface Characterization Analyser from Micromeritics using liquid N_2 at -196 °C. The samples was first degassed on a VacPrep 061 at 90 °C for 1 hour and then at 250 °C for 12 hours. The samples was then place on the instrument and degassed once again (in situ) at 90 °C for 1 hour and then at 250 °C for 15 hours. After degassing, liquid nitrogen at -196 °C was introduced. The BET equation was then used to evaluate the equilibrium points BET between the 0 – 0.22 P/P_0 range. From these results, the BET surface area was determined.

The particle size distribution of the Ni/Al_2O_3-SiO_2 catalyst was determined by means of a light scattering analysis technique using a high definition digital particle size analyser (Saturn DigiSizer 5200). Figure 4-3(a) shows the adsorption-desorption isotherm of the catalyst, while the particle size distribution is shown in Figure 4-3(b). A summary of the characteristics of the catalyst is given in Table 4-5.

TABLE 4-5 PROPERTIES OF Ni/Al_2O_3-SiO_2 CATALYST

CATALYST PROPERTY	VALUE
BET surface area	178 m^2/g
Per-unit mass pore volume	0.290 cm^3/g
Average pore size	6.567 nm
Average particle size	11.24 µm

a) Homogeneous catalyst (K_2CO_3)

Anhydrous potassium carbonate (K_2CO_3) with a purity of 99.5% was used as the homogeneous catalyst and was purchased from Merck (product number: SAAR5041950EM).

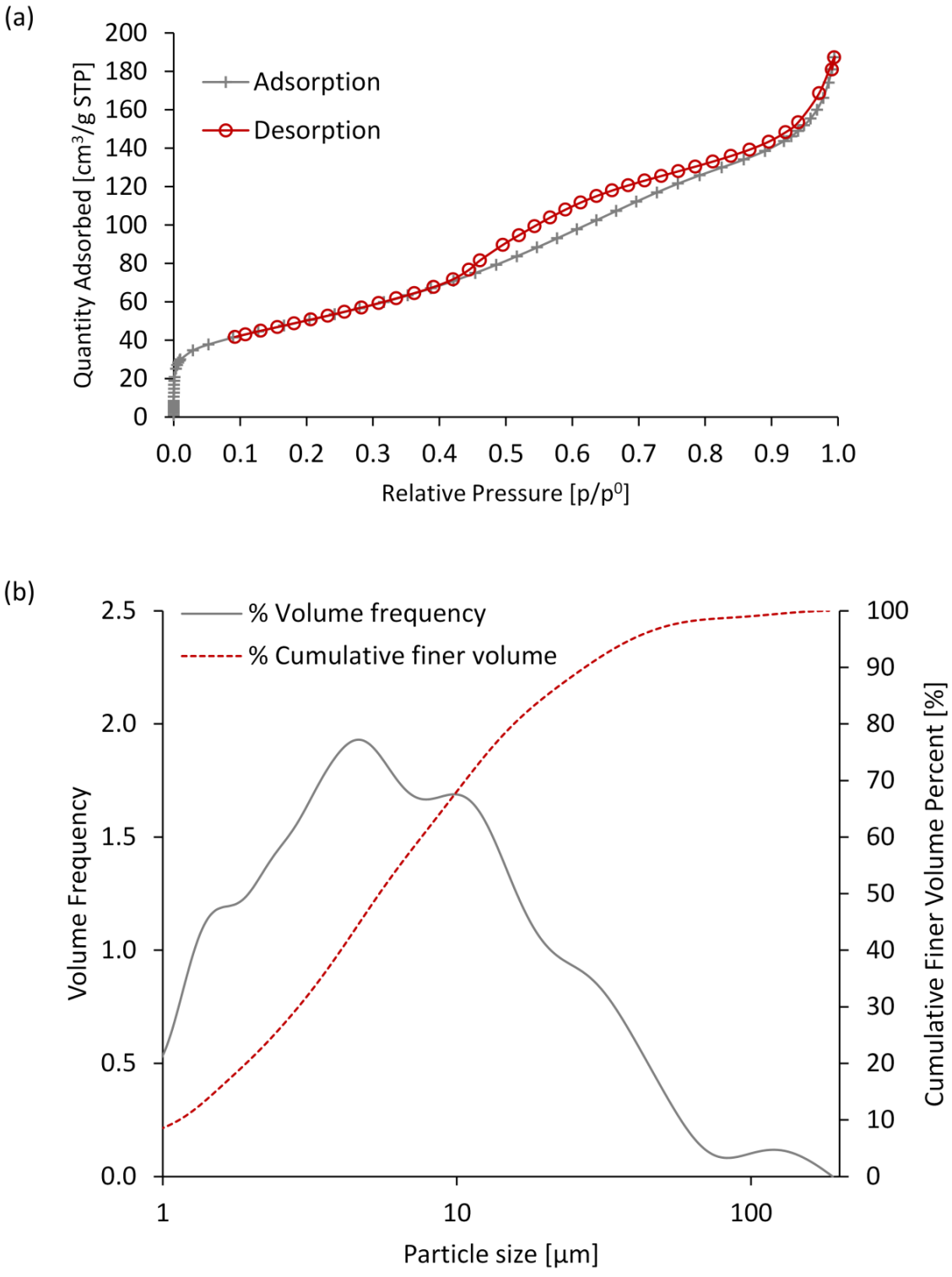

FIGURE 4-3 (A) ADSORPTION-DESORPTION ISOTHERMS FOR NI/AL_2O_3-SiO_2 CATALYST; (B) PARTICLE SIZE DISTRIBUTION OF NI/AL_2O_3-SiO_2 CATALYST

4.4 Batch Reactor Apparatus

SCWG experiments were carried out in a small batch reactor system with a total volume of 49 cm^3. Unless otherwise stated, the parts were obtained from HiP (High Pressure Equipment Company, USA) and made from stainless steel (SS316). Figure 4-4 shows a schematic of the reactor and additional components. A more detailed drawing of the reactor setup is shown in Figure C-1.

The reactor consists of standard medium pressure tubing with an internal volume of 41 cm^3. The outer diameter of the reactor tube is 25.4 mm (1”), the inner diameter is 14.3 mm (9/16") and the length is 254 mm (10”). A type K thermocouple (WIKA, SS310) with a diameter of 3.2 mm (1/8”) is attached to the bottom of the reactor to ensure sufficient contact with the reactor media. A pressure relief valve (factory set at 40 MPa), pressure transmitter with a cooling element (rated from 0 – 40 MPa purchased from WIKA) and a needle valve are connected to a ¼” medium pressure cross piece. The reactor is connected to the cross piece *via* a 152.4 mm (6”) long medium pressure tube with an outer diameter of 6.4 mm (¼”) and inner diameter of 2.73 mm (0.109”). The pressure transmitter and thermocouple are connected to a pressure and temperature indicator (WIKA) and a S210 HUATO data logger (WIKA). More detail regarding all the reactor parts are given in Section C.1 in Appendix C.

4.5 Experimental Procedure

Figure 4-4 shows a schematic of the entire experimental setup and procedure. A brief description of the experimental procedure for a typical experiment will follow. See Section C.1 in Appendix C for a more detailed explanation of the steps followed.

In order to control the feedstock and catalyst loading (i.e. the feedstock-to-water ratio, as well as the catalyst-to-feedstock ratio of each experiment), the specific feed material was dried overnight at 105 °C before each experiment. A known mass of the dried feed material, catalyst, and distilled water were added to the reactor, with relative quantities depending on the desired feedstock and catalyst loading (feedstock loadings were calculated on a catalyst free base). The total amount of feedstock and water added for each experiment was 6.016 g for each

experiment. This mass of feedstock-water mixture ensured that, when the reactor content reached 450 °C, the pressure in the reactor was always above 25 MPa.

Once the feedstock, water and catalyst were loaded into the reactor, the reactor was closed tightly with a torque wrench. Air was removed with a vacuum pump (Welch Gem 1.0). Next, the reactor was pressurised with pure nitrogen to 2.1 – 2.3 MPa, serving as a leak test. The pressure and temperature in the reactor after pressurisation with N_2 was logged and used to calculate the moles of N_2 added to the reactor. This was done by addressing the non-ideality of a gas at elevated pressures with the Pitzer correlation Eq. 4-1, as described in Smith et al. (2005) (see Section C.4 in Appendix C).

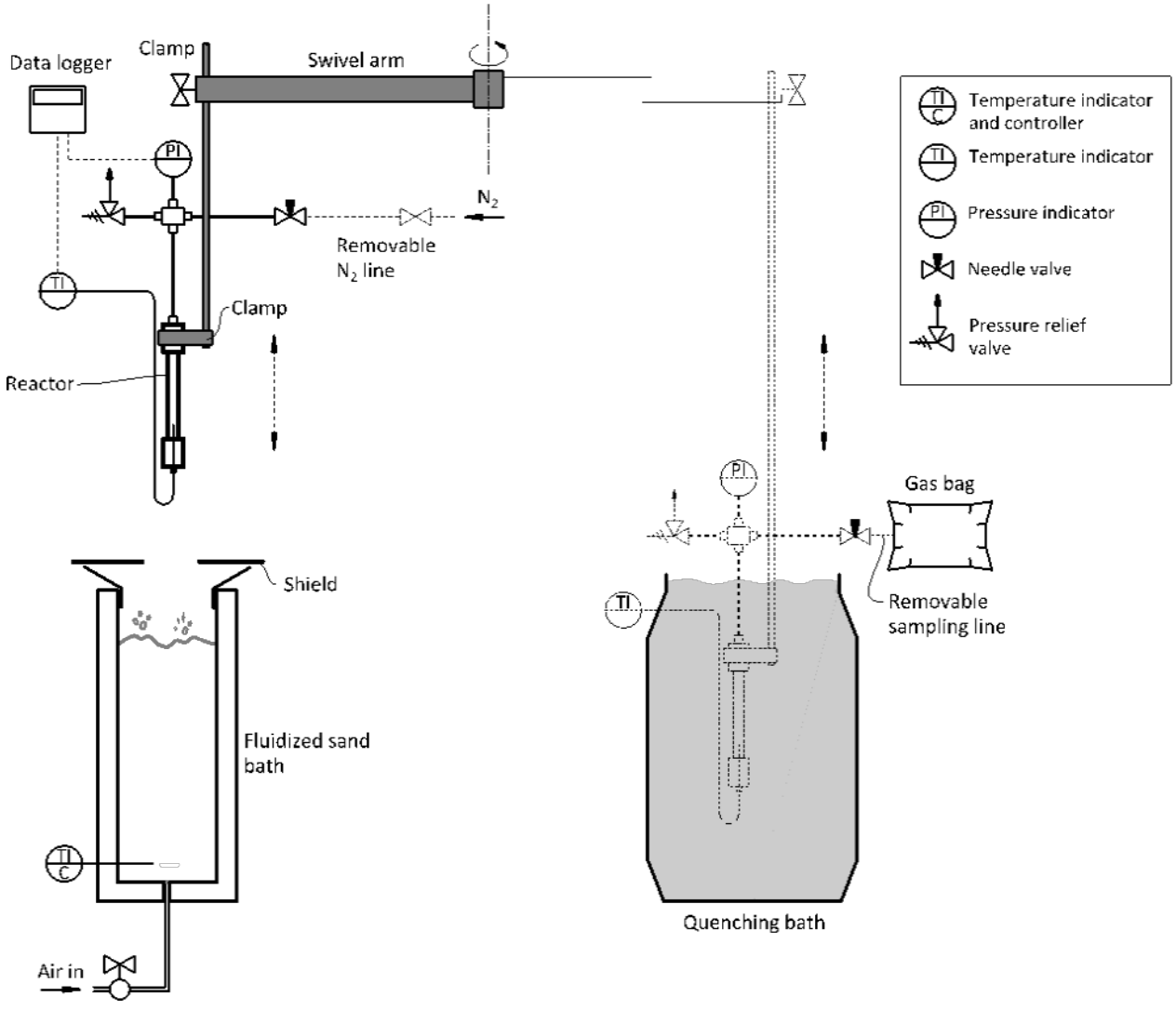

FIGURE 4-4 SCHEMATIC SHOWING THE EXPERIMENTAL SETUP

$$n_{N_2} = \frac{P(V_{reactor} - V_{feed})}{z_{N_2} RT} \quad 4\text{-}1$$

A mechanical swivel arm was used to place the reactor vertically into a pre-heated Techne SBL-2D sand bath fitted with a TC-8D temperature controller. The reactor was then heated to the specific reaction temperature of 450 °C at an average heating rate of approximately 40 °C/min. The "hold time" started as soon as the reactor reached 450 °C. After the selected hold time (0, 15, 30, 60 or 120 minutes), the reactor was removed from the sand bath and quenched to room temperature in a cold water bath. Once the reactor temperature reached room temperature, the pressure and temperature were noted and the gaseous product was collected in a pre-evacuated gas bag (purchased from SKC) through the needle valve. The temperature and pressure were logged continuously throughout the duration of each experiment, as shown Figure 4-5(a). The typical P-T profile during the heat-up and cool-down phases compared to the isochoric P-T curve of water are shown in Figure 4-5(b). In order to minimise the possible catalytic effect of the reactor wall, the reactor was used numerous times prior to the experiments, using glucose as feedstock material.

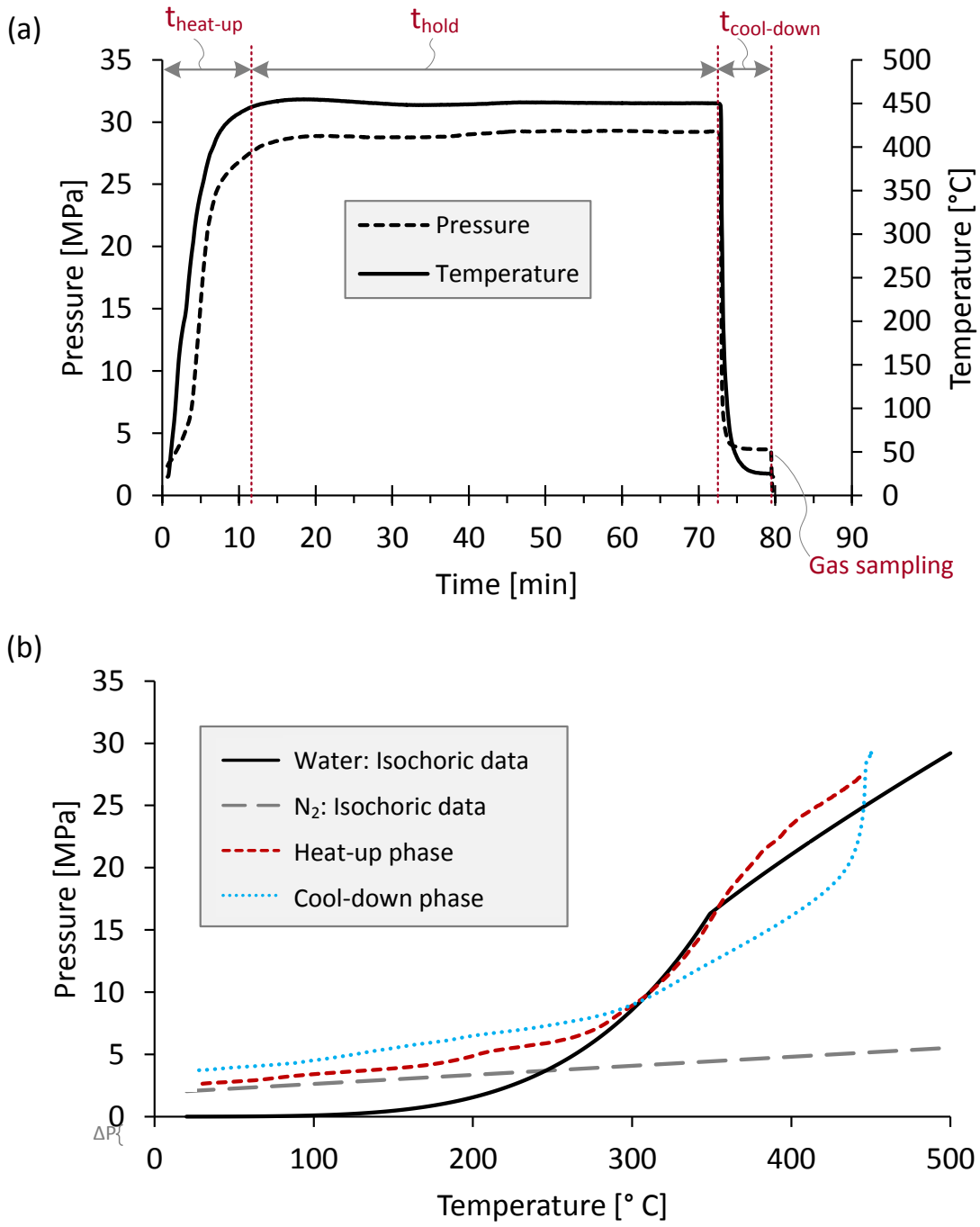

FIGURE 4-5 TYPICAL TEMPERATURE/PRESSURE PROFILES OBTAINED FOR A TYPICAL EXPERIMENT (HEAT-UP AND COOL-DOWN DATA FROM EXPERIMENT PWS18 – SEE CHAPTER 5. WATER AND N_2 ISOCHORIC DATA FROM LEMMON ET AL. (2011)).

4.6 Separation and Analysis of Products

4.6.1 Product gas analysis

In order to determine the molar fractions in the gas phase, a gas chromatograph (GC) method had to be established. This was done using an off-line Varian CP 3380 gas chromatograph fitted with a thermal conductivity detector (TCD). A Carbonex® 1000 (Supelco) packed column (15 ft. x $^1/_8$”) made from stainless steel with a 60/80 mesh was used. Argon (at a flow rate of 26.9 cm^3/min) was used as the carrier gas. The gases were firstly separated in the packed column and then quantified on the basis of their thermal conductivity by means of the TCD. A gas mixture purchased from Afrox with a known composition of N_2, H_2, CO, CH_4 and CO_2 as well as the pure N_2, H_2, CO, CH_4, CO_2, C_2H_6 and C_2H_4 were used as external standards for calibration purposes. Section C.3 Appendix C for a detailed description of the GC method used together with the calibration curves obtained for each gas product.

During an analysis, the oven temperature was maintained at 120 °C for 6 minutes for the detection of H_2, N_2, CO and CH_4 after which it was increased to 225 °C at a heating rate of 20 °C/min and again maintained for 10 minutes for the detection of CO_2, C_2H_4 and C_2H_6.

Thermodynamic predictions have shown that the presence of higher molecular weight gases (such as C_2H_4, C_2H_6, C_3H_6, C_3H_8 and C_4H_{10}) in the product gas should be negligible (as shown in Chapter 3 of this dissertation). Nevertheless, various authors have shown that small quantities of these gases may sometimes be present in the gas product (Castello et al., 2013; Zöhrer and Vogel, 2013). In the first part of this work with primary paper sludge as feed material (results presented in Chapter 5), the product gas was only analysed for N_2, H_2, CO, CH_4 and CO_2 in each experiment. These five gases comprised 97 – 100% of the total gas product for all the experiments. The composition of the gas phase presented in Chapter 5 and Chapter 6 is on a N_2-free basis, consisting of H_2, CO, CH_4 and CO_2, with C_{2+} gases being the balance. This assumption did however not affect the accuracy of the moles of H_2, CH_4, CO and CO_2 produced, as these were determined relative to the moles of N_2 in the product gas. For the second part of the work when pyrolysis char and *E.grandis* were used as feed material (results presented in Chapter 6),

the gas product was also analysed for ethylene (C_2H_4) and ethane (C_2H_6). The gas analyses were performed in duplicate with a standard error of less than 3% for all analyses.

The total moles of product gas, as well as the moles of each gas produced could then be determined relative to the moles of N_2 added to the reactor during the pressurisation step. Furthermore, the moles of each gas dissolved in the liquid phase after gas sampling was determined by means of Henry's law using Eq. 4-2 and 4-3. Values for the temperature dependence constant and the Henry's law constant for solubility in water at 298.15 K (k_H^0) for each gas were obtained from Sanders (2015) and are given in Table 4-6.

TABLE 4-6 HENRY'S CONSTANT DATA (FROM SANDERS (2015))

GAS COMPONENT	k_H^0 [MOL/KG.MPA]	$\frac{dlnk_H}{d\left(\frac{1}{T_{end}}\right)}$
H_2	7.8 x 10^{-5}	500
N_2	6.0 x 10^{-5}	1300
CO	9.9 x 10^{-5}	1300
CH_4	1.4 x 10^{-4}	1600
CO_2	3.5 x 10^{-3}	2400
C_2H_6	1.9 x 10^{-4}	2300
C_2H_4	4.7 x 10^{-3}	1800

$$n_{i,dissolved} = k_H m_{H_2O} y_i P_{end} \quad 4\text{-}2$$

$$k_H(T) = k_H^0 exp\left[\frac{dlnk_H}{d\left(\frac{1}{T_{end}}\right)}\left(\frac{1}{T_{end}} - \frac{1}{298.15}\right)\right] \quad 4\text{-}3$$

4.6.2 LIQUID PHASE ANALYSES

After analysing the gas, the reactor was opened and the content was emptied into a clean, dry beaker, yielding a solid/liquid phase product. This solid/liquid product was filtered with a pre-weighed 0.45 µm cellulose acetate filter paper (from Amtast). The filtered liquid phase (water soluble phase, WSP) was weighed, after which the total organic carbon (TOC) and total carbon

(TC) content were determined by an independent laboratory with an Analytik Jena CN (according to the SALM.25 standard and by means of thermocatalytic oxidation method).

The emptied reactor was subsequently rinsed with pure methanol (from Merck) to remove any remaining solids from the reactor. The methanol-solid mixture was filtered over the same filter paper as the WSP, yielding another liquid phase (methanol soluble phase, MSP) and a solid phase (consisting of recovered catalyst and/or char product). The water content of the MSP was measured by means of Karl Fischer titration with a 701 Titrino unit.

4.6.3 Solid Phase Analyses

The solid phase was dried overnight at 105 °C in a vacuum oven, cooled in a desiccator and weighed. The solid phase (char and/or recovered catalyst) was analysed for its carbon, hydrogen and nitrogen content with an elemental analyser (TruSpec Micro from LECO). Using all these results, a total mass balance could be calculated, as well as the total yield of each phase (gas, WSP, MSP and solid). Furthermore, the carbon fractions reporting to the solid, aqueous liquid (WSP) and gas phases were determined for each experiment. Hence, the fractions of carbon reporting to both the MSP were assumed to be the balance. In the cases when the C_2H_6 and C_2H_4 content were not analysed for in the gas phase, the balance was assumed to be the fraction of carbon reporting to both the MSP and C_{2+} gases.

4.7 Data Interpretation and Calculations

Figure 4-6 shows a schematic of the experimental procedure followed to separate and analyse the reaction products as well as to calculate the overall mass balance and the carbon balance. A detailed example of the sample calculations for a typical experiment is given in Section C.4 in Appendix C.

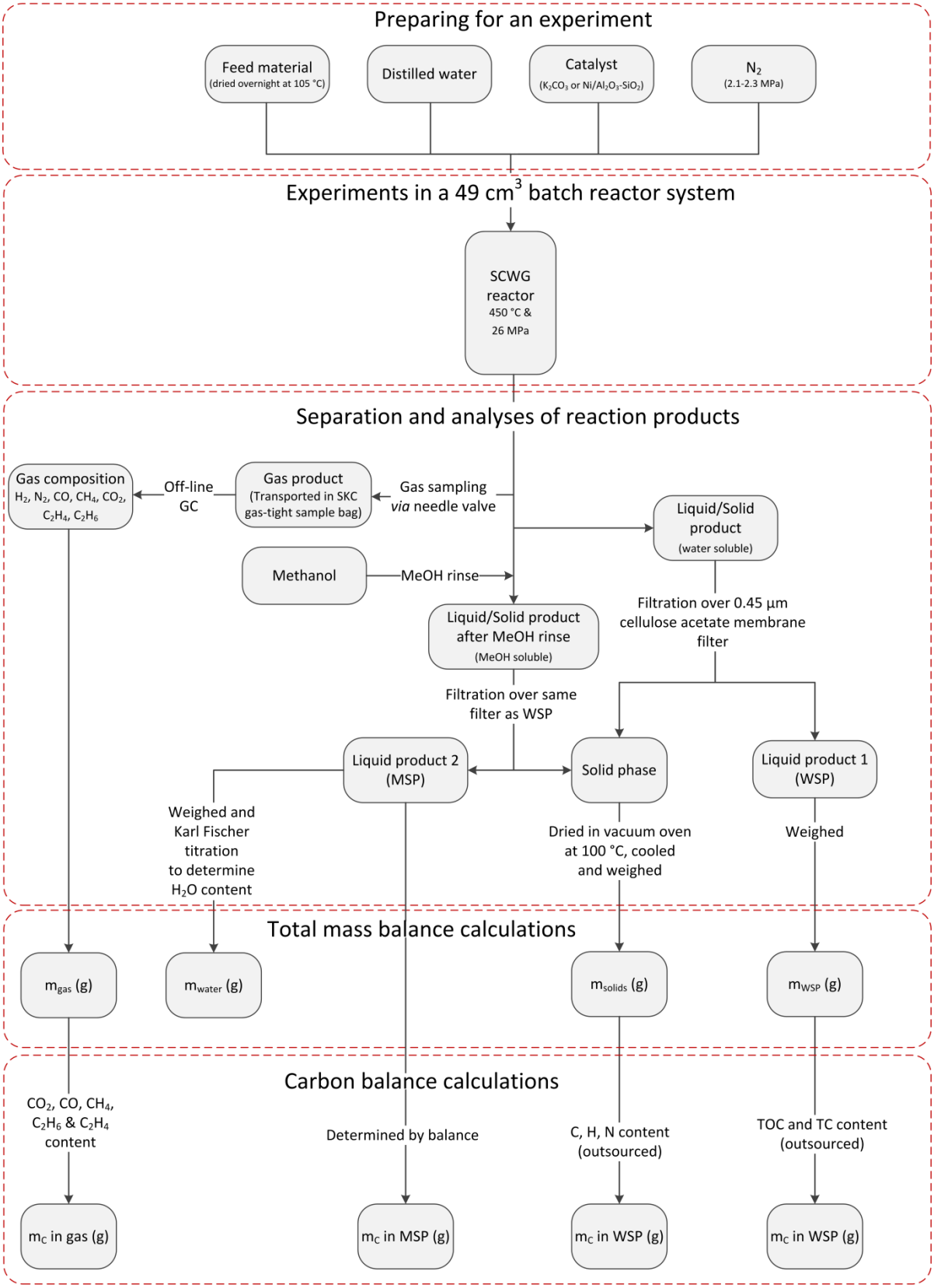

FIGURE 4-6 FLOW SHEET SHOWING THE SEPARATION AND ANALYSIS OF REACTION PRODUCTS

The molar composition of the product gas on a N_2-free basis (y_i) was determined by Eq. 4-4.

$$y_i = \frac{n_i}{n_{total\ gas\ without\ N_2}} \quad 4\text{-}4$$

The individual molar gas yield (Y_i) is defined the moles of a specific gas produced per kg of dry feed material used in the experiment:

$$Y_i[\frac{mol}{kg_{feed,dry}}] = \frac{n_i}{m_{feed,dry}} \quad 4\text{-}5$$

The gasification efficiency (GE) is defined as the mass of gas produced per mass of dry feed material used in the experiment:

$$GE\ [\%] = \frac{m_{gas,total,N_2free}}{m_{feed,dry}} \times 100 \quad 4\text{-}6$$

The carbon gasification efficiency (CE) is defined as the moles of carbon in the gas product per moles of carbon in the dry feed material:

$$CE\ [\%] = \frac{n_{CH_4} + n_{CO_2} + n_{CO}}{n_{C,feed,dry}} \times 100 \quad 4\text{-}7$$

The hydrogen gasification efficiency (HE) is defined as the moles of hydrogen in the gas product (specifically in CH_4 and H_2) per moles of hydrogen in the dry feed material:

$$HE\ [\%] = \frac{2n_{H_2} + 4n_{CH_4}}{n_{H,feed,dry}} \times 100 \quad 4\text{-}8$$

The energy recovery to the gas phase (ER) is defined as the lower heating value of the product gas per lower heating value of the dry feed material:

$$ER\ [\%] = \frac{\sum m_{i,gas} LHV_{i,gas}}{m_{PWS} LHV_{PWS,dry}} \times 100 \quad 4\text{-}9$$

The hydrogen selectivity (S_{H_2}) is defined of the moles of hydrogen in H_2 per moles of hydrogen in CH_4:

$$S_{H_2} = \frac{n_{H_2}}{2n_{CH_4}} \quad 4\text{-}10$$

4.8 Experimental Design

Experiments were conducted using different feedstock material (PWS, *E.grandis* and pyrolysis chars SP1, VP1, SP3 or VP3). Reaction time and catalyst type and loading were used as factors. K_2CO_3 was selected as the homogeneous catalyst and the commercially available Ni/Al_2O_3-SiO_2 catalyst was chosen as the heterogeneous catalyst. Experiments were conducted at different catalyst loads (0 – 1 g/g_{PWS}) and different reaction times (15 – 120 min) in a batch reactor, using either K_2CO_3 or Ni/Al_2O_3-SiO_2 as catalyst. This was done in order to investigate the possible kinetic effects of each type of feed material. The experimental conditions under which the experiments using PWS as feed material were conducted are provided in Table 4-7, Table 4-8 and Table 4-9.

Table 4-7 Details of experiments conducted with PWS to investigate the effect of catalyst loading

Parameter	Value
Catalyst type	K_2CO_3 or Ni/Al_2O_3-SiO_2
Catalyst loading	0, 0.1, 0.5 and 1 $g/g_{PWS,dry}$
Hold time	60 min
Temperature	450 °C
PWS concentration	10 wt.% (dry)

Table 4-8 Details of experiments conducted with PWS to investigate the effect of hold time

Parameter	Value
Catalyst type	No catalyst, K_2CO_3 or Ni/Al_2O_3-SiO_2
Catalyst loading	0 and 0.5 $g/g_{PWS,dry}$
Hold time	15, 30, 60 and 120 min
Temperature	450 °C
PWS concentration	10 wt.% (dry)

TABLE 4-9 DETAILS OF EXPERIMENTS CONDUCTED WITH PWS TO INVESTIGATE THE EFFECT OF DRY FEED CONCENTRATION

PARAMETER	VALUE
Catalyst type	Ni/Al_2O_3-SiO_2
Catalyst loading	0.5 $g/g_{PWS,dry}$
Hold time	60 min
Temperature	450 °C
PWS concentration	2.5, 5, 10 and 20 wt.% (dry)

Experiments using *E.grandis* wood chips and pyrolysis chars SP1, VP1, SP3 and VP3 as feed material were also conducted under various operating conditions (see Table 4-10, Table 4-11 and Table 4-12).

TABLE 4-10 DETAILS OF EXPERIMENTS CONDUCTED WITH *E.GRANDIS* AND PYROLYSIS CHAR TO INVESTIGATE THE EFFECT OF FEEDSTOCK TYPE

PARAMETER	VALUE
Feed type	*E.grandis* (EG), SP1, VP1, SP3 and VP3
Catalyst type	No catalyst, K_2CO_3 or Ni/Al_2O_3-SiO_2
Catalyst loading	0, or 0.5 $g/g_{PWS,dry}$
Hold time	60 min
Temperature	450 °C
Feed concentration	10 wt.% (dry)

TABLE 4-11 DETAILS OF EXPERIMENTS CONDUCTED WITH *E.GRANDIS* AND PYROLYSIS CHAR TO INVESTIGATE THE EFFECT OF NI/AL_2O_3-SIO_2 LOADING

PARAMETER	VALUE
Feed type	*E.grandis* (EG), SP1 and SP3
Catalyst type	Ni/Al_2O_3-SiO_2
Catalyst loading	0, 0.1, 0.5 and 1 $g/g_{PWS,dry}$
Hold time	60 min
Temperature	450 °C
Feed concentration	10 wt.% (dry)

TABLE 4-12 DETAILS OF EXPERIMENTS CONDUCTED WITH *E.GRANDIS* AND PYROLYSIS CHAR TO INVESTIGATE THE EFFECT OF HOLD TIME

PARAMETER	VALUE
Feed type	*E.grandis* (EG), SP1 and SP3
Catalyst type	Ni/Al_2O_3-SiO_2
Catalyst loading	0.5 $g/g_{feed,dry}$
Hold time	At T = 400 °C, 0, 15, 30 and 60 min
Temperature	450 °C
Feed concentration	10 wt.% (dry)

4.9 OUTCOME OF THIS CHAPTER

This chapter provided an overview of the materials and methods used during the experimental work as well as the conditions at which each experiment was conducted. The results of these 20 experiments, using PWS as feed material, are presented and discussed in Chapter 5. In addition, the reproducibility of the experiments are presented and discussed in Section 5.3.2. Furthermore, the results of the 35 experiments using *E.grandis* and pyrolysis char as feed material are presented and discussed in Chapter 6.

Chapter 5

SCWG OF PRIMARY PAPER SLUDGE**

5.1 INTRODUCTION

The aim of this chapter is to determine how close to the calculated equilibrium gas yields one can come during SCWG of primary paper waste sludge (PWS) by applying a reasonable catalyst loading and reaction time. Furthermore, the feasibility of using primary paper waste sludge as feed material for SCWG at a low operating temperature was also assessed (refer back to ***Objective 2*** in Section 1.3).

More specifically, the work presented in this chapter compares the thermodynamically predicted gas yields and gasification efficiencies for primary paper sludge from a South African kraft mill with experimentally measured values using a homogeneous (K_2CO_3) and heterogeneous (Ni/Al_2O_3-SiO_2) catalyst. The method developed in Chapter 3 was used to determine the thermodynamic limits of the PWS at various operating conditions. Furthermore, twenty experiments at various hold times (15 – 120 min), K_2CO_3 and Ni/Al_2O_3-SiO_2 loadings (0 – 1 g/g_{PWS}) and feedstock concentrations (2.5 – 20 wt.%) were conducted at an operating temperature of 450 °C. Additionally, the energy-recovery potential of SCWG of primary paper sludge at a low operating temperature (450 °C) is presented for the first time. H_2, CH_4, CO and CO_2 yields were measured and compared with calculated thermodynamic equilibrium yields.

** Part of this chapter has been published in: Louw, J., Schwarz, C.E., Burger, A.J., *Catalytic supercritical water gasification of primary paper sludge using a homogeneous and heterogeneous catalyst: Experimental vs thermodynamic equilibrium results*. Bioresource Technology, Vol 201 (2016), pp 111-120.

5.2 Determining the Thermodynamic Equilibrium Limits for PWS

The contour plots developed in Chapter 3 were used to determine the thermodynamic limits for PWS at an operating temperature of 400 °C, 450 and 500 °C and feed concentrations of 5, 10, 15 and 20 wt.%. The ranges for the thermodynamic gas yields and gasification efficiencies of PWS at 400, 450 and 500 °C are shown in Table 5-1, Table 5-2 and Table 5-3, respectively.

When considering the two energy-rich gases formed during SCWG, *viz.* H_2 and CH_4, maximum H_2 yields are expected at low feed concentrations and high operating temperatures, while the opposite is true for CH_4. Hence, in order to obtain reasonable yields for both H_2 and CH_4 and to minimise the CO_2 yield, it was decided to conduct experiments at a temperature of 450 °C and PWS feed concentration of 10 wt.%. Figure D-1 in Appendix D provides a graph of the yields of each gas at the different operating temperatures and feed concentrations. Figure 5-1 and Figure 5-2 at an operating temperature of 450 °C and dry feed concentration of 10 wt.%. PWS is indicated with a bullet point on each of the graphs.

Table 5-1 Results for the thermodynamic limits for SCWG of PWS when operating at 400 °C and 25 MPa

Feed Concentration	5 wt.%	10 wt.%	15 wt.%	20 wt.%
Yields [mol/kg$_{feed,daf}$]				
Total	40 – 45	40 – 45	40 – 45	35 – 40
H_2	4 – 6	2 – 4	0 – 2	0 – 2
CH_4	18 – 21	18 – 21	18 – 21	18 – 21
CO	0.014 – 0.016	0.014 – 0.016	0.014 – 0.016	0.016 – 0.018
CO_2	20 – 22	18 – 20	18 – 20	18 – 20
Energy				
ER [%]	95 – 100	90 – 95	90 – 95	
HHV [MJ/kg$_{feed,daf}$]	18 – 21	15 – 18	15 – 18	15 – 18
Q_{req} [MJ/kg$_{feed,daf}$]	68 – 71	41 – 44	31 – 34	28 – 31
Q_{req} [MJ/kg$_{feed,total}$]	3.4 – 3.55	4.1 – 4.4	4.65 – 5.1	5.6 – 6.2

TABLE 5-2 RESULTS FOR THE THERMODYNAMIC LIMITS FOR SCWG OF PWS WHEN OPERATING AT 450 °C AND 25 MPA

FEED CONCENTRATION	5 WT.%	10 WT.%	15 WT.%	20 WT.%
Yields [mol/kg$_{feed,daf}$]				
Total	50 – 55	45 – 50	40 – 45	40 – 45
H_2	10 – 11	4 – 5	3 – 4	2 – 3
CH_4	18 – 21	18 – 21	18 – 21	18 – 21
CO	0.040 – 0.045	0.045 – 0.050	0.045 – 0.050	0.045 – 0.050
CO_2	20 – 22	20 – 22	20 – 22	20 – 22
Energy				
ER [%]	95 – 100	95 – 100	95 – 100	95 – 100
HHV [MJ/kg$_{feed,daf}$]	18 – 21	15 – 18	15 - 18	16 – 20
Q_{req} [MJ/kg$_{feed,daf}$]	78 – 82	44 – 47	35 – 38	28 – 31
Q_{req} [MJ/kg$_{feed,total}$]	3.9 – 4.1	4.4 – 4.7	5.25 – 5.7	5.6 – 6.2

TABLE 5-3 RESULTS FOR THE THERMODYNAMIC LIMITS FOR SCWG OF PWS WHEN OPERATING AT 500 °C AND 25 MPA

FEED CONCENTRATION	5 WT.%	10 WT.%	15 WT.%	20 WT.%
Yields [mol/kg$_{feed,daf}$]				
Total	55 – 60	50 – 55	45 – 50	45 – 50
H_2	15 – 18	9 – 12	6 – 9	4 – 6
CH_4	15 – 18	15 – 18	18 – 21	18 – 21
CO	0.117 – 0.130	0.112 – 0.126	0.112 – 0.126	0.120 – 0.135
CO_2	22 – 24	22 – 24	20 – 22	20 – 22
Energy				
ER [%]	95 – 100	95 – 100	95 – 100	90 – 95
HHV [MJ/kg$_{feed,daf}$]	18 – 21	18 – 21	15 – 18	15 – 18
Q_{req} [MJ/kg$_{feed,daf}$]	77 – 80	44 – 47	34 – 37	31 – 34
Q_{req} [MJ/kg$_{feed,total}$]	3.85 – 4.4	4.4 – 4.7	5.1 – 5.55	6.2 – 6.8

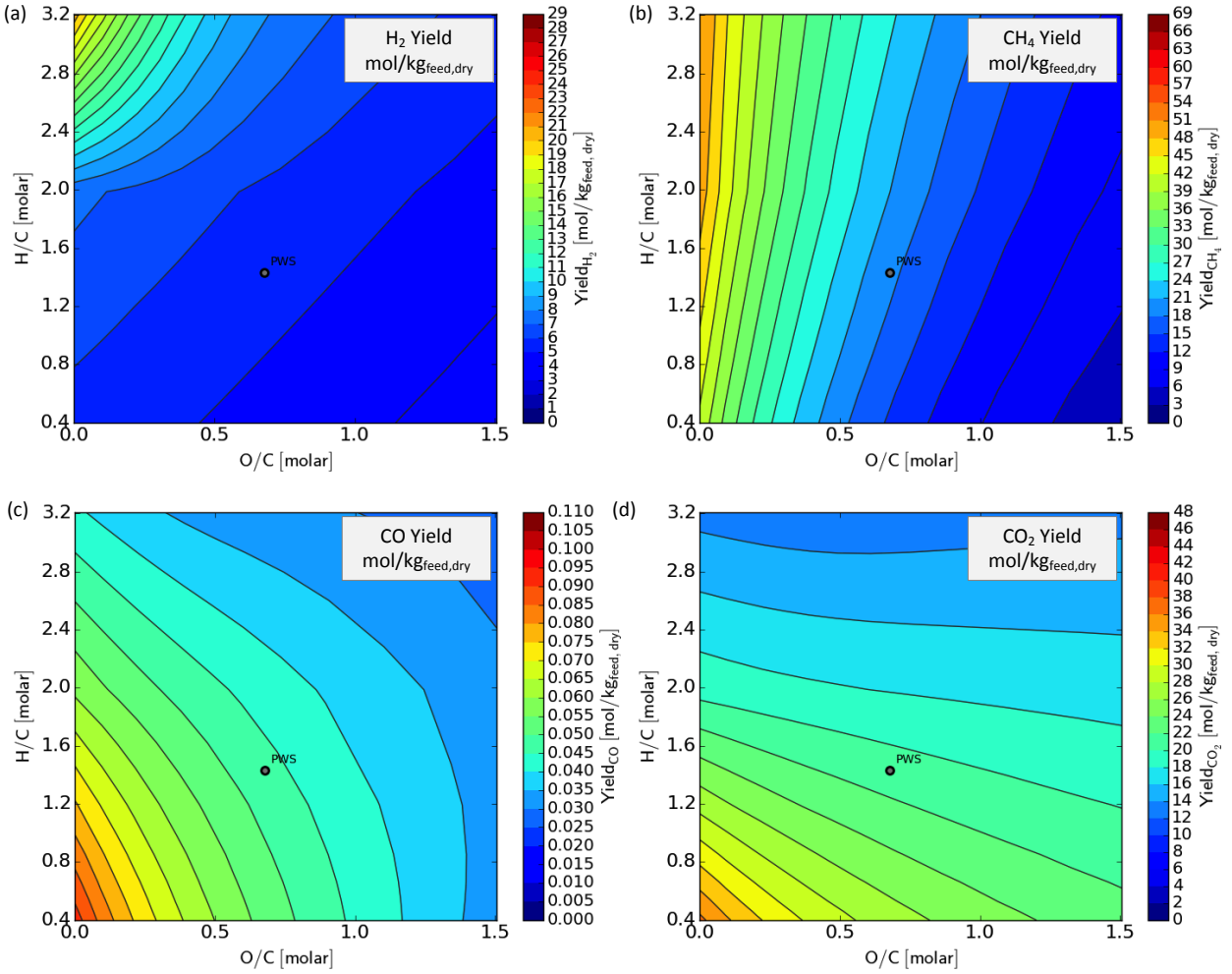

FIGURE 5-1 GENERALISED CONTOUR PLOT COMBINED WITH A VAN KREVELEN DIAGRAMS SHOWING THE EFFECT OF FEEDSTOCK COMPOSITION ON THE CALCULATED THERMODYNAMIC EQUILIBRIUM YIELDS AT 450 °C AND FEEDING 10 WT.% DRY MATTER CONTENT: (A) H_2 YIELD, (B) CH_4 YIELD, (C) CO YIELD, (D) CO_2 YIELD.

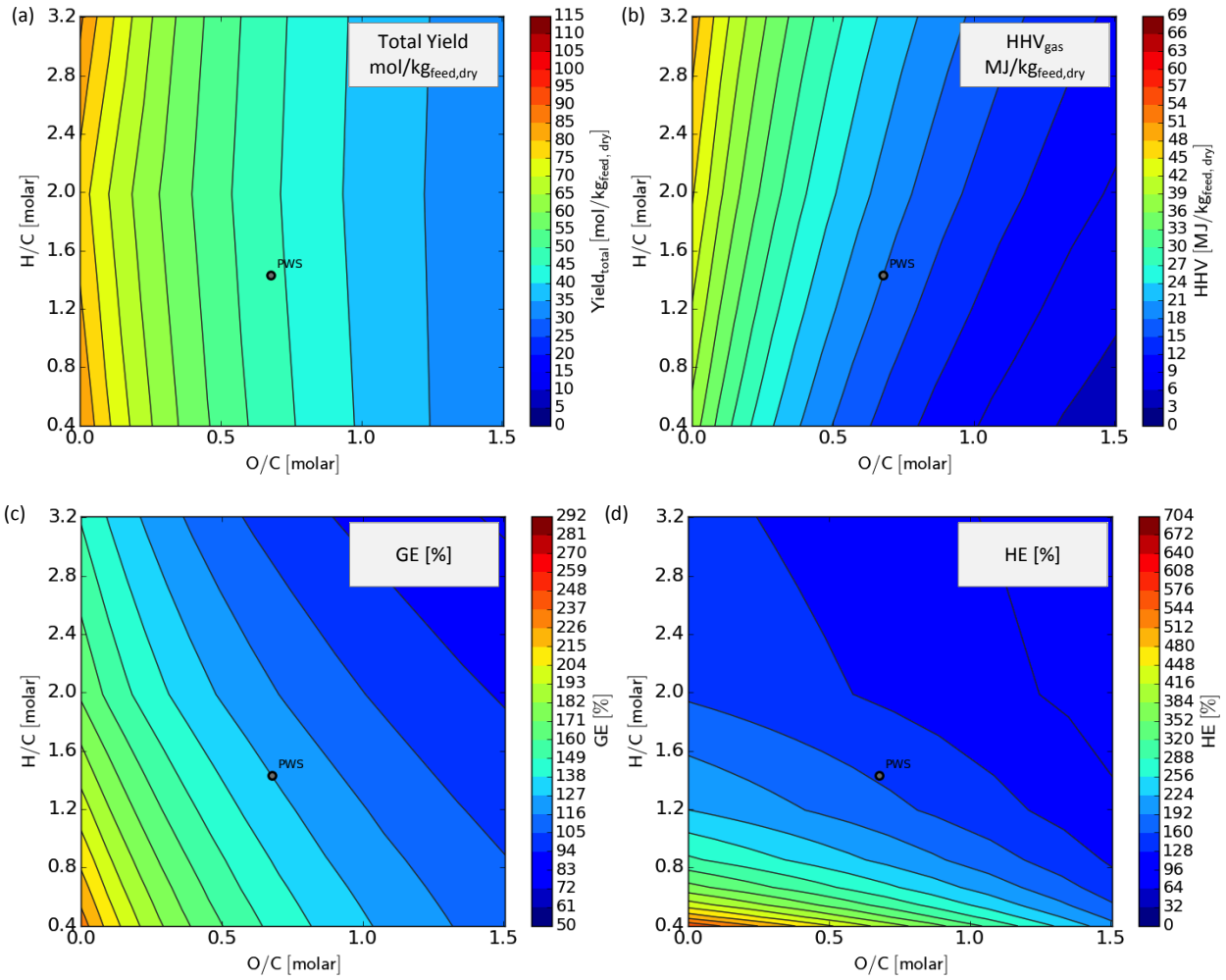

FIGURE 5-2 GENERALISED CONTOUR PLOT COMBINED WITH A VAN KREVELEN DIAGRAMS SHOWING THE EFFECT OF FEEDSTOCK COMPOSITION ON THE CALCULATED THERMODYNAMIC EQUILIBRIUM YIELDS AT 450 °C AND FEEDING 10 WT.% DRY MATTER CONTENT: (A) TOTAL GAS YIELD, (B) HHV OF PRODUCT GAS, (C) GASIFICATION EFFICIENCY (GE), AND (D) HYDROGEN EFFICIENCY (HE).

5.3 RESULTS AND DISCUSSION

Table 5-6 provides a summary for experimental conditions, mass balance results, gasification efficiencies and energy recovery for each experiment. Due to batch reactor operations, the pressure before cooling down the reactor was directly related to the gasification efficiency and the reaction temperature (see Table 5-6). Hence, for the cases when high gasification efficiencies were achieved (PWS06, PWS07, PWS09 and PWS18), the pressure in the reactor, before cooling down, was higher than in the cases when the conversion of carbon to the gas phase were low (PWS15 and PWS16 for example).

5.3.1 THERMODYNAMIC EQUILIBRIUM YIELDS

Due to the isochoric nature of the experimental setup (*i.e.*, constant volume), the pressure in a SCWG batch reactor cannot be kept constant. It was estimated that the pressure in the reactor will be 25.5 MPa once the temperature reaches 450 °C, assuming no gasification has taken place. This was done by considering the density of water and PWS at 450 °C (assuming the density of PWS is the same of that of water) and the mass of water and PWS loaded, as described by Castello et al. (2013). The final pressure in the reactor after an experiment should therefore typically be higher than 25.5 MPa. Hence it was decided to conduct the thermodynamic equilibrium calculations at a pressure of 27 MPa. Previous work showed that the pressure does not significantly influence the thermodynamic equilibrium results between 25 and 27 MPa (Withag et al., 2012).

The Aspen Plus® process model developed in Chapter 3 was used to calculate the exact thermodynamic equilibrium yields at 450 °C, 27 MPa and 10 wt.% (as appose to the ranges specified in Table 5-2). This was done in order to be able to compare the experimentally determined yields with the thermodynamic yields (see Table 5-4 and Table 5-5).

TABLE 5-4 CALCULATED THERMODYNAMIC EQUILIBRIUM YIELDS AND GAS COMPOSITION FOR PWS AT 450 °C, 27 MPA AND 10 WT.%

GAS COMPONENT	YIELDS [MOL/KG$_{PWS}$]	GAS COMPOSITION [MOLE %]
H_2	4.90	11.23
CO	0.04	0.10
CH_4	18.47	42.36
CO_2	20.20	46.31
Total	43.61	100

TABLE 5-5 CALCULATED THERMODYNAMIC EQUILIBRIUM EFFICIENCIES FOR PWS AT 450 °C, 27 MPA AND 10 WT.%

PERFORMANCE INDICATOR	VALUE
Gasification efficiency [%]	127.09
Carbon efficiency [%]	99.99
Hydrogen efficiency [%]	151.25
Energy recovery [%]	99.70
HHV_{gas} [MJ/kg_{PWS}]	17.86

5.3.2 REPRODUCIBILITY OF EXPERIMENTAL RESULTS

Variability in experimental results were to be expected, due to slight differences in the heat-up rates, the heterogeneous nature of the feedstock material, typical uncertainties associated with product analyses, etc. Due to the high cost of product analyses and limited amount of feed material, experiments could not be conducted in triplicate. Nevertheless, in order to verify experimental repeatability, triplicate runs were executed at each of three different operating conditions (PWS01a, PWS01b and PWS01c; PWS10a, PWS10b and PWS10c; PWS12a, PWS12b and PWS12c – see Table 5-6).

Figure 5-3(a) shows the variation in the gas yields at each of the three conditions, while corresponding variations in the TC and TOC content of the WSP are indicated in Figure 5-3(b). The variation in the gasification efficiencies can be observed in Table 5-6. Corresponding error bars are also indicated in the figures in the rest of this chapter.

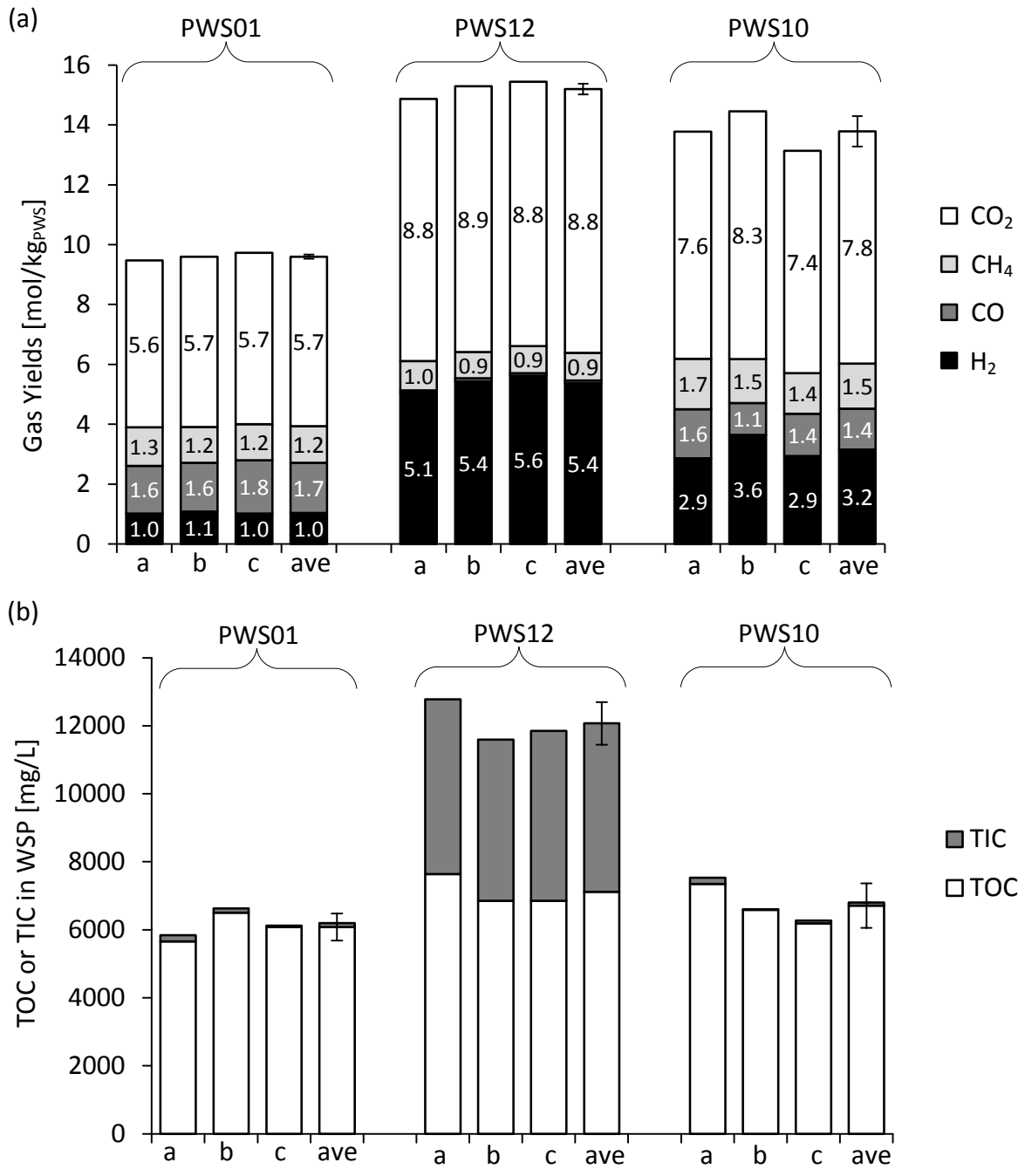

FIGURE 5-3 (A) REPRODUCIBILITY OF GAS YIELDS ACHIEVED DURING TRIPLICATE EXPERIMENTAL RUNS OF PWS01 (60 MINUTES HOLD TIME, NO CATALYST), PWS12 (15 MINUTES HOLD TIME, 0.5 G/G_{PWS} K_2CO_3) AND PWS10 (60 MINUTES HOLD TIME, 0.1 G/G_{PWS} NI/AL_2O_3-SIO_2 ADDED); (B) REPRODUCIBILITY OF TOC AND TC IN WSP ACHIEVED DURING TRIPLICATE EXPERIMENTAL RUNS OF PWS01, PWS12 AND PWS10, RESPECTIVELY.

TABLE 5-6 SUMMARY OF MAIN RESULTS AND EXPERIMENTAL CONDITIONS FOR EACH RUN

EXP. NAME	PWS CONC. [WT.%]	CATALYST		EXP. CONDITIONS[A]		TIME [MIN]		$\dot{\xi}$[B]	MASS BAL. [%]	GAS COMP. [%][C]	GASIFICATION EFFICIENCIES			
		TYPE	LOAD [g/g_{PWS}]	T_{END} [°C]	P_{END} [MPA]	$T_{HEAT-UP}$	T_{HOLD}				GE [%]	CE [%]	HE [%]	ER [%]
PWS01a	10.0	None	-	450.8	25.9	11	59	-	85	100	33.2	21.8	13.0	10.8
PWS01b	10.0	None	-	450.1	26.9	11	60	-	90	97	34.7	22.7	13.3	10.9
PWS01c	10.0	None	-	449.5	26.6	10	60	-	96	99	34.3	22.5	12.4	10.7
PWS02	10.2	K_2CO_3	0.1	450.8	25.9	13	59	-	85	100	41.5	25.1	20.7	11.8
PWS03	10.5	None	0.5	451.1	26.2	12	59	-	91	99	49.7	29.9	34.6	18.2
PWS04	10.5	K_2CO_3	0.5	450.4	26.4	12	118	-	93	100	53.8	33.1	40.7	21.9
PWS05	10.6	K_2CO_3	0.5	450.1	25.9	12	29	-	91	100	46.0	26.9	28.0	14.1
PWS06	10.6	Ni	0.5	451.3	28.1	n.d.[D]	59	1.7	89	99	109.8	83.5	127.4	81.7
PWS07	10.1	Ni	0.5	451.3	27.8	13	118	0.9	92	100	112.8	85.9	126.6	82.1
PWS09	10.6	Ni	0.5	452.2	28.8	10	29	3.3	90	99	106.8	78.7	120.4	75.2
PWS10a	10.2	Ni	0.1	451.0	26.6	13	59	8.6	92	98	43.8	28.2	22.5	15.6
PWS10b	10.2	Ni	0.1	449.9	26.5	14	60	8.6	96	100	45.1	29.6	23.8	14.7
PWS10c	10.2	Ni	0.1	449.7	27.3	13	60	8.6	97	100	41.7	28.0	20.4	13.7
PWS11	10.6	Ni	0.5	454.4	27.5	12	15	5.1	92	99	98.5	71.4	109.2	67.1
PWS12a	10.6	K_2CO_3	0.5	454.0	25.7	13	15	-	99	100	43.9	25.4	25.4	12.6
PWS12b	10.6	K_2CO_3	0.5	450.2	25.1	14	15	-	93	100	44.4	26.6	26.0	12.7
PWS12c	10.6	K_2CO_3	0.5	451.3	24.7	13	15	-	98	100	44.3	26.4	26.8	13.1
PWS14	10.0	None	-	450.8	26.7	11	30	-	93	99	32.2	21.1	11.0	9.8
PWS15	10.0	None	-	450.5	26.8	14	15	-	99	100	30.2	19.7	8.8	8.5
PWS16	10.0	None	-	450.3	26.9	12	120	-	94	98	37.5	24.4	17.3	12.7
PWS17	20.0	Ni	0.5	450.0	27.9	13	59	1.7	87	99	77.5	57.9	77.0	50.6
PWS18	10.0	Ni	1.0	450.0	29.2	13	59	0.9	92	99	119.8	90.0	128.4	82.9
PWS19	10.1	K_2CO_3	1.0	450.0	27.2	10	60	-	91	99	47.9	28.5	39.5	20.0
PWS20	2.5	Ni	0.5	449.7	27.6	15	60	1.7	91	97	103.2	68.2	124.8	68.3
PWS21	5.0	Ni	0.5	450.1	27.8	14	59	1.7	92	98	112.4	82.3	131.8	80.9

[A]before cool-down; [B]$g.g^{-1}.h^{-1}$; [C]N_2, H_2, CO, CH_4 and CO_2; [D]not determined

5.3.3 Deviation from Equilibrium yields

The slight deviation from equilibrium yields and incomplete carbon conversion, even at high Ni/Al_2O_3-SiO_2 loadings and long reaction times (PWS18 and PWS07), may be attributed to various factors. The fact that no agitation was employed during experiments might have limited the extent of the reactions taking place. Some particles may get trapped underneath the heavier catalyst particles, resulting in insufficient contact between particles.

Another contributing factor may be the heat-up rate. Various authors have shown that formation of furfurals occur during the heat-up phase, which may result in char formation via polymerisation (Barbier et al., 2011; Sınağ et al., 2004). Hence, once these char products have formed it may require much longer reaction times to convert them to gases, as shown by Castello et al. (2014). Furthermore, a temperature gradient in the experimental setup due to the fact that the top part of the experimental setup was not submerged in the sand bath, may also play a role in the deviation from the equilibrium results. Some lighter molecules may get trapped in the cooler top part of the reactor setup and not take any further part in the reactions, as described by Zöhrer and Vogel (2013).

5.3.4 Effect of Catalyst Type and Catalyst Loading

Table 5-7 shows a comparison of the results for non-catalytic SCWG of PWS (experiment PWS01), and catalytic SCWG using 1 g/g K_2CO_3 (experiment PWS19) and 1 g/g_{PWS} Ni/Al_2O_3-SiO_2 (experiment PWS18) at a hold time of 60 minutes.

a) Effect of K_2CO_3 loading on SCWG of PWS

From Table 5-7 and Figure 5-4(a) it is evident that the addition of K_2CO_3 enhanced the formation of H_2 and CO_2, while not significantly affecting the formation of CH_4. The H_2 selectivity and H_2 content of the gas phase were directly related to the K_2CO_3 loading, while the CO content was inversely related to the K_2CO_3 loading (see Figure 5-4(a) and Figure 5-4(b)). This confirms the catalytic effect of K_2CO_3 on the water-gas shift reaction, while not significantly affecting the methane forming reactions (Guo et al., 2007; Xu et al., 2013). Within the investigated range of K_2CO_3 loadings, maximum GE, CE and CH_4 yield were achieved at 0.5 g/g_{PWS} (Figure 5-4(a) and

Figure 5-5(a)). However, a loading of 1 g/g_{PWS} resulted in a maximum H_2 yield and selectivity, HE and ER.

TABLE 5-7 RESULTS OF NON-CATALYTIC AND CATALYTIC (1 G/G_{PWS} CATALYST LOADING) SCWG OF 10 WT.% PWS AT 450 °C AND 60 MIN HOLD TIME (DRY BASIS)

	CATALYST			THERMODYNAMIC EQUILIBRIUM
	NONE (PWS01)[E]	K_2CO_3 (PWS19)	NI (PWS18)	
Gas Yield [mol/kg$_{PWS}$]				
H_2	1.04	7.47	5.79	4.90
CO	1.67	0.06	0.00	0.04
CH_4	1.23	1.73	14.87	18.47
CO_2	5.66	9.25	19.96	20.20
Total	9.51	18.50	40.62	43.61
Gas Composition [mole %]				
H_2	10.56	39.74	14.61	11.23
CO	16.98	0.30	0.00	0.10
CH_4	12.47	9.20	37.44	42.36
CO_2	51.95	44.42	46.01	46.31
Efficiencies [%]				
GE	33.72	47.92	119.79	127.09
CE	22.10	28.51	89.95	99.99
HE	12.62	39.51	128.41	151.25
ER	10.62	19.98	82.90	99.70
HHV_{gas} [MJ/kg$_{PWS}$]				17.86
Selectivity [mole/mole]				
S_{H_2}	0.43	2.16	0.19	0.13

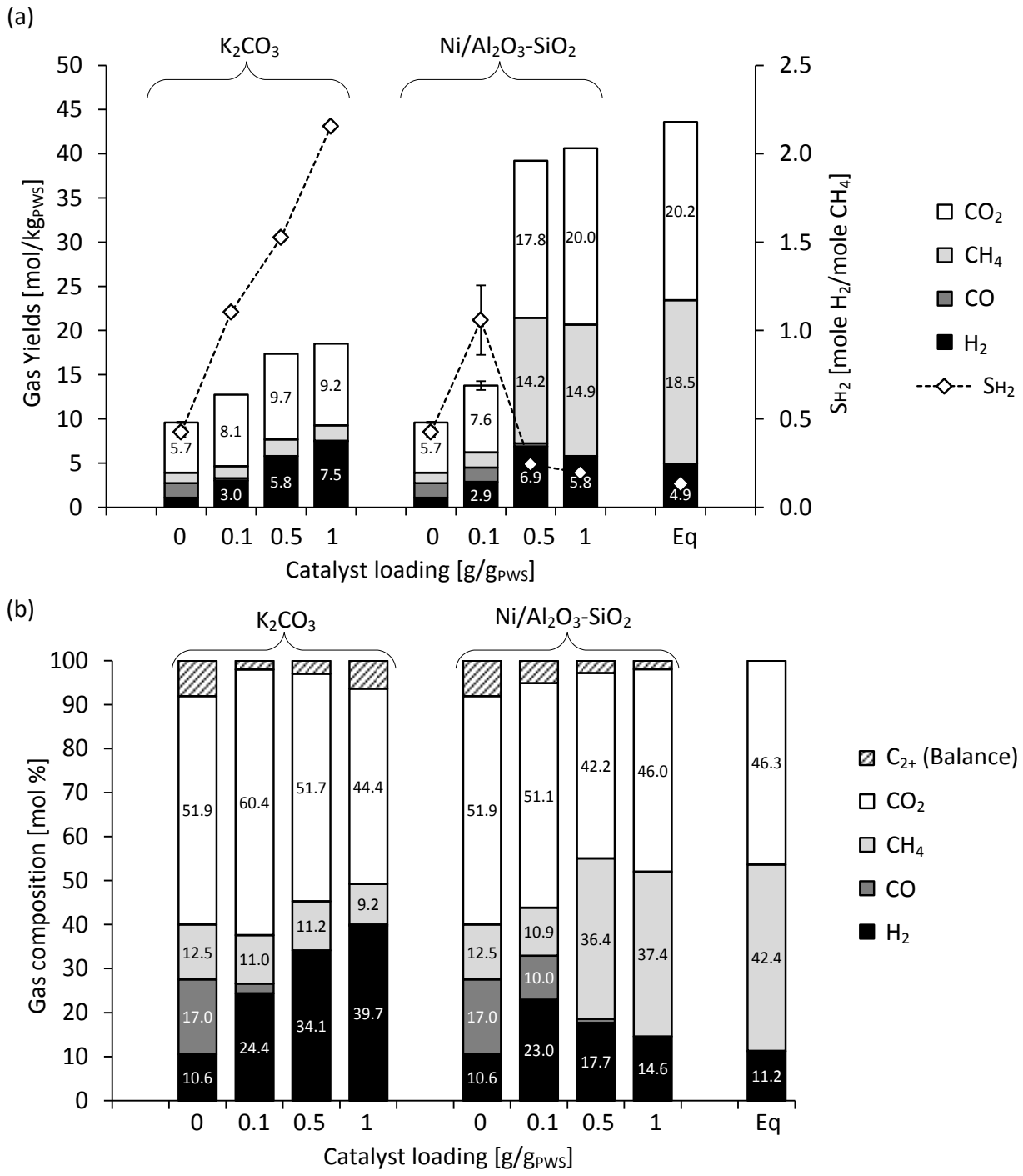

FIGURE 5-4 EFFECT OF CATALYST LOADING DURING SCWG OF 10 WT.% PWS AT 450 °C AND 60 MIN HOLD TIME ON (A) GAS YIELDS; (B) GAS COMPOSITION;

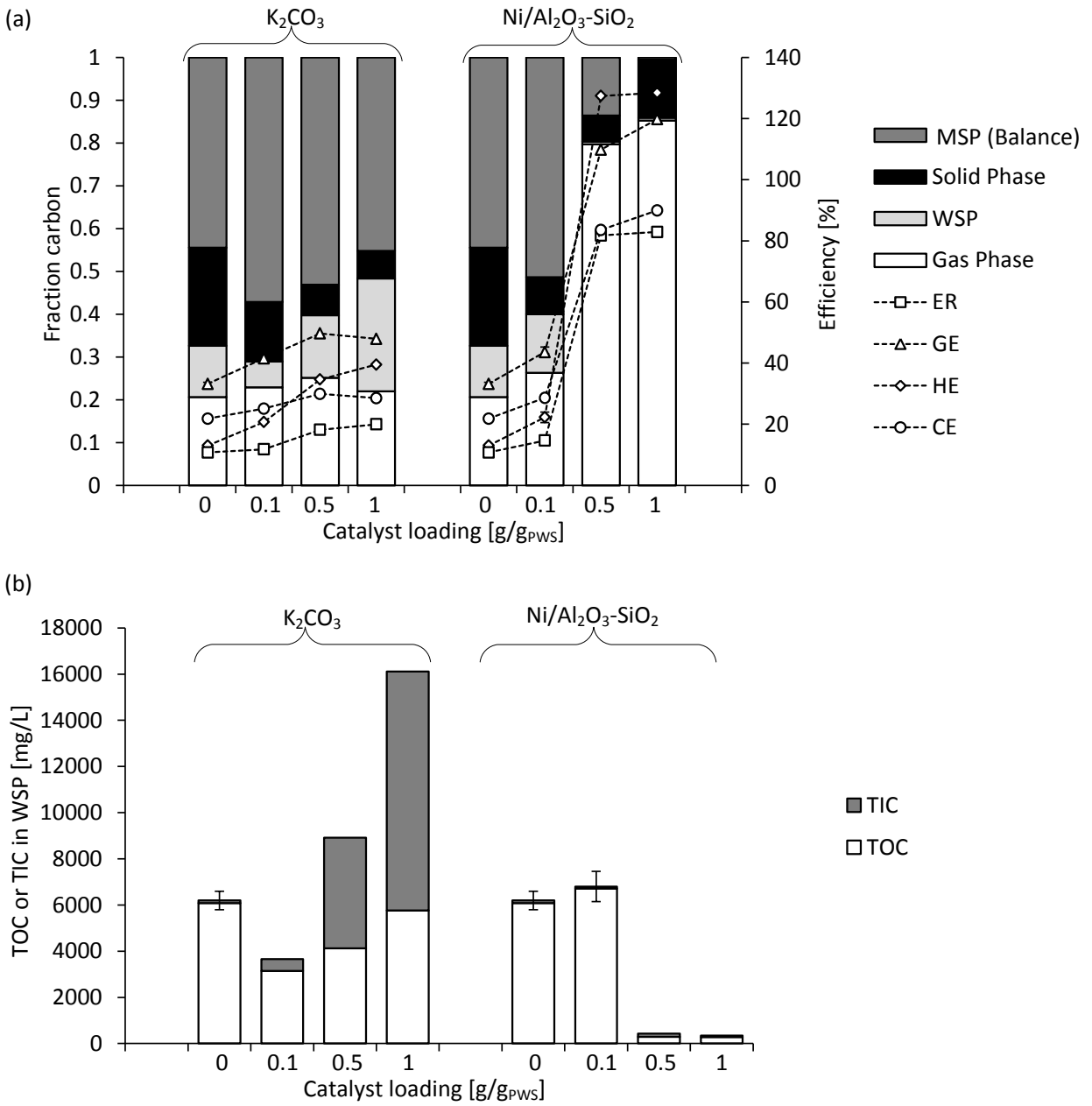

FIGURE 5-5 EFFECT OF CATALYST LOADING DURING SCWG OF 10 WT.% PWS AT 450 °C AND 60 MIN HOLD TIME ON (A) CARBON DISTRIBUTION BETWEEN PHASES, GE, CE, HE AND ER; (B) CARBON CONCENTRATION IN THE WSP.

Guo et al. (2007) also noted an increase in the gas yields with an increase in the K_2CO_3 loading between 0 and 0.8 $g/g_{cellulose}$ during SCWG of 10 wt.% cellulose at 500 °C. However, they found a best loading of 0.2 $g/g_{cellulose}$ K_2CO_3 was optimal for maximum H_2 and CH_4 yields. It may well be that their lower optimum loading – compared to this work – was due to a higher operating temperature of 500 °C. Furthermore, in this study, real biomass was used as feed material

(consisting of a mixture of cellulose, hemicellulose, lignin and ash), compared to pure cellulose used by Guo et al. (2007). Yoshida et al. (2004) showed that the presence of lignin in the feed material can inhibit the gasification efficiency. This suggests that higher catalyst loadings may be required when biomass material containing lignin (such as PWS) is used as feedstock material for SCWG compared to pure cellulose.

The increase in TIC concentration in the WSP with an increase in K_2CO_3 loading (Figure 5-5(b)) can be ascribed to the increase in the CO_3^{2-} concentration as K_2CO_3 typically dissolves in the water to form K^+ and CO_3^{2-} ions. The slight increase in the TOC with an increase in the K_2CO_3 loading from 0.1 to 1 g/g_{PWS} might be due to the fact that K_2CO_3 catalysed the formation of intermediate organic acid products such as HCOOH. It is suspected that, at longer hold times, the TOC will decrease as these intermediate products are converted to H_2 and CO_2 (see Section 5.3.5). Char formation typically decreased with an increase in the K_2CO_3 loading. Xu et al. (2013) also reported a decrease in the char yield with an increase in the K_2CO_3 loading during SCWG of sewage sludge at 450 °C.

b) Effect of Ni/Al_2O_3-SiO_2 loading on SCWG of PWS

The yields of H_2, CH_4 and CO_2 increased significantly when the Ni/Al_2O_3-SiO_2 loading was increased from 0.1 to 0.5 g/g_{PWS} (Figure 5-4(a)). A further increase in the loading did not have such a noteworthy effect on the gas yields. Interestingly, the hydrogen selectivity and CO yield initially increased after which it decreased at Ni/Al_2O_3-SiO_2 loadings above 0.1 g/g_{PWS}. This suggests that, at lower catalyst loadings, the formation of H_2 and CO *via* steam reforming (Eq. 2-2) was favoured. However, at higher catalyst loadings the formation of CH_4 *via* the methanation of CO and/or CO_2 became more prominent. Concerning the gas composition, when Ni/Al_2O_3-SiO_2 loadings of 0.5 or higher were used, a gas product composition relatively close to the calculated equilibrium gas composition was achieved (see Figure 5-4(b)).

Initially, the fraction of carbon reporting to the MSP and C_{2+} gases, as well as the WSP, increased up to a loading of 0.1 g/g_{PWS} (see Figure 5-5(a) and (b)). However, at the higher Ni/Al_2O_3-SiO_2 loadings, less carbon reported to the MSP and WSP, while the formation of H_2, CH_4 and CO_2 was greatly enhanced. This suggests that enough active sites were available on the catalyst surface for both the water-gas shift reaction and methanation reaction to take place. This also confirms

the findings by Minowa and Inoue (1999) that the gasification of water-soluble products to H_2, CO_2 and CH_4 is in competition with polymerisation of water soluble products at low catalyst loadings. Yoshida et al. (2004) also reported higher carbon yields to the MSP at lower catalyst loadings (0.4 $g/g_{cellulose+lignin}$) compared to higher catalyst loadings (1.2 $g/g_{cellulose+lignin}$) for the gasification of lignin and cellulose mixtures at 400 °C using a commercial nickel catalyst.

The slightly higher carbon fraction reporting to the solid phase at a catalyst loading of 1 g/g_{PWS}, suggests that carbon monoxide disproportionation might have taken place on the catalyst surface *via* the Boudouard reaction (Eq. 5-1), as described by Yoshida et al. (2004). The BET surface area of the catalyst and solid product recovered when 1 g/g_{PWS} loading was used was 74.9 m^2/g compared to 178 m^2/g of the fresh catalyst, confirming the possible loss of active sites on the catalyst surface due to carbon formation. Maximum CE of 90% and ER of 82.9% were achieved at a loading of 1 g/g_{PWS} (Figure 5-5(a)). This corresponds to a residence time dependent biomass-to-catalyst ratio ($\dot{\xi}$) of 1.7 $g.g^{-1}.h^{-1}$ (experiment PWS18).

$$2CO \rightarrow CO_2 + C_{(s)} \qquad 5\text{-}1$$

The highest CE of 90% is significantly higher than values reported in literature where Ni/Al_2O_3-SiO_2 was used as catalyst (see Table 2-5). Taylor et al. (2009) reported a CE of 50% during SCWG of cellulose at 500 °C. Youssef et al. (2010) reported a significantly higher CE of 78% when glucose was used as feed material at an operating temperature of 500 °C. A very low CE of 28% was reported by Guan et al. (2014) at 500 °C using lignin as feed material. Although the use of 0.5 and 1 g/g_{PWS} Ni/Al_2O_3-SiO_2 catalyst greatly enhanced the gasification efficiencies compared to non-catalytic SCWG and alkali-catalysed SCWG, complete conversion of carbon to the gas phase was not achieved. Furthermore, the gas composition and gas yields also deviated somewhat from the calculated equilibrium gas composition (especially the CH_4 content).

c) Comparison between K_2CO_3 and Ni/Al_2O_3-SiO_2

Overall, at catalyst loadings above 0.5 g/g_{PWS}, the addition of Ni/Al_2O_3-SiO_2 resulted in much higher gasification efficiency and energy recovery compared to when K_2CO_3 was added. Additionally, the CH_4 and CO_2 yields were more than 10 mol/kg_{PWS} higher when using Ni/Al_2O_3-SiO_2 (at 0.5 and 1 g/g_{PWS} loadings), hence, resulting in almost 60% higher CE compared to the

same loadings when K_2CO_3 was used. Although somewhat higher H_2 yields were achieved when the K_2CO_3 catalyst was used, the HE achieved with the Ni/Al_2O_3-SiO_2 catalyst was still almost 90% higher due to the significantly higher CH_4 yields. As could be ascertained, no previous study has compared the use of Ni/Al_2O_3-SiO_2 and K_2CO_3 as potential catalysts for SCWG of PWS. However, Guo et al. (2007) compared the use of 1 g/g Raney nickel and 1 g/g K_2CO_3 during SCWG of peanut shells at 450 °C and 20 minute reaction time. Their results also showed a significantly higher CH_4 and total gas yields when Raney nickel was added.

5.3.5 Effect of hold time

a) Gas yields and H_2 selectivity

The slight increase in the H_2 yield and H_2 selectivity during non-catalytic SCWG with an increase in the hold time (Figure 5-6(a)) confirms the possible catalytic effect of the reactor wall (due to the fact that nickel is present in the stainless steel) and/or the presence of inorganic material in the PWS on the water-gas shift reaction, as described by Castello et al. (2013). The relatively low gas yields achieved even at a long reaction time of 120 minutes during the non-catalytic runs, confirms the findings of previous authors that a catalyst is required to achieve high gasification efficiencies at a low gasification temperature such as 450 °C (Azadi et al., 2012; Hao et al., 2005). Although similar trends were observed, the H_2 and CH_4 yields achieved during non-catalytic SCWG of PWS at 450 °C were significantly lower than the yields obtained by Chen et al. (2013) during SCWG of 9 wt.% sewage sludge at 450 °C in a batch reactor. It must however be noted that the sewage sludge used in their study had an ash (inorganic) content of 29% compared to the 5.8 % PWS used here. Various authors have suggested that the presence of inorganic matter in the feedstock material may lead to higher gas yields (especially H_2) (Rönnlund et al., 2011; L. Zhang et al., 2010b).

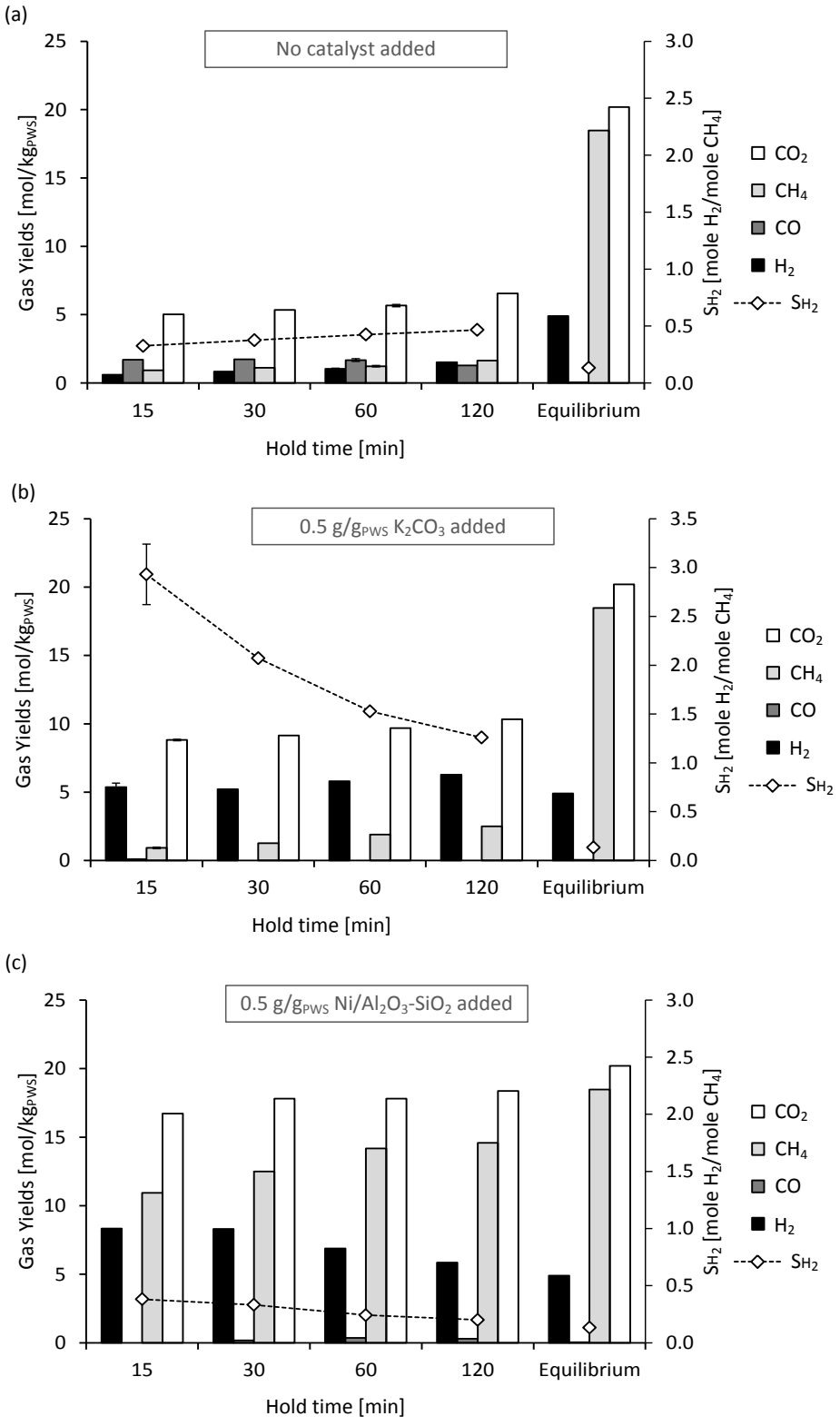

FIGURE 5-6 EFFECT OF HOLD TIME ON GAS YIELDS DURING SCWG OF 10 WT.% PWS AT 450 °C ON (A) NON-CATALYTIC SCWG GAS YIELDS; (B) CATALYTIC (0.5 G/G_{PWS} K_2CO_3) SCWG GAS YIELDS; (C) CATALYTIC (0.5 G/G_{PWS} NI/AL_2O_3-SIO_2);

The steady increase in the H_2 and CO_2 yields achieved with an increase in the hold time – up to 120 minutes – with K_2CO_3 as catalyst (Figure 5-6(b)) once again confirms that K_2CO_3 catalyses the water-gas shift reaction, even at a relatively short reaction time of 15 minutes. The decrease in the H_2 selectivity at longer hold times suggests that the formation of CH_4 became more prominent later-on *via* the hydrogenation of CO and H_2. Hence, the formation of H_2 was more predominant during the early stages of the experiment (*i.e.* within the heat-up phase and the first 15 minutes) which occurred *via* the steam reforming and water-gas shift reaction.

When Ni/Al_2O_3-SiO_2 was added, the H_2 yield decreased steadily while the CH_4 yield increased with an increased in hold time (Figure 5-6(c)). Furthermore, the H_2 selectivity decreased from 0.38 to 0.20 (a value close to the equilibrium calculated value of 0.13). The formation of CH_4 might have also occurred *via* the Sabatier reaction, which is the combination of the water gas shift reaction and the methanation reaction, commonly occurring in the presence of a nickel catalyst (Minowa and Ogi, 1998; Waldner and Vogel, 2005).

b) Gas composition

During non-catalytic SCWG, the CO content of the product gas decreased with an increase in the hold time (see Figure 5-7).

The CO content was however still an order of magnitude higher than in the two catalytic cases. Therefore, although the reactor wall might have catalysed the water-gas shift reaction to some degree, its effect was rather insignificant compared to the catalytic effect of both K_2CO_3 and Ni/Al_2O_3-SiO_2. During alkali-catalysed SCWG, both the H_2 and CO_2 content decreased with an increase in the hold time. Furthermore, the CH_4 content in the product increased significantly from 7 mole % at 15 minutes to 13.4 mole % at 120 minutes. This confirms that H_2 and CO_2 formation was favoured at short reaction times while CH_4 formation became more favoured at longer reaction times. During nickel catalysed SCWG, the H_2 content decreased and CH_4 content increased with an increase in the hold time to 120 minutes. At a hold time of 120 minutes a gas product with composition relatively close to the equilibrium calculated composition was obtained.

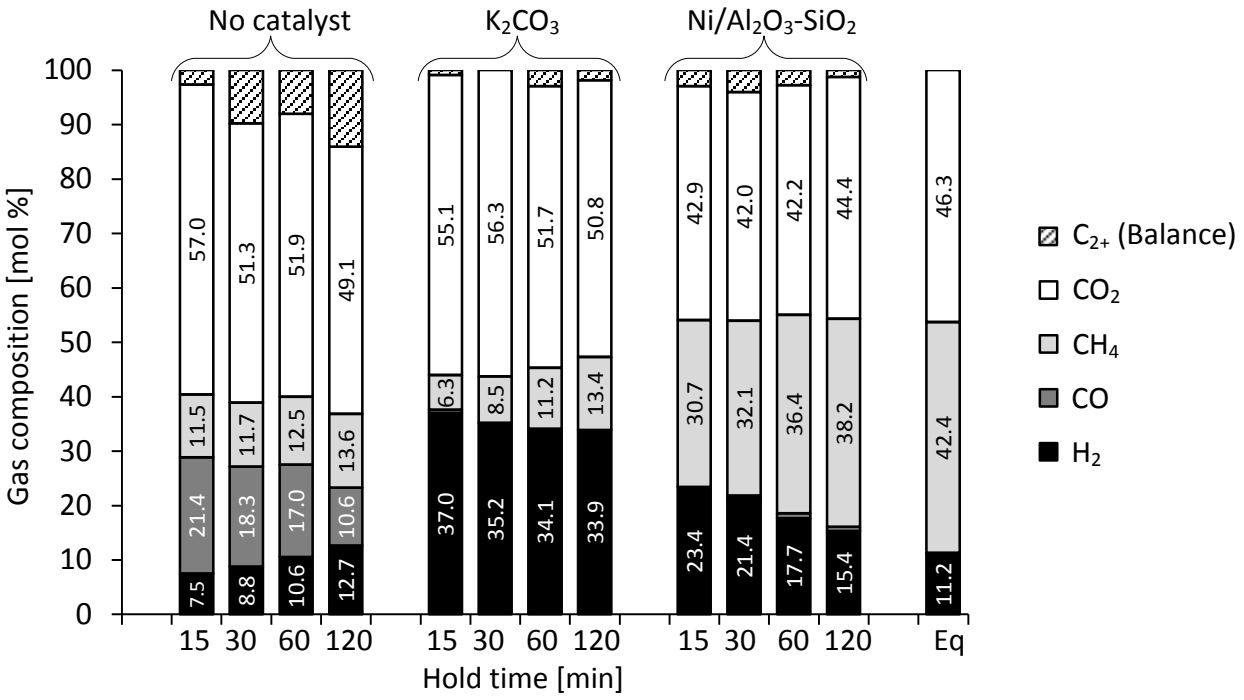

FIGURE 5-7 EFFECT OF HOLD TIME ON GAS COMPOSITION DURING SCWG OF 10 WT.% PWS AT 450 °C (0.5 G/G_{PWS} CATALYST LOADING)

c) Carbon distribution between the gas, liquid and solid phases

For both the non-catalysed case and the alkali-catalysed case, the TOC in the WSP, and, consequently, the fraction of carbon reporting to the WSP decreased steadily with an increase in the hold times (see Figure 5-8(a) and (b)). No significant change in the carbon fraction reporting to the solid phase as a function of time was observed during the non-catalytic and alkali-catalysed experiments. However, the fraction of carbon reporting to the gas phase increased as the hold time was increased for these two cases. This suggests that gasification of water soluble products occurred. The liquid phase product collected after all the experiments with Ni/Al_2O_3-SiO_2 were clear and the TOC was below 675 mg/L (which is more than ten times lower than for the non-catalysed case). The fraction of carbon reporting to the solid phase decreased significantly as the hold time was increased from 15 to 60 minutes when Ni/Al_2O_3-SiO_2 was added. A slight increase in the carbon fraction reporting to the solid phase was observed at a hold time of 120 minutes. This was accompanied with a slight decrease in the CO yield, which, once again suggests the formation of solid carbon on the catalyst surface *via* the Boudouard reaction (Eq. 5-1).

d) Gasification Efficiencies

Although the GE, CE, ER and HE typically increased with an increase in the hold time for all three cases, the use of Ni/Al_2O_3-SiO_2 greatly increased the GE (113%), CE (86%), ER (82%) and HE (127% - see Figure 5-8(b)). The corresponding residence time dependent biomass-to-catalyst ratio was 1.7 $g.g^{-1}h^{-1}$. Furthermore, although the GE and HE were notably higher for all the hold times when K_2CO_3 was used as catalyst, if compared to non-catalytic experiments, the CE for the catalysed and non-catalysed cases was comparable. This strongly suggests that, if high carbon conversions are desired (*i.e.* high CH_4 yields) during SCWG at 450 °C, K_2CO_3 would not be a suitable catalyst, despite long reaction times of up to 120 minutes.

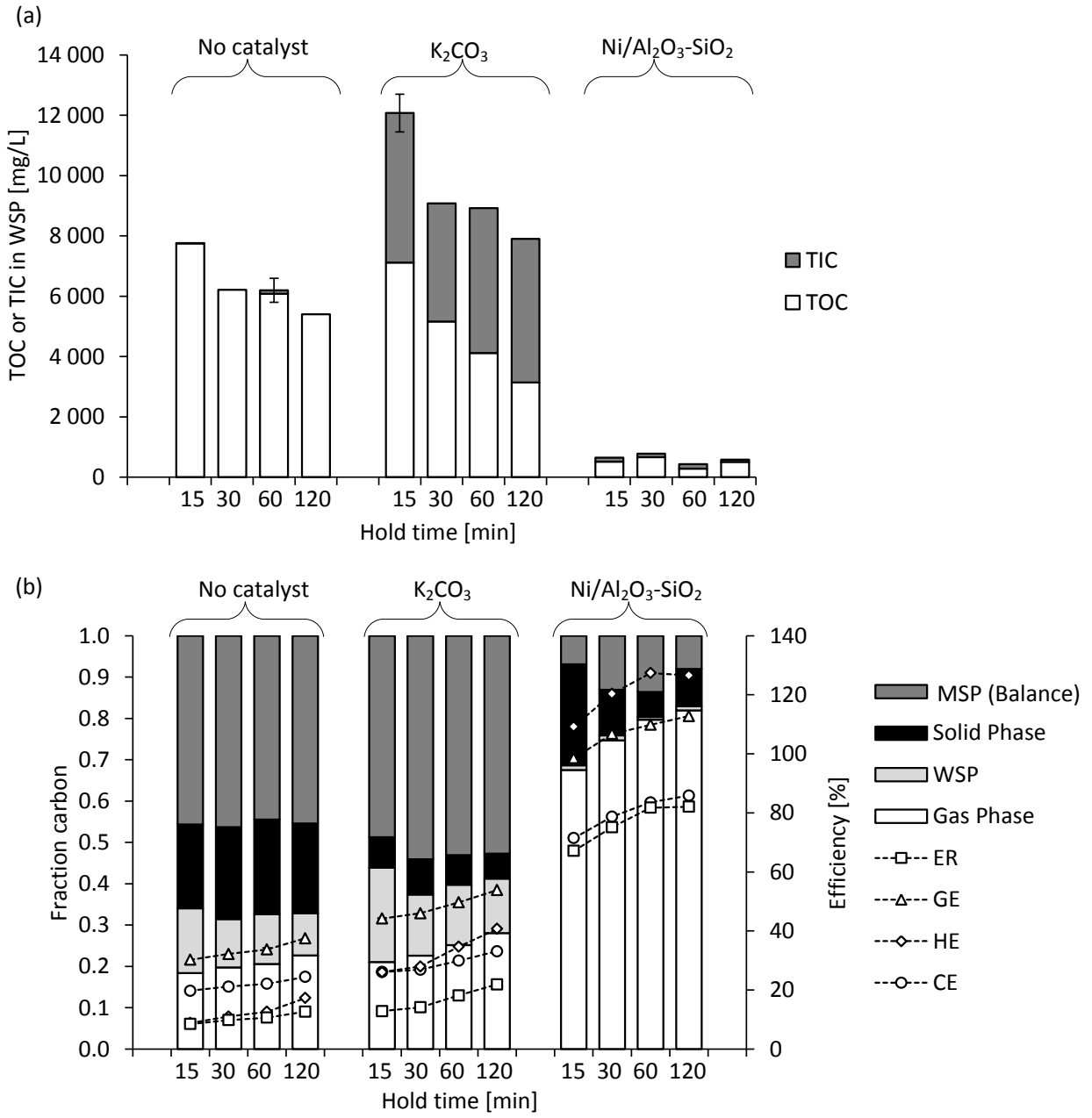

FIGURE 5-8 EFFECT OF HOLD TIME ON THE (A) CARBON CONCENTRATION IN THE WSP; (B) CARBON DISTRIBUTION BETWEEN PHASES, GE, CE, HE AND ER DURING SCWG OF PWS AT 450 °C.

5.3.6 Effect of PWS feed concentration during Ni/Al_2O_3-SiO_2 catalysed SCWG

Further experiments were conducted in order to show the change in the gas yields and gas composition when the PWS concentration in the feed were varied between 2.5, 5, 10 and 20 wt.%. These experiments were conducted in the presence of Ni/Al_2O_3-SiO_2 catalyst and a holding time of 60 min.

The experimental gas yields and gas composition followed the same trend as the predicted equilibrium yields at a feed concentration of up to 10 wt.% (Figure 5-9). However, contrary to equilibrium results, a further increase in the feed concentration to 20 wt.%, resulted in a decrease in the CH_4 yield, while the CH_4 content in the gas phase increased only slightly. Additionally, a significantly higher fraction of carbon ultimately reported to the WSP and solid phase (Figure 5-10(a) and (b)). Consequently, the ER and CE achieved at 20 wt.% and 2.5 wt.% were also notably lower than that achieved at a feedstock concentration of 5 and 10 wt.%. These observations may be due to insufficient mixing and poor mass transfer, typically associated with small tube-like batch reactors. Also, some feedstock particles might have been trapped below the catalyst particles, not coming into sufficient contact with other particles.

The results suggest that longer reaction times or higher catalyst loadings might be required at higher dry matter concentrations to achieve higher carbon conversion efficiencies. Hence, values for $\dot{\xi}$ obtained at a specific dry matter concentration for almost complete carbon conversion would not necessarily apply for other dry matter concentrations. At a low PWS feed concentration of 2.5 wt.%, a highest H_2 yield and H_2 selectivity was achieved. However, highest GE (112%) and HE (132%) were achieved at a PWS concentration of 5 wt.% while a highest CH_4 yield (14.2 mol/kg_{PWS}), CE (84%) and ER (82%) was achieved at a PWS concentration of 10 wt.%.

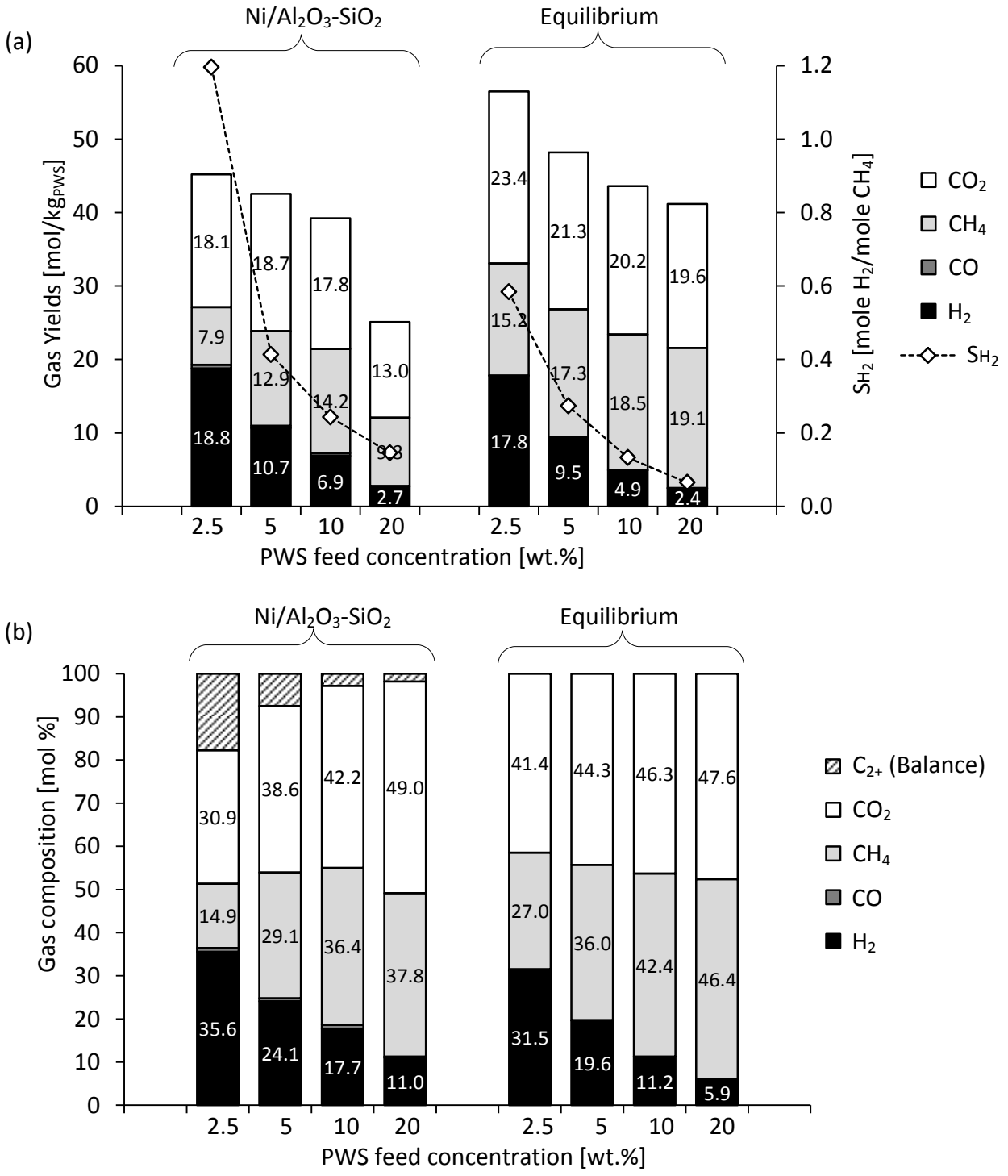

FIGURE 5-9 EFFECT OF DRY MATTER CONTENT DURING CATALYTIC SCWG OF PWS AT 450 °C, HOLD TIME OF 60 MIN WITH 0.5 G/G_{PWS} ADDED Ni/Al_2O_3-SiO_2 ON THE (A) GAS YIELDS; (B) PRODUCT GAS COMPOSITION

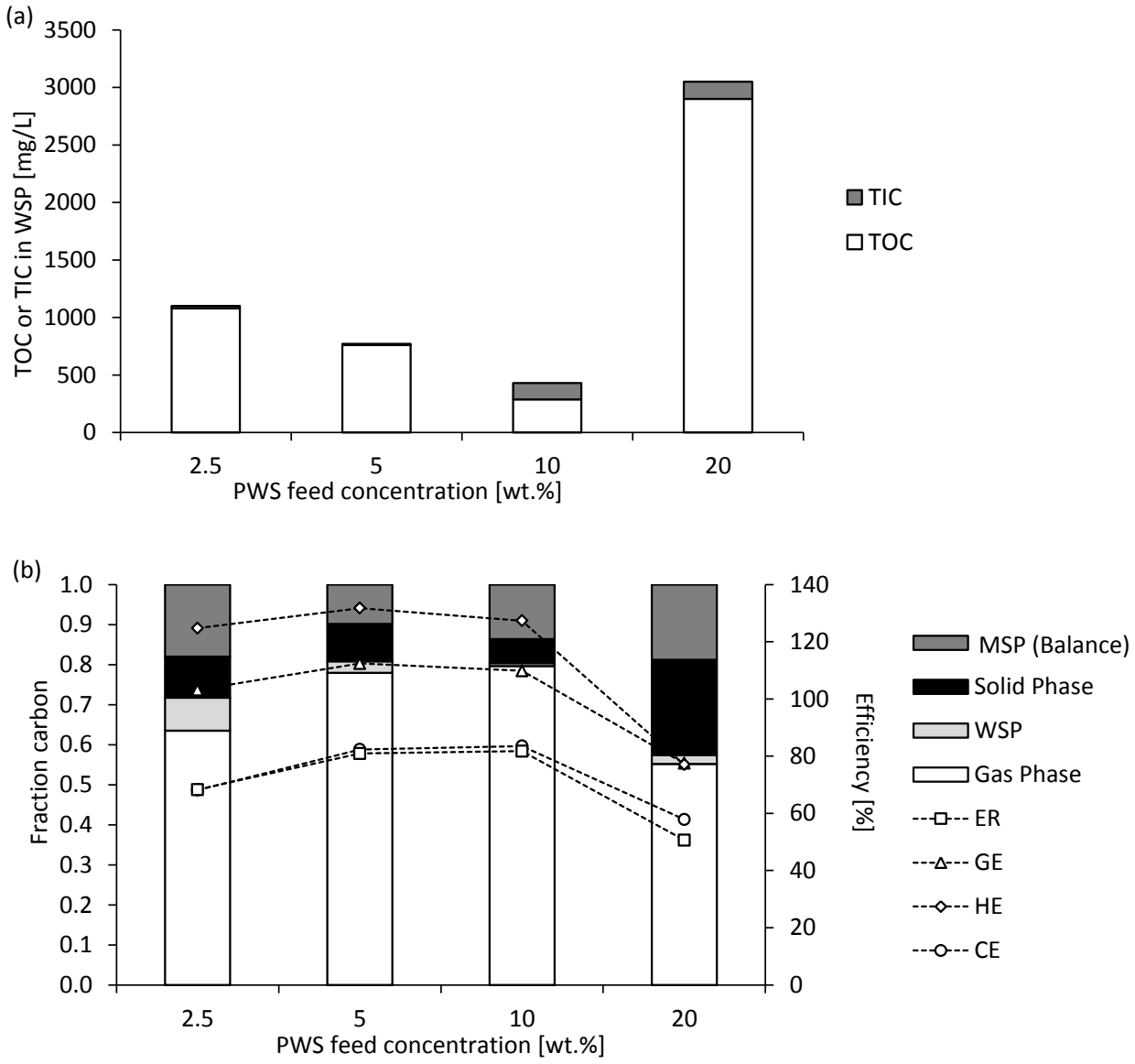

FIGURE 5-10 EFFECT OF DRY MATTER CONTENT DURING CATALYTIC SCWG OF PWS AT 450 °C, HOLD TIME OF 60 MIN WITH 0.5 G/G_{PWS} ADDED NI/AL_2O_3-SIO_2 ON THE (A) CARBON CONCENTRATION IN THE WSP; (D) CARBON DISTRIBUTION BETWEEN PHASES, GE, CE, HE AND ER.

5.3.7 Energy potential from SCWG of Primary Paper Sludge based on thermodynamic equilibrium calculations

Clearly, a catalyst is required to enhance the gasification efficiencies during SCWG of PWS at 450 °C. A product gas with a HHV of 13 – 13.3 MJ/$kg_{PWS,dry}$ can then be produced at an operating temperature of 450 °C when feeding a PWS concentration of 10 wt.% and with a residence time dependent biomass-to-catalyst ratio ($\dot{\xi}$) < 1.7. This corresponds to a possible ER of 81 – 83% from PWS at these conditions. The HHV of the product gas produced in this study is comparable to that produced in a study by Rönnlund et al., 2011 and Myréen et al., 2011 (13.4 MJ/kg_{PWS}) during SCWG of primary paper sludge at 600 °C. They suggested that integration of SCWG of primary paper sludge into an existing craft paper mill can increase the thermal efficiency of the mill by 50 %.

However, considering only the HHV of the products (gas, bio-oil or char) and ER of the products relative to the feed material is not sufficient to characterise the thermal efficiency of a process. One also needs to consider the heating of the feed material to the reaction temperature, the heating required for the reactor to operate isothermally (due to the endothermic nature of the SCWG reactions) as well as possibility of heat integration within the process. Hence, although the experimental results presented here show great potential in terms of energy recovery from primary paper sludge *via* SCWG, a thorough energy analysis will be required to determine the nett thermal energy that a craft mill will gain from SCWG.

In order to determine the thermodynamic limit for the overall energy efficiency of SCWG using PWS as feed material, the Aspen Plus® process model developed in Chapter 3 was used (refer back to Figure 3-3 for a schematic flow diagram of the process model). The overall efficiency of the process ($\eta_{overall}$ – Eq. 5-2) was determined as the energy produced during the process ($\dot{E}_{produced}$) divided by the energy added during the process ($\dot{E}_{added}$).

$$\eta_{overall} = \frac{\sum \dot{E}_{out}}{\sum \dot{E}_{in}} \qquad 5\text{-}2$$

The energy produced and energy added added comprises of chemical energy ($\dot{E}_{chemical}$), heat energy ($\dot{E}_{heat}$) and work energy ($\dot{E}_{work}$). $\dot{E}_{chemical,produced}$ was assumed to be equal to the LHV of the product gas, while $\dot{E}_{chemical,added}$ was assumed to be equal to the LHV of PWS (Eq. 5-3 and 5-4).

$$\dot{E}_{chemical,produced} = \dot{m}_{H_2} LHV_{H_2} + \dot{m}_{CH_4} LHV_{CH_4} + \dot{m}_{CO} LHV_{CO} \quad 5\text{-}3$$

$$\dot{E}_{chemical,added} = \dot{m}_{PWS} LHV_{PWS} \quad 5\text{-}4$$

The overall efficiency of the process was consequently determined by means of Eq. 5-5.

$$\eta_{overall} = \frac{\dot{m}_{H_2} LHV_{H_2} + \dot{m}_{CH_4} LHV_{CH_4} + \dot{m}_{CO} LHV_{CO} + \frac{HR}{100}\dot{Q}_{Cooler}}{\dot{m}_{PWS} LHV_{PWS} + \dot{Q}_{Heater} + \dot{Q}_{Netto} + \dot{W}_{pump}} \quad 5\text{-}5$$

Where:

- HR is the percentage heat recovered from the reactor product stream
- $\dot{Q}_{Cooler}$ is the duty of the cooler
- $\dot{Q}_{Heater}$ is the duty of the pre-heater
- $\dot{Q}_{Netto}$ is the nett heat of reaction
- $\dot{W}_{pump}$ is the duty of the pump

It was assumed that no work is recovered from the process. Furthermore, not all of the heat from the reactor product stream (S-5 in Figure 3-3) will be recovered. Hence, in order to determine the effect of the HR on the overall energy efficiency, the HR was varied between 0 and 100%. The operating temperature and dry feed concentration were also varied between 400 and 500 °C and 2.5 and 20 wt.%, respectively.

Figure 5-11 shows the results for the overall energy efficiency for the different conditions investigated. When 100% of the heat can be recovered, an overall energy efficiency of 62 – 88% can be achieved, depending on the dry feed concentration (Figure 5-11(a)). When 75%, 50% or 25% of the heat is recovered, an overall efficiency of 55 – 68%, 49 – 50% and 30 – 42% can be achieved, respectively. When no heat is recovered, the overall efficiency ranges between 12 and 36% (Figure 5-11(e)). At an operating temperature of 450 °C and dry feed concentration of

10 wt.%, the overall efficiency ranges between 71 and 27%, depending on the percentage of heat recovered.

These calculations are based on the assumption of thermodynamic equilibrium and provide the thermodynamic limit of the overall efficiency when no work is recovered during the process and the heat recovered ranges between 0 and 100%.

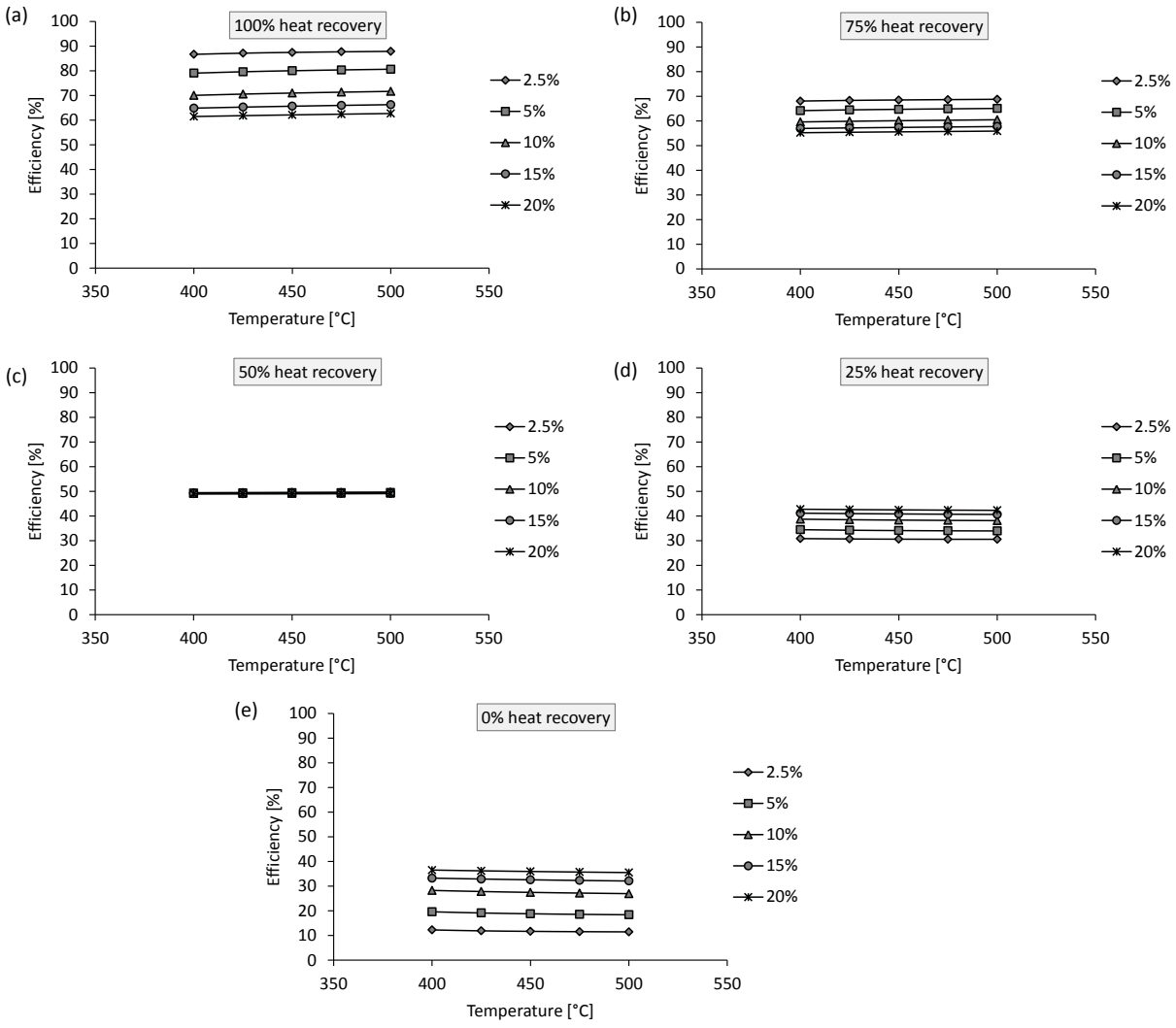

FIGURE 5-11 OVERALL EFFICIENCY FOR SCWG OF PWS AT HEAT RECOVERIES OF (A) 100%; (B) 75%; (C) 50%; (D) 25%; (E) 0%

5.4 OUTCOME OF THIS CHAPTER

The aim of this chapter was to determine how close one can come to the calculated thermodynamic equilibrium yields when using primary paper waste sludge as feed material. This investigation was conducted within a reasonable catalyst loading and reaction time. In addition, the feasibility of using primary paper sludge as feed material for SCWG was also assessed (refer back to ***Objective 2*** in Section 1.3).

The key conclusions drawn from this chapter are summarised as follows:

- A gas product relatively close to the calculated thermodynamic composition, with a HHV of 13.2 MJ/kg_{PWS}, can be produced when a time-dependent biomass-to-catalyst ratio of 1.7 $g_{PWS}.g^{-1}h^{-1}$ is applied during SCWG of primary paper sludge with Ni/Al_2O_3-SiO_2 catalyst.
- Significantly higher conversion of carbon to the gas phase can be achieved with a heterogeneous metal catalyst (Ni/Al_2O_3-SiO_2) than with a homogeneous catalyst (K_2CO_3) using PWS at feed material at an operating temperature of 450 °C.
- Confirming results from literature, the addition of K_2CO_3 as catalyst enhances the water-gas shift reaction, thus resulting in H_2 yields as high as 7.5 mol/kg_{PWS}.
- Confirming results from literature, the addition of Ni/Al_2O_3-SiO_2 as catalyst greatly enhances steam reforming and hydrogenation reactions, resulting in CH_4 and H_2 yields as high as 14.9 mol/kg_{PWS} and 5.8 mol/kg_{PWS}, respectively.
- Thermodynamic equilibrium calculations show that an overall energy efficiency up to 60% can be achieved when PWS is gasified in SCW at a temperature of 450 °C and a dry feed concentration of 10 wt.% (assuming that 75% of the heat from the heat in the product stream can be recovered).

Chapter 6

SCWG OF *E.GRANDIS* AND RELATED PYROLYSIS CHAR: EFFECT OF FEEDSTOCK COMPOSITION††

6.1 INTRODUCTION

The aim of this chapter is to determine the possible kinetic influence of the composition of the feedstock material (specifically the volatile matter content and the O/C ratio) on the gas yields and gasification efficiencies during SCWG. Furthermore, the possible usage of *E.grandis* wood and various wood-derived pyrolysis char material as feed material for SCWG was also assessed (Refer back to ***Objective 3*** in Section 1.3).

Various char products produced during slow and vacuum pyrolysis of *E.grandis* wood chips were used as feed material for SCWG experiments. Furthermore, the *E.grandis* wood chips themselves were also gasified in SCW for comparison. The O/C and H/C ratio of the char products and the *E.grandis* wood chips varied from 0.44 to 1.46 and from 0.23 to 0.75, respectively. Furthermore, the volatile content of these materials varied between 26.6 and 83.3 wt.% (refer back to Figure 4-1, Table 4-2 and Table 4-3 in Chapter 4 for the exact composition of these feed materials).

---

†† Part of the work presented in this chapter has been accepted for publication in Bioresource Technology: Louw, J., Schwarz, C.E., Burger, A.J., *Supercritical water gasification of Eucalyptus grandis and related pyrolysis char: Effect of feedstock composition*. Bioresource Technology, Vol 216 (2016), pp 1030-1039 (DOI: 10.1016/j.biortech.2016.06.062)

The experimental gas yields achieved with and without use of a homogeneous catalyst (K_2CO_3) and heterogeneous catalyst (Ni/Al_2O_3-SiO_2) were compared to the calculated thermodynamic equilibrium yields and efficiencies. The experiments were also conducted at various Ni/Al_2O_3-SiO_2 catalyst loadings and reaction times (refer to Table 4-10, Table 4-11 and Table 4-12 in Section 4.8 for the experimental design).

6.2 Effect of Feedstock Elemental Composition on the Thermodynamic Equilibrium Yields at 450 °C

The effect of the feedstock composition on the thermodynamic calculated yields and gasification efficiencies was evaluated. This was done using the method developed in Chapter 3. The thermodynamic gas yields and gasification efficiencies in terms of the H/C and O/C ratios (molar) are shown in Figure 6-1 and Figure 6-2. The bullet points on each graph indicate the respective thermodynamic equilibrium yields and gasification efficiencies of the *E.grandis* (EG) and pyrolysis char material (SP1, VP1, SP3 and VP3). The exact calculated thermodynamic equilibrium results, using the composition of each of the feed material in the Aspen Plus® model, are also summarised in Table 6-1.

At the conditions under consideration (450 °C, 27 MPa and 10 wt.% dry solids loading), the H_2 yields for *E.grandis* wood chips and pyrolysis chars (SP1, SP3, VP1 and VP3) are in the same range, specifically around 5 mol/$kg_{feed,dry}$ – see Figure 6-1(a). However, the calculated CH_4, CO, CO_2 and total yields, as well as the gasification efficiencies differ significantly at these conditions. From a thermodynamic perspective, it follows that pyrolysis char SP3 and VP3 should produce the highest CH_4 yield (29 – 30 mol/$kg_{feed,dry}$), GE (187 – 198%), HE (426 – 474%) and as a gas product with the highest HHV (27 – 28 MJ/$kg_{feed,dry}$). The significantly higher thermodynamic equilibrium CH_4 yields, gasification efficiencies and HHV of the product gas are due to the lower O/C ratio in SP3 and VP3 compared to that of *E.grandis*, VP1 and SP1 (*i.e.* the higher carbon content and lower oxygen content). Hence, more carbon is available for the formation of CO_2, CO and CH_4 for SP3 and VP3. However, these calculations only consider thermodynamics and ignore important kinetic effects. Therefore, the actual kinetic effects and/or limitation of the various feedstock materials at these experimental conditions have been measured experimentally, as described in Section 6.3.

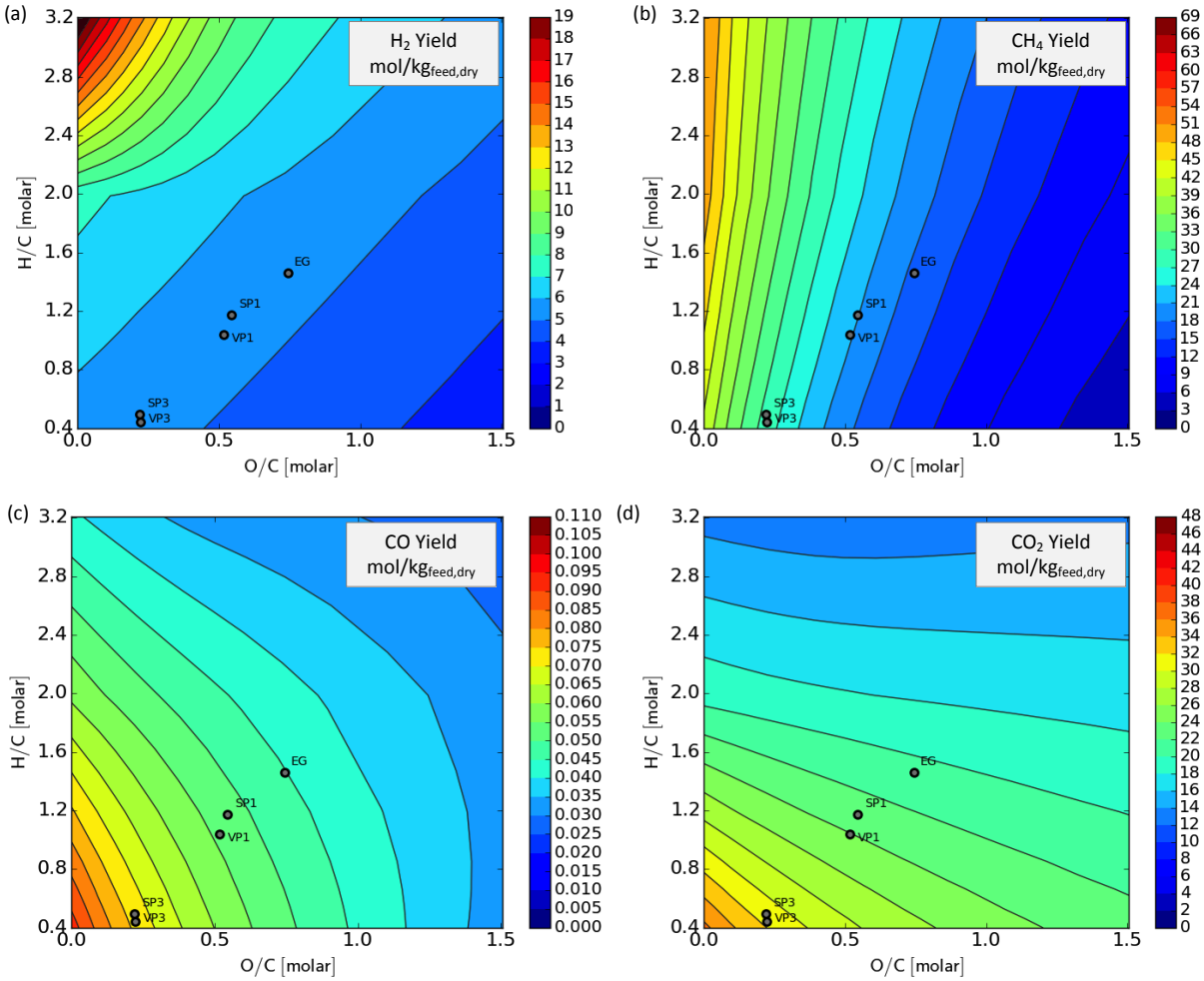

FIGURE 6-1 GENERALISED CONTOUR PLOT COMBINED WITH A VAN KREVELEN DIAGRAMS SHOWING THE EFFECT OF FEEDSTOCK COMPOSITION ON THE CALCULATED THERMODYNAMIC EQUILIBRIUM YIELDS AT 450 °C, 25 MPA AND FEEDING 10 WT.% DRY MATTER CONTENT: (A) H_2 YIELD, (B) CH_4 YIELD, (C) CO YIELD, (D) CO_2 YIELD.

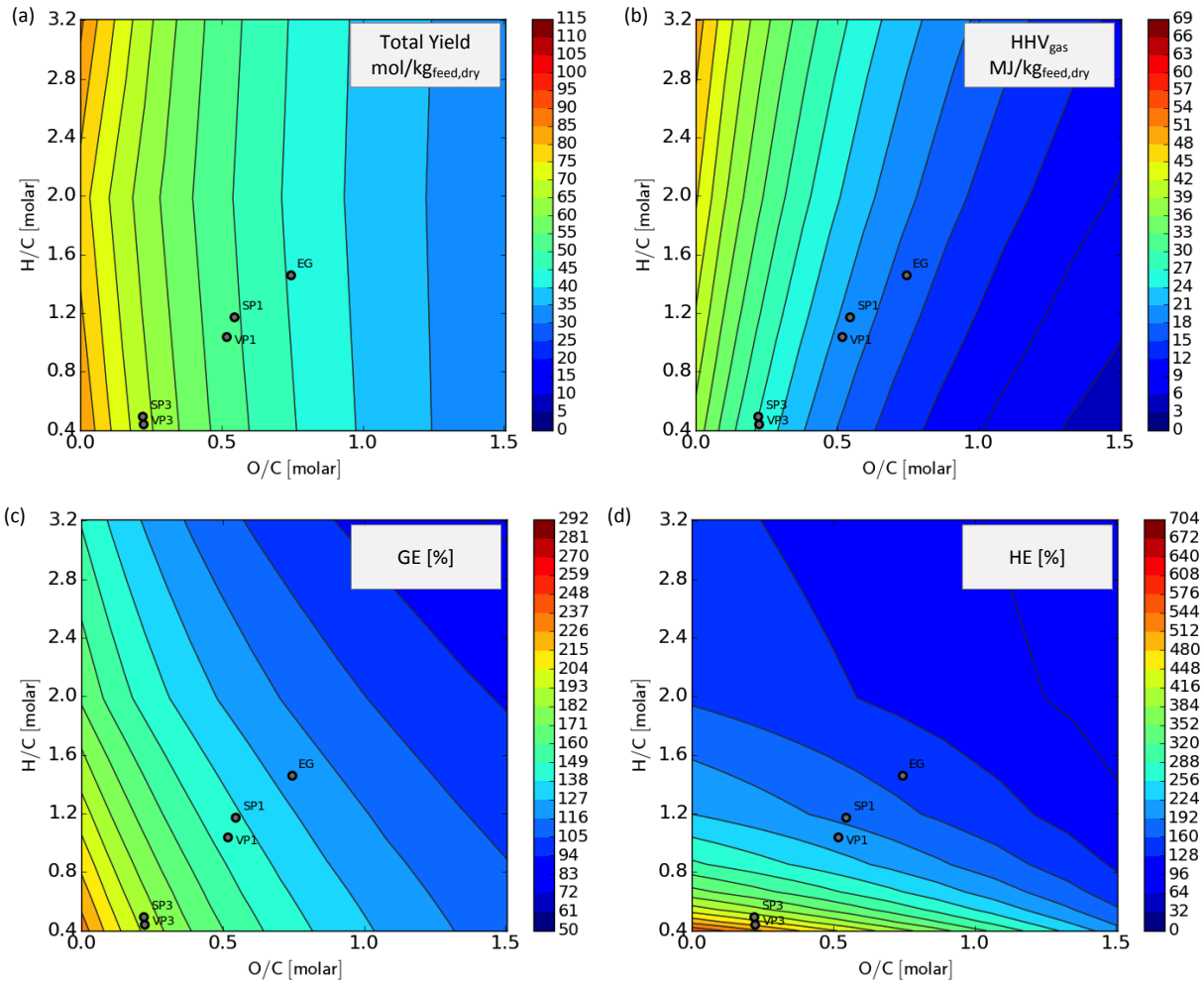

FIGURE 6-2 GENERALISED CONTOUR PLOT COMBINED WITH A VAN KREVELEN DIAGRAMS SHOWING THE EFFECT OF FEEDSTOCK COMPOSITION ON THE CALCULATED THERMODYNAMIC EQUILIBRIUM YIELDS AT 450 °C, 25 MPA AND FEEDING 10 WT.% DRY MATTER CONTENT: (A) TOTAL GAS YIELD, (B) HHV OF PRODUCT GAS, (C) GASIFICATION EFFICIENCY (GE), AND (D) HYDROGEN EFFICIENCY (HE).

TABLE 6-1 CALCULATED THERMODYNAMIC EQUILIBRIUM RESULTS FOR SCWG OF 10 WT.% DRY SOLID CONCENTRATION OF *E.GRANDIS* AND PYROLYSIS CHARS SP1, VP1, VP3 AND SP3 AT 450 °C AND 27 MPA

	EG	SP1	VP1	VP3	SP3
***Gas Composition* [mole %]**					
H_2	11.01	9.84	9.55	7.43	7.28
CO	0.10	0.11	0.11	0.11	0.11
CH_4	41.43	43.48	42.79	44.22	46.32
CO_2	47.45	46.58	47.55	48.24	46.29
***Gas Yield* [mol/$kg_{biomass,daf}$]**					
H_2	4.86	4.95	4.90	4.90	4.95
CO	0.05	0.05	0.05	0.07	0.07
CH_4	18.27	21.88	21.95	29.18	29.72
CO_2	20.93	23.45	24.39	31.83	31.43
Total	44.11	50.34	51.29	65.98	66.17
***Efficiencies* [%]**					
GE	124.96	139.44	143.69	188.08	187.20
CE	100.0	100.0	100.0	100.0	100.0
HE	144.65	183.23	202.79	473.98	426.23
ER	99.55	95.28	95.55	97.45	97.23
H_2 Selectivity	0.13	0.11	0.11	0.08	0.08
HHV [MJ/$kg_{feed,dry}$]	18.65	20.92	20.96	27.41	27.9

6.3 EXPERIMENTAL RESULTS

Experiments were conducted under three catalytic conditions – without the use of a catalyst; in the presence of a homogeneous catalyst (0.5 g/$g_{feed,dry}$ K_2CO_3); and using a heterogeneous catalyst (0.5 g/$g_{feed,dry}$ Ni/Al_2O_3-SiO_2) – each at a hold time of 60 minutes. Furthermore, experiments were also conducted at Ni/Al_2O_3-SiO_2 loadings of 0, 0.1, 0.5 and 1 g/$g_{feed,dry}$ Ni/Al_2O_3-SiO_2, and various hold times between 0 – 60 minutes using *E.grandis* and pyrolysis chars SP1 and SP3 as feed material (refer to back to Table 4-10, Table 4-11 and Table 4-12 in Section 4.8 for the experimental design). Table 6-2 provides a summary of the experimental results for each of the 35 experiments conducted.

TABLE 6-2 SUMMARY OF MAIN RESULTS AND EXPERIMENTAL CONDITIONS FOR EACH RUN

EXP. NO	EXP. NAME	FEED	CATALYST		T_{END} [D] [°C]	P_{END} [D] [MPA]	$T_{HEAT-UP}$	T_{HOLD}	$Y_{TOTAL\ GAS}$ [E]	MASS BAL. [%]	GASIFICATION EFFICIENCIES [%]				C IN WSP [MG/L]	
			TYPE	LOAD[C]							GE	CE	HE	ER	TOC	TIC
1	EG04	EG	-	-	450.8	27.1	10.3	60.4	11.0	93.0	33.6	23.9	17.1	13.7	7860	50
2	EG11	EG	K_2CO_3	0.50	451.8	26.9	12.9	60.2	19.7	91.0	50.7	33.8	40.2	20.8	4120	4800
3	EG03	EG	Ni	0.50	450.8	27.4	14.7	59.5	42.5	94.5	115.5	92.2	130.9	84.0	1100	b.d.l.[f]
4	CH07	SP1	-	-	449.4	25.6	16.2	59.1	9.5	96.2	30.7	17.8	15.9	8.6	5460	150
5	CH29	SP1	K_2CO_3	0.50	452.0	26.6	14.5	60.3	17.4	91.4	47.7	27.5	35.5	14.7	b.d.l.	b.d.l.
6	CH06	SP1	Ni	0.50	450.0	28.3	9.5	59.3	45.7	89.9	124.5	85.9	153.9	78.6	474	42
7	CH12	VP1	-	-	450.9	25.7	16.0	60.0	8.9	96.3	30.1	16.5	14.5	6.8	4490	30
8	CH31	VP1	K_2CO_3	0.50	450.3	27.2	14.5	59.7	17.3	90.7	45.9	25.4	39.8	14.6	b.d.l.	b.d.l.
9	CH10	VP1	Ni	0.50	450.4	27.9	14.2	59.7	38.0	95.2	105.2	70.0	138.7	63.9	480	14
10	CH14	SP3	-	-	451.6	26.2	10.3	59.7	4.8	92.9	17.8	7.0	9.9	2.1	b.d.l.	b.d.l.
11	CH32	SP3	K_2CO_3	0.50	450.8	26.0	14.3	59.7	7.2	99.7	21.5	9.3	25.3	4.8	874	6596
12	CH09	SP3	Ni	0.50	452.2	26.0	14.0	60.0	12.9	90.5	35.0	14.8	54.9	10.5	b.d.l.	93
13	CH13	VP3	-	-	451.0	25.6	16.0	59.9	6.1	98.9	23.7	9.4	12.8	2.6	b.d.l.	b.d.l.
14	CH30	VP3	K_2CO_3	0.50	450.7	25.9	21.8	59.4	8.0	91.3	26.3	10.5	24.3	4.1	528	6402
15	CH11	VP3	Ni	0.50	449.1	26.9	15.3	59.7	14.2	92.3	41.4	16.9	58.1	9.8	b.d.l.	b.d.l.
16	EG09	EG	Ni	0.1	451.2	27.2	16.6	60.1	24.6	95.4	64.9	47.0	53.6	32.5	10700	240
17	EG10	EG	Ni	1.0	450.6	28.6	15.2	59.4	42.4	105.0	117.5	92.0	123.7	79.0	1780	10
18	EG07	EG	Ni	0.5	403.3	23.8	6.4	0.0	21.8	89.8	59.3	41.4	44.4	26.2	12370	60
19	EG08	EG	Ni	0.5	450.3	27.7	12.2	0.0	35.4	97.1	96.3	72.1	89.2	54.7	8590	20
20	EG06	EG	Ni	0.5	450.6	27.6	15.0	15.0	37.9	98.3	99.6	75.9	103.3	62.5	5440	20
21	EG05	EG	Ni	0.5	451.8	28.7	9.9	30.5	41.4	95.0	108.7	81.8	117.5	72.1	2500	50

[c] $g/g_{feed,dry}$

[d] Temperature and pressure in reactor before cool down

[e] $mol/kg_{feed,dry}$

[f] below detection limit

TABLE 6-2 CONTINUED - SUMMARY OF MAIN RESULTS AND EXPERIMENTAL CONDITIONS FOR EACH RUN

EXP. NO	EXP. NAME	FEED	CATALYST		T_{END}[D] [°C]	P_{END}[D] [MPA]	$T_{HEAT-UP}$	T_{HOLD}	$Y_{TOTAL\ GAS}$[E]	MASS BAL. [%]	GASIFICATION EFFICIENCIES [%]				C IN WSP [MG/L]	
			TYPE	LOAD[C]							GE	CE	HE	ER	TYPE	LOAD[C]
22	EG03	EG	Ni	0.5	450.8	27.4	14.7	59.5	42.5	91.2	115.5	92.2	130.9	84.0	1100	b.d.l.
23	CH24	SP1	Ni	0.1	450.0	28.1	16.1	59.1	28.7	97.3	78.3	51.8	83.8	41.7	3800	50
24	CH22	SP1	Ni	1.0	450.9	29.0	14.9	59.7	45.1	90.9	126.1	87.3	151.0	77.7	480	72
25	CH18	SP1	Ni	0.5	405.3	23.0	6.4	0.0	15.9	90.4	46.0	27.0	32.5	15.2	7380	80
26	CH17	SP1	Ni	0.5	450.1	26.9	16.0	0.0	35.1	95.7	95.6	63.6	106.8	53.0	2750	80
27	CH08	SP1	Ni	0.5	450.4	27.8	13.0	15.0	40.2	93.7	109.1	73.8	130.3	65.8	472	39
28	CH15	SP1	Ni	0.5	450.8	28.2	14.7	29.6	41.3	93.6	112.7	78.1	139.1	71.0	b.d.l.	b.d.l.
29	CH16	SP1	Ni	0.5	451.2	282.8	27.6	119.9	46.7	88.9	128.4	89.5	159.8	82.0	b.d.l.	b.d.l.
30	CH28	SP3	Ni	0.1	450.0	26.9	15.0	60.0	13.2	92.3	35.1	15.2	59.8	11.6	50	70
31	CH27	SP3	Ni	1.0	451.6	26.2	16.9	60.6	13.5	97.3	38.4	15.6	51.2	9.7	b.d.l.	b.d.l.
32	CH20	SP3	Ni	0.5	403.1	22.6	6.2	0.0	4.8	104.3	13.3	4.9	14.0	2.2	b.d.l.	b.d.l.
33	CH19	SP3	Ni	0.5	450.3	25.7	13.8	0.0	8.5	90.7	24.1	9.8	31.3	5.8	236	126
34	CH26	SP3	Ni	0.5	448.1	25.7	13.8	14.9	11.4	95.6	32.2	13.4	44.8	8.6	1	87
35	CH25	SP3	Ni	0.5	451.3	26.4	14.7	30.6	11.9	92.1	34.0	14.3	48.2	9.4	78	92

[c] $g/g_{feed,dry}$

[d] Temperature and pressure in reactor before cool down

[e] $mol/kg_{feed,dry}$

[f] below detection limit

6.3.1 Effect of Elemental Composition and Volatile Matter Content of Feed Material

The results for the gas yields and gasification efficiencies for catalytic and non-catalytic SCWG using both K_2CO_3 and Ni/Al_2O_3-SiO_2 using *E.grandis* (EG), and pyrolysis chars SP1, VP1, VP3 and SP3 are shown in Figure 6-3, Figure 6-4, Figure 6-5, Figure 6-6 and Figure 6-7, respectively.

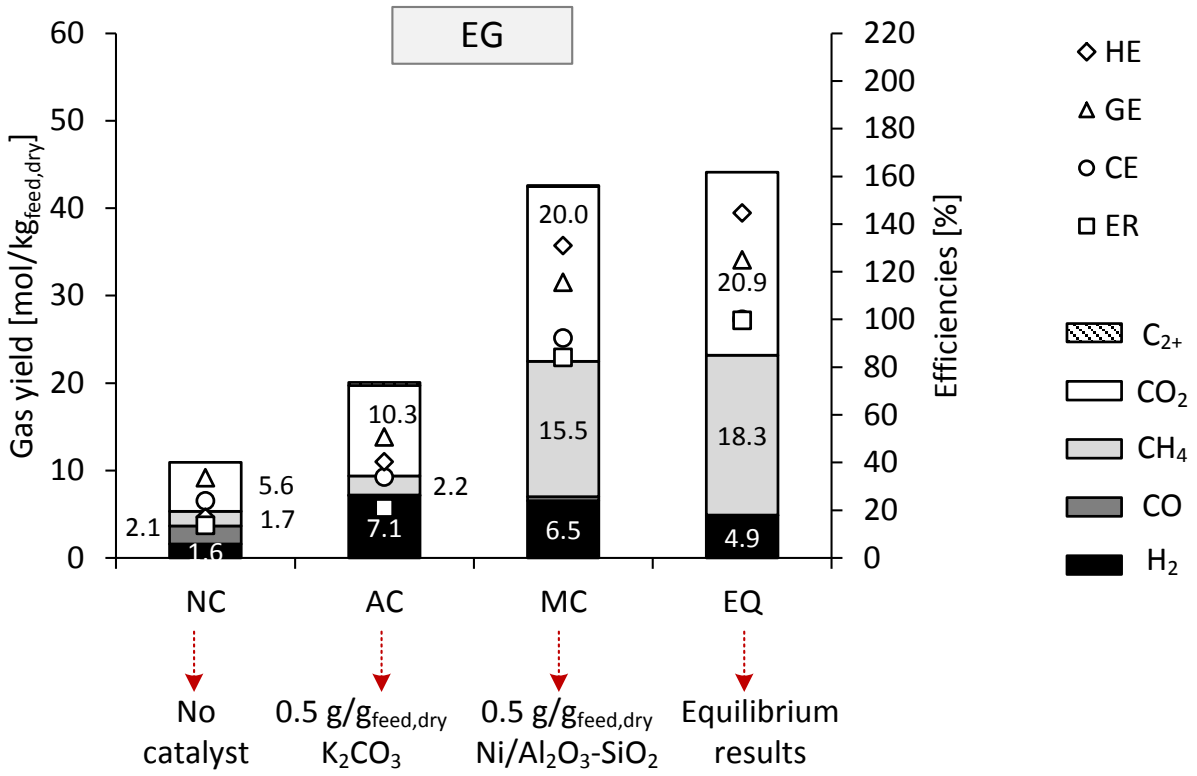

Figure 6-3 Experimental and Equilibrium results for *E.Grandis* (EG) showing the effect of the addition of 0.5 g/g K_2CO_3 and 0.5 g/g Ni/Al_2O_3-SiO_2 on the gas yields and gasification efficiencies

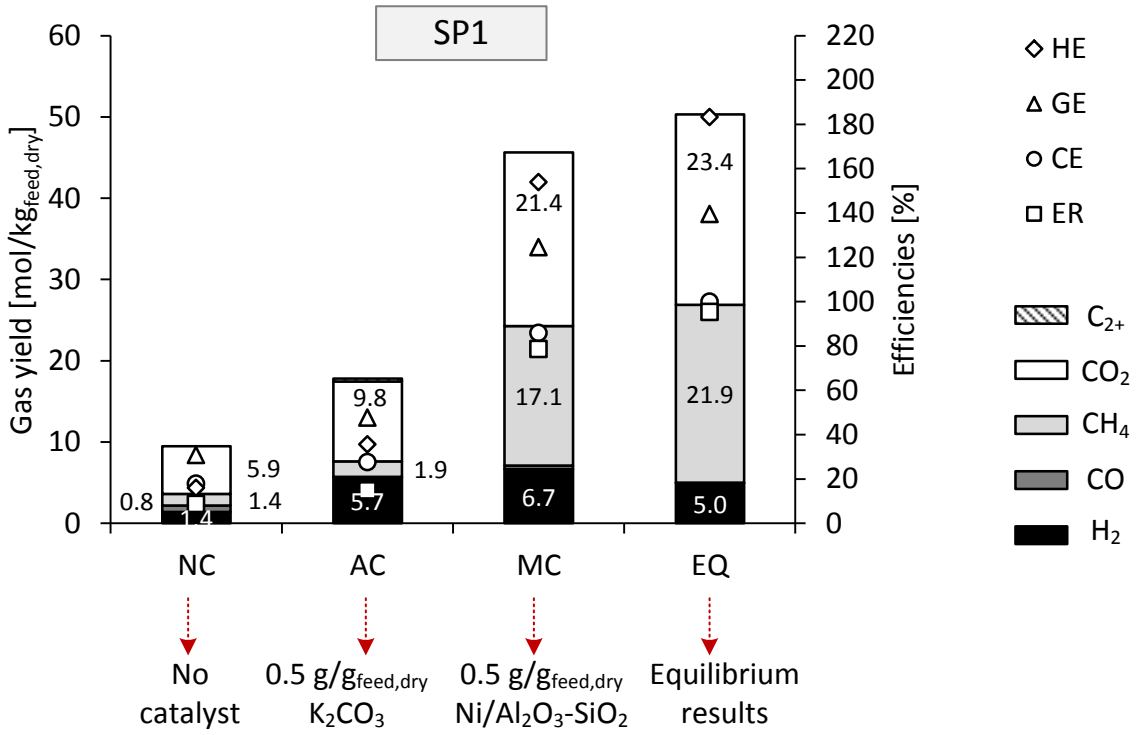

FIGURE 6-4 EXPERIMENTAL AND EQUILIBRIUM RESULTS FOR SP1 SHOWING THE EFFECT OF THE ADDITION OF 0.5 G/G K_2CO_3 AND 0.5 G/G NI/AL_2O_3-SIO_2 ON THE GAS YIELDS AND GASIFICATION EFFICIENCIES

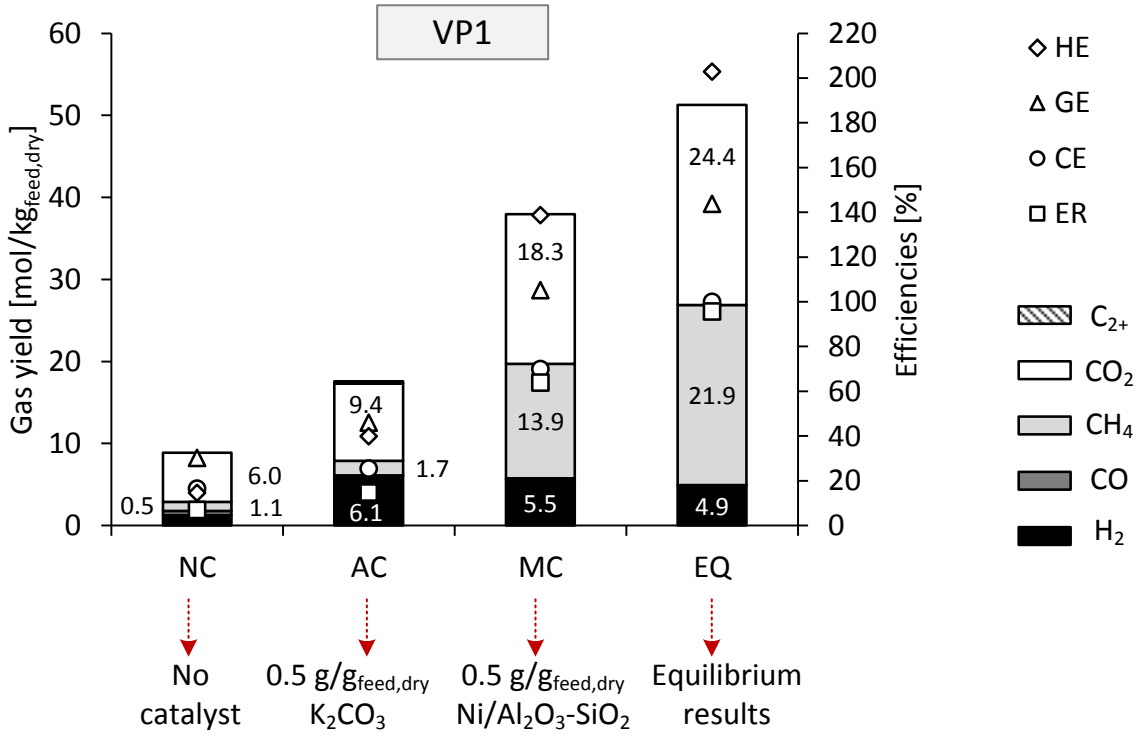

FIGURE 6-5 EXPERIMENTAL AND EQUILIBRIUM RESULTS FOR VP1 SHOWING THE EFFECT OF THE ADDITION OF 0.5 G/G K_2CO_3 AND 0.5 G/G NI/AL_2O_3-SIO_2 ON THE GAS YIELDS AND GASIFICATION EFFICIENCIES

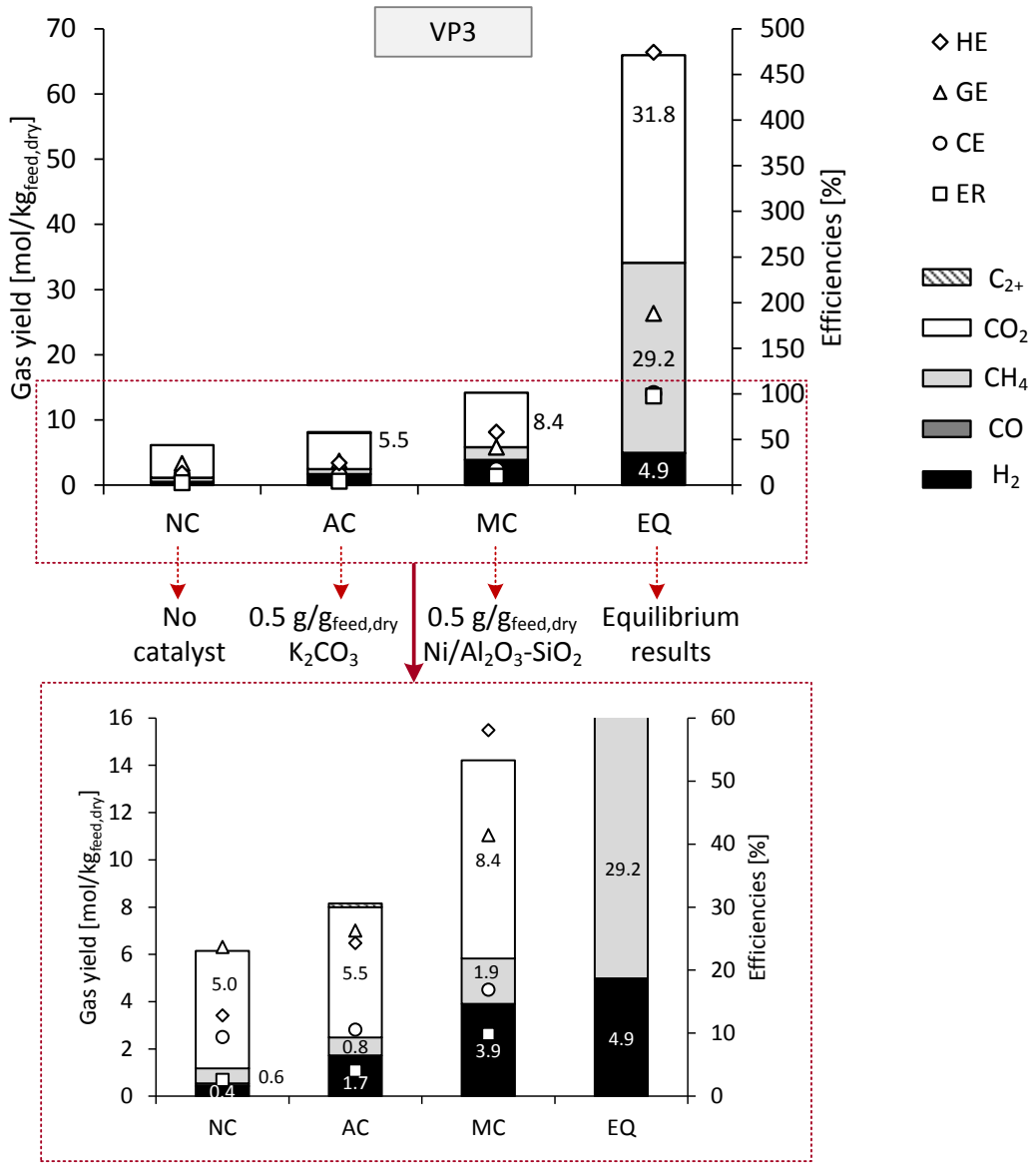

FIGURE 6-6 EXPERIMENTAL AND EQUILIBRIUM RESULTS FOR VP3 SHOWING THE EFFECT OF THE ADDITION OF 0.5 G/G K_2CO_3 AND 0.5 G/G NI/AL_2O_3-SIO_2 ON THE GAS YIELDS AND GASIFICATION EFFICIENCIES

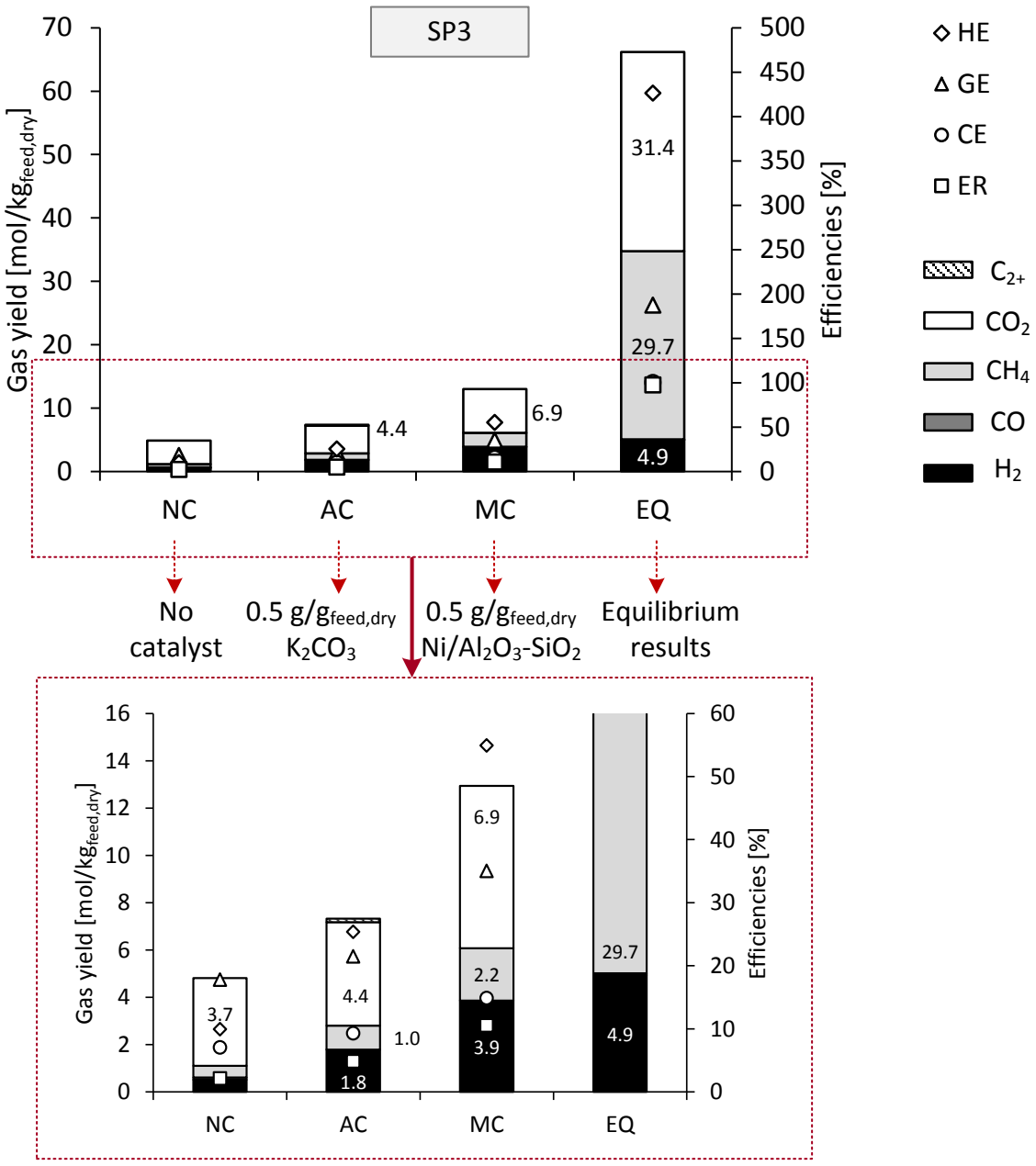

FIGURE 6-7 EXPERIMENTAL AND EQUILIBRIUM RESULTS FOR SP3 SHOWING THE EFFECT OF THE ADDITION OF 0.5 G/G K_2CO_3 AND 0.5 G/G NI/AL_2O_3-SIO_2 ON THE GAS YIELDS AND GASIFICATION EFFICIENCIES

The use of both K_2CO_3 and Ni/Al_2O_3-SiO_2 as catalyst enhanced the formation of H_2 for all five feedstock material compared to the non-catalytic cases. The addition of K_2CO_3 did not have a significant catalytic effect on the formation of CH_4 for any of the feedstock material used. The addition of Ni/Al_2O_3-SiO_2, however, resulted in CH_4 yields approximately ten times higher than the non-catalytic cases when *E.grandis* and pyrolysis char SP1 and VP1 were used as feedstock material. The results indicate that the addition of Ni/Al_2O_3-SiO_2 enhances the formation of CH_4 and H_2 *via* the steam reforming and methanation of CO and CO_2, while the addition of K_2CO_3 enhances the formation of H_2 *via* the water-gas shift reaction. These results are in agreement with the results showing the difference in the catalytic effect of K_2CO_3 and Ni/Al_2O_3-SiO_2 for the SCWG of primary paper sludge (as presented in Chapter 5 of this dissertation).

During SCWG of *E.grandis* wood chips (Figure 6-3), gas yields and gasification efficiencies relatively close to the calculated thermodynamic equilibrium yields could be achieved with the addition of Ni/Al_2O_3-SiO_2, with almost 93% of the carbon in the feed material converted to the gas phase. The energy recovery was 83% and gas with a HHV of 14 $MJ/kg_{feed,dry}$ could be produced.

Pyrolysis char SP1 (Figure 6-4) produced similar results than *E.grandis* during catalytic (with both K_2CO_3 as well as Ni/Al_2O_3-SiO_2 addition) and non-catalytic experiments. Although a higher maximum CH_4 yield was achieved compared to experiments with *E.grandis* (17.1 $mol/kg_{feed,dry}$ for SP1 compared to 15.5 $mol/kg_{feed,dry}$ for *E.grandis*), only 86% of the carbon in the feed material was converted to the gas phase. A product gas with a HHV of 15.4 $MJ/kg_{feed,dry}$ was produced, resulting in an energy recovery of 79%. SCWG of VP1 (Figure 6-5) in the presence of K_2CO_3 catalyst, produced results similar to SCWG of SP1 in the presence of K_2CO_3. However, in the presence of Ni/Al_2O_3-SiO_2, SP1 produced better yields and gasification efficiencies than VP1 (CE: 70 %, ER: 64% and HHV: 12.5 $MJ/kg_{feed,dry}$).

In contrast to the results obtained with *E.grandis*, SP1 and VP1 as feed materials, experiments using VP3 and SP3 resulted in very low gas yields and poor gasification efficiencies, even with the addition of a catalyst (see Figure 6-6 and Figure 6-7). Although the addition of both K_2CO_3 and Ni/Al_2O_3-SiO_2 did result in an increase in the gas yields and gasification efficiencies, the respective yields were still very far from the calculated equilibrium values. For example, only

14% (for VP3) and 17% (for SP3) of the carbon in the feed material were converted to the gas phase with the addition of Ni/Al_2O_3-SiO_2. Furthermore, the addition of Ni/Al_2O_3-SiO_2 resulted in CH_4 yields only two times higher than the non-catalytic cases, compared to the ten times higher yields achieved when using *E.grandis*, SP1, or VP1 as feed material.

Minowa and Ogi (1998) were the first to describe the reaction mechanism of cellulose over a nickel catalyst in sub- and supercritical water. They suggested that cellulose undergoes hydrolysis to form water soluble products, which in turn are either gasified to H_2, CO, CO_2 and CH_4 over a nickel catalyst or undergo polymerisation to oil and char. Carbon monoxide (CO) is an intermediate product formed during the steam reforming reaction of water soluble products (Eq. 6-1). It is needed for the formation of both H_2 *via* the water-gas shift reaction (Eq. 6-2) and CH_4 *via* methanation of H_2 with CO (Eq. 6-3). Hence, if no water soluble products have formed, steam reforming of these water soluble products cannot take place, and the only way in which CO can then be formed is *via* the steam reforming of solid carbon, as proposed by Matsumura et al. (1997) (Eq. 6-4).

$$CH_xO + (1-y)H_2O \rightarrow CO + (\frac{x}{2} + 1 - y)H_2 \quad \text{6-1}$$

$$CO + H_2O \rightleftharpoons CO_2 + H_2 \quad \text{6-2}$$

$$CO + 3H_2 \rightleftharpoons CH_4 + H_2O \quad \text{6-3}$$

$$C + H_2O \rightarrow H_2 + CO \quad \text{6-4}$$

The CO yield was the highest during the experiments when no catalyst was added for each of the five different feedstock material (see Table 6-3). While the CO yields were significantly lower in experiments with Ni/Al_2O_3-SiO_2 catalyst, it was even lower in experiments with K_2CO_3 catalyst. The highest CO yields were achieved during the non-catalytic experiments. Furthermore, the CO yield also decreased as the O/C ratio in the feed material decreased (as can be seen in Table 6-3). No CO was detected in the product gas when VP3 and SP3 were used as feed material during catalytic SCWG. This indicates that all of the CO formed during the

steam reforming reaction was consumed (either *via* the water-gas shift reaction or the methanation reaction), and that the formation of CO was the limiting reaction.

TABLE 6-3 CO YIELD (MOL/$KG_{FEED,DRY}$) DURING NON-CATALYTIC AND CATALYTIC SCWG OF *E.GRANDIS* AND PYROLYSIS CHARS SP1, VP1, VP3 AND SP3.

CATALYST	EG	SP1	VP1	VP3	SP3
None	2.09	0.80	0.51	0.10	0.10
0.5 $g/g_{dry,feed}$ K_2CO_3	0.08	0.07	0.04	0.00	0.00
0.5 $g/g_{dry,feed}$ Ni/Al_2O_3-SiO_2	0.49	0.46	0.26	0.00	0.00
O/C ratio in feed material	0.75	0.55	0.52	0.23	0.22
Volatile matter content [wt.%]	83.3	74.6	68.3	30.7	26.6

Castello et al. (2014) did not detect any CO in the product gas during the SCWG of hydrochar either. However, they found that the CH_4 yield increased five times after a reaction time of 16 hours compared to a reaction time of 60 minutes during the SCWG of hydrochar at 400 °C and 30 MPa, but the CH_4 yield was still 20 times lower than their calculated equilibrium values. Their results suggest that CH_4 formation occurred *via* the decarboxylation reaction of acetic acid to form CH_4 and CO_2.

Figure 6-8(a)-(c) show the gasification efficiency (GE), hydrogen efficiency (HE) and energy recovery (ER) as a function of the O/C ratio in the feedstock material for non-catalytic SCWG, K_2CO_3 catalysed SCWG and Ni/Al_2O_3-SiO_2 catalysed SCWG, respectively. Typically, the lower the O/C in the feed material, the lower the efficiencies. However, using SP1 and VP1 as feed materials resulted in higher hydrogen efficiencies compared to *E.grandis*. It must be noted that the HE and GE can exceed 100%, as the H_2 that is formed during SCWG may also originate from the excess water present. Hence, the GE and HE cannot be directly correlated to the dry feed material. The CE, however, cannot exceed 100%, as all the carbon in the system must have originated from the dry feed material.

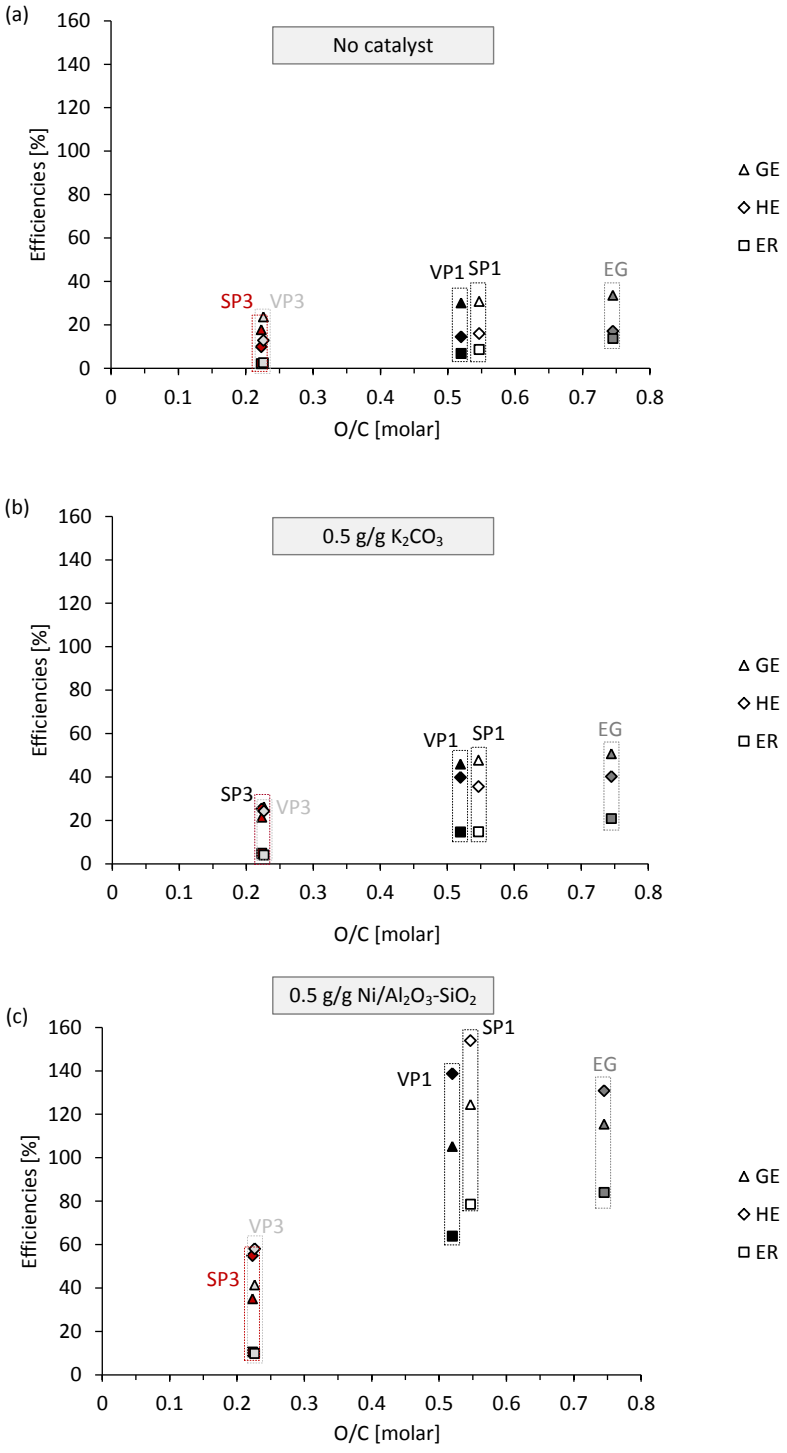

FIGURE 6-8 EXPERIMENTAL RESULTS SHOWING THE EFFECT OF O/C RATIO IN THE FEED MATERIAL ON THE GASIFICATION EFFICIENCIES DURING SCWG AT 450 °C AND HOLD TIME OF 60 MIN: (A) NO ADDED CATALYST, (B) 0.5 $G/G_{FEED,DRY}$ K_2CO_3, AND (C) 0.5 $G/G_{FEED,DRY}$ NI/AL_2O_3-SIO_2.

Figure 6-9(a) and (b) show the CE as a function of the volatile matter content and the O/C ratio of the feed material, respectively. Typically, lower CE's were achieved when materials with lower O/C ratios were used as feed material. This means that the lower the oxygen content in the feed material (or the higher the carbon content), the more difficult it was to convert the carbon in the feed material to the gas phase. Therefore, although thermodynamics dictate that feed material with lower O/C ratios should result in higher gasification efficiencies and CH_4 yields, there are clear kinetic limitations in practice.

What is interesting is that a linear relationship between the O/C ratio and CE as well as the volatile matter and the CE was found to be true for each of the three cases, depending on the catalyst type.

Typically, the feedstock material with higher volatile matter (*i.e.*, higher fixed carbon content) resulted in a higher percentage of carbon conversion to the gas phase. This shows that, although thermodynamic equilibrium calculations assume that 100% of the carbon in the feed material should be converted to the gas phase, the volatile matter and fixed carbon content plays a significant role in how easily a specific material will gasify in SCW at the specific operating conditions. Hence, the high percentage of fixed carbon in pyrolysis chars SP3 and VP3 might have acted as a kinetic sink, which may require much longer reaction times for gasification in SCW. During SCWG of various sludges, Zhang et al. (2010b) also found that the sludge with the lowest volatile matter content resulted in the lowest gas yields and gasification efficiencies.

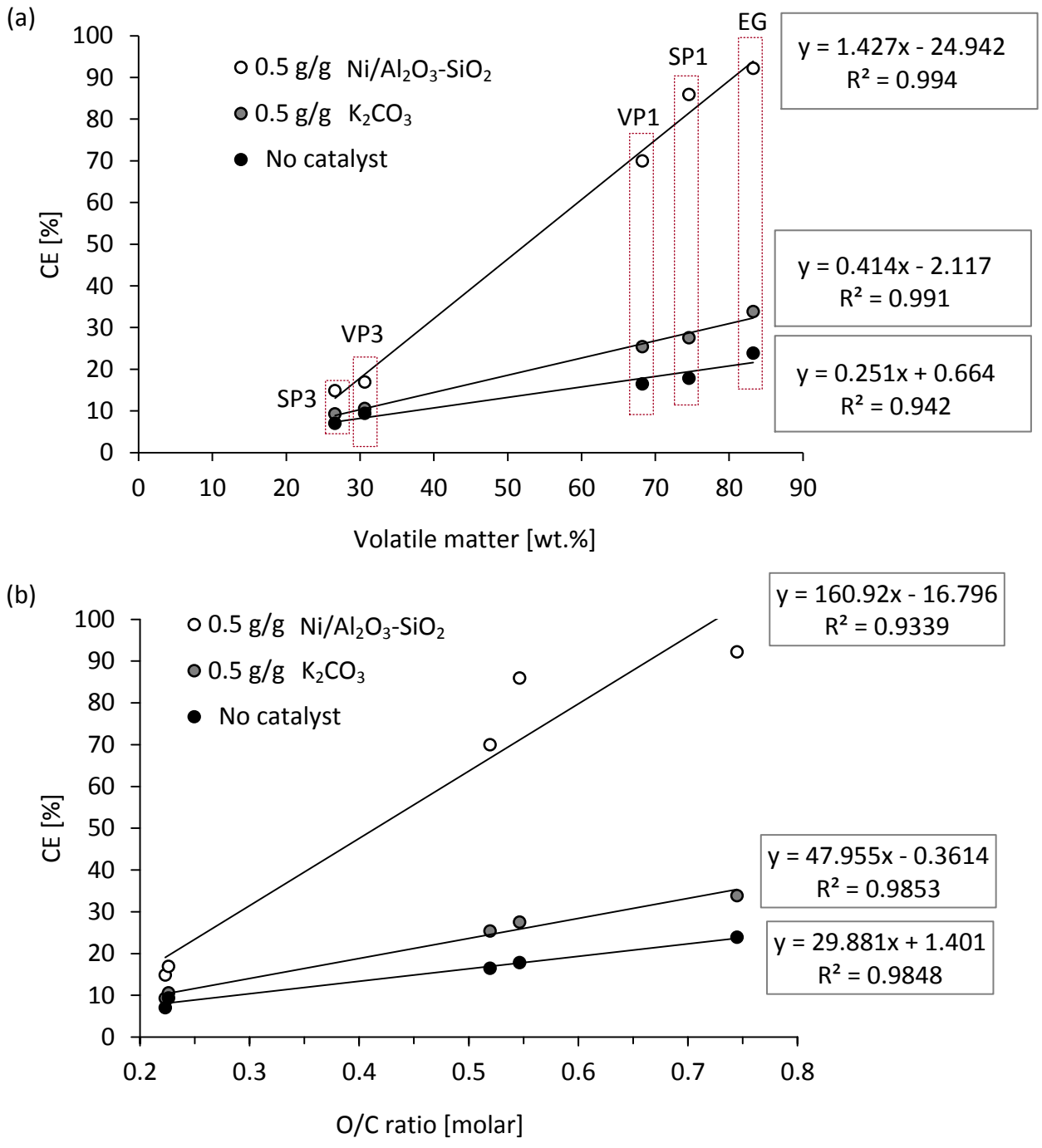

FIGURE 6-9 EFFECT OF THE VOLATILE MATTER IN THE FEEDSTOCK MATERIAL ON THE CARBON GASIFICATION EFFICIENCIES DURING CATALYTIC AND NON-CATALYTIC SCWG AT 450 °C

6.3.2 Effect of Ni/Al_2O_3-SiO_2 Loading

The effect of Ni/Al_2O_3-SiO_2 loading on the gas composition, gas yields and gasification efficiencies using *E.grandis*, pyrolysis char SP1 and SP3 as feed material are shown in Figure 6-10, Figure 6-11 and Figure 6-12, respectively. Product gas composition and gas yields relatively close to the equilibrium values together with carbon gasification efficiencies of 87% and 92% were achieved when *E.grandis* and pyrolysis char SP1 were used as feed material at the highest catalyst loading of 1 $g/g_{feed,dry}$. However, only 15% of the carbon in the feed material was converted to the gas phase when pyrolysis char SP3 was gasified using the highest catalyst loading of 1 $g/g_{feed,dry}$.

An initial increase in the catalyst loading resulted in a significant increase in the H_2 content and yield for all three feed materials. A further increase in the catalyst loading to 0.5 and 1 $g/g_{feed,dry}$, did not seem to have a significant effect on the H_2 yield. The initial increase in the catalyst loading also resulted in an increase in the carbon concentration in the WSP (see Table 6-2) when *E.grandis* and pyrolysis char SP1 were used as feed material. The same trend was observed when the effect of Ni/Al_2O_3-SiO_2 loading was investigated during the SCWG of primary paper sludge, as reported in the previous chapter of this dissertation. However, when pyrolysis char SP3 was used as feed material, the carbon concentration in the WSP was always below the detection limit (< 0.05 mole %). This, together with the low gas yields and gasification efficiencies achieved, even at a high catalyst loading of 1 $g/g_{feed,dry}$, indicates that the formation of water soluble products did not occur during SCWG of pyrolysis char SP3.

The CH_4 yield and content in the gas phase also typically increased with an increase in the catalyst loading for all three cases, with the most significant increase in the CH_4 yield observed when pyrolysis char SP1 was used as feed material. When *E.grandis* and pyrolysis char SP1 were gasified, an increase in the catalyst loading from 0.5 to 1 $g/g_{feed,dry}$ did not result in a significant increase in the gas yields and gasification efficiencies. When pyrolysis char SP3 was gasified, an increase in the catalyst loading from 0.1 to 0.5 and 1 $g/ g_{feed,dry}$ did not result in a significant change in the gas yields or gasification efficiencies.

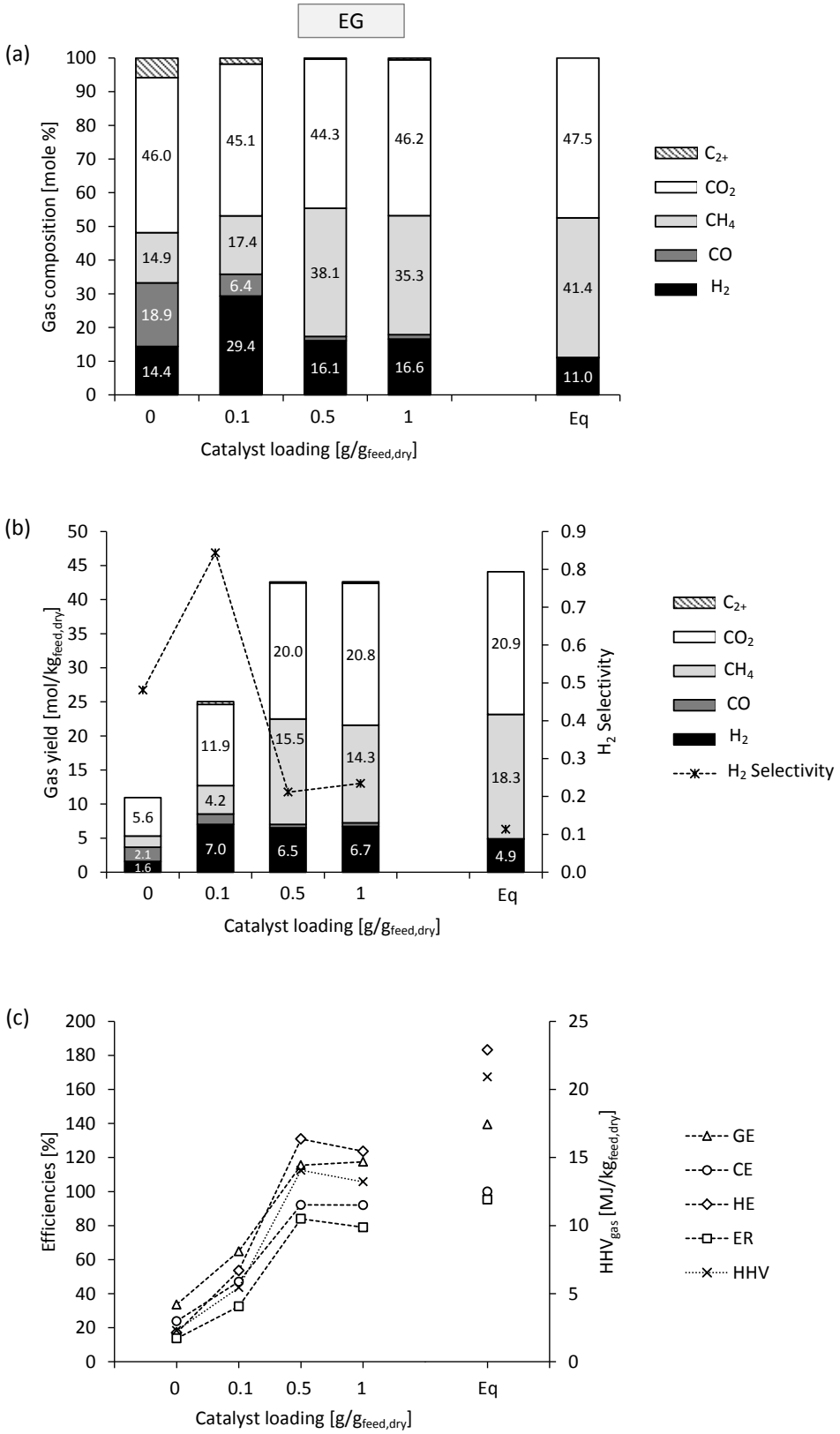

FIGURE 6-10 EFFECT OF NI/AL_2O_3-SIO_2 (A) PRODUCT GAS COMPOSITION, (B) GAS YIELDS AND H_2 SELECTIVITY, AND (C) GASIFICATION EFFICIENCIES DURING SCWG OF *E.GRANDIS* AT 450 °C (HOLD TIME OF 60 MIN)

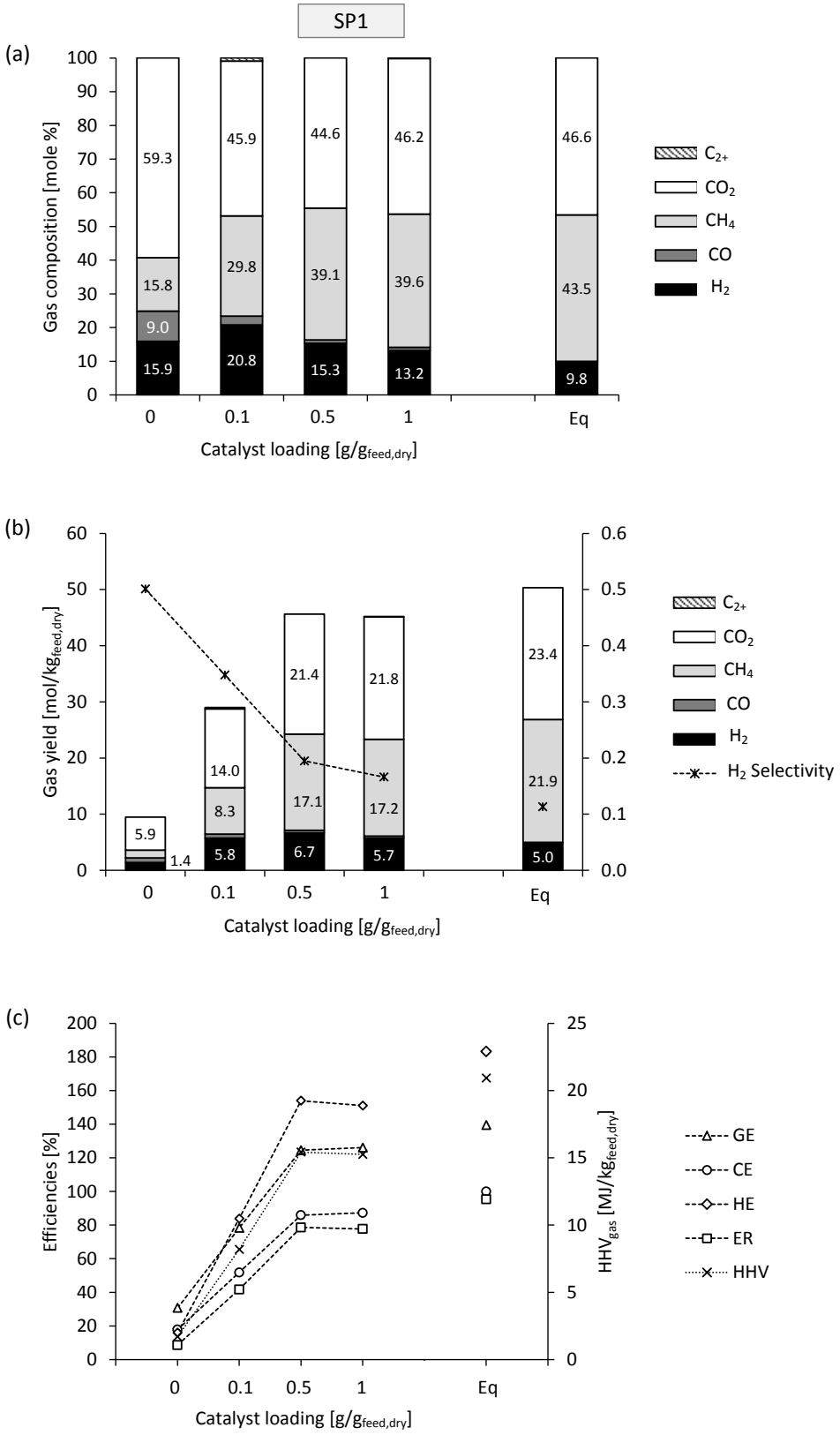

FIGURE 6-11 EFFECT OF NI/AL_2O_3-SIO_2 (A) PRODUCT GAS COMPOSITION, (B) GAS YIELDS AND H_2 SELECTIVITY, AND (C) GASIFICATION EFFICIENCIES DURING SCWG OF SP1 AT 450 °C (HOLD TIME OF 60 MIN)

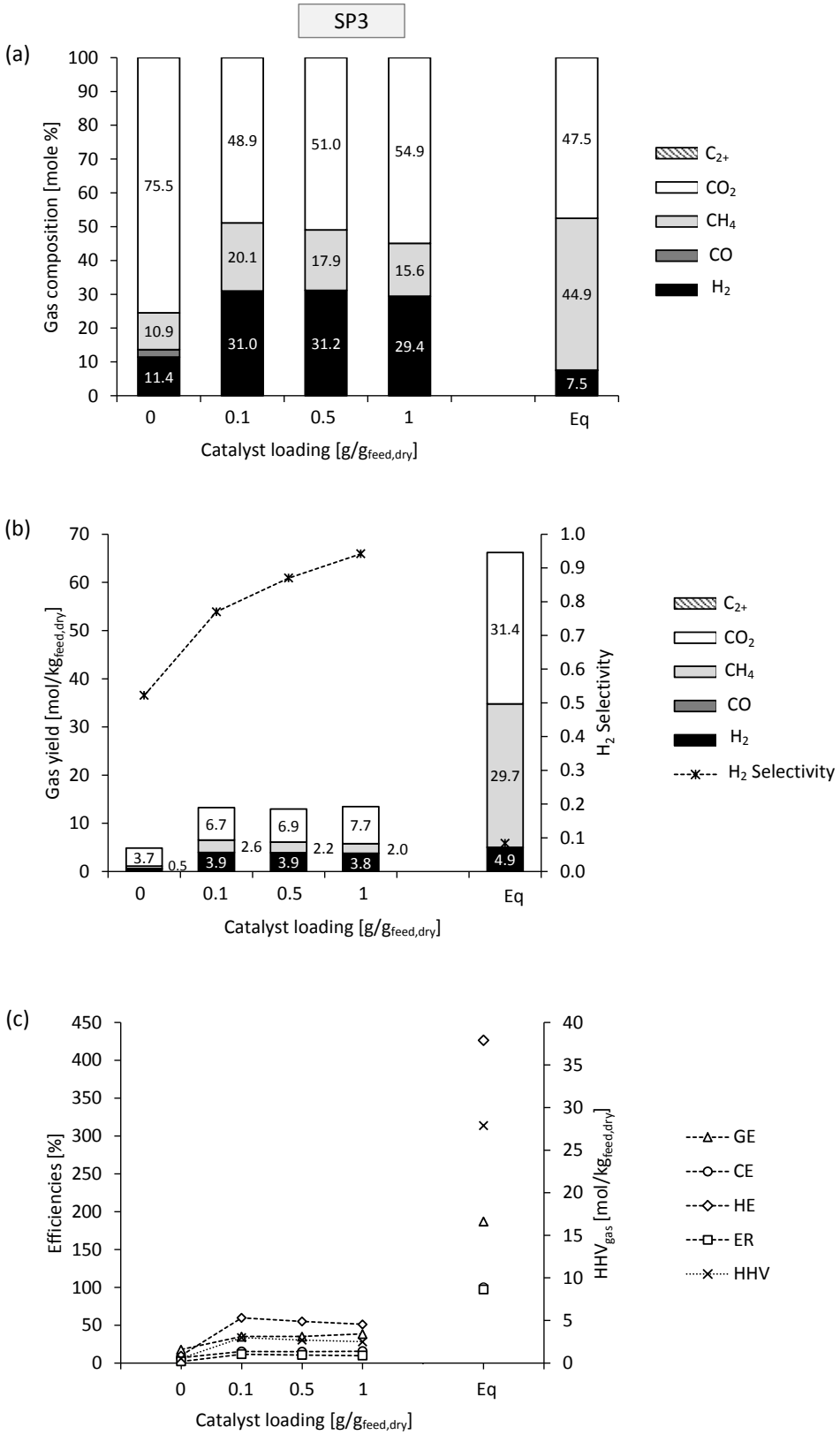

FIGURE 6-12 EFFECT OF NI/AL_2O_3-SIO_2 (A) PRODUCT GAS COMPOSITION, (B) GAS YIELDS AND H_2 SELECTIVITY, AND (C) GASIFICATION EFFICIENCIES DURING SCWG OF SP3 AT 450 °C (HOLD TIME OF 60 MIN)

An indication that a different mechanism was prevalent during the SCWG of the *E.grandis*, pyrolysis char SP1 and pyrolysis char SP3 is the variation in the trends of the H_2 selectivity as a function of the catalyst loading for each of these materials (see Figure 6-10(b), Figure 6-11(b) and Figure 6-12(b)). A similar trend in the H_2 selectivity was found when *E.grandis* was gasified compared to the results with primary paper sludge at the same conditions (as presented in Chapter 5 - see Figure 5-4). The decrease in the H_2 selectivity with an increase in the catalyst loading during SCWG of pyrolysis char SP1 shows that the formation of CH_4 was favoured over the formation of H_2 as the catalyst loading was increased. The increase in the H_2 selectivity with an increase in the catalyst load during SCWG of pyrolysis char SP3 shows that the formation of H_2 was favoured over that of CH_4. Furthermore, no CO was detected in the gas product during SCWG of pyrolysis char SP3 with an increase in the catalyst loading above 0.1 $g/g_{feed,dry}$. This further indicates that, although CH_4 yields of up to 33 $mol/kg_{feed,dry}$ were predicted for pyrolysis char SP3 at thermodynamic equilibrium, not enough CO formed to react with H_2 for the formation of CH_4, despite the high catalyst loading.

6.3.3 Effect of Reaction Time

Figure 6-13, Figure 6-14 and Figure 6-15 show the variation in the gas composition, gas yields and gasification efficiencies with an increase in the hold time. For each of these experiments, 0.5 $g/g_{feed,dry}$ Ni/Al_2O_3-SiO_2 was added as catalyst. The first data point in each of these graphs indicate the results during the heat-up phase when the temperature has reached 400 °C, while the second point shows the results once the temperature reached 450 °C , *i.e.* at a hold time of 0 minutes.

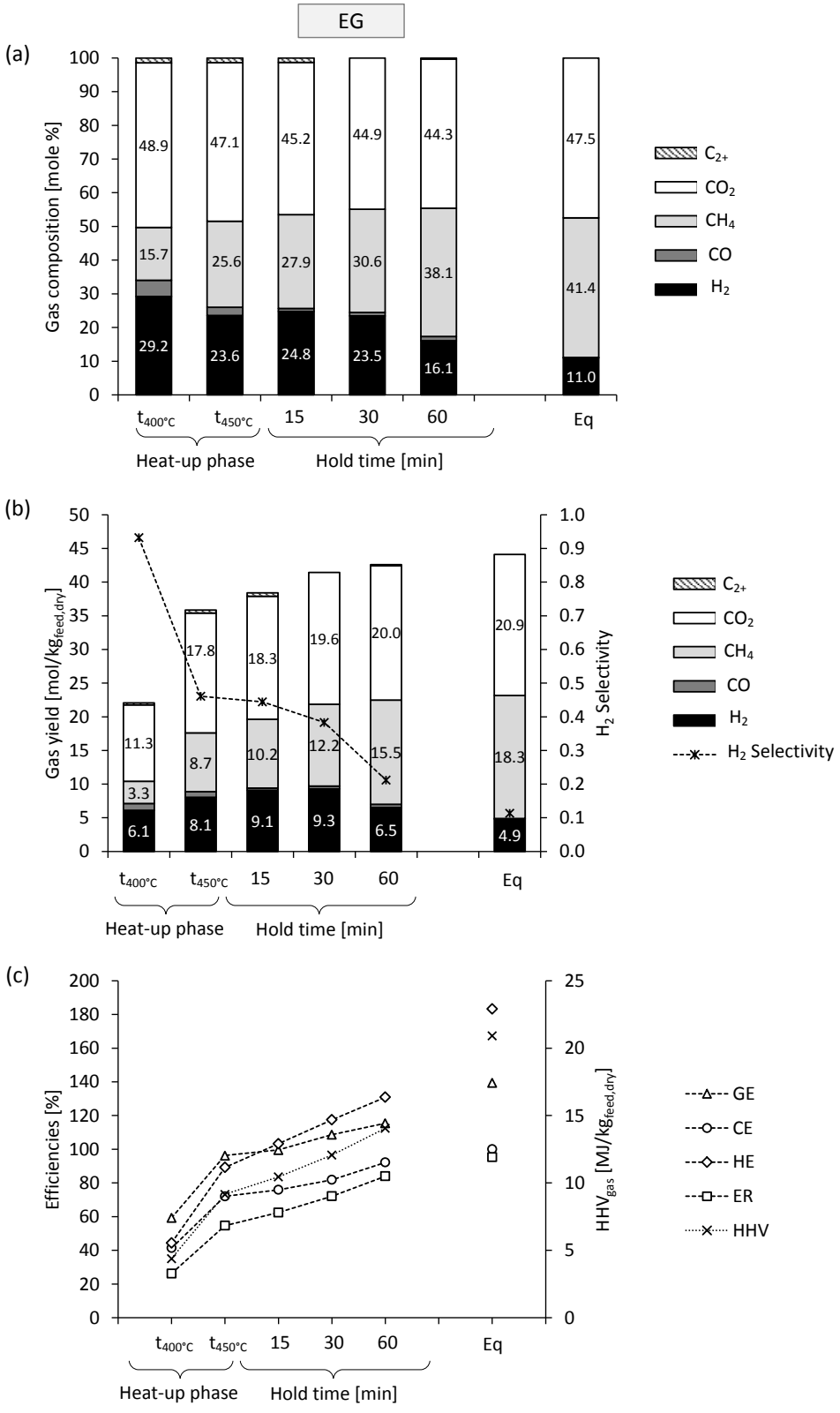

FIGURE 6-13 EFFECT OF HOLD TIME ON THE (A) PRODUCT GAS COMPOSITION, (B) GAS YIELDS AND H_2 SELECTIVITY, AND (C) GASIFICATION EFFICIENCIES DURING SCWG OF *E.GRANDIS* AT 450 °C (NI/AL_2O_3-SIO_2 LOADING OF 0.5 G/$G_{FEED,DRY}$)

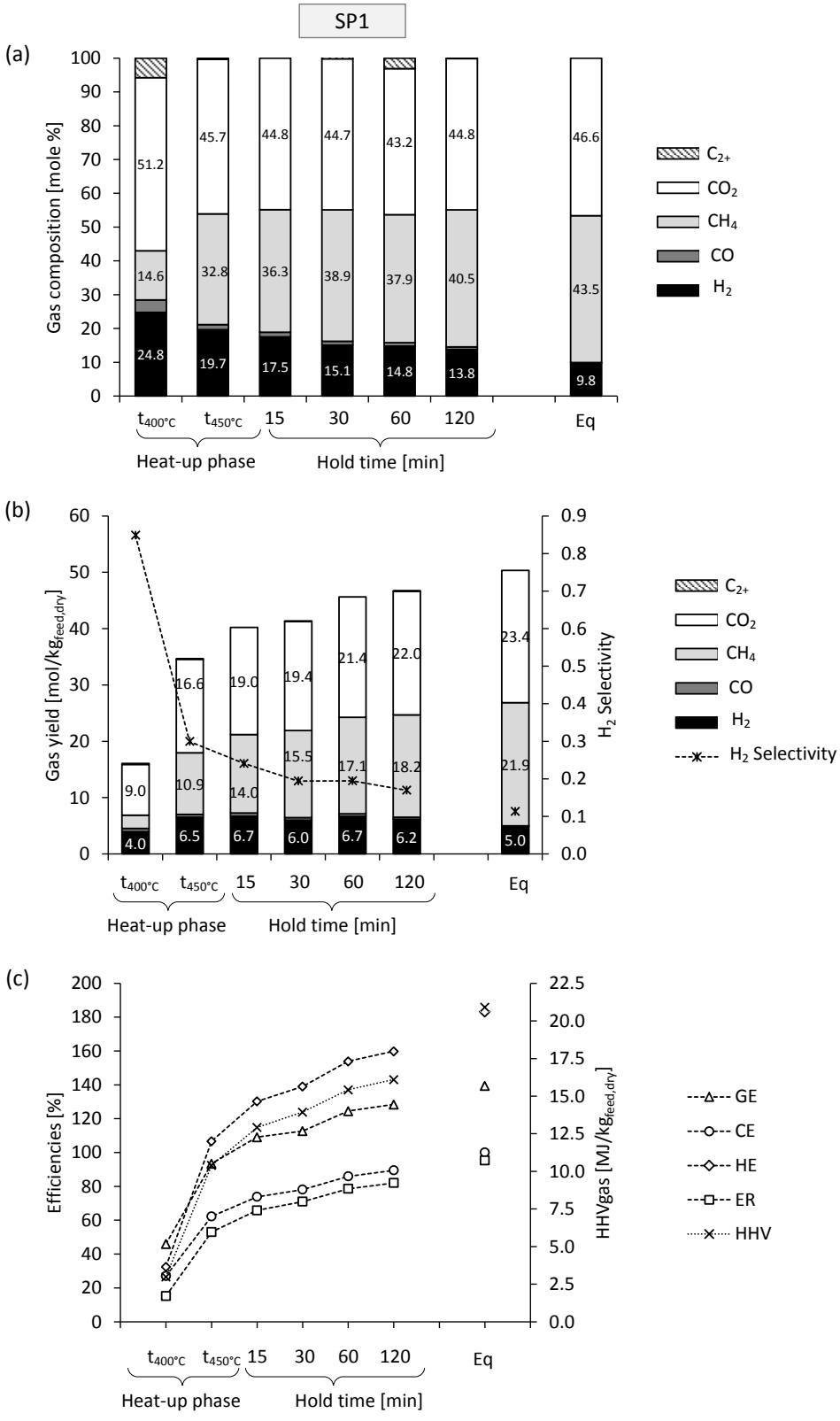

FIGURE 6-14 EFFECT OF HOLD TIME ON THE (A) PRODUCT GAS COMPOSITION, (B) GAS YIELDS AND H_2 SELECTIVITY, AND (C) GASIFICATION EFFICIENCIES DURING SCWG OF SP1 AT 450 °C (NI/AL_2O_3-SIO_2 LOADING OF 0.5 G/$G_{FEED,DRY}$)

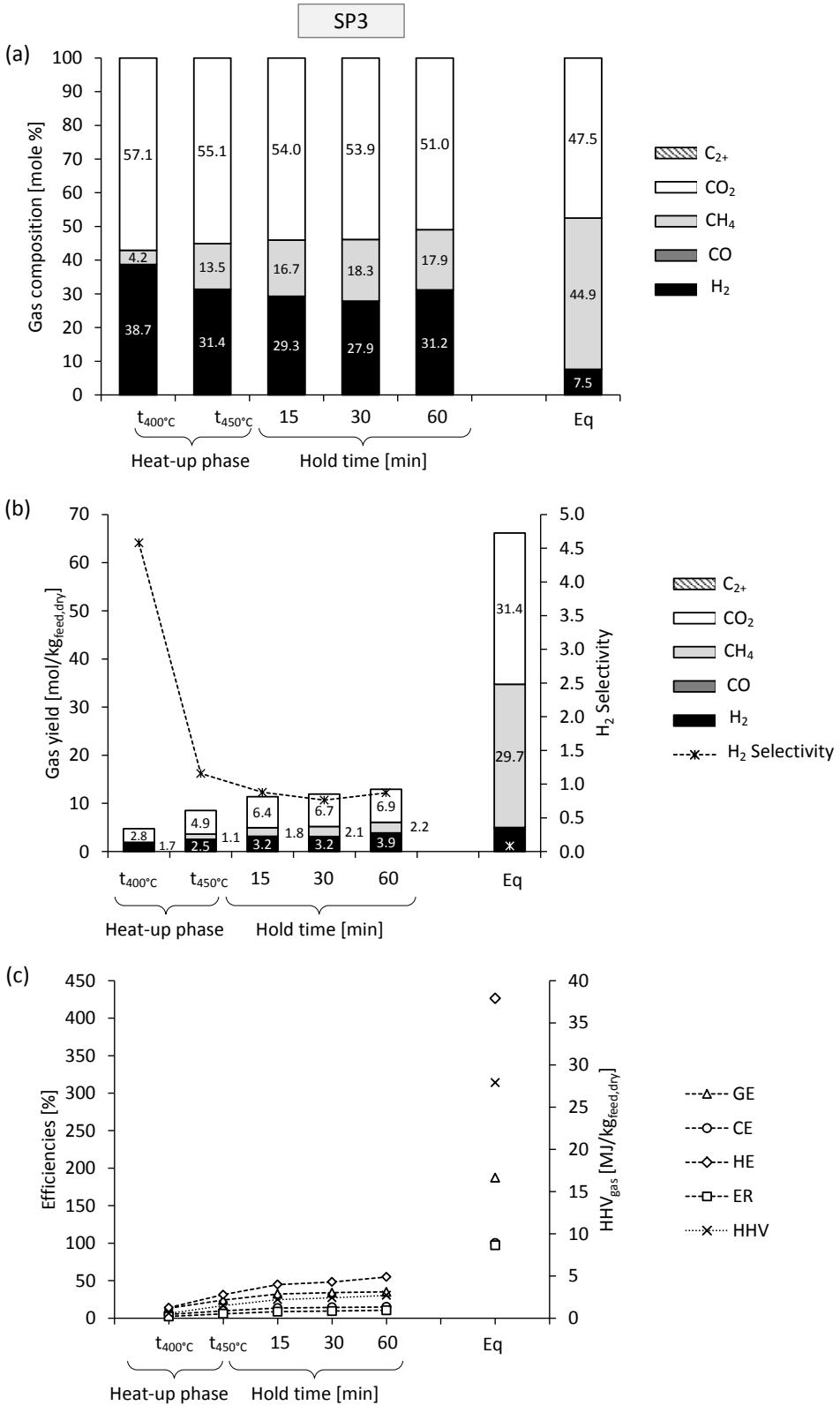

FIGURE 6-15 EFFECT OF HOLD TIME ON THE (A) PRODUCT GAS COMPOSITION, (B) GAS YIELDS AND H_2 SELECTIVITY, AND (C) GASIFICATION EFFICIENCIES DURING SCWG OF SP3 AT 450 °C (NI/AL_2O_3-SIO_2 LOADING OF 0.5 G/$G_{FEED,DRY}$)

What is of particular interest is that, when *E.grandis* was used as feed material, 42% of the carbon in the feed material was had already been converted to the gas phase once the temperature had reached 400 °C - approximately 6.4 minutes after the reactor was placed in the sand bath. Furthermore, after the temperature had reached the reaction temperature of 450 °C, 72% of the carbon in the feed material had already been converted to the gas phase. Hence, a significant portion of the gasification process occurred during the heat-up phase. The CE during the heat-up phase was somewhat lower when pyrolysis char SP1 was gasified compared to when *E.grandis* was gasified. Once the temperature reached 400 °C, 27% of the carbon was converted, while 63% had been converted once the temperature reached 450 °C. However, during SCWG of SP3, only 5% and 9% of the carbon in the feed material was converted to the gas phase once the temperature reached 400 and 450 °C, respectively.

The gasification efficiencies and the HHV of the product gas steadily increased with an increase in the hold time for each feedstock material (Figure 6-13(c), Figure 6-14(c) and Figure 6-15(c)). When SP1 was gasified, an additional experiment at a longer hold time of 120 minutes was conducted. Doubling the hold time to 120 minutes only resulted in a 3% increase in the carbon gasification efficiency and a 4% increase in the energy recovery. Furthermore, a product gas with a HHV of 16 MJ/kg_{feed} was produced after a hold time of 120 minutes, compared to that of 15.4 MJ/kg_{feed} at a hold time of 60 min. Despite a longer hold time of 120 minutes, the gas yields were still somewhat lower than the calculated equilibrium values.

Once the reactor reached 400 °C during the SCWG of *E.grandis*, the H_2 yield was already 6 mol/$kg_{feed,dry}$, while it increased to 8 mol/$kg_{feed,dry}$ as the temperature was increased to 450 °C. This is significantly higher than the H_2 yield at the same temperatures when pyrolysis char SP1 was gasified (3.9 mol/$kg_{feed,dry}$ at 400 °C and 6.5 mol/$kg_{feed,dry}$ at 450 °C). However, after a hold time of 60 min, no significant difference was observed between the H_2 yield obtained during SCWG of *E.grandis* compared to that of pyrolysis char SP1.

The CO yield during SCWG of *E.grandis* and pyrolysis char SP1 ranged between 0.3 and 1 mol/$kg_{feed,dry}$. However, no CO was detected in the product gas at any of the various hold times during SCWG of pyrolysis char SP3, hence the low CH_4 yield, even at a hold time of 60 minutes. The reason why no CO was detected when pyrolysis char SP3 was used as feed material can

once again be ascribed to the low O/C ratio of pyrolysis char SP3 (0.22) compared to that of *E.grandis* (0.74) and pyrolysis char SP1 (0.55). Hence, less oxygen is available for the formation of CO *via* steam reforming. Furthermore, the volatile matter content in pyrolysis char SP3 is also significantly lower than that of pyrolysis char SP1 and *E.grandis*, suggesting a direct link between the oxygen content in the feed material and its volatile matter content.

6.4 Outcome of This Chapter

The aim of this chapter was to determine the possible kinetic effects associated with the feedstock composition (in terms of the O/C content and volatile matter content) during SCWG of *E.grandis* wood chips and various related pyrolysis chars (***Objective 3***).

SCWG of pyrolysis char SP1 resulted in gas yields and gasification efficiencies relatively close to the equilibrium yields. The high oxygen content in pyrolysis char SP1 (39.6%), and the high volatile matter content (75%), resulted in higher initial formation of water soluble products, which in turn allowed for sufficient formation of CO *via* the steam reforming of water soluble products. Compared to experimental results from more conventional SCWG feedstock such as *E.grandis* (as presented in this chapter) and primary paper sludge (as presented in Chapter 5), pyrolysis char SP1 resulted in relatively similar gas yields and gasification efficiencies. However, pyrolysis char SP3 resulted in significantly lower gas yields and gasification efficiencies compared to *E.grandis* and primary paper sludge.

Clearly, although thermodynamic modelling may predict promising results in terms of calculated equilibrium CH_4 yields and gasification efficiencies (as in the case of pyrolysis char SP3), it can be highly misleading without considering the proximate analysis of the feed material. During Gibbs-free energy minimisation using the non-stoichiometric approach, one only requires prior knowledge of the elemental analysis (*i.e.*, the ultimate analysis), operating temperature and pressure (Smith and Missen, 1982). Hence, the proximate analysis (*i.e.*, volatiles matter and fixed carbon) is not considered in the calculations of the equilibrium yields. Furthermore, thermodynamic equilibrium calculations assume that infinite time is available for the process to reach equilibrium state.

Therefore, although thermodynamic predictions show that SCWG of a feed material with low oxygen content (such as the pyrolysis char SP3 produced during slow pyrolysis of *E.grandis*) could result in CH_4 yields as high as 30 mol/$kg_{feed,dry}$ and a product gas with a HHV of 28 MJ/$kg_{feed,dry}$, low levels of volatile matter in the feed material may dictate differently. At low volatile matter concentrations, the formation of CO *via* steam reforming of the water soluble product will be limited, which in turn will result in low actual CH_4 yields.

Key novel findings from this chapter are:

- As shown in Chapter 3 of this dissertation, thermodynamically, feed material with a low molar O/C ratio will result in maximum CH_4 yields during SCWG at 450 °C and 27 MPa.
- Using pyrolysis char with a low O/C ratio (0.15) and low volatile matter content (27 wt.%) as feed material for SCWG experiments resulted in gas yields far from the calculated equilibrium yields, even at a high catalyst loading of 1 g/$g_{feed,dry}$.
- A linear relationship between the carbon gasification efficiency and the volatile matter content in the feed material was found to be true for non-catalytic and catalytic SCWG, using both K_2CO_3 and Ni/Al_2O_3-SiO_2 as catalysts.
- A linear relationship between the carbon gasification efficiency and the O/C ratio in the feed material was found to be true for non-catalytic and catalytic (K_2CO_3 and Ni/Al_2O_3-SiO_2) SCWG.

Chapter 7

CONCLUSIONS AND RECOMMENDED FUTURE WORK

7.1 REVIEWING THE OBJECTIVES OF THIS RESEARCH

The overall aim of this research project was to provide an improved understanding and new insight into the thermodynamic and practical kinetic behaviour during SCWG of wood-related products sourced at three different stages of the wood utility cycle, namely *E.grandis* wood chips, primary paper waste sludge and wood-based pyrolysis char.

In order to achieve the main aim of this study, the following three objectives were devised:

1. ***To develop a method, based on the assumption of thermodynamic equilibrium, to aid in the selection of appropriate operating conditions for a specific feed material, in terms of its elemental composition (more specifically, the O/C and H/C ratio of the feed material).***

   Although various authors investigated the effect of operating conditions on the ***thermodynamic equilibrium*** results, no in-depth investigation on the combined effect of the ***elemental composition*** of the feed material and operation conditions have been reported so far. Knowing the effect of the composition of the feed material on the thermodynamic equilibrium results can aid in the selection of suitable feedstock material for SCWG prior to conducting experimental work. Therefore, a new method is presented in this dissertation to select appropriate operating conditions, based on thermodynamic equilibrium calculations, for SCWG of a specific feed material.

2. ***To determine whether the calculated thermodynamic equilibrium yields can be achieved by applying a reasonable catalyst loading and reaction time when using primary paper waste sludge (PWS) as feed material for SCWG (specifically at a low operating temperature).***

   Thermodynamic equilibrium studies do not consider possible kinetic effects such as ***catalyst type***, ***catalyst loading*** and ***reaction time***. Therefore, a combined theoretical and experimental study using ***primary paper sludge*** as feed material for SCWG and showing the effect of the aforementioned practical kinetic effects, are provided in this dissertation.

3. ***To determine the possible kinetic influence of the feedstock composition (O/C ratio and volatile matter content) on the gas yields and gasification efficiencies by using wood (E.grandis) and various wood-derived pyrolysis chars as feed material for SCWG.***

   Thermodynamic equilibrium studies do not consider the proximate analysis composition (*i.e.* ***fixed carbon*** and ***volatile composition***) of the feed material. This dissertation now provides additional insight through a combined thermodynamic and experimental study using ***E.grandis*** **wood** ***chips*** and related ***pyrolysis char*** as feed material. It specifically elaborates on the effect of the volatile matter content on the experimental yields. It also provides practical insights into the effect of ***feedstock composition*** (proximate and ultimate analysis) on both the experimental and thermodynamic equilibrium yields.

7.2 Objective 1: Development of a Method To Aid In The Selection of Feedstock material for SCWG

An accurate process model for SCWG was developed based on the assumption of thermodynamic equilibrium. Using the Peng-Robinson equation of state with Boston-Mathias modification provided results sufficiently close to existing experimental data obtained from literature.

From the results, generalised contour plots in the form of the well-known Van Krevelen diagrams (molar O/C and H/C ratios of the feed material) were developed for performance indicators such as individual gas yields, energy recovery and calorific value of the product gas.

These generalised contour plots can be used as a method to determine the thermodynamic limits at various operating temperatures (400, 450, 500, 600, 700 and 800 °C) and dry feed concentrations (5, 10, 15 and 20 wt.%) when any material within the following composition ranges is considered as possible feed material for SCWG:

- Carbon content: 34 – 86 wt.%
- Hydrogen content: 3.3 – 13 wt.%
- Oxygen content: 9.6 – 61 wt.%

The highest thermodynamic equilibrium CH_4 yields and lowest CO_2 yields are achieved at a lower operating temperature (400 °C) and a higher dry feedstock concentration (20 wt.%). Furthermore, the highest H_2 yields and a product gas with the highest calorific value can be produced when operating at the highest temperature (800 °C) and lowest feed concentrations (5 wt.%).

The highest thermodynamic equilibrium H_2 and CH_4 yields as well as a gas product with the highest calorific value can be achieved when feed material with a low oxygen content is gasified in SCW. Hence, modified biomass material with lower oxygen content, such as pyrolysis char, shows great potential as possible feed material for SCWG, based on the thermodynamic equilibrium results.

7.3 Objective 2: SCWG of Primary Paper Sludge: Effect of Reaction Time and Catalyst Type and Loading

SCWG experiments were conducted in a small-scale batch reactor setup using primary paper waste sludge (PWS), originating from a typical South African kraft mill, as feed material. Various aspects of the possible kinetic effects such as catalyst type, catalyst loading and reaction time were investigated at a low operating temperature of 450 °C. The experimental results were compared to thermodynamic equilibrium results and the possible energy efficiency of using PWS as feed material for SCWG was assessed.

The heterogeneous nature of the feed material, amongst other, caused some variation in results of tests performed under similar conditions. Nevertheless, accepted reproducibilities were

achieved with the small-scale batch reactor system. The maximum standard error for the total gas yield and TOC of the liquid phase product was 4% and 8%, respectively.

K_2CO_3 catalyses the water-gas shift reaction since the addition of up to 1 g/g_{PWS} K_2CO_3 as resulted in a 6.7 times increase in the H_2 yield and only a 1.5 times increase in the CH_4 yield during SCWG of PWS. Furthermore, the addition if Ni/Al_2O_3-SiO_2 greatly enhances formation of both CH_4 and H_2 (steam reforming and methanation reactions) as the addition of up to 1 g/g_{PWS} Ni/Al_2O_3-SiO_2 resulted in a 5.3 times increase in the H_2 yield and a 12.5 times increase in the CH_4 yield.

When applying a time-dependent-biomass-to-catalyst ratio ($\dot{\xi}$) of 1.7 $g_{PWS}.g^{-1}.h^{-1}$ during catalytic SCWG with Ni/Al_2O_3-SiO_2, a gas product with a composition close to the calculated equilibrium composition was produced. At these conditions, a carbon conversion efficiency of 86 – 90 % was achieved and a gas product with a calorific value of 13.2 MJ/kg_{PWS} was produced.

Process simulations based on thermodynamic equilibrium assumptions showed that, when operating at 450 °C and a dry feed concentration of 10 wt.%, an overall energy efficiency of 60% can be achieved when assuming a heat recovery of 75%.

7.4 Objective 3: SCWG of *E.grandis* and related Pyrolysis Char – Effect of Feedstock Composition

Possible kinetic effects such as feedstock composition, reaction time, catalyst type and catalyst loading were investigated in order to determine how closely the practical results, at a reasonable reaction time and catalyst loading, could approximate the calculated thermodynamic equilibrium values. Experiments using *E.grandis* wood chips and related pyrolysis chars as feed material were conducted at a dry feed concentration of 10 wt.% and temperature of 450 °C. These feed material differed in terms of their elemental composition (ultimate analysis) and volatile matter content (proximate analysis).

The proximate analysis of the feed material (fixed carbon and volatile matter content) does not affect the thermodynamic equilibrium gas yields, as thermodynamic equilibrium calculations only take into account the elemental composition of the feed material. However, the volatile matter content affects the experimental gas yields and gasification efficiencies to a great extent.

The lower the volatile matter in the feed material (*i.e.* the higher the fixed carbon content), the lower the experimental gasification efficiencies and the further the experimental yields will deviate from the thermodynamic equilibrium yields.

Thermodynamically, the feed material with the lower O/C ratios will result in the highest CH_4 yield, gasification efficiencies and a product gas with the highest calorific value. However, experimentally, the CH_4 yields and gasification efficiencies are limited and resulted in the lowest CH_4 yields and gasification efficiencies.

Although, according to thermodynamic equilibrium predictions, pyrolysis char with a low oxygen and volatile matter content seems like a promising feed material for SCWG, experimental results showed that the decreased concentration of volatile matter in such chars may have an adverse effect on the gasification performance.

For the investigated feedstock composition ranges, a linear relationship existed between the experimentally determined carbon gasification efficiencies for non-catalytic and catalytic SCWG (using both K_2CO_3 and Ni/Al_2O_3-SiO_2) and the volatile matter as well as the O/C ratio of the feed material.

7.5 Original Contributions

The original contributions within the research field of SCWG can be summarised as follows:

1. ***A method which can aid in the selection of appropriate feedstock for SCWG prior to experimental studies was developed. This method is based on thermodynamic equilibrium calculations for SCWG at different operating temperatures (400 – 800 °C) and dry feed concentrations (5 – 20 wt.%).***
    a. Generalised contour plots for the thermodynamic product yields, in the form of the well-known Van Krevelen diagrams for various performance indicators at various operating conditions were generated. These plots can be used to determine the thermodynamic equilibrium yields at various operating conditions when using a material with a known elemental composition as feed material for SCWG.

b. Based on the calculated thermodynamic equilibrium H_2 and CH_4 yields, modified biomass material with lower oxygen content (such as pyrolysis char) showed great potential as a possible feedstock for SCWG.

2. ***New insight on the kinetic vs. thermodynamic equilibrium behaviour was provided for SCWG of various wood-related feed materials including primary paper sludge, E.grandis wood chips and wood-based pyrolysis char.***

   a. Thermodynamically, feed material with a low molar O/C ratio and low volatile matter content, such as pyrolysis char, will result in high CH_4 yields and high gasification efficiencies. However, SCWG of pyrolysis char at these conditions resulted in experimental gas yields and gasification efficiencies far from the calculated equilibrium yields, even at high catalyst loading (1 $g/g_{feed,dry}$) and the long reaction time (1 hour).

   b. A linear relationship between the carbon gasification efficiency and both the O/C ratio and the volatile matter content of the feed material was found to be true for non-catalytic and catalytic (K_2CO_3 and Ni/Al_2O_3-SiO_2) SCWG.

7.6 Publication list

7.6.1 Journal Publications

The contributions made by this research have been published in and submitted to a peer reviewed journal, namely Bioresource Technology:

- Louw, J., Schwarz, C.E., Knoetze, J.H., Burger, A.J., *Thermodynamic modelling of supercritical water gasification: Investigating the effect of biomass composition to aid in the selection of appropriate feedstock material*, **Bioresource Technology, Vol 174 (2014), pp 11-23** (DOI: 10.1016/j.biortech.2014.09.129).
- Louw, J., Schwarz, C.E. and Burger, A.J., *Catalytic supercritical water gasification of primary paper sludge using a homogeneous and heterogeneous catalyst: Experimental vs thermodynamic equilibrium results*, **Bioresource Technology, Vol 201 (2016), pp 111-120** (DOI: 10.1016/j.biortech.2015.11.043).

- Louw, J., Schwarz, C.E. and Burger, A.J., *Supercritical water gasification of Eucalyptus grandis and related pyrolysis char: Effect of feedstock composition*, **Bioresource Technology, Vol 216 (2016), pp 1030 - 1039** (DOI: 10.1016/j.biortech.2016.06.062).

7.6.2 Conference Talks and Poster Presentations

Presentations at international conferences include:

- Louw, J., Schwarz, C.E. and Burger, A.J. *Process Modelling of Supercritical Water Gasification of Phenolic-based biomass.* **Poster Presentation at 6th International Symposium on High Pressure Process Technology, Belgrade, Serbia, September 8-11, 2013**.
- Louw, J., Schwarz, C.E. and Burger, A.J. *Methodology for Selecting Appropriate Feedstock Material for Biomass Gasification in Supercritical Water by Means of Process Modelling.* **Keynote Presentation at 14th EMSF – European Meeting on Supercritical Fluids, Marseille, France. May 18-21, 2014.**
- Louw, J., Schwarz, C.E., Knoetze, J.H. and Burger, A.J., *Process modelling of combined supercritical water gasification (SCWG) and supercritical water oxidation (SCWO) of paper sludge for hydrogen production.* **Poster presentation at ICCT/SAIChE 2014, Durban, South Africa, July 27 – August 1, 2014**.
- Louw, J., Schwarz, C.E. and Burger, A.J., *Comparison of thermodynamic and experimental yields during supercritical water gasification of biomass, biomass waste and pyrolysis char.* **Poster Presentation at 15th EMSF – European Meeting on Supercritical Fluids, 2016, Essen, Germany, May 8-11, 2016**.

7.7 Recommended Future Work

Based on the conclusions drawn, possible future work to expand the current state of the art of SCWG was identified. The developed thermodynamic equilibrium process model may be expanded in order to include the effect of the inorganic material (ash) as well as the volatile and fixed carbon content in the feed material. Hence, a 'quasi'-equilibrium model can be developed. Furthermore, the process model can also be expanded into a more detailed model with heat

integration and gas separation columns in order to determine the effect of feed composition on the process energy and exergy efficiency of the process.

Concerning the experimental work, the commercially available Ni/Al_2O_3-SiO_2 catalyst can be tested for catalyst durability and stability in SCWG applications. Its reactivity during reuse as well as exposing it to longer reaction times can also be investigated. Furthermore, methods of employing sufficient mixing during experiments in these small-scale batch reactor systems should be investigated. Impregnation of the feed material on the catalyst can also be investigated to improve the contact between the catalyst and the feed material. A thorough investigation on the different reaction rates obtained with the different catalyst and feed material combination will also be of great interest.

This study only focussed on the experimental results at one specific operating condition, namely 450 °C, 27 MPa and dry feed concentration of 10 wt.%. Future work should consider operating at higher temperatures and longer reaction times which might result in higher gas yields and gasification efficiencies and experimental yields closer to the thermodynamic calculated yields.

The effect of the properties of the feed material in terms of the elemental composition and the proximate analysis composition on the kinetics was investigated in this study. Taking into account other properties of the feed material such as the porosity will be of great interest for future work.

A more thorough energy and exergy analysis study for the possibility of harnessing energy from primary paper sludge *via* SCWG is also recommended. Furthermore, a comparative study between SCWG, pyrolysis and a combination there-off, depending on the feed type, can also be of great interest. The possibilities of integrating pyrolysis and SCWG by using suitable pyrolysis char and/or condensate as feed material for SCWG may provide an interesting study.

A comparative study between SCWG and conventional gasification at a variety of operating conditions and feedstock compositions will also be useful to compare the relative suitability of each technology for production of an energy-rich product gas.

REFERENCES

Aboyade, A.O., Carrier, M., Meyer, E.L., Knoetze, H., Görgens, J.F., 2013. Slow and pressurized co-pyrolysis of coal and agricultural residues. Energy Convers. Manag. 65, 198–207.

Acelas, N.Y., López, D.P., Brilman, D.W.F., Kersten, S.R.A., Kootstra, A.M.J., 2014. Supercritical water gasification of sewage sludge: Gas production and phosphorus recovery. Bioresour. Technol. 174, 167–175.

Afif, E., Azadi, P., Farnood, R., 2011. Catalytic hydrothermal gasification of activated sludge. Appl. Catal. B Environ. 105, 136–143.

Aida, T.M., Shiraishi, N., Kubo, M., Watanabe, M., Smith, R.L., 2010. Reaction kinetics of d-xylose in sub- and supercritical water. J. Supercrit. Fluids 55, 208–216.

Antal, M.J., Allen, S.G., Schulman, D., Xu, X., Divilio, R.J., 2000. Biomass gasification in supercritical water. Ind. Eng. Chem. Res. 39, 4040–4053.

Azadi, P., Farnood, R., 2011. Review of heterogeneous catalysts for sub- and supercritical water gasification of biomass and wastes. Int. J. Hydrog. Energy 36, 9529–9541.

Azadi, P., Farnood, R., Vuillardot, C., 2011. Estimation of heating time in tubular supercritical water reactors. J. Supercrit. Fluids 55, 1038–1045.

Azadi, P., Khan, S., Strobel, F., Azadi, F., Farnood, R., 2012. Hydrogen production from cellulose, lignin, bark and model carbohydrates in supercritical water using nickel and ruthenium catalysts. Appl. Catal. B Environ. 117–118, 330–338.

Azadi, P., Khodadadi, A.A., Mortazavi, Y., Farnood, R., 2009. Hydrothermal gasification of glucose using Raney nickel and homogeneous organometallic catalysts. Fuel Process. Technol. 90, 145–151.

Azadi, P., Otomo, J., Hatano, H., Oshima, Y., Farnood, R., 2010. Hydrogen production by catalytic near-critical water gasification and steam reforming of glucose. Int. J. Hydrog. Energy 35, 3406–3414.

Bajpai, P., 2015. Generation of Waste in Pulp and Paper Mills, in: Management of Pulp and Paper Mill Waste. Springer International Publishing, Cham, pp. 9–17.

Barati, M., Babatabar, M., Tavasoli, A., Dalai, A.K., Das, U., 2014. Hydrogen production via supercritical water gasification of bagasse using unpromoted and zinc promoted Ru/γ-Al2O3 nanocatalysts. Fuel Process. Technol. 123, 140–148.

Barbier, J., Charon, N., Dupassieux, N., Loppinet-Serani, A., Mahé, L., Ponthus, J., Courtiade, M., Ducrozet, A., Fonverne, A., Cansell, F., 2011. Hydrothermal conversion of glucose in a batch reactor. A detailed study of an experimental key-parameter: The heating time. J. Supercrit. Fluids 58, 114–120.

Basu, P., 2010a. Introduction, in: Biomass Gasification Design Handbook. Elsevier, pp. 1–25.

Basu, P., 2010b. Hydrothermal Gasification of Biomass, in: Biomass Gasification Design Handbook. Elsevier, pp. 229–267.

Basu, P., Mettanant, V., 2009. Biomass gasification in supercritical water - a review. Int. J. Chem. React. Eng. 7.

Blasi, C.D., Galgano, A., Meier, D., Brodzinski, I., Malmros, O., 2007. Supercritical gasification of wastewater from updraft wood gasifiers. Biomass Bioenergy 31, 802–811.

Bobleter, O., 1994. Hydrothermal degradation of polymers derived from plants. Prog. Polym. Sci. 19, 797–841.

Boukis, N., Diem, V., Habicht, W., Dinjus, E., 2003. Methanol reforming in supercritical water. Ind. Eng. Chem. Res. 42, 728–735.

Boukis, N., Galla, U., Muller, H., Dinjus, E., 2007. Biomass gasification in supercritical water, experimental progress achieved with the Verena pilot plant. Presented at the 15th European Biomass Conference & Exhibition, Berlin, Germany.

Bröll, D., Kaul, C., Krämer, A., Krammer, P., Richter, T., Jung, M., Vogel, H., Zehner, P., 1999. Chemistry in Supercritical Water. Angew. Chem. Int. Ed. 38, 2998–3014.

Bühler, W., Dinjus, E., Ederer, H., Kruse, A., Mas, C., 2002. Ionic reactions and pyrolysis of glycerol as competing reaction pathways in near- and supercritical water. J. Supercrit. Fluids 22, 37–53.

Byrd, A.J., Pant, K., Gupta, R.B., 2008. Hydrogen production from glycerol by reforming in supercritical water over Ru/Al2O3 catalyst. Fuel 87, 2956–2960.

Byrd, A.J., Pant, K.K., Gupta, R.B., 2007. Hydrogen production from ethanol by reforming in supercritical water using Ru/Al_2O_3 catalyst. Energy Fuels 21, 3541–3547.

Cao, C., Guo, L., Jin, H., Guo, S., Lu, Y., Zhang, X., 2013. The influence of alkali precipitation on supercritical water gasification of glucose and the alkali recovery in fluidized-bed reactor. Int. J. Hydrog. Energy 38, 13293–13299.

Cao, C., Guo, L., Yin, J., Jin, H., Cao, W., Jia, Y., Yao, X., 2015. Supercritical Water Gasification of Coal with Waste Black Liquor as Inexpensive Additives. Energy Fuels 29, 384–391.

Carrier, M., Hugo, T., Gorgens, J., Knoetze, H., 2011. Comparison of slow and vacuum pyrolysis of sugar cane bagasse. J. Anal. Appl. Pyrolysis 90, 18–26.

Castello, D., Fiori, L., 2012. Kinetics modeling and main reaction schemes for the supercritical water gasification of methanol. J. Supercrit. Fluids 69, 64–74.

Castello, D., Fiori, L., 2011. Supercritical water gasification of biomass: Thermodynamic constraints. Bioresour. Technol. 102, 7574–7582.

Castello, D., Kruse, A., Fiori, L., 2015. Low temperature supercritical water gasification of biomass constituents: Glucose/phenol mixtures. Biomass Bioenergy 73, 84–94.

Castello, D., Kruse, A., Fiori, L., 2014. Supercritical water gasification of hydrochar. Chem. Eng. Res. Des. 92, 1864–1875.

Castello, D., Kruse, A., Fiori, L., 2013. Biomass gasification in supercritical and subcritical water: The effect of the reactor material. Chem. Eng. J. 228, 535–544.

Chakinala, A.G., Brilman, D.W.F. (Wim), van Swaaij, W.P.M., Kersten, S.R.A., 2010. Catalytic and non-catalytic supercritical water gasification of microalgae and glycerol. Ind. Eng. Chem. Res. 49, 1113–1122.

Chen, J., Lu, Y., Guo, L., Zhang, X., Xiao, P., 2010. Hydrogen production by biomass gasification in supercritical water using concentrated solar energy: System development and proof of concept. Int. J. Hydrog. Energy 35, 7134–7141.

Chen, Y., Guo, L., Cao, W., Jin, H., Guo, S., Zhang, X., 2013a. Hydrogen production by sewage sludge gasification in supercritical water with a fluidized bed reactor. Int. J. Hydrog. Energy 38, 12991–12999.

Chen, Y., Guo, L., Jin, H., Yin, J., Lu, Y., Zhang, X., 2013b. An experimental investigation of sewage sludge gasification in near and super-critical water using a batch reactor. Int. J. Hydrog. Energy 38, 12912–12920.

Cheng, L., Zhang, R., Bi, J., 2004. Pyrolysis of a low-rank coal in sub- and supercritical water. Fuel Process. Technol. 85, 921–932.

Cherad, R., Onwudili, J.A., Williams, P.T., Ross, A.B., 2014. A parametric study on supercritical water gasification of Laminaria hyperborea: A carbohydrate-rich macroalga. Bioresour. Technol. 169, 573–580.

Chheda, J.N., Huber, G.W., Dumesic, J.A., 2007. Liquid-Phase Catalytic Processing of Biomass-Derived Oxygenated Hydrocarbons to Fuels and Chemicals. Angew. Chem. Int. Ed. 46, 7164–7183.

Chowdhury, M.B.I., Hossain, M.M., Charpentier, P.A., 2011. Effect of supercritical water gasification treatment on Ni/La_2O_3-Al_2O_3-based catalysts. Appl. Catal. Gen. 405, 84–92.

Chuntanapum, A., Matsumura, Y., 2010. Char formation mechanism in supercritical water gasification process: A study of model compounds. Ind. Eng. Chem. Res. 49, 4055–4062.

Crnkovic, P.M., Koch, C., Ávila, I., Mortari, D.A., Cordoba, A.M., Moreira dos Santos, A., 2012. Determination of the activation energies of beef tallow and crude glycerin combustion using thermogravimetry. Biomass Bioenergy 44, 8–16.

Crocker, M., 2010. Thermochemical conversion of biomass to liquid fuels and chemicals [WWW Document]. URL http://site.ebrary.com/id/10627725

Demirbas, A., 2004. Hydrogen-rich gas from fruit shells via supercritical water extraction. Int. J. Hydrog. Energy 29, 1237–1243.

DiLeo, G.J., Neff, M.E., Kim, S., Savage, P.E., 2008. Supercritical water gasification of phenol and glycine as models for plant and protein biomass. Energy Fuels 22, 871–877.

Ding, N., Azargohar, R., Dalai, A.K., Kozinski, J.A., 2014. Catalytic gasification of glucose to H_2 in supercritical water. Fuel Process. Technol. 127, 33–40.

D'Jesús, P., Artiel, C., Boukis, N., Kraushaar-Czarnetzki, B., Dinjus, E., 2005. Influence of Educt Preparation on Gasification of Corn Silage in Supercritical Water. Ind. Eng. Chem. Res. 44, 9071–9077.

D'Jesus, P., Boukis, N., Kraushaarczarnetzki, B., Dinjus, E., 2006. Gasification of corn and clover grass in supercritical water. Fuel 85, 1032–1038.

Elliott, D.C., 2008. Catalytic hydrothermal gasification of biomass. Biofuels Bioprod. Biorefining 2, 254–265.

Encinar, J.M., González, J.F., Rodríguez, J.J., Ramiro, M.J., 2001. Catalysed and uncatalysed steam gasification of eucalyptus char: influence of variables and kinetic study. Fuel 80, 2025–2036.

Feng, W., Van der Kooi, H., De Swaan Arons, J., 2004. Biomass conversions in subcritical and supercritical water: driving force, phase equilibria, and thermodynamic analysis. Chem. Eng. Process. 43, 1459–1467.

Finlayson, B.A., 2014. Introduction to chemical engineering computing: using the latest user interface with Aspen Plus 8.0, 2. ed. ed. Wiley, Hoboken, NJ.

Fiori, L., Valbusa, M., Castello, D., 2012. Supercritical water gasification of biomass for H2 production: Process design. Bioresour. Technol. 121, 139–147.

Freitas, A.C., Guirardello, R., 2013. Thermodynamic analysis of supercritical water gasification of microalgae biomass for hydrogen and syngas production. Chem. Eng. Trans. 553–558.

Friedl, A., Padouvas, E., Rotter, H., Varmuza, K., 2005. Prediction of heating values of biomass fuel from elemental composition. Anal. Chim. Acta 544, 191–198.

Furusawa, T., Sato, T., Sugito, H., Miura, Y., Ishiyama, Y., Sato, M., Itoh, N., Suzuki, N., 2007. Hydrogen production from the gasification of lignin with nickel catalysts in supercritical water. Int. J. Hydrog. Energy 32, 699–704.

Garcia Jarana, M.B., Sanchez-Oneto, J., Portela, J., Nebotsanz, E., Martinezdelaossa, E., 2008. Supercritical water gasification of industrial organic wastes. J. Supercrit. Fluids 46, 329–334.

Gasafi, E., Reinecke, M.-Y., Kruse, A., Schebek, L., 2008. Economic analysis of sewage sludge gasification in supercritical water for hydrogen production. Biomass Bioenergy 32, 1085–1096.

Gassner, M., Vogel, F., Heyen, G., Maréchal, F., 2011. Optimal process design for the polygeneration of SNG, power and heat by hydrothermal gasification of waste biomass: Thermo-economic process modelling and integration. Energy Environ. Sci. 4, 1726.

Gavrilscu, D., 2008. Energy from biomass in pulp and paper mills. Environ. Eng. Manag. J. 7, 537–546.

Ge, Z., Jin, H., Guo, L., 2014. Hydrogen production by catalytic gasification of coal in supercritical water with alkaline catalysts: Explore the way to complete gasification of coal. Int. J. Hydrog. Energy 39, 19583–19592.

Godsmark, R., 2015. Forestry South Africa Roundwood Sales Analysis for the 2014 Financial Year.

Gong, M., Zhu, W., Xu, Z.R., Zhang, H.W., Yang, H.P., 2014a. Influence of sludge properties on the direct gasification of dewatered sewage sludge in supercritical water. Renew. Energy 66, 605–611.

Gong, M., Zhu, W., Zhang, H.W., Ma, Q., Su, Y., Fan, Y.J., 2014b. Influence of NaOH and Ni catalysts on hydrogen production from the supercritical water gasification of dewatered sewage sludge. Int. J. Hydrog. Energy 39, 19947–19954.

Goodwin, A.K., Rorrer, G.L., 2011. Modeling of Supercritical Water Gasification of Xylose to Hydrogen-Rich Gas in a Hastelloy Microchannel Reactor. Ind. Eng. Chem. Res. 50, 7172–7182.

Goodwin, A.K., Rorrer, G.L., 2010. Reaction rates for supercritical water gasification of xylose in a micro-tubular reactor. Chem. Eng. J. 163, 10–21.

Goodwin, A.K., Rorrer, G.L., 2009. Conversion of Xylose and Xylose−Phenol Mixtures to Hydrogen-Rich Gas by Supercritical Water in an Isothermal Microtube Flow Reactor. Energy Fuels 23, 3818–3825.

Goodwin, A.K., Rorrer, G.L., 2008. Conversion of Glucose to Hydrogen-Rich Gas by Supercritical Water in a Microchannel Reactor. Ind. Eng. Chem. Res. 47, 4106–4114.

Guan, Q., Mao, T., Zhang, Q., Miao, R., Ning, P., Gu, J., Tian, S., Chen, Q., Chai, X.-S., 2014. Catalytic gasification of lignin with $Ni/Al_2O_3–SiO_2$ in sub/supercritical water. J. Supercrit. Fluids 95, 413–421.

Guan, Q., Savage, P.E., Wei, C., 2012a. Gasification of alga Nannochloropsis sp. in supercritical water. J. Supercrit. Fluids 61, 139–145.

Guan, Q., Wei, C., Savage, P.E., 2012b. Kinetic model for supercritical water gasification of algae. Phys. Chem. Chem. Phys.

Guo, L., Cao, C., Lu, Y., 2010. Supercritical Water Gasification of Biomass and Organic Wastes, in: Biomass. InTech, pp. 165–182.

Guo, L., Lu, Y., Zhang, X., Ji, C., Guan, Y., Pei, A., 2007. Hydrogen production by biomass gasification in supercritical water: A systematic experimental and analytical study. Catal. Today 129, 275–286.

Guo, S., Guo, L., Cao, C., Yin, J., Lu, Y., Zhang, X., 2012. Hydrogen production from glycerol by supercritical water gasification in a continuous flow tubular reactor. Int. J. Hydrog. Energy.

Guo, Y., Wang, S.Z., Xu, D.H., Gong, Y.M., Ma, H.H., Tang, X.Y., 2010. Review of catalytic supercritical water gasification for hydrogen production from biomass. Renew. Sustain. Energy Rev. 14, 334–343.

Gutiérrez Ortiz, F.J., Ollero, P., Serrera, A., 2011a. Thermodynamic analysis of the autothermal reforming of glycerol using supercritical water. Int. J. Hydrog. Energy 36, 12186–12199.

Gutiérrez Ortiz, F.J., Ollero, P., Serrera, A., Sanz, A., 2011b. Thermodynamic study of the supercritical water reforming of glycerol. Int. J. Hydrog. Energy 36, 8994–9013.

Hameed, B., Din, A., Ahmad, A., 2007. Adsorption of methylene blue onto bamboo-based activated carbon: Kinetics and equilibrium studies. J. Hazard. Mater. 141, 819–825.

Hao, X.H., Guo, L.J., Mao, X., Zhang, X.M., Chen, X.J., 2003. Hydrogen production from glucose used as a model compound of biomass gasified in supercritical water. Int. J. Hydrog. Energy 28, 55–64.

Hao, X.H., Guo, L.J., Zhang, X.M., Guan, Y., 2005. Hydrogen production from catalytic gasification of cellulose in supercritical water. Chem. Eng. J. 110, 57–65.

Hendry, D., Venkitasamy, C., Wilkinson, N., Jacoby, W., 2011. Exploration of the effect of process variables on the production of high-value fuel gas from glucose via supercritical water gasification. Bioresour. Technol. 102, 3480–3487.

Huelsman, C.M., Savage, P.E., 2012. Intermediates and kinetics for phenol gasification in supercritical water. Phys. Chem. Chem. Phys. 14, 2900.

Jin, H., Guo, L., Guo, J., Ge, Z., Cao, C., Lu, Y., 2015. Study on gasification kinetics of hydrogen production from lignite in supercritical water. Int. J. Hydrog. Energy.

Jin, H., Lu, Y., Guo, L., Zhang, X., Pei, A., 2014. Hydrogen Production by Supercritical Water Gasification of Biomass with Homogeneous and Heterogeneous Catalyst. Adv. Condens. Matter Phys. 2014, 1–9.

Joubert, J.-E., 2013. Pyrolysis of Eucalyptus grandis (Master of Science in Engineering). Stellenbosch University, Stellenbosch.

Kambo, H.S., Dutta, A., 2015. A comparative review of biochar and hydrochar in terms of production, physico-chemical properties and applications. Renew. Sustain. Energy Rev. 45, 359–378.

Kersten, S.R.A., Potic, B., Prins, W., Van Swaaij, W.P.M., 2006. Gasification of Model Compounds and Wood in Hot Compressed Water. Ind. Eng. Chem. Res. 45, 4169–4177.

Kıpçak, E., Sögüt, O.O., Akgün, M., 2011. Hydrothermal gasification of olive mill wastewater as a biomass source in supercritical water. J. Supercrit. Fluids 57, 50–57.

Kruse, A., 2009. Hydrothermal biomass gasification. J. Supercrit. Fluids 47, 391–399.

Kruse, A., 2008. Supercritical water gasification. Biofuels Bioprod. Biorefining 2, 415–437.

Kruse, A., Dinjus, E., 2007a. Hot compressed water as reaction medium and reactant: Properties and synthesis reactions. J. Supercrit. Fluids 39, 362–380.

Kruse, A., Dinjus, E., 2007b. Hot compressed water as reaction medium and reactant: 2. Degradation reactions. J. Supercrit. Fluids 41, 361–379.

Kruse, A., Forchheim, D., Gloede, M., Ottinger, F., Zimmermann, J., 2010. Brines in supercritical biomass gasification: 1. Salt extraction by salts and the influence on glucose conversion. J. Supercrit. Fluids 53, 64–71.

Kruse, A., Henningsen, T., Sınağ, A., Pfeiffer, J., 2003. Biomass Gasification in Supercritical Water: Influence of the Dry Matter Content and the Formation of Phenols. Ind. Eng. Chem. Res. 42, 3711–3717.

Kruse, A., Krupka, A., Schwarzkopf, V., Gamard, C., Henningsen, T., 2005. Influence of Proteins on the Hydrothermal Gasification and Liquefaction of Biomass. 1. Comparison of Different Feedstocks. Ind. Eng. Chem. Res. 44, 3013–3020.

Kruse, A., Meier, D., Rimbrecht, P., Schacht, M., 2000. Gasification of Pyrocatechol in Supercritical Water in the Presence of Potassium Hydroxide. Ind. Eng. Chem. Res. 39, 4842–4848.

Lan, R., Jin, H., Guo, L., Ge, Z., Guo, S., Zhang, X., 2014. Hydrogen Production by Catalytic Gasification of Coal in Supercritical Water. Energy Fuels 28, 6911–6917.

Lee, I.G., Ihm, S.K., 2010. Hydrogen Production by SCWG Treatment of Wastewater from Amino Acid Production Process. Ind. Eng. Chem. Res. 49, 10974–10980.

Lee, I.G., Kim, M.S., Ihm, S.K., 2002. Gasification of Glucose in Supercritical Water. Ind. Eng. Chem. Res. 41, 1182–1188.

Lemmon, E.W., McLinden, M.O., Friend, D.G., 2011. Thermophysical Properties of Fluid Systems, in: Linstrom, P.J., Mallard, W.G. (Eds.), NIST Chemistry WebBook, NIST Standard Reference Database Number 69. National Institute of Standards and Technology, Gaithersburg MD, 20899.

Leslie, A.D., Mencuccini, M., Perks, M., 2012. The potential for Eucalyptus as a wood fuel in the UK. Appl. Energy 89, 176–182.

Li, S., Lu, Y., Guo, L., Zhang, X., 2011. Hydrogen production by biomass gasification in supercritical water with bimetallic Ni–M/γAl2O3 catalysts (M = Cu, Co and Sn). Int. J. Hydrog. Energy 36, 14391–14400.

Li, Y., Guo, L., Zhang, X., Jin, H., Lu, Y., 2010. Hydrogen production from coal gasification in supercritical water with a continuous flowing system. Int. J. Hydrog. Energy 35, 3036–3045.

Louw, J., Schwarz, C.E., Knoetze, J.H., Burger, A.J., 2014. Thermodynamic modelling of supercritical water gasification: Investigating the effect of biomass composition to aid in the selection of appropriate feedstock material. Bioresour. Technol. 174, 11–23.

Lu, Y., Guo, L., Ji, C., Zhang, X., Hao, X., Yan, Q., 2006. Hydrogen production by biomass gasification in supercritical water: A parametric study. Int. J. Hydrog. Energy 31, 822–831.

Lu, Y., Guo, L., Zhang, X., Yan, Q., 2007. Thermodynamic modeling and analysis of biomass gasification for hydrogen production in supercritical water. Chem. Eng. J. 131, 233–244.

Lu, Y., Li, S., Guo, L., 2013. Hydrogen production by supercritical water gasification of glucose with Ni/CeO_2/Al_2O_3: Effect of Ce loading. Fuel 103, 193–199.

Lu, Y., Li, S., Guo, L., Zhang, X., 2010. Hydrogen production by biomass gasification in supercritical water over Ni/γAl_2O_3 and Ni/CeO_2-γAl_2O_3 catalysts. Int. J. Hydrog. Energy 35, 7161–7168.

Lu, Y., Savage, P.E., 2015. Supercritical water gasification of lipid-extracted hydrochar to recover energy and nutrients. J. Supercrit. Fluids 99, 88–94.

Lu, Y., Zhu, Y., Li, S., Zhang, X., Guo, L., 2014. Behavior of nickel catalysts in supercritical water gasification of glucose: Influence of support. Biomass Bioenergy 67, 125–136.

Luterbacher, J.S., Fröling, M., Vogel, F., Maréchal, F., Tester, J.W., 2009. Hydrothermal Gasification of Waste Biomass: Process Design and Life Cycle Asessment. Environ. Sci. Technol. 43, 1578–1583.

Madenoğlu, T.G., Kurt, S., Sağlam, M., Yüksel, M., Gökkaya, D., Ballice, L., 2012. Hydrogen production from some agricultural residues by catalytic subcritical and supercritical water gasification. J. Supercrit. Fluids 67, 22–28.

Madenoğlu, T.G., Sağlam, M., Yüksel, M., Ballice, L., 2013. Simultaneous effect of temperature and pressure on catalytic hydrothermal gasification of glucose. J. Supercrit. Fluids 73, 151–160.

Marias, F., Letellier, S., Cezac, P., Serin, J.P., 2011. Energetic analysis of gasification of aqueous biomass in supercritical water. Biomass Bioenergy 35, 59–73.

Marrone, P.A., Hong, G.T., 2009. Corrosion control methods in supercritical water oxidation and gasification processes. J. Supercrit. Fluids 51, 83–103.

Marshall, W.L., Franck, E.U., 1981. Ion product of water substance, 0-1000 °C, 1-10,000 Bars. New international formulation and its backgrounds. J. Phys. Chem. Ref. Data 10, 295–304.

Matsumura, Y., Minowa, T., Potic, B., Kersten, S.R.A., Prins, W., van Swaaij, W.P.M., Van der Beld, B., Elliott, D.C., Neuenschwander, G.G., Kruse, A., Antal, M.J.J., 2005. Biomass gasification in near- and super-critical water: Status and prospects. Biomass Bioenergy 29, 269–292.

Matsumura, Y., Sasaki, M., Okuda, K., Takami, S., Ohara, S., Umetsu, M., Adschiri, T., 2006. Supercritical water treatment of biomass for energy and material recovery. Combust. Sci. Technol. 178, 509–536.

Matsumura, Y., Xu, X., Antal, M.J., 1997. Gasification characteristics of an activated carbon in supercritical water. Carbon 35, 819–824.

McGowan, T.F. (Ed.), 2009. Biomass and Alternate Fuel Systems: An Engineering and Economic Guide. John Wiley & Sons, Ltd, New Jersey, USA.

McKendry, P., 2002. Energy production from biomass (part 1): overview of biomass. Bioresour. Technol. 83, 37–46.

Menon, V., Rao, M., 2012. Trends in bioconversion of lignocellulose: Biofuels, platform chemicals & biorefinery concept. Prog. Energy Combust. Sci. 38, 522–550.

Miller, A., Hendry, D., Wilkinson, N., Venkitasamy, C., Jacoby, W., 2012. Exploration of the gasification of Spirulina algae in supercritical water. Bioresour. Technol. 119, 41–47.

Minowa, T., Inoue, S., 1999. Hydrogen production from biomass by catalytic gasification in hot compressed water. Renew. Energy 16, 1114–1117.

Minowa, T., Ogi, T., 1998. Hydrogen production from cellulose using a reduced nickel catalyst. Catal. Today 45, 411–416.

Minowa, T., Ogi, T., Dote, Y., Yokoyama, S., 1994. Methane production from cellulose by catalytic gasification. Renew. Energy 5, 813–815.

Modell, M., 1985. Gasification and Liquefaction of Forest Products in Supercritical Water, in: Overend, R.P., Milne, T.A., Mudge, L.K. (Eds.), Fundamentals of Thermochemical Biomass Conversion. Springer Netherlands, Dordrecht, pp. 95–119.

Muangrat, R., Onwudili, J.A., Williams, P.T., 2010a. Influence of alkali catalysts on the production of hydrogen-rich gas from the hydrothermal gasification of food processing waste. Appl. Catal. B Environ. 100, 440–449.

Muangrat, R., Onwudili, J.A., Williams, P.T., 2010b. Alkali-promoted hydrothermal gasification of biomass food processing waste: A parametric study. Int. J. Hydrog. Energy 35, 7405–7415.

Munetsuna, H., Tamai, M., Noda, Y., Matsumura, Y., 2010. Supercritical Water Gasification Staged at Intervals for Hydrogen Fermentation Residue of Food Waste. J. Jpn. Inst. Energy 89, 1173–1178.

Myréen, L., Ronnlund, I., Westerlund, T., 2011. Integration of supercritical water gasification (SCWG) in pulp and paper production - A feasibility study of integration options. Chem. Eng. Trans. 25, 429–434.

Nakagawa, H., Namba, A., Sharma, A., Miura, K., 2007. Production of Fuel Gas through the Hydrothermal Gasification of Wastewater Using Highly Active Carbon-Base Catalyst. J. Chem. Eng. Jpn. 40, 1210–1215.

Nakamura, A., Kiyonaga, E., Yamamura, Y., Shimizu, Y., Minowa, T., Noda, Y., Matsumura, Y., 2008. Gasification of Catalyst-Suspended Chicken Manure in Supercritical Water. J. Chem. Eng. Jpn. 41, 433–440.

Onwudili, J.A., Lea-Langton, A.R., Ross, A.B., Williams, P.T., 2013. Catalytic hydrothermal gasification of algae for hydrogen production: Composition of reaction products and potential for nutrient recycling. Bioresour. Technol. 127, 72–80.

Osada, M., Hiyoshi, N., Sato, O., Arai, K., Shirai, M., 2007. Reaction Pathway for Catalytic Gasification of Lignin in Presence of Sulfur in Supercritical Water. Energy Fuels 21, 1854–1858.

Park, K.C., Tomiyasu, H., 2003. Gasification reaction of organic compounds catalyzed by RuO2 in supercritical water. Chem. Commun. 694–695.

Pei, A., Guo, L., Jin, H., 2007. Experimental research on catalysts and their catalytic mechanism for hydrogen production by gasification of peanut shell in supercritical water. Front. Energy Power Eng. China 1, 451–456.

Penninger, J., Rep, M., 2006. Reforming of aqueous wood pyrolysis condensate in supercritical water. Int. J. Hydrog. Energy 31, 1597–1606.

Peterson, A.A., Vogel, F., Lachance, R.P., Fröling, M., Antal, Jr., M.J., Tester, J.W., 2008. Thermochemical biofuel production in hydrothermal media: A review of sub- and supercritical water technologies. Energy Environ. Sci. 1, 32.

Phyllis2, 2012. Phyllis2, database for biomass and waste [WWW Document]. Energy Res. Cent. Neth. URL https://www.ecn.nl/phyllis2 (accessed 11.30.12).

Prins, M., Ptasinski, K., Janssen, F., 2007. From coal to biomass gasification: Comparison of thermodynamic efficiency. Energy 32, 1248–1259.

Promdej, C., Chuntanapum, A., Matsumura, Y., 2010. Effect of Temperature on Tarry Material Production of Glucose in Supercritical Water Gasification. J. Jpn. Inst. Energy 89, 1179–1184.

Qian, L., Wang, S., Xu, D., Guo, Y., Tang, X., Wang, L., 2015. Treatment of sewage sludge in supercritical water and evaluation of the combined process of supercritical water gasification and oxidation. Bioresour. Technol. 176, 218–224.

Ramsurn, H., Kumar, S., Gupta, R.B., 2011. Enhancement of Biochar Gasification in Alkali Hydrothermal Medium by Passivation of Inorganic Components Using $Ca(OH)_2$. Energy Fuels 25, 2389–2398.

Reddy, S.N., Nanda, S., Dalai, A.K., Kozinski, J.A., 2014. Supercritical water gasification of biomass for hydrogen production. Int. J. Hydrog. Energy 39, 6912–6926.

Resende, F.L.P., Fraley, S.A., Berger, M.J., Savage, P.E., 2008. Noncatalytic Gasification of Lignin in Supercritical Water. Energy Fuels 22, 1328–1334.

Resende, F.L.P., Savage, P.E., 2010. Kinetic model for noncatalytic supercritical water gasification of cellulose and lignin. AIChE J. 2412–2420.

Rönnlund, I., Myréen, L., Lundqvist, K., Ahlbeck, J., Westerlund, T., 2011. Waste to energy by industrially integrated supercritical water gasification – Effects of alkali salts in residual by-products from the pulp and paper industry. Energy 36, 2151–2163.

Saha, B.C., 2003. Hemicellulose bioconversion. J. Ind. Microbiol. Biotechnol. 30, 279–291.

Saisu, M., Sato, T., Watanabe, M., Adschiri, T., Arai, K., 2003. Conversion of Lignin with Supercritical Water−Phenol Mixtures. Energy Fuels 17, 922–928.

Sanders, R., 2015. Henry's Law Constants, in: Linstrom, P.J., Mallard, W.G. (Eds.), NIST Chemistry WebBook, NIST Standard Reference Database Number 69. National Institute of Standards and Technology, Gaithersburg MD, 20899.

Schmieder, H., Abeln, J., Boukis, N., Dinjus, E., Kruse, A., Kluth, M., Petrich, G., Sadri, E., Schacht, M., 2000. Hydrothermal gasification of biomass and organic wastes. J. Supercrit. Fluids 17, 145–153.

Schubert, M., Aubert, J., Müller, J.B., Vogel, F., 2012. Continuous salt precipitation and separation from supercritical water. Part 3: Interesting effects in processing type 2 salt mixtures. J. Supercrit. Fluids 61, 44–54.

Schubert, M., Regler, J.W., Vogel, F., 2010a. Continuous salt precipitation and separation from supercritical water. Part 1: Type 1 salts. J. Supercrit. Fluids 52, 99–112.

Schubert, M., Regler, J.W., Vogel, F., 2010b. Continuous salt precipitation and separation from supercritical water. Part 2. Type 2 salts and mixtures of two salts. J. Supercrit. Fluids 52, 113–124.

Sealock, L.J., Elliott, D.C., 1991. Method for the catalytic conversion of lignocellulosic material. 5019135.

Selvi Gökkaya, D., Saglam, M., Yüksel, M., Ballice, L., 2015. Supercritical water gasification of phenol as a model for plant biomass. Int. J. Hydrog. Energy.

Sınağ, A., Kruse, A., Rathert, J., 2004. Influence of the Heating Rate and the Type of Catalyst on the Formation of Key Intermediates and on the Generation of Gases During Hydropyrolysis of Glucose in Supercritical Water in a Batch Reactor. Ind. Eng. Chem. Res. 43, 502–508.

Sınağ, A., Kruse, A., Schwarzkopf, V., 2003. Key Compounds of the Hydropyrolysis of Glucose in Supercritical Water in the Presence of K2CO3. Ind. Eng. Chem. Res. 42, 3516–3521.

Sluiter, A., Hames, B., Ruiz, R., Scarlata, C., Templeton, D., Crocker, D., 2011. Determination of structural carbohydrates and lignin in biomass (Laboratory Analytical Procedure (LAP) No. NREL/TP-510-42618). National Renewable Energy Laboratory.

Sluiter, A., Ruiz, R., Scarlata, C., Sluiter, J., Templeton, D., 2005. Determination of extractives in biomass (Laboratory Analytical Procedure (LAP) No. NREL/TP-510-42619). National Renewable Energy Laboratory.

Smith, J.M., Van Ness, H.C., Abbott, M.M., 2005. Introduction to chemical engineering thermodynamics, 7. ed., International ed. ed, McGraw-Hill chemical engineering series. McGraw-Hill, Boston, Mass.

Smith, W.R., Missen, R.W., 1982. Chemical reaction equilibrium analysis: theory and algorithms. Wiley-Interscience, New York.

Stucki, S., Vogel, F., Ludwig, C., Haiduc, A.G., Brandenberger, M., 2009. Catalytic gasification of algae in supercritical water for biofuel production and carbon capture. Energy Environ. Sci. 2, 535.

Su, Y., Zhu, W., Gong, M., Zhou, H., Fan, Y., Amuzu-Sefordzi, B., 2015. Interaction between sewage sludge components lignin (phenol) and proteins (alanine) in supercritical water gasification. Int. J. Hydrog. Energy 40, 9125–9136.

Susanti, R.F., Dianningrum, L.W., Yum, T., Kim, Y., Lee, B.G., Kim, J., 2012. High-yield hydrogen production from glucose by supercritical water gasification without added catalyst. Int. J. Hydrog. Energy 37, 11677–11690.

Susanti, R.F., Veriansyah, B., Kim, J.D., Kim, J., Lee, Y.W., 2010. Continuous supercritical water gasification of isooctane: A promising reactor design. Int. J. Hydrog. Energy 35, 1957–1970.

Tang, H., Kitagawa, K., 2005. Supercritical water gasification of biomass: thermodynamic analysis with direct Gibbs free energy minimization. Chem. Eng. J. 106, 261–267.

Tapah, B.F., Santos, R.C.D., Leeke, G.A., 2014. Processing of glycerol under sub and supercritical water conditions. Renew. Energy 62, 353–361.

Taylor, A.D., DiLeo, G.J., Sun, K., 2009. Hydrogen production and performance of nickel based catalysts synthesized using supercritical fluids for the gasification of biomass. Appl. Catal. B Environ. 93, 126–133.

Uematsu, M., Franck, E.U., 1980. Static dielectric constant of water and steam. J. Phys. Chem. Ref. Data 9, 1291–1306.

Uras, Ü., Carrier, M., Hardie, A.G., Knoetze, J.H., 2012. Physico-chemical characterization of biochars from vacuum pyrolysis of South African agricultural wastes for application as soil amendments. J. Anal. Appl. Pyrolysis 98, 207–213.

Vaezi, M., Passandideh-Fard, M., Moghiman, M., Charmchi, M., 2012. On a methodology for selecting biomass materials for gasification purposes. Fuel Process. Technol. 98, 74–81.

van Bennekom, J.G., Venderbosch, R.H., Assink, D., Heeres, H.J., 2011. Reforming of methanol and glycerol in supercritical water. J. Supercrit. Fluids 58, 99–113.

Van Krevelen, D.W., 1950. Graphical-statistical method for the study of structure and reaction processes of coal. Fuel 29, 269–284.

Vogel, F., Waldner, M.H., Rouff, A.A., Rabe, S., 2007. Synthetic natural gas from biomass by catalytic conversion in supercritical water. Green Chem. 9, 616.

Voll, F.A.P., Rossi, C.C.R.S., Silva, C., Guirardello, R., Souza, R.O.M.A., Cabral, V.F., Cardozo-Filho, L., 2009. Thermodynamic analysis of supercritical water gasification of methanol, ethanol, glycerol, glucose and cellulose. Int. J. Hydrog. Energy 34, 9737–9744.

Vostrikov, A.A., Fedyaeva, O.N., Shishkin, A.V., Dubov, D.Y., Sokol, M.Y., 2008. Conversion of municipal sewage sludge in supercritical water. Solid Fuel Chem. 42, 384–393.

Waldner, M.H., 2007. Catalytic hydrothermal gasification of biomass for the production of synthetic natural gas (Ph.D. Thesis). Eidgenössische Technische Hochschule/Paul Scherrer Institute, Zurich, Switzerland.

Waldner, M.H., Vogel, F., 2005. Renewable Production of Methane from Woody Biomass by Catalytic Hydrothermal Gasification. Ind. Eng. Chem. Res. 44, 4543–4551.

Watanabe, M., Inomata, H., Arai, K., 2002. Catalytic hydrogen generation from biomass (glucose and cellulose) with ZrO2 in supercritical water. Biomass Bioenergy 22, 405–410.

Wei, C., Hu, C., Wu, C., Yan, B., 2006. Supercritical gasification for the treatment of o-cresol wastewater. J. Environ. Sci. 18, 644–649.

Weiss-Hortala, E., Kruse, A., Ceccarelli, C., Barna, R., 2010. Influence of phenol on glucose degradation during supercritical water gasification. J. Supercrit. Fluids 53, 42–47.

Wilkinson, N., Wickramathilaka, M., Hendry, D., Miller, A., Espanani, R., Jacoby, W., 2012. Rate determination of supercritical water gasification of primary sewage sludge as a replacement for anaerobic digestion. Bioresour. Technol. 124, 269–275.

Williams, P.T., Onwudili, J., 2006. Subcritical and Supercritical Water Gasification of Cellulose, Starch, Glucose, and Biomass Waste. Energy Fuels 20, 1259–1265.

Williams, P.T., Onwudili, J., 2005. Composition of Products from the Supercritical Water Gasification of Glucose: A Model Biomass Compound. Ind. Eng. Chem. Res. 44, 8739–8749.

Withag, J.A.M., Smeets, J.R., Bramer, E.A., Brem, G., 2012. System model for gasification of biomass model compounds in supercritical water – A thermodynamic analysis. J. Supercrit. Fluids 61, 157–166.

World Bioenergy Association, 2014. WBA Global Bioenergy Statistics 2014.

Xu, X., Antal, M.J., 1998. Gasification of sewage sludge and other biomass for hydrogen production in supercritical water. Environ. Prog. 17, 215–220.

Xu, Z.R., Zhu, W., Gong, M., Zhang, H.W., 2013. Direct gasification of dewatered sewage sludge in supercritical water. Part 1: Effects of alkali salts. Int. J. Hydrog. Energy 38, 3963–3972.

Xu, Z.R., Zhu, W., Li, M., 2012. Influence of moisture content on the direct gasification of dewatered sludge via supercritical water. Int. J. Hydrog. Energy 37, 6527–6535.

Yakaboylu, O., Harinck, J., Gerton Smit, K.G., de Jong, W., 2013. Supercritical water gasification of manure: A thermodynamic equilibrium modeling approach. Biomass Bioenergy 59, 253–263.

Yakaboylu, O., Harinck, J., Smit, K., de Jong, W., 2015. Supercritical Water Gasification of Biomass: A Literature and Technology Overview. Energies 8, 859–894.

Yakaboylu, O., Harinck, J., Smit, K.G., de Jong, W., 2014. Supercritical water gasification of biomass: A thermodynamic model for the prediction of product compounds at equilibrium state. Energy Fuels 28, 2506–2522.

Yamaguchi, A., Hiyoshi, N., Sato, O., Bando, K.K., Osada, M., Shirai, M., 2009. Hydrogen production from woody biomass over supported metal catalysts in supercritical water. Catal. Today 146, 192–195.

Yan, Q., Guo, L., Lu, Y., 2006. Thermodynamic analysis of hydrogen production from biomass gasification in supercritical water. Energy Convers. Manag. 47, 1515–1528.

Yanagida, T., Minowa, T., Nakamura, A., Matsumura, Y., Noda, Y., 2008. Behavior of Inorganic Elements in Poultry Manure during Supercritical Water Gasification. J. Jpn. Inst. Energy 87, 731–736.

Yanagida, T., Minowa, T., Shimizu, Y., Matsumura, Y., Noda, Y., 2009. Recovery of activated carbon catalyst, calcium, nitrogen and phosphate from effluent following supercritical water gasification of poultry manure. Bioresour. Technol. 100, 4884–4886.

Yanik, J., Ebale, S., Kruse, A., Saglam, M., Yüksel, M., 2008. Biomass gasification in supercritical water: II. Effect of catalyst. Int. J. Hydrog. Energy 33, 4520–4526.

Yanik, J., Ebale, S., Kruse, A., Saglam, M., Yuksel, M., 2007. Biomass gasification in supercritical water: Part 1. Effect of the nature of biomass. Fuel 86, 2410–2415.

Yesodharan, S., 2002. Supercritical water oxidation: An environmentally safe method for the disposal of organic wastes. Curr. Sci. 82, 1112–1122.

Yong, T.L.-K., Matsumura, Y., 2012a. Catalytic Gasification of Poultry Manure and Eucalyptus Wood Mixture in Supercritical Water. Ind. Eng. Chem. Res. 51, 5685–5690.

Yong, T.L.-K., Matsumura, Y., 2012b. Reaction Kinetics of the Lignin Conversion in Supercritical Water. Ind. Eng. Chem. Res. 51, 11975–11988.

Yoshida, T., Matsumura, Y., 2009. Reactor Development for Supercritical Water Gasification of 4.9 wt% Glucose Solution at 673 K by Using Computational Fluid Dynamics. Ind. Eng. Chem. Res. 48, 8381–8386.

Yoshida, T., Matsumura, Y., 2001. Gasification of Cellulose, Xylan, and Lignin Mixtures in Supercritical Water. Ind. Eng. Chem. Res. 40, 5469–5474.

Yoshida, T., Oshima, Y., Matsumura, Y., 2004. Gasification of biomass model compounds and real biomass in supercritical water. Biomass Bioenergy 26, 71–78.

Yoshida, Y., Dowaki, K., Matsumura, Y., Matsuhashi, R., Li, D., Ishitani, H., Komiyama, H., 2003. Comprehensive comparison of efficiency and CO2 emissions between biomass energy conversion technologies—position of supercritical water gasification in biomass technologies. Biomass Bioenergy 25, 257–272.

Youssef, E.A., Chowdhury, M.B.I., Nakhla, G., Charpentier, P., 2010. Effect of nickel loading on hydrogen production and chemical oxygen demand (COD) destruction from glucose oxidation and gasification in supercritical water. Int. J. Hydrog. Energy 35, 5034–5042.

Yu, D., Aihara, M., Antal, M.J., 1993. Hydrogen production by steam reforming glucose in supercritical water. Energy Fuels 7, 574–577.

Yu-Wu, Q.M., Weiss-Hortala, E., Barna, R., 2013. Hydrothermal conversion of glucose in multiscale batch processes. Analysis of the gas, liquid and solid residues. J. Supercrit. Fluids 79, 76–83.

Zhang, L., Xu, C., Champagne, P., 2010a. Overview of recent advances in thermo-chemical conversion of biomass. Energy Convers. Manag. 51, 969–982.

Zhang, L., Xu, C., Champagne, P., 2010b. Energy recovery from secondary pulp/paper-mill sludge and sewage sludge with supercritical water treatment. Bioresour. Technol. 101, 2713–2721.

Zhang, R., Jiang, W., Cheng, L., Sun, B., Sun, D., Bi, J., 2010. Hydrogen production from lignite via supercritical water in flow-type reactor. Int. J. Hydrog. Energy 35, 11810–11815.

Zhu, W., Xu, Z.R., Li, L., He, C., 2011. The behavior of phosphorus in sub- and super-critical water gasification of sewage sludge. Chem. Eng. J. 171, 190–196.

Zöhrer, H., Vogel, F., 2013. Hydrothermal catalytic gasification of fermentation residues from a biogas plant. Biomass Bioenergy 53, 138–148.

Appendix A

ADDITIONAL INFORMATION: THERMODYNAMIC MODELLING

A.1 Biomass Feedstock Properties

TABLE A-1 ULTIMATE ANALYSIS AND HHV OF BIOMASS MATERIAL USED (DATA FROM PHYLLIS2 (2012))

NO.	FEEDSTOCK MATERIAL NAME	ULTIMATE ANALYSIS						HHV_{MILNE} [MJ/KG]	PHYLLIS #
		C	H	O	N	S	Cl		
1	Sewage Sludge	25.50	4.96	18.50	3.25	1.12	0.02	12.34	#1513
2	Black Liquor	29.20	4.40	31.10	0.14	4.90	0.06	11.99	#1394
3	Grape Pomace	54.94	5.83	32.73	2.09	0.21	0.00	22.22	#1485
4	Olive Residue	39.64	5.03	37.17	1.59	0.08	0.30	15.31	#2176
5	Paper Sludge	23.80	3.34	26.81	0.09	0.16	0.06	8.93	#2746
6	Cow Manure	22.10	2.90	11.50	1.10	0.10	0.00	9.51	#2773
7	Char Sugarcane Bagasse	81.50	3.10	9.10	0.80	0.00	0.00	30.62	#2344
8	Micro Algae Spirulina	52.73	7.22	28.85	8.01	0.49	0.18	23.48	#1921
9	Pig Manure	43.66	4.18	33.51	2.47	0.48	0.50	15.93	#1715
10	Ethanol	52.14	13.13	34.73	0.00	0.00	0.00	30.97	#1264
11	Spent Coffee	57.00	7.60	32.90	2.10	0.10	0.00	25.29	#1788
12	Sugar Cane Bagasse	45.45	5.26	36.65	0.23	0.05	0.04	17.86	#2806
13	Animal Blood	50.50	7.70	25.45	13.80	0.50	0.65	22.70	#2693
14	Beet Pulp	35.50	4.74	34.09	1.28	0.00	0.00	13.85	#1361
15	Bitiminius Coal	76.73	4.69	10.52	1.41	0.40	0.06	30.87	#1145
16	Chlorella Residue after Ethanol extraction	50.57	6.82	22.41	11.62	0.77	0.00	22.18	#2335

TABLE A-1 CONTINUED - ULTIMATE ANALYSIS AND HHV OF BIOMASS MATERIAL USED (DATA FROM PHYLLIS2 (2012))

NO.	FEEDSTOCK MATERIAL NAME	ULTIMATE ANALYSIS						HHV_{MILNE} [MJ/KG]	PHYLLIS #
		C	H	O	N	S	Cl		
17	Lignite Coal	63.54	4.52	28.95	0.70	0.31	0.02	24.05	#2847
18	Cotton gin Waste	49.03	4.71	35.08	1.45	0.36	0.00	18.46	#382
19	Flax stalk	49.10	6.10	40.45	1.30	0.12	0.06	19.76	#3163
20	Switchgrass	46.89	5.58	41.51	0.58	0.11	0.50	18.60	#701
21	Olive Waste	46.42	5.62	34.38	1.76	0.16	0.00	18.78	#3348
22	Chicken Manure	38.10	5.60	30.90	3.50	0.60	0.00	16.05	#2774
23	Cattle Manure (fresh)	29.15	3.55	20.75	2.25	0.61	1.35	11.54	#1886
24	Pig Manure (digestate, dried)	44.38	5.57	37.90	2.22	0.48	1.46	17.52	#2903
25	Sheep Manure	40.60	5.10	30.70	2.10	0.60	0.00	16.44	#2772
26	Coffee Husks	49.40	6.10	41.20	0.81	0.07	0.03	19.84	#2882
27	Grape Skins and seeds	48.33	5.95	37.75	1.93	0.00	0.00	19.50	#2862
28	Mango peel	41.60	7.04	46.00	0.91	0.08	0.09	17.80	#2922
29	Oil Palm empty fruit bunch pith	41.61	5.92	43.72	0.23	0.98	0.00	16.70	#2897
30	Soybean Oil cake	38.80	5.47	41.86	6.64	0.00	0.00	14.90	#2848
31	Sugar cane fibre	44.50	5.18	33.84	0.51	0.16	0.43	17.71	#2807
32	Humus from digested MSW	32.37	3.83	26.91	1.21	0.39	0.65	12.41	#2132
33	MSW compost	33.78	3.71	20.29	1.83	0.68	4.68	13.45	#3345
34	Organic wet fraction municipal waste	33.96	4.04	26.27	1.73	1.54	0.90	13.31	#3198
35	Dutch organic domestic waste	25.84	3.32	20.56	1.29	0.00	0.19	10.20	#1716
36	Cellulose	43.30	6.50	49.30	0.20	0.00	0.04	17.41	#1720
37	Leather waste	49.31	8.52	22.12	12.42	1.83	0.45	23.98	#2930
38	Lingnin from softwood	62.17	5.89	31.11	0.15	0.06	0.00	25.23	#2000
39	Waste paper	49.31	7.07	34.86	0.70	0.15	0.00	21.79	#709
40	Solid Recoved fuel	56.90	8.30	29.10	0.18	0.11	0.00	26.80	#3097
41	Munisipal Solid Waste	49.23	8.15	23.73	1.82	0.25	0.00	24.30	#2920
42	Refuse Derived Fuel (RDF)	40.75	7.57	38.59	0.28	0.53	0.53	19.11	#1386

TABLE A-1 CONTINUED - ULTIMATE ANALYSIS AND HHV OF BIOMASS MATERIAL USED (DATA FROM PHYLLIS2 (2012))

NO.	FEEDSTOCK MATERIAL NAME	ULTIMATE ANALYSIS						HHV_{MILNE} [MJ/KG]	PHYLLIS #
		C	H	O	N	S	Cl		
43	Apple pulp	49.56	8.43	38.87	0.97	0.05	0.00	23.23	#2292
44	Olive mill effluent (OME) concentrate	46.00	6.20	33.50	0.80	1.26	0.00	19.65	#2297
45	Paper Residue sludge	23.60	3.08	26.51	0.72	0.12	0.10	8.48	#670
46	Paper mill Sludge Cake	24.31	3.31	43.11	0.40	0.03	0.00	7.13	#917
47	Paper residue sludge granules	22.90	2.94	25.75	0.72	0.34	0.02	8.16	#940
48	Straw	44.34	5.48	39.11	0.09	0.13	0.94	17.70	#3059
49	Torrified Wood chips	48.76	5.08	34.84	0.41	0.03	0.02	20.73	#3503
50	Palm leaves	47.98	5.26	36.61	1.17	0.02	0.00	18.67	#3350
51	Methanol	37.50	12.50	50.00	0.00	0.00	0.00	23.31	#1962
52	Glucose	40.01	6.71	53.28	0.00	0.00	0.00	16.12	#1181
53	Crude Glycerin	50.20	9.70	37.50	2.60	0.00	0.00	25.13	n/a[a]
54	Glycerol	39.13	8.76	52.12	0.00	0.00	0.00	18.66	n/a[b]

[a]Data from Crnkovic et al. (2012)
[b]Calculated

TABLE A-2 PROXIMATE ANALYSIS OF ALL 54 FEEDSTOCK MATERIAL CONSIDERED ON A DRY BASIS (DATA FROM PHYLLIS2 (2012))

NO.	FEEDSTOCK MATERIAL NAME	FC	VM	ASH
1	Sewage Sludge	2.30	51.10	46.60
2	Black Liquor	13.00	46.80	40.20
3	Grape Pomace	21.40	74.40	4.20
4	Olive Residue	19.20	64.60	16.20
5	Paper Sludge	1.21	53.05	45.74
6	Cow Manure	7.10	30.60	62.30
7	Char Sugarcane Bagasse	79.10	15.40	5.50
8	Micro Algae Spirulina	15.68	81.80	2.52
9	Pig Manure	21.90	62.90	15.20
10	Ethanol	n/a	n/a	n/a
11	Spent Coffee	13.30	86.40	0.30
12	Sugar Cane Bagasse	10.26	77.36	12.38
13	Animal Blood	4.80	93.80	1.40
14	Beet Pulp	14.11	61.50	24.39
15	Bitiminius Coal	61.30	32.50	6.20
16	Chlorella Residue after Ethanol extraction	15.39	76.70	13.83
17	Lignite Coal	46.97	49.20	3.83
18	Cotton gin Waste	8.48	82.16	9.36
19	Flax stalk	18.27	78.80	2.93
20	Switchgrass	16.21	79.19	4.59
21	Olive Waste	19.36	68.98	11.66
22	Chicken Manure	9.62	69.13	21.25
23	Cattle Manure (fresh)	4.56	53.10	42.34
24	Pig Manure (digestate, dried)	20.20	64.90	14.90
25	Sheep Manure	13.90	65.20	20.90
26	Coffee Husks	12.86	74.80	2.50
27	Grape Skins and seeds	27.87	66.09	6.04
28	Mango peel	24.10	71.53	4.37

TABLE A-2 CONTINUED - PROXIMATE ANALYSIS OF ALL 54 FEEDSTOCK MATERIAL CONSIDERED ON A DRY BASIS (DATA FROM PHYLLIS2 (2012))

NO.	FEEDSTOCK MATERIAL NAME	FC	VM	ASH
29	Oil Palm empty fruit bunch pith	21.26	71.20	7.54
30	Soybean Oil cake	16.49	76.55	6.96
31	Sugar cane fibre	12.71	71.61	15.68
32	Humus from digested MSW	13.77	51.59	34.64
33	MSW compost	6.70	53.59	39.71
34	Organic wet fraction municipal waste	10.68	52.36	36.96
35	Dutch organic domestic waste	11.00	40.20	48.80
36	Cellulose	10.96	88.30	0.74
37	Leather waste	16.90	77.30	5.80
38	Lingnin from softwood	26.24	73.14	0.62
39	Waste paper	9.18	82.90	7.92
40	Solid Recoved fuel	9.80	85.30	4.90
41	Munisipal Solid Waste	10.58	72.60	16.82
42	Refuse Derived Fuel (RDF)	12.25	76.00	11.75
43	Apple pulp	18.20	79.00	2.80
44	Olive mill effluent (OME) concentrate	0.30	84.00	15.70
45	Paper Residue sludge	2.44	48.70	45.86
46	Paper mill Sludge Cake	11.26	59.90	28.84
47	Paper residue sludge granules	7.30	45.40	47.30
48	Straw	18.51	74.40	7.09
49	Torrified Wood chips	24.68	72.20	3.12
50	Palm leaves	12.14	79.05	8.81
51	Methanol	n/a	n/a	n/a
52	Glucose	12.90	87.10	0.00
53	Crude Glycerin	0.00	95.56	4.44
54	Glycerol	n/a	n/a	n/a

A.2 PR-BM Property Method applying Gibbs-free Energy Minimisation

The following section provides a summary of the equations employed in Aspen Plus® when the PR-BM property method. The PR-BM property method uses the Peng-Robinson equation with the Boston and Mathias alpha function and the standard mixing rules. A brief summary of the equations employed by Aspen Plus® follows:

The Peng-Robinson equation of state is given in Eq. A-1:

$$P = \frac{RT}{(c + V_m) - b} - \frac{a}{(V_m + c)(V_m + c + b) + b(V_m + c - b)} \quad \text{A-1}$$

Where P is the system pressure, T is the system temperature, R is the universal gas constant and V_m is the molar volume.

The values of b and c are calculated by means of the standard mixing rule using the mole fraction (x_i) of each component:

$$b = \sum_i x_i b_i \quad \text{A-2}$$

$$c = \sum_i x_i c_i \quad \text{A-3}$$

The value of b_i for each component is determined using Eq. A-4 where $T_{c,i}$ and $P_{c,i}$ are the critical temperature and pressure of the individual components, respectively.

$$b_i = 0.07780 \frac{RT_{c,i}}{P_{c,i}} \quad \text{A-4}$$

The value of c_i can be determined using Eq. A-5, where $z_{RA,i}$ is the regressed parameter. In this case, the default values of $z_{RA,i}$ in Aspen Plus® were used.

$$c_i = 0.40768 \frac{RT_{c,i}}{P_{c,i}} \left(0.29441 - z_{RA,i}\right) \quad \text{A-5}$$

The value of a is calculated as follows:

$$a = a_0 + a_1 \tag{A-6}$$

$$a_0 = \sum_i \sum_j x_i x_j (a_i a_j)^{0.5} (1 - k_{ij}) \tag{A-7}$$

$$a_1 = \sum_{i=1}^{n} x_i \left(\sum_{j=1}^{n} x_j \left((a_i a_j)^{1/2} l_{i,j} \right)^{1/3} \right)^3 \tag{A-8}$$

In Eq. A-7 and A-8 k_{ij} and l_{ij} are temperature dependent binary interaction parameters calculated as follows:

$$k_{ij} = {k_{ij}}^{(1)} + {k_{ij}}^{(2)} T + \frac{{k_{ij}}^{(3)}}{T} \tag{A-9}$$

Where, $k_{ij} = k_{ji}$

$$l_{ij} = {l_{ij}}^{(1)} + {l_{ij}}^{(2)} T + \frac{{l_{ij}}^{(3)}}{T} \tag{A-10}$$

Where, $l_{ij} \neq l_{ji}$

Generally, these binary interaction parameters should be determined by means of regression for the best results. However, the Aspen Physical Property System has built-in values for these parameters for a wide variety of component pairs. In this study, the default values in the databank was used.

The value of a_i for each component can be determined using Eq. A-11:

$$a_i = 0.45724 \alpha_i \frac{R^2 T_{c,i}^2}{P_{c,i}} \tag{A-11}$$

At supercritical conditions, the Boston-Mathias modification of the alpha function (α_i) is adopted:

$$\alpha_i = \left[\exp\left[c_i\left(1 - T_{r_i}^{d_i}\right)\right]\right]^2 \quad \text{A-12}$$

$$d_i = \left(1 + \frac{m_i}{2}\right) \quad \text{A-13}$$

$$c_i = 1 - \frac{1}{d_i} \quad \text{A-14}$$

$$m_i = 0.3764 + 1.5226\omega_i - 0.26992\omega^2 \quad \text{A-15}$$

At subcritical conditions, the original expression for alpha function is used:

$$\alpha_i(T) = \left[1 + m_i\left(1 - T_{r,i}^{1/2}\right)\right]^2 \quad \text{A-16}$$

A.3 Gibbs Free Energy Minimisation

This section provides a summary of how the Gibbs free energy minimisation is applied using the Peng-Robinson EoS (as described byTang and Kitagawa (2005)).

The Peng-Robinson equation (Eq. A-1) can be rewritten as a third-order polynomial using the compressibility factor Z:

$$Z^3 - (1 - B^*)Z^2 + (A^* - 2B^* - 3B^{*2})Z - (A^*B^* - B^{*2} - B^{*3}) = 0 \quad \text{A-17}$$

$$A^* = \frac{aP}{R^2T^2} \quad \text{A-18}$$

$$B^* = \frac{bP}{RT} \quad \text{A-19}$$

The partial fugacity coefficient for all of the species i can be determined as follows:

$$\phi_i = \frac{1}{Z} exp\left(\frac{1}{RT}\int_V^\infty \frac{\partial P}{\partial n_i}|T, V, n_{j(j\neq i)} - \frac{RT}{V}dV\right) \quad \text{A-20}$$

The Gibbs free energy of a system is the sum of the chemical potential (μ_i) of each component:

$$G = \sum_{i}^{i=k} n_i \mu_i \qquad \text{A-21}$$

Eq. A-21 can be rewritten as follows:

$$G = \sum_{i}^{k} n_i \Delta G_i^o + RT \sum_{i}^{k} n_i ln x_i + RT \sum_{i}^{k} n_i ln \phi_i + RT \sum_{i}^{k} n_i lnP \qquad \text{A-22}$$

$$\Delta G_i^o = \Delta H_{f,i}^o + \int_{298}^{T} c_{p_i}(T)dt - T\Delta S_{f,i}^o - T\int_{298}^{T} \frac{c_{p_i}(T)}{T} dt \qquad \text{A-23}$$

Eq. A-22 is then the function which is minimised and it is subjected to the following constraints:

- Non-linear equality constraint (Eq. A-24):

$$Z^3 - (1 - B^*)Z^2 + (A^* - 2B^* - 3B^{*2})Z - (A^*B^* - B^{*2} - B^{*3}) = 0 \qquad \text{A-24}$$

- Linear equality constraint for the conservation of the individual molecules (Eq. A-25), where N_{e_i} is the moles a certain element (j) in component i:

$$\sum_i^k N_{j_i} n_i = N_e \quad (e = 1, 2, 3 \ldots M) \qquad \text{A-25}$$

- Linear inequality constraint (Eq. A-26) for the conservation of the moles of individual components in which the moles of an individual component cannot be less than zero or more than the possible total maximum of moles of the specific species:

$$0 \leq n_i \leq n_{i,total\ possible} \qquad \text{A-26}$$

A.4 Properties of all 120 cases of feed material used

Table A-3 provides the properties of the feed material for each of the cases when the C, H and O content were varied in terms of their C/H ratio.

TABLE A-3 COMPOSITION OF FEED MATERIAL OF EACH OF THE 120 CASES USED

CASE	MASS COMPOSITION [WT.%]								MOLAR RATIOS		HHV
	C/H	C	H	O	N	S	CL	TOTAL	H/C	O/C	[MJ/KG]
1	2	20.00	10.00	66.79	0.5	2.3	0.4	100.0	5.96	2.51	12.12
2	2	22.97	11.48	62.34	0.5	2.3	0.4	100.0	5.96	2.04	15.63
3	2	25.93	12.97	57.89	0.5	2.3	0.4	100.0	5.96	1.68	19.14
4	2	28.90	14.45	53.44	0.5	2.3	0.4	100.0	5.96	1.39	22.64
5	2	31.87	15.93	48.99	0.5	2.3	0.4	100.0	5.96	1.15	26.15
6	2	34.84	17.42	44.54	0.5	2.3	0.4	100.0	5.96	0.96	29.66
7	2	37.80	18.90	40.09	0.5	2.3	0.4	100.0	5.96	0.80	33.17
8	2	40.77	20.38	35.64	0.5	2.3	0.4	100.0	5.96	0.66	36.67
9	2	43.74	21.87	31.18	0.5	2.3	0.4	100.0	5.96	0.54	40.18
10	2	46.70	23.35	26.73	0.5	2.3	0.4	100.0	5.96	0.43	43.69
11	2	49.67	24.84	22.28	0.5	2.3	0.4	100.0	5.96	0.34	47.19
12	2	52.64	26.32	17.83	0.5	2.3	0.4	100.0	5.96	0.25	50.70
13	2	55.61	27.80	13.38	0.5	2.3	0.4	100.0	5.96	0.18	54.21
14	2	58.57	29.29	8.93	0.5	2.3	0.4	100.0	5.96	0.11	57.72
15	2	64.51	32.25	0.03	0.5	2.3	0.4	100.0	5.96	0.00	64.73
16	6	20.00	3.33	73.46	0.5	2.3	0.4	100.0	1.99	2.76	2.51
17	6	24.20	4.03	68.56	0.5	2.3	0.4	100.0	1.99	2.13	5.45
18	6	28.39	4.73	63.67	0.5	2.3	0.4	100.0	1.99	1.68	8.39
19	6	32.59	5.43	58.77	0.5	2.3	0.4	100.0	1.99	1.35	11.34
20	6	36.78	6.13	53.88	0.5	2.3	0.4	100.0	1.99	1.10	14.28
21	6	40.98	6.83	48.98	0.5	2.3	0.4	100.0	1.99	0.90	17.22
22	6	45.17	7.53	44.09	0.5	2.3	0.4	100.0	1.99	0.73	20.17
23	6	49.37	8.23	39.19	0.5	2.3	0.4	100.0	1.99	0.60	23.11
24	6	53.57	8.93	34.30	0.5	2.3	0.4	100.0	1.99	0.48	26.05
25	6	57.76	9.63	29.40	0.5	2.3	0.4	100.0	1.99	0.38	28.99
26	6	61.96	10.33	24.51	0.5	2.3	0.4	100.0	1.99	0.30	31.94
27	6	66.15	11.03	19.61	0.5	2.3	0.4	100.0	1.99	0.22	34.88

TABLE A-3 CONTINUED - COMPOSITION OF FEED MATERIAL OF EACH OF THE 120 CASES USED

CASE	MASS COMPOSITION [WT.%]								MOLAR RATIOS		HHV [MJ/KG]
	C/H	C	H	O	N	S	CL	TOTAL	H/C	O/C	
28	6	70.35	11.72	14.72	0.5	2.3	0.4	100.0	1.99	0.16	37.82
29	6	74.55	12.42	9.82	0.5	2.3	0.4	100.0	1.99	0.10	40.76
30	6	82.94	13.82	0.03	0.5	2.3	0.4	100.0	1.99	0.00	46.65
31	10	20.00	2.00	74.79	0.5	2.3	0.4	100.0	1.19	2.81	0.59
32	10	24.53	2.45	69.81	0.5	2.3	0.4	100.0	1.19	2.14	3.33
33	10	29.06	2.91	64.82	0.5	2.3	0.4	100.0	1.19	1.67	6.07
34	10	33.59	3.36	59.84	0.5	2.3	0.4	100.0	1.19	1.34	8.81
35	10	38.12	3.81	54.85	0.5	2.3	0.4	100.0	1.19	1.08	11.56
36	10	42.65	4.27	49.87	0.5	2.3	0.4	100.0	1.19	0.88	14.30
37	10	47.19	4.72	44.89	0.5	2.3	0.4	100.0	1.19	0.71	17.04
38	10	51.72	5.17	39.90	0.5	2.3	0.4	100.0	1.19	0.58	19.78
39	10	56.25	5.62	34.92	0.5	2.3	0.4	100.0	1.19	0.47	22.52
40	10	60.78	6.08	29.93	0.5	2.3	0.4	100.0	1.19	0.37	25.27
41	10	65.31	6.53	24.95	0.5	2.3	0.4	100.0	1.19	0.29	28.01
42	10	69.84	6.98	19.97	0.5	2.3	0.4	100.0	1.19	0.21	30.75
43	10	74.37	7.44	14.98	0.5	2.3	0.4	100.0	1.19	0.15	33.49
44	10	78.90	7.89	10.00	0.5	2.3	0.4	100.0	1.19	0.10	36.23
45	10	87.96	8.80	0.03	0.5	2.3	0.4	100.0	1.19	0.00	41.72
46	14	20.00	1.43	75.36	0.5	2.3	0.4	100.0	0.85	2.83	-0.24
47	14	24.69	1.76	70.34	0.5	2.3	0.4	100.0	0.85	2.14	2.41
48	14	29.37	2.10	65.32	0.5	2.3	0.4	100.0	0.85	1.67	5.05
49	14	34.06	2.43	60.30	0.5	2.3	0.4	100.0	0.85	1.33	7.69
50	14	38.75	2.77	55.27	0.5	2.3	0.4	100.0	0.85	1.07	10.34
51	14	43.44	3.10	50.25	0.5	2.3	0.4	100.0	0.85	0.87	12.98
52	14	48.12	3.44	45.23	0.5	2.3	0.4	100.0	0.85	0.71	15.62
53	14	52.81	3.77	40.21	0.5	2.3	0.4	100.0	0.85	0.57	18.27

TABLE A-3 CONTINUED - COMPOSITION OF FEED MATERIAL OF EACH OF THE 120 CASES USED

CASE	MASS COMPOSITION [WT.%]								MOLAR RATIOS		HHV [MJ/KG]
	C/H	C	H	O	N	S	CL	TOTAL	H/C	O/C	
54	14	57.50	4.11	35.18	0.5	2.3	0.4	100.0	0.85	0.46	20.91
55	14	62.19	4.44	30.16	0.5	2.3	0.4	100.0	0.85	0.36	23.56
56	14	66.87	4.78	25.14	0.5	2.3	0.4	100.0	0.85	0.28	26.20
57	14	71.56	5.11	20.12	0.5	2.3	0.4	100.0	0.85	0.21	28.84
58	14	76.25	5.45	15.10	0.5	2.3	0.4	100.0	0.85	0.15	31.49
59	14	80.93	5.78	10.07	0.5	2.3	0.4	100.0	0.85	0.09	34.13
60	14	90.31	6.45	0.03	0.5	2.3	0.4	100.0	0.85	0.00	39.42
61	18	20.00	1.11	75.68	0.5	2.3	0.4	100.0	0.66	2.84	-0.69
62	18	24.78	1.38	70.64	0.5	2.3	0.4	100.0	0.66	2.14	1.89
63	18	29.56	1.64	65.59	0.5	2.3	0.4	100.0	0.66	1.67	4.48
64	18	34.33	1.91	60.55	0.5	2.3	0.4	100.0	0.66	1.32	7.06
65	18	39.11	2.17	55.51	0.5	2.3	0.4	100.0	0.66	1.07	9.65
66	18	43.89	2.44	50.46	0.5	2.3	0.4	100.0	0.66	0.86	12.23
67	18	48.67	2.70	45.42	0.5	2.3	0.4	100.0	0.66	0.70	14.82
68	18	53.44	2.97	40.38	0.5	2.3	0.4	100.0	0.66	0.57	17.40
69	18	58.22	3.23	35.33	0.5	2.3	0.4	100.0	0.66	0.46	19.99
70	18	63.00	3.50	30.29	0.5	2.3	0.4	100.0	0.66	0.36	22.57
71	18	67.78	3.77	25.25	0.5	2.3	0.4	100.0	0.66	0.28	25.16
72	18	72.56	4.03	20.20	0.5	2.3	0.4	100.0	0.66	0.21	27.74
73	18	77.33	4.30	15.16	0.5	2.3	0.4	100.0	0.66	0.15	30.33
74	18	82.11	4.56	10.12	0.5	2.3	0.4	100.0	0.66	0.09	32.91
75	18	91.67	5.09	0.03	0.5	2.3	0.4	100.0	0.66	0.00	38.09
76	22	20.00	0.91	75.88	0.5	2.3	0.4	100.0	0.54	2.85	-0.99
77	22	24.84	1.13	70.82	0.5	2.3	0.4	100.0	0.54	2.14	1.56
78	22	29.67	1.35	65.77	0.5	2.3	0.4	100.0	0.54	1.66	4.11
79	22	34.51	1.57	60.71	0.5	2.3	0.4	100.0	0.54	1.32	6.65
80	22	39.35	1.79	55.65	0.5	2.3	0.4	100.0	0.54	1.06	9.20

TABLE A-3 CONTINUED - COMPOSITION OF FEED MATERIAL OF EACH OF THE 120 CASES USED

CASE	MASS COMPOSITION [WT.%]								MOLAR RATIOS		HHV [MJ/KG]
	C/H	C	H	O	N	S	CL	TOTAL	H/C	O/C	
81	22	44.18	2.01	50.60	0.5	2.3	0.4	100.0	0.54	0.86	11.75
82	22	49.02	2.23	45.54	0.5	2.3	0.4	100.0	0.54	0.70	14.29
83	22	53.86	2.45	40.48	0.5	2.3	0.4	100.0	0.54	0.56	16.84
84	22	58.69	2.67	35.43	0.5	2.3	0.4	100.0	0.54	0.45	19.39
85	22	63.53	2.89	30.37	0.5	2.3	0.4	100.0	0.54	0.36	21.94
86	22	68.37	3.11	25.31	0.5	2.3	0.4	100.0	0.54	0.28	24.48
87	22	73.21	3.33	20.26	0.5	2.3	0.4	100.0	0.54	0.21	27.03
88	22	78.04	3.55	15.20	0.5	2.3	0.4	100.0	0.54	0.15	29.58
89	22	82.88	3.77	10.14	0.5	2.3	0.4	100.0	0.54	0.09	32.12
90	22	92.55	4.21	0.03	0.5	2.3	0.4	100.0	0.54	0.00	37.22
91	26	20.00	0.77	76.02	0.5	2.3	0.4	100.0	0.46	2.85	-1.19
92	26	24.88	0.96	70.95	0.5	2.3	0.4	100.0	0.46	2.14	1.33
93	26	29.76	1.14	65.89	0.5	2.3	0.4	100.0	0.46	1.66	3.85
94	26	34.64	1.33	60.82	0.5	2.3	0.4	100.0	0.46	1.32	6.37
95	26	39.51	1.52	55.76	0.5	2.3	0.4	100.0	0.46	1.06	8.89
96	26	44.39	1.71	50.69	0.5	2.3	0.4	100.0	0.46	0.86	11.41
97	26	49.27	1.90	45.62	0.5	2.3	0.4	100.0	0.46	0.70	13.93
98	26	54.15	2.08	40.56	0.5	2.3	0.4	100.0	0.46	0.56	16.45
99	26	59.03	2.27	35.49	0.5	2.3	0.4	100.0	0.46	0.45	18.97
100	26	63.91	2.46	30.43	0.5	2.3	0.4	100.0	0.46	0.36	21.49
101	26	68.78	2.65	25.36	0.5	2.3	0.4	100.0	0.46	0.28	24.01
102	26	73.66	2.83	20.29	0.5	2.3	0.4	100.0	0.46	0.21	26.53
103	26	78.54	3.02	15.23	0.5	2.3	0.4	100.0	0.46	0.15	29.05
104	26	83.42	3.21	10.16	0.5	2.3	0.4	100.0	0.46	0.09	31.57
105	26	93.18	3.58	0.03	0.5	2.3	0.4	100.0	0.46	0.00	36.60
106	30	20.00	0.67	76.12	0.5	2.3	0.4	100.0	0.40	2.86	-1.34
107	30	24.91	0.83	71.05	0.5	2.3	0.4	100.0	0.40	2.14	1.16

TABLE A-3 CONTINUED - COMPOSITION OF FEED MATERIAL OF EACH OF THE 120 CASES USED

CASE	MASS COMPOSITION [WT.%]								MOLAR RATIOS		HHV
	C/H	C	H	O	N	S	CL	TOTAL	H/C	O/C	
108	30	29.82	0.99	65.98	0.5	2.3	0.4	100.0	0.40	1.66	3.66
109	30	34.73	1.16	60.90	0.5	2.3	0.4	100.0	0.40	1.32	6.16
110	30	39.64	1.32	55.83	0.5	2.3	0.4	100.0	0.40	1.06	8.66
111	30	44.55	1.48	50.76	0.5	2.3	0.4	100.0	0.40	0.86	11.16
112	30	49.46	1.65	45.69	0.5	2.3	0.4	100.0	0.40	0.69	13.66
113	30	54.36	1.81	40.61	0.5	2.3	0.4	100.0	0.40	0.56	16.16
114	30	59.27	1.98	35.54	0.5	2.3	0.4	100.0	0.40	0.45	18.66
115	30	64.18	2.14	30.47	0.5	2.3	0.4	100.0	0.40	0.36	21.16
116	30	69.09	2.30	25.39	0.5	2.3	0.4	100.0	0.40	0.28	23.66
117	30	74.00	2.47	20.32	0.5	2.3	0.4	100.0	0.40	0.21	26.15
118	30	78.91	2.63	15.25	0.5	2.3	0.4	100.0	0.40	0.15	28.65
119	30	83.82	2.79	10.18	0.5	2.3	0.4	100.0	0.40	0.09	31.15
120	30	93.64	3.12	0.03	0.5	2.3	0.4	100.0	0.40	0.00	36.15

Appendix B

ADDITIONAL RESULTS: THERMODYNAMIC MODELLING

B.1 Comparison between mass and molar basis results

The results were initially presented on a mass basis in terms of the oxygen content (wt.%) and the C:H ratio (wt.% C per wt.% H) and published in Louw et al. (2014). However, it was decided to present the results on a molar basis in this dissertation. A comparison between the results on a molar and mass basis for an operating temperature of 700 °C and a feed concentration of 5 wt.% are shown in Figure B-1 to Figure B-4.

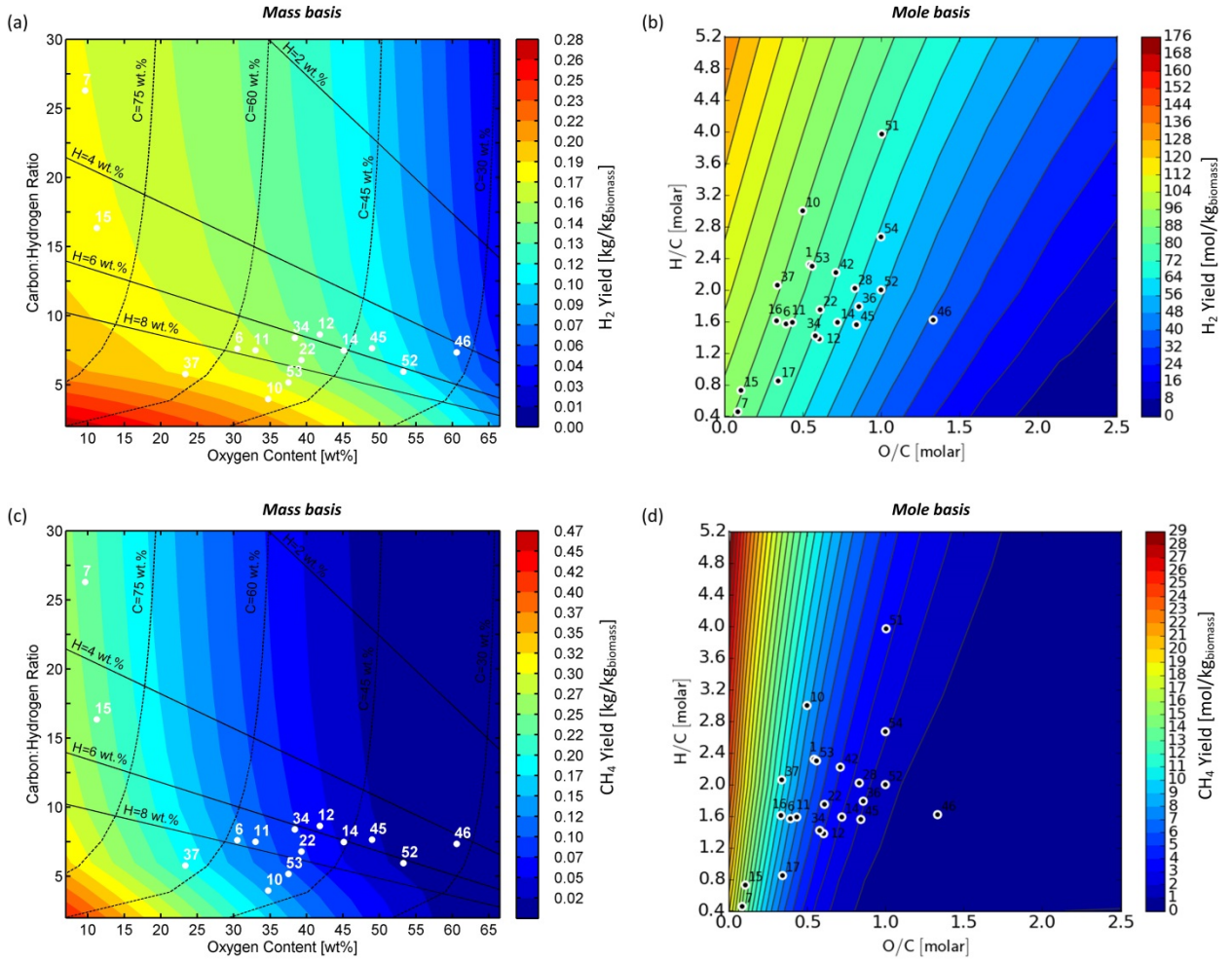

FIGURE B-1 COMPARISON OF CONTOUR PLOTS ON A MASS AND MOLE BASIS FOR H_2 AND CH_4 YIELDS (OPERATING TEMPERATURE OF 700 °C AND FEED CONCENTRATION OF 5 WT.%)

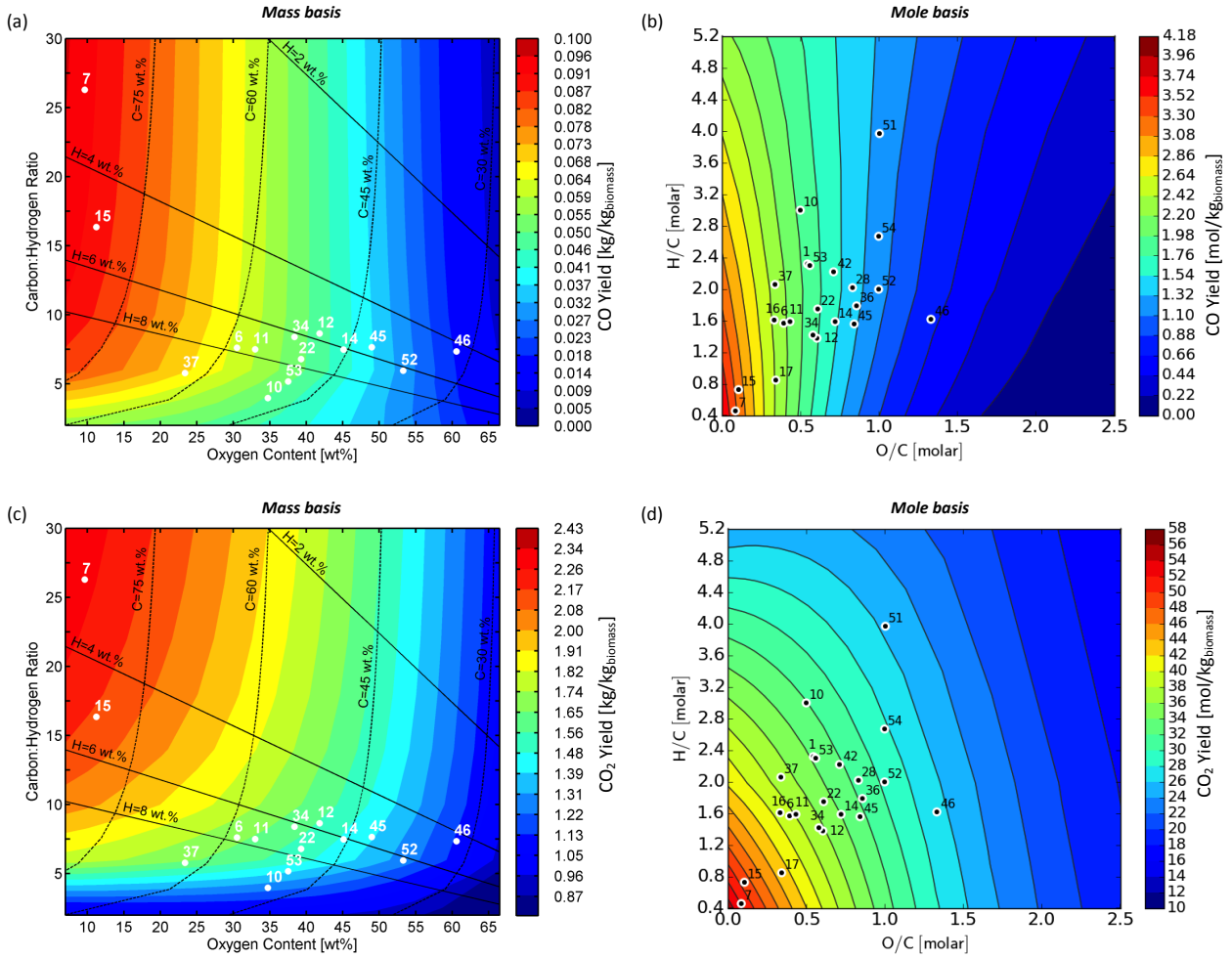

FIGURE B-2 COMPARISON OF CONTOUR PLOTS ON A MASS AND MOLE BASIS FOR CO AND CO_2 YIELDS (OPERATING TEMPERATURE OF 700 °C AND FEED CONCENTRATION OF 5 WT.%)

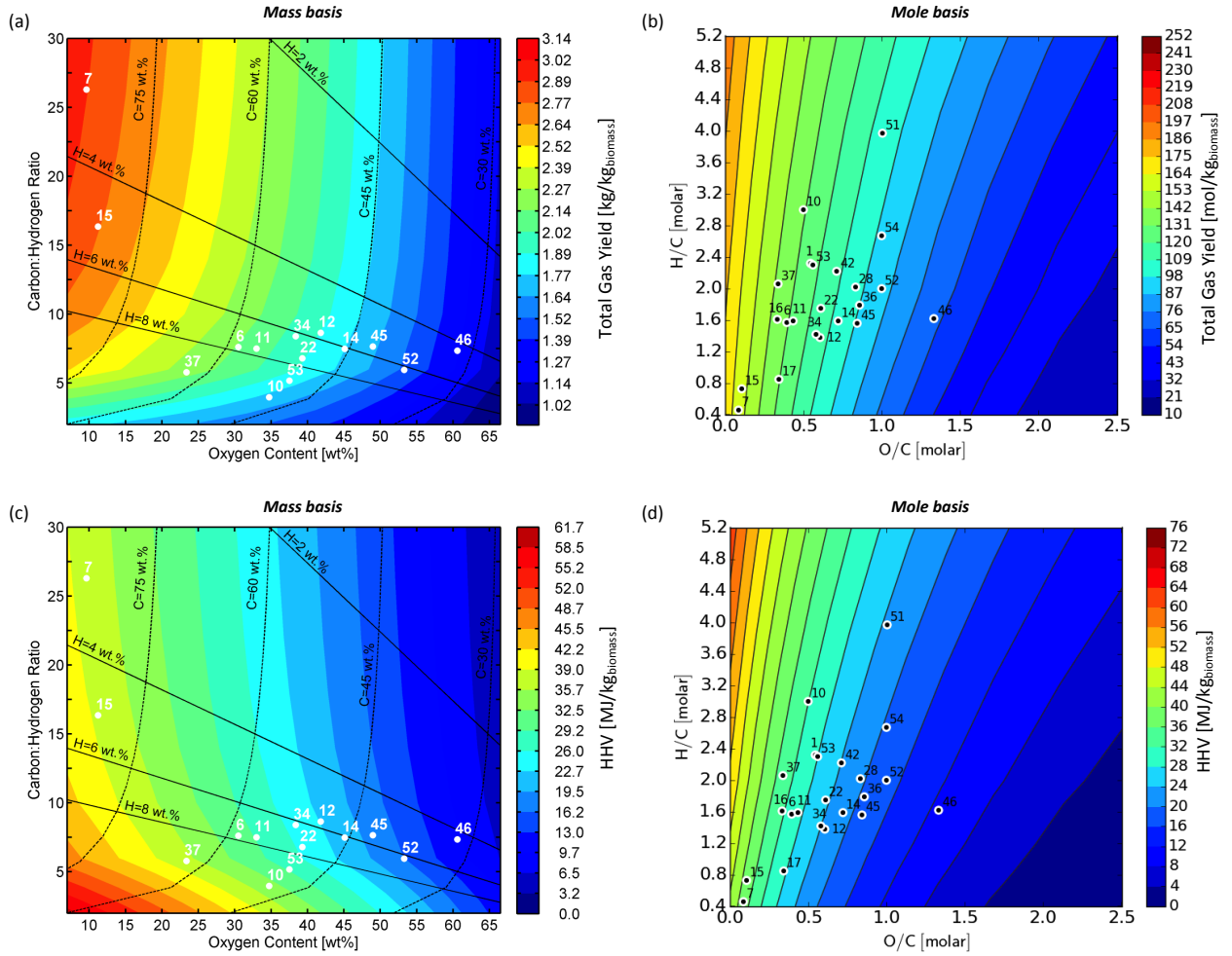

FIGURE B-3 COMPARISON OF CONTOUR PLOTS ON A MASS AND MOLE BASIS FOR THE TOTAL GAS YIELD AS WELL AS THE HHV OF THE GAS PRODUCED (OPERATING TEMPERATURE OF 700 °C AND FEED CONCENTRATION OF 5 WT.%)

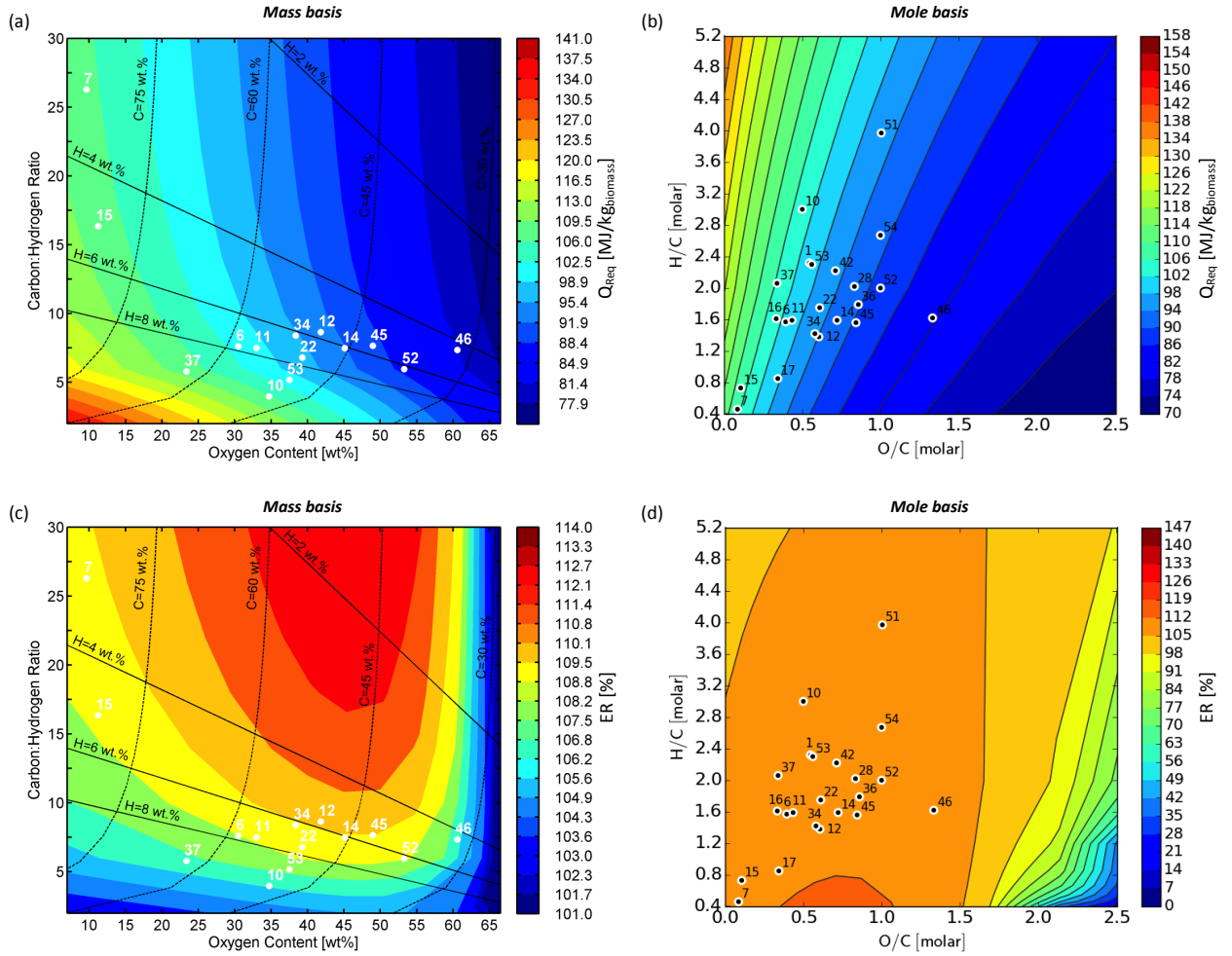

FIGURE B-4 COMPARISON OF CONTOUR PLOTS ON A MASS AND MOLE BASIS FOR THE HEAT REQUIRED FOR ISOTHERMAL OPERATION (Q_{REQ}) AS WELL AS THE ENERGY RECOVERY (ER) (OPERATING TEMPERATURE OF 700 °C AND FEED CONCENTRATION OF 5 WT.%)

B.2 Additional results

B.2.1 Gas composition 400 °C

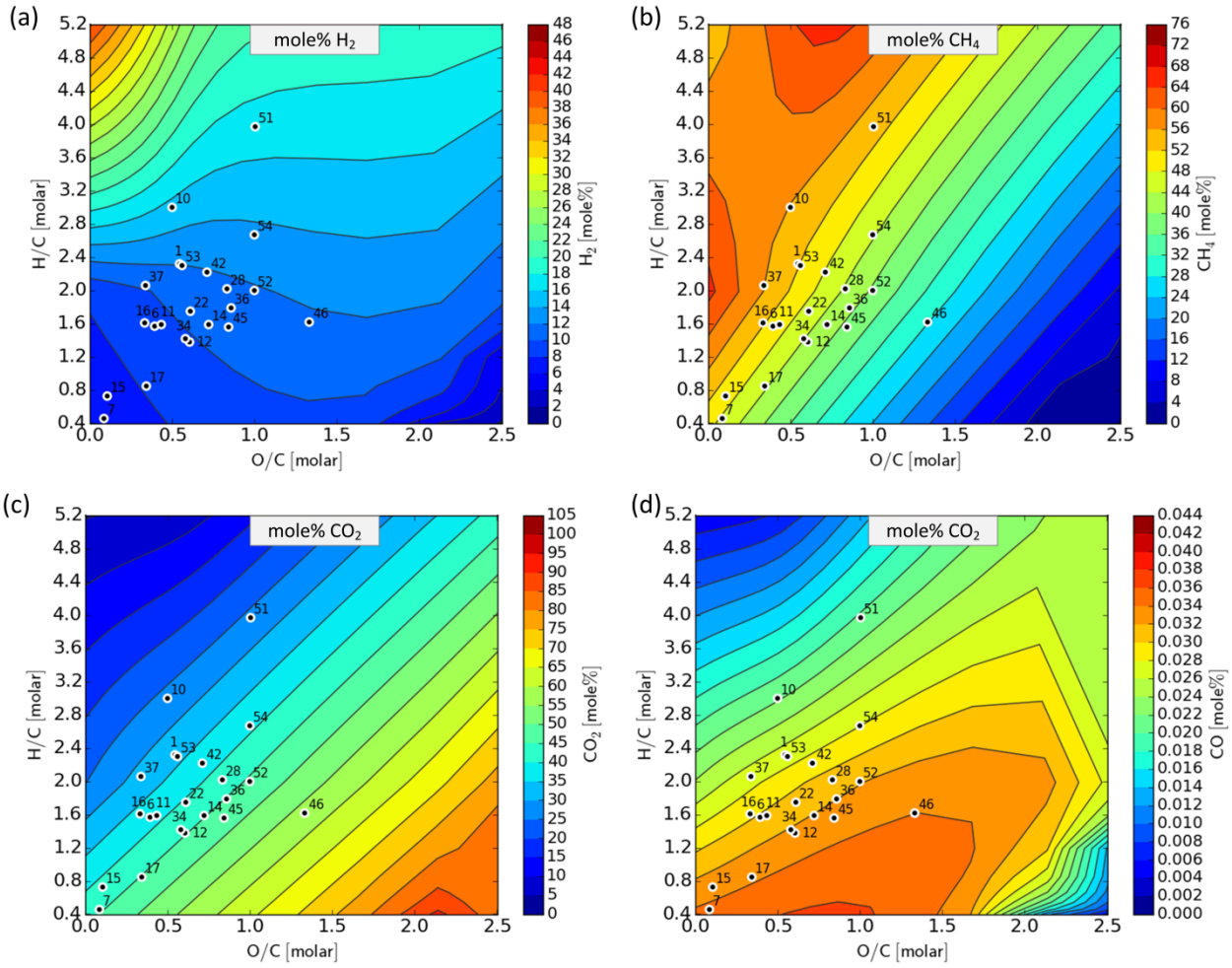

FIGURE B-5 EFFECT OF FEEDSTOCK COMPOSITION OF PRODUCT GAS COMPOSITION AT 400 °C AND DRY FEED CONCENTRATION OF 5 WT.%

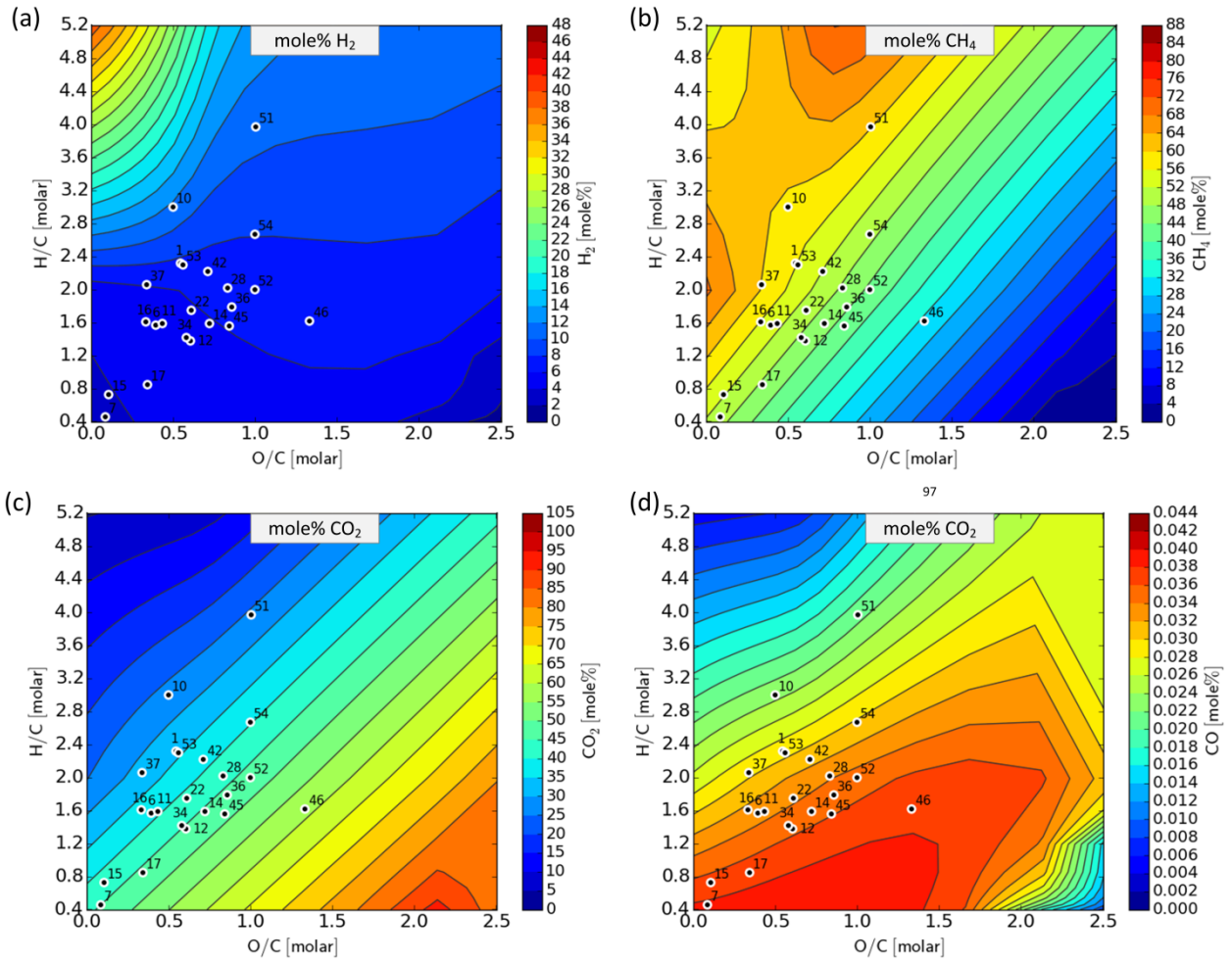

FIGURE B-6 EFFECT OF FEEDSTOCK COMPOSITION OF PRODUCT GAS COMPOSITION AT 400 °C AND DRY FEED CONCENTRATION OF 10 WT.%

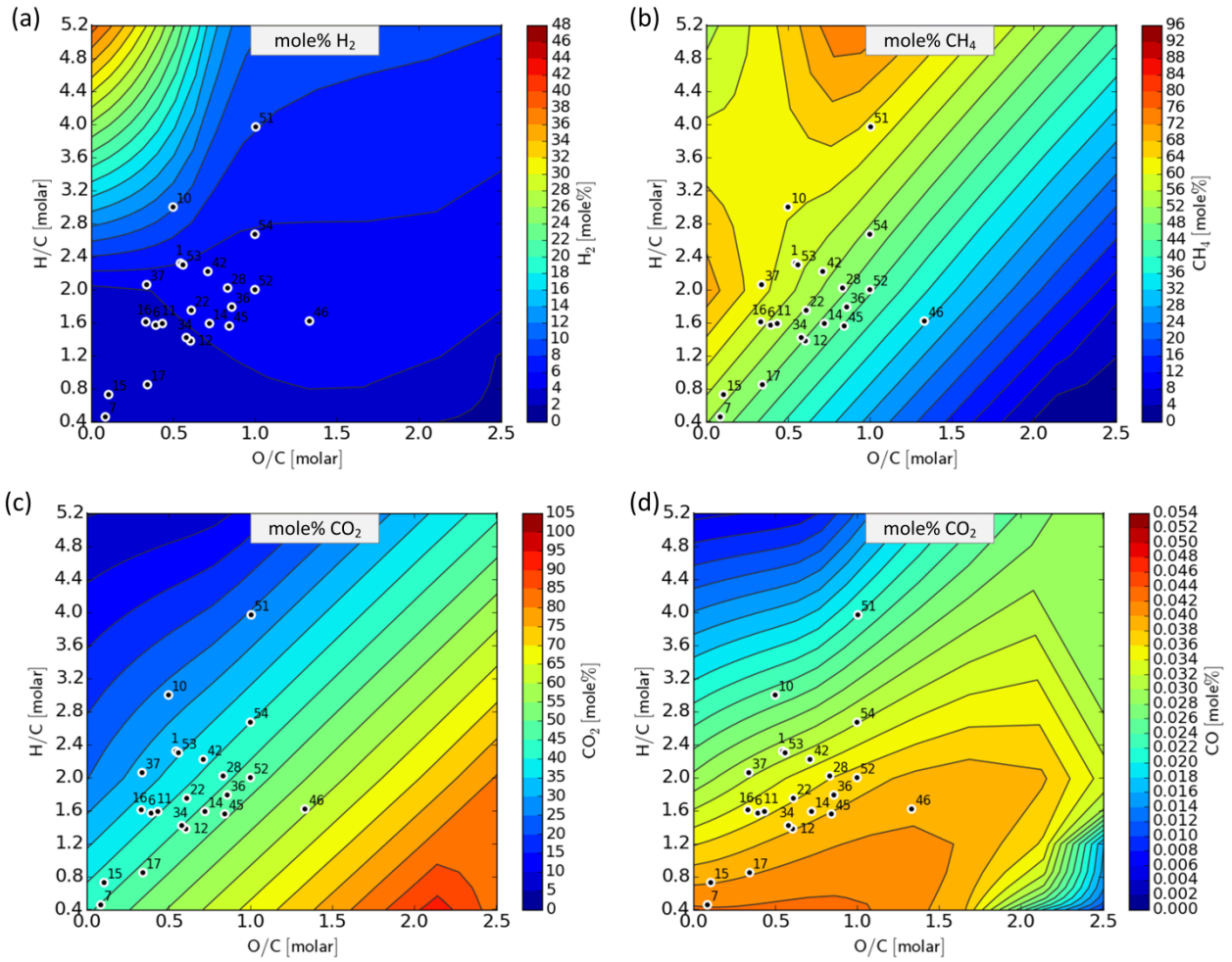

FIGURE B-7 EFFECT OF FEEDSTOCK COMPOSITION OF PRODUCT GAS COMPOSITION AT 400 °C AND DRY FEED CONCENTRATION OF 15 WT.%

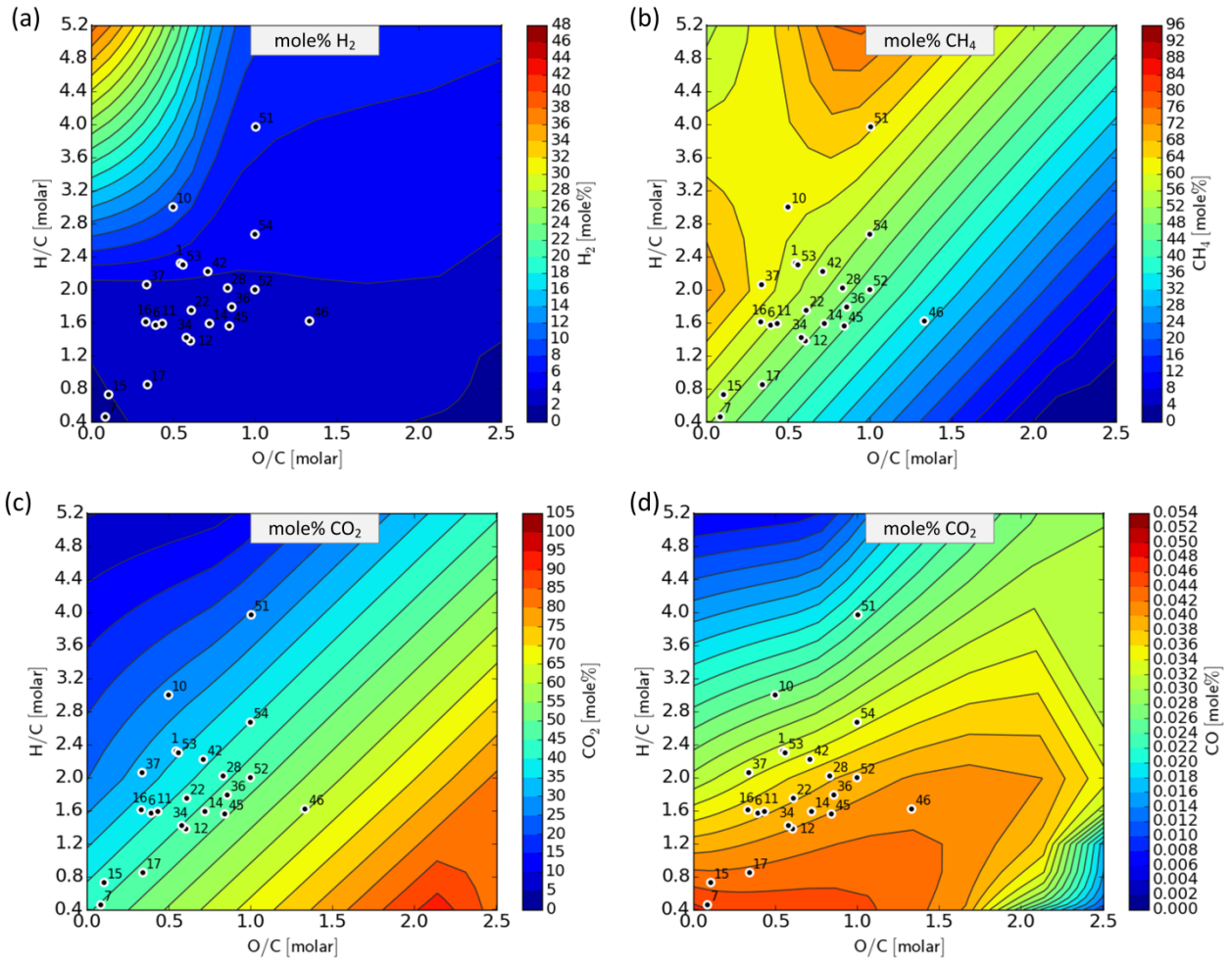

FIGURE B-8 EFFECT OF FEEDSTOCK COMPOSITION OF PRODUCT GAS COMPOSITION AT 400 °C AND DRY FEED CONCENTRATION OF 20 WT.%

B.2.2 Gas composition 600 °C

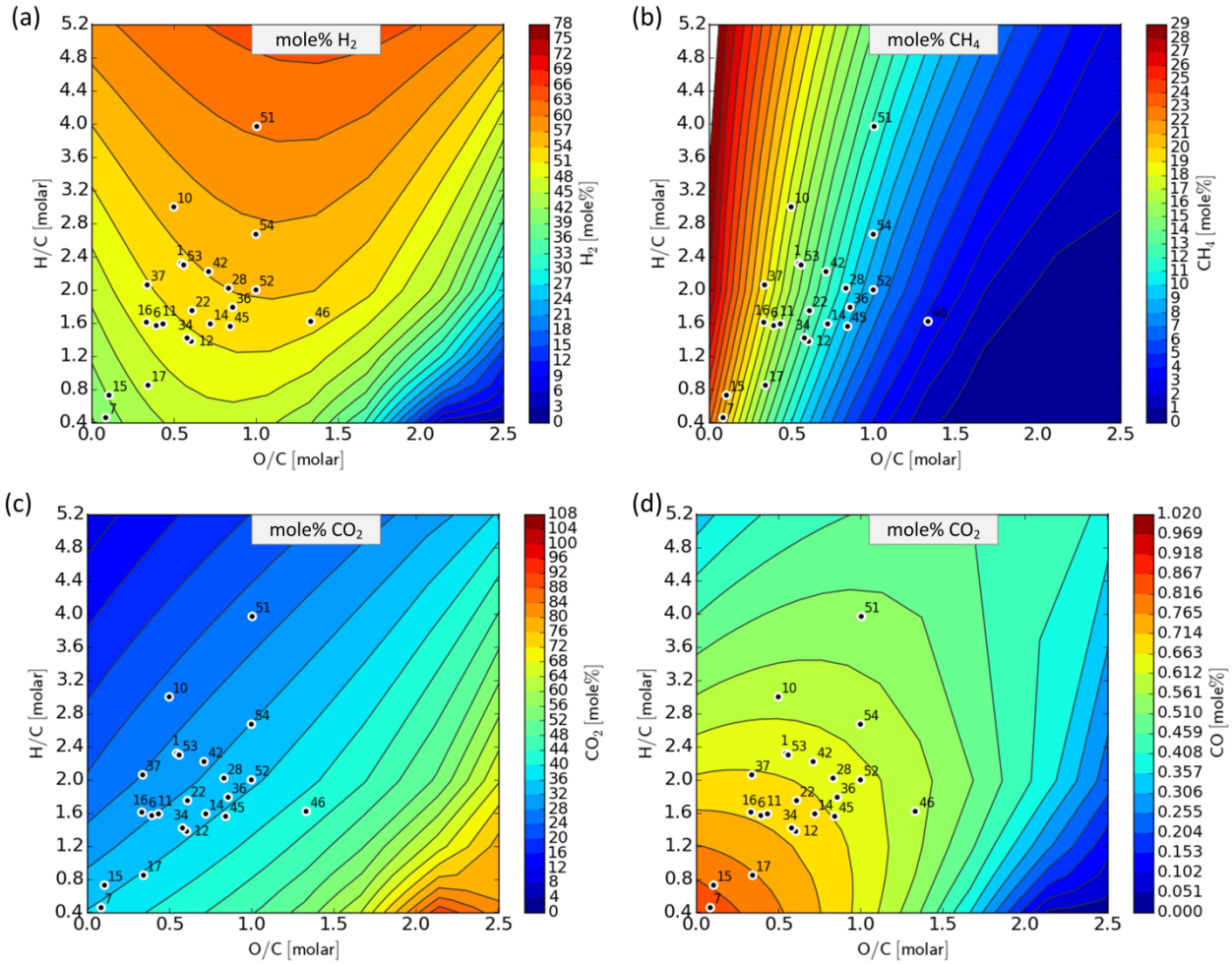

FIGURE B-9 EFFECT OF FEEDSTOCK COMPOSITION OF PRODUCT GAS COMPOSITION AT 600 °C AND DRY FEED CONCENTRATION OF 5 WT.%

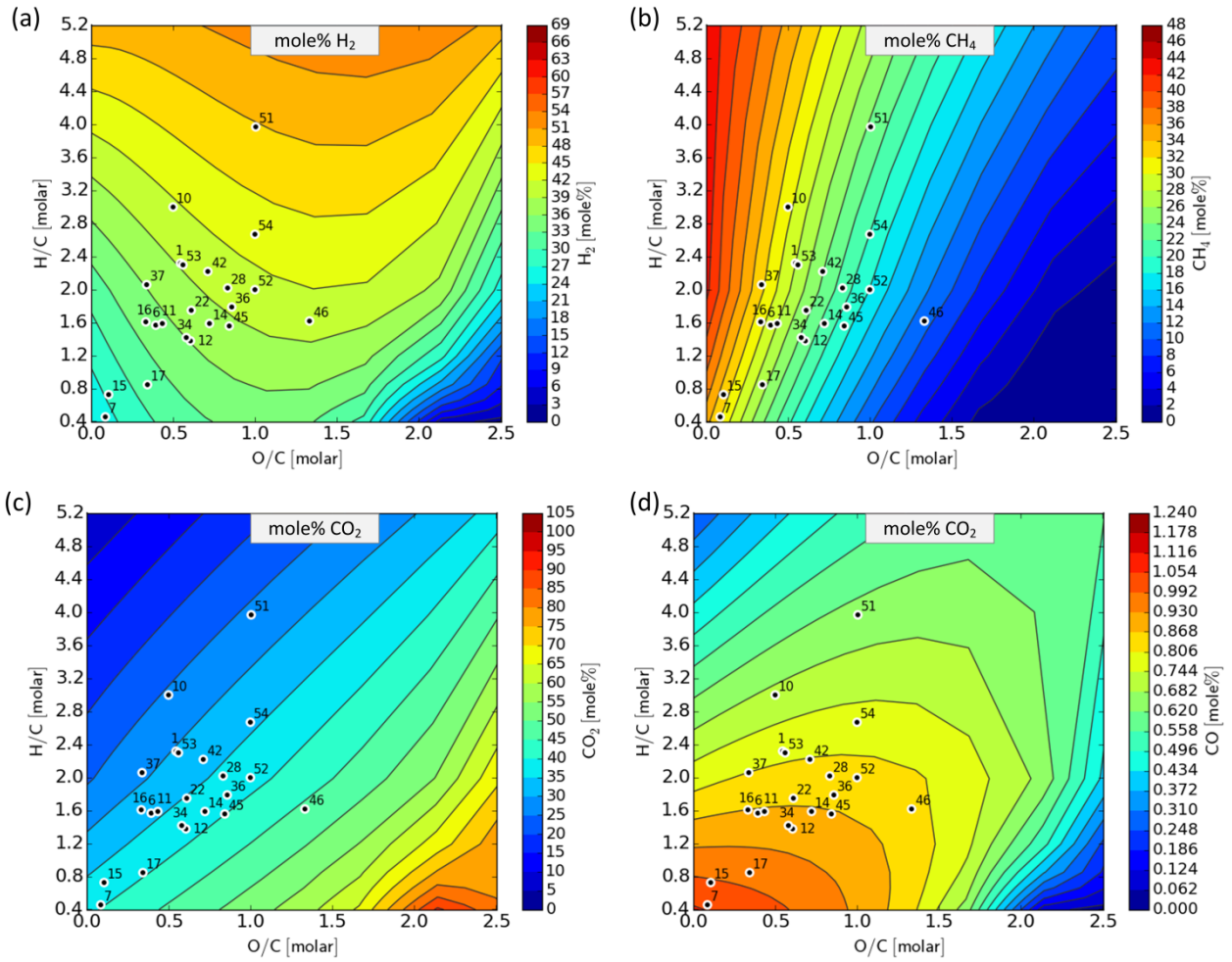

FIGURE B-10 EFFECT OF FEEDSTOCK COMPOSITION OF PRODUCT GAS COMPOSITION AT 600 °C AND DRY FEED CONCENTRATION OF 10 WT.%

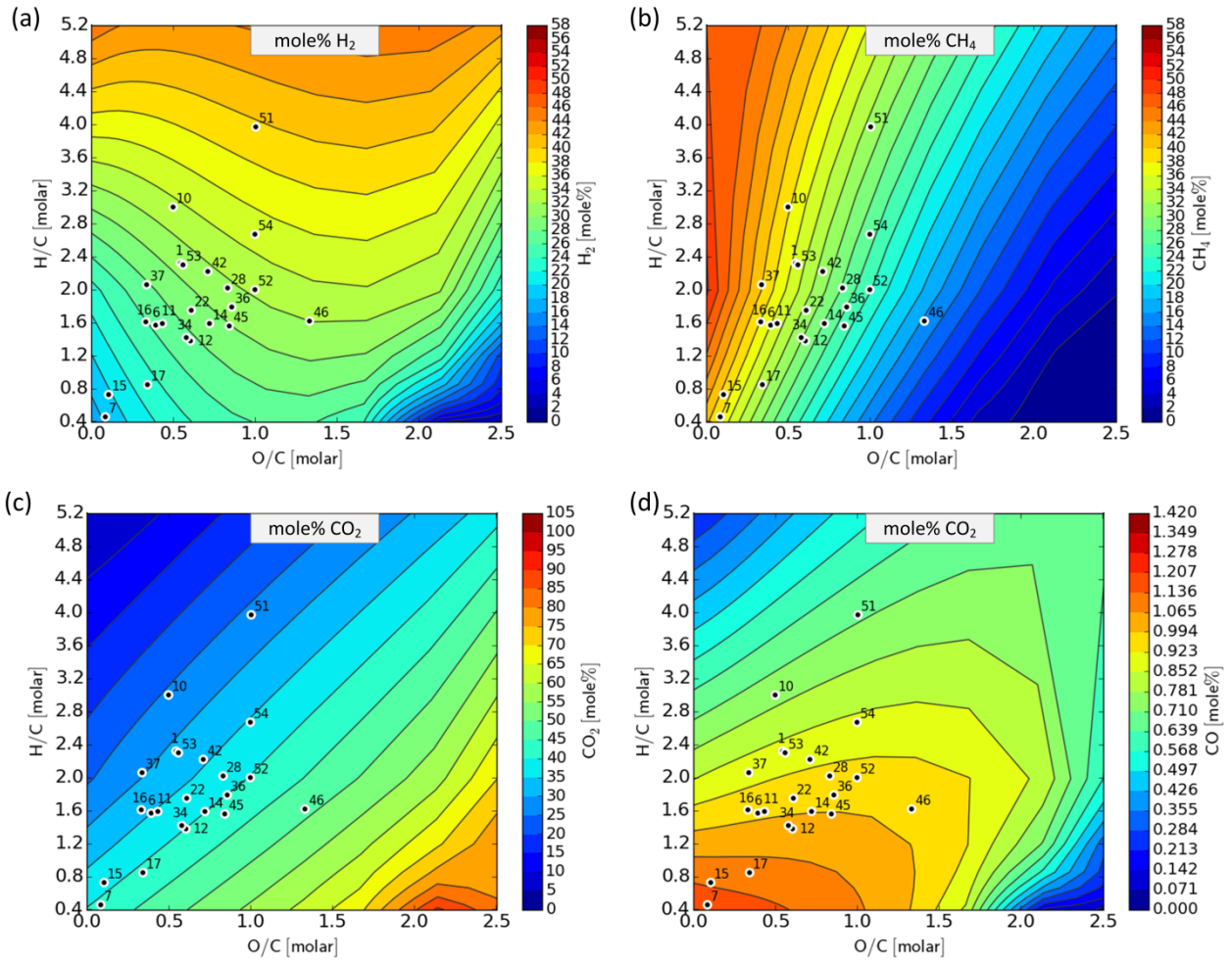

FIGURE B-11 EFFECT OF FEEDSTOCK COMPOSITION OF PRODUCT GAS COMPOSITION AT 600 °C AND DRY FEED CONCENTRATION OF 15 WT.%

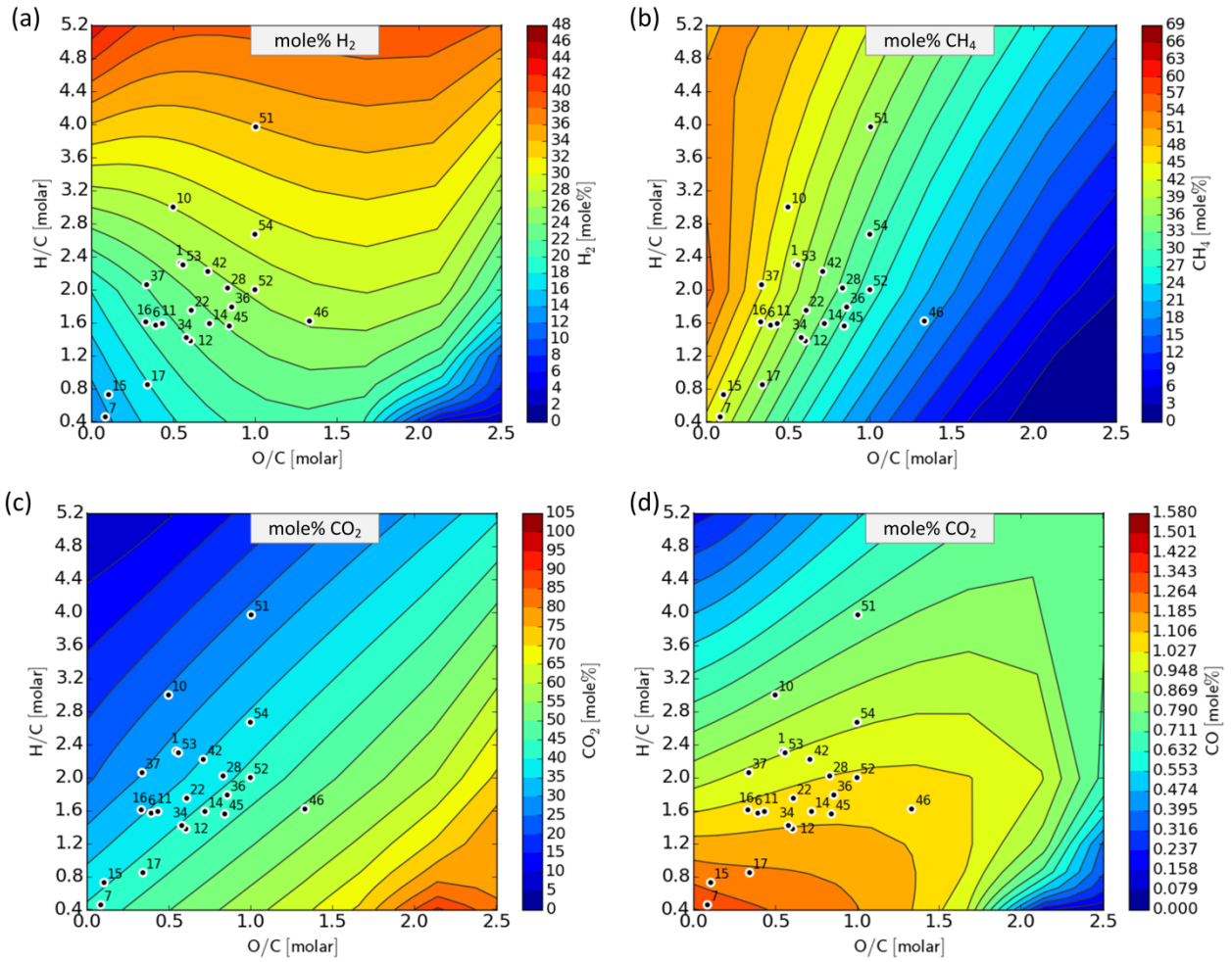

FIGURE B-12 EFFECT OF FEEDSTOCK COMPOSITION OF PRODUCT GAS COMPOSITION AT 600 °C AND DRY FEED CONCENTRATION OF 20 WT.%

B.2.3 Gas composition 800 °C

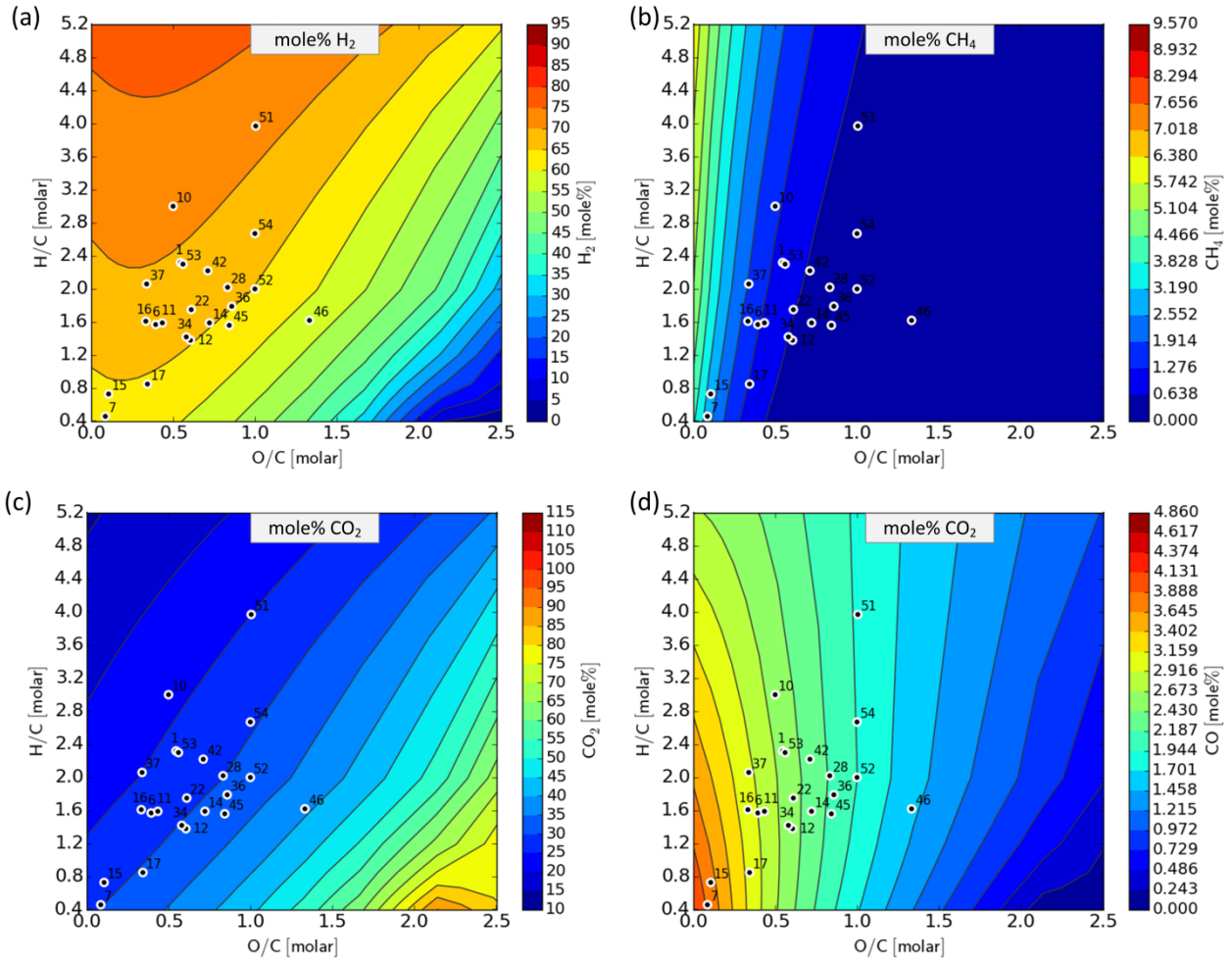

FIGURE B-13 EFFECT OF FEEDSTOCK COMPOSITION OF PRODUCT GAS COMPOSITION AT 800 °C AND DRY FEED CONCENTRATION OF 5 WT.%

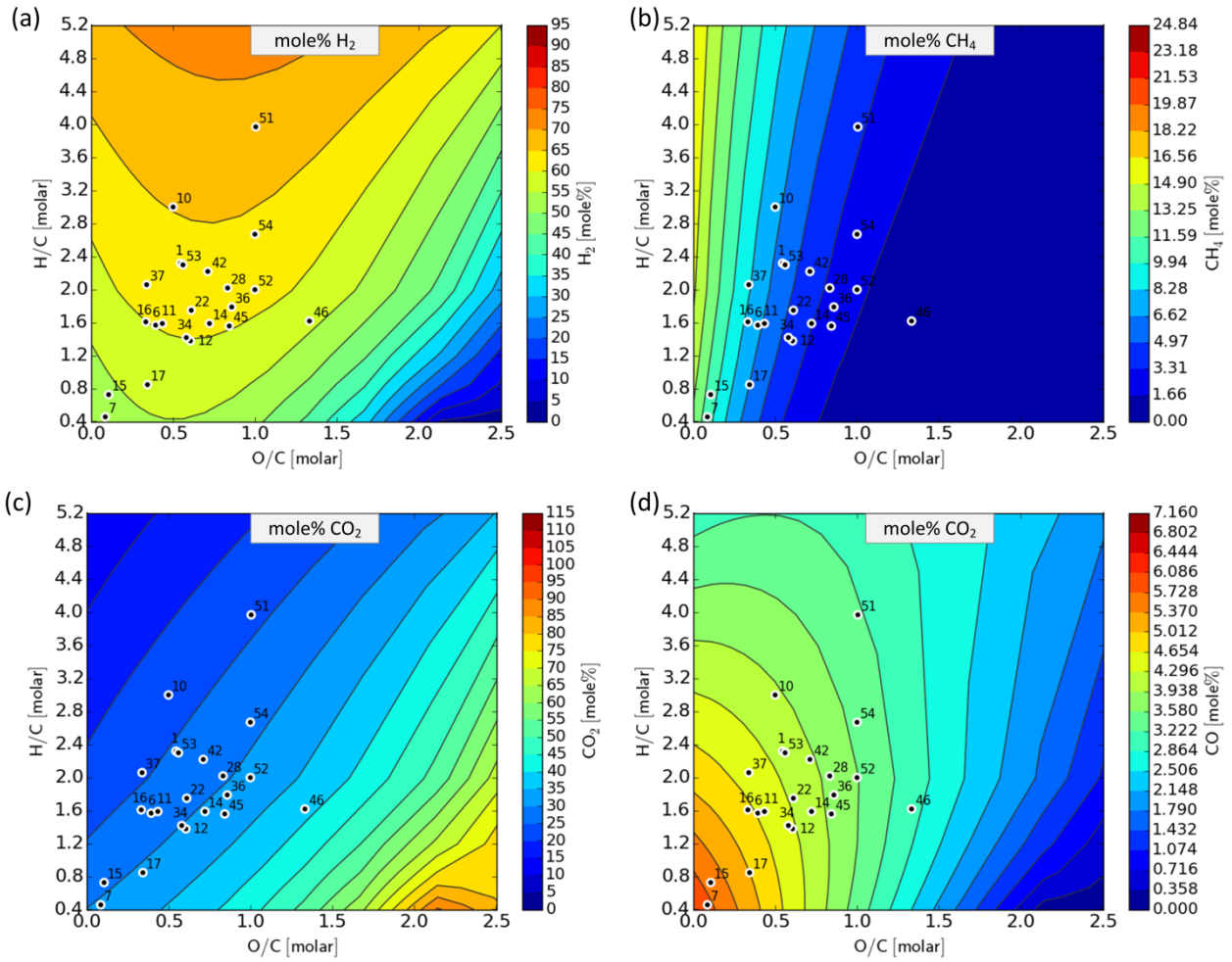

FIGURE B-14 EFFECT OF FEEDSTOCK COMPOSITION OF PRODUCT GAS COMPOSITION AT 800 °C AND DRY FEED CONCENTRATION OF 10 WT.%

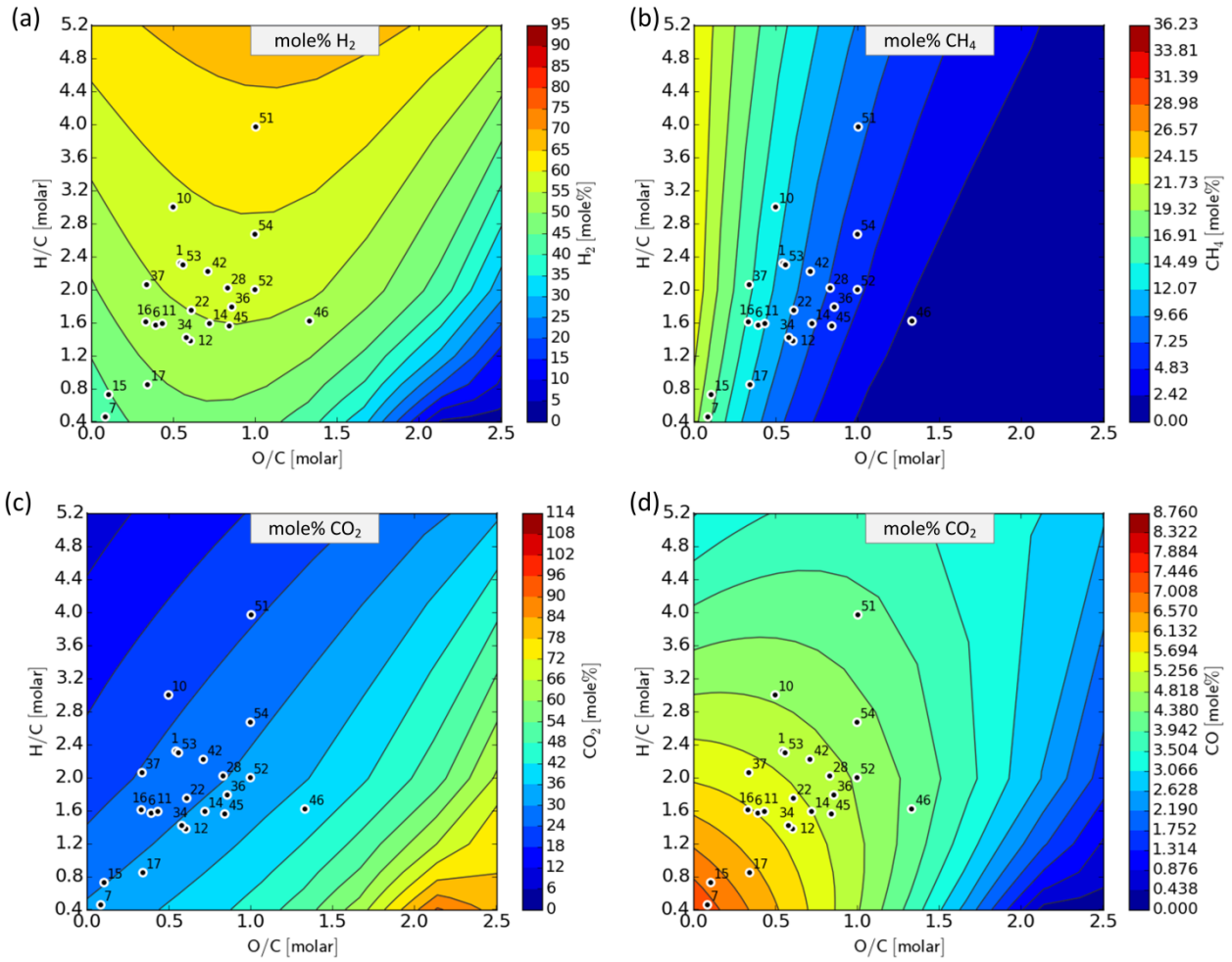

FIGURE B-15 EFFECT OF FEEDSTOCK COMPOSITION OF PRODUCT GAS COMPOSITION AT 800 °C AND DRY FEED CONCENTRATION OF 15 WT.%

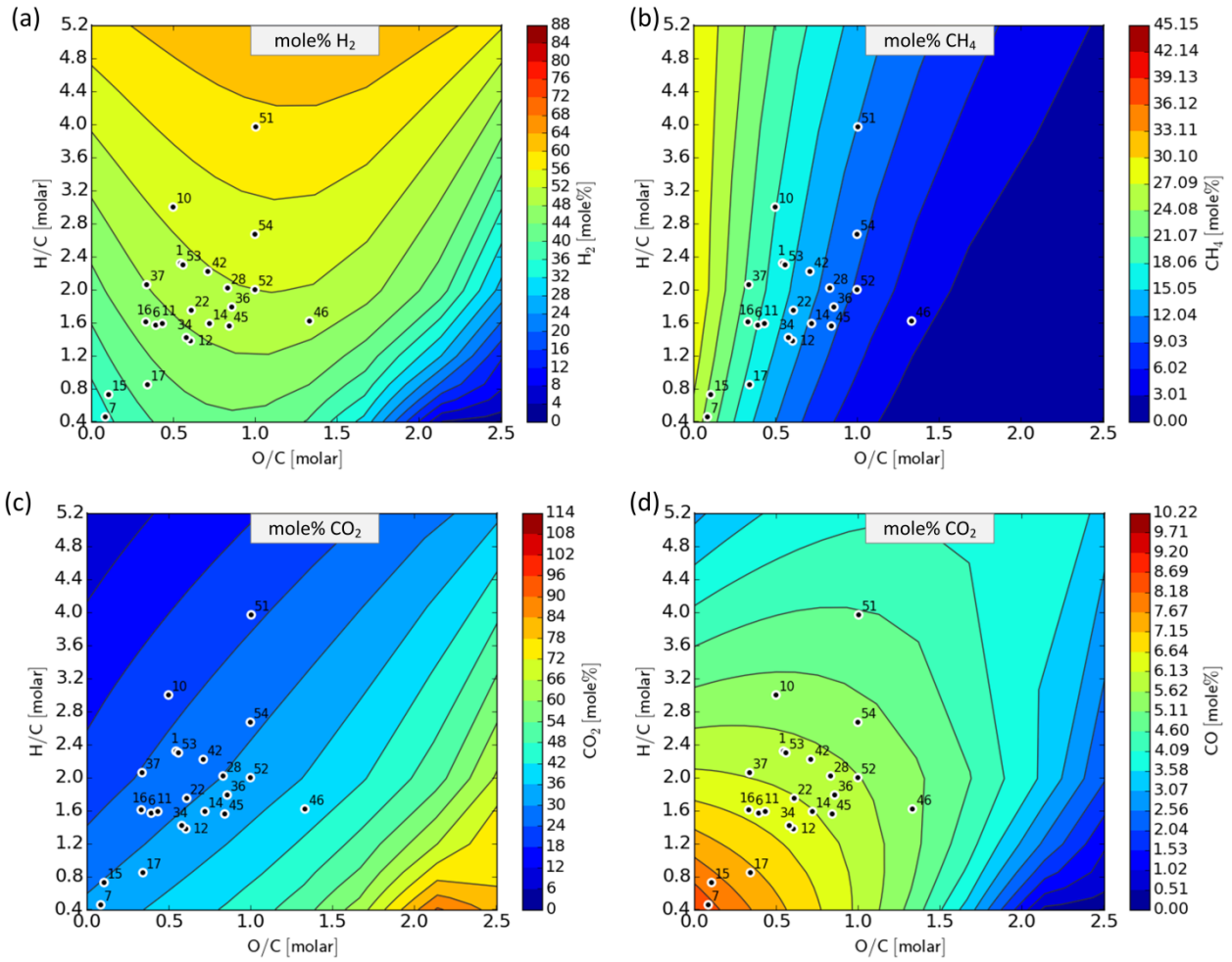

FIGURE B- 16 EFFECT OF FEEDSTOCK COMPOSITION OF PRODUCT GAS COMPOSITION AT 800 °C AND DRY FEED CONCENTRATION OF 20 WT.%

B.3 Result at 450 °C and 25 MPa

B.3.1 Total gas yield at 450 °C and 25 MPa

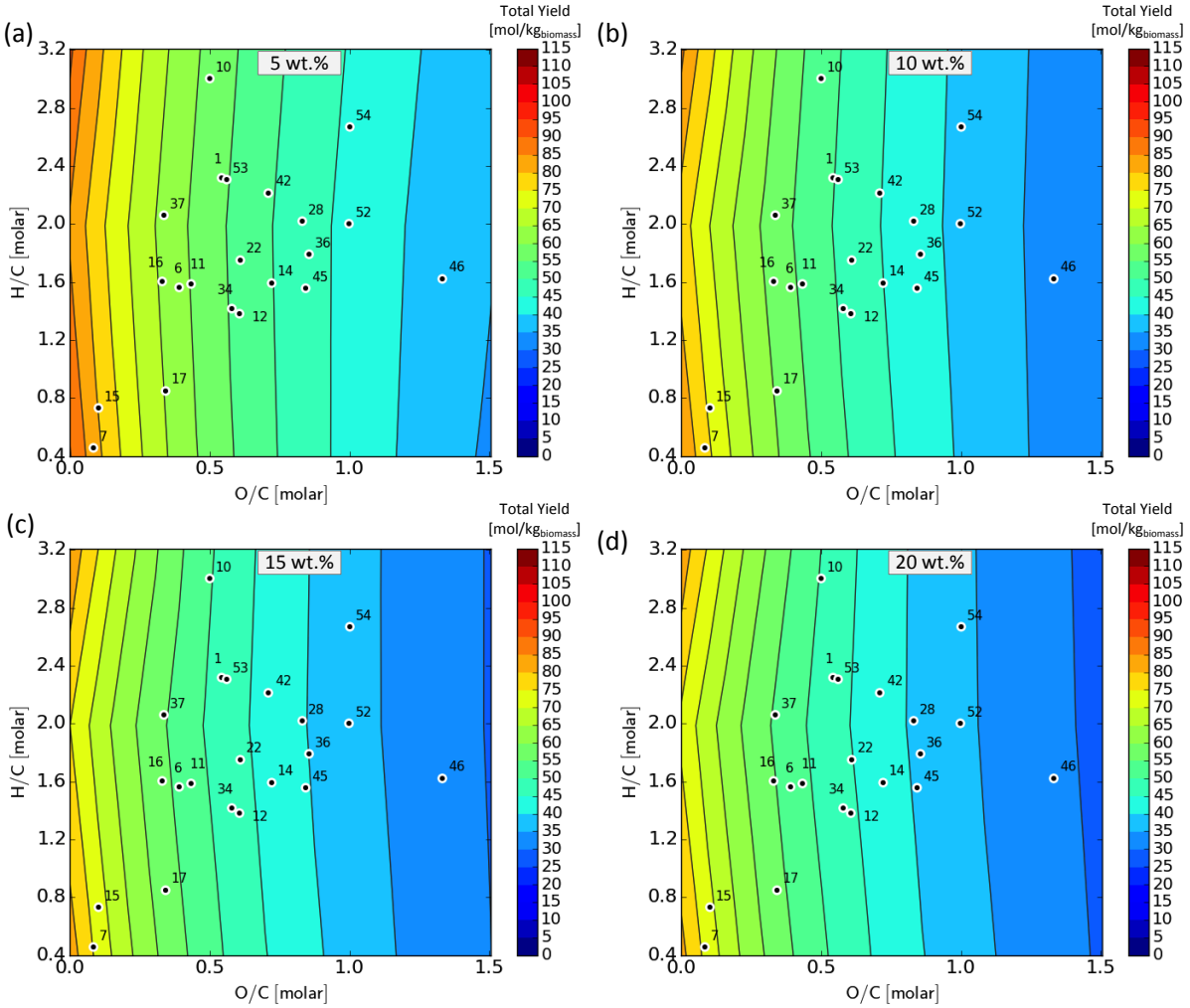

FIGURE B-17 EFFECT OF FEEDSTOCK COMPOSITION ON THE TOTAL THERMODYNAMIC EQUILIBRIUM GAS YIELD DURING SCWG AT 450 °C AND 25 MPA

B.3.2 H_2 yield at 450 °C and 25 MPa

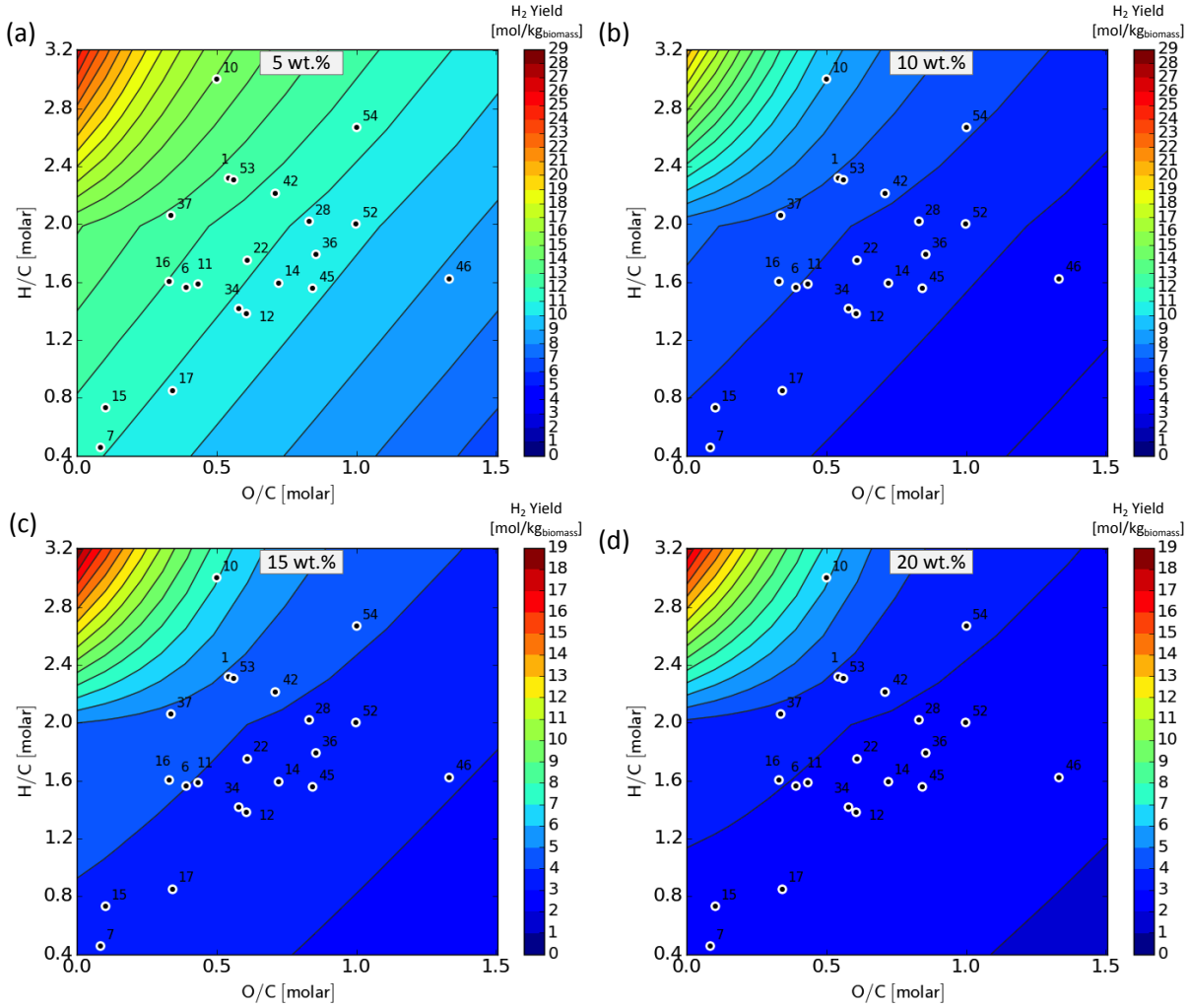

FIGURE B-18 EFFECT OF FEEDSTOCK COMPOSITION ON THE THERMODYNAMIC EQUILIBRIUM H_2 YIELD DURING SCWG AT 450 °C AND 25 MPA

B.3.3 CH_4 yield at 450 °C and 25 MPa

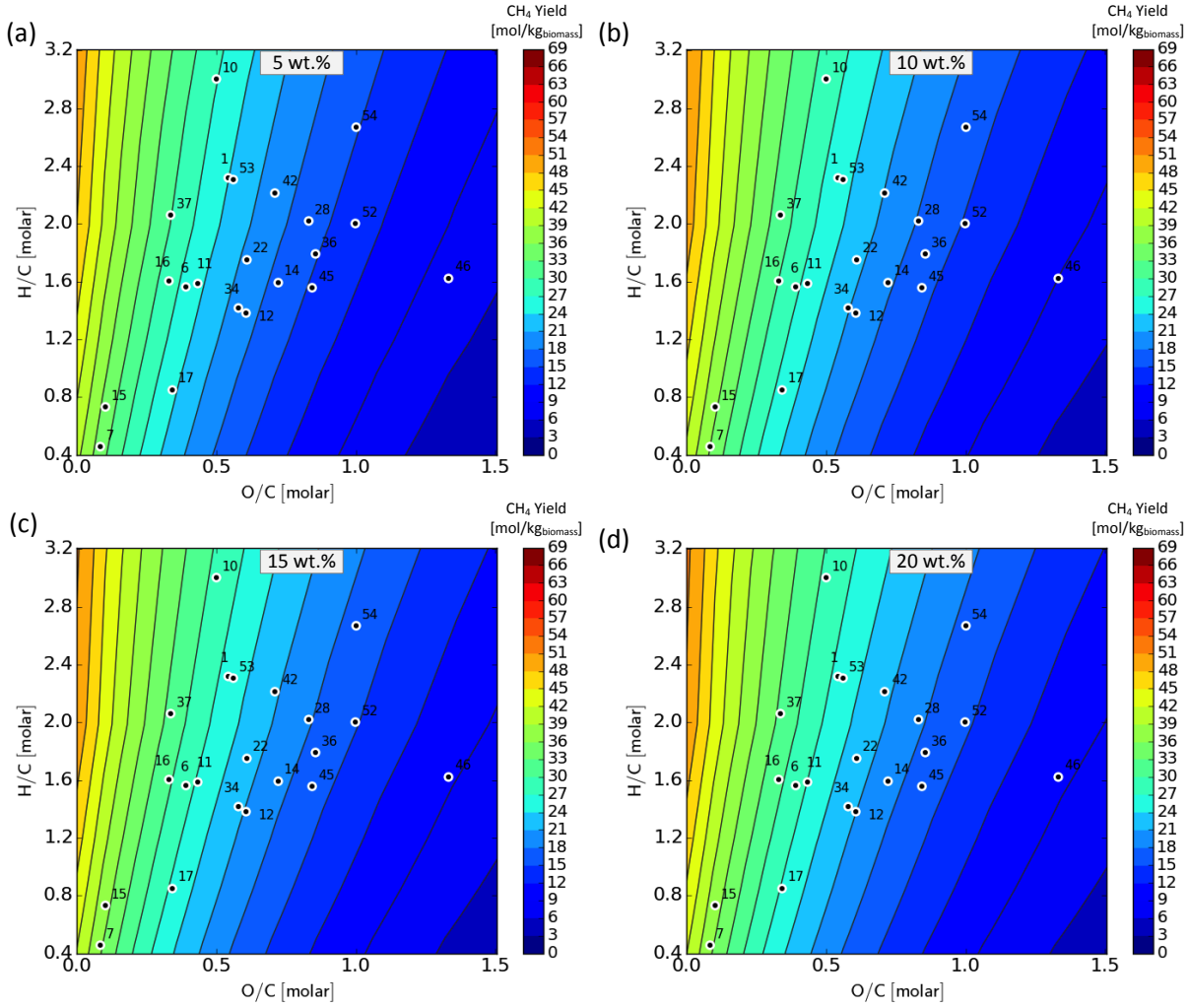

FIGURE B-19 EFFECT OF FEEDSTOCK COMPOSITION ON THE THERMODYNAMIC EQUILIBRIUM CH_4 YIELD DURING SCWG AT 450 °C AND 25 MPA

B.3.4 CO Yield at 450 °C and 25 MPa

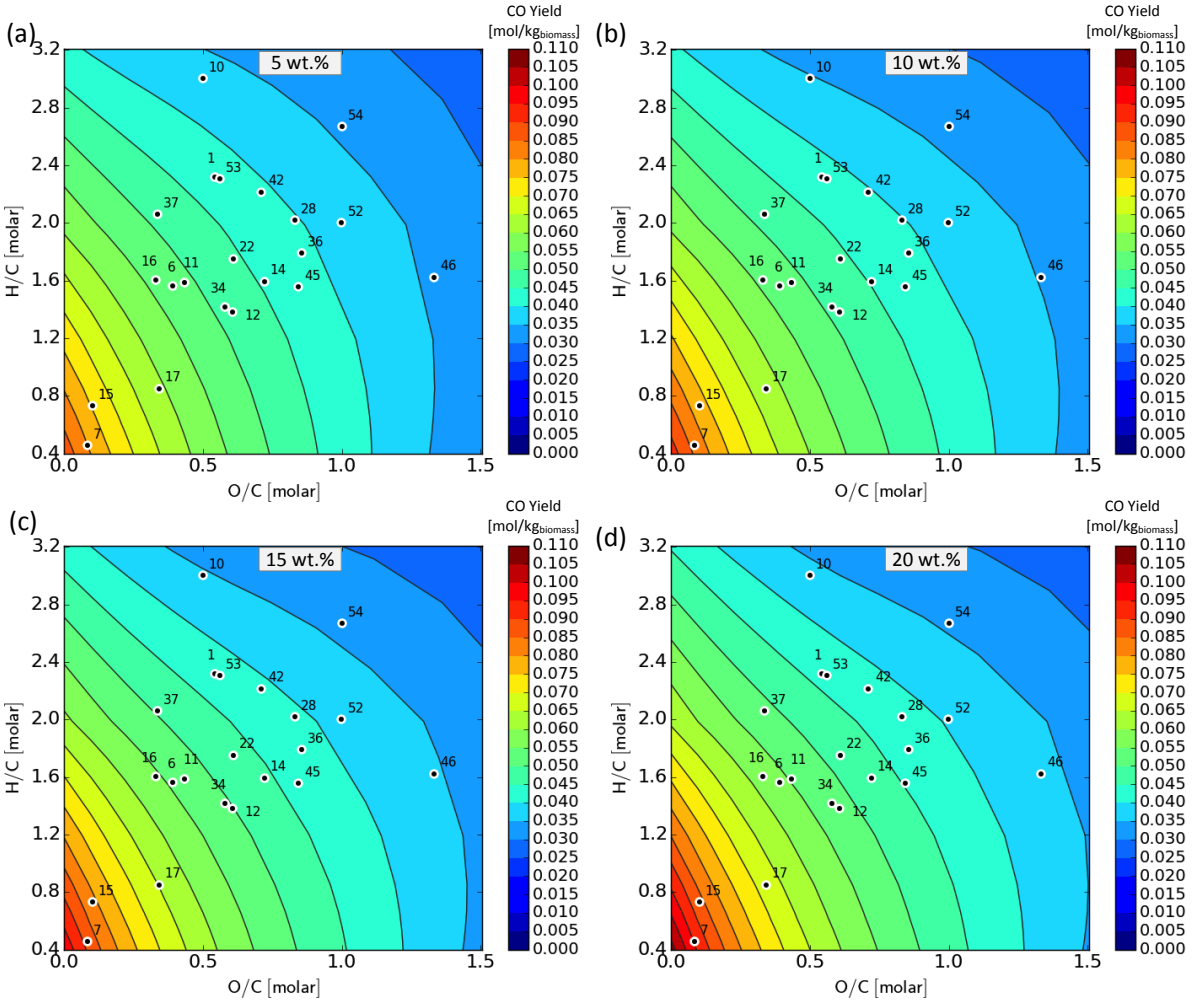

FIGURE B-20 EFFECT OF FEEDSTOCK COMPOSITION ON THE THERMODYNAMIC EQUILIBRIUM CO YIELD DURING SCWG AT 450 °C AND 25 MPA

B.3.5 CO_2 yield at 450 °C and 25 MPa

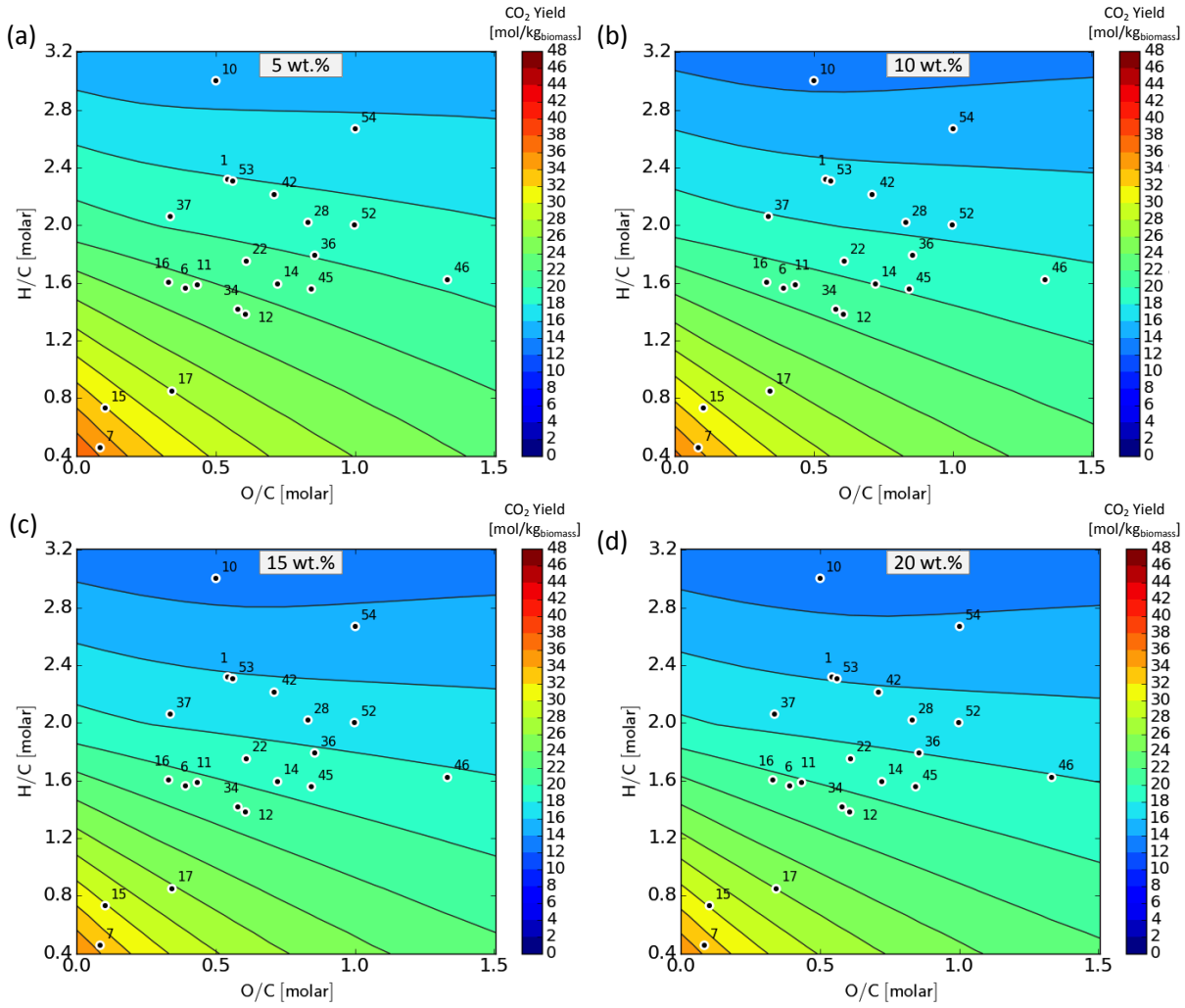

FIGURE B-21 EFFECT OF FEEDSTOCK COMPOSITION ON THE THERMODYNAMIC EQUILIBRIUM CO_2 YIELD DURING SCWG AT 450 °C AND 25 MPA

B.3.6 HHV of product gas at 450 °C and 25 MPa

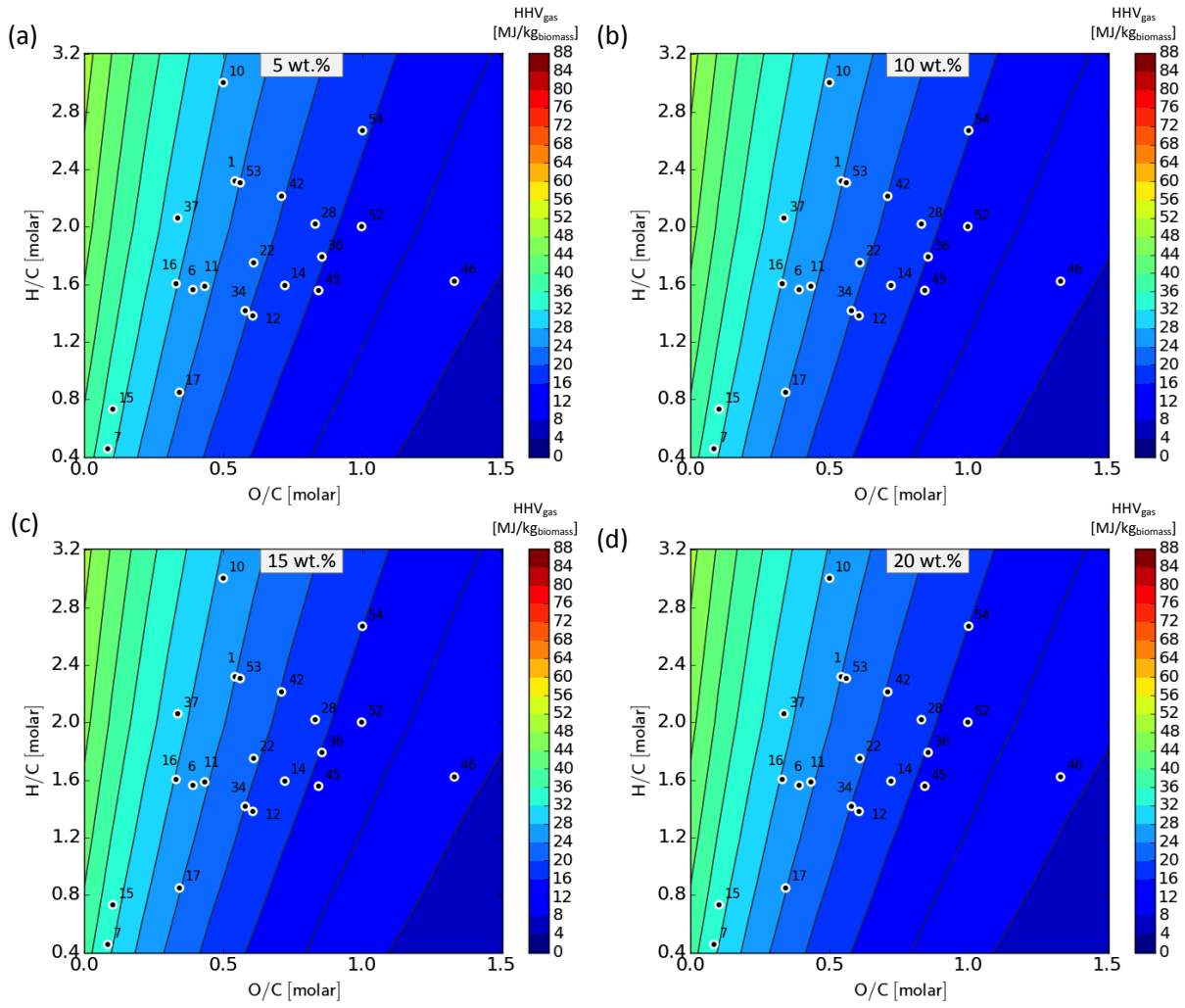

FIGURE B-22 EFFECT OF FEEDSTOCK COMPOSITION ON THE THERMODYNAMIC EQUILIBRIUM HHV OF THE PRODUCT GAS DURING SCWG AT 450 °C AND 25 MPA

B.3.7 Heat required for isothermal operation at 450 °C and 25 MPa

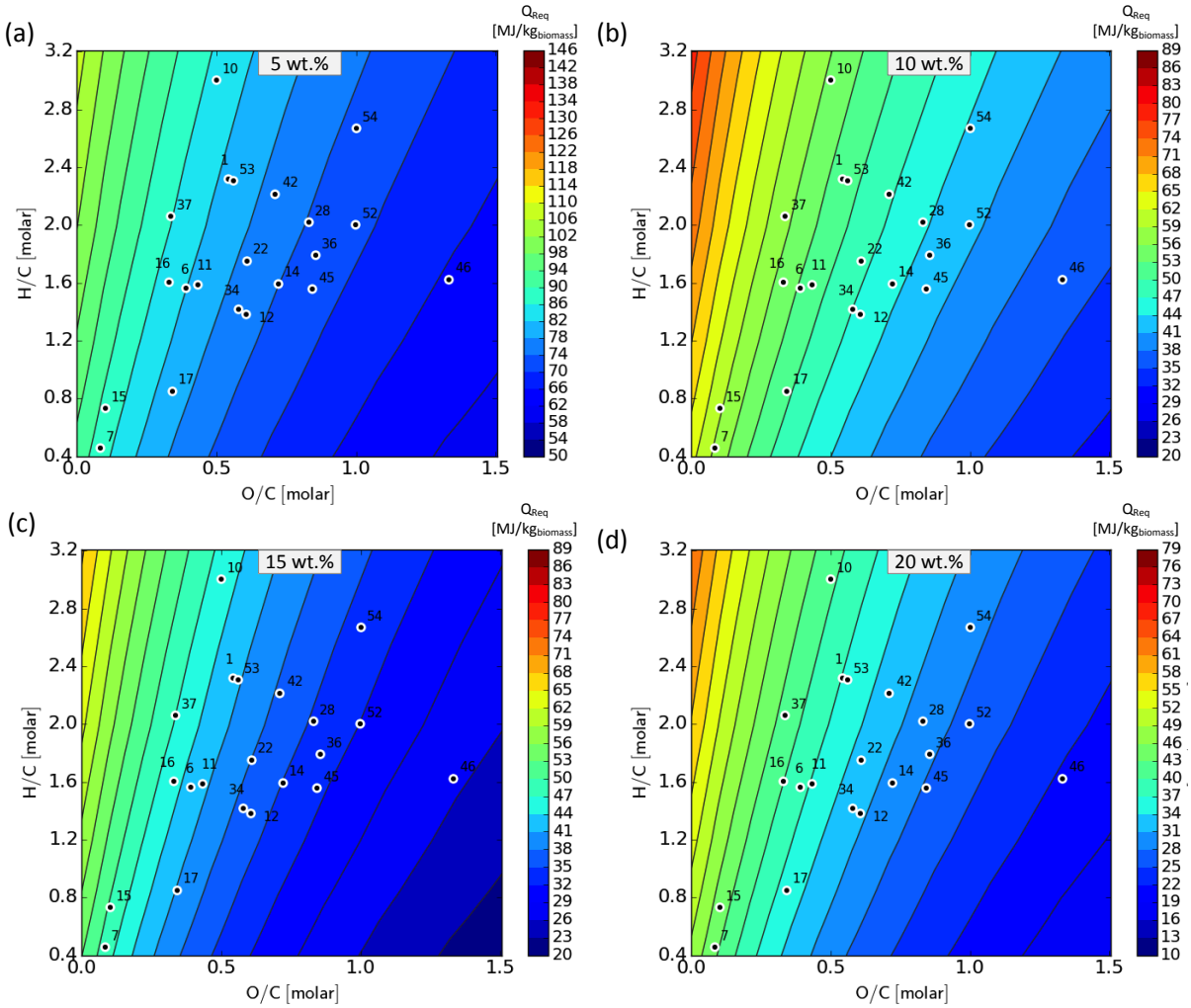

FIGURE B-23 EFFECT OF FEEDSTOCK COMPOSITION ON THE HEAT REQUIRED FOR ISOTHERMAL OPERATION AT 450 °C AND 25 MPA

B.4 Results at 500 °C and 25 MPa

B.4.1 Total gas yield at 500 °C and 25 MPa

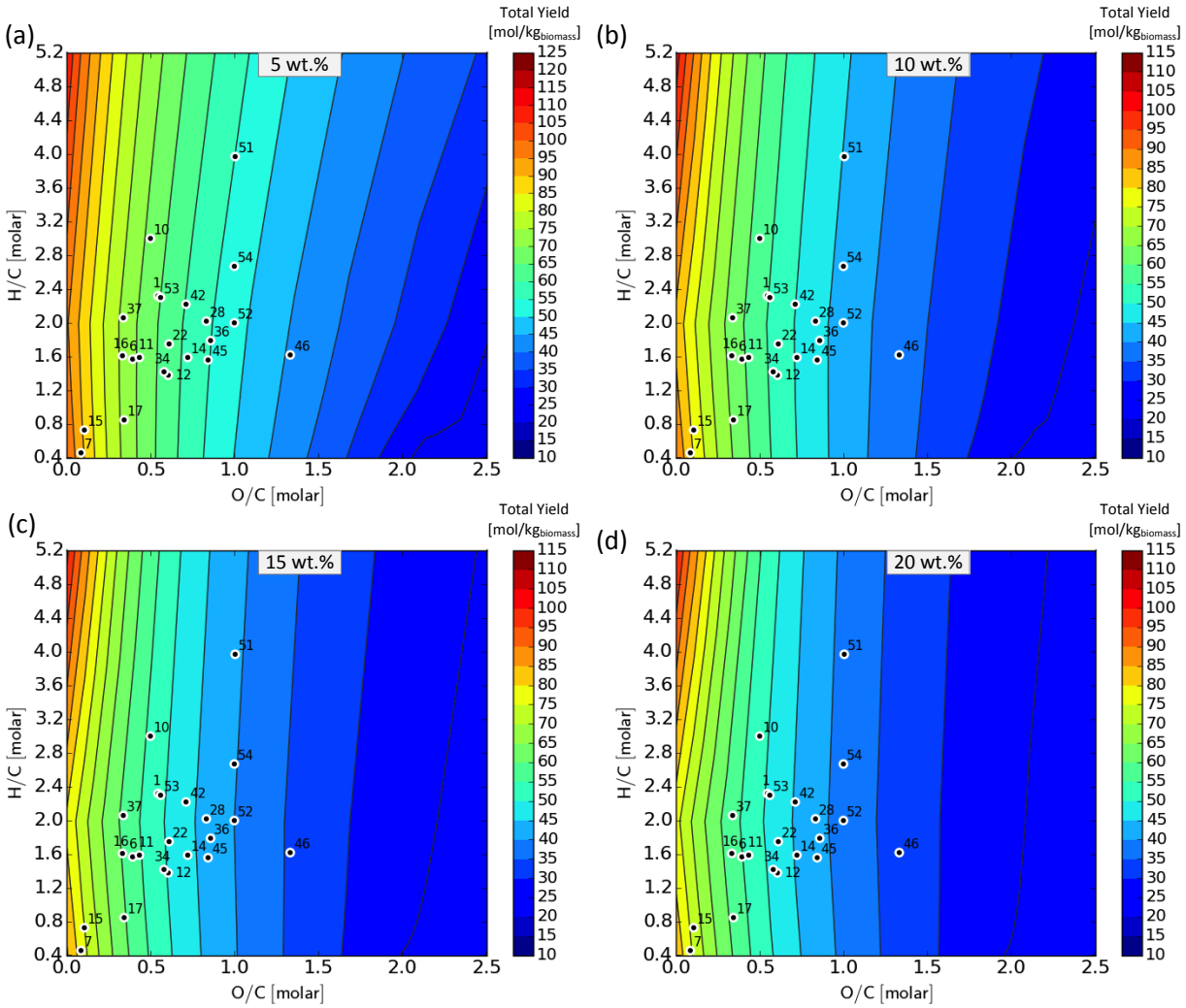

FIGURE B-24 EFFECT OF FEEDSTOCK COMPOSITION ON THE TOTAL THERMODYNAMIC EQUILIBRIUM GAS YIELD DURING SCWG AT 500 °C AND 25 MPA

B.4.2 H_2 yield at 500 °C and 25 MPa

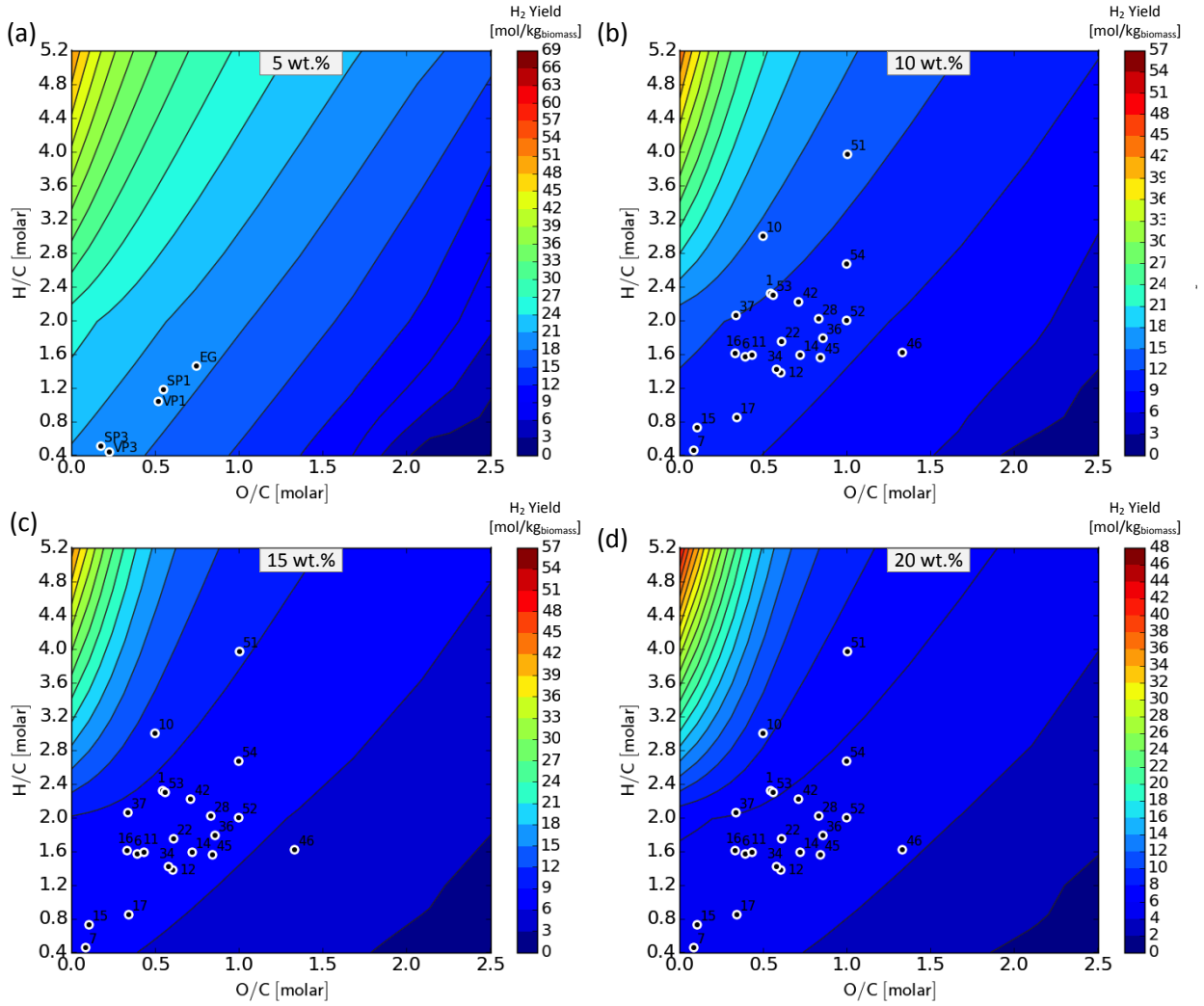

FIGURE B-25 EFFECT OF FEEDSTOCK COMPOSITION ON THE THERMODYNAMIC EQUILIBRIUM H_2 YIELD DURING SCWG AT 500 °C AND 25 MPA

B.4.3 CH_4 yield at 500 °C and 25 MPa

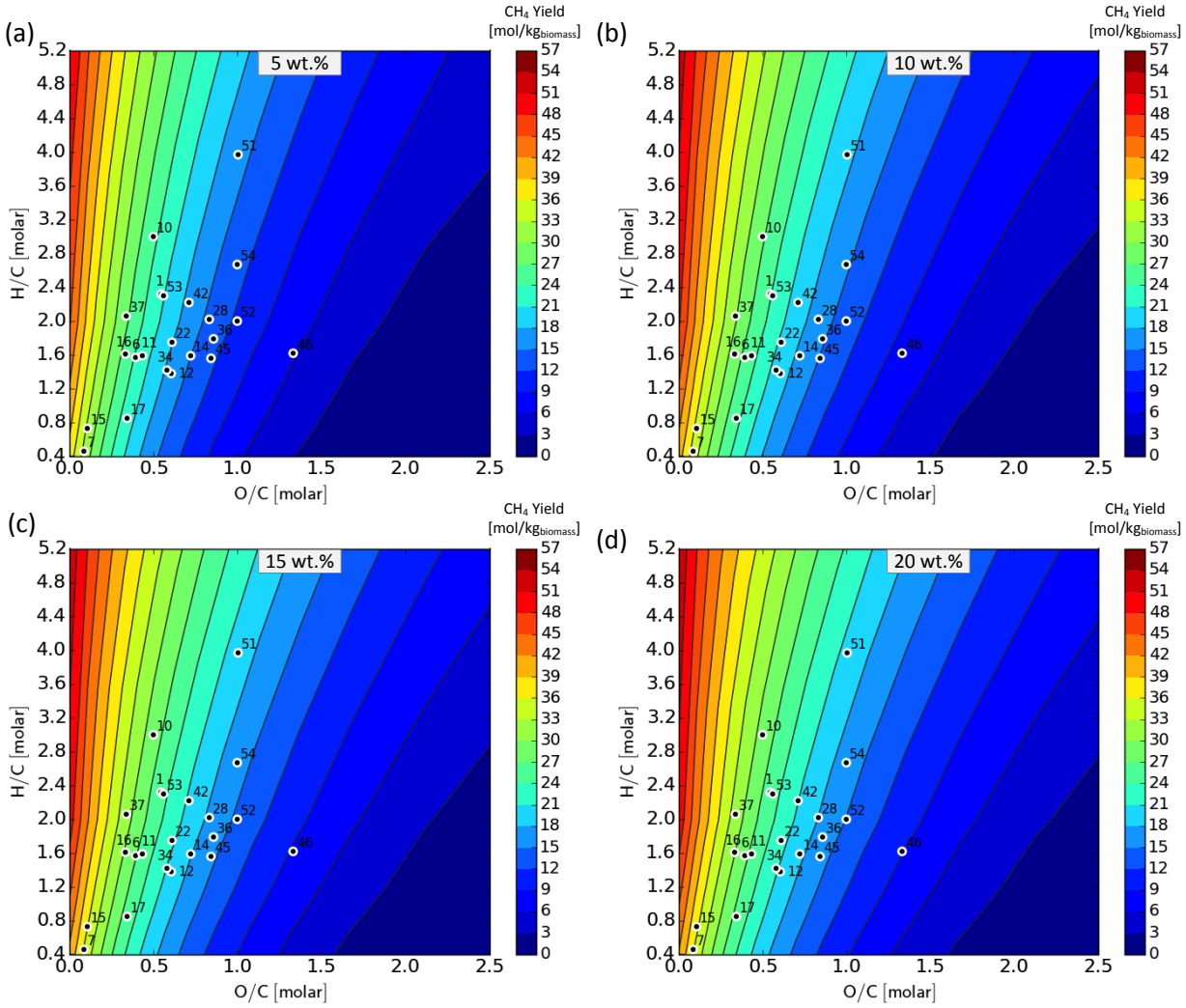

FIGURE B-26 EFFECT OF FEEDSTOCK COMPOSITION ON THE THERMODYNAMIC EQUILIBRIUM CH_4 YIELD DURING SCWG AT 500 °C AND 25 MPA

B.4.4 CO Yield at 500 °C and 25 MPa

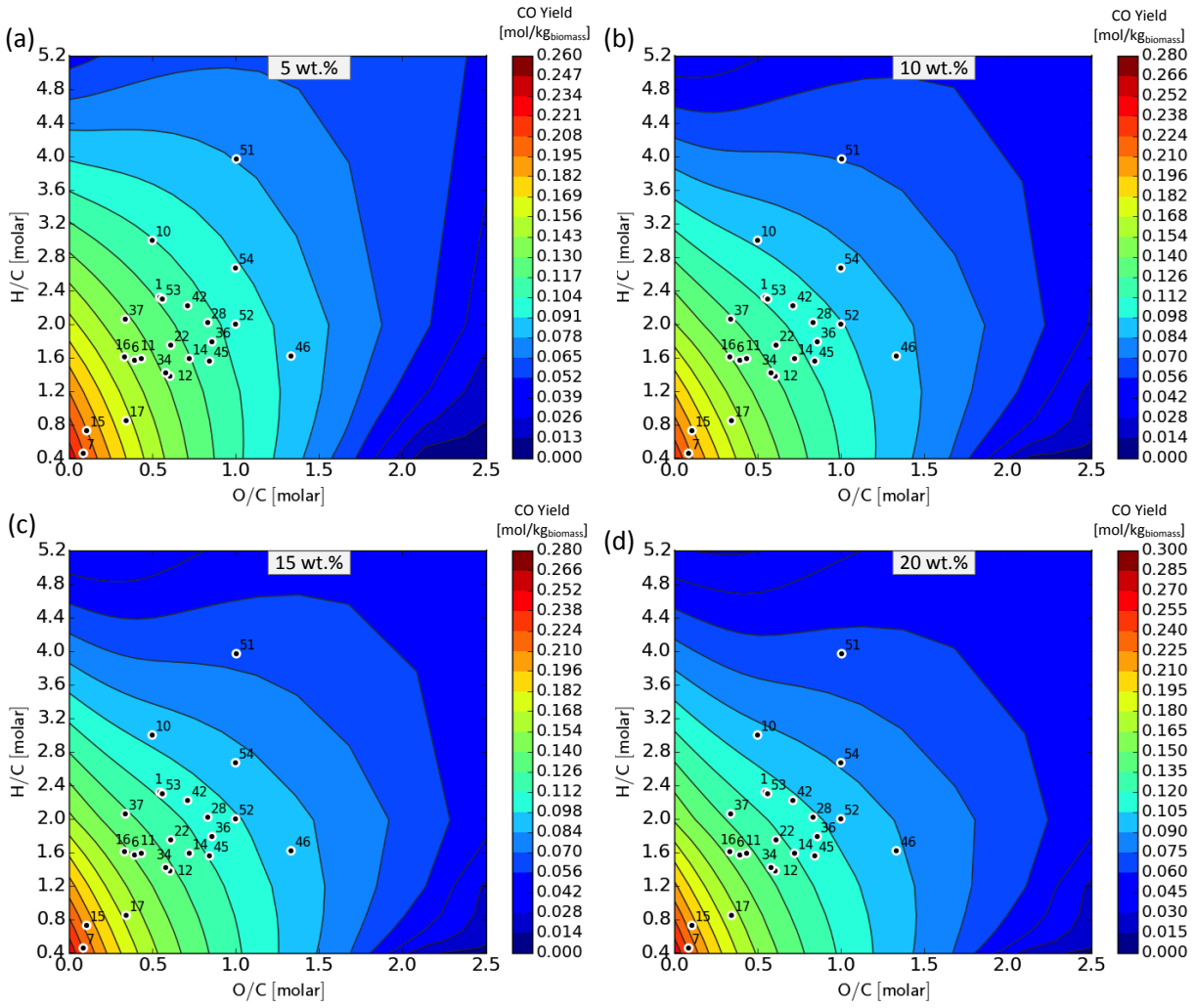

FIGURE B-27 EFFECT OF FEEDSTOCK COMPOSITION ON THE THERMODYNAMIC EQUILIBRIUM CO YIELD DURING SCWG AT 500 °C AND 25 MPA

B.4.5 CO_2 yield at 500 °C and 25 MPa

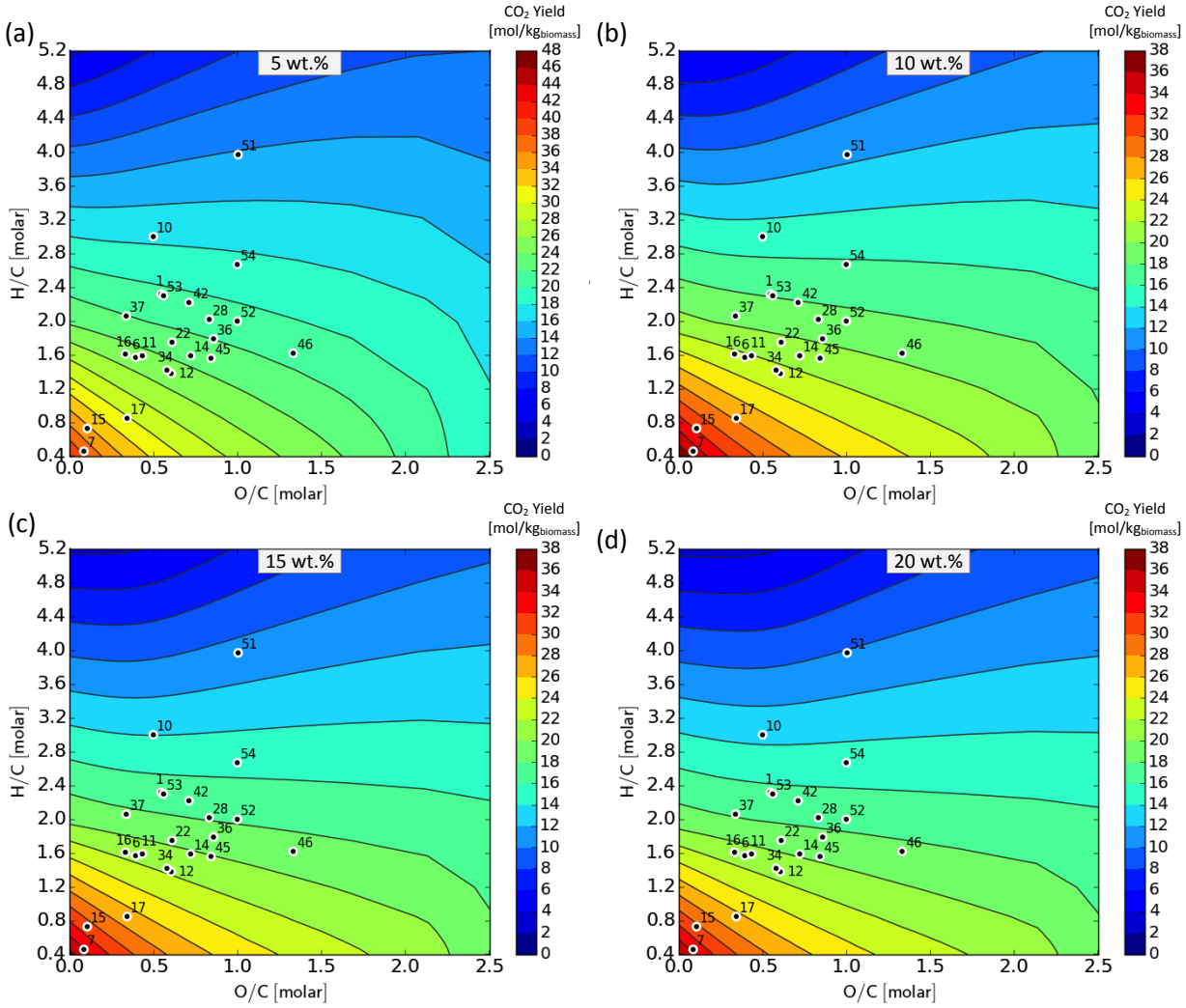

FIGURE B-28 EFFECT OF FEEDSTOCK COMPOSITION ON THE THERMODYNAMIC EQUILIBRIUM CO_2 YIELD DURING SCWG AT 500 °C AND 25 MPA

B.4.6 HHV of product gas at 500 °C and 25 MPa

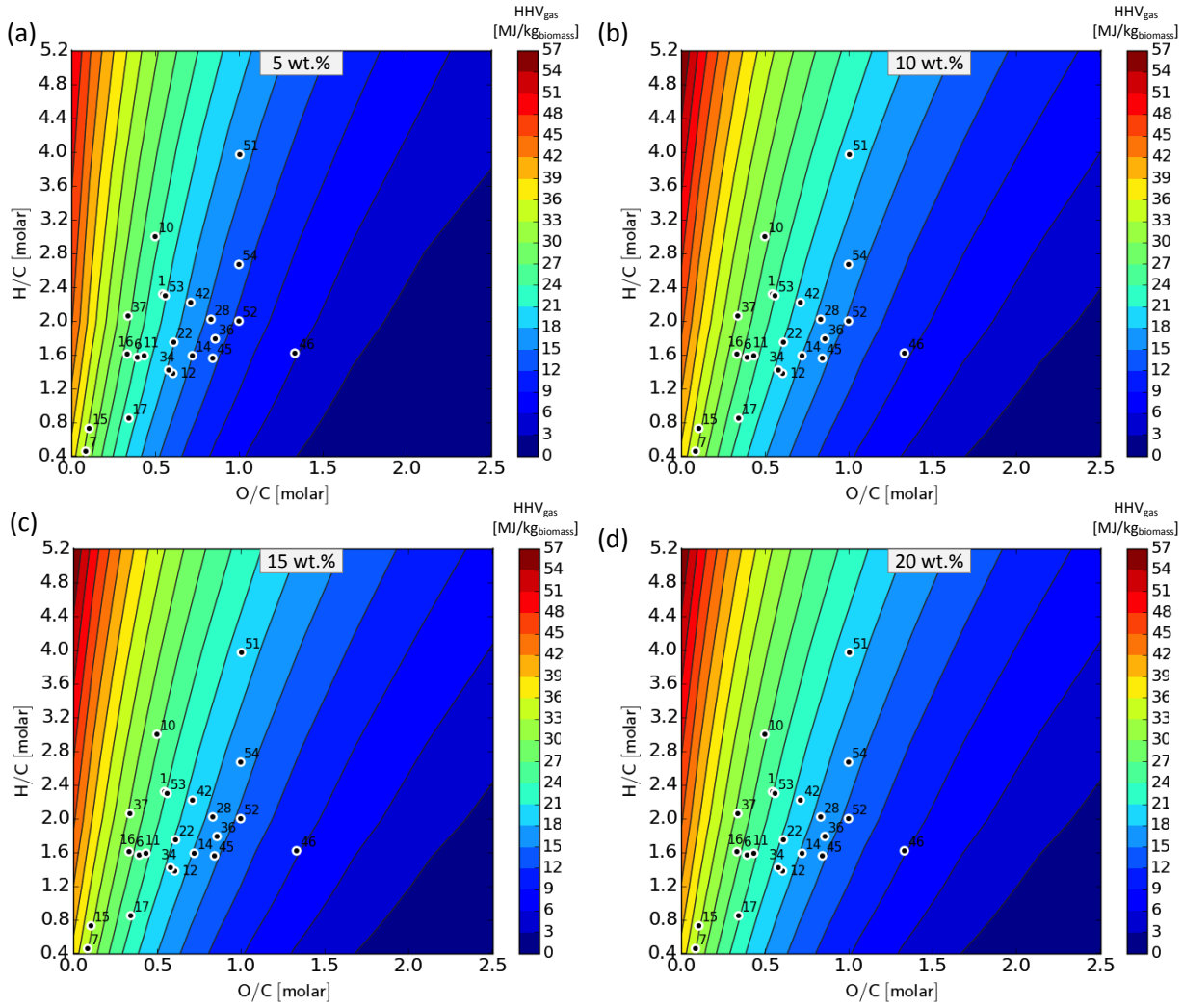

FIGURE B-29 EFFECT OF FEEDSTOCK COMPOSITION ON THE THERMODYNAMIC EQUILIBRIUM HHV OF THE PRODUCT GAS DURING SCWG AT 500 °C AND 25 MPA

B.4.7 Heat required for isothermal operation at 500 °C and 25 MPa

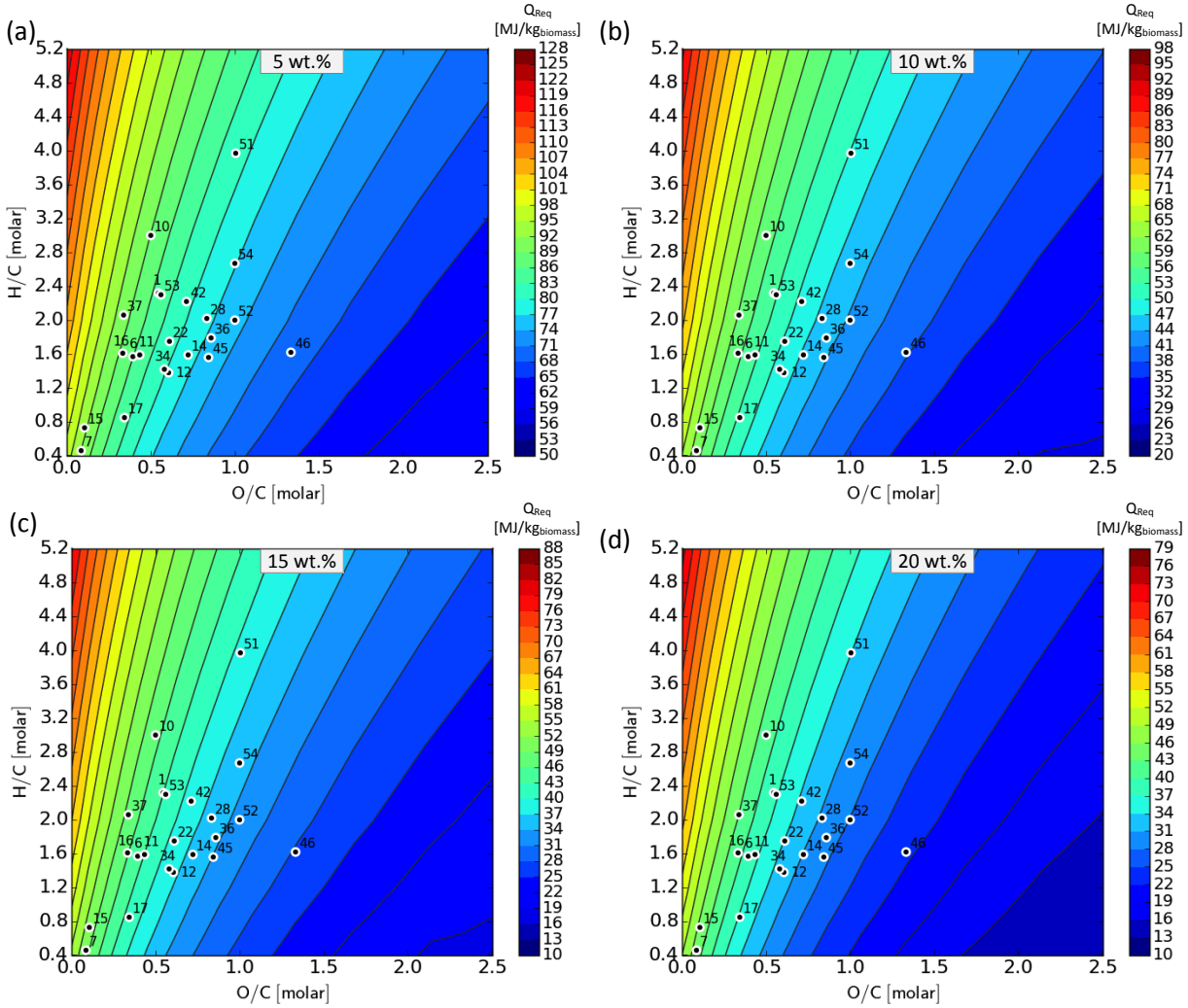

FIGURE B-30 EFFECT OF FEEDSTOCK COMPOSITION ON THE HEAT REQUIRED FOR ISOTHERMAL OPERATION AT 500 °C AND 25 MPA

B.4.8 Energy Recovery (ER) at 500 °C and 25 MPa

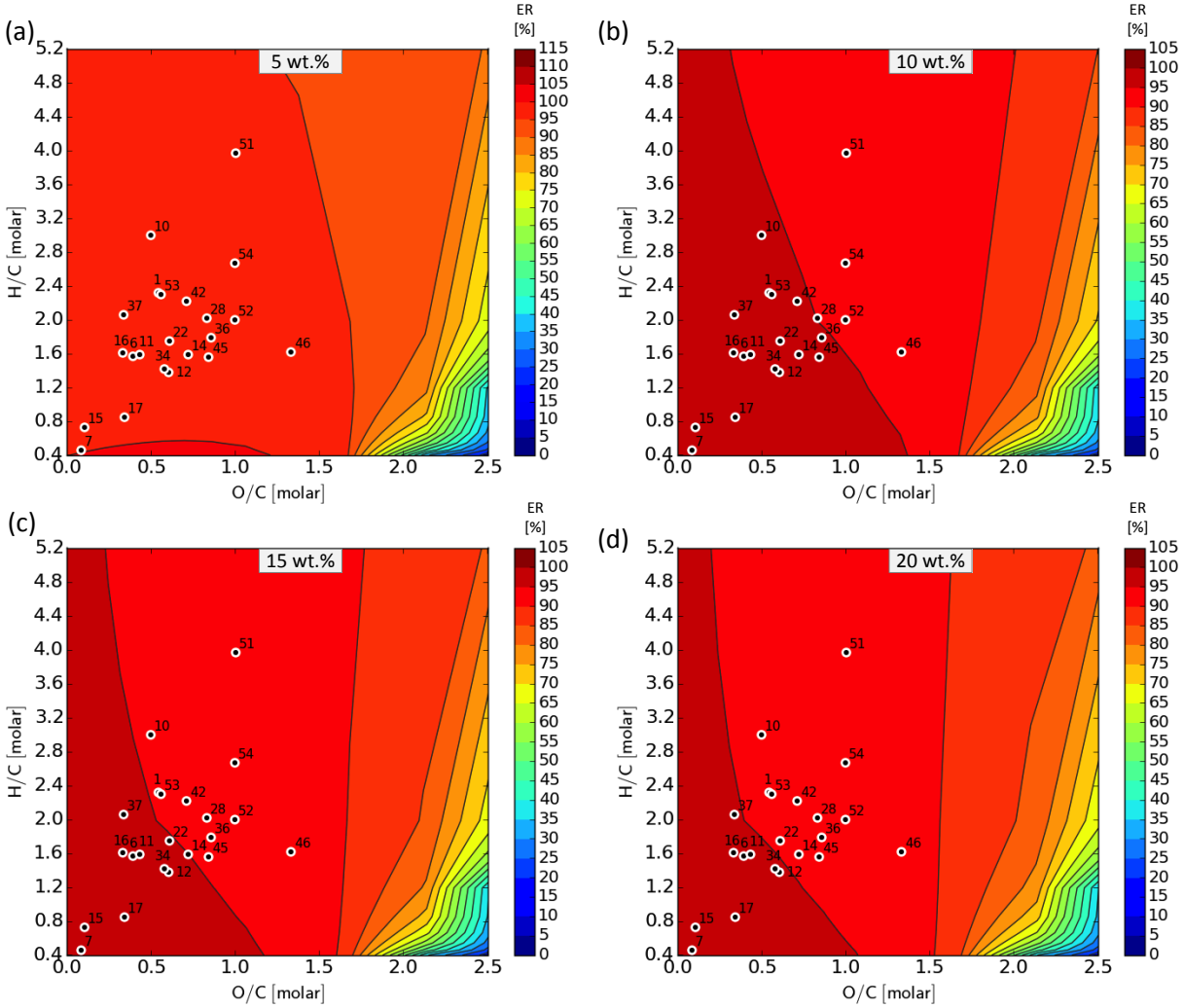

FIGURE B-31 EFFECT OF FEEDSTOCK COMPOSITION ON THE ENERGY RECOVERY DURING SCWG AT 500 °C AND 25 MPA

B.5 Additional results at 700 °C and 25 MPa

B.5.1 Total gas yield at 700 °C and 25 MPa

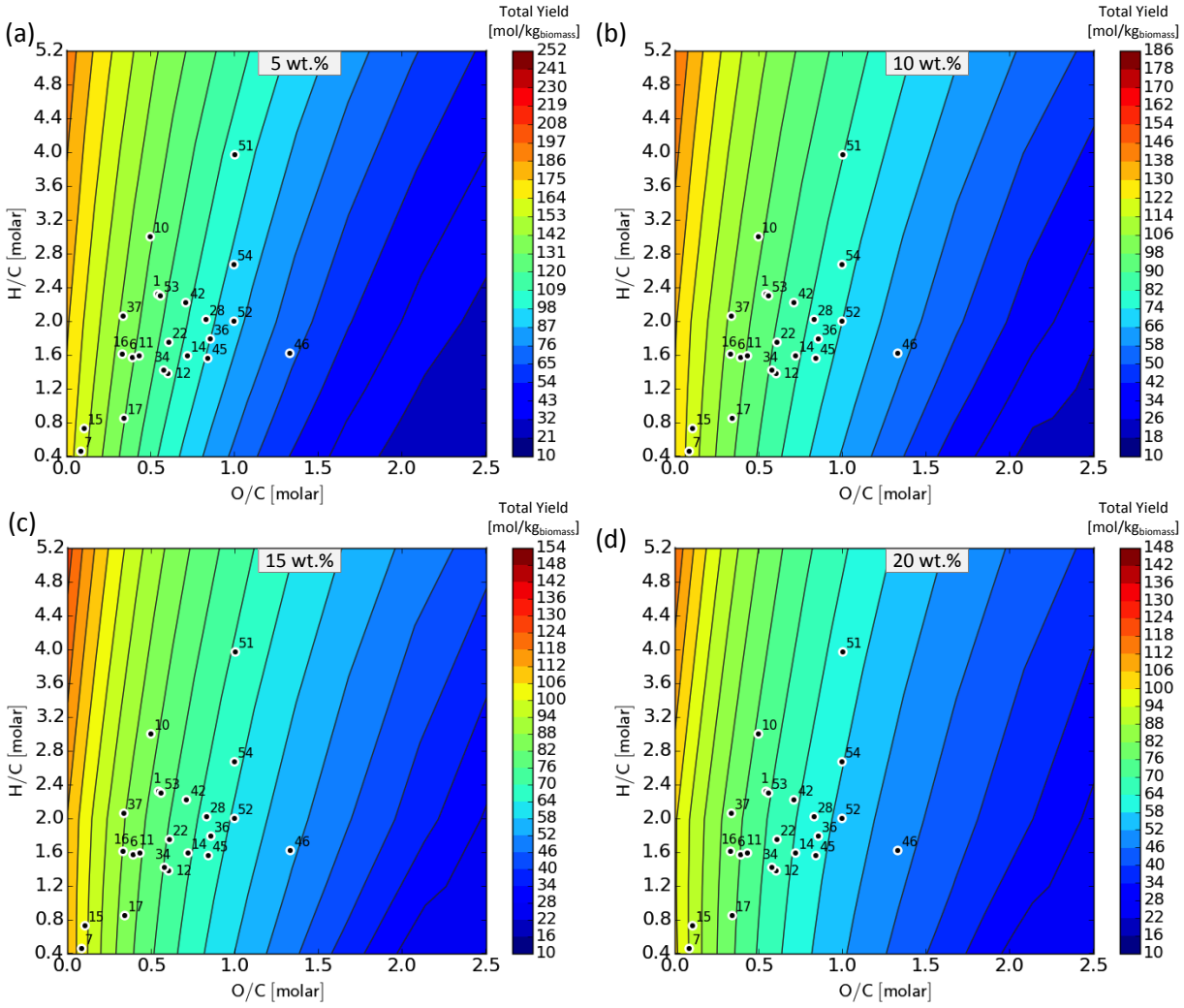

FIGURE B-32 EFFECT OF FEEDSTOCK COMPOSITION ON THE TOTAL THERMODYNAMIC EQUILIBRIUM GAS YIELD DURING SCWG AT 700 °C AND 25 MPA

B.5.2 H_2 yield at 700 °C and 25 MPa

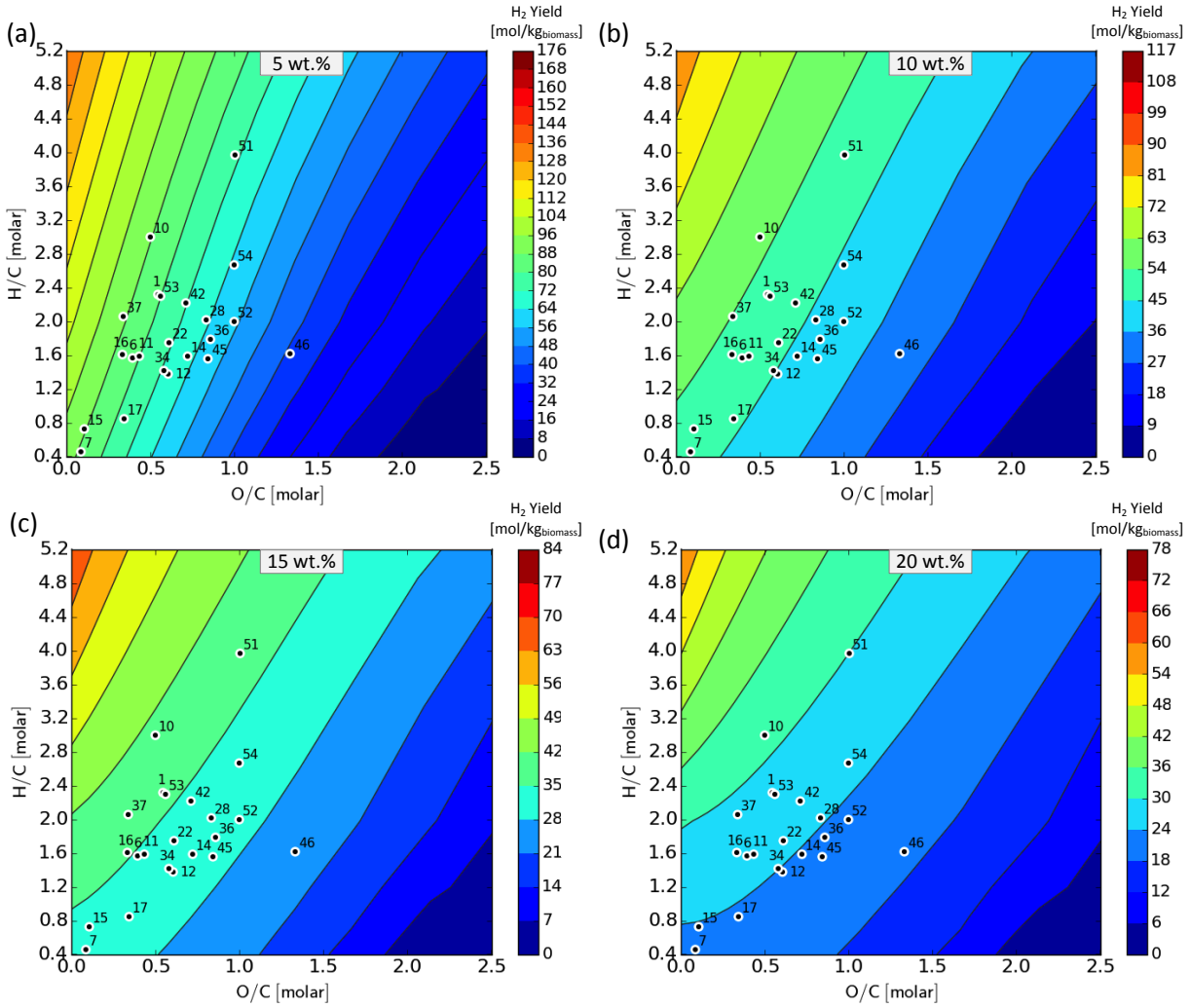

FIGURE B-33 EFFECT OF FEEDSTOCK COMPOSITION ON THE THERMODYNAMIC EQUILIBRIUM H_2 YIELD DURING SCWG AT 700 °C AND 25 MPA

B.5.3 CH_4 yield at 700 °C and 25 MPa

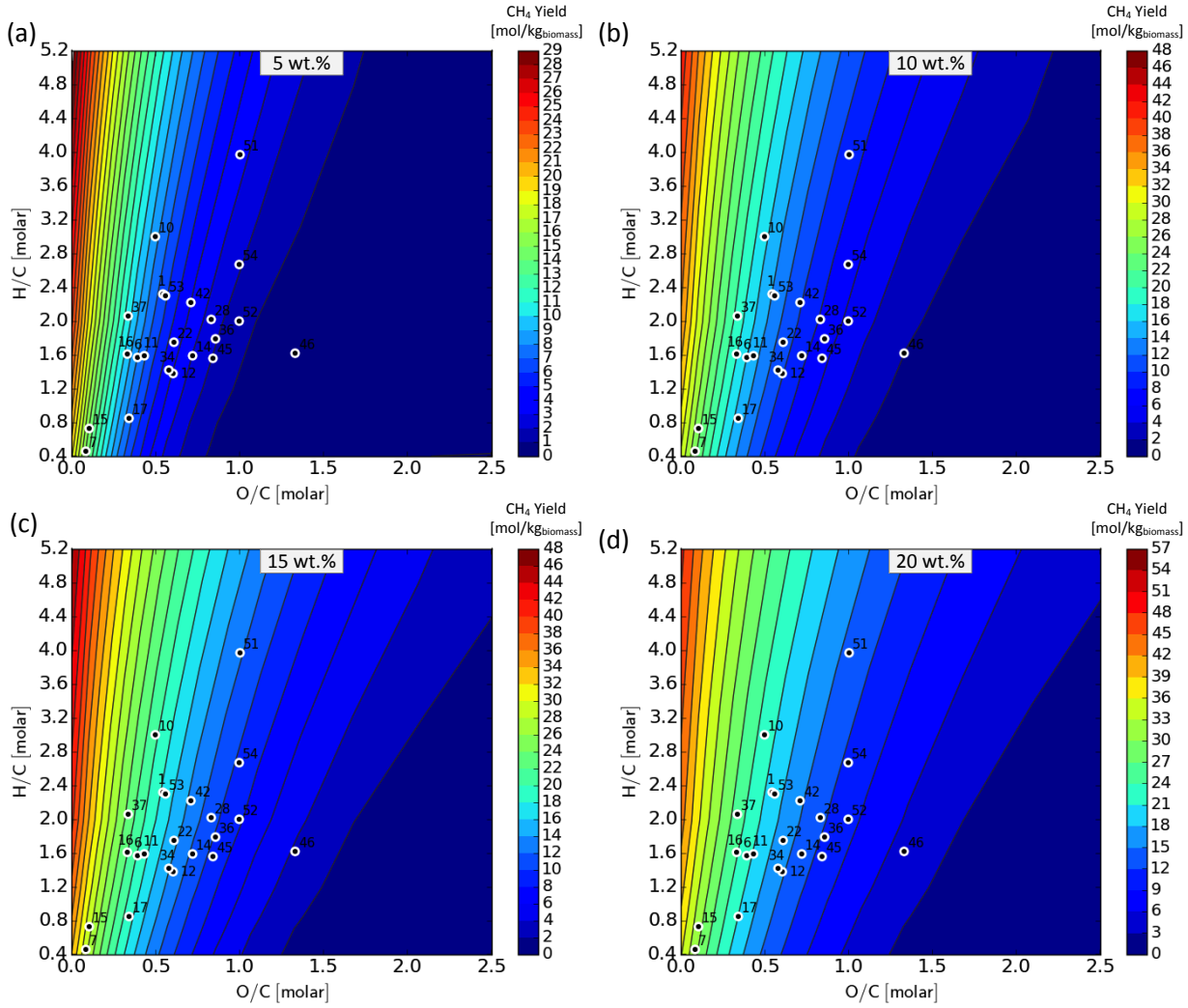

FIGURE B-34 EFFECT OF FEEDSTOCK COMPOSITION ON THE THERMODYNAMIC EQUILIBRIUM CH_4 YIELD DURING SCWG AT 700 °C AND 25 MPA

B.5.4 CO Yield at 700 °C and 25 MPa

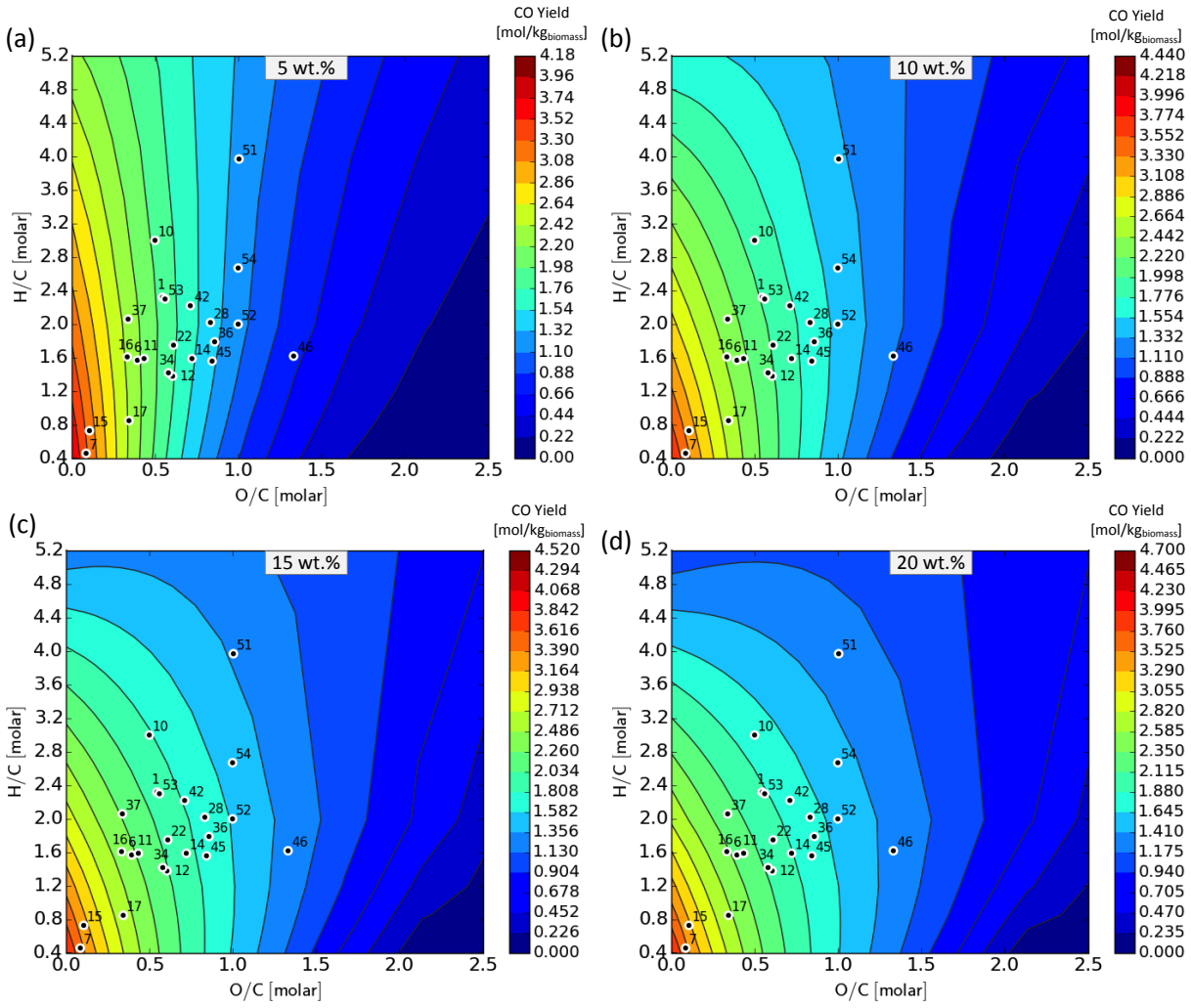

FIGURE B-35 EFFECT OF FEEDSTOCK COMPOSITION ON THE THERMODYNAMIC EQUILIBRIUM CO YIELD DURING SCWG AT 700 °C AND 25 MPA

B.5.5 CO_2 yield at 700 °C and 25 MPa

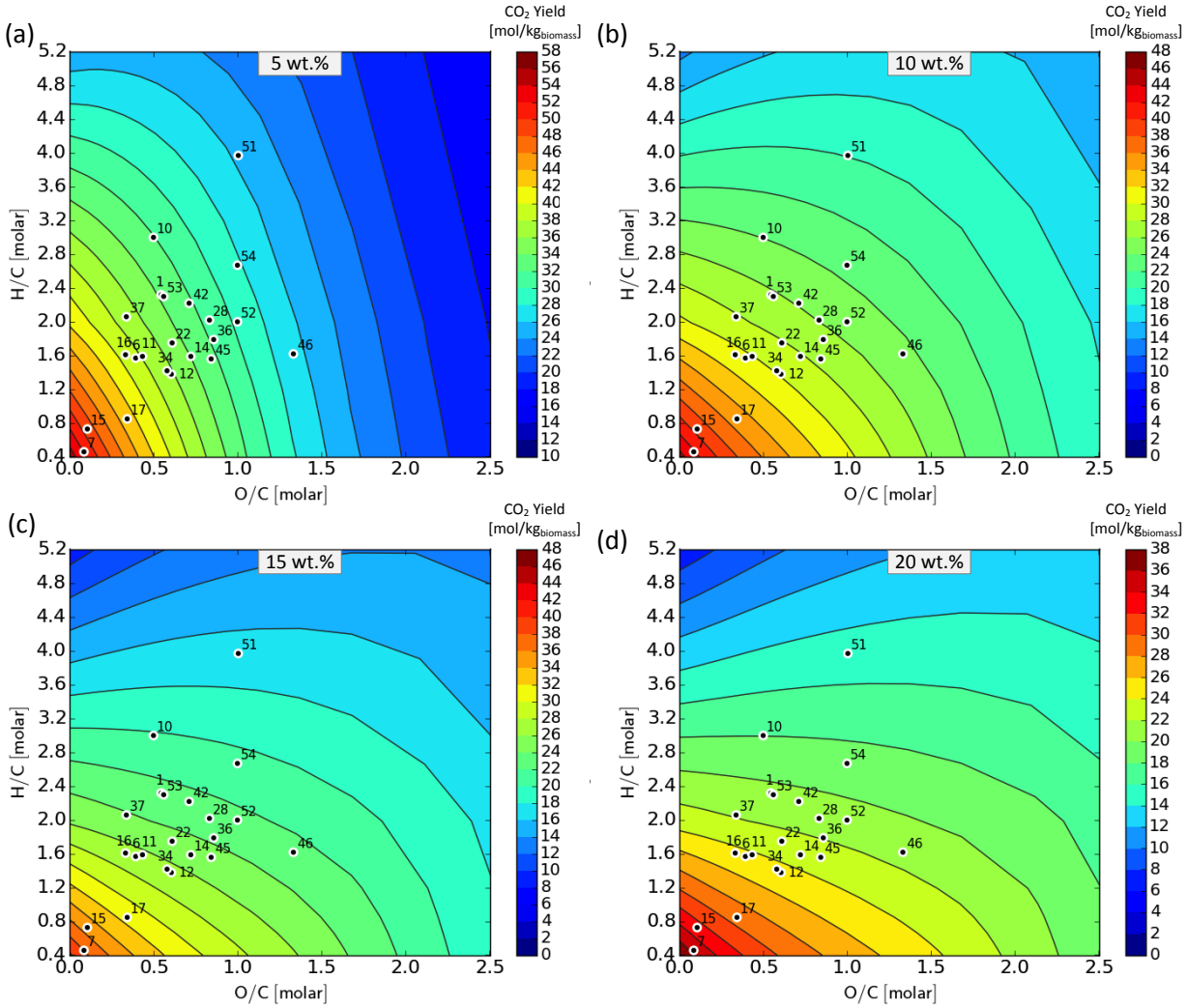

FIGURE B-36 EFFECT OF FEEDSTOCK COMPOSITION ON THE THERMODYNAMIC EQUILIBRIUM CO_2 YIELD DURING SCWG AT 700 °C AND 25 MPA

B.5.6 HHV of product gas at 700 °C and 25 MPa

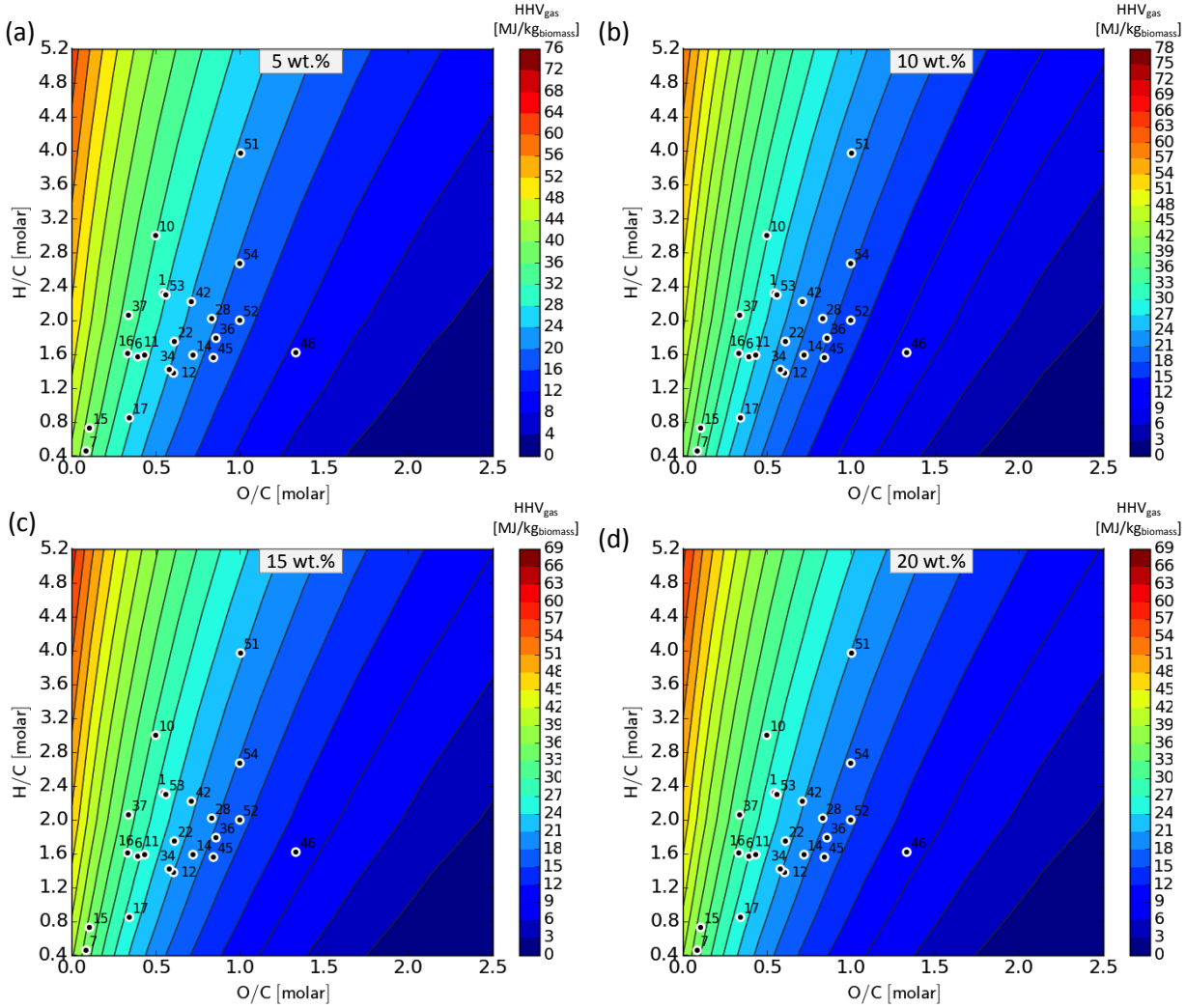

FIGURE B-37 EFFECT OF FEEDSTOCK COMPOSITION ON THE THERMODYNAMIC EQUILIBRIUM HHV OF THE PRODUCT GAS DURING SCWG AT 700 °C AND 25 MPA

B.5.7 Heat required for isothermal operation at 700 °C and 25 MPa

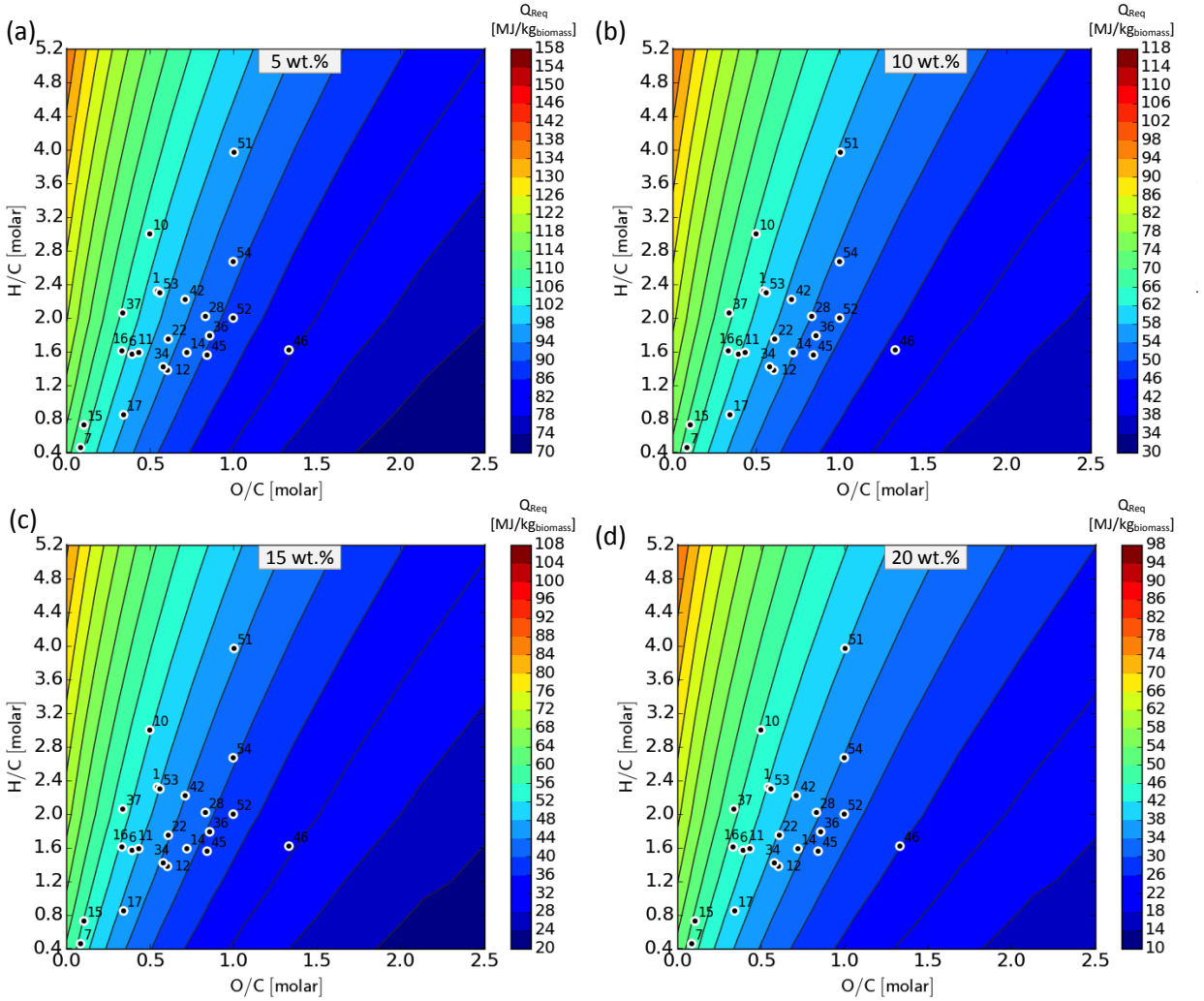

FIGURE B-38 EFFECT OF FEEDSTOCK COMPOSITION ON THE HEAT REQUIRED FOR ISOTHERMAL OPERATION AT 700 °C AND 25 MPA

B.5.8 Energy Recovery (ER) at 700 °C and 25 MPa

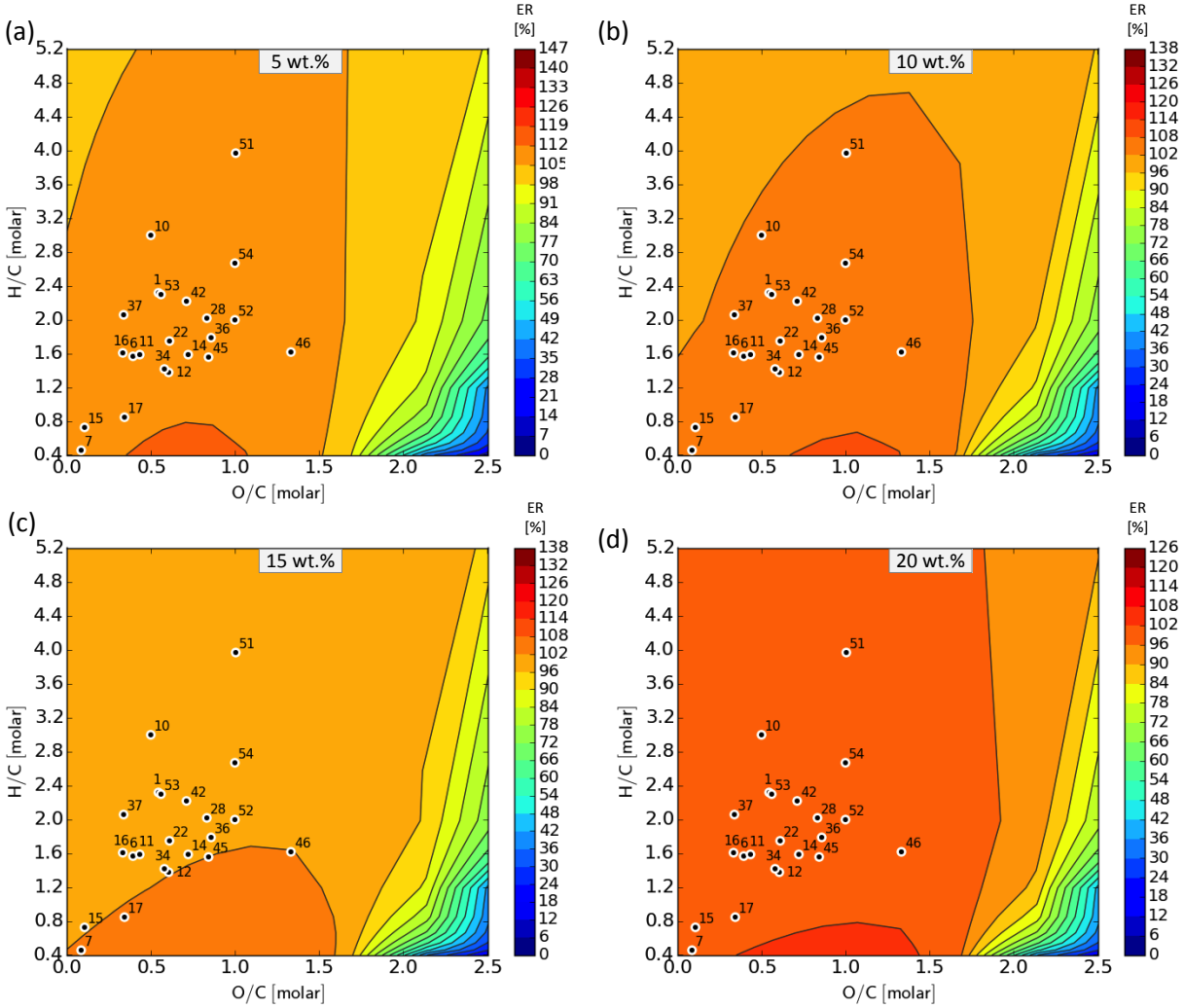

FIGURE B- 39 EFFECT OF FEEDSTOCK COMPOSITION ON THE ENERGY RECOVERY DURING SCWG AT 700 °C AND 25 MPA

Appendix C

Detailed Experimental Setup and Procedure

C.1 Experimental setup

Figure C-1 and Table C-1 shows a 3D drawing and details of batch reactor setup used during experiments.

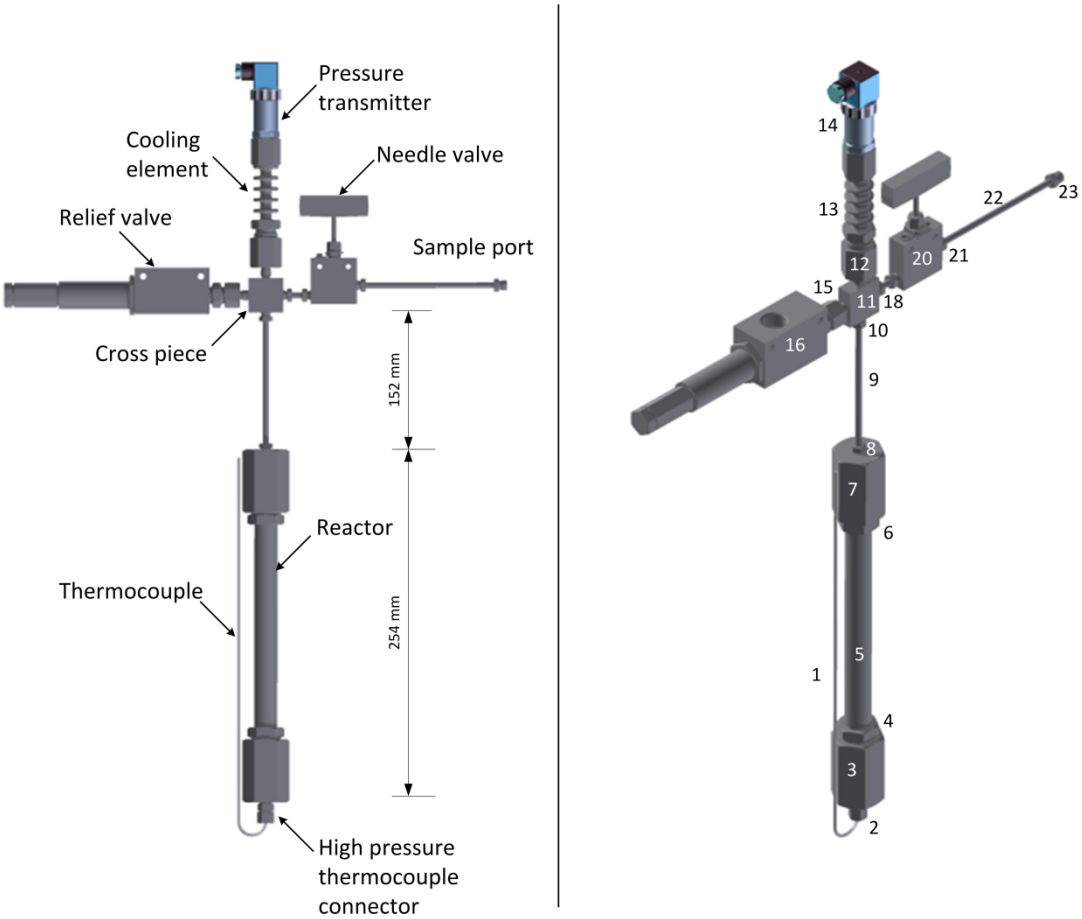

FIGURE C-1 DETAILED 3D DRAWING OF THE BATCH REACTOR SETUP

TABLE C-1 DETAILS OF THE REACTOR PARTS

PART #	DESCRIPTION	MOC	SUPPLIER	PART #
1	1/8" Type K Thermocouple (1000 mm long)	SS310	WIKA	n/a
2	High pressure thermocouple connector (1/4" HP male x 1/8" TS female)	SS316	HiP[a]	15-21AF2HM4-T
3	1" MP Female to ¼" HP Female coupling	SS316	HiP	20-21LF16HF4
4	1" MP Gland	SS316	HiP	20-2LM16
4b	1" MP Collar	SS316	HiP	20-2L16
5	1" MP Nipple (10" long, ID 9/16")	SS316	HiP	20-LM16-10
6	1" MP Gland	SS316	HiP	20-2LM16
6b	1" MP Collar	SS316	HiP	20-2L16
7	1" MP Female to ¼" MP Female coupling	SS316	HiP	20-21LF4LF16
8	¼" MP Gland	SS316	HiP	20-2LM4
9	¼" MP Nipple (6" long)	SS316	HiP	20-LM4-6
10	¼" MP Gland	SS316	HiP	20-2LM4
11	¼" MP Cross piece	SS316	HiP	20-24LF4
12	½" NPT Female to ¼" MP Male	SS316	HiP	20-21NFDLM4
13	½" NPT to ½" BSP cooling element for pressure transducer	SS316	WIKA	W4-1461621
14	S-10-A Pressure transmitter (0 – 40 MPa, 4 – 20 mA, 2 wire)		WIKA	W210400B
15	¼" MP Male to 9/16" HP Male	SS316	HiP	20-21LM4HM9
16	Factory set pressure relief valve (set to 40 MPa)	SS316	HiP	402633-10
17	¼" MP Gland	SS316	HiP	20-2LM4
18	¼" MP Male to ¼" MP Male	SS316	HiP	20-21LM4LM4
19	¼" MP Gland	SS316	HiP	20-2LM4
20	¼" MP 2-way straight needle valve	SS316	HiP	20-11LF4
21	¼" MP Gland	SS316	HiP	20-2LM4
22	¼" MP Nipple (6" long)	SS316	HiP	20-LM4-6
23	¼" Swagelok coupling	SS316	Swagelok	

[a]HiP = High Pressure Equipment Company

C.2 Detailed Experimental Procedure

This section is a step-by-step description of the experimental procedure followed during a typical experimental run.

C.2.1 Drying of feed material

- Dry the appropriate feedstock material overnight in an oven at 105 °C
- On the morning when conducting an experiment, remove dried sample from oven, switch off the oven and place the sample in a desiccator to cool down.

C.2.2 Switching on the sand bath

- Open the air valve to the sand bath and ensure that the air is flowing through
- Switch on the sand bath and set the temperature to 460 °C
- Allow approximately 1.5 hours for the sand bath to heat to 460 °C

C.2.3 Preparing the reactor for an experiment

- Ensure that the reactor parts are clean and dry
- Apply anti-seize assembly compound to the 1" gland (part #4 – see Figure C-1) before tightening it with a 1", together with the 1" nipple (part #5) to the adaptor (part #3) using a spanner with the appropriate mouth size
- Attach the thermocouple and thermocouple connector (part #2) to the adaptor (part #3)
- Insert the reactor vertically into the bench-top vice grip to ensure

C.2.4 Loading the reactor

- Once the dried feedstock sample is cooled, weigh the appropriate amount of feedstock sample, catalyst and water in a weighing boat (in the case of catalyst and feedstock) or beaker (in the case of water) and add it to the reactor
- Apply anti-seize assembly compound to the other gland (part #6) before connecting it, together with the adaptor (part #7) to the rest of the reactor
- Attach the ¼" tubing (part 9) to the reactor
- Remove the reactor from the bench-top vice

C.2.5 Attaching the reactor to the mechanical swivel arm

- Attach the reactor to the cross piece (part #11) *via* the other end of the ¼" tubing
- Attach the clamps holding the reactor to the mechanical swivel arm
- Attach the thermocouple, pressure transmitter and logger plugs to the appropriate plugs in the indicator box

C.2.6 Purging and pressurising the reactor

- Start the logger by pressing the "log" button on the logger
- Attach the vacuum pump line to the reactor setup (*via* part #23) and ensure that the needle valve (part #20) is closed tightly
- Switch on the vacuum pump and slowly open the needle valve in order to remove the air in the reactor setup
- Close the valve once the pressure reaches approximately -0.9 bar(g) and remove the vacuum pump
- Attach the tube connected to the N_2 bottle to the reactor
- Purge the line between the N_2 bottle and the reactor setup with N_2
- Once the line is purged, close the purge valve and open the valve on the N_2 bottle regulator to allow a pressure of about 2.5 MPa in the line
- Open the needle valve attached to the reactor (part 20) slowly to allow the reactor to be pressurised with N_2
- Close the needle valve once the pressure in the reactor has reached 2.1 MPa (21 bar)
- Close the valve to the regulator and allow the line between the N_2 bottle and the needle valve to vent and remove the adaptor connecting the N_2 bottle to the reactor setup
- Allow the pressure and temperature in the reactor to stabilise (approximately 5 minutes) and check the reactor for any leaks by allowing another 5 minutes by noting any drop in the pressure in the reactor
- If no leak is detected, the experiment can proceed. If a leak is detected, open the needle valve slowly to remove the N_2 from the system and check if all the reactor parts are attached tightly enough

C.2.7 Starting an experiment

- Ensure that the cold water bath is in the correct position and contains enough water.
- Once the sand bath has reached the set temperature, lower the reactor into the sand bath by means of the mechanical swivel arm using the appropriate personal protective equipment (heat resistant gloves and a face shield)
- Once the reactor is fully submerged in the sand, tighten the mechanical arm to ensure the reactor is supported and place the two-parts of the radiation shield over the sand bath opening and place the Perspex shield between yourself and the reactor
- Check the pressure and temperature during the heat-up phase. If the pressure drops during the heat-up phase, a leakage occurred. The reactor should then be removed from the sand bath and quenched in the cold water bath and a new experiment should be started
- Set the timer to the appropriate "hold time". The "hold time" starts once the reactor temperature reaches a temperature 5 °C less than the set point temperature of 450 °C (*i.e.* when the temperature reaches 445 °C)

C.2.8 Quenching the reactor

- Once the predetermined "hold time" is over, move the Perspex shield and remove reactor from the sand bath by means of the mechanical swivel arm and place it in the cold water bath (while wearing the appropriate PPE)
- During the cooling stage, pour some cold water over the top parts of the reactor (except for the pressure transmitter) to minimise the temperature gradient in the system
- Once the temperature and pressure in the system have stabilised, remove the reactor from the water bath by means of the mechanical swivel arm and allow another 5 minutes for the reactor to reach ambient temperature

C.2.9 Gas sampling

- While waiting for the reactor to cool to ambient temperature, connect a gas sample bag to the vacuum pump in order to remove the air

- Attach the gas bag to the reactor setup and open the needle valve slowly in order to transfer the gas product in the reactor setup to the gas bag
- Close the valve of the gas sample bag tightly as soon as the pressure in the reactor has reached ambient pressure
- Transport the gas sample bag containing the product gas to the gas chromatograph as soon as the sample was withdrawn

C.2.10 Separation of reactor products

- After analysing the gas phase, remove the reactor from the mechanical swivel arm by loosening part #9 ($^1/_4$" nipple) from the cross piece (part #11)
- Place the reactor in the bench-top vice
- Weigh 3 empty, dry beakers (beaker #1, #2 and #3)
- Weigh a dry cellulose acetate filter paper and watch glass
- Place the cellulose acetate filter paper on the vacuum filter
- Loosen part #9, #7 and #6 from the reactor
- Empty the reactor content into beaker #1
- Transfer the content of beaker #1 to the vacuum filter
- Attach the vacuum filter to the vacuum line and allow the liquid content to filter through
- Once all the liquid have filtered through, remove the vacuum line from the filter
- Empty the liquid filtrate into beaker #2 and weigh
- Empty the content of beaker #2 into a clean, dry falcon tube and mark it clearly with the experiment name (this is the water soluble product – WSP)
- Rinse the reactor with methanol and empty the content into beaker #1
- Transfer the content of beaker #1 to the vacuum filter
- Attach the vacuum filter to the vacuum line and allow the liquid content to filter through
- Once all the liquid have filtered through, remove the vacuum line from the filter
- Transfer the liquid content to beaker #3 and weigh (this is the methanol soluble phase)

- After weighing, transfer the methanol soluble phase to a vile marked with the experiment name and determine the water content of the methanol soluble phase by means of Karl Fischer Titration
- Remove the cellulose acetate filter paper from the vacuum filter and place it back on the watch glass and weigh
- Place the watch glass with the cellulose acetate filter in the vacuum oven and dry overnight at 80 °C, cool down in the desiccator and weigh
- Loosen all the parts of the reactor and rinse it with acetone and distilled water
- Allow the reactor parts to dry overnight or place it in the drying oven at 50 °C for approximately 2 hours

C.3 Gas Analysis

C.3.1 GC Setup and Method

Gas analyses were performed by means of a Varian CP3380 gas chromatograph equipped with a thermal conductivity detector (TCD) and a Suelco® Carbonex 1000 packed column (15 ft. x 1/8") made from stainless steel with a 60/80 mesh. Argon, at a flow rate of 26.9 mL/min was used as carrier gas. Table C-2 shows the specifications of the GC method. Figure C- 3 shows the thermal conductivity of N_2, H_2, CO, CH_4, CO_2, C_2H_6 and C_2H_4 as a function of temperature at atmospheric pressure.

The oven temperature program which was used can be summarised as follows:

- Step 1: Hold oven temperature at 120 °C for 6 minutes – this allows for the detection of H_2, N_2, CO and CH_4;
- Step 2: Ramp oven temperature to 225 °C at a heating rate of 20 °C/min – this allows for the detection of CO_2;
- Step 3: Hold oven temperature at 225 °C for 10 minutes – this allows for the detection of C_2H_4 and C_2H_6;
- Step 4: Cool down oven temperature to 120 °C.

In order to inject more accurate sample volumes, a 6-port valve was added to the GC, fitted with a sample loop with a fixed volume. Figure C-2 shows the two possible positions of the valve (Position A and Position B).

TABLE C-2 DETAILS CONCERNING THE GC METHOD USED

GC METHOD SPECIFICATIONS	
GC	Varian CP3380
Column Type	Supelco® Carbonex 1000
Detector	TCD
TCD Temperature	160 °C
Filament Temperature	250 °C
Filament current	102 mA
Range	0.05
Injector Temperature	90 °C
Carrier Gas	Ar
Carrier Gas flow rate	26.8 mL/min
Reference Gas flow rate	26.9 mL/min

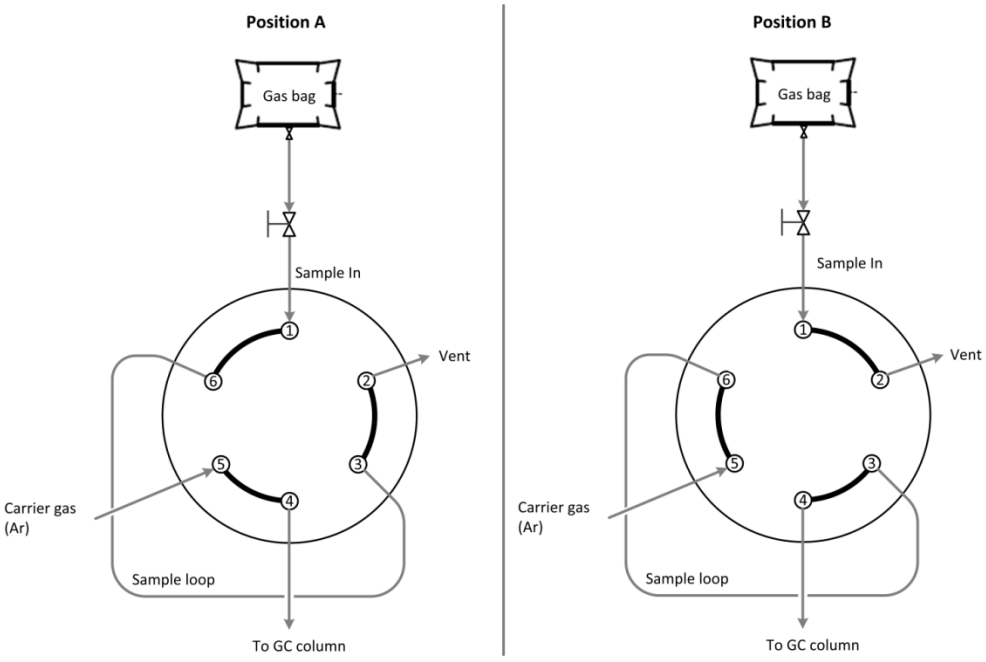

FIGURE C-2 GC SAMPLE LOOP SETUP

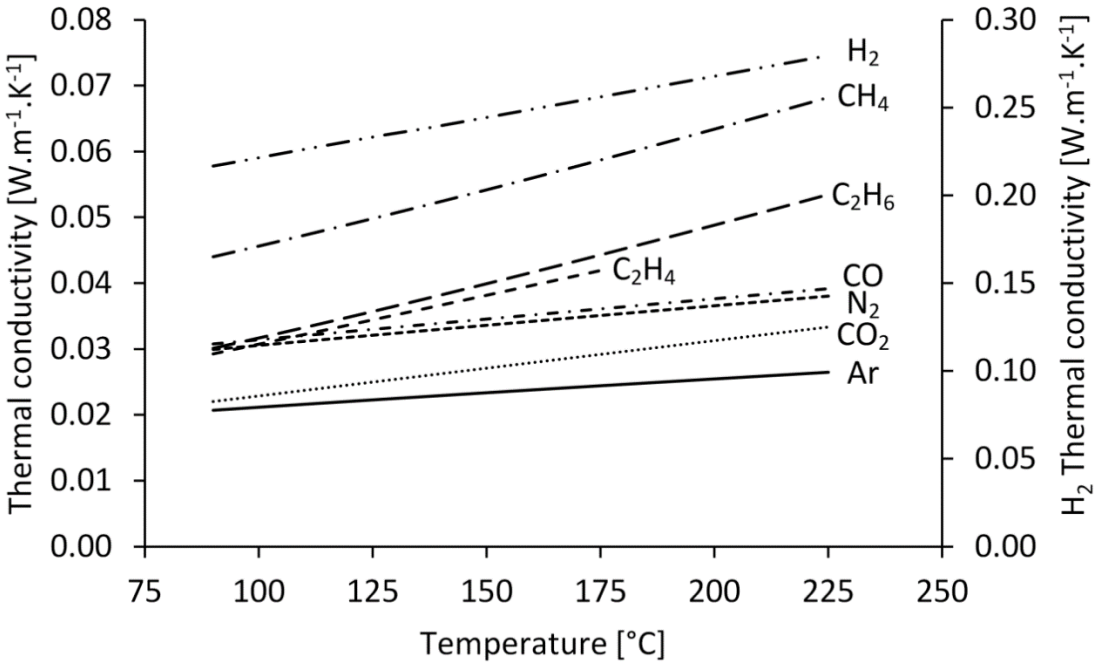

FIGURE C- 3 THERMAL CONDUCTIVITY OF GASES AS A FUNCTION OF TEMPERATURE AT ATMOSPHERIC PRESSURE (DATA FROM LEMMON ET AL. (2011))

Initially, the sample valve was kept at Position A. The gas bag filled with the product gas was attached to GC line. By opening the gas bag valve and the valve in the sample line, the sample loop line was purged with the product gas by applying pressure on the gas bag with one's hand. The line vented to a column filled with water. After purging the line for approximately 3 – 4 minutes, the valve position was changed to Position B to allow the product gas in the sample loop to be carried away with the carrier gas to the GC column. After 5 seconds in Position B, the valve was changed back to Position A. Analyses were performed in duplicate.

C.3.2 Calibration procedure

Two separate sets of calibrations were done for the gas analyses. The first calibration was done in December 2014. During August 2015, a slight shift in the peak heights in the gas mixture were noticed, and a second set of calibrations were consequently done.

The first set of calibrations was done with pure N_2, H_2, CH_4, CO and CO_2 as well as a gas mixture purchased from Afrox containing N_2, H_2, CO, CH_4 and CO_2. For the second calibration set, the GC

column was additionally calibrated for C_2H_6 and C_2H_4 using pure C_2H_6 and C_2H_4. Calibrations were done on a molar basis using four sample loops with fixed volumes of 50, 100, 188 and 580 µL.

Before the calibration curves for each gas could be generated, the elution time of each gas product had to be determined. This was done by analysing each respective pure gas on its own (see Table C-3) using the smallest sample loop (50 µL) in the GC valve. Once the elution time was established, the response peak area of each of the pure gases using each of the four sample loops were determined by analysing each of the pure gases. The moles of gas in each of the sample loops were then calculated using the ideal gas law.

The calibration gas mixture from Afrox (see Table C-4) was then analysed using each of the 4 different sample loops. The moles of each of the gases in each of the sample loops were calculated using the ideal gas law as well as the gas composition of the product gas (as determined by the supplier using the international standard method ISO 6143). The analysis of each of the pure gases and gas mixture was done 3 times for each sample loop size. The average of the three response areas relating to each sample loop size was then used to construct a calibration curve for each of the product gases by fitting a straight line or 2nd order polynomial which passes through the origin through the points.

TABLE C-3 ELUTION TIME OF EACH GAS COMPONENT ON THE COLUMN

GAS COMPONENT	ELUTION TIME ON COLUMN [MIN]
H_2	1.06 – 1.10
N_2	2.05 – 2.08
CO	2.51 – 2.53
CH_4	4.9 – 5.1
CO_2	8.5 – 8.7
C_2H_4	16.0 – 16.3
C_2H_6	19.2 – 19.5

Figure C-4 to Figure C-10 shows the constructed calibration curves for each of the gas products. The error bars (as the standard deviation of each of the three analyses for each point) are also

shown in the figures. In most cases, the reproducibility was very good with the standard error being less than 2% for all cases. Hence, the error bars are not always visible.

TABLE C-4 COMPOSITION OF THE GAS MIXTURE USED AS CALIBRATION GAS

GAS COMPONENT	COMPOSITION IN GAS MIXTURE [MOLE %]
H_2	9.7 %
N_2	59.2 %
CO	5.2 %
CH_4	10.3 %
CO_2	15.6 %

C.3.3 Calibration Curves

Figure C-4 to Figure C-10 shows the calibration curves and response equations used for each component.

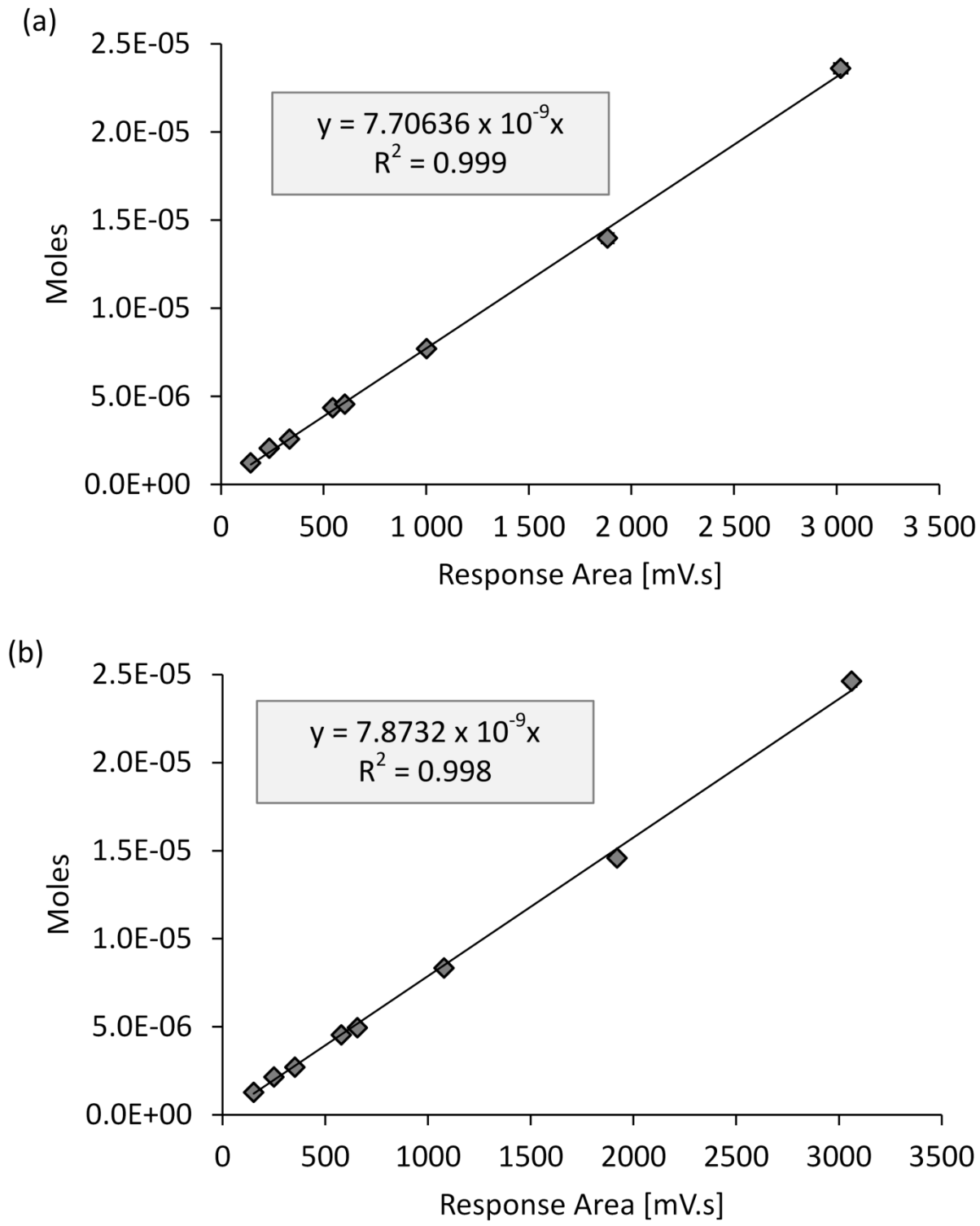

FIGURE C-4 (A) CALIBRATION CURVES FOR N_2 FOR CALIBRATION DONE DURING DECEMBER 2014 AND (B) CALIBRATION CURVES FOR H_2 FOR CALIBRATION DONE DURING AUGUST 2015

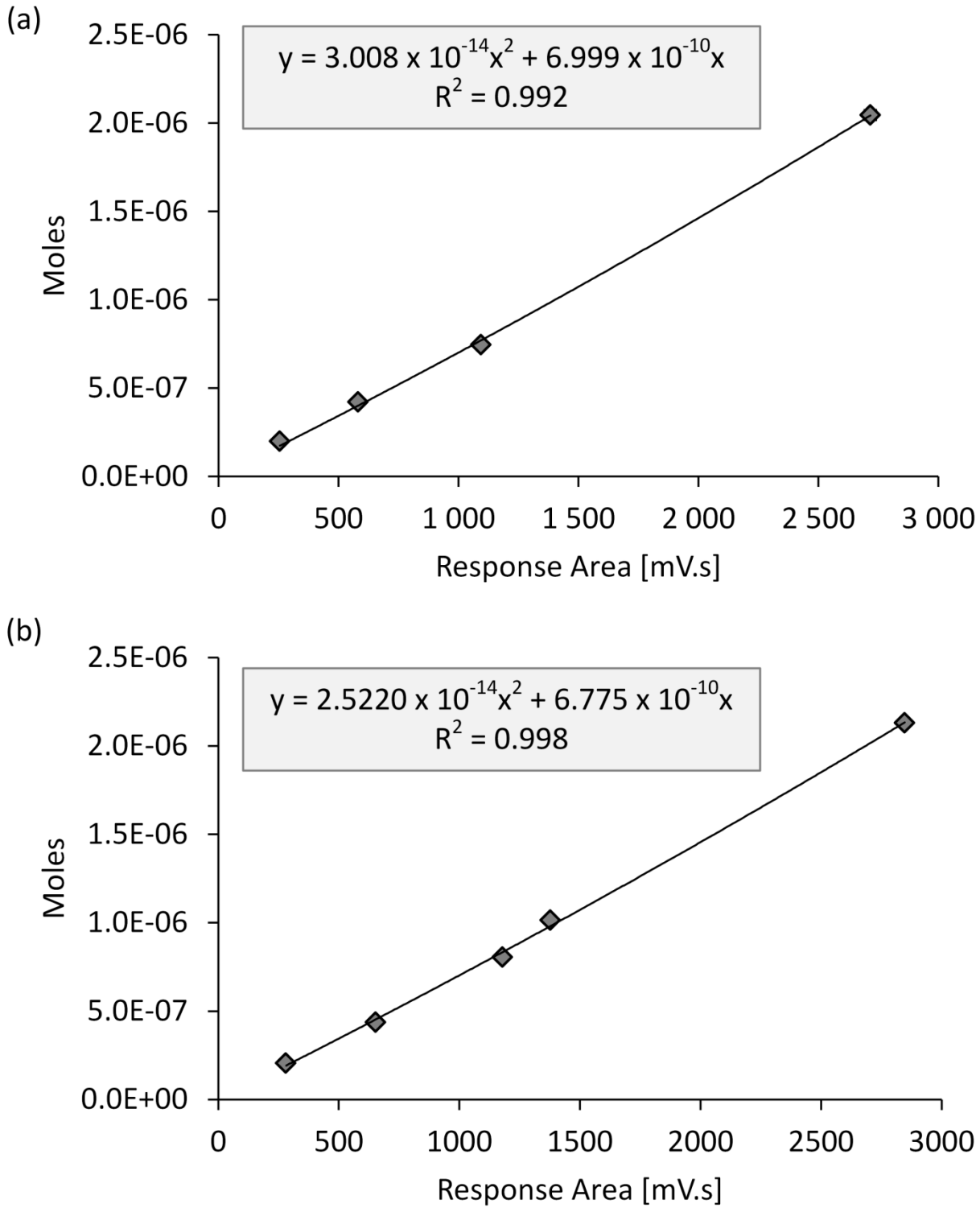

FIGURE C-5 (A) CALIBRATION CURVES FOR H_2 FOR CALIBRATION DONE DURING DECEMBER 2014 AND (B) CALIBRATION CURVES FOR H_2 FOR CALIBRATION DONE DURING AUGUST 2015

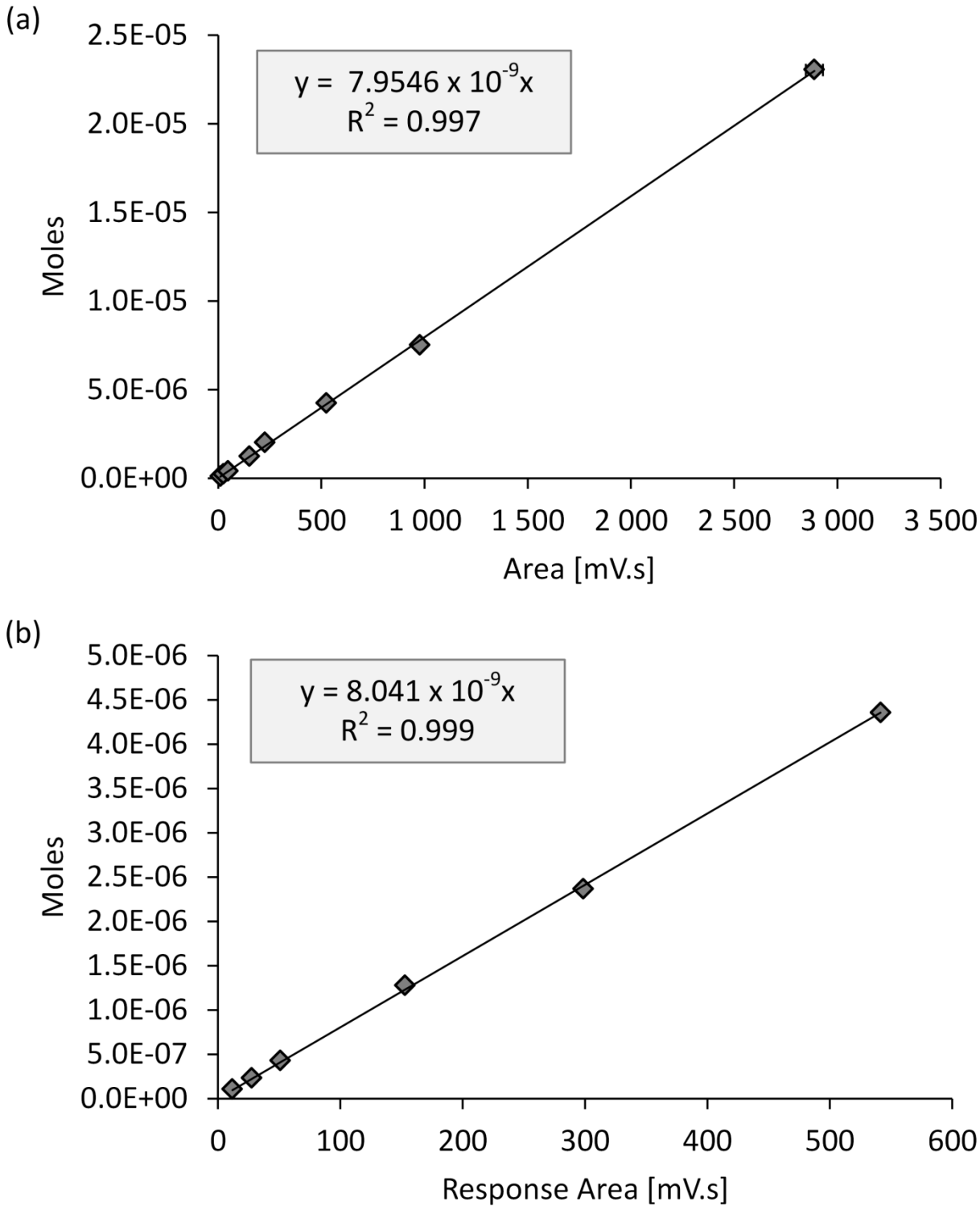

FIGURE C-6 (A) CALIBRATION CURVES FOR CO FOR CALIBRATION DONE DURING DECEMBER 2014 AND (B) CALIBRATION CURVES FOR CO FOR CALIBRATION DONE DURING AUGUST 2015

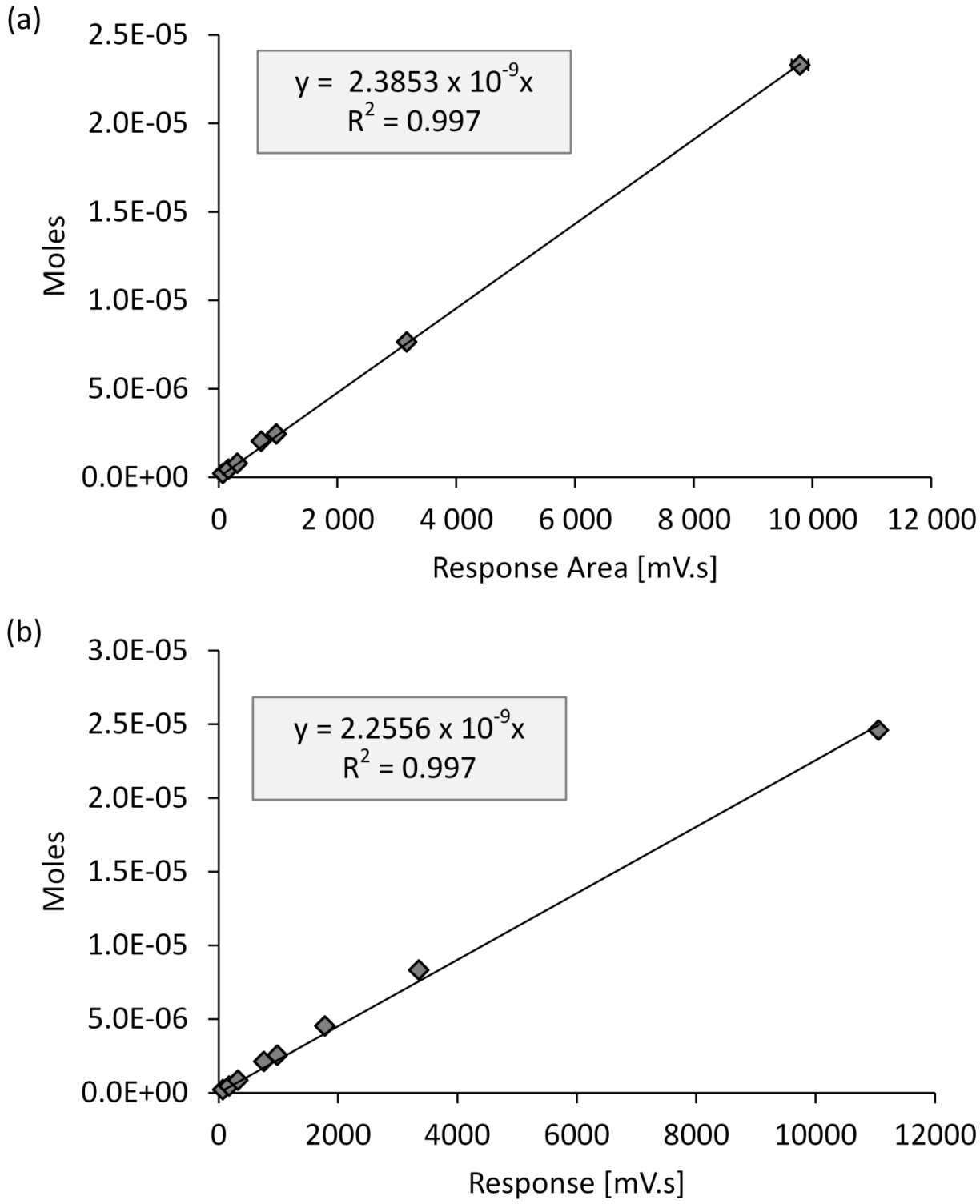

FIGURE C-7 (A) CALIBRATION CURVES FOR CH_4 FOR CALIBRATION DONE DURING DECEMBER 2014 AND (B) CALIBRATION CURVES FOR CH_4 FOR CALIBRATION DONE DURING AUGUST 2015

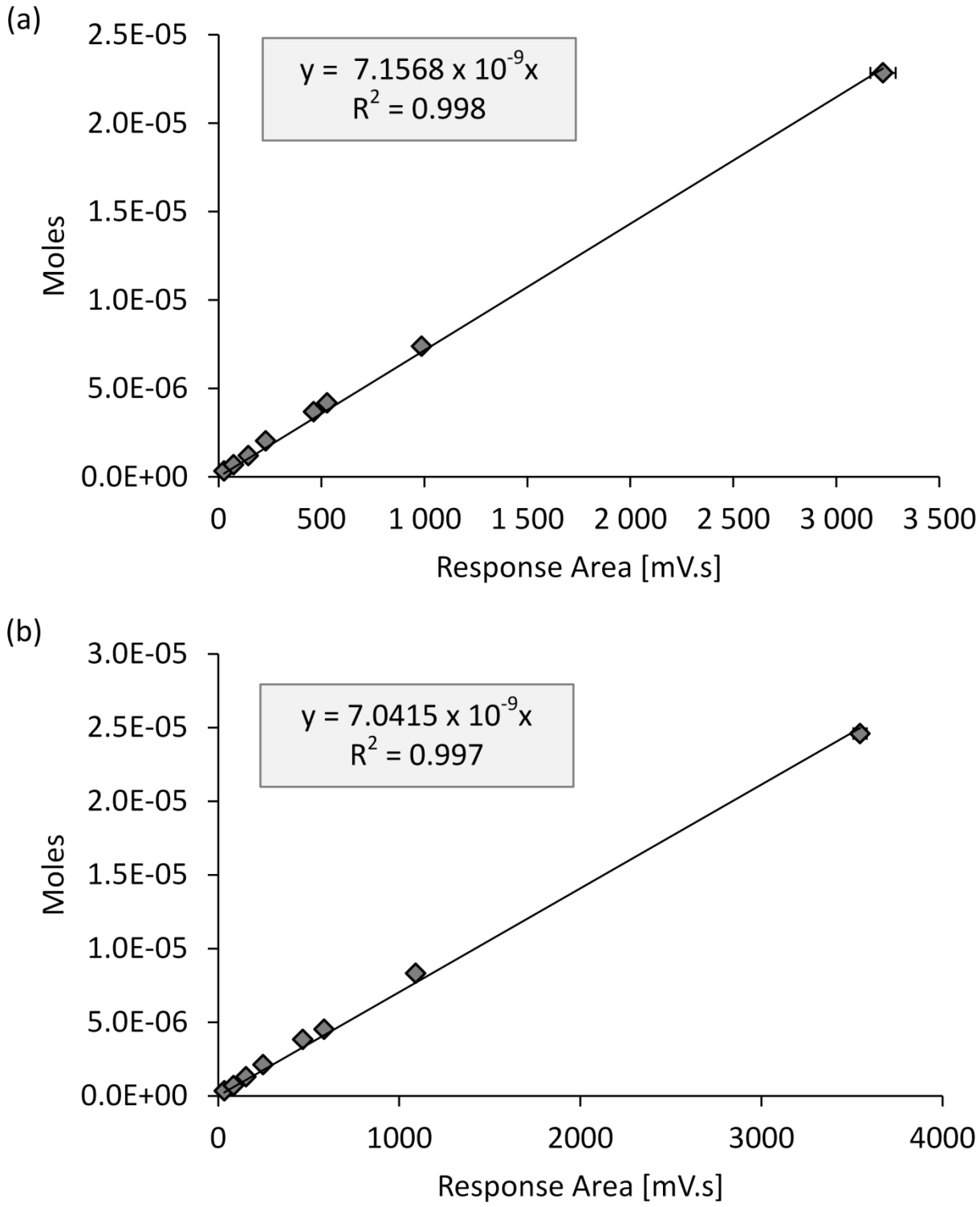

FIGURE C-8 (A) CALIBRATION CURVES FOR CO_2 FOR CALIBRATION DONE DURING DECEMBER 2014 AND (B) CALIBRATION CURVES FOR CO_2 FOR CALIBRATION DONE DURING AUGUST 2015

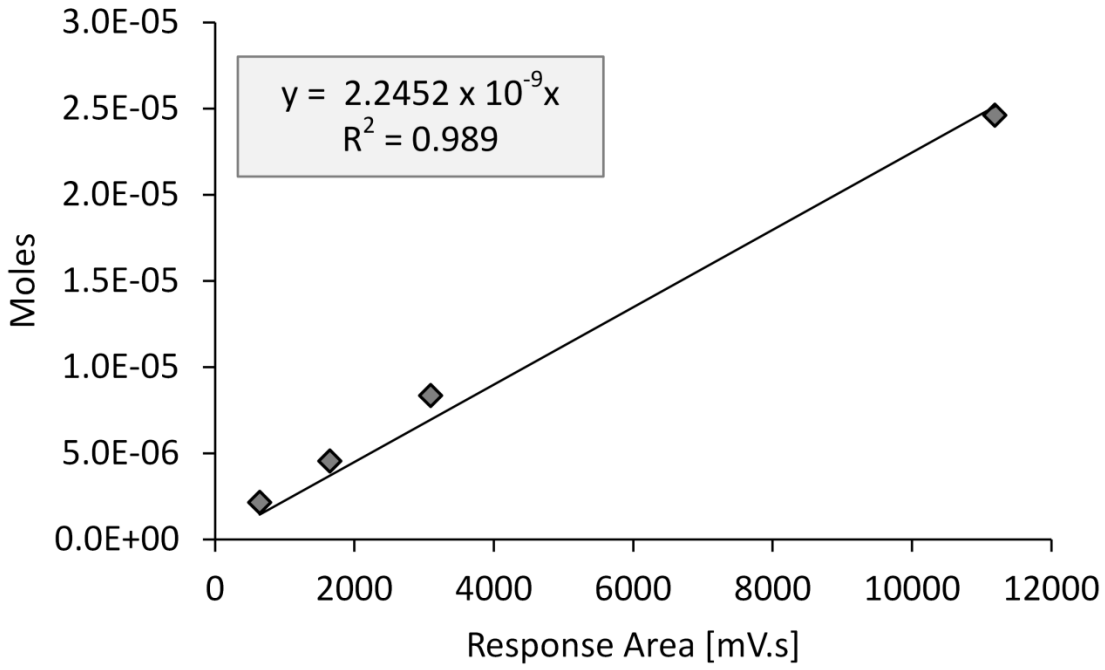

FIGURE C-9 CALIBRATION CURVES FOR C_2H_4 FOR CALIBRATION DONE DURING AUGUST 2015

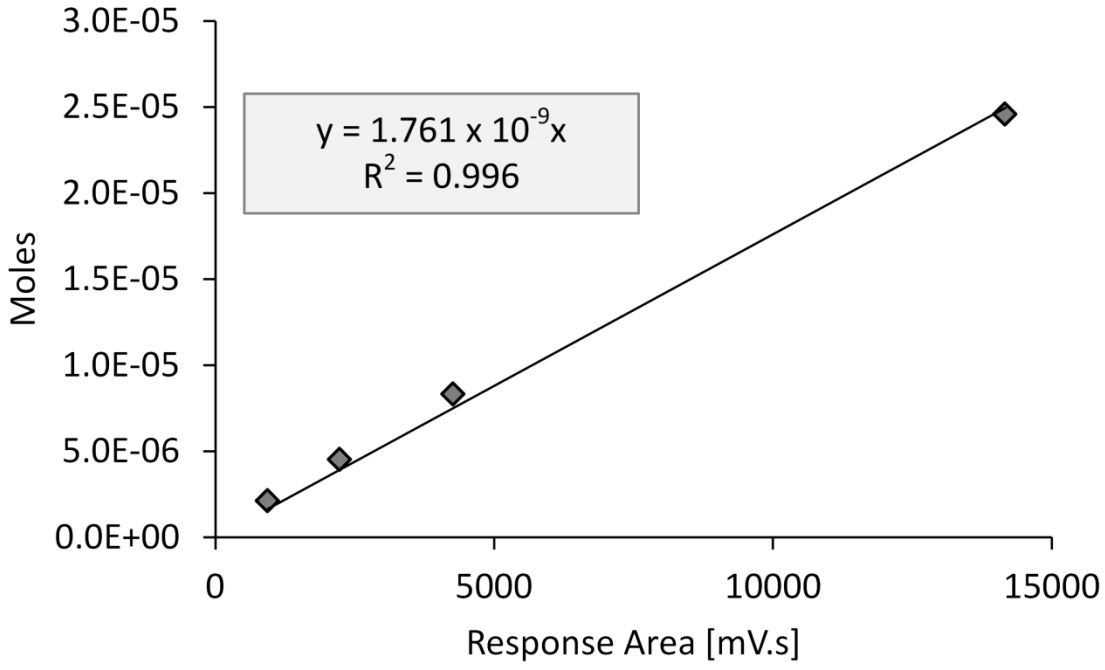

FIGURE C-10 CALIBRATION CURVES FOR C_2H_6 FOR CALIBRATION DONE DURING AUGUST 2015

C.4 Detailed Sample Calculations

This section contains the detailed calculations performed for a typical experimental run (experiment PWS18).

C.4.1 Calculating the total mass of feed material and catalyst added to the reactor

$$m_{total,in} = m_{PWS,dry} + m_{water} + m_{Ni/Al_2O_3-SiO_2} \quad \text{C-1}$$

$m_{PWS,dry} = 0.6000$ g

$m_{PWS,dry} = 0.6000$ g

$m_{water} = 5.4278$ g

$m_{Ni/Al_2O_3-SiO_2} = 0.59998$ g

$m_{total,in} = 0.6000 + 5.4278 + 0.59998 = 6.6276$ g

$m_{PWS,dry} + m_{water} = 0.6000 + 5.4278 = 6.0278$ g

C.4.2 Calculating the head-space of the reactor available after the feed material, water and catalyst have been added

$$V_{reactor,head-space} = V_{Total} - V_{feed+water+catalyst} \quad \text{C-2}$$

Assume the density of the slurry mixture (ρ_{slurry}) is the same as the density of water:

($\rho_{slurry} = \rho_{water} = 0.997$ g/mL)

$$V_{feed+water+catalyst} = \frac{m_{total}}{\rho_{water}} = \frac{0.6000}{0.997} = 6.648 \text{ mL}$$

$V_{reactor,head-space} = 49 - 6.648 = 42.35$ mL

Assume the volume of N_2 added to the reactor after pressurisation is equal to the heat-space volume of the reactor:

$V_{N_2} = V_{reactor,head-space} = 42.35$ mL

C.4.3 Calculating the moles of N_2 added to the reactor during pressurisation

The moles of N_2 added during pressurisation were calculated by taking into account the non-ideal behaviour of N_2 at elevated pressures.

$$n_{N_2,pressure} = \frac{PV_{N_2}}{z_{N_2}RT} \quad \text{C-3}$$

The temperature and pressure after purging and pressurising the reactor with N_2 (T_1 and P_1) are obtained from the logged data:

$T_1 = 21°C = 294.55\ K$

$P_1 = 23.72\ bar(a)$

Calculating the compressibility factor (Z) of N_2 at the specific temperature and pressure by means of the Pitzer correlation:

$$Z = 1 + \beta^0 \frac{P_r}{T_r} + \omega\beta' \frac{P_r}{T_r} \quad \text{C-4}$$

$$T_r = \frac{T_1}{T_{c,N_2}} \quad \text{C-5}$$

$$P_r = \frac{P_1}{P_{c,N_2}} \quad \text{C-6}$$

$$\beta^0 = 0.083 - \frac{0.422}{T_r^{1.6}} \quad \text{C-7}$$

$$\beta' = 0.139 - \frac{0.172}{T_r^{4.2}} \quad \text{C-8}$$

$$T_r = \frac{294.55}{126.2} = 2.334$$

$$P_r = \frac{23.72}{34} = 0.698$$

$$\omega_{N_2} = 0.038$$

$$\beta^0 = 0.083 - \frac{0.422}{2.334^{1.6}} = -0.0257$$

$$\beta' = 0.139 - \frac{0.172}{2.334^{4.2}} = 0.1341$$

$$Z_{N_2} = 1 - 0.0257\frac{0.698}{2.334} + 0.038(0.1341)\frac{0.698}{2.334} = 0.994$$

$$n_{N_2,pressure} = \frac{23.72 \times 42.35}{0.994 \times 83.1451 \times 294.55} = 0.0413 \text{ moles}$$

C.4.4 Determining the gas composition after gas analysis

Calculate the actual total moles in the 187.5 µL sample loop ($\boldsymbol{n_{SL,total}}$) used for gas analysis, assuming ideal gas behaviour at atmospheric pressure:

$$n_{SL,total} = \frac{PV_{SL}}{RT} \quad \text{C-9}$$

$$n_{SL,total} = \frac{1.014 \times 187.5 \times 10^{-3}}{83.1451 \times 298.25} = 7.6792 \times 10^{-6} \text{ moles}$$

TABLE C- 5 CALIBRATION EQUATIONS FOR EACH PRODUCT GAS

GAS	GC RESPONSE PEAK AREAS [MV.S]	CALIBRATION EQUATION
H_2	595.24	$n_{H_2,SL} = 3.01 \times 10^{-14}(A_{H_2})^2 + 6.9998 \times 10^{-10} A_{H_2}$
N_2	632.69	$n_{N_2,SL} = 7.70636 \times 10^{-10} A_{N_2}$
CO	Below detection limit	$n_{CO,SL} = 7.95459 \times 10^{-9} A_{CO}$
CH_4	440.05	$n_{CH_4,SL} = 2.3853 \times 10^{-9} A_{CH_4}$
CO_2	180.23	$n_{CO_2,SL} = 7.1568 \times 10^{-9} A_{CO_2}$

$$n_{H_2,SL} = 3.01 \times 10^{-14}(595.24)^2 + 6.9998 \times 10^{-10}(595.24) = 4.09 \times 10^{-7} \text{moles}$$

$$n_{N_2,SL} = 7.70636 \times 10^{-10}(632.69) = 4.88 \times 10^{-6} \text{ moles}$$

$$n_{CO,SL} = 7.95459 \times 10^{-9}(0) = 0 \text{ moles}$$

$$n_{CH_4,SL} = 2.3853 \times 10^{-9}(440.05) = 1.05 \times 10^{-6}$$

$$n_{CO_2,SL} = 7.1568 \times 10^{-9}(180.23) = 1.29 \times 10^{-6} \text{ moles}$$

$$n_{total,SL,1} = n_{H_2,SL} + n_{N_2,SL} + n_{CO,SL} + n_{CH_4,SL} + n_{CO_2,SL} = 7.6248 \times 10^{-6} \; moles$$

$$n_{C_2^+} = n_{SL,total} - n_{total,SL,1} = 7.6792 \times 10^{-6} - 7.6248 \times 10^{-6} = 5.445510^{-8} \text{ moles}$$

$$n_{\%of\ SL} = n_{\%N_2+H_2+CO+CH_4+CO_2} = \frac{n_{total,SL,1}}{n_{SL,total}} = \frac{7.6248 \times 10^{-6}}{7.6792 \times 10^{-6}} \times 100 = 99.29\%$$

$$n_{\%,C_2^+} = 100\% - 99.29\% = 0.71\%$$

Calculating the composition of the gas product as analysed by the GC ($\boldsymbol{y_i}$)

$$y_i = \frac{n_{i,SL}}{n_{SL,total}} \qquad \text{C-10}$$

$$y_{N_2} = \frac{n_{N_2,SL}}{n_{SL,total}} = \frac{4.88\times10^{-6}}{7.6792\times10^{-6}} = 0.6349$$

$$y_{H_2} = \frac{n_{H_2,SL}}{n_{SL,total}} = \frac{4.09\times10^{-7}}{7.6792\times10^{-6}} = 0.0533$$

$$y_{CO} = \frac{n_{CO,SL}}{n_{SL,total}} = \frac{0}{7.6792\times10^{-6}} \approx 0$$

$$y_{CH_4} = \frac{n_{CH_4,SL}}{n_{SL,total}} = \frac{1.05\times10^{-6}}{7.6792\times10^{-6}} = 0.1367$$

$$y_{CO_2} = \frac{n_{CO_2,SL}}{n_{SL,total}} = \frac{1.29\times10^{-6}}{7.6792\times10^{-6}} = 0.1680$$

C.4.5 Calculating the total moles of gas

Calculating the total moles of gas produced relative to the amount of N_2 added to the reactor ($n_{gas\ phase,total}$):

$$n_{gas\ phase,total} = \frac{n_{N_2,pressure}}{y_{N_2}} \qquad \text{C-11}$$

$$n_{gas\ phase,total} = \frac{0.0413}{0.6349} = 0.06501 \text{ moles}$$

$$n_{i,gas} = y_i n_{gas\ phase,total} \qquad \text{C-12}$$

$$n_{H_2} = 0.0533(0.06501) = 0.0035 \text{ moles}$$

$$n_{CO} = 0(0.06501) = 0$$

$$n_{CH_4} = 0.1367(0.06501) = 0.0089 \text{ moles}$$

$$n_{CO_2} = 0.168(0.06501) = 0.0109 \text{ moles}$$

C.4.6 Calculating the total mass of water soluble products

$$m_{WSP,total} = m_{WSP,filtration} + m_{WSP,KF} + m_{WSP,solids} \quad \text{C-13}$$

$$m_{WSP,filtration} = m_{beaker,full,WSP} - m_{beaker,empty,WSP} \quad \text{C-14}$$

$$m_{WSP,filtration} = 70.1898 - 68.7252 = 1.4646 \text{ g}$$

$$m_{MeOH,total} = m_{MeOH,filtration} + m_{MeOH,solids} \quad \text{C-15}$$

$$m_{MeOH,filtration} = m_{beaker,full,MeOH,filtration} - m_{beaker,full,MeOH,filtration} \quad \text{C-16}$$

$$m_{MeOH,filtration} = 91.9278 - 63.8265 = 28.1013 \text{ g}$$

$$m_{WSP,KF} = \frac{wt.\%H_2O,KF}{100} \times m_{MeOH,filtration} \quad \text{C-17}$$

The water concentration in the MeOH-rich phase as determined *via* Karl-Fischer titration was $11.796\ wt.\%$ ($wt.\%H_2O,KF$):

$$m_{WSP,KF} = \frac{11.796}{100} \times 28.1013 = 3.3146 \text{ g}$$

$$m_{MeOH,solids} = m_{watchglass+filterpaper,wet} - m_{watchglass+filterpaper,dried} \quad \text{C-18}$$

$$m_{MeOH,solids} = 13.2620 - 12.5649 = 0.6971 \text{ g}$$

$$m_{MeOH,total} = 0.6971 + 28.1013 = 28.7984 \text{ g}$$

$$m_{WSP,solids} = \frac{wt.\%H_2O,KF}{100} \times m_{MeOH,solids} \quad \text{C-19}$$

$$m_{WSP,solids} = \frac{11.796}{100} \times 0.6971 = 0.0822 \text{ g}$$

$$m_{WSP,total} = 1.4646 + 3.3149 + 0.0822 = 4.862 \text{ g}$$

C.4.7 Calculating the total mass of the solid and liquid products

$$m_{solids} = m_{watchglass+filterpaper+solids,dried} - m_{watchglass+filterpaper,empty} \quad \text{C-20}$$

$$m_{solids} = 12.5649 - 11.9832 \text{ g} = 0.582 \text{ g}$$

$$m_{solid\ and\ liquid} = m_{solids} + m_{WSP,total} \quad \text{C-21}$$

$$m_{solid/liquid} = 0.582 + 4.866 = 5.4481\ \text{g}$$

Calculating the volume that the liquid/solid product occupied in the reactor ($V_{solid/liquid}$):

$$V_{solid/liquid} = \frac{m_{solid/liquid}}{\rho_{water}} \quad \text{C-22}$$

$$V_{solid/liquid} = \frac{5.4481}{0.997} = 5.465\ \text{mL}$$

C.4.8 Calculating the moles of gas dissolved in liquid phase

Calculating the moles of gas dissolved ($\boldsymbol{n_{i,dissolved}}$) in the liquid phase by means of Henry's law:

$$n_{i,dissolved} = k_H m_{WSP,total} y_i P_{end} \quad \text{C-23}$$

$$k_H(T) = k_H^0 exp\left[\frac{dlnk_H}{d\left(\frac{1}{T_{end}}\right)}\left(\frac{1}{T_{end}} - \frac{1}{298.15}\right)\right] \quad \text{C-24}$$

TABLE C-6 CONSTANTS FOR EACH GAS TO USE IN HENRY'S LAW CALCULATIONS (DATA FROM SANDERS (2015))

GAS COMPONENT	k_H^0 [MOL/KG.BAR]	$\frac{dlnk_H}{d\left(\frac{1}{T_{end}}\right)}$
H_2	7.80E-07	500
N_2	6.00E-07	1300
CO	9.90E-07	1300
CH_4	1.40E-06	1600
CO_2	3.50E-05	2400

$$k_H(T)_{N_2} = 6.0\times10^{-7} exp\left[1300\left(\frac{1}{298.25} - \frac{1}{298.15}\right)\right] = 5.99\times10^{-7}\ \text{mol.g}^{-1}.\text{bar}^{-1}$$

$$n_{N_2,dissolved} = 5.99\times10^{-7}\times4.866\times0.6349\times37.02 = 6.85\times10^{-5}\ \text{moles}$$

$$k_H(T)_{H_2} = 7.8\times10^{-7} exp\left[500\left(\frac{1}{298.25} - \frac{1}{298.15}\right)\right] = 7.8\times10^{-7}\ \text{mol.g}^{-1}.\text{bar}^{-1}$$

$$n_{H_2,dissolved} = 7.80\times10^{-7}\times4.866\times0.0533\times37.02 = 7.49\times10^{-6}\ \text{moles}$$

$$n_{CO,dissolved} \approx 0\ \text{moles}$$

$$k_H(T)_{CH_4} = 1.4\times10^{-6} exp\left[1600\left(\frac{1}{298.25} - \frac{1}{298.15}\right)\right] = 1.4\times10^{-6}\ \text{mol.g}^{-1}.\text{bar}^{-1}$$

$$n_{CH_4,dissolved} = 1.4\times10^{-6}\times4.866\times0.0.1367\times37.02 = 3.44\times10^{-5}\ \text{moles}$$

$$k_H(T)_{CO_2} = 3.5\times10^{-5} exp\left[2400\left(\frac{1}{298.25} - \frac{1}{298.15}\right)\right] = 3.49\times10^{-5}\ \text{mol.g}^{-1}.\text{bar}^{-1}$$

$$n_{CO_2,dissolved} = 3.49\times10^{-5}\times4.866\times0.168\times37.02 = 1.06\times10^{-3}\ \text{moles}$$

Calculating the total moles of gas dissolved ($\boldsymbol{n_{total\ gas\ dissolved}}$) in the liquid phase:

$$n_{total\ gas\ dissolved} = n_{N_2,dissolved} + n_{H_2,dissolved} + n_{CO,dissolved} + n_{CH_4,dissolved} + n_{CO_2,dissolved}$$

$$n_{total\ gas\ dissolved} = 7.49\times10^{-6} + 6.85\times10^{-5} + 0 + 3.44\times10^{-5} + 1.06\times10^{-3}$$

$$n_{total\ gas\ dissolved} = 1.17\times10^{-3}\ \text{moles}$$

C.4.9 Calculating the total moles and mass of each gas product produced

$$n_{i,total} = n_i + n_{i,dissolved} \qquad \text{C-25}$$

$$m_{i,total} = n_{i,total}\times MW_i \qquad \text{C-26}$$

$$n_{N_2,total} = 4.13\times10^{-2} + 6.85\times10^{-5} = 4.13\times10^{-2}\ \text{moles}$$

$$m_{N_2} = 4.13\times10^{-2}\times28.0134 = 1.1582\ \text{g}$$

$$n_{H_2,total} = 3.47\times10^{-3} + 7.49\times10^{-6} = 3.47\times10^{-3}\ \text{moles}$$

$$m_{H_2} = 4.13\times10^{-2}\times2.0158 = 0.0070\ \text{g}$$

$$n_{CO,total} \approx 0\ \text{moles}$$

$$m_{CO} \approx 0\ \text{g}$$

$$n_{CH_4,total} = 8.89\times10^{-3} + 3.44\times10^{-5} = 8.92\times10^{-3}\ \text{moles}$$

$$m_{CH_4} = 8.92\times10^{-3}\times16.0316 = 0.1430\ \text{g}$$

$$n_{CO_2,total} = 1.09\times10^{-2} + 1.06\times10^{-3} = 1.20\times10^{-2}\ \text{moles}$$

$$m_{CO_2} = 1.20\times10^{-2}\times44.01 = 0.5270\ \text{g}$$

Calculating the total mass of the gas produced ($m_{gas,total}$):

The total mass of the gas produced ($m_{gas,total}$, excluding N_2 and C_2+ gases) can then be calculated as follows:

$$m_{gas,total} = m_{H_2} + m_{CO} + m_{CH_4} + m_{CO_2} \quad \text{C-27}$$

$$m_{gas,total} = 0.0070 + 0 + 0.143 + 0.527 = 0.6771 \text{ g}$$

C.4.10 Performing the total mass balance

$$m_{total,in} = m_{water} + m_{PWS,dry} + m_{catalyst} \quad \text{C-28}$$

$$m_{total,in} = 0.6000 + 5.4278 + 0.59998 = 6.6276 \text{ g}$$

$$m_{total,out} = m_{WSP} + m_{gas,total} + m_{solids} \quad \text{C-29}$$

$$m_{total,out} = 4.8618 + 0.6771 + 0.5817 = 6.1205 \text{ g}$$

The % mass balance ($\%MB$) was calculated as follows:

$$\%MB = \frac{m_{total,out}}{m_{total,in}} \times 100 \quad \text{C-30}$$

$$\%MB = \frac{6.1205}{6.6276} \times 100 = 92.42\%$$

C.4.11 Calculating the total and individual gas yields

The total yields of each of the product gases (Y_i) as well as the total gas yield ($Y_{total,gas}$) can then be calculated:

$$Y_i = \frac{n_i}{m_{PWS,dry}} \times 1000 \quad \text{C-31}$$

$$Y_{total,gas} = \frac{n_{total}}{m_{PWS,dry}} \quad \text{C-32}$$

$$Y_{H_2} = \frac{3.47 \times 10^{-3}}{0.600} \times 1000 = 5.79 \text{ mol/kg}_{\text{PWS,dry}}$$

$$Y_{CO} = \frac{0}{0.600} \times 1000 = 0 \text{ mol/kg}_{\text{PWS,dry}}$$

$$Y_{CH_4} = \frac{8.92 \times 10^{-3}}{0.600} \times 1000 = 14.87 \text{ mol/kg}_{\text{PWS,dry}}$$

$$Y_{CO_2} = \frac{1.20 \times 10^{-2}}{0.600} \times 1000 = 19.96 \text{ mol/kg}_{\text{PWS,dry}}$$

$$Y_{total,gas} \times 1000 = \frac{2.44 \times 10^{-2}}{0.600} = 40.62 \text{ mol/kg}_{\text{PWS,dry}}$$

C.4.12 Calculating the gasification efficiencies

The gasification efficiency (GE) was calculated as follows:

$$GE\ [\%] = \frac{m_{gas,total}}{m_{PWS,daf}} \times 100 \quad \text{C-33}$$

$$m_{PWS,daf} = m_{PWS,dry} - \left(\frac{wt.\%_{ash,PWS}}{100} \times m_{PWS,dry}\right) \quad \text{C-34}$$

$$m_{PWS,daf} = 0.6000 - \left(\frac{5.8}{100} \times 0.6000\right) = 0.5652 \text{ g}$$

$$GE\ [\%] = \frac{0.6771}{0.5652} \times 100 = 119.8\%$$

The carbon gasification efficiency (CE) was calculated as follows:

$$CE\ [\%] = \frac{n_{CH_4} + n_{CO_2} + n_{CO}}{n_{C,PWS}} \times 100 \quad \text{C-35}$$

$$n_{C,PWS} = \frac{m_{C,PWS}}{MW_C} \quad \text{C-36}$$

$$m_{C,PWS} = m_{PWS,daf} \times \frac{wt.\%_{C,daf}}{100} \quad \text{C-37}$$

$$m_{C,PWS} = 0.5652 \times \frac{49.37}{100} = 0.2790 \text{ g}$$

$$n_{C,PWS} = \frac{0.2790}{12.011} = 0.0232 \text{ moles}$$

$$CE\ [\%] = \frac{8.92 \times 10^{-3} + 1.20 \times 10^{-2} + 0}{0.0232} \times 100 = 89.95\%$$

The hydrogen gasification efficiency (HE) was calculated as follows:

$$HE\ [\%] = \frac{2n_{H_2} + 4n_{CH_4}}{n_{H,PWS,dry}} \times 100 \quad \text{C-38}$$

$$n_{H,PWS} = \frac{m_{H,PWS}}{MW_H} \quad \text{C-39}$$

$$m_{H,PWS} = m_{PWS,daf} \times \frac{wt.\%_{H,daf}}{100} \quad \text{C-40}$$

$$m_{H,PWS} = 0.5652 \times \frac{5.92}{100} = 0.0335 \text{ g}$$

$$n_{H,PWS} = \frac{0.0335}{1.0079} = 0.0332 \text{ moles}$$

$$HE\ [\%] = \frac{2(3.47 \times 10^{-3}) + 4(8.92 \times 10^{-3})}{0.0332} \times 100 = 128.41\%$$

C.4.13 Calculating the Energy Recovery

The energy recovery in the gas phase (ER) was calculated as follows:

$$ER[\%] = \frac{LHV_{gas,tot}}{LHV_{PWS,dry,tot}} \quad \text{C-41}$$

Calculating the lower heating value of the product gas ($LHV_{gas,tot}$):

$$LHV_{gas,tot} = \sum m_{i,gas} LHV_{i,gas} \quad \text{C-42}$$

$$LHV_{gas,tot} = m_{H_2} LHV_{H_2} + m_{CH_4} LHV_{CH_4} + m_{CO} LHV_{CO} \quad \text{C-43}$$

$$LHV_{gas,tot} = [0.007(119.96) + 0.143(50.03) + 0(10.10)] \times 1000 = 7.99 \text{ kJ}$$

Calculating the LHV of the dry feed ($LHV_{PWS,dry,tot}$):

$$LHV_{PWS,dry,tot} = m_{PWS,dry} \times LHV_{PWS,dry} \quad \text{C-44}$$

$$LHV_{PWS,dry,tot} = \frac{0.600}{1000} \times 16.07 \times 1000 = 9.64 \text{ kJ}$$

$$ER[\%] = \frac{7.99}{9.64} \times 100 = 82.86\%$$

C.4.14 Calculating the higher and lower heating value of the product gas

The HHV_{gas} and LHV_{gas} of the gas product per kg of PWS fed was calculated as follows:

$$HHV_{gas} = \frac{\sum m_{i,gas} HHV_{i,gas}}{m_{PWS,dry}} \quad \text{C-45}$$

$$HHV_{gas} = \frac{m_{H_2} HHV_{H_2} + m_{CH_4} HHV_{CH_4} + m_{CO} HHV_{CO}}{m_{PWS,dry}} \quad \text{C-46}$$

$$HHV_{gas} = \frac{0.007(141.79) + 0.143(55.52) + 0(10.10)}{0.600} = 14.89 \text{ MJ/kg}_{\text{PWS}}$$

$$LHV_{gas} = \frac{7.99\times10^{-3}}{0.600} = 13.3\ \mathrm{MJ/kg_{PWS}}$$

C.4.15 Calculating the hydrogen selectivity

The hydrogen selectivity (S_{H_2}) was calculated as follows:

$$S_{H_2} = \frac{n_{H_2}}{2n_{CH_4}} \quad \text{C-47}$$

$$S_{H_2} = \frac{3.47\times10^{-3}}{2\times8.92\times10^{-3}} = 0.19$$

C.4.16 Performing the carbon balance calculations

$$m_{C,in} = m_{C,PWS} \quad \text{C-48}$$

$$m_{C,PWS} = \frac{\%C_{PWS,daf}}{100}\times m_{PWS,daf} \quad \text{C-49}$$

$$m_{C,out} = m_{C,WSP} + m_{C,solid} + m_{C,gas} \quad \text{C-50}$$

$$m_{C,PWS} = \frac{49.37}{100}\times0.5652 = 0.2790\ \mathrm{g}$$

The total organic carbon (TOC) and total carbon (TC) content of the WSP as analysed by means of the SALM.25 standard method using the thermocatalytic oxidation method), is 346 and 278 mg/L, respectively.

$$m_{C,WSP} = \frac{m_{WSP}}{\rho_{water}}\times TC_{WSP} \quad \text{C-51}$$

$$m_{C,WSP} = \frac{4.8618}{0.997\times1000}\times\frac{346}{1000} = 0.00169\ \mathrm{g}$$

The total carbon content in the solid phase (catalyst + char product) was determined with an elemental analyser as 6.529 wt.%.

$$m_{C,solid} = wt.\%C_{solid\ product}\times m_{solid} \quad \text{C-52}$$

$$m_{C,solid} = 6.529\times0.582 = 0.03798\ \mathrm{g}$$

The total mass of carbon in the gas phase is the sum of the carbon in the CO, CO_2 and CH_4:

$$m_{C,gas} = m_{C,CH_4} + m_{C,CO_2} + m_{C,CO} \quad \text{C-53}$$

$$m_{C,gas} = MW_C\left(n_{C,CH_4} + n_{C,CO_2} + n_{C,CO}\right) \quad \text{C-54}$$

$$m_{C,gas} = 12.011(8.89\times10^{-3} + 1.09\times10^{-2} + 0) = 0.2379 \text{ g}$$

Total mass of carbon out:

$$m_{C,out} = 0.00169 + 0.03798 + 0.2379 = 0.2775 \text{ g}$$

Calculating the % carbon balance:

$$\%CB = \frac{m_{c,out}}{m_{c,in}}\times100 \quad \text{C-55}$$

$$\%CB = \frac{0.2775}{0.2790}\times100 = 99.5\%$$

Calculating the mass of carbon in the MSP and C2+ gases as the balance:

$$m_{C,MSP+C_{2+gas}} = m_{C,in} - m_{C,out} \quad \text{C-56}$$

$$m_{C,MSP+C_{2+gas}} = 0.2790 - 0.2775 = 0.001 \text{ g}$$

C.4.17 Calculating the fraction of carbon yielded in each phase

$$Y_{C,gas} = \frac{m_{C,gas}}{m_{C,in}} \quad \text{C-57}$$

$$Y_{C,WSP} = \frac{m_{C,WSP}}{m_{C,in}} \quad \text{C-58}$$

$$Y_{C,solid} = \frac{m_{C,solid}}{m_{C,in}} \quad \text{C-59}$$

$$Y_{C,MSP+C_{2+gas}} = \frac{m_{C,MSP+C_{2+gas}}}{m_{C,in}} \quad \text{C-60}$$

$$Y_{C,gas} = \frac{0.2379}{0.2790} = 0.852$$

$$Y_{C,WSP} = \frac{0.00169}{0.2790} = 0.0061$$

$$Y_{C,solid} = \frac{0.03798}{0.2790} = 0.136$$

$$Y_{C,gas} = \frac{0.001}{0.2790} = 0.0053$$

Appendix D

Additional Results for SCWG of PWS

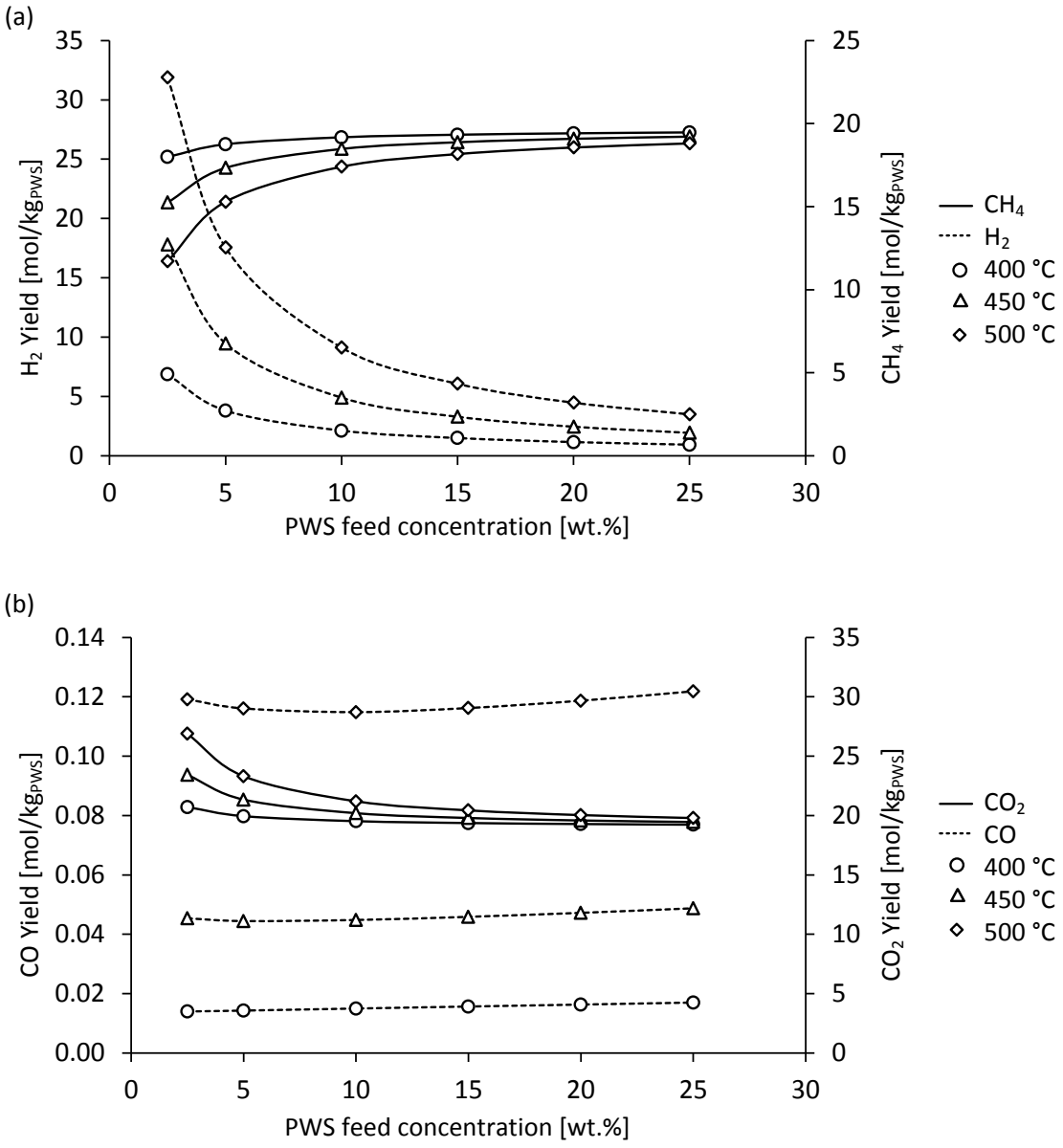

Figure D-1 (a) Theoretical equilibrium H_2 and CH_4 yields of SCWG of 10 wt.% PWS at 450 °C and 27 MPa; (b) Theoretical equilibrium CO and CO_2 yields of SCWG of 10 wt.% PWS and 25 MPa.